

Computational Social Sciences

Petter Holme
Jari Saramäki *Editors*

Temporal Network Theory

 Springer

Computational Social Sciences

Computational Social Sciences

A series of authored and edited monographs that utilize quantitative and computational methods to model, analyze and interpret large-scale social phenomena. Titles within the series contain methods and practices that test and develop theories of complex social processes through bottom-up modeling of social interactions. Of particular interest is the study of the co-evolution of modern communication technology and social behavior and norms, in connection with emerging issues such as trust, risk, security and privacy in novel socio-technical environments.

Computational Social Sciences is explicitly transdisciplinary: quantitative methods from fields such as dynamical systems, artificial intelligence, network theory, agent-based modeling, and statistical mechanics are invoked and combined with state-of-the-art mining and analysis of large data sets to help us understand social agents, their interactions on and offline, and the effect of these interactions at the macro level. Topics include, but are not limited to social networks and media, dynamics of opinions, cultures and conflicts, socio-technical co-evolution and social psychology. Computational Social Sciences will also publish monographs and selected edited contributions from specialized conferences and workshops specifically aimed at communicating new findings to a large transdisciplinary audience. A fundamental goal of the series is to provide a single forum within which commonalities and differences in the workings of this field may be discerned, hence leading to deeper insight and understanding.

Series Editor:

Elisa Bertino Purdue University, West Lafayette, IN, USA	Larry S. Liebovitch Queens College, City University of New York, Flushing, NY, USA
Claudio Cioffi-Revilla George Mason University, Fairfax, VA, USA	Sorin A. Matei Purdue University, West Lafayette, IN, USA
Jacob Foster University of California, Los Angeles, CA, USA	Anton Nijholt University of Twente, Enschede, The Netherlands
Nigel Gilbert University of Surrey, Guildford, UK	Andrzej Nowak University of Warsaw, Warsaw, Poland
Jennifer Golbeck University of Maryland, College Park, MD, USA	Robert Savit University of Michigan, Ann Arbor, MI, USA
Bruno Gonçalves New York University, New York, NY, USA	Flaminio Squazzoni University of Brescia, Brescia, Italy
James A. Kitts University of Massachusetts Amherst, MA, USA	Alessandro Vinciarelli University of Glasgow, Glasgow, Scotland, UK

More information about this series at <http://www.springer.com/series/11784>

Petter Holme • Jari Saramäki
Editors

Temporal Network Theory



Springer

Editors

Petter Holme 

Tokyo Tech World Research Hub
Initiative (WRHI)
Institute of Innovative Research
Tokyo Institute of Technology
Tokyo, Japan

Jari Saramäki

Department of Computer Science
Aalto University
Espoo, Finland

ISSN 2509-9574

Computational Social Sciences

ISBN 978-3-030-23494-2

<https://doi.org/10.1007/978-3-030-23495-9>

ISSN 2509-9582 (electronic)

ISBN 978-3-030-23495-9 (eBook)

© Springer Nature Switzerland AG 2019

This work is subject to copyright. All rights are reserved by the Publisher, whether the whole or part of the material is concerned, specifically the rights of translation, reprinting, reuse of illustrations, recitation, broadcasting, reproduction on microfilms or in any other physical way, and transmission or information storage and retrieval, electronic adaptation, computer software, or by similar or dissimilar methodology now known or hereafter developed.

The use of general descriptive names, registered names, trademarks, service marks, etc. in this publication does not imply, even in the absence of a specific statement, that such names are exempt from the relevant protective laws and regulations and therefore free for general use.

The publisher, the authors, and the editors are safe to assume that the advice and information in this book are believed to be true and accurate at the date of publication. Neither the publisher nor the authors or the editors give a warranty, express or implied, with respect to the material contained herein or for any errors or omissions that may have been made. The publisher remains neutral with regard to jurisdictional claims in published maps and institutional affiliations.

This Springer imprint is published by the registered company Springer Nature Switzerland AG.

The registered company address is: Gewerbestrasse 11, 6330 Cham, Switzerland

Preface

Great minds think alike! Many researchers have gotten the idea that there is structure in the times of when things happen, in addition to network structure, that can be exploited in modeling and data analysis. This, we believe, is inevitable in any active, interdisciplinary field and not necessarily a bad thing, especially because great minds don't think identically. There is a multitude of frameworks, mathematical representations, data structures, and visualization methods that are, on the one hand, equivalent (there are one-to-one mappings between them) and, on the other hand, emphasizing different aspects of the data. The main motivation behind this book is to show these different ways of thinking about temporal networks.

Our second motivation is to showcase the field of temporal networks 6–7 years after our previous edited volume *Temporal Networks* (in the Springer Complexity series). At the time that book was published, temporal networks felt like an immature subfield that had just figured out that it was sufficiently different from (static) network science and that it could not simply bake the same cake over and over again, this time sprinkling temporal information on top. Now, 3/4 of a decade later, temporal networks still feels like an immature subfield, struggling to break free from the ideas of static network science. Where this will end is not completely clear. Maybe some great mind, relaxing in the hammock with this book, will be able to unify the many directions taken. Or there may be a future where the current diversity of ideas will provide ingredients for cooking great science. Either way, temporal networks is a field that is younger than its age.

We hope this book will inspire new methods and discoveries and perhaps guide applied researchers to useful approaches. We also hope that this is the last time that the preface of a Springer temporal networks volume claims that temporal networks is a young field!

Tokyo, Japan
Espoo, Finland
August 2019

Petter Holme
Jari Saramäki

Contents

A Map of Approaches to Temporal Networks	1
Petter Holme and Jari Saramäki	
Fundamental Structures in Temporal Communication Networks.....	25
Sune Lehmann	
Weighted, Bipartite, or Directed Stream Graphs for the Modeling of Temporal Networks	49
Matthieu Latapy, Clémence Magnien, and Tiphaine Viard	
Modelling Temporal Networks with Markov Chains, Community Structures and Change Points	65
Tiago P. Peixoto and Martin Rosvall	
Visualisation of Structure and Processes on Temporal Networks	83
Claudio D. G. Linhares, Jean R. Ponciano, Jose Gustavo S. Paiva, Bruno A. N. Travençolo, and Luis E. C. Rocha	
Weighted Temporal Event Graphs	107
Jari Saramäki, Mikko Kivelä, and Márton Karsai	
Exploring Concurrency and Reachability in the Presence of High Temporal Resolution	129
Eun Lee, James Moody, and Peter J. Mucha	
Metrics for Temporal Text Networks	147
Davide Vega and Matteo Magnani	
Bursty Time Series Analysis for Temporal Networks	161
Hang-Hyun Jo and Takayuki Hiraoka	
Challenges in Community Discovery on Temporal Networks.....	181
Remy Cazabet and Giulio Rossetti	
Information Diffusion Backbone	199
Huijuan Wang and Xiu-Xiu Zhan	

Continuous-Time Random Walks and Temporal Networks	219
Renaud Lambiotte	
Spreading of Infection on Temporal Networks: An Edge-Centered Perspective	235
Andreas Koher, James P. Gleeson, and Philipp Hövel	
The Effect of Concurrency on Epidemic Threshold in Time-Varying Networks	253
Tomokatsu Onaga, James P. Gleeson, and Naoki Masuda	
Dynamics and Control of Stochastically Switching Networks: Beyond Fast Switching	269
Russell Jeter, Maurizio Porfiri, and Igor Belykh	
The Effects of Local and Global Link Creation Mechanisms on Contagion Processes Unfolding on Time-Varying Networks	305
Kaiyuan Sun, Enrico Ubaldi, Jie Zhang, Márton Karsai, and Nicola Perra	
Supracentrality Analysis of Temporal Networks with Directed Interlayer Coupling	325
Dane Taylor, Mason A. Porter, and Peter J. Mucha	
Approximation Methods for Influence Maximization in Temporal Networks	345
Tsuyoshi Murata and Hokuto Koga	
Index	369

A Map of Approaches to Temporal Networks



Petter Holme  and Jari Saramäki

1 Overview

If we want to make sense of large, complicated systems via the data they leave behind, we need ways of systematically simplifying them. Such simplifications typically need to be very drastic. A common first step is to represent the system as a network that only stores information on which units are connected to which other units. In order to investigate the World Wide Web with this approach, one would neglect the content, the owner, the time of creation, and the number of downloads of a webpage, and instead, only consider individual webpages and how they are linked together. The second step is to apply the methods of network science to find important nodes or clusters of nodes with some special role or function, or to study how the wiring of the network controls some dynamical system. The fundamental idea of this book is that one can learn more about a system if one does not, at the first step of simplification, discard information about when things happen. Consequently, one needs to modify the second step and develop a science of temporal networks that exploits this additional information.

The fundamental idea of retaining the information about time is evidently not a hard one to get. Temporal networks have been invented and reinvented many times. Researchers have proposed many mathematical and computational frameworks—some equivalent, some not. This is probably inevitable for such an extraordinarily interdisciplinary field of science—temporal networks have been

P. Holme (✉)

Tokyo Tech World Research Hub Initiative (WRHI), Institute of Innovative Research,
Tokyo Institute of Technology, Tokyo, Japan
e-mail: holme@cns.pi.titech.ac.jp

J. Saramäki

Department of Computer Science, Aalto University, Espoo, Finland
e-mail: jari.saramaki@aalto.fi

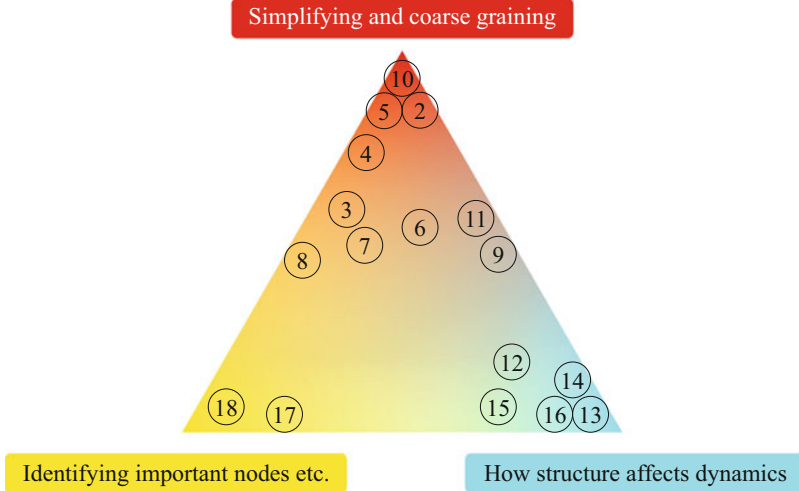


Fig. 1 A schematic map of the chapters of this book, positioned with respect to the three main research themes within the study of temporal networks

applied to neuroscience, transportation problems, social theory [13], control theory [53], ecology [100], and many more areas. The many existing frameworks could be frustrating for a newcomer to temporal networks. Part of our idea with this book was to showcase this diversity, see the chapters “Fundamental Structures in Temporal Communication Networks”, “Weighted, Bipartite, or Directed Stream Graphs for the Modeling of Temporal Networks”, and “Dynamics and Control of Stochastically Switching Networks: Beyond Fast Switching” for very different ways of thinking about networks in time.

Even if you encounter a problem where both the network and the temporal aspects should play a role, there is no general recipe to follow. The goal of this introductory chapter is to provide a rough map of the field—what types of questions researchers have been interested in, and what results there are out there. We will also try to place the subsequent chapters on their correct locations on this map (Fig. 1). This chapter is not a catalogue of techniques or an introduction to a comprehensive and self-consistent theory. For readers interested in that, our review papers [33, 35] the book by Masuda and Lambiotte [58] or by Batagelj et al. [10] will be a better read.

2 Temporal Network Data

In this section, we discuss the many subtleties about how to represent a system as a temporal network in a meaningful way.

2.1 Events

The fundamental building blocks of temporal networks are events (or contacts, links, or dynamic links). These represent units of interaction between a pair of nodes at specified times. Often, they take the form of triples (i, j, t) showing that nodes i and j are in contact at time t . Sometimes the time can be an interval, rather than just a moment.

As we will see throughout this book, temporal-network modeling is far from a straightforward generalization of static networks—often, it is fundamentally different. As a first example, we note that events are not always a straightforward generalization of links of the static networks. Take e-mail communication as an example. In static network modeling, one typically assumes that the links (between people that have exchanged email) indicate social relationships. These links can be viewed as the underlying infrastructure for e.g. information spreading since people who know each other exchange information. The links are there not only for one email to be sent but represent persistent opportunities for spreading events for the duration of the relationship. In contrast, an event in a temporal e-mail network is simply one e-mail being sent, and this is something that usually happens for the explicit purpose of spreading information. But there are also systems other than e-mail communication where events are more like links of static networks. Consider, for example, transportation systems, where the bus, train or flight connections are really opportunities to travel that happen whether a certain person needs to use them or not. As we will see, different approaches treat these two interpretations of events differently.

2.2 Boundaries

In the natural sciences, we can sometimes model time as a dimension, if not exactly like space then at least similar to it. For temporal networks, the binary connections and the time are more fundamentally different concepts. The simplest way of seeing this is to consider the network's boundaries (between what is contained in a data set and what is not). Regarding time, a temporal network data set almost always covers a time interval, and the interval is the same for all nodes. The structural boundaries of the network dimension are usually less controlled. Similar to cohort studies in the social sciences, one would like to have a selection of nodes that is as tight-knit as possible, typically defined by common features. For example, Ref. [93] is based on data from voluntary participants among the freshmen of a university—better than a random group of people, but worse than the complete group of freshmen.

Boundaries become a problem when one wants to control the size of a data set. If a temporal network is too large to handle or one wants to understand the effects of size, how should one reduce the size of the network without changing its structure? One could reduce the number of nodes by random sub-sampling, or perhaps simply

truncate the data in the temporal dimension. However, both these approaches would introduce biases. While there are ways of correcting some of those [48], it is hard to avoid problems. For example, if one truncates the data, there might not be enough time for a spreading process to saturate before the sampling interval is over. If one deletes nodes, or events, one introduces other biases. The proper way of resampling a temporal network must simultaneously vary the number of nodes and the sampling duration, but exactly how is still an open question.

2.3 Connectivity

It is fundamental to any kind of network modeling that being indirectly connected through a path is relevant to dynamic processes. This is true for temporal networks as well, but the connections have to happen along time-respecting paths of contacts (with strictly increasing timestamps). Indirect connections through time-respecting paths are not transitive (see Fig. 2)—even if one can get from A to B and B to C, it might still be impossible to go from A to C because one would arrive at B too late

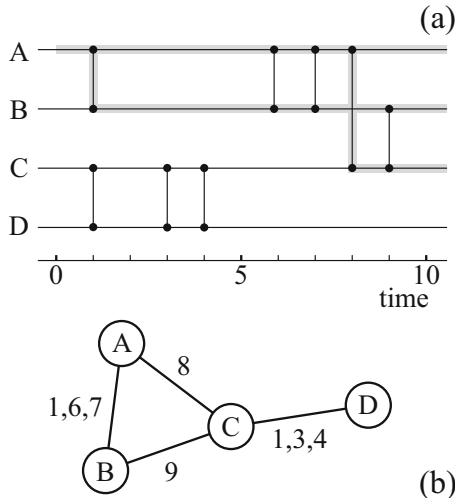


Fig. 2 An illustration of two ways to visualize small temporal networks that can be convenient for reasoning about measures and methods. Panel (a) shows a time-line graph where an epidemic outbreak starting at node A is indicated by grey lines. In almost all cases, paths between nodes (that follow events) in temporal networks need to go forward in time (to the right in the plot). (b) shows the same data, but plotted projected onto a static graph. The latter visualization highlights the underlying static network structure at the expense of the temporal information. The former, the time-line plot, can capture many types of temporal structures but is inconvenient for network structure

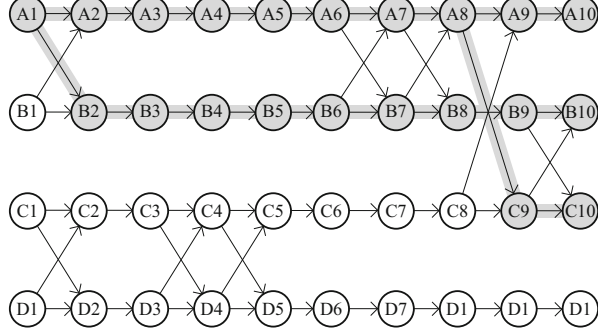


Fig. 3 A time-node representation of the data in Fig. 2. This is a (directed, acyclic) static graph containing the same information as in Fig. 2 but the meaning of nodes and edges is different

for a further connection to be possible. Contrary to this, all static networks, directed networks included, are transitive.

Another important difference to static networks is that connectivity itself is temporal: even if there is a path from A to B now, whether direct or indirect, there might be none a second later. Therefore, the statement “A is connected to B” is not necessarily even meaningful unless the time (interval) of this connection is specified. The above issues mean that one can never reduce a temporal network into a static one without losing information or changing the meaning of the nodes (cf. Fig. 3).

Since many static network tools are based on paths and distances, researchers have sought to generalize these concepts to static networks. Once again, the addition of a temporal dimension makes this task much more complicated. The most common generalization of distance is *latency (temporal distance)* [50]—the time it would take to reach j from i starting at time t and following only time-respecting paths. For a longer discussion about paths and connectivity, see Refs. [33, 35, 58].

3 Simplifying and Coarse-Graining Temporal Networks

Even if representing data as a temporal network means that information has to be discarded for the sake of simplification, this is often not enough to get an understanding of the large-scale organization of the system. There are many ideas how to further simplify a temporal network that we will discuss in this section.

3.1 Projections to Static Networks

Perhaps the most obvious way of simplifying a temporal network is to turn it into a static network. In fact, many classical examples of static networks like citation

networks or affiliation studies (like the “Southern Women” study of 1941 [18]) have temporal link information, but the time is ignored by simply only studying the network of all aggregated contacts or separate “snapshot” graphs that represent different times.

If one, from time-stamped data, constructs a binary static network where nodes are only linked or not, it is obvious that a lot of information is lost. A better option is to include information on the number or frequency of connections between pairs of nodes, leading to weighted networks. In this case, the link weights can provide important insights into the network structure (see, e.g., [7, 68]). However, including links between all nodes that have been in contact can in some cases result in a very dense network. In this case, one can threshold the network, discarding the weakest links, or extract the backbone of the network [86].

It is obvious that the above weighted-network approach is not really temporal, because if one manipulates the times of the contacts, the outcome will remain the same. The simplest static networks that truly encode some temporal effects are *reachability graphs*. These graphs have a directed edge (i, j) if one can reach j from i via a time-respecting path.

Another way of creating sparser static networks than thresholding weighted graphs is to aggregate contacts within a time window [49]. While the thresholded graphs contain information about the contacts that are the most common in the whole sampling interval, time-window graphs emphasize shorter time-scales, and their sequence captures at least part of the network dynamics. Indeed, tuning the duration of the time windows can be a way to understand the organization of the data [85]. Yet a similar idea is to construct networks where links represent ongoing relationships [30]—pairs of nodes that, at some point in time, have had contacts before and will have them again.

One more elaborate way of reducing temporal networks to static ones is the extraction of backbones specifically with respect to spreading processes on temporal networks [103] and the chapter “Information Diffusion Backbone”. By this approach, links in the resultant network correspond to node pairs that are likely to infect each other in an epidemic outbreak.

As mentioned above, these approaches can never retain all temporal features of the original data. Nevertheless, analyzing temporal networks by making them static is rather attractive because there is a plethora of methods for static-network analysis. One way of circumventing the problem of information loss is to use more elaborate mappings, where temporal networks are mapped onto static network structures whose nodes and links represent something else than the original network’s nodes and links. One example is temporal event graphs, whose nodes correspond to the original network’s events (see [47, 61] and the chapter “Weighted Temporal Event Graphs” of this book).

One common approach that can also be interpreted as static-network projection is to use multilayer networks, as in the chapter “Supracentrality Analysis of Temporal Networks with Directed Interlayer Coupling” of this book: time is sliced into consequent intervals, and the layers of a multilayer network correspond to networks aggregated for each interval. Once the layers are coupled (e.g. with a directed

link from a node to its future self), one can then apply (static) multilayer network methods to the system. Importantly, the layers in such a projection are ordered by time.

Finally, temporal network data can also be projected to *higher-order network models* that retains some information of the flows over the network. The Chapter “Modelling Temporal Networks with Markov Chains, Community Structures and Change Points” discusses such approaches.

3.2 Separating the Dynamics of Contacts, Links and Nodes

Instead of reducing temporal network data to static networks, one can try to retain some but not all of the temporal features. One example is the statistics of times between contacts. It was early recognized that often, the times between events, both for nodes and links, have heavy-tailed distributions [30, 40] (they are *bursty* [5, 42]). Subsequent studies (e.g. Ref. [43, 63]) found that this burstiness of inter-event times slows down spreading processes: simulated spreading that takes place on bursty networks is slower than it is on networks where the burstiness has been artificially removed. However, the result is the same when the heavy-tailed inter-event times are part of the dynamical process itself: when a spreading process with power-law distributed waiting times is placed on a static network [62], it is slow too. This is related to how events are interpreted (see Sect. 2.1 and the chapter “Continuous-Time Random Walks and Temporal Networks”): are they separated from the process and just passive conduits for it, as in spreading on top of bursty event sequences, or are the events actively generated by the process, as one could interpret the combination of spreading with broad waiting times and a static network? Figure 4a, b illustrate homogeneous and heterogeneous (bursty) link dynamics on top of a static network. See also the chapter “Bursty Time Series Analysis for Temporal Networks” that goes deeper into this issue. Note that under some conditions, burstiness may also speed up spreading [37, 77].

Another way of simplifying temporal networks is to ignore contact dynamics and just think of links as present between the first and last observation of a contact in the data and ignore the precise timing of contacts [34]. Compared to simplifying the system as bursty dynamics on top of static networks, this picture emphasizes longer time structures such as the general growth and decline of activity in the data. Figure 4c illustrates a data set that is well-modeled by links appearing and disappearing, disregarding the interevent time statistics.

3.3 Mesoscopic Structures

In science in general, “mesoscopic” refers to the scales between macroscopic and microscopic. In network science, this would mean structures larger than nodes but smaller than the entire network, and indeed, the term is often used in the context of

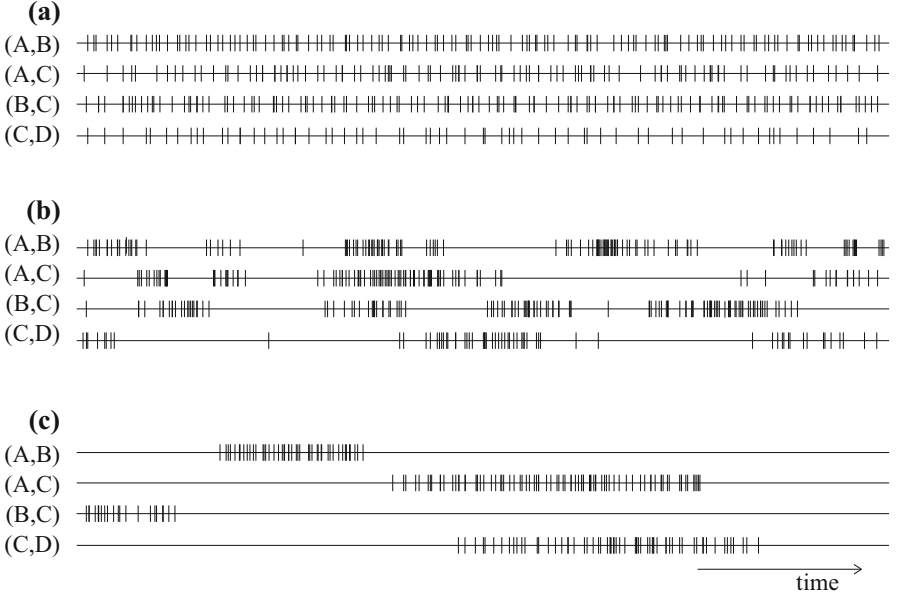


Fig. 4 Three scenarios of temporal edge structure. The figures show time lines of contacts along edges in a four-node graph. Panel **(a)** shows a scenario with narrow distributed inter-event times; **(b)** shows a bursty edge dynamics; **(c)** shows a scenario with a turnover of edges—where the time between the beginning of the sampling to the first contact, or from the last contact to the end of the sampling, is too long to be explained by the interevent time distributions

grouping nodes into classes based on how they are connected to each other and the rest of the network. The primary example of mesoscopic structures is community structure—that some networks have clear groups that are strongly connected within and weakly connected between each other [84].

Most methods for community detection in static networks divide the network so that every node belongs to one group only (the chapter “Challenges in Community Discovery on Temporal Networks”). The straightforward extension of this idea to temporal networks would be to let nodes belong to different groups at different times, but only to a single group at each point in time [79]. This is also the most common assumption in the literature, see e.g. Refs. [65, 69, 81]. This view focuses on the individual nodes and seeks to group them in some principled way. If one, on the other hand, focuses on the communities instead of the nodes and prioritizes definitions that give interpretable communities (one temporal-network community could for example represent one seminar, one concert, etc.), it makes sense not to require every node to be member of a group at every point in time [85], as in the chapter “Fundamental Structures in Temporal Communication Networks”.

Other mesoscopic structures, such as core-periphery structures [78], have been less studied for temporal networks (even though there are some works—e.g. [75] uses core-periphery analysis to understand ant-plant networks). Finally, *temporally*

connected components (see chapter “Weighted Temporal Event Graphs” and [47]) span the structural scale from mesoscopic to macroscopic, both in terms of network structure and with respect to time.

3.4 Fundamental Structures

In the chapter “Fundamental Structures in Temporal Communication Networks” and Ref. [85], Lehmann et al. discuss the traces that the six fundamental interaction types leave on temporal networks. Chapter “Fundamental Structures in Temporal Communication Networks” presents a division of the interaction types in the configuration of participants (one-to-one, one-to-many and many-to-many) and synchronicity (synchronous and asynchronous). In the limit of a short time interval projection of a temporal network data set, these different communication events contribute with different subgraphs—synchronous one-to-many communication yields a star graph, and synchronous many-to-many communication yields a clique. By tuning the time window, one can identify the timescales of influence of these “fundamental structures”.

4 Important Nodes, Links and Events

Perhaps the most common question for static networks is to find important nodes (where “important” should be interpreted in a very broad sense). This question is just as relevant for temporal networks. This is maybe the topic where the approaches borrowed from the static-network toolbox are most applicable to temporal networks. One major difference is that it is meaningful to talk about the importance of contacts (in addition to nodes and links) for temporal networks [96]. Another difference is that the most principled, general measures of importance are time-dependent, simply because in most contexts a node can become more or less important in time.

4.1 Generalizing Centrality Measures

A huge number of papers have been devoted to the generalization of classical centrality measures to temporal networks, see Refs. [70, 98] and the chapters “Metrics for Temporal Text Networks” and “Supracentrality Analysis of Temporal Networks with Directed Interlayer Coupling”. In many cases—for distance-based centrality measures—they have taken the obvious approach of replacing distances by latency. Since temporal networks are typically less connected (in the sense that the fraction of nodes that are reachable through time-respecting paths is smaller than the corresponding quantity in static networks), centrality measures

have to work in fragmented networks. This means that one needs to combine information about how many nodes can be reached with information on how easily they can be reached (or whatever rationale the corresponding static centrality measure has). One example would be to generalize closeness centrality by averaging reciprocal latencies, rather than taking the inverse of the averages [97]. This is, however, an arbitrary combination of two aspects of centrality and quite typical for straightforward generalizations of static concepts to temporal networks—they become less principled than their static counterparts.

4.2 Controllability

The rationales of centrality measures comes from reasoning about dynamic systems—you can reach other nodes quickly from central nodes; central nodes are in the middle of heavy traffic; etc. The purpose of measuring centrality is typically to rank the nodes and perhaps list the most central ones. Finding *control nodes* involves a slightly different thinking. Instead of ranking the nodes, the control nodes are minimal sets of nodes needed to be manipulated in order for the entire network to reach a certain state. Ref. [53] and subsequent works show that temporal networks can facilitate controllability—i.e. the system can be controlled with less energy and by fewer nodes if it has temporal heterogeneities.

4.3 Vaccination, Sentinel Surveillance, and Influence Maximization

The problems of vaccination, sentinel surveillance, and influence maximization are related to questions about spreading phenomena. Similarly to controllability, one assumes some objective and some sort of intervention to the underlying temporal-network structure. In this case, however, the objective is typically to minimize or maximize the number of nodes reached by some spreading dynamics (like infectious disease, word-of-mouth marketing, etc.).

The *vaccination* problem is to select nodes that would minimize or slow down disease spreading as much as possible. Typically one assumes that the vaccinated nodes are deleted from the system so that they can no longer become infected and spread the disease. Unlike centrality measures, but similarly to controllability, it usually makes no sense to talk about the importance of individual nodes with respect to the vaccination procedure—vaccinating one or a few nodes in a large network would have no measurable effect on the epidemics. Instead, the importance of nodes comes from the membership of a group that is vaccinated [27]. Another important point is that one can typically not assume knowledge about the entire network of contacts—only the interactions that could reliably be reported by individuals can serve as input for vaccination protocols. For example, Refs. [24, 91] propose vaccination protocols that exploit temporal structures.

The *influence maximization* problem deals with finding seed nodes for spreading dynamics that maximize the number of reached nodes [45]. The prime application is viral marketing, but to protect against outbreaks that have not yet entered a population influence maximization is also interesting for network epidemiology. The nodes that are important for vaccination and influence maximization do not necessarily have to be the same—optimal node sets for vaccination typically fragment the network efficiently, whereas influence maximization emphasizes efficiently splitting the network into subnetworks of influence. The first problem is akin to *network attack* or *network dismantling* [11], and the second to finding a *vertex cover* [20]. To exploit temporal structures, one can identify nodes in a heightened state of activity or nodes that reliably influence others (chapter “Approximation Methods for Influence Maximization in Temporal Networks”).

Sentinel surveillance assumes that one can put sensors (sentinels) on the nodes. The task is to choose locations of the sensors such that disease outbreaks are discovered as reliably or quickly as possible. This is probably the least studied of these three problems on temporal networks—we are only aware of Ref. [4]. On the other hand, it is practically a more important problem since it is currently in use in health care systems [2]. Ref. [4] tests how efficient temporal network protocols originally developed for vaccination are for the problem of sentinel surveillance.

4.4 Robustness to Failure and Attack

A problem that is very much overlapping with influence maximization etc. is network robustness. The scenario is that some adversary is trying to destroy a network. This adversary can have different amounts of information or resources to carry out the attack, which yields different versions of the problem. With no information about the network, the problem reduces to *node percolation* (or *robustness to failure*). With perfect information but limited computational resources the problem is equivalent to network dismantling. It is both interesting to study optimal heuristics for this problem and what network structures that are contributing to the robustness of a network. For temporal networks, this problem was studied in Refs. [83, 99], but there should be several ways of extending their work and in general temporal-network robustness seems to be an understudied area. This may have to do with the fact that the temporal dimension makes the whole framework of percolation more complicated (see chapter “Weighted temporal event graphs”).

5 How Structure Affects Dynamics

For models of disease spreading, heterogeneous, heavy-tailed degree distributions are known to speed up the dynamics [9]. One line of research in temporal network studies is to identify similar relations between the structure of the data and dynamics taking place over the contacts.

The types of dynamics people have been studying on underlying temporal networks include disease spreading of different kinds (the chapters “Exploring Concurrency and Reachability in the Presence of High Temporal Resolution”, “Information Diffusion Backbone”, “Spreading of Infection on Temporal Networks: An Edge-Centered Perspective”, “The effect of concurrency on epidemic threshold in time-varying networks”, and “The Effects of Local and Global Link Creation Mechanisms on Contagion Processes Unfolding on Time-Varying Networks”) [22], threshold models of complex contagion [3, 95], random walks (the chapter “Continuous-Time Random Walks and Temporal Networks”) [19, 58, 82, 89], navigation processes [51], synchronization (the chapter “Dynamics and Control of Stochastically Switching Networks: Beyond Fast Switching”) and even game-theoretic models [14, 104].

5.1 Simulating Disease Spreading

Disease spreading typically follows standard compartmental models developed by applied mathematicians [12, 29]. Such models divide a population into classes with respect to the disease and then state transition rules between the classes. The key transition rule that exists in all compartmental models is the *contagion event* where a susceptible individual becomes infected when in contact with an infectious individual. In the two canonical and most well-studied models—the SIS (susceptible–infectious–susceptible) and SIR (susceptible–infectious–recovered) models—the contagion event is paired with the recovery of individuals (in SIS, recovered individuals become susceptible again, whereas in SIR they become immune to the disease or die). The probability that a contact between a susceptible individual and an infectious individual results in contagion is usually a parameter of the model, and it is assumed to be the same for all contacts (which is an assumption done for convenience and not realism).

Many assumptions are needed for simulating compartmental model on a temporal network of contacts [21, 57]. Unless modelling bio-terrorism or the spread of something else than a disease, it makes no sense to select more than one seed. With no prior knowledge about the entry into the population, one should choose this seed uniformly at random. By the same principle, one should choose the time of infection uniformly randomly as well. This could of course lead to the outbreak not being able to reach all nodes, so that the measured outbreak sizes are an average of outbreak sizes of different times. For this reason, some authors choose to start the outbreak early in the interval their data covers, even though that introduces a bias if e.g. the activity in the data grows [76]. Another commonly used approach is to use periodic boundary conditions and repeat the data from the beginning (e.g., in Ref. [43]).

Another important consideration is the duration of the infectious period. In the mathematical epidemiology literature, it is usually taken to be exponentially distributed to achieve the Markov property (that the probability to recover is independent of the time since the infection). Markovian SIR and SIS are not only

easier to analyze analytically, but also allow for some tricks to speed up simulation code (see github.com/pholme for very fast, even-driven code for the Markovian SIR on temporal networks). Some studies use a constant duration of infection for all nodes. To the best of our knowledge, no studies have tried duration distributions inferred from data.

Another decision that anyone simulating disease spreading (or random walks) on temporal networks needs to make is what to do with contacts happening in the same time step. There are, as we see it, two principled solutions. Either one assumes that this allowed, in which case one then needs to pick contacts with the same time stamp in a random order and average over different randomizations; or one assumes the disease cannot spread via an intermediate node in a single time step. This is effectively to assume an SEIS or SEIR model (E stands for *exposed*, which means that the individual will become infectious in the future, but is not yet infectious), with the duration of the E state being less than the time resolution of the temporal network.

Another slight difference in approaches, especially in studies where the underlying temporal network is generated by a model, is that of *link-centric* and *node-centric* compartmental models. In node-centric models [39, 59], the time to the next contact that could spread the disease is determined at a contagion event. In link-centric models [37, 101] the contacts are generated independently of the propagation of the disease. The node-centric model simplifies analytical calculations whereas the link-centric model is conceptually simpler and perhaps more realistic (even though the assumption that the contact dynamics is independent of what spreads on the network is probably often invalid).

Typically, papers about disease spreading have focused on understanding how network structure affects the final outbreak size [34, 57, 62]. Some, however, have studied early outbreak characteristics such at the basic reproductive number R_0 (the expected number of others an infectious individual would infect in a completely susceptible population) [55, 76]. From a medical point of view, there is no obvious choice between these two—even though the societal concern is to minimize the outbreak size. The outbreak size is also a consequence of interventions that are not modelled by the canonical disease-spreading models such as SIS and SIR, and thus the early phase of the disease, which is better summarized by R_0 , could be more informative.

Random-walk studies have focused on the *mean first passage time*—the expected time since the beginning of a walk that the walker reaches a node—and *reachability*—the probability a that node is reached by a walker starting at a random node [58, 82]. Another topic of interest has been how topological and temporal structure affects the speed of diffusion [19]. As opposed to spreading of disease, there is no directly obvious real-world phenomenon that would be well-modeled by random walks on temporal networks; however, random walks equal diffusion, and diffusion can be considered a fundamental process in any system. Often, the random walk process is simply used as a probe of the temporal network structure.

5.2 Tuning Temporal Network Structure by Randomization

The most straightforward way of understanding the impact of temporal network structure on dynamic processes is of course to tune it and monitor the response on some quantity describing the dynamics. There were important contributions (also involving temporal structures) in this direction even before the turn-of-the-millennium network boom. For example, Morris and Kretzschmar studied the effect of concurrency, or overlapping relations, on outbreak sizes [64].

The most common way of investigating the effect of structures on temporal network is to use randomization schemes. This approach starts with empirical networks and then destroys some specific correlation by randomizing it away. For example, one can randomly swap the time stamps of contacts or replace the time stamps with a random time stamp chosen uniformly between the first and last of the original data [31]. The former randomization is more restrictive in that it preserves the overall activity pattern and per-node and per-link inter-event time statistics (see Fig. 5). Randomization schemes turns out to be much more versatile for temporal networks than for static ones. Ref. [23] gives a comprehensive theory of almost 40 different randomization schemes. By applying increasingly restrictive methods to

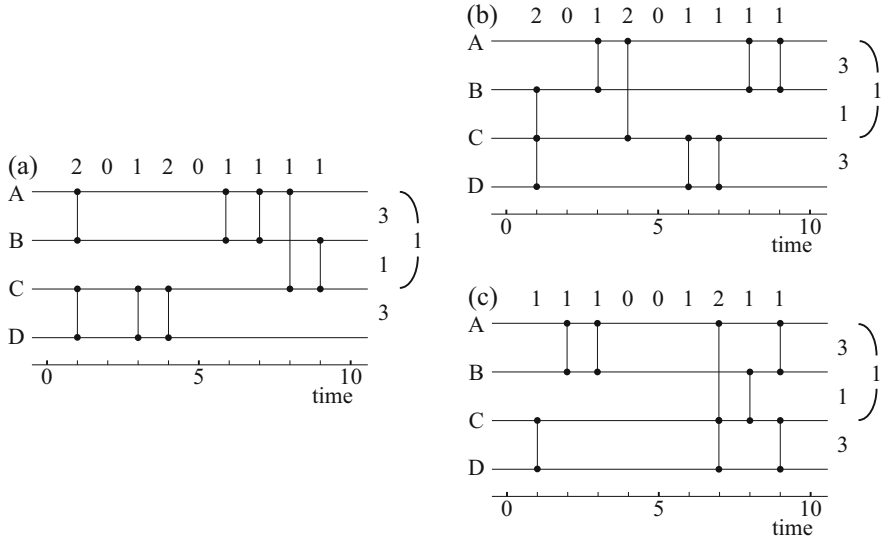


Fig. 5 Illustrating two types of randomization procedures. Panel (a) shows a temporal network that is randomized by randomly swapping time stamps (b) and by replacing time stamps by random ones (c). The randomization in (b) preserves both the number of contacts per time (the numbers above) and the number of contacts per pair of nodes (the numbers to the right). The randomization procedure of panel (c) preserves the number of contacts per pair of nodes, but not the number of contacts per time

real data sets one can see how much structure is needed to recreate the behavior of the original temporal network.

In general, the terminology of temporal networks is ambiguous. The topic itself sometimes goes under the names “dynamic networks”, “temporal graphs”, or “time-varying networks”. The randomization schemes above are no exception—Ref. [31] calls the scheme of Fig. 5b “permuted times”, Ref. [43] calls it “shuffled times” and Ref. [23] calls it “shuffled timestamps”.

5.3 Models of Temporal Networks

Another way of tuning temporal network structure, other than randomization, is by generative models. Generative models of temporal networks serve a different role than for static networks. Static network science, traditionally used models of network evolution as proof-of concept models for theories about emergent properties, like power-law degree distributions [6] or community structure [25]. For temporal networks, there are common structures combining temporal and network structures in a non-trivial way that also is non-trivial to explain. Nevertheless, models of temporal networks are needed, if for nothing else then to generate underlying data sets for controlled experimentation. In this section, we will mention some of the central developments in this area. For a more complete overview, see Ref. [33].

The most straightforward approach to generate a temporal network is to generate a static network and assign a sequence of contacts to every link. For example, Ref. [32] uses the following procedure:

1. Construct a simple graph by first generating an instance of the configuration model [66] and merging multiple links and self-links from it.
2. For every link, randomly generate an interval when contacts can happen.
3. Generate a sequence of contacts following an interevent time distribution.
4. Match time sequence of contacts to the active intervals of the links.

This model is illustrated in Fig. 6.

Perra et al. [74] proposed a model of temporal networks—the *activity driven model*—that is even simpler than the above with the advantage that it is analytically tractable. Let G_t denote a simple graph at time t . Their generation algorithm proceeds as follows:

1. Increment the time to t and let G_t be empty.
2. Activate a node i with probability $a_i \Delta t$. Connect i to m other randomly chosen distinct nodes.

This model has been fundamental to analytical studies of processes on temporal networks, see e.g. Refs. [28, 44, 55, 56, 73, 92, 94].

Starnini et al. [90] use a two-dimensional random walk model where there the chance of approaching node i is proportional to an increasing attractiveness

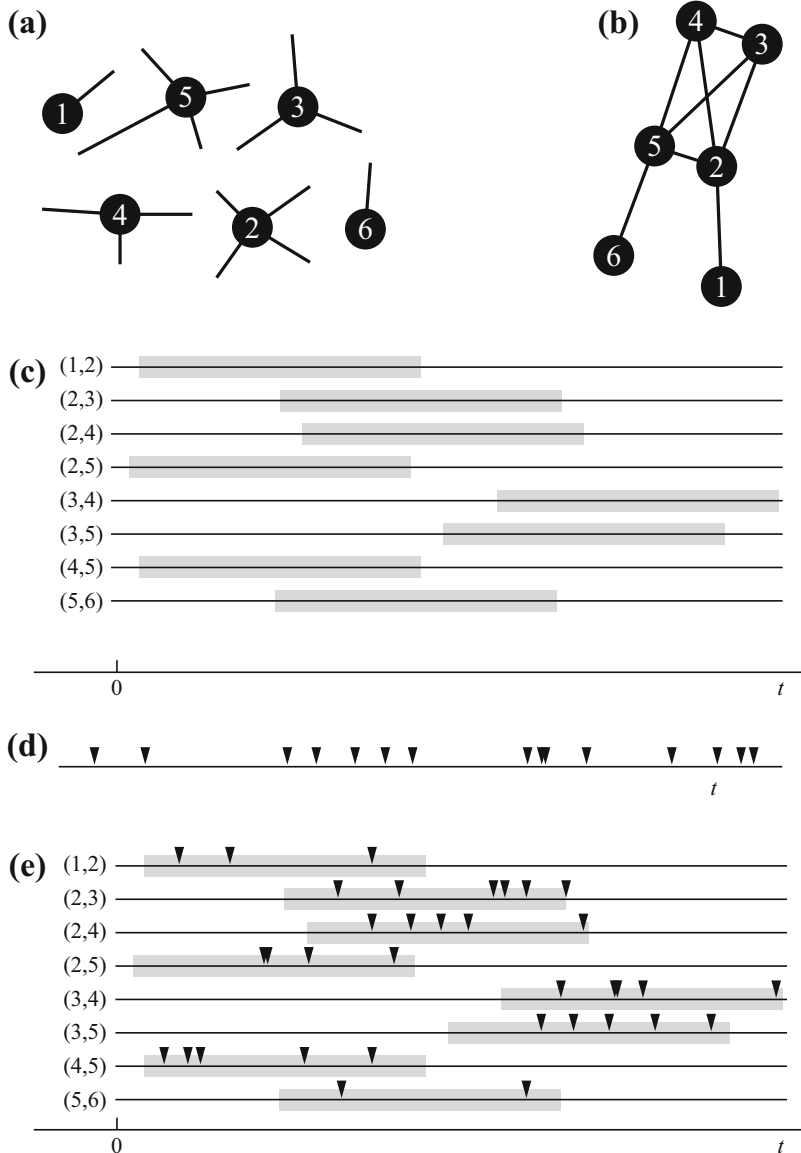


Fig. 6 Illustrating a simple generative model for temporal networks, used in Refs. [32] and [76]. First one generates a static network from the configuration model by creating desired degrees from a probability distribution (a) and matching them up in random pairs (b). Then one generates intervals for the links showing when they are active (c). Finally, one generates a time series of interevent times (d) and matches it to the active intervals. Panel (e) shows the final temporal network. This figure is adapted from Ref. [33]

parameter a_i . This means that the more attracted a walker is to its neighbors, the slower its walk becomes (simulating acquaintances stopping to talk when they meet on the street). Furthermore, they also allow people not to socialize by having occasional inactive periods. Zhang et al. [105] propose a similar model, but without an explicit representation of space.

Another model of temporal networks of social contacts was proposed in Ref. [102]. The authors introduced a model where both nodes and links can be activated by temporal effects. In their model, a link can be active or inactive and further characterized by the time $\tau_{(i,j)}$ since the last time it changed state. Similarly, node i uses the time τ_i since it last was involved in a contact as a basis for its decisions. The network is initialized to N nodes and all links inactive. A node can activate a link with probability depending on τ . The link is chosen from the nodes i that are currently not in contact with i with a probability depending on the τ s of the neighbors. An active link is inactivated with a rate that is also dependent on τ .

Refs. [60] and [15] use a Hawkes process to model a similar situation to the one considered by Starnini et al. [90] above. Ref. [60] argue that there is a positive correlation between consecutive interevent times in empirical data that cannot be modeled by interevent times alone. Their model works by defining an event rate by

$$v + \sum_{i:t_i \leq t} \phi(t - t_i) \quad (1)$$

where ϕ is an exponentially decreasing memory kernel and v is a base event rate. Even with an exponentially decaying kernel, the interevent time distribution becomes broader than exponential. Similar to Refs. [60] and [15], Ref. [16] introduced a model of temporal networks based on stochastic point processes. In their model, nodes form and break links following a Bernoulli process with memory. Similar to the Hawkes process mentioned above, the probability of an event between i and j increases with the number of recent events that happened between i and j . Specifically, Ref. [16] takes the probability of a link to activate or deactivate at time t to be proportional to the number of such events in a time window.

6 Other Topics

There are of course some themes in the temporal network literature that do not fit into the above three categories. Two examples are generalizations of *link prediction* [54] and *network reconstruction* [67, 72] to temporal networks. The motivation of both these topics is that real data is often erroneous and incomplete. In static networks, link prediction refers to the problem of finding the linkless pair of nodes that is most likely to be a false negative (falsely not having a link). In the context of temporal networks, this could be reformulated as either the question of what will be the next contact (given the information up to a point), or which contact was missing in the past. We are not aware of any paper addressing these particular

problems. Instead of solving these purely temporal network questions, there is a large body of literature on link prediction in static networks with a turnover of nodes and links—see e.g. Ref. [1] and references therein—i.e., assuming a slower changing network that elsewhere in this chapter.

Network reconstruction, in general, is the problem of inferring a network from secondary, incomplete, or noisy data [67, 72]. So far, we are not aware of such temporal-network studies similar to the static network case. There are papers about the technical difficulties of inferring temporal network contacts from electronic sensors [8, 93] and papers about how to reconstruct static networks from temporal network data [32, 49], but we are aware of no papers that would predict false positive and negative data in a contact sequence.

7 Future Perspectives

Temporal network studies has been a vivid sub-discipline of network science for around a decade. Some issues of the early days have been settled, while others still remain. This period has seen a shift from research that simply extends static-network ideas to temporal networks to methods that are unique to temporal networks. Still, the overall research directions are more or less the same as for static networks (cf. Fig. 1)—questions about identifying important nodes, how to further simplify temporal networks, and how their structure affect dynamics. Are there such larger research directions that make sense for temporal networks but not static ones? An obvious idea would be to focus on questions that involve time more directly. Yet only rarely have researchers asked what the optimal time to do something is, or what the optimal duration to expose the system to some treatment is, etc. Change-point detection (finding the time when a system changes between qualitatively different states) is one exception [71]. There are also papers about time series analysis of temporal networks [38, 87], but these typically do not ask questions about time like the ones above.

Perhaps the crudest assumption of temporal network modeling to date (as mentioned in Sect. 2.1) is that the existence of a contact is independent of the dynamic system of interest. As an example, there are many modeling studies of information spreading on top of empirical temporal networks (e.g. mobile-phone or e-mail data [3, 41, 43]). Of course, information spreading via e-mails or calls does really happen, but one cannot usually view it as a random process on top of some temporal contact structure that is independent of the information. While one can imagine less important information spreading this way—“By the way, put on that Finnish heavy metal when uncle Fredrik comes to visit, he will appreciate it”—usually, calls are made and e-mails are sent with the explicit purpose of spreading information. Therefore, information spreading influences or even drives the contact structure. How should one then model information spreading on temporal networks? One possibility would be to give up using empirical data as the basis for the analysis; such an approach would be similar to *adaptive networks* [26]. One could also go for

data that contains the content of the messages or conversations instead of only their metadata; in this case, it might be possible to understand the relationship between the temporal network of contacts and the spreading dynamics. Evidently, such data is hard to come by for privacy reasons, but interestingly, early studies of electronic communications did analyze both the content and the structure of spreading [17]. There are also communication channels where everything is public, such as Twitter.

One research direction with plenty of room for improvement is temporal-network visualization. Figure 2 illustrates some of the challenges where Fig. 2a gives a reasonable feeling for the temporal structures but none for the network structure, and for Fig. 2b the situation is reversed. One can probably rule out a type of visualization that manages to show all information and convey all different aspects of structure, but there should be methods that discard some information but still reveal important structures. Also animated visualization (that has the obvious limitation that not all the information is shown at once) probably has room for improvement. Some such methods are discussed in chapter “Visualisation of Structure and Processes on Temporal Networks”. The “alluvial diagrams” of Ref. [80] are another interesting approach. Evidently there are some available methods, but what we wish for is an even wider selection to choose from.

Yet another fundamental challenge for temporal networks is how to properly rescale or subsample a data set. Many methods, in particular those inspired by statistical physics, rely on ways to consistently change the size of a network. This is a challenge even for static networks—simply making subgraphs based on a random set of nodes will most likely change the structure of a network (other than Erdős-Rényi random graphs) [52]. The same goes for more elaborate ways of reducing the size of a network by merging nodes [46, 88]—there is no guarantee that such manipulation will retain the structure of networks. For temporal networks, one might think that at least the temporal dimension could be rescaled by sampling windows of different sizes, but this is not trivial either because it could change whether or not a dynamic process has the time to reach a certain state or not. For the purpose of finite-size scaling such as used in the study of critical phenomena [36], one would need a way to link the size of the network and the duration of the temporal network.

Finally, as mentioned earlier in this chapter, we feel that there is a lot to do regarding temporal-network robustness and fragility, with applications ranging from network security to public health and to the efficient planning of robust public-transport systems. This is an area where it is possible to go beyond static-network analogies. As an example, while a static network may just fragment when chosen nodes are attacked/immunized, the range of responses of a temporal network is much broader: the network may remain temporally connected in principle but the average latency of time-respecting paths may grow high enough to make them useless. Or, the system’s latency could temporarily grow to make it temporarily disconnected: consider, e.g., congestion in a public transport system. Furthermore, the range of possible attack or immunization strategies can be much broader too: interventions to events, attacks that aim to generally increase latency, interventions at specific times, sequences of timed interventions at different nodes or contacts, and so on. Likewise, when the aim is to improve network robustness, interventions are

not limited to network topology alone. As an example, for improving the reliability of public-transport systems, one could only modify the temporal sequences of connections and their time-domain statistics to minimize the disruption caused by random deviations from the planned schedules, or one could aim at maximal synchronization of connections to minimize the latency of time-respecting paths.

Acknowledgements PH was supported by JSPS KAKENHI Grant Number JP 18H01655. JS acknowledges support from the Academy of Finland, project “Digital Daily Rhythms” (project n:o 297195).

References

1. Ahmed, N.M., Chen, L.: An efficient algorithm for link prediction in temporal uncertain social networks. *Inf. Sci.* **331**, 120–136 (2016)
2. Arita, I., Nakane, M., Kojima, K., Yoshihara, N., Nakano, T., El-Gohary, A.: Role of a sentinel surveillance system in the context of global surveillance of infectious diseases. *Lancet Infect. Dis.* **4**(3), 171–177 (2004)
3. Backlund, V.P., Saramäki, J., Pan, R.K.: Effects of temporal correlations on cascades: threshold models on temporal networks. *Phys. Rev. E* **89**, 062815 (2014)
4. Bai, Y., Yang, B., Lin, L., Herrera, J.L., Du, Z., Holme, P.: Optimizing sentinel surveillance in temporal network epidemiology. *Sci. Rep.* **7**(1), 4804 (2017)
5. Barabási, A.-L.: The origin of bursts and heavy tails in human dynamics. *Nature* **435**, 207–211 (2005)
6. Barabási, A.-L., Albert, R.: Emergence of scaling in random networks. *Science* **286**, 509–512 (1999)
7. Barrat, A., Barthélémy, M., Pastor-Satorras, R., Vespignani, A.: The architecture of complex weighted networks. *Proc. Natl. Acad. Sci. U.S.A.* **101**, 3747–3752 (2004)
8. Barrat, A., Cattuto, C.: Temporal networks of face-to-face human interactions. In: P. Holme, J. Saramäki (eds.) *Temporal Networks*, pp. 191–216. Springer, Berlin (2013)
9. Barthélémy, M., Barrat, A., Pastor-Satorras, R., Vespignani, A.: Velocity and hierarchical spread of epidemic outbreaks in scale-free networks. *Phys. Rev. Lett.* **92**, 178701 (2004)
10. Batagelj, V., Doreian, P., Ferligoj, A., Kejzar, N.: *Understanding Large Temporal Networks and Spatial Networks: Exploration, Pattern Searching, Visualization and Network Evolution*. Wiley, London (2014)
11. Braunstein, A., Dall’Asta, L., Semerjian, G., Zdeborová, L.: Network dismantling. *Proc. Natl. Acad. Sci. U.S.A.* **113**(44), 12368–12373 (2016)
12. Britton, T.: Stochastic epidemic models: A survey. *Math. Biosci.* **225**(1), 24–35 (2010)
13. Brudner, L.A., White, D.R.: Class, property, and structural endogamy: visualizing networked histories. *Theory Soc.* **26**(2), 161–208 (1997)
14. Cho, J.H., Gao, J.: Cyber war game in temporal networks. *PLoS One* **11**(2), 1–16 (2016)
15. Cho, Y.S., Galstyan, A., Brantingham, P.J., Tita, G.: Latent self-exciting point process model for spatial-temporal networks. *Discrete Contin. Dynam. Syst. B* **19**(5), 1335–1354 (2014)
16. Colman, E.R., Vukadinović Greetham, D.: Memory and burstiness in dynamic networks. *Phys. Rev. E* **92**, 012817 (2015)
17. Danowski, J.A., Edison-Swift, P.: Crisis effects on intraorganizational computer-based communication. *Commun. Res.* **12**(2), 251–270 (1985)
18. Davis, A., Gardner, B.B., Gardner, M.R.: *Deep South*. The University of Chicago Press, Chicago (1941)

19. Delvenne, J.C., Lambiotte, R., Rocha, L.E.C.: Diffusion on networked systems is a question of time or structure. *Nat. Commun.* **6**, 7366 (2015)
20. Dinur, I., Safra, S.: On the hardness of approximating vertex cover. *Ann. Math.* **162**(1), 439–485 (2005)
21. Enright, J., Kao, R.R.: Epidemics on dynamic networks. *Epidemics* **24**, 88–97 (2018)
22. Fefferman, N.H., Ng, K.L.: How disease models in static networks can fail to approximate disease in dynamic networks. *Phys. Rev. E* **76**, 031919 (2007)
23. Gauvin, L., Génois, M., Karsai, M., Kivelä, M., Takaguchi, T., Valdano, E., Vestergaard, C.L.: Randomized reference models for temporal networks (2018). arXiv:1806.04032
24. Génois, M., Vestergaard, C.L., Fournet, J., Panisson, A., Bonmarin, I., Barrat, A.: Data on face-to-face contacts in an office building suggest a low-cost vaccination strategy based on community linkers. *Netw. Sci.* **3**(3), 326–347 (2015)
25. Grönlund, A., Holme, P.: Networking the seeder model: group formation in social and economic systems. *Phys. Rev. E* **70**, 036108 (2004)
26. Gross, T., Sayama, H. (eds.): *Adaptive Networks*. Springer, Berlin (2009)
27. Gu, J., Lee, S., Saramäki, J., Holme, P.: Ranking influential spreaders is an ill-defined problem. *Europhys. Lett.* **118**(6), 68002 (2017)
28. Han, D., Sun, M., Li, D.: Epidemic process on activity-driven modular networks. *Phys. A* **432**, 354–362 (2015)
29. Hethcote, H.W.: The mathematics of infectious diseases. *SIAM Rev.* **42**, 599 (2000)
30. Holme, P.: Network dynamics of ongoing social relationships. *Europhys. Lett.* **64**, 427–433 (2003)
31. Holme, P.: Network reachability of real-world contact sequences. *Phys. Rev. E* **71**, 046119 (2005)
32. Holme, P.: Epidemiologically optimal static networks from temporal network data. *PLoS Comput. Biol.* **9**, e1003142 (2013)
33. Holme, P.: Modern temporal network theory: a colloquium. *Eur. Phys. J. B* **88**, 234 (2015)
34. Holme, P., Liljeros, F.: Birth and death of links control disease spreading in empirical contact networks. *Sci. Rep.* **4**, 4999 (2014)
35. Holme, P., Saramäki, J.: Temporal networks. *Phys. Rep.* **519**, 97–125 (2012)
36. Hong, H., Ha, M., Park, H.: Finite-size scaling in complex networks. *Phys. Rev. Lett.* **98**(25), 258701 (2007)
37. Horváth, D.X., Kertész, J.: Spreading dynamics on networks: the role of burstiness, topology and non-stationarity. *New J. Phys.* **16**(7), 073037 (2014)
38. Huang, Q., Zhao, C., Zhang, X., Wang, X., Yi, D.: Centrality measures in temporal networks with time series analysis. *Europhys. Lett.* **118**(3), 36001 (2017)
39. Jo, H.H., Perotti, J.I., Kaski, K., Kertész, J.: Analytically solvable model of spreading dynamics with non-poissonian processes. *Phys. Rev. X* **4**, 011041 (2014)
40. Johansen, A.: Probing human response times. *Phys. A* **330**, 286–291 (2004)
41. Karimi, F., Holme, P.: Threshold model of cascades in empirical temporal networks. *Phys. A Stat. Mech. Appl.* **392**(16), 3476–3483 (2013)
42. Karsai, M., Jo, H.H., Kaski, K. (eds.): *Bursty Human Dynamics*. Springer, Berlin (2018)
43. Karsai, M., Kivelä, M., Pan, R.K., Kaski, K., Kertész, J., Barabási, A.L., Saramäki, J.: Small but slow world: how network topology and burstiness slow down spreading. *Phys. Rev. E* **83**, 025102(R) (2011)
44. Karsai, M., Perra, N., Vespignani, A.: Time varying networks and the weakness of strong ties. *Sci. Rep.* **4**, 4001 (2014)
45. Kempe, D., Kleinberg, J., Tardos, É.: Maximizing the spread of influence through a social network. In: *Proceedings of the Ninth ACM SIGKDD International Conference on Knowledge Discovery and Data Mining*, pp. 137–146. ACM, New York (2003)
46. Kim, B.J.: Geographical coarse graining of complex networks. *Phys. Rev. Lett.* **93**, 168701 (2004)
47. Kivelä, M., Cambe, J., Saramäki, J., Karsai, M.: Mapping temporal-network percolation to weighted, static event graphs. *Sci. Rep.* **8**, 12357 (2018)

48. Kivelä, M., Porter, M.A.: Estimating interevent time distributions from finite observation periods in communication networks. *Phys. Rev. E* **92**, 052813 (2015)
49. Krings, G., Karsai, M., Bernhardsson, S., Blondel, V.D., Saramäki, J.: Effects of time window size and placement on the structure of an aggregated communication network. *EPJ Data Sci.* **1**(1), 4 (2012)
50. Lamport, L.: Time, clocks, and the ordering of events in a distributed system. *Commun. ACM* **21**, 558–565 (1978)
51. Lee, S.H., Holme, P.: Navigating temporal networks. *Phys. A Stat. Mech. Appl.* **513**, 288–296 (2019)
52. Lee, S.H., Kim, P.J., Jeong, H.: Statistical properties of sampled networks. *Phys. Rev. E* **73**, 016102 (2006)
53. Li, A., Cornelius, S.P., Liu, Y.Y., Wang, L., Barabási, A.L.: The fundamental advantages of temporal networks. *Science* **358**, 1042–1046 (2017)
54. Liben-Nowell, D., Kleinberg, J.: The link-prediction problem for social networks. *J. Am. Soc. Inf. Sci. Technol.* **58**(7), 1019–1031 (2007)
55. Liu, S., Perra, N., Karsai, M., Vespignani, A.: Controlling contagion processes in activity driven networks. *Phys. Rev. Lett.* **112**, 118702 (2014)
56. Liu, S.Y., Baronchelli, A., Perra, N.: Contagion dynamics in time-varying metapopulation networks. *Phys. Rev. E* **87**, 032805 (2013)
57. Masuda, N., Holme, P.: Predicting and controlling infectious disease epidemics using temporal networks. *F1000Prime Rep.* **5**, 6 (2015)
58. Masuda, N., Lambiotte, R.: A Guide to Temporal Networks. World Scientific, Singapore (2016)
59. Masuda, N., Rocha, L.E.C.: A Gillespie algorithm for non-markovian stochastic processes. *SIAM Rev.* **60**, 95–115 (2018)
60. Masuda, N., Takaguchi, T., Sato, N., Yano, K.: Self-exciting point process modeling of conversation event sequences. In: P. Holme, J. Saramäki (eds.) *Temporal Networks*, pp. 245–264. Springer, Berlin (2013)
61. Mellor, A.: The temporal event graph. *J. Complex Netw.* **6**, 639–659 (2018)
62. Min, B., Goh, K.I., Vazquez, A.: Spreading dynamics following bursty human activity patterns. *Phys. Rev. E* **83**, 036102 (2011)
63. Miritello, G., Moro, E., Lara, R.: Dynamical strength of social ties in information spreading. *Phys. Rev. E* **83**, 045102 (2011)
64. Morris, M., Kretzschmar, M.: Concurrent partnerships and transmission dynamics in networks. *Soc. Netw.* **17**(3), 299–318 (1995). Social networks and infectious disease: HIV/AIDS
65. Mucha, P.J., Richardson, T., Macon, K., Porter, M.A., Onnela, J.P.: Community structure in time-dependent, multiscale, and multiplex networks. *Science* **328**, 876–878 (2010)
66. Newman, M.E.J.: Networks: An Introduction. Oxford University Press, Oxford (2010)
67. Newman, M.E.J.: Estimating network structure from unreliable measurements. *Phys. Rev. E* **98**(6), 062321 (2018)
68. Onnela, J.P., Saramäki, J., Hyvönen, J., Szabó, G., Lazer, D., Kaski, K., Kertész, J., Barabási, A.L.: Structure and tie strengths in mobile communication networks. *Proc. Natl. Acad. Sci.* **104**, 7332–7336 (2007)
69. Palla, G., Barabási, A.L., Vicsek, T.: Quantifying social group evolution. *Nature* **446**, 664–667 (2007)
70. Pan, R.K., Saramäki, J.: Path lengths, correlations, and centrality in temporal networks. *Phys. Rev. E* **84**, 016105 (2011)
71. Peel, L., Clauset, A.: Detecting change points in the large-scale structure of evolving networks. In: Twenty-Ninth AAAI Conference on Artificial Intelligence (2015)
72. Peixoto, T.P.: Network reconstruction and community detection from dynamics (2019). arXiv:1903.10833
73. Perra, N., Baronchelli, A., Mocanu, D., Gonçalves, B., Pastor-Satorras, R., Vespignani, A.: Random walks and search in time-varying networks. *Phys. Rev. Lett.* **109**, 238701 (2012)

74. Perra, N., Gonçalves, B., Pastor-Satorras, R., Vespignani, A.: Activity driven modeling of time varying networks. *Sci. Rep.* **4**, 4001 (2014)
75. Rico-Gray, V., Díaz-Castelazo, C., Ramírez-Hernández, A., Guimaraes, P.R., Holland, J.N.: Abiotic factors shape temporal variation in the structure of an ant–plant network. *Arthropod Plant Interact.* **6**(2), 289–295 (2012)
76. Rocha, L.E.C., Blondel, V.D.: Bursts of vertex activation and epidemics in evolving networks. *PLoS Comput. Biol.* **9**(3), 1–9 (2013)
77. Rocha, L.E.C., Liljeros, F., Holme, P.: Simulated epidemics in an empirical spatiotemporal network of 50,185 sexual contacts. *PLoS Comput. Biol.* **7**, 1–9 (2011)
78. Rombach, M.P., Porter, M.A., Fowler, J.H., Mucha, P.J.: Core-periphery structure in networks. *SIAM J. Appl. Math.* **74**(1), 167–190 (2014)
79. Rossetti, G., Cazabet, R.: Community discovery in dynamic networks: a survey. *ACM Comput. Surv.* **51**, 35 (2018)
80. Rosvall, M., Bergstrom, C.T.: Mapping change in large networks. *PLoS One* **5**(1), e8694 (2010)
81. Rosvall, M., Esquivel, A.V., Lancichinetti, A., West, J.D., Lambiotte, R.: Memory in network flows and its effects on spreading dynamics and community detection. *Nat. Commun.* **5**, 4630 (2014)
82. Saramäki, J., Holme, P.: Exploring temporal networks with greedy walks. *Eur. Phys. J. B* **88**(12), 334 (2015)
83. Scellato, S., Leontiadis, I., Mascolo, C., Basu, P., Zafer, M.: Evaluating temporal robustness of mobile networks. *IEEE Trans. Mob. Comput.* **12**(1), 105–117 (2013)
84. Schaub, M.T., Delvenne, J.C., Rosvall, M., Lambiotte, R.: The many facets of community detection in complex networks. *Appl. Netw. Sci.* **2**(1), 4 (2017)
85. Sekara, V., Stopczynski, A., Lehmann, S.: Fundamental structures of dynamic social networks. *Proc. Natl. Acad. Sci. U.S.A.* **113**(36), 9977–9982 (2016)
86. Serrano, M.Á., Boguná, M., Vespignani, A.: Extracting the multiscale backbone of complex weighted networks. *Proc. Natl. Acad. Sci. U.S.A.* **106**(16), 6483–6488 (2009)
87. Sikdar, S., Ganguly, N., Mukherjee, A.: Time series analysis of temporal networks. *Eur. Phys. J. B* **89**(1), 11 (2016)
88. Song, C., Havlin, S., Makse, H.A.: Origins of fractality in the growth of complex networks. *Nat. Phys.* **2**(4), 275 (2006)
89. Starnini, M., Baronchelli, A., Barrat, A., Pastor-Satorras, R.: Random walks on temporal networks. *Phys. Rev. E* **85**(5), 056115 (2012)
90. Starnini, M., Baronchelli, A., Pastor-Satorras, R.: Modeling human dynamics of face-to-face interaction networks. *Phys. Rev. Lett.* **110**, 168701 (2013)
91. Starnini, M., Machens, A., Cattuto, C., Barrat, A., Pastor-Satorras, R.: Immunization strategies for epidemic processes in time-varying contact networks. *J. Theor. Biol.* **337**, 89–100 (2013)
92. Starnini, M., Pastor-Satorras, R.: Temporal percolation in activity-driven networks. *Phys. Rev. E* **89**, 032807 (2014)
93. Stopczynski, A., Sekara, V., Sapiezynski, P., Cuttone, A., Madsen, M.M., Larsen, J.E., Lehmann, S.: Measuring large-scale social networks with high resolution. *PLoS One* **9**, e95978 (2014)
94. Sun, K., Baronchelli, A., Perra, N.: Contrasting effects of strong ties on sir and sis processes in temporal networks. *Eur. Phys. J. B* **88**(12), 326 (2015)
95. Takaguchi, T., Masuda, N., Holme, P.: Bursty communication patterns facilitate spreading in a threshold-based epidemic dynamics. *PLoS One* **8**, e68629 (2013)
96. Takaguchi, T., Sato, N., Yano, K., Masuda, N.: Importance of individual events in temporal networks. *New J. Phys.* **14**(9), 093003 (2012)
97. Tang, J., Leontiadis, I., Scellato, S., Nicosia, V., Mascolo, C., Musolesi, M., Latora, V.: Applications of temporal graph metrics to real-world networks. In: P. Holme, J. Saramäki (eds.) *Temporal Networks*, pp. 135–159. Springer, Berlin (2013)

98. Taylor, D., Myers, S.A., Clauset, A., Porter, M.A., Mucha, P.J.: Eigenvector-based centrality measures for temporal networks. *Multiscale Model. Simul.* **15**(1), 537–574 (2017)
99. Trajanovski, S., Scellato, S., Leontiadis, I.: Error and attack vulnerability of temporal networks. *Phys. Rev. E* **85**, 066105 (2012)
100. Ushio, M., Hsieh, C.H., Masuda, R., Deyle, E.R., Ye, H., Chang, C.W., Sugihara, G., Kondoh, M.: Fluctuating interaction network and time-varying stability of a natural fish community. *Nature* **554**, 360–363 (2018)
101. Vazquez, A., Rácz, B., Lukács, A., Barabási, A.L.: Impact of non-poissonian activity patterns on spreading processes. *Phys. Rev. Lett.* **98**, 158702 (2007)
102. Vestergaard, C.L., Génois, M., Barrat, A.: How memory generates heterogeneous dynamics in temporal networks. *Phys. Rev. E* **90**, 042805 (2014)
103. Zhan, X.X., Hanjalic, A., Wang, H.: Information diffusion backbones in temporal networks. *Sci. Rep.* **9**, 6798 (2019)
104. Zhang, Y., Wen, G., Chen, G., Wang, J., Xiong, M., Guan, J., Zhou, S.: Gaming temporal networks. *IEEE Trans. Circuits Syst. Express Briefs* **66**(4), 672–676 (2019)
105. Zhang, Y.Q., Li, X., Liang, D., Cui, J.: Characterizing bursts of aggregate pairs with individual poissonian activity and preferential mobility. *IEEE Commun. Lett.* **19**(7), 1225–1228 (2015)

Fundamental Structures in Temporal Communication Networks



Sune Lehmann

1 Introduction

Temporal networks provide an important methodology for modeling a range of dynamical systems [31–33]. A central category of temporal networks is *communication networks*, which—in this context—I define to be networks that facilitate or represent communication between human beings. Frequently analyzed examples of communication networks are networks of face-to-face contacts between individuals [18, 95], phone calls and text messages [71], online social networks such as Facebook [106, 107] or Twitter [69], and networks of email messages [26]. But communication networks could also represent other types of human communication, such as broadcast networks (e.g. television or newspapers) or communication via letters or books. While the framework discussed here is presented in the context of human communication networks, in many cases the validity of the framework extends beyond networks of human communication to describe networks of machine-machine communication, biological signaling, etc.

2 Network Structure of Communication Events

The main realization underlying the ideas presented here is that each human communicative act is shaped by the medium in which it takes place. As modern communication tools have developed, the richness of the ways human beings can communicate with one another has grown. What is perhaps less recognized in the

S. Lehmann (✉)

Technical University of Denmark, DTU Compute, Lyngby, Denmark

e-mail: sljo@dtu.dk

Table 1 Six prototypical communicative practices and real-world examples of each practice

	Synchronous	Asynchronous
One-to-one	Phone call ^a , voice chat	Text message, letter
One-to-many	Broadcast radio and TV	Book, newspaper, webpage
Many-to-many	Face-to-face, online chatroom	Online social network, wiki

^aIt is, of course, possible to set up a conference call, but one-to-one calls are so prevalent within this medium of communication that I allow myself to use phone calls as an example of one-to-one communication

field of network theory is that each new medium for communication sets its own particular constraints for the network structure of communication events within that medium. In the field of communication studies, a key question is to understand how the technological evolution impacts human communication. Therefore, within that field, the many possible types of human communication—old and new—have been boiled down to six fundamental prototypical communicative practices¹ [36] shown in Table 1.

2.1 *Synchronous vs. Asynchronous*

In the vertical split, Table 1 makes a distinction between synchronous and asynchronous communication. In the case of synchronous communication, both parties are active and engaged. E.g. during a phone call. Conversely, in the case of asynchronous communication, a message is initiated at some time by the sender and then received later at some time by the recipient(s). For example, in the case of one-to-one communication, the recipient reading a text message or a letter.

2.2 *One-to-One, One-to-Many, Many-to-Many*

Along the horizontal splits, each row in Table 1 refers to the configuration of participants in a given communication act and the nature of their interaction. This division of communicative behaviors into one-to-one, one-to-many, and many-to-many is quite natural and recognized beyond communication theory; these distinctions are used, for example, in the analysis of computer networks [6, 39], when negotiating contracts [83], within marketing [28], or as design patterns/data models in database design [38].

¹In their formulation within the field of communication these practices are not connected to the underlying communication networks (or their dynamics); rather, the prototypical practices are used as a way to categorize real-world communication and understand their impact on, e.g. communication practices.

2.3 Connecting to Network Theory

Bringing this framework, which was developed to organize different types of communication, into the realm of temporal network theory, I propose that we think of each prototypical type of communication as defining a ***dynamic class*** of network and that very real-world communication network can be modeled as belonging to one of these six classes.

The key concept which distinguishes the six classes is their ***fundamental structures***. We arrive at the fundamental structures by first noticing that each row in Table 1, corresponds to an archetypal network structure: one-to-one interactions correspond to *dyads*, one-to-many interactions can be represented as *star graphs* (or *trees*), and the many-to-many interactions match the network structure of *cliques*. When also incorporating the temporal aspect (synchronous/asynchronous), we arrive at the network representations of the six prototypical communicative practices, the fundamental structures.

The fundamental structures are temporal-topological network patterns, with each pattern corresponding to a communication event (a phone call, a meeting, a text message) in that network. We can then model the entire network as sequences of instances of fundamental structures. Since each class is characterized by its fundamental structure, we name the each class according to their fundamental structure: synchronous, one-to-one, synchronous, one-to-many, . . . asynchronous, many-to-many.

Let me provide some examples to give a sense of what I mean. In the synchronous, one-to-one class (e.g. the phone call network, see Fig. 1A), fundamental structures are individual dyads, with some duration given by its start and end time. In synchronous, one-to-many networks (e.g. a live-stream), the duration of the communication event is set by the node which is broadcasting, whereas receiving nodes may participate for only part of the communication event’s duration. Finally, in

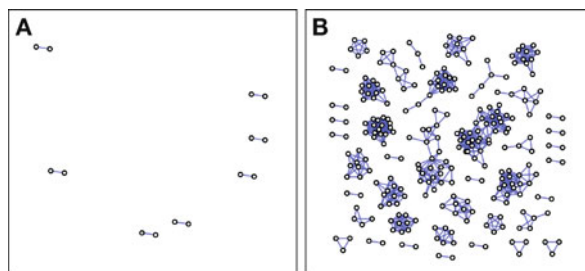


Fig. 1 Cross-sections of fundamental structures are revealed in brief snapshots of networks from the SensibleDTU project [100]. (a) A 1 min time-slice from the phone call network at peak activity; the network is entirely composed of dyads. (b) Social interactions over 5 min in the face-to-face contact network. Here the network is disconnected and well-approximated by non-overlapping cliques

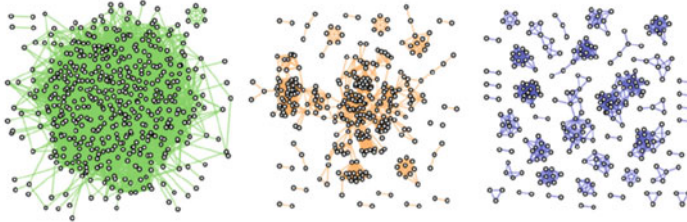


Fig. 2 Three views of the contact network. **Left** (green), all interactions aggregated over 24 h. **Middle** (orange), interactions during 1 h. **Right** (blue), interactions in a 5-min window

the synchronous, many-to-many class (Fig. 1B), where the fundamental structure is a sequence of cliques (see Fig. 2 for another example), the start of the communication event is set by the first participant(s) connecting—and the end occurs when the last participant(s) stop communicating. An example of this class is face-to-face networks, where a fundamental structure could represent a group of friends meeting for dinner at a restaurant.

In all of the synchronous classes, infinitesimally thin temporal slices of the communication event reveal the network pattern characteristic of that class. That is, a *dyad*, *tree*, or *clique* for the one-to-one, one-to-many, and many-to-many class respectively. I illustrate this point in Fig. 1, where I show brief snapshots (thin temporal slices) of the network of phone-calls (synchronous, one-to-one) which consists of disconnected dyads, each dyad corresponding to an ongoing conversation (see Fig. 1a), whereas a slice of face-to-face meetings is well approximated as disconnected cliques (see Fig. 1b). Getting a bit ahead of myself, I note that, already at this point, it is clear from inspection that from the point of view of a dynamical process, the possible network flows in the two networks shown in Fig. 1 are going to be very different.

Let us now consider examples of networks from the asynchronous classes. Here one-to-one communication events still involves dyads, and an event starts, when a person sends a message. The communication ends when the recipient receives the message at some later time. In the asynchronous, one-to-many class, a communication event starts when some communication is initiated (and that node becomes *active*): a book is published, a web-page is launched, etc. Now, recipients can engage with that active node at any point until the sender-node is no longer active/available—and thus ending that fundamental structure. Finally the asynchronous, many-to-many class. Here, again a node becomes active (starting the communication event), and other nodes can engage with the active node *as well as all other nodes in that conversation*. The fundamental structure ends when original post ceases to be available (although activity may end sooner than that). Examples of networks from the asynchronous, many-to-many class is a post on a message board,

or a post on Facebook.² In the case of the asynchronous classes, infinitesimally thin time-slices of the fundamental structures are empty, only revealing the active nodes, since the interactions themselves typically are instantaneous and do not have a duration.

Summarizing the discussion above, the key concepts are

- **Dynamic Classes.** Each dynamic class is the set of networks characterized by a certain type of fundamental structure. There are six dynamic classes, cf. Table 1.
- **Fundamental Structures.** A fundamental structure is the topological-temporal network representation the archetypical communication pattern within a class of network. Each communication event corresponds to an instance of the fundamental structure characterizing that network.

A useful way to think about real-world communication networks is as a sequences of instances of fundamental structure from a single class. In this sense we can think of each of the fundamental structures as *generating a class of networks*.

These distinctions prove to be important because while two networks originating from different classes aggregated over time may have similar topological properties, a difference in network class may have profound impact on the network dynamics and for processes unfolding on the network (cf. Fig. 1). Stated differently: *When we consider the networks on much shorter time-scales than those typically considered in the literature, networks from the six classes are radically different.*

I cover this point in detail below, arguing that there are a number of advantages associated with thinking about temporal networks as sequences of fundamental structures—and that while the impact is on many aspects of how we model temporal networks, the unfolding of dynamics are particularly important. Further, I argue below that when we compare analyses of various real-world networks, we should only expect similar behavior when we compare networks within the same dynamic class, and that we should aggregate statistics within each class of network separately.

2.4 The Case of Many-to-Many, Synchronous Networks

Before we move on, let me start by showing how the fundamental structures can lead to clean, simple descriptions of temporal communication networks. A few years

²It is not guaranteed that all posts become a full discussion between all readers—and if no-one comments, such posts could display a one-to-many structure. I discuss this below.

ago—without realizing the connection to a larger framework—my group analyzed a network from the class of synchronous, many-to-many interactions [95], arising from person-to-person interactions (estimated using Bluetooth-signal strength [94]) in a large, densely connected network [100].

The key realization arose from simply plotting the contact-network at increasingly higher temporal resolution. The green hairball (Fig. 2, left panel) shows connections between everyone who has spent time together, aggregated across an entire day. The orange network (Fig. 2, middle panel) shows contacts aggregated over an hour, and the blue network (Fig. 2, right panel) shows the interactions during a 5-min time slice. The discovery originates from the blue network. There, we can directly observe cross-sections of the fundamental structures: groups (well approximated by cliques) of people spending time together.

This was a case where analyzing the network became *easier* by including higher resolution temporal data (in our case, no community detection was necessary). Usually it is the opposite. Usually, our descriptions become more complex when we have to account for more detailed data, especially temporal data [31, 33, 60]. I take the fact that *more* data simplified this particular problem to mean that we were on to something: in this case, the fundamental structures constitute a quite natural representation of the network.

This way of representing the network also provided a way to understand the temporal evolution of the network. Simply matching up cross-sections of the fundamental structures across time-slices, we could then construct the full fundamental structures (the individual communication events) for this class of network. We called the result *gatherings*—the temporal representation of a meeting between a group of individuals (see Fig. 3 for an examples of gatherings in two

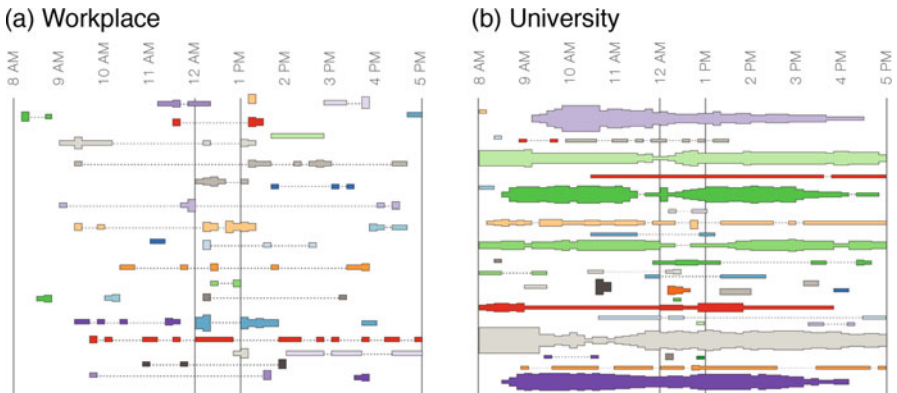


Fig. 3 An example of fundamental structures in real-time, many-to-many networks. In both panels, time runs from left to right, and each horizontal colored band represents a fundamental structure in that network (a sequence of cliques matched up over time). Therefore, each horizontal colored band is basically a representation of a group of people meeting, with the width of each band proportional to the number of participants at that time. Here we show these fundamental structures in two social settings (**a**) a Workplace network [24], (**b**) in the SensibleDTU data [100]

real-world networks). Gatherings represent the fundamental structure of many-to-many, synchronous networks. Studying the properties of gatherings allowed us to estimate the relevant time-scales and spatial behaviors of the fundamental structures in this systems, e.g. how individual nodes interact with the gatherings. Turning our attention to time-scales of weeks and months, we could study the patterns of meetings (gatherings) among the same people beyond single meetings. Thus, we could model the network dynamics as sequences of—and relationships between—such gatherings. This provided a dramatic simplification allowing us, for example, to make predictions about the temporal trajectories of individual nodes through the social network [95]. We have since developed more sophisticated methods for identifying communities in this class of networks [1].

I include this example here to showcase the potential of the fundamental structures to organize our modeling of a certain network, and I hope that it will be possible to make similar progress for the remaining five dynamic classes. Connecting to the more general point of within-class versus between-class comparisons, it is also important to emphasize, that while the descriptions and algorithms developed in Refs. [1, 95] are excellent when analyzing networks in the synchronous, many-to-many class, they are not suited for describing networks in the remaining network classes (because they assume an underlying many-to-many, synchronous network structure).

3 Frequently Asked Questions

In this *Frequently Asked Questions* (FAQ) section, I go over a few questions that have come up frequently when I have discussed the ideas in the paper with other researchers.

3.1 What Do You Mean ‘Framework’!?

It is important to point out that the dynamic classes and associated fundamental structures are emphatically *not* a mathematical framework (for example, the classes are neither disjoint, nor complete). Instead what I aim to do here, is to point out new, meaningful structures in dynamic networks. These structures are organized around the idea of *communication events*, which in turn can be roughly classified into six prototypical forms of communication. In this sense, aspects of the framework are qualitative, focusing on providing useful taxonomy of classes of networks in the real world.

Nevertheless, as I argue in detail below, the fundamental structures impose a set of important constraints on dynamics for networks belonging to each class (with different constraints in different classes). These constraints impact many aspects of

how we currently model and analyze temporal networks, and therein lies the value of the framework. Much more on this in the epilogue.

3.2 Is the Framework All Done and Ready to Use?

A very important point to make in this FAQ section is to admit that there is still a big piece of the framework missing. Specifically, that, while in the case of the synchronous classes, understanding the temporal evolution of single communication events is relatively straightforward (as witnessed by our progress in the case of synchronous, many-to-many networks [95]), the temporal structure of fundamental structures of networks from the asynchronous classes is non-trivial since identification of (and method of analysis for) individual acts of communication is less clear.

In these cases, for example, while there is a well-defined end-time for each fundamental structure (when the active node ceases to be available), structures themselves can still cease to show any link-activity much before that, for example an old Facebook post which it is technically possible to comment on, but which nobody will ever find again. Or a book, which nobody will ever read again, but which is still available on many bookshelves. Further, in the many-to-many, asynchronous classes (which includes many important online social networks, such as Twitter and Facebook), there seems to be almost a spectrum running from one-to-many to many-to-many, depending on the amount of discussion associated with a post: posts without activity resembling trees, while vigorous discussions result in more clique-like structures.

3.3 Is It Just for Communication Networks?

While we focus here on modeling communication networks, it is likely that the distinctions, concepts, and methods developed for each of the classes summarized in Table 1 are valid in domains outside human communication, for example dynamics of signaling networks in biology such as protein–protein interaction networks [90], gene regulatory networks [105], and metabolic networks [37]. I also expect that the results developed in this project can be extended to networks of computer-to-computer communication [93].

3.4 Isn't All This Obvious?

The distinctions pointed out in Table 1 may appear so self-evident that a reader might ask why they are currently not a part of modeling temporal networks. I believe that the reason the network classes have remained unnoticed in the context of

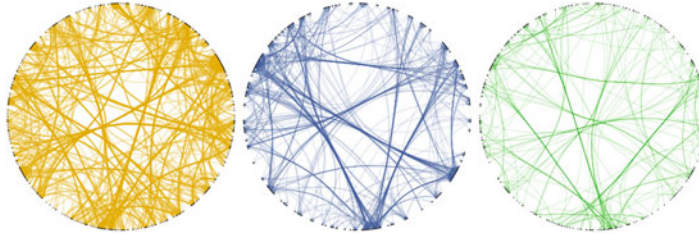


Fig. 4 Three networks defined on the same set of approximately 500 nodes from the SensibleDTU project [100], with links aggregated over 1 week; node-positions are the same in all three panels. From left to right the three panels show networks of physical proximity, telecommunication, and Facebook interactions. Data from [67]. While from different dynamic classes, in aggregated form, all three networks have similar topological properties

network science because time aggregation has obscured the fundamental differences in *generating processes* between networks with distinct fundamental structures.

As noted above, at the level of aggregation used in the literature, the many distinct networks (face-to-face, phone calls, text messages, emails, Twitter, Facebook, Snapchat, Instagram, discussion forums, etc.) that we participate in have common properties (see Fig. 4). These common properties are due to the simple fact that all these networks reflect the same underlying object: the social network of relationships between human beings. But as the cross sections of fundamental structures displayed in Fig. 2 shows, these networks are fundamentally different from each other on short time-scales. These differences are due to the characteristics of (and design-choices behind) each communication platform, which inevitably encodes one of the prototypical forms of communication in Table 1.

There are many traces of the fundamental structures in the recent literature. My group's work on communities in face-to-face networks [1, 95] discussed above proposes a new way of analyzing the class of synchronous, many-to-many networks, but does not realize its place in a larger framework. Elsewhere, recent work focusing on *simplicial complexes* explores the same class, both in terms of network structures [80] and implications for spreading processes [35], again without noting that these networks are not necessarily representative of temporal networks generally; without explicitly pointing out that networks from different classes need different methods of analysis. From another angle, it has been pointed out by many authors, see for example [49, 85], that time integrating techniques can introduce biases in understanding spreading processes as we will discuss later.

In the next section, we explore the consequences of the presence of the six classes on selected topics within temporal network analysis. Because each structure severely constrains possible network configurations, the fundamental motifs have a profound impact on the current state-of-the-art in temporal networks research.

4 Consequences for Analysis and Modeling

An immediate and important realization that flows from constraints imposed by the fundamental structures is that many important high-order network structures are strongly influenced by their network class.

I include an overview of five key topics below to illustrate the implications for existing temporal network theory. This list is not exhaustive, but simply intended to give the reader some examples of where I think the dynamic classes could be useful for developing new descriptions of temporal networks.

4.1 Randomization

A common approach to understand the effect of temporal structure in networks is to use *randomization* techniques to probe the impact of a structural feature of the network.

A simple example from static network theory to explain the logic of randomization: In their seminal paper [110], Watts and Strogatz argued that real world networks are ‘small worlds’, characterized by high clustering and short path lengths. But what does ‘high’ and ‘short’ mean in the sentence above? To make their point, Watts and Strogatz created ‘random’ counterparts to their real-world networks which contained the same number of nodes and links as the empirical networks, but with links placed randomly among nodes. They found that the empirical networks had both clustering and path-lengths that were orders of magnitude different (higher and lower, respectively) from their random counterparts. In static networks, the degree distribution is also often conserved [59].

The purpose of randomization is similar in temporal networks, but the possible randomization schemes are *much* richer [20, 32]. The idea is still: We want to estimate the effect of a specific temporal network property and remove that property (through randomization) to measure the effect. One may shuffle time-stamps (to understand the importance of ordering), replace time-stamps with random times drawn from a uniform distribution (to understand the importance of circadian patterns), shuffle links (in order to destroy topological structures), reverse time (to understand importance of causal sequences), etc. The idea is then to simulate a process of interest on the temporal network and compare the dynamics of that process with the same process run on ensembles of networks that are increasingly randomized relative to the original network [31].

Because the fundamental structures (as I have argued above) correspond to individual communication events, it is not always meaningful to randomize the networks according to the strategies mentioned above—*this generally results in*

*configurations of links that could not possibly appear in real communication networks.*³

Thus, a fruitful area for future research is to develop randomization schemes which respect the fundamental structures and understand how the fundamental structures impact the existing work on network randomizations [20]. A framework for randomization that respects the network classes would be analogous to the way that most randomizations in static networks respect degree distributions [59] (or higher-order structures [57, 72]), the key topological feature in these networks.

4.2 Generative Models

Closely related to randomization is the idea of using the fundamental structures to build new synthetic networks.

The idea of using simple models that reproduce some properties of the system under study and its dynamics, has been another important method for understanding complex dynamical systems [64]. Realistic synthetic data is important because we can use such synthetic temporal networks to study dynamic processes. The synthetic networks provide access to arbitrary amounts of data where we (a) understand the network's temporal changes (because we have created them) and (b) create ensembles of networks to study variability in outcome given a particular dynamic (contrary to the case of real-networks, we typically only have a single instance).

Thus, a plethora of models that generate temporal networks have also been investigated. The simplest approach is probably the ‘graph sequence approach’, which—time-slice by time-slice—selects nodes according to a heavy-tailed probability distribution and connect them to a fixed number of neighbors [79]. Due to its simplicity, this model has been the subject of much analytical work [43, 54, 55, 78, 99, 101] and extended in a number of ways [13, 52, 58, 66, 102]. Another simple approach is to generate a static network using an algorithm for generating static network (e.g. the configuration model [70]) and define activation patterns for links [30, 86]. Yet another approach is the work on simplicial complexes [35, 80], discussed above. Networks can also be generated based on an ensemble of two-dimensional random walkers with links forming when walkers are nearby each other [98, 112]. Other interesting approaches ‘grow’ network topologies according to local rules [4, 109]. Although they focus on larger (meso-scale) structures, we can even think of generative models for communities as models for networks [21, 62, 75–77, 108]. Adding temporal correlations, based on the notion that there is a positive correlation between inter-event times in empirical data is the motivation

³Another, related issue is that the communication events (fundamental structures) themselves, often are the very thing that spread information/opinions. They are not always (as many modeling papers assume) an underlying infrastructure on which the spreading occurs.

behind using Hawkes processes [10, 61], an approach which has also been used for predicting, for example, retweet dynamics [47].⁴

In the case of all these existing generative models, analyses based on synthetic datasets may have little relevance for real-world problems *because the models do not incorporate the constraints on dynamics imposed by the fundamental structures*.

The framework of dynamic classes, however, offers a completely new way of generating synthetic temporal networks. Since the fundamental structures are a manifestation of each network’s real-world generative process, we can create network models by simply creating time-sequences of realistic fundamental structures for a given. The usefulness of such models can be tested using statistical methods [12].

4.3 Link Prediction and Link Activity

Another dynamic network property strongly influenced by network class is the pattern of how links are active/non-active, and activity correlations between sets of links in a network [19, 42]. In face-to-face networks, these patterns are typically dominated by long-duration meetings between groups of individuals [95], whereas in text message networks back-and-forth dynamics are common [92].

Closely related the link-activities is temporal link prediction [53]. Here, the objective is to model patterns of link occurrences and use machine-learning to predict subsequent occurrences of links in the network based on local/global features of nodes/links. In static network theory, link prediction (especially within computer science) is a large topic [56], which focuses on predicting the presence of links that have been artificially removed or removed due to noise of some kind. In temporal networks, the objective is rephrased to—for example—predict all or some links in the next time-step [17].

Based our understanding of the differences in link-activities in different classes, it is clear that the fundamental structures offer a way to understand why features for link-prediction can vary strongly from network to network. There is simply a massive difference between predicting future links in a synchronous, many-to-many network, where temporal cross-sections are cliques and structures typically persist for hours, relative to e.g. text chat networks (asynchronous, one-to-one), where individuals can be in multiple ongoing conversations and text-snippets are short. In turn, this means that link prediction algorithms [53, 56] trained on one class of networks will fare poorly on networks belonging to other classes, since features will change dramatically depending on network class. These caveats become especially important when link-prediction is used to infer values for missing data [11, 27, 45]

⁴These latter models are closely related to the inter-fundamental structure activity in asynchronous, many-to-many networks.

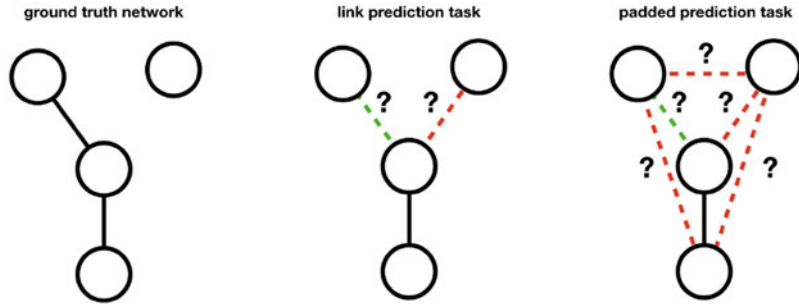


Fig. 5 Impossible links and link prediction performance. In this one-to-many scenario, the only possible links connects central node to the three neighbors. In the left panel we see the ground truth network. In the middle panel, we see the links that we are, in fact, relevant to consider when evaluating the performance of link-prediction. In the rightmost panel, we show the ‘padded’ network, which most current algorithms base their performance metrics on. The padded task, however, includes a number of links that could not possibly occur. We are not interested in the classifier’s performance on these links, and therefore an algorithm’s ability to predict/not predict their presence, should not be a part of the performance evaluation

Another consequence for link prediction is that current performance estimations may be misleading. This is because, depending on the dynamic class of network, not all links are possible to realize.

When performing a link prediction task, we feed the classifier examples of removed links (‘true’ examples) and examples of links that never existed (‘false’ examples), we then evaluate whether the classifier can tell which links exist and which do not. What we learn from the dynamic classes, is that there are, in fact, two types on non-links: actual false examples and ‘impossible’ links—links that cannot occur because they are not possible given the constraints imposed by fundamental structures in that network. This problem is important in one-to-many networks, where message recipients cannot communicate amongst each other, and there are many such impossible links. Link prediction algorithms should only consider actual false examples and not the impossible links, see Fig. 5 for an illustration of this problem in a one-to-many network.

4.4 Spreading Processes

Spreading processes are profoundly impacted by the fundamental structures. Let us begin the discussion on spreading by considering epidemic spreading. Perhaps the most studied type of dynamical systems on temporal networks is epidemic spreading, realizing compartment models, such as SIS (susceptible-infected-susceptible), SIR (susceptible-infected-recovered), etc on the temporal network [31, 32]. In terms of disease spreading, the key quantity is the fraction of available Susceptible-Infected links at any given time. This fraction varies strongly depending on the

network class [67], which in turn means that we can expect spreading dynamics to unfold differently within different classes.

For example, a central finding when simulating epidemics on temporal networks is that adding the temporal dimension has a strong impact on disease spreading in nearly all networks, relative to simulating the disease on a static network. In some cases the disease speeds up (relative to null models) and in others it slows down, depending on a complex interplay between structure and topology (see [31] for a discussion). This raises the intriguing possibility that perhaps some classes (e.g. one-to-one networks) might have slower epidemics than their randomized counterparts, while other classes (e.g. many-to-many networks) might have more rapidly spreading epidemics than their randomized versions.

If we look beyond epidemic spreading, there is experimental evidence that there are subtle differences in spreading processes across various domains [3, 7, 88, 111] and that opinions, behaviors, and information spread in different ways than diseases [8, 88]. When multiple sources of exposure to an innovation are required for a transmission to take place, we call the process *complex contagion*. In terms of modeling complex contagion processes on temporal networks, a key framework is threshold models, [25] where infection probability increases as a function of the fraction of infected neighbors. These have been generalized to temporal networks [2, 40, 41, 63, 103].

The class of network has an even more profound impact on complex contagion processes than on simple disease spreading. Consider, for example, a threshold model [25], where the probability of infection depends on which fraction of a node's neighbors are infected. Compared to phone-call networks, for example, threshold models have fundamentally different outcomes in face-to-face networks, where large groups of individuals routinely gather [35]. In the phone call network, forming connections to a large fraction of one's network might take several months. See Fig. 6 for an illustration of this discussion. Thus, if we want to understand contagion on a specific network, we must first understand the class of fundamental structures to which the network belongs.

4.5 Communities

Communities in static networks are groups of nodes with a high density of internal connections. Community detection in static networks never settled on a common definition of the term community (there is a strong analogy to clustering in machine learning [46]). Thus, generalizations to temporal networks also allow for substantial variability in approaches. The simplest strategy for identifying temporal communities is to first separate the list of time-stamped edges into sequence of static snapshots, independently cluster each layer, and then match the communities across the layers to find the temporal communities [29, 44, 73, 81, 95, 104]. A number of approaches can directly cluster the entire stack of temporal layers; these include

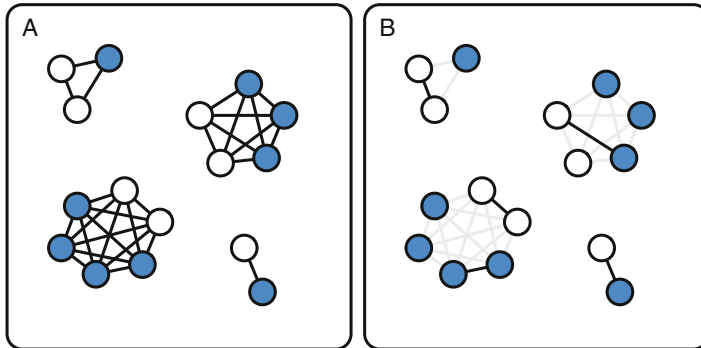


Fig. 6 A cartoon illustrating why complex contagion (e.g. the threshold model) behaves differently in different classes of networks. **(a)** Shows the meetings in a many-to-many realtime network (face-to-face meetings). **(b)** Shows phone calls (one-to-one synchronous network) among the same nodes at some point in time. Imagine that blue nodes are infected. In the many-to-many network, simultaneous information about a large set of neighbors is available for extended periods of time allowing for an accurate overview of opinions in the network. In the phone network nodes might need to wait extensively to access the state of some neighbors, allowing for much more difficulty in establishing an accurate state of knowledge

three-way matrix factorization [21], time-node graphs [96], and stochastic block models [21, 62, 76].⁵

From the perspective of the temporal structures, the central issue with community detection is that the appropriate community detection method varies strongly depending on a network's dynamic class. In synchronous, many-to-many networks, temporal continuity is a key feature of communities. And as we have already discussed, communities in face-to-face networks (dynamic class: synchronous, many-to-many) form more or less instantaneously as a group of fully connected nodes that connect at a certain time [95] and form gatherings that can be easily tracked over time. In this sense, communities in face-to-face networks are straightforward to identify—they are literally the fundamental structures of such systems.

Identifying communities in other dynamic classes, is a completely different exercise. For example, in the phone call (dynamic class: synchronous, one-to-one) or Facebook networks (dynamic class: asynchronous, many-to-many), communities become gradually observable as calls or messages aggregate over time. In the latter case, communities have to do with other network properties than the temporal

⁵These methods, however, do not incorporate explicit dependencies between layers. To take into account interdependencies, some methods cluster multilayer networks using interlayer links that represent specific causal or correlational dependencies between the layers [5, 9, 14, 15, 51, 68, 97]. These interlayer dependencies are of key importance in the context of modeling fundamental structures since the temporal aspect of the fundamental structures impose important (and class dependent) interlayer correlations among nodes belonging to the same fundamental structure over time. Using the Infomap framework [89], we have recently developed a model for interlayer dependencies for synchronous, many-to-many networks [1].

sequence. Here, my interactions are driven by the order in which posts were published rather than organized by social context (as is the case in the synchronous networks). To give a concrete example, I might retweet a work-related post about *p*-values, then ‘like’ a post about the Finnish heavy metal band Nightwish, published by a friend, and finally comment on a political statement from a family member. Thus, in most asynchronous systems, activity aggregates around *active nodes* (posts) rather than social contexts. *This means that interactions within communities are not necessarily correlated in time.* A fact which must be taken into consideration when we construct methods for detecting communities. At the same time, we know from the literature that communities do exist in these networks [73, 82, 106].

As in the FAQ, the temporal evolution of the fundamental structures within the asynchronous classes is under-determined in the framework as it currently stands. Similarly, exactly how to identify communities in these dynamical classes is not clear to me. The central point I wish to make related to communities, however, is that methods related to identifying communities in temporal networks will likely need to be different depending on the network’s dynamical class.

5 Conclusion

The lesson that i hope arises across the five key examples above is that networks within each of the dynamic classes must be analyzed and modeled separately; that comparisons of statistics between networks are only meaningful for networks belonging to the same class. This is because the class itself (and not just the actual systems that are represented through the temporal network), strongly impacts almost all known temporal network metrics.

Zooming out further, three key points emerge from the full discussion of the dynamic classes and their fundamental structures.

1. Firstly, I argued that it is meaningful to divide all communication networks into six dynamic classes (Fig. 1). This distinction originates from communication studies [36] but is not yet recognized within network science.
2. Secondly, I pointed out that a networks class strongly influences its temporal evolution and alters dynamic processes on that network. This implies that we cannot meaningfully compare results for networks belonging to different classes.
3. Thirdly, I tried to motivate the idea that the dynamic classes provide a promising new framework for modeling temporal communication networks. This is because every communication network can be seen as *sequences of individual communication events*. Thus, we can model every such network as generated by many instances of a single fundamental structure. In this sense, the six classes provide us the foundation for a new framework for both measuring and modeling temporal networks.

These three key take-homes lead me to consider the role that I hope the dynamical classes will play in the field of temporal networks. An important element that is

currently missing from the field of temporal network theory is a set of topological properties to measure and devise statistics for. This lack of agreed-upon-structures is eloquently pointed out by Petter Holme in his excellent review of temporal network science [31], where he writes:

In the history of static network theory, **measuring network structure has been driving the field**. For example, after Barabási and coworkers discovered how common scale-free (i.e. power-law-like) degree distributions are (...), there was a huge effort both to measure degree distribution and to model their emergence.

For temporal networks, **similar ubiquitous structures are yet to be discovered, perhaps they do not even exist**. This has led the research in temporal networks down a slightly different path, where the focus is more on dynamic systems on the network and how they are affected by structure, and less on discovering common patterns or classifying networks. [my emphases]

Now, allow me to speculate wildly for a bit. I do not think that it is impossible that the fundamental structures could be analogues to the ‘ubiquitous structures’ mentioned in the quote for the case of temporal networks. Perhaps the six dynamic classes will allow us to think about structure in temporal networks in a new and more principled way.

Finding such structures is important because, in static networks, a deeper understanding of the *structure* of the network, has allowed us to reason in principled ways about their *function*—and for most applications outside pure science, function is what we care about. As the quote illustrates, temporal network science has had to follow a different path, focused more on simulation, for example observing how dynamical processes unfold. As a consequence, we still do not have a coherent picture of the key mechanisms in temporal networks. While still unproven at this point, I think that the fundamental structures carry the promise of being the ubiquitous structures that Holme posits are ‘yet to be discovered’. Therefore I hope that the new perspective provided by the dynamic classes will give rise to new statistical models, algorithms and research questions.

Epilogue: More FAQs

There’s a couple of more questions that have come up frequently in discussions of the framework, but which slowed down the flow of the paper, so I have moved them here, to the epilogue, for readers who might share these particular questions.

What About Mathematical Completeness?

A graph-theory inclined reader may ask: ‘In what sense is this a mathematical framework?’ With follow-ups such as ‘Are the classes disjoint? Can a dynamic

network belong to multiple classes? Can a network's class change over time?" They might proceed 'Are the classes complete? Can all possible networks be divided into one of the six classes? Is it possible to construct networks that fall outside the taxonomy in Table 1?"

Here, the answer is that this is not a framework/theory in a graph theoretical sense. I think of the six classes as a *model* in the physics sense of the word.

Let me explain by way of an analogy. In the early days of quantum mechanics, Geiger and Marsden (directed by Rutherford), decided to shoot some α -particles into a thin sheet of gold foil [22, 23]. They noticed that a vast majority of the particles went straight through the gold foil, but that a small fraction were scattered at a wide range of angles. This was a highly unexpected and very non-classical behavior. To explain these strange experimental observations, Rutherford proposed a new *model*, qualitative at first, that atoms have a tiny and heavy nucleus, surrounded by a cloud of electrons (departing from the then popular 'plum pudding model'⁶ of the atom, proposed in 1904 by J.J. Thompson). Based on Rutherford's model for the atom's structure, other scientists were able to develop better descriptions, eventually leading to the quantum mechanical framework that we teach undergrads today.

I think of the framework presented here as a model in the same sense as Rutherford's (no comparison otherwise). Just like the model of a dense core with mostly empty space around it was a way to organize subsequent observations and provide structure to the theories/models to follow it, the dynamical classes are a way to organize our study of networks and to provide constraints/structure for the next steps of theory-building.⁷

But How Is This Different from Temporal Motifs?

Motifs are a structural characteristic closely connected to fundamental structures, and have been the focus of much research. This area features multiple generalizations of the motifs in static networks [65]—small subgraphs that occur more or less frequently than one might expect in an appropriate null model. Typically, the strategy is to count the temporal subgraphs occurring within some interval Δt [48, 113]. Findings suggest that certain tit-for-tat motifs and triangles are over-represented in phone networks (dynamic class: synchronous, one-to-one networks) and may shape processes such as spreading [16, 58, 87, 91]. Recently, highly efficient methods have resulted in accurate motif-counts for very large networks [74]. Other motif-like structures have been explored, for example graphlets, which are equivalence classes of Δt -causal subgraphs [34]. Of particular relevance to

⁶Yes, that was real thing.

⁷By the way, as far as I can tell, the classes are not disjoint and not complete. Further, real networks are not necessarily a perfect fit to their classes. But as I hope to have convinced the reader by way of the analogy above ... that's not the point.

the framework presented here is work on structure prediction [50] and related algorithms for efficiently counting isomorphic temporal subgraphs [84].

From the perspective of fundamental structures, there are two issues with temporal sub-graph counting approaches. The key issue is that current methods do not measure individual communication events. The sliding window based approach, which identifies the network structures that arise within some time Δt does not recognize that the fundamental structures have a natural beginning and end. As a consequence, these methods do not identify and aggregate statistics for the fundamental structures, rather ending up with aggregate statistics for smaller structures which are incidental to the fundamental structures. To be concrete: In the example we discussed above (Fig. 2), a motif-based method would find many triangles in the face-to-face networks, but not realize that the network consists of disjoint cliques, which could be matched up over time. A second problem in some of the large comparative studies is that the notion of network classes are not considered. This can lead to non-meaningful comparisons of motif-counts between networks belonging to separate classes (see [74] for an example).

Acknowledgements I would like to thank Arkadiusz Arek Stopczynski, Enys Mones, Hjalmar Bang Carlsen, Laura Alessandretti, James Bagrow, Petter Holme, Piotr Sapiezynski, Sebastiano Piccolo, Ulf Aslak Jensen, and Yong-Yeol Ahn for fruitful discussions and generous comments on the manuscript text (list sorted alphabetically by first name). Special thanks to Piotr for the link prediction example. This work was supported by the Independent Research Fund Denmark.

References

1. Aslak, U., Rosvall, M., Lehmann, S.: Constrained information flows in temporal networks reveal intermittent communities. Preprint arXiv:1711.07649 (2017)
2. Backlund, V.P., Saramäki, J., Pan, R.K.: Effects of temporal correlations on cascades: threshold models on temporal networks. *Phys. Rev. E* **89**(6), 062815 (2014)
3. Backstrom, L., Huttenlocher, D., Kleinberg, J., Lan, X.: Group formation in large social networks: membership, growth, and evolution. In: Proceedings of the 12th ACM SIGKDD International Conference, pp. 44–54 (2006)
4. Bagrow, J.P., Brockmann, D.: Natural emergence of clusters and bursts in network evolution. *Phys. Rev. X* **3**(2), 021016 (2013)
5. Bazzi, M., Porter, M.A., Williams, S., McDonald, M., Fenn, D.J., Howison, S.D.: Community detection in temporal multilayer networks, with an application to correlation networks. *Multiscale Model. Simul.* **14**(1), 1–41 (2016)
6. Carlberg, K., Crowcroft, J.: Building shared trees using a one-to-many joining mechanism. *ACM SIGCOMM Comput. Commun. Rev.* **27**(1), 5–11 (1997)
7. Centola, D.: The spread of behavior in an online social network experiment. *Science* **329**(5996), 1194–1197 (2010)
8. Centola, D., Macy, M.: Complex contagions and the weakness of long ties. *Am. J. Soc.* **113**(3), 702–734 (2007)
9. Chen, Y., Kawadia, V., Urgaonkar, R.: Detecting overlapping temporal community structure in time-evolving networks. arXiv preprint arXiv:1303.7226 (2013)
10. Cho, Y.S., Galstyan, A., Brantingham, P.J., Tita, G.: Latent self-exciting point process model for spatial-temporal networks. Preprint arXiv:1302.2671 (2013)

11. Clauset, A., Moore, C., Newman, M.E.: Hierarchical structure and the prediction of missing links in networks. *Nature* **453**(7191), 98 (2008)
12. Clegg, R.G., Parker, B., Rio, M.: Likelihood-based assessment of dynamic networks. *J. Complex Netw.* **4**(4), 517–533 (2016)
13. Cui, J., Zhang, Y.Q., Li, X.: On the clustering coefficients of temporal networks and epidemic dynamics. In: 2013 IEEE International Symposium on Circuits and Systems (ISCAS), pp. 2299–2302. IEEE, Piscataway (2013)
14. De Bacco, C., Power, E.A., Larremore, D.B., Moore, C.: Community detection, link prediction, and layer interdependence in multilayer networks. *Phys. Rev. E* **95**(4), 042317 (2017)
15. De Domenico, M., Lancichinetti, A., Arenas, A., Rosvall, M.: Identifying modular flows on multilayer networks reveals highly overlapping organization in interconnected systems. *Phys. Rev. X* **5**(1), 011027 (2015)
16. Delvenne, J.C., Lambiotte, R., Rocha, L.E.: Diffusion on networked systems is a question of time or structure. *Nature Commun.* **6**, 7366 (2015)
17. Dhote, Y., Mishra, N., Sharma, S.: Survey and analysis of temporal link prediction in online social networks. In: 2013 International Conference on Advances in Computing, Communications and Informatics (ICACCI), pp. 1178–1183. IEEE, Piscataway (2013)
18. Eagle, N., Pentland, A., Lazer, D.: Inferring social network structure using mobile phone data. *Proc. Natl. Acad. Sci.* **106**, 15274–15278 (2007)
19. Eckmann, J.P., Moses, E., Sergi, D.: Entropy of dialogues creates coherent structures in e-mail traffic. *Proc. Natl. Acad. Sci. U.S.A.* **101**(40), 14333–14337 (2004)
20. Gauvin, L., Génois, M., Karsai, M., Kivelä, M., Takaguchi, T., Valdano, E., Vestergaard, C.L.: Randomized reference models for temporal networks. Preprint arXiv: 1806.04032 (2018)
21. Gauvin, L., Panisson, A., Cattuto, C.: Detecting the community structure and activity patterns of temporal networks: a non-negative tensor factorization approach. *PLoS One* **9**(1), e86028 (2014)
22. Geiger, H., Marsden, E.: On a diffuse reflection of the α -particles. *Proc. R. Soc. Lond. A* **82**(557), 495–500 (1909)
23. Geiger, H.: The scattering of α -particles by matter. *Proc. R. Soc. Lond. A* **83**(565), 492–504 (1910)
24. Génois, M., Vestergaard, C.L., Fournet, J., Panisson, A., Bonmarin, I., Barrat, A.: Data on face-to-face contacts in an office building suggest a low-cost vaccination strategy based on community linkers. *Netw. Sci.* **3**(3), 326–347 (2015)
25. Granovetter, M.: Threshold models of collective behavior. *Am. J. Sociol.* **83**(6), 1420 (1978)
26. Guimera, R., Danon, L., Diaz-Guilera, A., Giralt, F., Arenas, A.: Self-similar community structure in a network of human interactions. *Phys. Rev. E* **68**(6), 065103 (2003)
27. Guimerà, R., Sales-Pardo, M.: Missing and spurious interactions and the reconstruction of complex networks. *Proc. Natl. Acad. Sci.* **106**(52), 22073–22078 (2009)
28. Gummesson, E.: From one-to-one to many-to-many marketing. In: Service Excellence in Management: Interdisciplinary Contributions, Proceedings from the QUIS 9 Symposium, Karlstad University Karlstad, Sweden, pp. 16–25. Citeseer (2004)
29. He, J., Chen, D.: A fast algorithm for community detection in temporal network. *Phys. A Stat. Mech. Appl.* **429**, 87–94 (2015)
30. Holme, P.: Epidemiologically optimal static networks from temporal network data. *PLoS Comput. Biol.* **9**(7), e1003142 (2013)
31. Holme, P.: Modern temporal network theory: a colloquium. *Eur. Phys. J. B* **88**(9), 234 (2015)
32. Holme, P., Saramäki, J.: Temporal networks. *Phys. Rep.* **519**, 97–125 (2012)
33. Holme, P., Saramäki, J.: Temporal Networks. Springer, Berlin (2013)
34. Hulovatyy, Y., Chen, H., Milenković, T.: Exploring the structure and function of temporal networks with dynamic graphlets. *Bioinformatics* **31**(12), i171–i180 (2015)
35. Iacopini, I., Petri, G., Barrat, A., Latora, V.: Simplicial models of social contagion. arXiv preprint arXiv:1810.07031 (2018)

36. Jensen, K.B., Helles, R.: The internet as a cultural forum: implications for research. *New Media Soc.* **13**(4), 517–533 (2011)
37. Jeong, H., Tombor, B., Albert, R., Oltvai, Z.N., Barabási, A.L.: The large-scale organization of metabolic networks. *Nature* **407**(6804), 651 (2000)
38. Jewett, T.: Database Design with UML and SQL, 3rd edn. (2011). <http://www.tomjewett.com/dbdesign>
39. Jo, J., Kim, J.: Synchronized one-to-many media streaming with adaptive playout control. In: *Multimedia Systems and Applications V*. International Society for Optics and Photonics, vol. 4861, pp. 71–83 (2002)
40. Karimi, F., Holme, P.: A temporal network version of wattss cascade model. In: *Temporal Networks*, pp. 315–329. Springer, Berlin (2013)
41. Karimi, F., Holme, P.: Threshold model of cascades in empirical temporal networks. *Phys. A Stat. Mech. Appl.* **392**(16), 3476–3483 (2013)
42. Karsai, M., Kaski, K., Kertész, J.: Correlated dynamics in egocentric communication networks. *PLoS One* **7**(7), e40612 (2012)
43. Karsai, M., Perra, N., Vespignani, A.: Time varying networks and the weakness of strong ties. *Sci. Rep.* **4**, 4001 (2014)
44. Kauffman, J., Kittas, A., Bennett, L., Tsoka, S.: DyCoNet: a geph plugin for community detection in dynamic complex networks. *PLoS One* **9**(7), e101357 (2014)
45. Kim, M., Leskovec, J.: The network completion problem: Inferring missing nodes and edges in networks. In: *Proceedings of the 2011 SIAM International Conference on Data Mining*, pp. 47–58. SIAM (2011)
46. Kleinberg, J.M.: An impossibility theorem for clustering. In: *Advances in neural information processing systems*, pp. 463–470 (2003)
47. Kobayashi, R., Lambiotte, R.: TiDeH: time-dependent hawkes process for predicting retweet dynamics. In: *ICWSM*, pp. 191–200 (2016)
48. Kovanen, L., Kaski, K., Kertész, J., Saramäki, J.: Temporal motifs reveal homophily, gender-specific patterns, and group talk in call sequences. *Proc. Natl. Acad. Sci.* **110**(45), 18070–18075 (2013)
49. Krings, G., Karsai, M., Bernhardsson, S., Blondel, V.D., Saramäki, J.: Effects of time window size and placement on the structure of an aggregated communication network. *EPJ Data Sci.* **1**(1), 4 (2012)
50. Lahiri, M., Berger-Wolf, T.Y.: Structure prediction in temporal networks using frequent subgraphs. In: *IEEE Symposium on Computational Intelligence and Data Mining, CIDM 2007*, pp. 35–42. IEEE, Piscataway (2007)
51. Larremore, D.B., Clauset, A., Buckee, C.O.: A network approach to analyzing highly recombinant malaria parasite genes. *PLoS Comput. Biol.* **9**(10), e1003268 (2013)
52. Laurent, G., Saramäki, J., Karsai, M.: From calls to communities: a model for time-varying social networks. *Eur. Phys. J. B* **88**(11), 301 (2015)
53. Liben-Nowell, D., Kleinberg, J.: The link-prediction problem for social networks. *J. Assoc. Inf. Sci. Technol.* **58**(7), 1019–1031 (2007)
54. Liu, S., Perra, N., Karsai, M., Vespignani, A.: Controlling contagion processes in activity driven networks. *Phys. Rev. Lett.* **112**(11), 118702 (2014)
55. Liu, S.Y., Baronchelli, A., Perra, N.: Contagion dynamics in time-varying metapopulation networks. *Phys. Rev. E* **87**(3), 032805 (2013)
56. Lü, L., Zhou, T.: Link prediction in complex networks: a survey. *Phys. A Stat. Mech. Appl.* **390**(6), 1150–1170 (2011)
57. Mahadevan, P., Krioukov, D., Fall, K., Vahdat, A.: Systematic topology analysis and generation using degree correlations. In: *ACM SIGCOMM Computer Communication Review*, vol. 36, pp. 135–146. ACM, New York (2006)
58. Mantzaris, A.V., Higham, D.J.: Inferring and calibrating triadic closure in a dynamic network. In: *Temporal Networks*, pp. 265–282. Springer, Berlin (2013)
59. Maslov, S., Sneppen, K.: Specificity and stability in topology of protein networks. *Science* **296**(5569), 910–913 (2002)

60. Masuda, N., Lambiotte, R.: A Guidance to Temporal Networks. World Scientific, Singapore (2016)
61. Masuda, N., Takaguchi, T., Sato, N., Yano, K.: Self-exciting point process modeling of conversation event sequences. In: Temporal Networks, pp. 245–264. Springer, Berlin (2013)
62. Matias, C., Miele, V.: Statistical clustering of temporal networks through a dynamic stochastic block model. *J. R. Stat. Soc. Ser. B Stat Methodol.* **79**(4), 1119–1141 (2017)
63. Michalski, R., Kajdanowicz, T., Bródka, P., Kazienko, P.: Seed selection for spread of influence in social networks: temporal vs. static approach. *N. Gener. Comput.* **32**(3–4), 213–235 (2014)
64. Miller, J.H., Page, S.E.: Complex Adaptive Systems: An Introduction to Computational Models of Social Life. Princeton University Press, Princeton (2009)
65. Milo, R., Shen-Orr, S., Itzkovitz, S., Kashtan, N., Chklovskii, D., Alon, U.: Network motifs: simple building blocks of complex networks. *Science* **298**(5594), 824–827 (2002)
66. Moinet, A., Starnini, M., Pastor-Satorras, R.: Burstiness and aging in social temporal networks. *Phys. Rev. Lett.* **114**(10), 108701 (2015)
67. Mones, E., Stopczynski, A., Hupert, N., Lehmann, S., et al.: Optimizing targeted vaccination across cyber–physical networks: an empirically based mathematical simulation study. *J. R. Soc. Interface* **15**(138), 20170783 (2018)
68. Mucha, P., Richardson, T., Macon, K., Porter, M., Onnela, J.P.: Community structure in time-dependent, multiscale, and multiplex networks. *Science* **328**(5980), 876–878 (2010)
69. Myers, S.A., Sharma, A., Gupta, P., Lin, J.: Information network or social network? The structure of the twitter follow graph. In: Proceedings of the 23rd International Conference on World Wide Web, pp. 493–498. ACM, New York (2014)
70. Newman, M.: Networks, An Introduction. Oxford University Press, Oxford (2010)
71. Onnela, J.P., Saramäki, J., Hyvönen, J., Szabó, G., Lazer, D., Kaski, K., Kertész, J., Barabási, A.L.: Structure and tie strengths in mobile communication networks. *Proc. Natl. Acad. Sci.* **104**(18), 7322–7336 (2007)
72. Orsini, C., Dankulov, M.M., Colomer-de Simón, P., Jamakovic, A., Mahadevan, P., Vahdat, A., Bassler, K.E., Toroczkai, Z., Boguñá, M., Caldarelli, G., et al.: Quantifying randomness in real networks. *Nat. Commun.* **6**, 8627 (2015)
73. Palla, G., Barabási, A., Vicsek, T.: Quantifying social group evolution. *Nature* **446**, 664–667 (2007)
74. Paranjape, A., Benson, A.R., Leskovec, J.: Motifs in temporal networks. In: Proceedings of the Tenth ACM International Conference on Web Search and Data Mining, pp. 601–610. ACM, New York (2017)
75. Peixoto, T.P.: Parsimonious module inference in large networks. *Phys. Rev. Lett.* **110**(14), 148701 (2013)
76. Peixoto, T.P.: Inferring the mesoscale structure of layered, edge-valued, and time-varying networks. *Phys. Rev. E* **92**(4), 042807 (2015)
77. Peixoto, T.P.: Model selection and hypothesis testing for large-scale network models with overlapping groups. *Phys. Rev. X* **5**(1), 011033 (2015)
78. Perra, N., Baronchelli, A., Mocanu, D., Gonçalves, B., Pastor-Satorras, R., Vespignani, A.: Random walks and search in time-varying networks. *Phys. Rev. Lett.* **109**(23), 238701 (2012)
79. Perra, N., Gonçalves, B., Pastor-Satorras, R., Vespignani, A.: Activity driven modeling of time varying networks. *Sci. Rep.* **2**, 469 (2012)
80. Petri, G., Barrat, A.: Simplicial activity driven model. *Phys. Rev. Lett.* **121**, 228301 (2018)
81. Pietilänen, A.K., Diot, C.: Dissemination in opportunistic social networks: the role of temporal communities. In: Proceedings of the Thirteenth ACM International Symposium on Mobile Ad Hoc Networking and Computing, pp. 165–174. ACM, Berlin (2012)
82. Porter, M.A., Onnela, J.P., Mucha, P.J.: Communities in networks. *Notices of the AMS* **56**(9), 1082–1097 (2009)
83. Rahwan, I., Kowalczyk, R., Pham, H.H.: Intelligent agents for automated one-to-many e-commerce negotiation. In: Australian Computer Science Communications, vol. 24, pp. 197–204. Australian Computer Society, Darlinghurst (2002)

84. Redmond, U., Cunningham, P.: Temporal subgraph isomorphism. In: Proceedings of the 2013 IEEE/ACM International Conference on Advances in Social Networks Analysis and Mining, pp. 1451–1452. ACM, New York (2013)
85. Ribeiro, B., Perra, N., Baronchelli, A.: Quantifying the effect of temporal resolution on time-varying networks. *Sci. Rep.* **3**, 3006 (2013)
86. Rocha, L.E., Blondel, V.D.: Bursts of vertex activation and epidemics in evolving networks. *PLoS Comput. Biol.* **9**(3), e1002974 (2013)
87. Rocha, L.E., Blondel, V.D.: Flow motifs reveal limitations of the static framework to represent human interactions. *Phys. Rev. E* **87**(4), 042814 (2013)
88. Romero, D.M., Meeder, B., Kleinberg, J.: Differences in the mechanics of information diffusion across topics: idioms, political hashtags, and complex contagion on twitter. In: Proceedings of the 20th International Conference on World Wide Web, pp. 695–704. ACM, New York (2011)
89. Rosvall, M., Bergstrom, C.: Maps of random walks on complex networks reveal community structure. *Proc. Natl. Acad. Sci.* **105**(4), 1118–1123 (2008)
90. Rual, J.F., Venkatesan, K., Hao, T., Hirozane-Kishikawa, T., Dricot, A., Li, N., Berriz, G.F., Gibbons, F.D., Dreze, M., Ayivi-Guedehoussou, N., et al.: Towards a proteome-scale map of the human protein–protein interaction network. *Nature* **437**(7062), 1173 (2005)
91. Saramäki, J., Holme, P.: Exploring temporal networks with greedy walks. *Eur. Phys. J. B* **88**(12), 334 (2015)
92. Saramaki, J., Moro, E.: From seconds to months: multi-scale dynamics of mobile telephone calls. *Eur. Phys. J. B* **88**, 1 (2015)
93. Schwartz, M.: Computer-Communication Network Design and Analysis, vol. 25. Prentice-Hall, Englewood Cliffs (1977)
94. Sekara, V., Lehmann, S.: The strength of friendship ties in proximity sensor data. *PLoS One* **9**(7), e100915 (2014)
95. Sekara, V., Stopczynski, A., Lehmann, S.: Fundamental structures of dynamic social networks. *Proc. Natl. Acad. Sci.* **113**(36), 9977–9982 (2016)
96. Speidel, L., Takaguchi, T., Masuda, N.: Community detection in directed acyclic graphs. *Eur. Phys. J. B* **88**(8), 203 (2015)
97. Stanley, N., Shai, S., Taylor, D., Mucha, P.J.: Clustering network layers with the strata multilayer stochastic block model. *IEEE Trans. Netw. Sci. Eng.* **3**(2), 95–105 (2016)
98. Starnini, M., Baronchelli, A., Pastor-Satorras, R.: Modeling human dynamics of face-to-face interaction networks. *Phys. Rev. Lett.* **110**(16), 168701 (2013)
99. Starnini, M., Pastor-Satorras, R.: Temporal percolation in activity-driven networks. *Phys. Rev. E* **89**(3), 032807 (2014)
100. Stopczynski, A., Sekara, V., Sapiezynski, P., Cuttone, A., Larsen, J.E., Lehmann, S.: Measuring large-scale social networks with high resolution. *PLoS One* **9**(4), e95978 (2014)
101. Sun, K., Baronchelli, A., Perra, N.: Contrasting effects of strong ties on SIR and SIS processes in temporal networks. *Eur. Phys. J. B* **88**(12), 326 (2015)
102. Sunny, A., Kotnis, B., Kuri, J.: Dynamics of history-dependent epidemics in temporal networks. *Phys. Rev. E* **92**(2), 022811 (2015)
103. Takaguchi, T., Masuda, N., Holme, P.: Bursty communication patterns facilitate spreading in a threshold-based epidemic dynamics. *PLoS One* **8**(7), e68629 (2013)
104. Tantipathananandh, C., Berger-Wolf, T., Kempe, D.: A framework for community identification in dynamic social networks. In: Proceedings of the 13th ACM SIGKDD International Conference on Knowledge Discovery and Data Mining, pp. 717–726. ACM, New York (2007)
105. Thieffry, D., Huerta, A.M., Pérez-Rueda, E., Collado-Vides, J.: From specific gene regulation to genomic networks: a global analysis of transcriptional regulation in escherichia coli. *Bioessays* **20**(5), 433–440 (1998)
106. Ugander, J., Backstrom, L., Marlow, C., Kleinberg, J.: Structural diversity in social contagion. *Proc. Natl. Acad. Sci.* **109**(16), 5962–5966 (2012)
107. Ugander, J., Karrer, B., Backstrom, L., Marlow, C.: The anatomy of the facebook social graph. arXiv preprint arXiv:1111.4503 (2011)

108. Valles-Catala, T., Massucci, F.A., Guimera, R., Sales-Pardo, M.: Multilayer stochastic block models reveal the multilayer structure of complex networks. *Phys. Rev. X* **6**(1), 011036 (2016)
109. Vestergaard, C.L., Génoin, M., Barrat, A.: How memory generates heterogeneous dynamics in temporal networks. *Phys. Rev. E* **90**(4), 042805 (2014)
110. Watts, D., Strogatz, S.: Collective dynamics of ‘small-world’ networks. *Nature* **393**, 440 (1998)
111. Weng, L., Menczer, F., Ahn, Y.Y.: Virality prediction and community structure in social networks. *Sci. Rep.* **3**, 2522 (2013)
112. Zhang, Y.Q., Li, X., Liang, D., Cui, J.: Characterizing bursts of aggregate pairs with individual poissonian activity and preferential mobility. *IEEE Commun. Lett.* **19**(7), 1225–1228 (2015)
113. Zhao, Q., Tian, Y., He, Q., Oliver, N., Jin, R., Lee, W.C.: Communication motifs: a tool to characterize social communications. In: Proceedings of the 19th ACM International Conference on Information and Knowledge Management, pp. 1645–1648. ACM, New York (2010)

Weighted, Bipartite, or Directed Stream Graphs for the Modeling of Temporal Networks



Matthieu Latapy, Clémence Magnien, and Tiphaine Viard

1 Introduction

Graph theory is one of the main formalisms behind network science. It provides concepts and methods for the study of networks, and it is fueled by questions and challenges raised by them. Its core principle is to model networks as sets of nodes and links between them. Then, a graph G is defined by a set of nodes V and a set of links $E \subseteq V \otimes V$ where each link is an unordered pair of nodes.¹ In many cases, though, this does not capture key features of the modeled network. In particular, links may be weighted or directed, nodes may be of different kinds, etc. One key strength of graph theory is that it easily copes with such situations by defining natural extensions of basic graphs, typically weighted, bipartite, or directed graphs. Classical concepts on graphs are then extended to these more complex cases.

Stream graphs were recently introduced as a formal framework for temporal networks [27], similar to what graph theory is to networks. A stream graph S is defined by a time set T , a node set V , a set of temporal nodes $W \subseteq T \times V$ and a set of temporal links $E \subseteq T \times V \otimes V$. See Fig. 1 for an illustration. Each node $v \in V$ has a set of presence times $T_v = \{t, (t, v) \in W\}$. Likewise, $T_{uv} = \{t, (t, uv) \in E\}$ is the set of presence times of link uv . Conversely, $V_t = \{v, (t, v) \in W\}$ and $E_t = \{uv, (t, uv) \in E\}$ are the set of nodes and links

¹Given any two sets X and Y , we denote by $X \times Y$ the cartesian product of X and Y , i.e. the set of all ordered pairs (x, y) such that $x \in X$ and $y \in Y$. We denote by $X \otimes Y$ the set of all unordered pairs composed of $x \in X$ and $y \in Y$, with $x \neq y$, that we denote by $xy = yx$.

M. Latapy (✉) · C. Magnien · T. Viard
CNRS, Laboratoire d’Informatique de Paris 6, Paris, France
e-mail: Matthieu.Latapy@lip6.fr

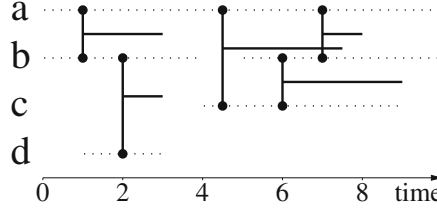


Fig. 1 An example of stream graph: $S = (T, V, W, E)$ with $T = [0, 10] \subseteq \mathbb{R}$, $V = \{a, b, c, d\}$, $W = [0, 10] \times \{a\} \cup ([0, 4] \cup [5, 10]) \times \{b\} \cup [4, 9] \times \{c\} \cup [1, 3] \times \{d\}$, and $E = ([1, 3] \cup [7, 8]) \times \{ab\} \cup [4.5, 7.5] \times \{ac\} \cup [6, 9] \times \{bc\} \cup [2, 3] \times \{bd\}$. In other words, $T_a = [0, 10]$, $T_b = [0, 4] \cup [5, 10]$, $T_c = [4, 9]$, $T_d = [1, 3]$, $T_{ab} = [1, 3] \cup [7, 8]$, $T_{ac} = [4.5, 7.5]$, $T_{bc} = [6, 9]$, $T_{bd} = [2, 3]$, and $T_{ad} = T_{cd} = \emptyset$

present at time t , leading to the graph at time t : $G_t = (V_t, E_t)$. The graph induced by S is $G(S) = (\{v, T_v \neq \emptyset\}, \{uv, T_{uv} \neq \emptyset\})$.

Stream graphs encode the same information as Time Varying Graphs (TVG) [13], Relational Event Models (REM) [11, 47], Multi-Aspect Graphs (MAG) [52, 53], or other models of temporal networks. Stream graphs emphasize the streaming nature of data, but all stream graph concepts may easily be translated to these other points of views.

A wide range of graph concepts have been extended to stream graphs [27]. The most basic ones are probably the number of nodes $n = \sum_{v \in V} \frac{|T_v|}{|T|}$ and the number of links $m = \sum_{uv \in V \otimes V} \frac{|T_{uv}|}{|T|}$. Then, the neighborhood of node v is $N(v) = \{(t, u), (t, uv) \in E\}$ and its degree is $d(v) = \frac{|N(v)|}{|T|}$. The average degree of S is the average degree of all nodes weighted by their presence time: $d(S) = \sum_{v \in V} \frac{|T_v|}{|W|} d(v)$.

Going further, the density of S is $\delta(S) = \frac{m}{\sum_{uv \in V \otimes V} |T_u \cap T_v|}$. It is the probability, when one chooses at random a time instant and two nodes present at that time, that these two nodes are linked together at that time. Then, a clique is a subset C of W such that for all (t, u) and (t, v) in C , u and v are linked together at time t in S , i.e. $(t, uv) \in E$. Equivalently, a subset of W is a clique of S if the substream it induces has density 1.

This leads to the definition of clustering coefficient in stream graphs: like in graphs, $cc(v)$ is the density of the neighborhood of v . Equivalently, $cc(v) = \sum_{uw \in V \otimes V} \frac{|T_{vu} \cap T_{vw} \cap T_{uw}|}{|T_{vu} \cap T_{vw}|}$. Likewise, the transitivity of S is the fraction of all 4-uplets (t, u, v, w) with (t, uv) and (t, vw) in E such that (t, uw) is also in E .

These concepts generalize graph concepts in the following sense. A stream S is called *graph-equivalent* if it has no dynamics: $G_t = G(S)$ for all t . In this case, each stream property of S is equal to the corresponding graph property of $G(S)$. For instance, the density of S is equal to the one of $G(S)$. Graphs may therefore be seen as special cases of stream graphs (the ones with no dynamics).

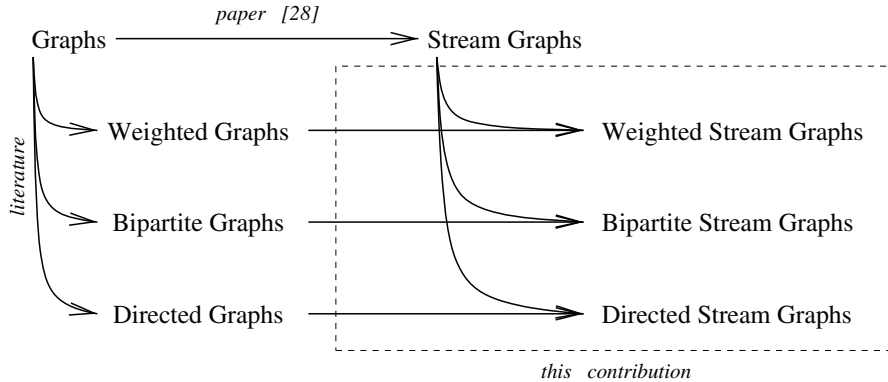


Fig. 2 The global positionning of this contribution with respect to state-of-the-art. Left: weighted, bipartite and directed extensions of graph properties are available in the scientific literature. Top: a generalization of graphs to stream graphs was proposed in [27]. Dotted rectangle: in this contribution, we extend weighted, bipartite and directed graph concepts to weighted, bipartite, and directed stream graphs, as well as standard stream graph concepts to the weighted, bipartite and directed cases, in a consistent way

Like for graphs, the stream graph formalism was designed to be readily extendable to weighted, directed, or bipartite cases. However, these extensions remain to be done, and this is the goal of the present contribution, summarized in Fig. 2.

Before entering in the core of this contribution, notice that the set of available graph concepts is huge, much larger than what may be considered here. We therefore focus on a the set of key properties succinctly summarized above. In particular, we do not consider path-related concepts, which would deserve a dedicated work of their own. Rather than being exhaustive, our aim is to illustrate how weighted, bipartite, or directed graph concepts may be generalized to stream graphs in a consistent way, and to provide a ground for further generalizations.

2 Weighted Stream Graphs

A **weighted graph** is a graph $G = (V, E)$ equipped with a weight function ω generally defined over E , and sometimes on V too. Then, $\omega(v)$ is the weight of node v and $\omega(uv)$ the one of link uv . Link weights may represent tie strength (in a friendship or collaboration network for instance) [35, 45], link capacity (in an road or computer network, for instance) [12, 45], or a level of similarity (in document or image networks, or gene networks for instance) [25, 54]. Node weights may represent reliability, availability, size, etc. As a consequence, weighted graphs are very important and they are used to model a wide variety of networks. In most cases, though, nodes are considered unweighted. We will therefore only consider weighted links in the following, except where specified otherwise.

Even when one considers a weighted graph $G = (V, E)$ equipped with the weight function ω , the properties of G itself (without weights) are of crucial interest. In addition, one may consider thresholded versions of G , defined as $G_\tau = (V_\tau, E_\tau)$ where $V_\tau = \{v \in V, \omega(v) \geq \tau\}$ and $E_\tau = \{uv \in E, \omega(uv) \geq \tau\}$, for various thresholds τ . This actually is a widely used way to deal with graph weights, formalized in a systematic way as early as 1969 [16]. However, one often needs to truly take weights into account, without removing any information. In particular, the importance of weak links is missed by thresholding approaches. In addition, determining appropriate thresholds is a challenge in itself [17, 45, 46].

As a consequence, several extensions of classical graph concepts have been introduced to incorporate weight information and deal directly with it. The most basic ones are the maximal, minimal, and average weights, denoted respectively by ω_{\max} , ω_{\min} and $\langle \omega \rangle$. The minimal weight ω_{\min} is often implicitly considered as equal to 0, and weights are sometimes normalized in order to ensure that $\omega_{\max} = 1$ [1, 20, 37, 54].

In addition to these trivial metrics, one of the most classical property probably is the weighted version of node degree, known as node strength [4, 5, 36]: $s(v) = \sum_{u \in N(v)} \omega(uv)$. Notice that the average node strength is equal to the product of the average node degree and the average link weight.

Strength is generally used jointly with classical degree, in particular to investigate correlations between degree and strength: if weights represent a kind of activity (like travels or communications) then correlations give information on how activity is distributed over the structure [5, 42]. One may also combine node degree and strength in order to obtain a measure of node importance. For instance, [39] uses a tuning parameter α and compute $d(v) \cdot \left(\frac{s(v)}{d(v)}\right)^\alpha$, but more advanced approaches exist [12].

Generalizing density, i.e. the number of present links divided by the total number of possible links, raises subtle questions. Indeed, it seems natural to replace the number of present links by the sum of all weights $\sum_{uv \in E} \omega(uv)$ like for strength, but several variants for the total sum of possible weights make sense. For instance, the literature on rich clubs [2, 40] considers that all present links may have the maximal weight, leading to $\sum_{uv \in E} \omega_{\max}$, or that all links may be present and have the maximal weight, leading to $\sum_{uv \in V \otimes V} \omega_{\max}$. In the special case where weights represent a level of certainty between 0 and 1 for link presence (1 if it is present for sure, 0 if it is absent for sure), then the weighted density may be defined as $\frac{\sum_{uv \in E} \omega(uv)}{|V \otimes V|}$ [57].

Various definitions of weighted clustering coefficients have been proposed, and [4, 44, 49] review many of them in details. The most classical one was proposed in [5]: $cc(v) = \frac{1}{s(v)(d(v)-1)} \sum_{i,j \in N(v), ij \in E} \frac{\omega(vi)+\omega(vj)}{2}$. A general approach was also proposed in [41]. Given a node v , it assigns a value to each triplet of distinct nodes (i, v, j) such that iv and vj are in E and to each such triplet such that ij is also in E . Then, $cc(v)$ is defined as the ratio between the sum of values of triplets in the second category and the one of triplets in the first category. In [41], considered values are the arithmetic mean, geometric mean, maximal value or minimal value

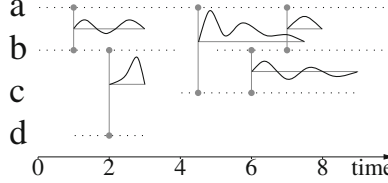


Fig. 3 An example of weighted stream graph. In this example, nodes are unweighted but links are weighted. Instead of just a straight horizontal line indicating link presence over time, we plot the weight value (assuming that 0 is indicated by the horizontal line)

of weights of involved links, depending on the application. One may also consider the product of weights, leading to $cc(v) = \frac{\sum_{i,j \in N(v), ij \in E} \omega(vi) \cdot \omega(vj) \cdot \omega(ij)}{\sum_{i \neq j \in N(v)} \omega(vi) \cdot \omega(vj)}$ as proposed in [1, 25, 54] with normalized weights.

Transitivity is generalized in a very similar way [41] by considering all triplets of distinct nodes (i, j, k) such that ij and jk are in E and each such triplet such that ik is also in E , instead of only the ones centered on a specific node v . If the associated value is the product of weight, this leads to $tr = \frac{\sum_{(i,j,k)} \omega(ij) \cdot \omega(jk) \cdot \omega(ik)}{\sum_{(i,j,k)} \omega(ij) \cdot \omega(jk)}$. If all weights are equal to 1 (*i.e.* the graph is unweighted) this is nothing but the transitivity in G .

Various other concepts have been generalized to weighted graphs, like for instance assortativity [5], and specific weighted graph concepts, like closeness and betweenness centralities [39], connectability [3], eigenvector centrality [36], or rich club coefficient [2, 40, 56]. We do not consider them here as our focus is on the most basic properties.

We define a **weighted stream graph** as a stream graph $S = (T, V, W, E)$ equipped with a weight function ω defined over W and E : if $(t, v) \in W$ then $\omega(t, v)$ is the weight of node v at time t , and if $(t, uv) \in E$ then $\omega(t, uv)$ is the weight of link uv at time t . See Fig. 3 for an illustration.

If a stream graph represents money transfers, then node weights may represent available credit and link weights may represent transfer amounts; if a stream represents travels, then node weights may represent available fuel, and link weights may represent speed; if a stream represents contacts between mobile device, node weights may represent battery charge and link weights may represent signal strength or link capacity; if a stream represents data transfers between computers then link weights may represent throughput or error rates; like for weighted graphs, countless situations may benefit from a weighted stream graph modeling.

As we will see in Sect. 3, weighted stream graphs also widely appear within bipartite graph studies. In addition, as explained in [27], Sect. 19, one often resorts to Δ -analysis for stream graph studies. Given a stream graph $S = (T, V, W, E)$ with $T = [x, y]$ and a parameter Δ , its most simple form consists in transforming S into $S_\Delta = (T', V, W', E')$ such that $T' = [x + \frac{\Delta}{2}, y - \frac{\Delta}{2}]$, $T'_v = T' \cap \{t, \exists t' \in [t - \frac{\Delta}{2}, t + \frac{\Delta}{2}], t' \in T_v\}$, and $T'_{uv} = T' \cap \{t, \exists t' \in [t - \frac{\Delta}{2}, t + \frac{\Delta}{2}], t' \in T_{uv}\}$.

Then, one may capture the amount of information in S leading to node and link presences in S_Δ with weights: $\omega(t, v) = |\{t, \exists t' \in [t - \frac{\Delta}{2}, t + \frac{\Delta}{2}], t' \in T_v\}|$ and $\omega(t, uv) = |\{t, \exists t' \in [t - \frac{\Delta}{2}, t + \frac{\Delta}{2}], t' \in T_{uv}\}|$.

Like for weighted graphs, in addition to S itself (without weights), one may consider the thresholded (unweighted) stream graphs $S_\tau = (T, V, W_\tau, E_\tau)$ where $W_\tau = \{(t, v) \in W, \omega(t, v) \geq \tau\}$ and $E_\tau = \{(t, uv) \in E, \omega(t, uv) \geq \tau\}$, for various thresholds τ . One may then study how the properties of S_τ evolve with τ .

The graph obtained from S at time t , $G_t = (V_t, E_t)$, is naturally weighted by the function $\omega_t(v) = \omega(t, v)$ and $\omega_t(uv) = \omega(t, uv)$. Likewise, the induced graph $G(S)$ is weighted by $\omega(v) = \frac{1}{|T|} \int_{t \in T_v} \omega(t, v) dt$ and $\omega(uv) = \frac{1}{|T|} \int_{t \in T_{uv}} \omega(t, uv) dt$. These definitions correspond to the average weight over time of each node and link. One may define similarly the minimal and maximal node and link weights, and go further by studying S through the weighted graph $G(S)$ and the time-evolution of weighted graph properties of G_t .

These approaches aim to take both the weight and the temporal aspect into account: from a weighted stream graph, the first one provides a family of (unweighted) stream graphs, one for each considered value of the threshold; the second one provides a series of (static) weighted graphs, one for each instant considered. In both cases, the actual combination of weight and time information is poorly captured. We will therefore define concepts that jointly deal with both weights and time. Like with weighted graphs, we simplify the presentation by assuming that only links are weighted (nodes are not).

Since the degree of node v in a stream graph S is $d(v) = \sum_{u \in V} \frac{|T_{uv}|}{|T|}$ and since the strength of node v in a weighted graph G is $s(v) = \sum_{u \in N(v)} \omega(uv)$, we define the strength of node v in a weighted stream graph S as $s(v) = \sum_{u \in V} \int_{t \in T_{uv}} \frac{\omega(t, uv)}{|T|} dt$. It is the degree of v where each neighbor is counted with respect to the weight of its links with v at the times when it is linked to v . It is related to the strength $s_t(v)$ of v in G_t as follows: $s(v) = \frac{1}{|T|} \int_{t \in T_v} s_t(v)$; it is the average strength of v over time.

With this definition, one may study correlations between degree and strength in stream graphs, as with graphs, and even directly use their combinations, like $d(v) \cdot \left(\frac{s(v)}{d(v)}\right)^\alpha$ where α is a parameter.

Unsurprisingly, generalizing density to weighted stream graphs raises the same difficulties as for weighted graphs. Still, proposed definitions for weighted graphs easily apply to weighted stream graphs. Indeed, the sum of all weights becomes $\sum_{uv \in V \otimes V} \int_{t \in T_{uv}} \omega(t, uv) dt$, and the maximal weight of possible links may be defined as $\sum_{uv \in V \otimes V} \int_{t \in T_{uv}} \omega_{\max} dt = \omega_{\max} \cdot |E|$ or $\sum_{uv \in V \otimes V} \int_{t \in T} \omega_{\max} dt = \omega_{\max} \cdot |V \otimes V|$. Like with weighted graphs, if all weights are in $[0, 1]$ then the weighted density may be defined by $\frac{\sum_{uv \in V \otimes V} \int_{t \in T_{uv}} \omega(t, uv) dt}{|T \otimes V \otimes V|}$.

Then, one may define the clustering coefficient of v as the weighted density (according to one of the definitions above or another one) of the neighborhood of v . One may also consider the time-evolution of one the weighted clustering coefficient in G_t , according to previously proposed definitions surveyed above.

Interestingly, one may also generalize the classical definition [5] as follows: $cc(v) = \frac{1}{2s(v)(d(v)-1)} \int_{t \in T_v} \sum_{i, j \in N_t(v), (t, ij) \in E} \omega(t, vi) + \omega(t, vj) dt$, which is the product of link weights of v with its pairs of neighbors when these neighbors are linked together.

The general approach of [41] also extends: one has to assign a value to each quadruplet (t, i, j, k) with i, j , and k distinct such that $(t, ij), (t, jk)$ are in E , and to each such quadruplet such that (t, ik) also is in E . As in the weighted graph case, the weighted stream graph clustering coefficient of node v , $cc(v)$ is then the ratio between the sum of values of quadruplets in the second category such that $j = v$ and the one of quadruplets in the first category such that $j = v$ too. If the value of a quadruplet is the product of the weights of involved links, we obtain $cc(v) = \frac{\int_{t \in T_v} \sum_{i, j \in N_t(v), (t, ij) \in E} \omega(t, vi) \cdot \omega(t, vj) \cdot \omega(t, ij) dt}{\int_{t \in T_v} \sum_{i \neq j \in N_t(v)} \omega(t, vi) \cdot \omega(t, vj)}$.

Likewise, we define the weighted stream graph transitivity as the ratio between the sum of values of all quadruplets in the second category above and the one of quadruplets in the first category. If the value of quadruplets is defined as the product of weights of involved links, this leads to $tr = \frac{\int_t \sum_{(i, j, k)} \omega(t, ij) \cdot \omega(t, jk) \cdot \omega(t, ik) dt}{\int_t \sum_{(i, j, k)} \omega(t, ij) \cdot \omega(t, jk) dt}$. If all weights are equal to 1 (i.e. the stream is unweighted), this is nothing but the stream graph transitivity defined in [27].

If S is a graph-equivalent stream weighted by a constant function over time, i.e. $\omega(t, v) = \omega(t', v)$ and $\omega(t, uv) = \omega(t', uv)$ for all t and t' , then it is equivalent to the weighted graph $G(S)$ weighted by $\omega(v) = \omega(t, v)$ and $\omega(uv) = \omega(t, uv)$ for any t ; we call it a weighted graph-equivalent weighted stream. The strength of v in S is equal to its strength in $G(S)$ if S is a weighted graph-equivalent weighted stream. The same is true for the different notions of density or clustering coefficient: the density of S is equal to the density of $G(S)$ and the clustering coefficient of a vertex v or the transitivity are equal to the clustering coefficient or transitivity in $G(S)$.

3 Bipartite Stream Graphs

A **bipartite graph** $G = (\top \cup \perp, E)$ is defined by a set of top nodes \top , a set of bottom nodes \perp with $\top \cap \perp = \emptyset$, and a set of links $E \subseteq \top \otimes \perp$: there are two different kinds of nodes and links may exist only between nodes of different kinds. Like weighted graphs, but maybe less known, bipartite graphs are pervasive and model many real-world data [23, 26]. Typical examples include relations between client and products [7], between company boards and their members [6, 43], and between items and their key features like movie-actor networks [33, 51] or publication-author networks [34, 35], to cite only a few.

Bipartite graphs are often studied through their top or bottom projections [10] $G_\top = (\top, E_\top)$ and $G_\perp = (\perp, E_\perp)$, defined by $E_\top = \cup_{v \in \perp} N(v) \otimes N(v)$ and $E_\perp = \cup_{v \in \top} N(v) \otimes N(v)$. In other words, in G_\top two (top) nodes are linked together if they have (at least) a (bottom) neighbor in common in G , and G_\perp is defined

symmetrically. Notice that, if $v \in \top$ (resp. $v \in \perp$), then $N(v)$ always is a (not necessarily maximal) clique in G_\perp (resp. G_\top).

Projections induce important information losses: the existence of a link or a clique in the projection may come from very different causes in the original bipartite graph. To improve this situation, one often considers *weighted* projections: each link uv in the projection is weighted by the number $\omega(uv) = N(u) \cap N(v)$ of neighbors u and v have in common in the original bipartite graph. One may then use weighted graph tools to study the weighted projections [5, 22, 36], but information losses remain important. In addition, projection are often much larger than the original bipartite graphs, which raises serious computational issues [26].

As a consequence, many classical graph concepts have been extended to deal directly with the bipartite case, see [8–10, 19, 26]. The most basic properties are $n_\top = |\top|$ and $n_\perp = |\perp|$, the number of top and bottom nodes. The definition of the number of links $m = |E|$ is the same as in classical graphs. The definitions of node neighborhoods and degrees are also unchanged. The average top and bottom degrees d_\top and d_\perp of G are the average degrees of top and bottom nodes, respectively.

With these notations, the bipartite density of G is naturally defined as $\delta(G) = \frac{m}{n_\top \cdot n_\perp}$: it is the probability when one takes two nodes that may be linked together that they indeed are. Then, a bipartite clique in G is a set $C_\top \cup C_\perp$ with $C_\top \subseteq \top$ and $C_\perp \subseteq \perp$ such that $C_\top \times C_\perp \subseteq E$. In other words, all possible links between nodes in a bipartite clique are present in the bipartite graph.

Several bipartite generalizations of the clustering coefficient have been proposed [26, 28, 29, 38, 55]. In particular:

- Latapy et al. [26] and Lind et al. [28] rely on the Jaccard coefficient defined over node pairs both either in \top or \perp : $cc(uv) = \frac{|N(u) \cap N(v)|}{|N(u) \cup N(v)|}$ or close variants. One then obtains the clustering coefficient of node v by averaging its Jaccard coefficient with all neighbors of its neighbors: $cc(v) = \frac{\sum_{u \in N(N(v)), u \neq v} cc(uv)}{|N(N(v))|}$.
- for each node v , [26] and [29] consider all triplets (u, v, w) of distinct nodes with u and w in $N(v)$ and define the redundancy $rc(v)$ as the fraction of such triplets such that there exists an other node in $N(u) \cap N(w)$.
- similarly, [38] proposes to consider all quintuplets (a, b, v, c, d) of distinct nodes with $b, c \in N(v)$, $a \in N(b)$ and $d \in N(c)$ and defines $cc^*(v)$ as the fraction of them such that there exists another node in $N(a) \cap N(d)$.

Transitivity is usually extended to bipartite graphs [26, 38, 43] by considering the set N of quadruplets of nodes (a, b, c, d) such that ab, bc and cd are in E and the set \bowtie of such quadruplets with in addition ad in E . Then, the transitivity is $tr(G) = \frac{|\bowtie|}{|N|}$. Like above, [38] also propose to consider the fraction of all quintuplets (a, b, c, d, e) of distinct nodes with ab, bc, cd, de in E such that there exists an other node f with af and ef in E .

We define a **bipartite stream graph** $S = (\mathcal{T}, \top \cup \perp, W, E)$ from a time interval T , a set of top nodes \top , a set of bottom nodes \perp with $\top \cap \perp = \emptyset$, and two sets $W \subseteq T \times (\top \cup \perp)$ and $E \subseteq T \times \top \otimes \perp$ such that $(t, uv) \in E$ implies $(t, u) \in W$ and $(t, v) \in W$. See Fig. 4 (left) for an illustration. Each instantaneous graph G_t , as

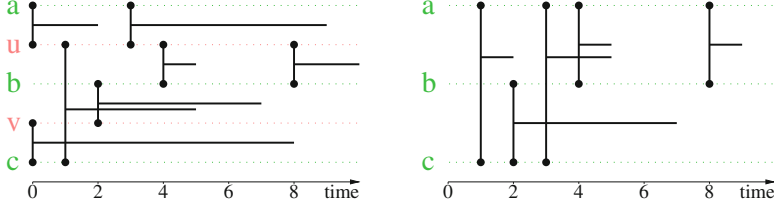


Fig. 4 Left: a bipartite stream graph $S = (T, \top \cup \perp, W, E)$ with $T = [0, 10]$, $\top = \{u, v\}$, $\perp = \{a, b, c\}$, $W = T \times (\top \cup \perp)$, and $E = ([0, 2] \cup [3, 9]) \times \{ua\} \cup ([4, 5] \cup [8, 10]) \times \{ub\} \cup [1, 5] \times \{uc\} \cup [2, 7] \times \{v, b\} \cup [0, 8] \times \{vc\}$. Right: its \perp -projection S_\perp . For instance, a and c are linked together from time 3 to 5 because they both have u in their neighborhood for this time period in S

well as the induced graph $G(S)$, are bipartite graphs with the same top and bottom nodes.

Bipartite stream graphs naturally model many situations, like for instance presence of people in rooms or other kinds of locations, purchases of products by clients, access to on-line services, bus presence at stations [15], traffic between a set of computers and the rest of the internet [48], or contribution of people to projects, such as software.

The classical definition of projections is easily extended, leading to $S_\top = (T, \top, W_\top, E_\top)$ and $S_\perp = (T, \perp, W_\perp, E_\perp)$, where $W_\top = W \cap (T \times \top)$, $W_\perp = W \cap (T \times \perp)$, $E_\top = \cup_{(t,v) \in W_\top} \{(t, uw) \text{ s.t. } (t, uv) \in E \text{ and } (t, vw) \in E\}$ and $E_\perp = \cup_{(t,v) \in W_\perp} \{(t, uw) \text{ s.t. } (t, uv) \in E \text{ and } (t, vw) \in E\}$. In other words, in S_\top two (top) nodes are linked together at a given time instant if they have (at least) a (bottom) neighbor in common in S at this time, and S_\perp is defined symmetrically. See Fig. 4 for an illustration. Notice that, if $v \in \top$ (resp. $v \in \perp$) then $N(v)$ always is a (not necessarily maximal) clique in S_\top (resp. S_\perp).

One may also generalize weighted projections by considering the number $\omega(t, uv) = |N_t(u) \cap N_t(v)|$ of neighbors u and v have in common at time t in the original bipartite stream graph. One then obtains weighted stream graphs, and may use the definitions proposed in Sect. 2 to study them. Still, this induces much information loss, which calls for the generalization of bipartite properties themselves.

The most immediate definitions are the numbers of top and bottom nodes: $n_\top = \sum_{v \in \top} \frac{|T_v|}{|T|} = \frac{|W \cap (T \times \top)|}{|T|}$ and $n_\perp = \sum_{v \in \perp} \frac{|T_v|}{|T|} = \frac{|W \cap (T \times \perp)|}{|T|}$, respectively. We then have $n = n_\top + n_\perp$. Like with graphs, the number of links, neighborhood of nodes, and their degree do not call for specific bipartite definitions. We however define the average top and bottom degrees d_\top and d_\perp of S as the average degrees of top and bottom nodes, respectively, weighted by their presence time in the stream: $d_\top(S) = \sum_{v \in \top} \frac{|T_v|}{|W|} d(v)$ and $d_\perp(S) = \sum_{v \in \perp} \frac{|T_v|}{|W|} d(v)$.

We define the bipartite density of S as $\delta(S) = \frac{m}{\sum_{u \in \top, v \in \perp} |T_u \cap T_v|}$: it is the probability when one takes two nodes when they may be linked together that they indeed are. A subset $C = C_\top \cup C_\perp$ of W , with $C_\top \subseteq T \times \top$ and $C_\perp \subseteq T \times \perp$, is

a clique in S if all possible links exist between nodes when they are involved in C : for all t , if (t, u) is in C_{\top} and v is in C_{\perp} then uv is in E .

Like with graphs, defining a bipartite stream graph clustering coefficient is difficult and leaves us with several reasonable choices:

- Extending the Jaccard coefficient to node pairs in a stream graph leads to an instantaneous definition: $cc_t(uv) = \frac{|N_t(u) \cap N_t(v)|}{|N_t(u) \cup N_t(v)|}$, which is nothing but $cc(uv)$ in G_t . It also leads to a global definition: $cc(uv) = \frac{|N(u) \cap N(v)|}{|N(u) \cup N(v)|} = \frac{\sum_{w \in T \cup \perp} |T_{uw} \cap T_{vw}|}{\sum_{w \in T \cup \perp} |T_{uw} \cup T_{vw}|}$. We may then define the bipartite clustering coefficient of node v by averaging its Jaccard coefficient with all neighbors of its neighbors, weighted by their co-presence time: $\frac{1}{|N(N(v))|} \sum_{u \in T \cup \perp} \frac{|T_u \cap T_v|}{|T|} cc(uv)$. Notice that $cc(uv) = 0$ if the neighborhoods of u and v do not intersect. This means that the sum actually is over nodes that are at some time neighbor of a neighbor of v , which is consistent with the bipartite graph definition.
- Redundancy is easier to generalize to stream graphs: for each node v , we consider all triplets (t, u, v, w) composed of a time instant t , a neighbor u of v at time t , v itself, and another neighbor w of v at time t , and we define $rc(v)$ as the fraction of such quadruplets such that there exists an other node linked to u and w at time t . In other words, $rc(v) = \frac{|\{(t, u, v, w), u \neq w, u, w \in N_t(v), \exists x \in N_t(u) \cap N_t(w), x \neq v\}|}{|\{(t, u, v, w), u \neq w, u, w \in N_t(v)\}|}$.
- Similarly, we propose a stream graph generalization of $cc^*(v)$ as the fraction of sextuplets (t, a, b, v, c, d) with a, b, v, c , and d all different from each other, $b \in N_t(v)$, $c \in N_t(v)$, $a \in N_t(b)$ and $d \in N_t(c)$ for which in addition there exists an other node in $N_t(a) \cap N_t(d)$.

Finally, if we denote by \mathbf{N} the set of quintuplets (t, a, b, c, d) such that (t, ab) , (t, bc) and (t, cd) are in E and the set \bowtie of such quintuplets with in addition (t, ad) in E , then the bipartite transitivity for stream graphs is $tr(G) = \frac{|\bowtie|}{|\mathbf{N}|}$ as before. Like for bipartite graphs, one may also consider the fraction of all sextuplets (t, a, b, c, d, e) where a, b, c, d , and e are distinct nodes with (t, ab) , (t, bc) , (t, cd) , (t, de) in E such that there exists an other node f with (t, af) and (t, ef) in E .

If S is a graph-equivalent bipartite stream, then its projections S_{\top} and S_{\perp} are also graph-equivalent streams, and their corresponding graphs are the projections of the graph corresponding to S : $G(S_{\perp}) = G(S)_{\perp}$ and $G(S_{\top}) = G(S)_{\top}$. In addition, the bipartite properties of S are equivalent to the bipartite properties of its corresponding bipartite graph: the density, Jaccard coefficient, redundancy, and cc^* , as well as transitivity values, are all equal to their graph counterpart in $G(S)$ if S is a graph-equivalent bipartite stream.

4 Directed Stream Graphs

A **directed graph** $G = (V, E)$ is defined by its set V of nodes and its set $E \subseteq V \times V$ of links: while links of undirected graphs are unordered pairs of distinct nodes, links in directed graphs are ordered pairs of nodes, not necessarily distinct:

$(u, v) \neq (v, u)$, and (v, v) is allowed and called a loop. Then, (u, v) is a link from u to v , and if both (u, v) and (v, u) are in E then the link is said to be symmetric.

Directed graphs naturally model the many situations where link asymmetry is important, like for instance dependencies between companies or species, citations between papers or web pages [31], friendship relations in many on-line social networks [32], or hierarchical relations of various kinds.

Directed graph are often studied as undirected graphs by ignoring link directions. However, this is not satisfactory in many cases: having a link to a node is very different from having a link from a node and, for instance, having links to many nodes is very different from having links from many nodes. As a consequence, many directed extensions of standard graph properties have been proposed to take direction into account, see for instance [50] Sect. 4.3 and [18, 24].

First, a node v in a directed graph has two neighborhoods: its out-going neighborhood $N^+(v) = \{u, (v, u) \in E\}$ and its in-coming neighborhood $N^-(v) = \{u, (u, v) \in E\}$. This leads to its out- and in-degrees $d^+(v) = |N^+(v)|$ and $d^-(v) = |N^-(v)|$. These definitions make it possible to study the role of nodes with high in- and out-degrees, as well as correlations between these metrics [21, 32]. Notice that $\sum_{v \in V} d^+(v) = \sum_{v \in V} d^-(v) = m$ is the total number of links, and so the average in- and out-degrees are equal to $\frac{m}{n}$.

The directed density of G is $\frac{m}{n^2}$ since in a directed graph (with loops) there are n^2 possible links. Then, a directed clique is nothing but a set of nodes all pairwise linked together with symmetrical links, which, except for loops, is equivalent to an undirected clique. One may also consider the fraction of loops present in the graph $\frac{|\{(v,v) \in E\}|}{n}$, as well as the fraction of symmetric links $\frac{|\{(u,v) \in E \text{ s.t. } (v,u) \in E\}|}{m}$.

With this definition of density, one may define the in- and out-clustering coefficient of node v as the density of its in-coming and out-going neighborhood. However, this misses the diversity of ways v may be linked to its neighbors and these neighbors may be linked together [18, 50]. Table 1 in [18] summarizes all possibilities and corresponding extensions of clustering coefficient. We focus here on two of these cases, that received more attention because they capture the presence of small cycles and the transitivity of relations. Given a node v , the cyclic clustering coefficient is the fraction of its pairs of distinct neighbors u and w with (u, v) and (v, w) in E , such that (w, u) also is in E , i.e. u, v and w form a cycle. The transitive coefficient of v consists in the fraction of its pairs of distinct neighbors u and w with (u, v) and (v, w) in E , such that (u, w) also is in E , i.e. the relation is transitive.

Finally, these extensions of node clustering coefficient directly translate to extensions of graph transitivity ratio. In the two cases explained above, this leads to the fraction of all triplets of distinct nodes (u, v, w) with (u, v) and (v, w) in E , such that in addition (w, v) is in E , or (v, w) is in E , respectively.

We define a **directed stream graph** $S = (T, V, W, E)$ from a time interval T , a set of nodes V , a set of temporal nodes $W \subseteq T \times V$, and a set of temporal links $E \subseteq T \times V \times V$: (t, u, v) in E means that there is a link from u to v at time t , which is different from (t, v, u) . We therefore make a distinction between $T_{u,v}$ the set $\{t, (t, u, v) \in E\}$ and $T_{v,u}$ the set $\{t, (t, v, u) \in E\}$. A loop is a triplet (t, v, v)

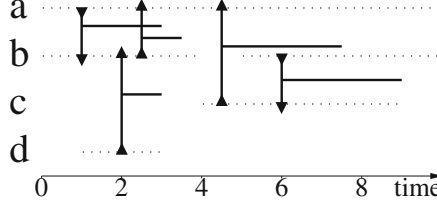


Fig. 5 An example of directed stream graph $S = (T, V, W, E)$ with $T = [0, 10] \subseteq \mathbb{R}$, $V = \{a, b, c, d\}$, $W = [0, 10] \times \{a\} \cup [0, 4] \cup [5, 10] \times \{b\} \cup [4, 9] \times \{c\} \cup [1, 3] \times \{d\}$, and $E = [1, 3] \times \{(a, b)\} \cup [2.5, 3.5] \times \{(b, a)\} \cup [4.5, 7.5] \times \{(c, a)\} \cup [6, 9] \times \{(b, c)\} \cup [2, 3] \times \{(d, b)\}$. Notice that $T_{a,b} = [1, 3] \neq T_{b,a} = [2.5, 3.5]$, and that links between a and b are symmetrical from time 2.5 to time 3

in E . If both (t, u, v) and (t, v, u) are in E , then we say that this temporal link is symmetric. See Fig. 5 for an illustration.

Directed stream graphs model the many situations where directed links occur over time and their asymmetry is important, like for instance money transfers, network traffic, phone calls, flights, moves from a place to another, and many others. In all these cases, both time information and link direction are crucial, as well as their interplay. For instance, a large number of computers sending packets at a given computer in a very short period of time is a typical signature of denial of service attack [30]. Instead, a computer sending packets to a large number of other computers in a short period of time is typical of a streaming server.

The directed stream graph $S = (T, V, W, E)$ may be studied through the standard stream graph $(T, V, W, \{(t, uv), (t, u, v) \in E \text{ or } (t, v, u) \in E\})$ obtained by considering each directed link as undirected. Likewise, S may be studied through its induced directed graph $G(S) = (\{v, \exists(t, v) \in W\}, \{(u, v), \exists(t, u, v) \in E\})$ and/or the sequence of its instantaneous directed graphs $G_t = (\{v, (t, v) \in W\}, \{(u, v), (t, u, v) \in E\})$. However, these approaches induce much information loss, and make it impossible to make subtle distinctions like the one described above for network traffic. This calls for generalizations of available concepts to this richer case.

We define the out-going neighborhood of node v as $N^+(v) = \{(t, u), (t, v, u) \in E\}$ and its in-coming neighborhood as $N^-(v) = \{(t, u), (t, u, v) \in E\}$. Its in-and out-degrees are $d^+(v) = \frac{|N^+(v)|}{|T|} = \sum_{u \in V} \frac{|T_{v,u}|}{|T|}$ and $d^-(v) = \frac{|N^-(v)|}{|T|} = \sum_{u \in V} \frac{|T_{u,v}|}{|T|}$. Like with directed graphs, the total number of links m is equal to $\sum_{v \in V} d^+(v)$ as well as to $\sum_{v \in V} d^-(v)$.

We extend the standard stream graph density $\frac{m}{\sum_{uv \in V \otimes V} |T_u \cap T_v|}$ into the directed stream graph density $\frac{m}{\sum_{(u,v) \in V \times V} |T_u \cap T_v|}$: it is the fraction of possible links that indeed exist. Then, a clique in a directed stream graph is a subset C of W such that for all (t, u) and (t, v) in C , both (t, u, v) and (t, v, u) are in E . These definitions are immediate extensions of standard stream graph concepts.

One may then define the in- and out-clustering coefficient of a node v as the density of its in- and out-neighborhoods in the directed stream graph. However, like for directed graphs, there are many possible kinds of interactions between neighbors of a node, which lead to various generalizations of clustering coefficient to directed stream graph. We illustrate this on the two definitions detailed above for a given node v . First, let us consider the set of quadruplets (t, u, v, w) with u, v and w distinct, such that (t, u, v) and (t, v, w) are in E . Then one may measure the cyclic clustering coefficient as the fraction of these quadruplets such that in addition (t, w, u) is in E , and the transitive clustering coefficient as the fraction of these quadruplets such that in addition (t, w, u) is in E .

Like with directed graphs, this leads to directed stream graph extensions of transitivity. In the two cases above, we define it as the fraction of quadruplets (t, u, v, w) with u, v and w distinct and with (t, u, v) and (t, v, w) in E , such that in addition (t, w, v) is in E , or (t, v, w) is in E , respectively.

If S is a directed graph-equivalent directed stream graph, i.e. $G_t = G(S)$ for all t , then all the properties of S defined above are equal to their directed graph counterpart in $G(S)$.

5 Conclusion

Previous works extended many graph concepts to deal with weighted, bipartite or directed graphs. In addition, graphs were generalized recently to stream graphs in order to model temporal networks in a way consistent with graph theory. In this contribution, we show that weighted, bipartite or directed graphs concepts may themselves be generalized to weighted, bipartite or directed stream graphs, in a way consistent with both their graph counterparts and the stream graph formalism. This opens the way to a much richer modeling of temporal networks, and more precise case studies, in a unified framework.

Such case studies may benefit from improved modeling with either weights, different sorts of nodes, or directed links, but may also combine these extensions together. For instance, money transfers between clients and sellers are best modeled by weighted bipartite directed stream graphs. The concepts we discussed then have to be extended even further, like what has already been done for graphs for instance with the directed strength $s^+(v) = \sum_{u \in N^+(v)} \omega(u, v)$ [39], the directed weighted clustering coefficient [14, 18], or for the study of weighted bipartite graphs [21].

One may also consider other kinds of graph extensions, like multigraphs, labelled graphs, hypergraphs, or multi-layer graphs for instance, which model important features of real-world data and already received much attention. We focused on weighted, bipartite and directed cases because they seem to be the most frequent in applications.

Likewise, we selected only a few key weighted, bipartite or directed properties in order to extend them to stream graphs. Many others remain to generalize, in particular path-related concepts like reachability, closeness, or betweenness, to cite only a few [39].

Acknowledgements This work is funded in part by the European Commission H2020 FET-PROACT 2016-2017 program under grant 732942 (ODYCCEUS), by the ANR (French National Agency of Research) under grants ANR-15-CE38-0001 (AlgoDiv), by the Ile-de-France Region and its program FUI21 under grant 16010629 (iTRAC).

References

1. Ahnert, S.E., Garlaschelli, D., Fink, T.M.A., Caldarelli, G.: Ensemble approach to the analysis of weighted networks. *Phys. Rev. E* **76**, 016101 (2007)
2. Alstott, J., Panzarasa, P., Rubinov, M., Bullmore, E.T., Vértes, P.E.: A unifying framework for measuring weighted rich clubs. *Sci. Rep.* **4**, 7258 (2014)
3. Amano, S.I., Ogawa, K.I., Miyake, Y.: Node property of weighted networks considering connectability to nodes within two degrees of separation. *Sci. Rep.* **8**, 8464 (2018)
4. Antoniou, I.E., Tsompa, E.T.: Statistical analysis of weighted networks. *Discret. Dyn. Nat. Soc.* **2008**, 375452 (2008)
5. Barrat, A., Barthélémy, M., Pastor-Satorras, R., Vespignani, A.: The architecture of complex weighted networks. *Proc. Natl. Acad. Sci.* **101**(11), 3747–3752 (2004)
6. Battiston, S., Catanzaro, M.: Statistical properties of corporate board and director networks. *Eur. Phys. J. B* **38**, 345–352 (2004)
7. Bernardes, D., Diaby, M., Fournier, R., Françoise, F., Viennet, E.: A social formalism and survey for recommender systems. *SIGKDD Explorations* **16**(2), 20–37 (2014)
8. Bonacich, P.: Technique for analyzing overlapping memberships. *Sociol. Methodol.* **4**, 176–185 (1972)
9. Borgatti, S.P., Everett, M.G.: Network analysis of 2-mode data. *Soc. Netw.* **19**(3), 243–269 (1997)
10. Breiger, R.L.: The duality of persons and groups. *Soc. Forces* **53**(2), 181–190 (1974)
11. Butts, C.T.: A relational event framework for social action. *Sociol. Methodol.* **38**(1), 155–200 (2008)
12. Candeloro, L., Savini, L.: A new weighted degree centrality measure: the application in an animal disease epidemic. *PLoS One* **11**, e0165781 (2016)
13. Casteigts, A., Flocciani, P., Quattrociocchi, W., Santoro, N.: Time-varying graphs and dynamic networks. *IJPEDS* **27**(5), 387–408 (2012)
14. Clemente, G.P., Grassi, R.: Directed clustering in weighted networks: a new perspective. *Chaos, Solitons Fractals* **107**, 26–38 (2018)
15. Curzel, J.L., Lüders, R., Fonseca, K.V.O. and Rosa, M.O.: Temporal performance analysis of bus transportation using link streams. *Math. Probl. Eng.* **2019**, 6139379 (2019)
16. Doreian, P.: A note on the detection of cliques in valued graphs. *Sociometry* **32**, 237–242 (1969)
17. Esfahlani, F.Z., Sayama, H.: A percolation-based thresholding method with applications in functional connectivity analysis. In: Cornelius, S., Coronges, K., Gonçalves, B., Sinatra, R., Vespignani, A. (eds.) *Complex Networks IX*, pp. 221–231. Springer, Cham (2018)
18. Fagiolo, G.: Clustering in complex directed networks. *Phys. Rev. E* **76**, 026107 (2007)
19. Faust, K.: Centrality in affiliation networks. *Soc. Netw.* **19**, 157–191 (1997)
20. Grindrod, P.: Range-dependent random graphs and their application to modeling large small-world proteome datasets. *Phys. Rev. E* **66**, 066702 (2002)
21. Guillaume, J.L., Le Blond, S., Latapy, M.: Statistical analysis of a P2P query graph based on degrees and their time-evolution. In: Proceedings of the 6th International Workshop on Distributed Computing (IWDC). Lecture Notes in Computer Sciences (LNCS). Springer, Berlin (2004)

22. Guillaume, J.L., Le Blond, S., Latapy, M.: Clustering in P2P exchanges and consequences on performances. In: Proceedings of the 4th International Workshop on Peer-to-Peer Systems (IPTPS). Lecture Notes in Computer Sciences (LNCS). Springer, Berlin (2005)
23. Guillaume, J.-L., Latapy, M.: Bipartite structure of *all* complex networks. *Inf. Process. Lett.* **90**(5), 215–221 (2004)
24. Hakimi, S.L.: On the degrees of the vertices of a directed graph. *J. Frankl. Inst.* **279**(4), 290–308 (1965)
25. Kalna, G., Higham, D.J.: A clustering coefficient for weighted networks, with application to gene expression data. *AI Commun.* **20**, 263–271 (2007)
26. Latapy, M., Magnien, C., Del Vecchio, N.: Basic notions for the analysis of large two-mode networks. *Soc. Netw.* **30**(1), 31–48 (2008)
27. Latapy, M., Viard, T., Magnien, C.: Stream graphs and link streams for the modeling of interactions over time. *Soc. Netw. Anal. Mining* **8**(1), 1–61 (2018)
28. Lind, P.G., González, M.C., Herrmann, H.J.: Cycles and clustering in bipartite networks. *Phys. Rev. E* **72**, 056127 (2005)
29. Lioma, C., Tarissan, F., Simonsen, J.G., Petersen, C., Larsen, B.: Exploiting the bipartite structure of entity grids for document coherence and retrieval. In: Proceedings of the 2016 ACM International Conference on the Theory of Information Retrieval (ICTIR ’16), pp. 11–20. ACM, New York (2016)
30. Mazel, J., Casas, P., Fontugne, R., Fukuda, K., Owezarski, P.: Hunting attacks in the dark: clustering and correlation analysis for unsupervised anomaly detection. *Int. J. Netw. Manag.* **25**(5), 283–305 (2015)
31. Meusel, R., Vigna, S., Lehmburg, O., Bizer, C.: The graph structure in the web—analyzed on different aggregation levels. *J. Web Sci.* **1**, 33–47 (2015)
32. Mislove, A., Marcon, M., Gummadi, K.P., Druschel, P. and Bhattacharjee, B.: Measurement and analysis of online social networks. In: Proceedings of the 7th ACM SIGCOMM Conference on Internet Measurement, pp. 29–42. ACM, New York (2007)
33. Newman, M.E., Strogatz, S.H., Watts, D.J.: Random graphs with arbitrary degree distributions and their applications. *Phys. Rev. E* **64**, 026118 (2001)
34. Newman, M.E.J.: Scientific collaboration networks: I. Network construction and fundamental results. *Phys. Rev. E* **64**, 016131 (2001)
35. Newman, M.E.J.: Scientific collaboration networks: II. Shortest paths, weighted networks, and centrality. *Phys. Rev. E* **64**, 016132 (2001)
36. Newman, M.E.J.: Analysis of weighted networks. *Phys. Rev. E* **70**, 056131 (2004)
37. Onnela, J.-P., Saramäki, J., Kertész, J., Kaski, K.: Intensity and coherence of motifs in weighted complex networks. *Phys. Rev. E* **71**, 065103 (2005)
38. Opsahl, T.: Triadic closure in two-mode networks: Redefining the global and local clustering coefficients. *Soc. Netw.* **35**(2), 159–167 (2013)
39. Opsahl, T., Agneessens, F., Skvoretz, J.: Node centrality in weighted networks: generalizing degree and shortest paths. *Soc. Netw.* **32**(3), 245–251 (2010)
40. Opsahl, T., Colizza, V., Panzarasa, P., Ramasco, J.J.: Prominence and control: the weighted rich-club effect. *Phys. Rev. Lett.* **101**, 168702 (2008)
41. Opsahl, T., Panzarasa, P.: Clustering in weighted networks. *Soc. Netw.* **31**(2), 155–163 (2009)
42. Panzarasa, P., Opsahl, T., Carley, K.M.: Patterns and dynamics of users’ behavior and interaction: network analysis of an online community. *J. Am. Soc. Inf. Sci. Technol.* **60**(5), 911–932 (2009)
43. Robins, G., Alexander, M.: Small worlds among interlocking directors: network structure and distance in bipartite graphs. *Comput. Math. Organ. Theory* **10**(1), 69–94 (2004)
44. Saramäki, J., Kivelä, M., Onnela, J.P., Kaski, K., Kertesz, J.: Generalizations of the clustering coefficient to weighted complex networks. *Phys. Rev. E* **75**(2), 027105 (2007)
45. Serrano, M.Á., Boguná, M., Vespignani, A.: Extracting the multiscale backbone of complex weighted networks. *Proc. Natl. Acad. Sci.* **106**(16), 6483–6488 (2009)

46. Smith, K., Azami, H., Parra, M.A., Starr, J.M., Escudero, J.: Cluster-span threshold: an unbiased threshold for binarising weighted complete networks in functional connectivity analysis. In: 2015 37th Annual International Conference of the IEEE Engineering in Medicine and Biology Society (EMBC), pp. 2840–2843. IEEE, Piscataway (2015)
47. Stadtfeld, C., Block, P.: Interactions, actors, and time: Dynamic network actor models for relational events. *Sociol. Sci.* **4**, 318–352 (2017)
48. Viard, T., Fournier-S'niehotta, R., Magnien, C., Latapy, M.: Discovering patterns of interest in IP traffic using cliques in bipartite link streams. In: Proceedings of Complex Networks IX, pp. 233–241. Springer, Cham (2018)
49. Wang, Y., Ghumare, E., Vandenbergh, R., Dupont, P.: Comparison of different generalizations of clustering coefficient and local efficiency for weighted undirected graphs. *Neural Comput.* **29**, 313–331 (2017)
50. Wasserman, S., Faust, K.: Social Network Analysis: Methods and Applications. Cambridge University Press, Cambridge (1994)
51. Watts, D., Strogatz, S.: Collective dynamics of small-world networks. *Nature* **393**, 440–442 (1998)
52. Wehmuth, K., Fleury, E., Ziviani, A.: On multiaspect graphs. *Theor. Comput. Sci.* **651**, 50–61 (2016)
53. Wehmuth, K., Ziviani, A., Fleury, E.: A unifying model for representing time-varying graphs. In: 2015 IEEE International Conference on Data Science and Advanced Analytics (DSAA 2015), Campus des Cordeliers, Paris, pp. 1–10 (2015)
54. Zhang, B., Horvath, S.: A general framework for weighted gene co-expression network analysis. *Stat. Appl. Genet. Mol. Biol.* **4**, 1544–6115 (2005)
55. Zhang, P., Wang, J., Li, X., Li, M., Di, Z., Fan, Y.: Clustering coefficient and community structure of bipartite networks. *Phys. A Stat. Mech. Appl.* **387**(27), 6869–6875 (2008)
56. Zlatic, V., Bianconi, G., Díaz-Guilera, A., Garlaschelli, D., Rao, F., Caldarelli, G.: On the rich-club effect in dense and weighted networks. *Eur. Phys. J. B* **67**(3), 271–275 (2009)
57. Zou, Z.: Polynomial-time algorithm for finding densest subgraphs in uncertain graphs. In: Proceedings of MLG Workshop (2013)

Modelling Temporal Networks with Markov Chains, Community Structures and Change Points



Tiago P. Peixoto and Martin Rosvall

1 Introduction

Recent advances in temporal network theory include modelling of the time-varying network structure [1, 2] as well as processes that take place on the dynamic structure, such as epidemic spreading [3–6]. However, most approaches rely on a characteristic time scale at which they describe the dynamics. These can be roughly divided into approaches that model temporal correlations of interactions through Markov chains with short-term memory [7, 8], and those that model the dynamics at longer times, usually through network snapshots [9–14] or discrete change points when the dynamics changes abruptly [15–17]. For example, when the network evolution is represented as a static Markov chain, such that new edges are placed based on the placement of the last few edges with fixed transition probabilities, the system eventually reaches equilibrium and cannot maintain any long-term memory.

With new introduction and conclusion sections, this chapter combines and reuses text and figures from Peixoto, T. P., & Rosvall, M. (2017). Modelling sequences and temporal networks with dynamic community structures. *Nature Communications*, 8, 582 and Peixoto, T. P., & Gauvin, L. (2018). Change points, memory and epidemic spreading in temporal networks. *Scientific Reports*, 8, 15511, both licensed under a Creative Commons Attribution 4.0 International License, <http://creativecommons.org/licenses/by/4.0/>.

T. P. Peixoto

Department of Mathematical Sciences, University of Bath, Bath, UK

ISI Foundation, Torino, Italy

e-mail: t.peixoto@bath.ac.uk

M. Rosvall (✉)

Integrated Science Lab, Department of Physics, Umeå University, Umeå, Sweden

e-mail: martin.rosvall@umu.se

Conversely, when the network evolution is represented by a sequence of snapshots, there is no attempt to model any short-term memory. Consequently, focus on one timescale blurs the other whereas in reality most systems exhibit dynamics in a wide range of timescales. Moreover, most systems also exhibit dynamics at multiple structural scales, including large-scale dynamic communities [8, 10].

In this chapter, we review two approaches that attempt to capture multiple aspects of temporal network dynamics with Markov chains inferred from data. The first approach identifies large-scale structures by parametrising the transition probabilities as well as the nodes into communities. The second approach describes non-stationary dynamics based on abrupt change points. Both approaches can detect short-term dynamical memory through arbitrary-order Markov chains and use a nonparametric Bayesian inference framework that prevents overfitting and yields efficient and effective algorithms.

We employ the multi-aspect approaches on empirical data and show that the most plausible models tend to combine short-term memory with large-scale structural and dynamical modular patterns and also many change points. The communities and change points work synergistically with the Markov chains, typically uncovering higher-order memory that is washed out by less flexible models. This effect suggests that a full dynamical description of large-scale modular structures that combines community structure and change points would further our understanding of temporal networks.

2 Temporal Networks as Markov Chains

We consider dynamical networks that can be represented as sequence of edges that are observed in time. This includes, for example, proximity events where an edge denotes when two individuals come in close contact at a specific point in time. More formally, we describe a sequence of discrete tokens, $s = \{x_t\}$, with $t \in \{1, \dots, E\}$ being by the relative time ordering of the tokens, and $x_t \in \{1, \dots, D\}$ the set of unique tokens with cardinality D . This description is applied to dynamical networks by considering each token as an edge, i.e., $x_t = (i, j)_t$, and hence $D = \binom{N}{2}$ is the total number of possible edges in a network with N nodes (see Fig. 1 for an illustration).

This sequential representation lends itself naturally to be modelled as a stationary Markov chain of order n , i.e., the sequence s occurs with probability

$$P(s|\mathbf{p}, n) = \prod_t p_{x_t, x_{t-1}} = \prod_{x, x} p_{x, x}^{a_{x, x}}, \quad (1)$$

where \mathbf{p} corresponds to the transition matrix, with elements $p_{x_t, x_{t-1}}$ being the probability of observing token x_t given the previous n tokens $\mathbf{x}_{t-1} = \{x_{t-1}, \dots, x_{t-n}\}$ in the sequence, and $a_{x, x}$ is the number of observed transitions from memory x to token x . Despite its simplicity, this model is able to reproduce arbitrary edge

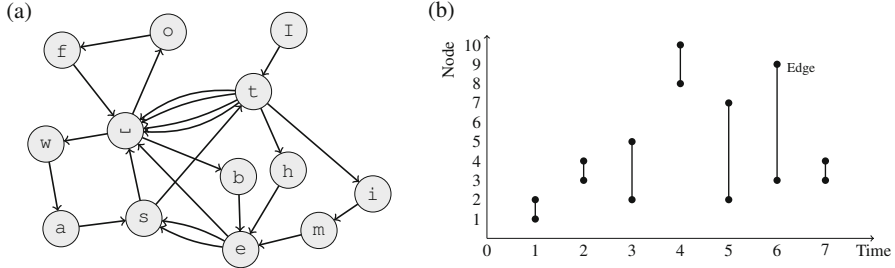


Fig. 1 The modelling of dynamical networks as Markov chains describe the transitions between “tokens” in a sequence, where the tokens are observed edges in the network. For example, (a) illustrates the transitions in the sequence “Itwasthebestoftimes” with letters as tokens and (b) illustrates the sequence {(1, 2), (4, 3), (5, 2), (10, 8), (7, 2), (9, 3), (3, 4)}

frequencies, determined by the steady-state distribution of the tokens x and temporal correlations between edges. This means that the model should be able to reproduce properties of the data that can be attributed to the distribution of number of contacts per edge, which are believed to be important, e.g. for epidemic spreading [18, 19]. However, due to its Markovian nature, the dynamics will eventually forgets its history, and converge to the limiting distribution (assuming the chain is ergodic and aperiodic). This latter property means that the model should be able to capture nontrivial statistics of waiting times only at a short timescale, comparable to the Markov order.

Given the above model, the simplest way to proceed would be to infer transition probabilities from data using maximum likelihood, i.e., maximizing Eq. (1) under the normalization constraint $\sum_x p_{x,x} = 1$. This yields

$$\hat{p}_{x,x} = \frac{a_{x,x}}{k_x}, \quad (2)$$

where $k_x = \sum_x a_{x,x}$ is the number of transitions originating from x . However, if we want to determine the most appropriate Markov order n that fits the data, the maximum likelihood approach cannot be used, as it will *overfit*, i.e., the likelihood of Eq. (1) will increase monotonically with n , favouring the most complicated model possible, and thus confounding statistical fluctuations with actual structure. Instead, the most appropriate way to proceed is to consider the Bayesian posterior distribution

$$P(n|s) = \frac{P(s|n)P(n)}{P(s)}, \quad (3)$$

which involves the integrated marginal likelihood [20]

$$P(s|n) = \int P(s|\mathbf{p}, n)P(\mathbf{p}|n)d\mathbf{p}, \quad (4)$$

where the prior probability $P(\mathbf{p}|n)$ encodes the amount of knowledge we have on the transitions \mathbf{p} before we observe the data. If we possess no information, we can be agnostic by choosing a uniform prior

$$P(\mathbf{p}|n) = \prod_x (D-1)! \delta\left(1 - \sum_x p_{x,x}\right), \quad (5)$$

where D is again the total number of tokens, and $\delta(x)$ is the Dirac delta function, which assumes that all transition probabilities are equally likely. Inserting Eqs. (1) and (5) in Eq. (4), and calculating the integral we obtain

$$P(\mathbf{s}|n) = \prod_x \frac{(D-1)!}{(k_x + D-1)!} \prod_x a_{x,x}!. \quad (6)$$

The remaining prior, $P(n)$, that represents our a priori preference to the Markov order, can also be chosen in an agnostic fashion in a range $[0, N]$, i.e.,

$$P(n) = \frac{1}{N+1}. \quad (7)$$

Since this prior is a constant, the upper bound N has no effect on the posterior of Eq. (3), provided it is sufficiently large to include most of the distribution.

Differently from the maximum-likelihood approach described previously, the posterior distribution of Eq. (3) will select the size of the model to match the statistical significance available, and will favour a more complicated model only if the data cannot be suitably explained by a simpler one, i.e., it corresponds to an implementation of Occam's razor that prevents overfitting.

Although elegant, this modelling approach turns out to be limited in capturing the dynamics observed in real systems. For example, when applied to a proximity network between students in a high school [21], it favours a “zero-order” $n = 0$ Markov chain, indicating that the edges occur independently at random in the sequence, as can be seen in Fig. 2. Rather than concluding that this uncovers a lack of temporal structure in the data, it is in fact a lot more plausible that this description is too simplistic and ill-suited to capture the actual underlying dynamics. One way of seeing this is by comparing properties of the data with artificial sequences generated by the fitted model. For example, if we generate temporal networks using the maximum-likelihood transition probabilities $\hat{p}_{x,x} = a_{x,x}/k_x$, and simulate an epidemic spreading dynamic on them, the observed behaviour is quite different from the same dynamics simulated on the empirical time-series, as can be seen in Fig. 3. Importantly, independently of the Markov order n —even those values that overfit—the simulated dynamics lacks the abrupt changes in the infection rate observed with the empirical data. This discrepancy exposes the inadequacy of simple Markov assumption considered above. However, as we will show below, this model can nevertheless be used as the basis for higher-order models that are in fact capable of capturing important aspects of the underlying dynamics. In the following, we

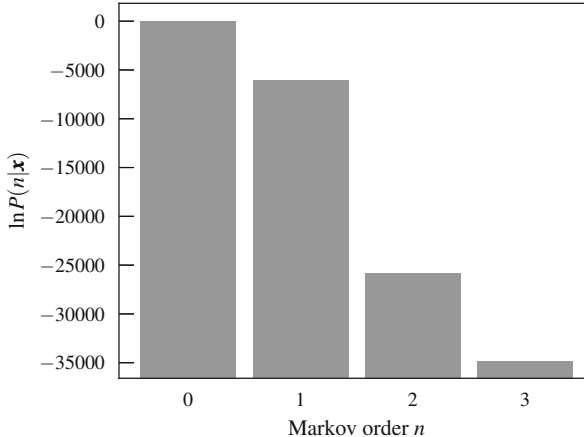


Fig. 2 Posterior distribution of the Markov order $P(n|x)$ (Eq. (3)) for a temporal network between students in a high school [21]

present two ways in which this can be done: (1) by parametrising the Markov chain using community structures [8], and (2) by introducing non-stationary Markov chains with latent change points [22].

3 Markov Chains with Communities

One of the main limitations of the Markov chain model considered previously is its relatively large number of parameters. For a network of N nodes, the transition matrix \mathbf{p} has $O(N^{2(n+1)})$ entries, which means that even for $n = 1$ we would still need to infer $O(N^4)$ parameters from data, requiring the length of the observed sequence to be compatible in size. If the size of the data is insufficient given the parameter space, overfitting is unavoidable, and the Bayesian posterior of Eq. (3) appropriately prefers a smaller model, e.g. with $n = 0$ for which the number of parameters is much smaller, $O(N^2)$. This situation can be improved by imposing latent structure in the transition matrix \mathbf{p} , which can be used to adaptively match the dimension of the model, for any given Markov order n , according to what is compatible with the data. The alternative we propose is to assume that both memories and tokens are distributed in disjoint groups (see Fig. 4). That is, $b_x \in [1, 2, \dots, B_N]$ and $b_x \in [B_N + 1, B_N + 2, \dots, B_N + B_M]$ are the group memberships of the tokens and memories uniquely assigned in B_N and B_M groups, respectively, such that the transition probabilities can be parametrised as

$$p_{x,x} = \theta_x \lambda_{b_x b_x}. \quad (8)$$

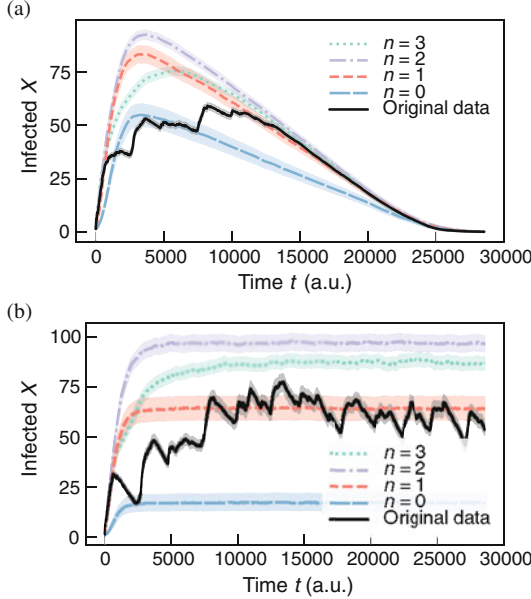


Fig. 3 Number of infected nodes over time $X(t)$ for a temporal network between students in a high-school [21] ($N = 126$), considering both the original data and artificial time-series generated from the fitted Markov model of a given order n , using (a) SIR and (b) SIS epidemic models. In all cases, the values were averaged over 100 independent realizations of the network model (for the artificial datasets) and dynamics. The shaded areas indicate the standard deviation of the mean. The values of the infection and recovery rates were chosen so that the spreading dynamics spans the entire time range of the dataset

Here θ_x is the relative probability at which token x is selected among those that belong to the same group, and λ_{rs} is the overall transition probability from memory group $s = b_x$ to token group $r = b_x$. Note that, in principle, the number of parameters in this model can be larger than the previous model, however this depends on the numbers of groups B_N and B_M , which is something that needs to be chosen to match the data, as will be done in our method.

In the case of Markov order $n = 1$ each token appears twice in the model, both as token and memory. An alternative and often useful approach for $n = 1$ is to consider a single unified partition for both tokens and memories, as shown in Fig. 4b and described in more detailed in Ref. [8]. In any case, the maximum likelihood parameter estimates are

$$\hat{\lambda}_{rs} = \frac{e_{rs}}{e_s}, \quad \hat{\theta}_x = \frac{k_x}{e_{b_x}}, \quad (9)$$

where e_{rs} is the number of observed transitions from group s to r , $e_s = \sum_t e_{ts}$ is the total outgoing transitions from group s if s is a memory group, or the total incoming transition if it is a token group. The labels r and s are used indistinguishably

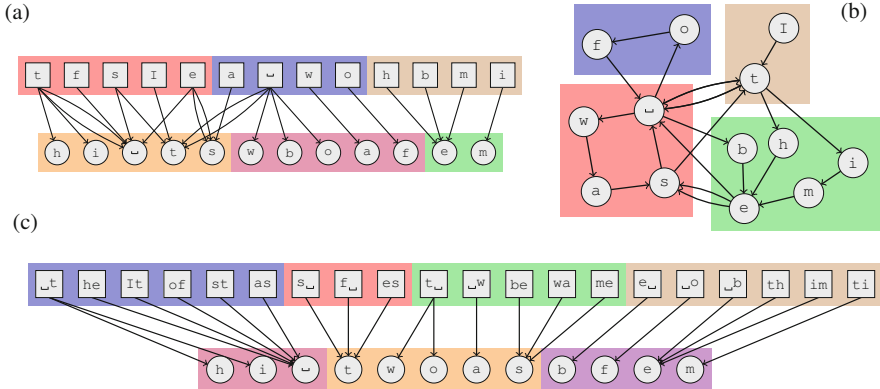


Fig. 4 Schematic representation of the Markov model with communities. The token sequence $\{x_t\} = \text{"It was the best of times"}$ represented with nodes for memories (top row) and tokens (bottom row), and with directed edges for transitions in different variations of the model. (a) A partition of the tokens and memories for an $n = 1$ model. (b) A unified formulation of an $n = 1$ model, where the tokens and memories have the same partition, and hence can be represented as a single set of nodes. (c) A partition of the tokens and memories for an $n = 2$ model

to denote memory and token groups, since it is only their numerical value that determines their kind. Finally, k_x is the total number of occurrences of token x . Putting this back in the likelihood of Eq. (1), we have

$$\ln \hat{P}(s|\mathbf{b}, \boldsymbol{\lambda}, \boldsymbol{\theta}, n) = \sum_{r < s} e_{rs} \ln \frac{e_{rs}}{e_r e_s} + \sum_x k_x \ln k_x. \quad (10)$$

As before, this maximum likelihood approach cannot be used if we do not know the order of the Markov chain, otherwise it will overfit. In fact, this problem is now aggravated by the potential larger number of model parameters. Therefore, we employ a Bayesian formulation and construct a generative process for the model parameters themselves. We do this by introducing prior probability densities for the parameters $P(\boldsymbol{\theta}|\boldsymbol{\alpha})$ and $P(\boldsymbol{\lambda}|\boldsymbol{\beta})$ for tokens and memories, respectively, with hyperparameter sets $\boldsymbol{\alpha}$ and $\boldsymbol{\beta}$, and computing the integrated likelihood

$$P(s|\mathbf{b}, n, \boldsymbol{\alpha}, \boldsymbol{\beta}) = \int P(s|\mathbf{b}, \boldsymbol{\lambda}, \boldsymbol{\theta}) P(\boldsymbol{\theta}|\boldsymbol{\alpha}) P(\boldsymbol{\lambda}|\boldsymbol{\beta}) d\boldsymbol{\theta} d\boldsymbol{\lambda}. \quad (11)$$

where we used \mathbf{b} as a shorthand for $\{b_x\}$ and $\{b_x\}$. Now, instead of inferring the hyperparameters, we can make a noninformative choice for $\boldsymbol{\alpha}$ and $\boldsymbol{\beta}$ that reflects our a priori lack of preference towards any particular model [23]. Doing so in this case yields a likelihood (for details, see Ref. [8]),

$$P(s|\mathbf{b}, n) = \left[\prod_r \frac{(n_r - 1)!}{(e_r + n_r - 1)!} \right] \left[\prod_s \frac{(B_N - 1)! \prod_r e_{rs}!}{(e_s + B_N - 1)!} \right] \prod_x k_x!, \quad (12)$$

where $n_r = \sum_x \delta_{b_x, r}$ is the number of tokens in group r . The Markov order and partitions can now be inferred from the posterior distribution

$$P(\mathbf{b}, n | \mathbf{s}) = \frac{P(\mathbf{s} | \mathbf{b}, n) P(\mathbf{b}) P(n)}{P(\mathbf{s})}, \quad (13)$$

where $P(\mathbf{s}) = \sum_{\mathbf{b}, n} P(\mathbf{s} | \mathbf{b}, n) P(\mathbf{b}) P(n)$ is an intractable constant, that fortunately does not need to be determined when either maximizing or sampling from the posterior distribution.

Before proceeding further with this model, we note that it still treats each possible edge as an individual token. However, this can be suboptimal if the networks are sparse, that is, if only a relatively small subset of all possible edges occur, and thus there are insufficient data to reliably fit the model. Furthermore, although it puts the tokens and memories into groups, it does not take into account any community structure present in the network, i.e., groups of nodes with similar connection patterns. In order to alleviate both problems, we adapt the model above by including an additional generative layer between the Markov chain and the observed edges. We do so by partitioning the *nodes* of the network into groups, that is, $c_i \in [1, C]$ determines the membership of node i in one of C groups, such that each edge (i, j) is associated with a label (c_i, c_j) . Then we define a Markov chain for the sequence of *edge labels* and sample the actual edges conditioned only on the labels. Since this reduces the number of possible tokens from $O(N^2)$ to $O(C^2)$, it has a more controllable number of parameters that can better match the sparsity of the data. We further assume that, given the node partitions, the edges themselves are sampled in a degree-corrected manner, conditioned on the edge labels,

$$P((i, j) | (r, s), \kappa, \mathbf{c}) = \begin{cases} \delta_{c_i, r} \delta_{c_j, s} \kappa_i \kappa_j & \text{if } r \neq s \\ 2\delta_{c_i, r} \delta_{c_j, s} \kappa_i \kappa_j & \text{if } r = s, \end{cases} \quad (14)$$

where κ_i determines the probability of a node being selected inside a group, with $\sum_{i \in r} \kappa_i = 1$. The total likelihood conditioned on the label sequence becomes

$$P(\{(i, j)_t\} | \{(r, s)_t\}, \kappa, \mathbf{c}) = \prod_t P((i, j)_t | (r, s)_t, \kappa). \quad (15)$$

Since we want to avoid overfitting the model, we once more use noninformative priors, but this time on $\{\kappa_i\}$, and integrate over them,

$$P(\{(i, j)_t\} | \{(r, s)_t\}, \mathbf{c}) = \int P(\{(i, j)_t\} | \{(r, s)_t\}, \kappa, \mathbf{c}) P(\kappa) d\kappa, \quad (16)$$

$$= \frac{\prod_i d_i! \prod_r 2^{m_{rr}}}{\prod_r m_r!} \prod_r \left(\binom{n_r}{m_r} \right)^{-1}, \quad (17)$$

where d_i is the degree of node i , and m_{rs} is the total number of edges between groups r and s , and $m_r = \sum_s m_{rs}$.

Combining this result with Eq. (12), we have the complete likelihood of the temporal network,

$$P(\mathbf{s}|\mathbf{c}, \mathbf{b}) = P(\{(i, j)_t\}|\{(r, s)_t\}, \mathbf{c}) P(\{(r, s)_t\}|\mathbf{b}), \quad (18)$$

conditioned only on the partitions, and remembering that $\mathbf{s} = \{(i, j)_t\}$. Finally, the full posterior distribution involves both kinds of partitions considered,

$$P(\mathbf{c}, \mathbf{b}, n|\mathbf{s}) = \frac{P(\mathbf{s}|\mathbf{c}, \mathbf{b}) P(\mathbf{c}) P(\mathbf{b}) P(n)}{P(\mathbf{s})}. \quad (19)$$

For details on the priors $P(\mathbf{c})$ and $P(\mathbf{b})$ and the algorithmic approach to maximise the posterior distribution, we refer to Ref. [8].

We employ this model in a variety of dynamic network datasets from different domains (for details, see Table 1 and Ref. [8]). In all cases, we infer models with $n > 0$ that identify many groups for the tokens and memories, meaning that the model succeeds in capturing temporal structures. In most cases, models with $n = 1$ best describe the data, implying that there is not sufficient evidence for higher-order memory, with exception of the network of chess moves, which is best described by

Table 1 Summary of inference results for empirical temporal networks

High school proximity ($N = 327, E = 5,818$)				Enron email ($N = 87, 273, E = 1, 148, 072$)				
n	C	B_N	B_M	Σ	C	B_N	B_M	Σ
0	10	—	—	89, 577	1, 447	—	—	19, 701, 405
1	10	9	9	82, 635	1, 596	2, 219	2, 201	13, 107, 399
2	10	6	6	86, 249	324	366	313	16, 247, 904
3	9	6	6	103, 453	363	333	289	26, 230, 928
APS citations ($N = 425, 760, E = 4, 262, 443$)				prosper.com loans ($N = 89, 269, E = 3, 394, 979$)				
0	3, 774	—	—	131, 931, 579	318	—	—	96, 200, 002
1	4, 426	6, 853	6, 982	94, 523, 280	267	1039	1041	59, 787, 374
2	4, 268	710	631	144, 887, 083	205	619	367	109, 041, 487
3	4, 268	454	332	228, 379, 667	260	273	165	175, 269, 743
Hospital contacts ($N = 75, E = 32, 424$)				Infectious sociopatterns ($N = 10, 972, E = 415, 912$)				
0	68	—	—	484, 121	4695	—	—	8, 253, 351
1	60	58	58	245, 479	5572	2084	2084	4, 525, 629
2	62	29	26	366, 351	5431	3947	3947	7, 503, 859
3	50	11	7	644, 083	1899	829	783	12, 527, 730
Internet AS ($N = 53, 387, E = 500, 106$)				Chess moves ($N = 76, E = 3, 130, 166$)				
0	187	—	—	19, 701, 403	72	—	—	66, 172, 128
1	185	131	131	10, 589, 136	72	339	339	58, 350, 128
2	132	75	43	14, 199, 548	72	230	266	58, 073, 342
3	180	87	79	22, 821, 016	72	200	205	76, 465, 862

Description length $\Sigma = -\log_2 P(\{(i, j)_t\}, \mathbf{c}, \mathbf{b})$ in bits and inferred number of node groups C , token groups B_N , and memory groups B_M for different data sets and different Markov order n . Values in grey correspond to the minimum of each column

a model with $n = 2$. We note that this only occurs when we use the intermediary layer where the Markov chain generates edge types instead of the edges. If we fit the original model without this modification, we indeed get much larger description lengths and we often fail to detect any Markov structure with $n > 0$ (not shown).

To illustrate how the model characterizes the temporal structure of these systems, we focus on the proximity network of high school students, which corresponds to the voluntary tracking of 327 students for a period of 5 days [24]. Whenever the distance between two students fell below a threshold, an edge between them was recorded at that time. In the best-fitting model for these data, the inferred groups for the aggregated network correspond exactly to the known division into 9 classes, except for the PC class, which was divided into two groups (Fig. 5). The groups show a clear assortative structure, where most connections occur within each class. The clustering of the edge labels in the second part of the model reveals the temporal dynamics. We observe that the edges connecting nodes of the same group cluster either in single-node or small groups, with a high incidence of self-loops. This means that if an edge that connects two students of the same class appears in the sequence, the next edge is most likely also inside the same class, indicating that the students of the same class are clustered in space and time. The remaining edges between students of different classes are separated into two large groups. This division indicates that the different classes meet each other at different times. Indeed, the classes are located in different parts of the school building and they typically go to lunch separately [24]. Accordingly, our method can uncover the associated dynamical pattern from the data alone.

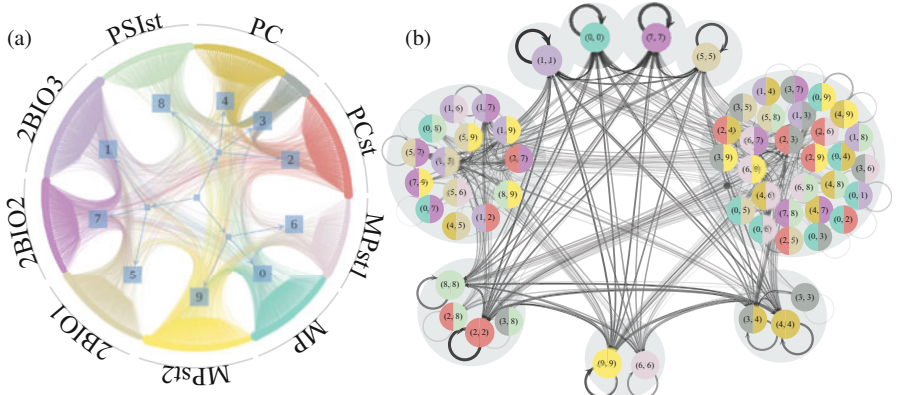


Fig. 5 Inferred temporal model for a high school proximity network [24]. **(a)** The static part of the model divides the high school students into $C = 10$ groups (square nodes) that almost match the known classes (text labels). **(b)** The dynamic part of the model divides the directed multigraph group pairs in **(a)** into $B_N = B_M = 9$ groups (grey circles). The model corresponds to an $n = 1$ unified Markov chain on the edge labels, where the memory and tokens have identical partitions, as described in detail Ref. [8]

4 Markov Chains with Change Points

The model considered previously succeeds in capturing both temporal and structural patterns in empirical dynamic networks, but it is still based on a Markov chain with stationary transition probabilities. As discussed before, this means long-term correlations are not used to inform the model, which can only aggregate temporal heterogeneities into an effective model that averages out possible changes in the transition probabilities over time. In this section we describe how to model changes in the dynamics by considering non-stationary transition probabilities $p_{x,x}$ that change abruptly at a given change point, but otherwise remain constant between change points. The occurrence of change points is governed by the probability q that one is inserted at any given time. The existence of M change points divide the time series into $M + 1$ temporal segments indexed by $l \in \{0, \dots, M\}$. The variable l_t indicates to which temporal segment a given time t belongs among the M segments. Thus, the conditional probability of observing a token x at time t in segment l_t is given by

$$P(x_t, l_t | \mathbf{x}_{t-1}, l_{t-1}) = p_{x,x}^{l_t} [q(1 - \delta_{l_t, l_{t-1}}) + (1 - q)\delta_{l_t, l_{t-1}}], \quad (20)$$

where $p_{x,x}^{l_t}$ is the transition probability inside segment l_t and q is the probability to transit from segment l to $l + 1$. The probability of a whole sequence $\mathbf{s} = \{x_t\}$ and $\mathbf{l} = \{l_t\}$ being generated is then

$$P(\mathbf{s}, \mathbf{l} | \mathbf{p}, q) = q^M (1 - q)^{E-M} \prod_{l,x,x} \left(p_{x,x}^l \right)^{a_{x,x}^l} \quad (21)$$

where $a_{x,x}^l$ is the number of transitions from memory x to token x in the segment l . Note that we recover the stationary model of Eq.(1) by setting $q = 0$. The maximum-likelihood estimates of the parameters are

$$\hat{p}_{x,x}^l = \frac{a_{x,x}^l}{k_x^l}, \quad \hat{q} = \frac{M}{E} \quad (22)$$

where $k_x^l = \sum_x a_{x,x}^l$ is the number of transitions originating from x in a segment l . But once more, we want to infer the model the segments \mathbf{l} in a Bayesian way, via the posterior distribution

$$P(\mathbf{l} | \mathbf{s}, n) = \frac{P(\mathbf{s}, \mathbf{l} | n)}{P(\mathbf{s} | n)}, \quad (23)$$

where the numerator is the integrated likelihood

$$P(\mathbf{s}, \mathbf{l} | n) = \int P(\mathbf{s}, \mathbf{l} | \mathbf{p}, q, n) P(\mathbf{p} | n) P(q) d\mathbf{p} dq \quad (24)$$

using uniform priors $P(q) = 1$, and

$$P(\mathbf{p}|n) = \prod_l P(\mathbf{p}_l|d_l, n)P(d_l), \quad (25)$$

with the uniform prior

$$P(\mathbf{p}_l|d_l, n) = \prod_x (D_l - 1)! \delta\left(\sum_x p_{x,\mathbf{x}}^l - 1\right). \quad (26)$$

and

$$P(d_l) = 2^{-D} \quad (27)$$

being the prior for the alphabet d_l of size D_l inside segment l , sampled uniformly from all possible subsets of the overall alphabet of size D . Performing the above integral, we obtain

$$P(\mathbf{x}, \mathbf{l}|n) = 2^{-D(M+1)} \frac{M!(E-M)!}{(E+1)!} \prod_l \prod_x \frac{(D_l - 1)!}{(k_x^l + D_l - 1)!} \prod_x a_{x,\mathbf{x}}^l!. \quad (28)$$

Like with the previous stationary model, both the order and the positions of the change points can be inferred from the joint posterior distribution

$$P(\mathbf{l}, n|\mathbf{x}) = \frac{P(\mathbf{x}, \mathbf{l}|n)P(n)}{P(\mathbf{x})}, \quad (29)$$

in a manner that intrinsically prevents overfitting. This constitutes a robust and elegant way of extracting this information from data, that contrasts with non-Bayesian methods of detecting change points using Markov chains that tend to be more cumbersome [25], and is more versatile than approaches that have a fixed Markov order [26].

The exact computation of the posterior of Eq. (23) would require the marginalization of the above distribution for all possible segments \mathbf{l} , yielding the denominator $P(\mathbf{x}|n)$, which is unfeasible for all but the smallest time series. However, it is not necessary to compute this value if we sample \mathbf{l} from the posterior using Monte Carlo. We do so by making move proposals $\mathbf{l} \rightarrow \mathbf{l}'$ with probability $P(\mathbf{l}'|\mathbf{l})$, and accepting it with probability a according to the Metropolis-Hastings criterion [27, 28]

$$a = \min\left(1, \frac{P(\mathbf{l}'|\mathbf{x}, n)P(\mathbf{l}|\mathbf{l}')}{P(\mathbf{l}|\mathbf{x}, n)P(\mathbf{l}'|\mathbf{l})}\right), \quad (30)$$

which does not require the computation of $P(\mathbf{x}|n)$ as it cancels out in the ratio. If the move proposals are ergodic, i.e., they allow every possible partition \mathbf{l} to be visited

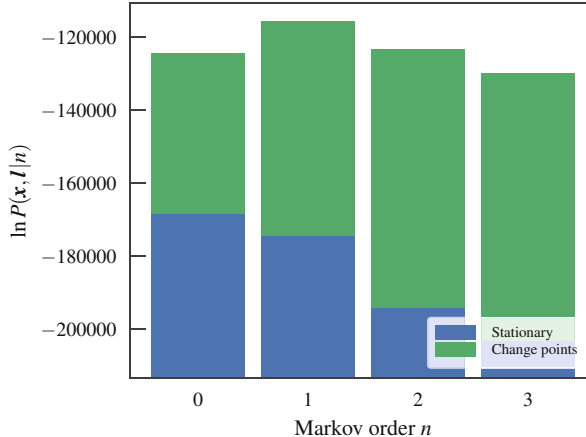


Fig. 6 Integrated joint likelihood $P(\mathbf{x}, \mathbf{I}|n)$ (Eq. (28)) for a temporal network between students in a high school [21], for the stationary (i.e., zero change points) and nonstationary models. For all values of n the likelihoods are higher for the nonstationary model (yielding a posterior odds ratio $\Lambda > 1$)

eventually, this algorithm will asymptotically sample from the desired posterior. We refer to Ref. [22] for more details about the algorithm, including the move proposals used.

Once a fit is obtained, we can compare the above model with the stationary one by computing the posterior odds ratio

$$\Lambda = \frac{P(\mathbf{l}, n|\mathbf{x})}{P(\mathbf{l}_0, n_0|\mathbf{x})} = \frac{P(\mathbf{x}, \mathbf{l}|n)}{P(\mathbf{x}, \mathbf{l}_0|n_0)}, \quad (31)$$

where \mathbf{l}_0 is the partition into a single interval (which is equivalent to the stationary model). A value $\Lambda > 1$ [i.e., $P(\mathbf{x}, \mathbf{l}|n) > P(\mathbf{x}, \mathbf{l}_0|n_0)$] indicates a larger evidence for the nonstationary model. As can be seen in Fig. 6, we observe indeed a larger evidence for the nonstationary model for all Markov orders. In addition to this, using this general model we identify $n = 1$ as the most plausible Markov order, in contrast to the $n = 0$ obtained with the stationary model. Therefore, identifying change points allows us not only to uncover patterns at longer timescales, but the separation into temporal segments enables the identification of statistically significant patterns at short timescales as well, which would otherwise remain obscured with the stationary model—even though it is designed to capture only these kinds of correlations.

The improved quality of this model is also evident when we investigate the epidemic dynamics, as shown in Fig. 7. In order to obtain an estimate of the number of infected based on the model, we generated different sequences of edges using the fitted segments and transition probabilities $\hat{p}_{x,x}^l = d_{x,x}^l / k_x^l$ in each of the segments estimated with Markov orders going from 0 to 3. We simulated SIR and

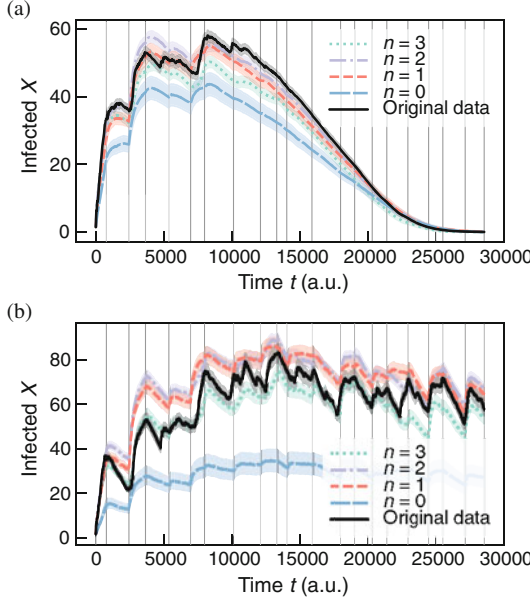


Fig. 7 Number of infected nodes over time $X(t)$ for a temporal network between students in a high-school [21] ($N = 126$), considering both the original data and artificial time-series generated from the fitted nonstationary Markov model of a given order n , using (a) SIR ($\beta = 0.41$, $\gamma = 0.005$) and (b) SIS ($\beta = 0.61$, $\gamma = 0.03$) epidemic models. The vertical lines mark the position of the inferred change points. In all cases, the values were averaged over 100 independent realizations of the network model (for the artificial datasets) and dynamics. The shaded areas indicate the standard deviation of the mean

SIS processes on top of the networks generated and averaged the number of infected over many instances. Looking at Fig. 7, we see that the inferred positions of the change points tend to coincide with the abrupt changes in infection rates, which show very good agreement between the empirical and generated time-series. For higher Markov order, the agreement improves, although the improvement seen for $n > 1$ is probably due to overfitting, given the results of Fig. 6. The fact that $n = 0$ provides the worst fit to the data shows that it is not only the existence of change points, but also the inferred Markov dynamics that contribute to the quality of the model in reproducing the epidemic spreading.

In order to examine the link between the structure of the network and the change points, we fitted a layered hierarchical degree-corrected stochastic block model [11, 29] to the data, considering each segment as a separate edge layer. Figure 8 shows that the density of connections between node groups vary in a substantial manner, suggesting that change point marks an abrupt transition in the typical kind of encounters between students—representing breaks between classes, meal time, etc. This yields an insight as to why these changes in pattern may slow down or speed up an epidemic spreading: if students are confined to their classrooms, contagion across classrooms is inhibited, but as soon they are free to move around the school grounds, so can the epidemic.

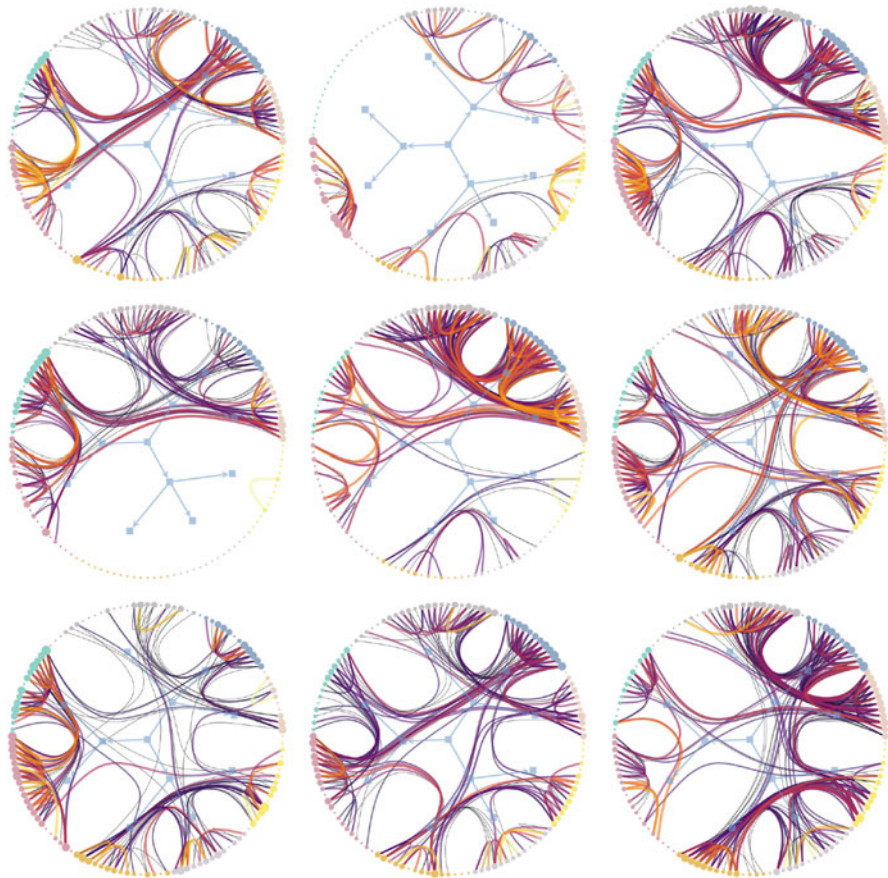


Fig. 8 Network structure inside the first nine segments of a temporal network between students in a high-school [21]. The segments were captured by a layered hierarchical degree-corrected stochastic block model [11] using the frequency of interactions as edge covariates [29] (indicated by colors), where each segment is considered as a different layer. The values of the infection and recovery rates were chosen so that the spreading dynamics spans the entire time range of the dataset

5 Conclusion

In this chapter, we reviewed two data-driven approaches to model temporal networks based on arbitrary-order Markov chains, while at the same time incorporating two kinds of higher-order structures: (1) the division of the transition probabilities and the nodes in the network into communities, and (2) the abrupt transition of the Markov transition probabilities at specific change points. In each case, we have described a Bayesian framework that allows the inference of communities, change points and Markov order from data in a manner that prevents overfitting, and enables the selection of competing models.

We have applied our approach to a variety of empirical dynamical networks, and we have evaluated the inferred models based on their capacity to compress the data and to reproduce the epidemic spreading observed with the original data. We have seen that the model with communities uncovers modular structure both in the network itself and in its dynamical patterns. In turn, the nonstationary model with change points accurately reproduces the highly-variable nature of the infection rate, with changes correlating strongly with the inferred change points.

Both modelling approaches can be extended to data with continuous time and with bursty dynamics by introducing waiting times as additional covariates, as described in Ref. [8].

There is no reason why community structure and change points cannot be considered together, which would allow, among other things, for a fully dynamical description of large-scale modular structures. In fact, there are approaches not based on Markov chains that do just that [15]. However, combining both models described here seems at first challenging, as the most direct approach yields a cumbersome model that is difficult to operate algorithmically. An elegant approach that combines both aspects simultaneously—thus allowing for the synergistic combination of multiple timescales and dynamic community structure—is a desirable area for future work.

Finally, it would be interesting to investigate how the approaches presented here can be extended from dynamics represented as a sequence of edges to scenarios where edges are allowed both to appear and disappear from the network.

Acknowledgement M.R. was supported by the Swedish Research Council grant 2016-00796.

References

1. Ho, Q., Song, L., Xing, E.P.: Evolving cluster mixed-membership blockmodel for time-varying networks. In: Proceedings of the International Conference on Artificial Intelligence and Statistics, vol. 15, pp. 342–350 (2011)
2. Perra, N., Gonçalves, B., Pastor-Satorras, R., Vespignani, A.: Activity driven modeling of time varying networks. *Sci. Rep.* **2**, 469 (2012)
3. Rocha, L.E. C., Liljeros, F., Holme, P.: Simulated epidemics in an empirical spatiotemporal network of 50,185 sexual Contacts. *PLoS Comput. Biol.* **7**, e1001109 (2011)
4. Valdano, E., Ferreri, L., Poletto, C., Colizza, V.: Analytical computation of the epidemic threshold on temporal networks. *Phys. Rev. X* **5**, 021005 (2015)
5. Génois, M., Vestergaard, C.L., Cattuto, C., Barrat, A.: Compensating for population sampling in simulations of epidemic spread on temporal contact networks. *Nat. Commun.* **6**, 8860 (2015)
6. Ren, G., Wang, X.: Epidemic spreading in time-varying community networks. *Chaos: Interdiscip. J. Nonlinear Sci.* **24**, 023116 (2014)
7. Scholtes, I. et al.: Causality-driven slow-down and speed-up of diffusion in non-Markovian temporal networks. *Nat. Commun.* **5**, 5024 (2014)
8. Peixoto, T.P., Rosvall, M.: Modelling sequences and temporal networks with dynamic community structures. *Nat. Commun.* **8**, 582 (2017)

9. Xu, K.S., Iii, A.O.H.: Dynamic stochastic blockmodels: statistical models for time-evolving networks. In: Greenberg, A.M., Kennedy, W.G., Bos, N.D. (eds.) *Social Computing, Behavioral-Cultural Modeling and Prediction. Lecture Notes in Computer Science*, vol. 7812, pp. 201–210. Springer, Berlin (2013)
10. Gauvin, L., Panisson, A., Cattuto, C.: Detecting the community structure and activity patterns of temporal networks: a non-negative tensor factorization approach. *PLoS One* **9**, e86028 (2014)
11. Peixoto, T.P.: Inferring the mesoscale structure of layered, edge-valued, and time-varying networks. *Phys. Rev. E* **92**, 042807 (2015)
12. Stanley, N., Shai, S., Taylor, D., Mucha, P.J. Clustering network layers with the strata multilayer stochastic block model. *IEEE Trans. Netw. Sci. Eng.* **3**, 95–105 (2016)
13. Ghasemian, A., Zhang, P., Clauset, A., Moore, C., Peel, L.: Detectability thresholds and optimal algorithms for community structure in dynamic networks. *Phys. Rev. X* **6**, 031005 (2016)
14. Zhang, X., Moore, C., Newman, M.E.J.: Random graph models for dynamic networks. *Eur. Phys. J. B* **90**, 200 (2017)
15. Peel, L., Clauset, A.: Detecting change points in the large-scale structure of evolving networks. In: Twenty-Ninth AAAI Conference on Artificial Intelligence (2015)
16. De Ridder, S., Vandermarliere, B., Ryckebusch, J.: Detection and localization of change points in temporal networks with the aid of stochastic block models. *J. Stat. Mech: Theory Exp.* **2016**, 113302 (2016)
17. Cornelis, M., Latouche, P., Rossi, F.: Multiple change points detection and clustering in dynamic networks. *Stat. Comput.* **28**, 989 (2018)
18. Gauvin, L., Panisson, A., Cattuto, C., Barrat, A.: Activity clocks: spreading dynamics on temporal networks of human contact. *Sci. Rep.* **3**, 3099 (2013)
19. Vestergaard, C.L., Géniois, M., Barrat, A.: How memory generates heterogeneous dynamics in temporal networks. *Phys. Rev. E* **90**, 042805 (2014)
20. Strelloff, C.C., Crutchfield, J.P., Hübner, A.W.: Inferring Markov chains: Bayesian estimation, model comparison, entropy rate, and out-of-class modeling. *Phys. Rev. E* **76**, 011106 (2007)
21. Fournet, J., Barrat, A.: Contact patterns among high school students. *PLoS One* **9**, e107878 (2014)
22. Peixoto, T.P., Gauvin, L.: Change points, memory and epidemic spreading in temporal networks. *Sci. Rep.* **8**, 15511 (2018)
23. Jaynes, E.T.: *Probability Theory: The Logic of Science* Cambridge University Press, Cambridge (2003)
24. Mastrandrea, R., Fournet, J., Barrat, A.: Contact patterns in a high school: a comparison between data collected using wearable sensors, contact diaries and friendship surveys. *PLoS One* **10**, e0136497 (2015)
25. Polansky, A.M.: Detecting change-points in Markov chains. *Comput. Stat. Data Anal.* **51**, 6013–6026 (2007)
26. Arnesen, P., Holsclaw, T., Smyth, P.: Bayesian detection of changepoints in finite-state Markov chains for multiple sequences. *Technometrics* **58**, 205–213 (2016)
27. Metropolis, N., Rosenbluth, A.W., Rosenbluth, M.N., Teller, A.H., Teller, E.: Equation of state calculations by fast computing machines. *J. Chem. Phys.* **21**, 1087 (1953)
28. Hastings, W.K.: Monte Carlo sampling methods using Markov chains and their applications. *Biometrika* **57**, 97–109 (1970)
29. Peixoto, T.P.: Nonparametric Bayesian inference of the microcanonical stochastic block model. *Phys. Rev. E* **95**, 012317 (2017)

Visualisation of Structure and Processes on Temporal Networks



Claudio D. G. Linhares, Jean R. Ponciano, Jose Gustavo S. Paiva,
Bruno A. N. Travençolo, and Luis E. C. Rocha

1 Introduction

Networks have been extensively used to model the connections and inter-dependencies between the parts of a system by using nodes and edges. Network models and measures are used to reproduce and identify patterns, or extract information, from the structure of connections in a multitude of disciplines, ranging from the social sciences to technologies, passing through biology, medicine, economics, business and engineering [1–3]. Network visualisation complements the network science toolbox by providing means to translate mathematical abstraction to visual patterns. It helps to understand the network structure, the network evolution, and processes taking place on the network [4]. The challenge however is to make visualisations that are informative and insightful.¹ Since Ramon Llull first introduced his ideas of connecting *concepts* to derive *consequences* by lines back in the twelfth century [5], we have been coping well with small and ordered networks (or graphs) such as those on road maps, companies' flight route maps, the London tube (arguably) or simple lattices (Fig. 1a). However, visual information scales with network size and density, and sociograms used to provide an intuitive graphic representation of social relations [6, 7] can quickly turn into ridiculograms

¹ Art-conscious researchers may also call for aesthetic visualisations.

C. D. G. Linhares · J. R. Ponciano · J. G. S. Paiva · B. A. N. Travençolo
Faculty of Computing, Federal University of Uberlândia, Uberlândia, Brazil

L. E. C. Rocha (✉)
Department of General Economics, Ghent University, Ghent, Belgium

Department of International Business and Economics, University of Greenwich, London, UK
e-mail: Luis.Rocha@UGent.be

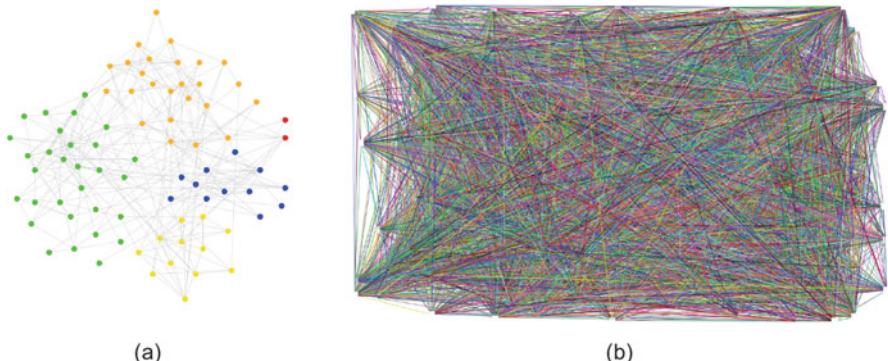


Fig. 1 The diagrams correspond to (a) a meaningful sociogram where some information about the structure can be retrieved and (b) a ridiculous sociogram where no meaningful information can be retrieved

that are a bunch of crossing lines resembling a cat’s hairball² (Fig. 1b). This effect is called visual clutter (i.e. excessive information or items in an image) in information visualisation [8]. Several methods exist to improve network visualisation to avoid or at least minimise the hairball curse and other issues [9]. Nevertheless, visualisation per se has its own limitations and is at risk of manipulation or unconscious bias. Simply changing the order of drawing nodes and edges, or making a 3D projection, may highlight or hide relevant features such as node clustering, the strength of connections, or the distance between nodes.

The increasing availability of high quality time-evolving network data revealed that structure may change faster than previously acknowledged. Such findings encouraged researchers to study more in-depth the temporal evolution of these complex networks. Such networks are characterised by the timings that nodes and edges are active. Although some networks are rather stable (e.g. road networks) or vary slowly in time (e.g. flight networks [10]), a number of social networks are highly dynamic, with an inflow and outflow of nodes and edges, periods of inactivity and bursts of interaction at small temporal scales in respect to the observation time [3, 11–13]. The temporal dimension adds an extra layer of complexity in such already hard-to-visualise patterns. The most rudimentary yet useful approach is to simply draw a sequence of snapshots containing the network structure at subsequent times [14, 15]. This method highlights the structure of connections at given times and gives insights about the activation of specific edges (and nodes) over time. It is particularly informative if nodes are (artificially or empirically) fixed in space. However, if layout strategies [9] are applied at each time step, patterns become less intuitive. Furthermore, the same issues of static network drawings,

²To our knowledge, the oldest available online record suggests that the term ridiculous was coined by Marc Vidal as early as 2007 (www.cs.unm.edu/~aaron/blog/archives/2007/05/ipam_random_and.htm).

such as node and edge overlaps, are observed. In addition, the mental map of the historical evolution of the network is lost due to the form of presenting the network. For example, in a movie generated using temporally ordered network snapshots, the screen updates at each time step and a viewer has to rely on his or her memory to recall previous network patterns. The use of transparency and three dimensional visualisation have been suggested to improve such methods [16]. This snapshot method is possibly mostly appropriate to study networks with weak temporal activity, e.g. when structural changes occur at a slower pace or when edges and nodes are persistently active, but may also aid identifying parts of the network that are more active at certain times (e.g. flashing broadcast) irrespective of the speed of structural changes.

Not only the quality but also the size of network data has increased. Some strategies have been proposed to handle larger evolving networks and include reducing their complexity by pre-processing the networks before visualisation. For example, one can observe the movement of nodes between network communities through alluvian diagrams where groups of nodes are clustered in communities, represented by temporally ordered blocks of varying sizes connected by stream fields representing the nodes moving between communities over time [17]. A number of variations of the alluvian diagrams have been used to visualise evolving communities [18]. Another methodological attempt focuses on visualising the evolution of the adjacency matrix of the network. The so-called matrix cube method draws a 2D grid (i.e. the adjacency matrix) where occupied cells represent an active edge between two nodes and then stacks up subsequent chessboards in the third dimension to show the evolving activity as blocks (i.e. cubes, instead of 2D occupied cells) [19]. The shortcoming of this (juxtaposed) snapshot method is to visualise the historical evolution of the network since internal blocks are frequently hidden in sparse networks. An intuitive approach to overcome this limitation is to create a 2D visualisation where all active nodes and edges are shown simultaneously with different nodes in different rows (as horizontal lines) and temporal edges (as vertical lines) connecting these nodes in the respective time steps that they are active. Although information about the connectivity is partly lost due to overlap of edges, it is then possible to get an overview of the node activity in time [20, 21].

In this Chapter, we first define the temporal networks (Sect. 2) and then introduce key concepts of information visualisation in the context of temporal networks with particular emphasis on algorithms to reduce edge overlap and methods to highlight the node activity over time (Sect. 3). These methods are then applied to real-world temporal networks to identify non-trivial activity patterns and are also used to visualise trajectories of random walkers and transmission paths of infection dynamics taking place on these evolving networks (Sect. 4). Key visual and computational scalability issues are discussed in Sect. 5 and conclusions and future research directions in Sect. 6.

2 Temporal Networks

This section introduces the concept of temporal networks, including the definition of essential parameters and measures that will be used throughout the Chapter. A temporal network with N nodes and E edges is defined by a set of nodes i connected by edges active at times t , i.e. (i, j, t) [3, 22]. Since t is discrete, an edge activation at time t means that the activation occurred in the interval $[t, t + \delta)$ where δ is the temporal resolution. Each of these intervals is called snapshot, or time step τ , and $\Upsilon = T/\delta$ is the total number of time steps.³ To simplify, here we remove multiple edges and self-edges per snapshot. Multiple edges could be summed and assigned as weight to a single edge at each snapshot. The times $t = 0$ and $t = T$ indicate respectively the start and end of the observation period. The adjacency matrix is dynamic with $a_{ij}(t) = 1$ if there is an edge between i and j at time t , and $a_{ij}(t) = 0$ otherwise. The set of nodes j connected to i forms the neighbourhood of i . The degree of node i at time t is given by $k_i(t)$, the accumulated degree is k_i and the strength is s_i :

$$k_i(t) = \sum_{j=0}^N a_{ij}(t) \quad (1)$$

$$k_i = \sum_{j=0}^N a'_{ij} \text{ where } a'_{ij} = \cup_{t=0}^T a_{ij}(t) \quad (2)$$

$$s_i = \sum_{t=0}^T \sum_{j=0}^N a_{ij}(t) \quad (3)$$

3 Visualisation on and of Temporal Networks

This section introduces the concept of layout and the use of Gestalt theory in the context of visualisation of temporal networks. It also discusses the main issue of visual clutter on network visualisation and directions to quantify and reduce this recurrent problem, including node re-ordering techniques, removal of edges and colouring of nodes.

3.1 Layouts

The layout is a fundamental visualisation concept that defines the way in which the parts of something are arranged in the visual space. In the case of a network,

³The snapshot τ coincides with time t if $\delta = 1$.

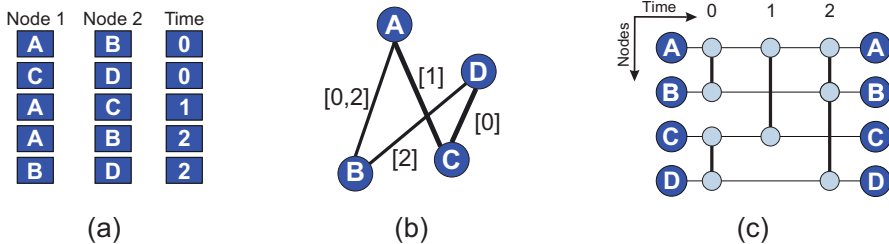


Fig. 2 Methods for representation of temporal networks: (a) tabular or ordered list; (b) node-edge diagram, the standard layout for static networks, with time stamps; (c) temporal or sequence view layout

the parts would be nodes and edges. An ordered list of contacts is a common way of representing temporal network data (Fig. 2a). Though convenient and optimal to store information and input statistical analysis, this tabular format is unhelpful if one wishes to visually identify temporal patterns for qualitative analysis. A number of more appropriate layouts, such as space-time cubes [23], circular methods [21], structural (the classic node-edge diagrams, see Fig. 2b) and sequence views [24, 25] (Fig. 2c), have been designed to facilitate visual analysis of temporal network data. There is no consensus on the best layout because each one has advantages and disadvantages on particular tasks. For example, matrix-based techniques are more suitable than node-edge diagrams for low-level tasks such as the estimation of the network density [26]. The structural and temporal layouts on the other hand are typically used to analyse the distribution of connections.

The structural layout is the conventional network representation in which the nodes (called instances in the discipline of information visualisation) are spatially placed on the layout with edges connecting them (Fig. 2b). Edges may contain a list of numbers representing the times they are active. This layout is recommended to get a global picture of the network since it facilitates identifying multiple structures at the same time. If the network has several nodes and edges, visual clutter may affect the perception of patterns. Visual clutter refers to excessive items or information close together due to edge and node overlap [8] (See Sect. 3.2). In network visualisation, it indicates excessive overlap of edges and nodes on the layout. To reduce clutter, a number of strategies can be employed to change nodes' positions. Popular methods include force-based and circular algorithms [25, 27, 28]. Such techniques are generally hopeless for temporal networks even if combined with animated graphs because it is difficult to maintain the mental map representation using the structural layout with networks that change in time [29]. In this layout, it is recommended to use nodes with fixed positions.

One effective layout for temporal networks places different nodes on non-overlapping horizontal lines with vertical lines (i.e. edges) linking different nodes. Nodes only appear as circles (or squares) at times they are active. The temporal evolution of the network structure follows the x-axis (Fig. 2c). In this case, the positions of nodes are fixed on space and are time-invariant to maintain the mental

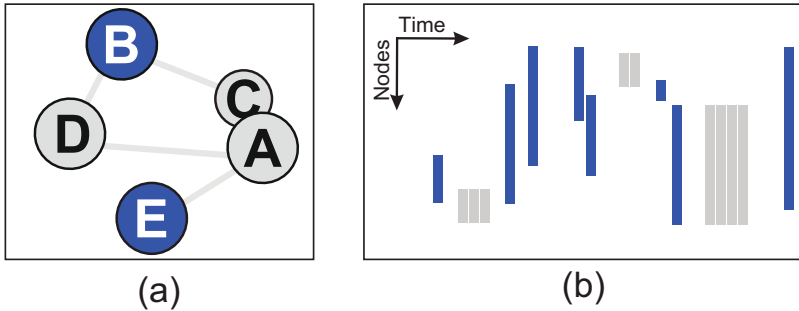


Fig. 3 Gestalt principles applied to structural and temporal complex network layouts: (a) structural layout with node overlap and multiple node colours; (b) Temporal layout with multiple colours, positions and lengths of edges

map necessary to identify relevant patterns. Originally introduced by Jerding and Stasko [20], this method is sometimes called massive sequence view (MSV) [30]. In this temporal layout, the edge length varies according to the distance between the two nodes in the layout (compare for example nodes *A* and *B*, and *B* and *D* in Fig. 2c). The varying edge length may mislead the interpretation of the visualisation since simple edge overlap frequently suggests regions with high connectivity where in fact only a few edges may be overlapping.

The Gestalt theory from psychology attempts to explain the human perception of the world and is a fundamental tool for optimal visual design and consequently information visualisation [31]. The most relevant principles of Gestalt theory that applies to the temporal layout is proximity, closure and similarity (Fig. 3). The proximity principle suggests that things that are close to one another lead us to perceive them as grouped together [31], as illustrated by nodes *A* and *C* in the static layout of Fig. 3a and the gray blocks in the temporal layout of Fig. 3b. However, the closure principle states that “*a closed contour tends to be seen as an object*” [31]. The same nodes *A* and *C* partially overlap but the brain visually separates them as distinct objects because of the closure of the contours (Fig. 3a). Similarly, the spatially close gray lines in the temporal layout are seen as separated blocks distinguishable due to white lines (Fig. 3b). Complementary, the similarity principle states that “*similar elements tend to be grouped together*” [31]. Even though nodes *B* and *E* are spatially distant, the human brain is able to distinguish them from the other nodes due to the common colour (Fig. 3a). For the same reason, the vertical lines in the temporal layout are also segregated by colour and easily distinguishable (Fig. 3b).

Redundant coding is typically used to improve the visualisation [31]. In the structural layout, for example, it can be implemented by combining the edge thickness with a gray-scale such that thicker lines indicate more connections between a pair of nodes and darker gray indicate higher edge overlap. Colours can be also used to highlight node features such as the network structure (e.g. degree) or node labels (e.g. political parties [32]). In the temporal layout, the colour gradient

technique is used to visualise the relationships among nodes within the same group (if nodes are labelled) or within the same network community, and to indicate the level of edge overlap at each time step. Furthermore, the state of nodes (e.g. occupied or not) or trajectories in the network can be highlighted through the use of different colours in the respective nodes and edges.

3.2 Visual Clutter

The main limitation of the temporal (and also of the structural) layout is the often excessive overlap of edges that creates visual clutter. Visual clutter is the excessive amount of information within a small area of an image. As pointed out in the previous section, visual clutter due to edge similarity and edge overlap limits any meaningful visualisation of information and visual analysis. This section describes algorithms to highlight visual information taking into account Gestalt principles to reduce clutter. There are 3 major classes of methods in the temporal layout: (1). node re-ordering (Fig. 4b), (2). smart sampling or filtering (partial removal) of edges or nodes (Fig. 4c), and (3). complete removal of edges (Fig. 4d).

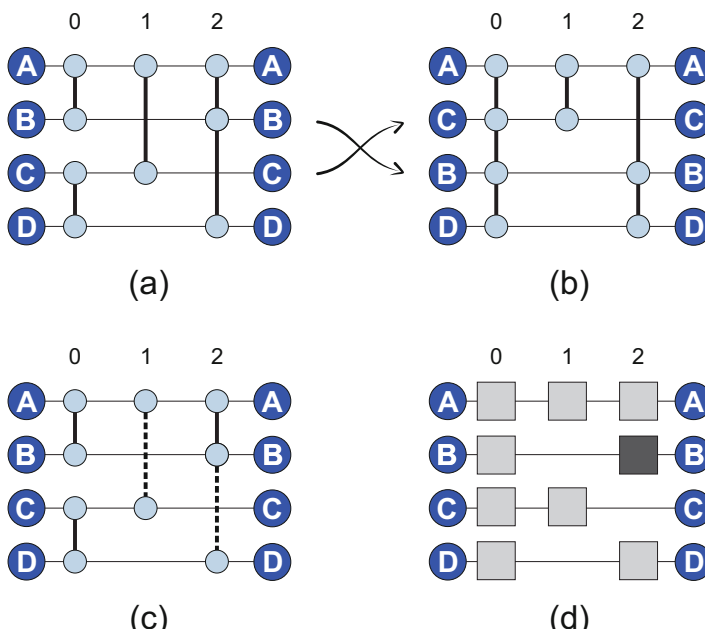


Fig. 4 Strategies to reduce visual clutter in the temporal layout: (a) Original temporal layout; (b) Node re-ordering; (c) Sampling edges; (d) Temporal activity map with all edges removed. The darker square indicates that node B has a higher degree (i.e. $k_B(2) = 2$) than the other nodes at other times (i.e. $k_i(t) = 1$, for $i \neq B$ and $t \neq 2$)

The baseline reference strategy is to place nodes in rows uniformly chosen at random. To highlight the order of appearance, nodes are sorted (e.g. from top to bottom) according to the timings of first connection (Fig. 4a). Similarly, nodes can be sorted according to the last time they are observed. These ordering strategies help to identify the birth, death and lifetime of nodes and edges [33], and to identify if node and edge activities are concentrated in time or spread all over the observation period [24]. Another useful strategy is to sort nodes according to labels or values (called lexicographic ordering [21, 24]). Labels may come from meta-data, e.g. same ward patients, classmates, age or income bands, or from the network structure, e.g. accumulated degree/strength (Sect. 2) [21], centrality or community structure [34]. The main advantage of such approach is to cluster nodes with similar features to facilitate cross-comparisons. For example, two nodes with similar (cumulative) degree may have different activity patterns, e.g. one node may concentrate activity within short periods (relatively lower persistence) whereas another may have a more uniform distributed pattern of connections (higher persistence). These strategies explore activity patterns for ordering without taking into account visual clutter.

Advanced strategies aim to reduce edge overlap to maximise the visual structural information. One strategy is to place nodes that are frequently in contact, or whose connections are recurrent in time, spatially close in the layout. This is named recurrent neighbours strategy (RN). In the RN strategy, the node i with highest strength s_i is initially placed in the centre and then the most connected neighbour j to i is placed right above i followed by placing the second most connected neighbour k to i right below i and so on until all neighbours of i are added on the layout. The next node j with highest strength is now selected and the same routine is repeated. The algorithm proceeds until all nodes are positioned on the layout. This iterative process keeps the highest density of edges in the central part of the layout,⁴ minimising the average length of edges and consequently the visual clutter [24]. In this solution, least important (i.e. least frequent) edges end up with relatively longer lengths that may be interpreted as more important. An inverted recurrent neighbour solution could solve this issue but then would add substantial edge overlapping, that should be avoided. An alternative hierarchical strategy (HS) for node ordering aiming to minimise both edge block overlap and average edge length has been also proposed in the literature [21]. In this case, the algorithm first uses a simulated annealing optimisation process to find the shortest combination of edges length based on the standard deviation of the lengths and then minimises the block overlapping, i.e. the groups of overlapping edges (vertical lines) [21]. Finally, edge overlap can be also minimised by filtering, i.e. by removing or hiding selected edges. Naive strategies include random removal of a fraction of edges to depopulate the layout yet keeping some structure (Fig. 4c) or simply reducing

⁴Somewhat similar to the force-directed graph drawing algorithm for the structural layout [9], except that in our case nodes' positions are fixed.

the temporal resolution δ to collapse edges [12]. In fact, small variations of the temporal resolution do not affect substantially network structure [12, 35] but can substantially decrease visual clutter. Another strategy consists in creating a sample of edges maintaining the edge distribution over time [36].

Since edges bring little information in the temporal layout, they can sometimes be completely removed to decrease the density of elements in a layout called temporal activity map (TAM)⁵ [24]. To improve the visualisation, nodes are drawn using squares instead of circles to provide a sense of continuity [31] and colours are used to show structural of dynamic information, as for example the degree $k_i(t)$ (Fig. 4d). The network structure is then used in the re-ordering algorithms, as those discussed above, or to assign values to nodes (e.g. network centrality) presented by colour gradients. This layout emphasises node activity since high activity is readily identified through the frequency of appearances (inactive nodes are not shown in the respective time steps). Activity can be further highlighted by assigning colours to nodes according to their level of connectivity (e.g. their degree $k_i(t)$ or strength s_i). This method and variations are particularly suitable to visualise communities in temporal networks [18].

3.3 Estimating Clutter on Temporal Networks

To quantify the performance of algorithms employed to reduce visual clutter in temporal networks, one can measure different image features like the number of overlapping edges, the edge length, and the number of edge intersections for one re-ordering algorithm and compare to the random case, i.e. when nodes are randomly placed in rows. The most intuitive measure is to count the number of overlapping edges in each time step τ ($\theta(\tau)$) and take the average $\langle \theta \rangle$ over all time steps Υ .⁶ If two edges overlap more than one time in the same time step, only one overlap is counted. The maximum overlap per time is thus equal to the number of edges at that time. This measure does not take into account that edges have different lengths and longer edges populate the layout more than shorter ones. To capture this feature, we define the length of edge (i, j) as $l_{ij} = n + 1$, where n is the number of nodes in-between the connected nodes i and j and estimate the average edge length $\langle l \rangle$ and standard deviation of edge lengths σ_l . Nevertheless, the edge length does not indicate whether a region of the image is visually dense. The average number of intersections $\langle \gamma \rangle$ is then used to count the number of times $\gamma(\tau)$ that two edges cross each other at each time step τ (in each horizontal line):

⁵This method is similar to heatmap grids [37].

⁶We use the notation of snapshots τ rather than time t to emphasise that measures take into account snapshots, see Sect. 2 for definitions.

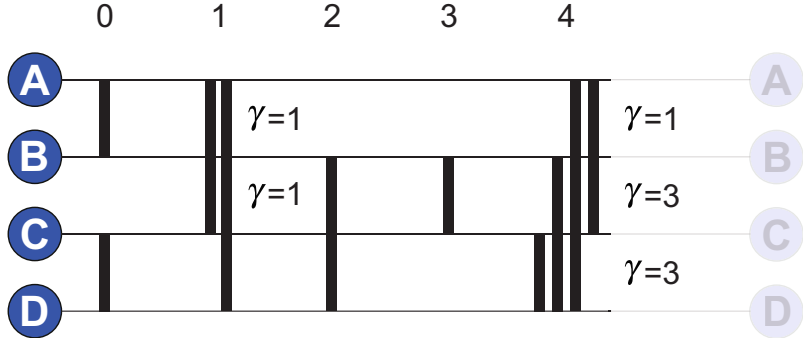


Fig. 5 Measuring the performance of re-ordering algorithms. In this sample temporal network, the number of snapshots is $\Upsilon = 5$. The average overlap is $\langle \theta \rangle = (0 + 2 + 0 + 0 + 4)/5 = 1.2$. The average edge length and standard deviation are respectively $\langle l \rangle = 18/10 = 1.8$ and $\sigma_l = 0.75$. The average number of intersections is $\langle \gamma \rangle = (0 + 2 + 0 + 0 + 7)/5 = 1.8$

$$\langle \theta \rangle = \frac{1}{\Upsilon} \sum_{\tau=0}^{\Upsilon} \theta(\tau) \quad (4)$$

$$\langle l \rangle = \frac{1}{E} \sum_{(i,j)} l_{ij} \quad (5)$$

$$\sigma_l = \frac{1}{E} \sqrt{\sum_{(i,j)} (l_{ij} - \langle l \rangle)^2} \quad (6)$$

$$\langle \gamma \rangle = \frac{1}{\Upsilon} \sum_{\tau=0}^{\Upsilon} \gamma(\tau) \quad (7)$$

Two edges with several intersections result on more visual clutter and thus larger and denser networks are expected to have a higher number of intersections and consequently higher visual clutter (Fig. 5).

4 Visual Insights

The visualisation techniques discussed in the previous sections can be applied to real-world network data to support visual analysis for insights about the evolution of the network structure and to identify patterns to guide further quantitative statistical analysis. The visualisation of the temporal network is particularly helpful when combined with the visualisation of node activity and dynamic processes taking place

on the network. This section shows a few case studies to illustrate the visualisation techniques based on three layouts containing (1) both nodes and edges (focus on structure), (2) nodes attributes (focus on temporal activity), and (3) nodes states linked to dynamic processes (focus on processes).

4.1 Network Data

Two different network data sets of social contacts will be used to illustrate the application of the methods. They correspond to face-to-face spatial proximity (within 1.5 m) interactions between two people wearing RFID badges and include typical real-world temporal structures. In both cases, contacts are scanned every 20 s (that is the maximum temporal resolution δ). The first network data set contains $E = 188,508$ contacts between $N = 327$ students collected during 5 days (between the 2nd and 6th of December 2013) in a high-school in Marseille, France [38]. The second network data set contains $E = 6980$ contacts between $N = 72$ people visiting the Science Gallery in Dublin, Ireland, during 1 day in 2009 [39].

4.2 Temporal Structure

The temporal or sequence view layout is a projection of the network on the plane where nodes are located in fixed horizontal lines and then linked by vertical edges at certain times. Therefore, edges on each time (i.e. at each temporal snapshot) necessarily overlap. Due to spatial constraints, a few active nodes per time step are already sufficient to produce a layout with high clutter due to edge overlap. Edges between spatially distant nodes also cost too much information in such layout since they occupy much space. The colour intensity correlates with the level of edge overlap such that lighter edges indicate relatively fewer connections at that time step in comparison to darker edges. For example, in the museum network, for random node location, the first part of the observation window shows dense information and suggests relatively higher activity followed by some periods of medium activity (Fig. 6a). An effective strategy to reduce information while keeping all edges on the layout is to simultaneously reduce overlap and the length of recurring edges. This is done by putting together nodes that interact often (i.e. recurrent neighbour—RN—strategy, see Sect. 3.2). The RN algorithm highlights the frequent interaction by positioning the most active nodes in the centre of the layout whereas less active nodes stay peripheral (Fig. 6b). It produces a cleaner layout that facilitates the identification of clusters of temporal activity. Since the longer the edge, the less frequent is the contact, one can readily see that activity in earlier times is less intense and involve less nodes than suggested by the random ordering. It is also visible that only a few pairs of nodes have intense activity (i.e. repeated connections) over time (e.g. before the period of high activity, there is a pair of nodes between the bottom

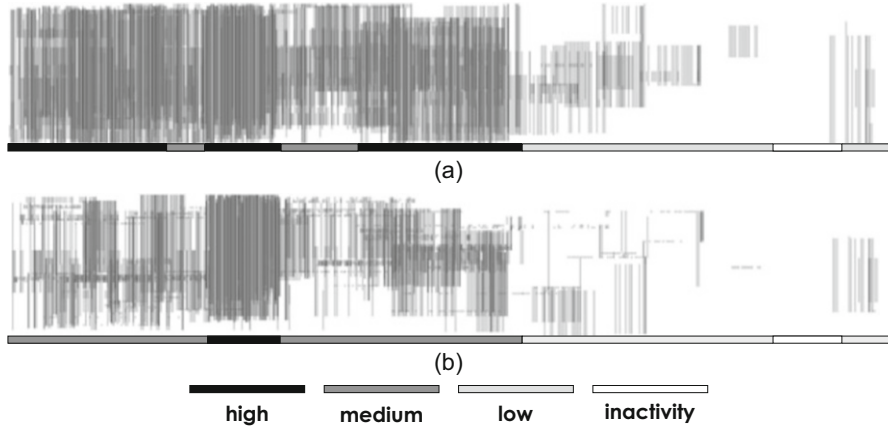


Fig. 6 Temporal layout for (a) random and (b) recurrent neighbour ordering of nodes for the museum data set. The re-ordering of nodes removes noise and helps to emphasise periods with different levels of activity over time. The temporal resolution is $\delta = 1$ min

and the mid-part of the layout, and after the period of high activity, there is a pair of nodes at the mid-part of the layout with recurrent contacts, Fig. 6b).

Reducing visual clutter (and thus layout information) is an essential step in network visualisation. To quantify the improvement of the RN algorithm, we apply measures of visual clutter (Sect. 3.3) in both data sets (museum and high-school) for various temporal resolutions δ (Table 1). In some cases, RN provides an improvement of up to 87% (and frequently above 40%) for both data sets. In the museum data, performance tends to decrease for lower temporal resolutions whereas in the school network, performance is generally maintained for most measures for various δ . This is likely a consequence of the persistent of edge activity in the high school case where all students arrive and leave at the same time and subsequent contacts are common (lower resolution simply collapse similar edges), whereas museum visitors, at least in this particular case, tend to come in groups, moving around (subsequent contacts are not so common and collapsing subsequent edges generate different visual patterns) and spending roughly the same time in the museum but starting at different times.

4.3 Temporal Activity

Another strategy to reduce information due to edge overlap is to completely remove the edges and focus on the nodes. In the temporal activity map strategy, the position of nodes can be defined by their connectivity through node re-ordering algorithms (e.g. degree or centrality) but edges are removed before showing the network. This layout reveals several relevant patterns during the network evolution, as for example,

Table 1 Statistical measures of visual clutter for the museum and high-school data sets using different temporal resolutions δ

Museum data set						
$\delta = 20\text{ s}$			$\delta = 1\text{ min}$			$\delta = 5\text{ min}$
	Random	RN	Random	RN	$\Delta(\%)$	Random
$\langle \theta \rangle$	5.04 ± 0.03	4.43	-12	10.83 ± 0.04	10.33	-5
$\langle l \rangle$	24 ± 1	10	-57	23 ± 2	13	-45
σ_l	17 ± 1	14	-14	17 ± 1	16	-5
$\langle l \rangle$	147.04 ± 10.09	48.49	-67	629.55 ± 74.21	355.40	-44
<i>High-school data set</i>						
$\delta = 20\text{ s}$			$\delta = 3\text{ min}$			$\delta = 10\text{ min}$
	Random	RN	Random	RN	$\Delta(\%)$	Random
$\langle \theta \rangle$	0.998 ± 0.002	0.92	-8	2.86 ± 0	2.82	-1
$\langle l \rangle$	109 ± 5	33	-69	108 ± 3	38	-65
σ_l	77 ± 3	64	-17	76 ± 2	71	-7
$\langle l \rangle$	356.4 ± 24.3	47.0	-87	3381.8 ± 168.7	640.8	-81

We measure the performance of RN re-ordering algorithm in comparison to the random case, $\Delta = 100(x_{RN} - x_{Random})/x_{Random}$ where x represents one measure for RN and the same measure for the random placement of nodes. The random cases are averaged over 10 realisations with \pm indicating the standard deviation. The values of Δ are rounded

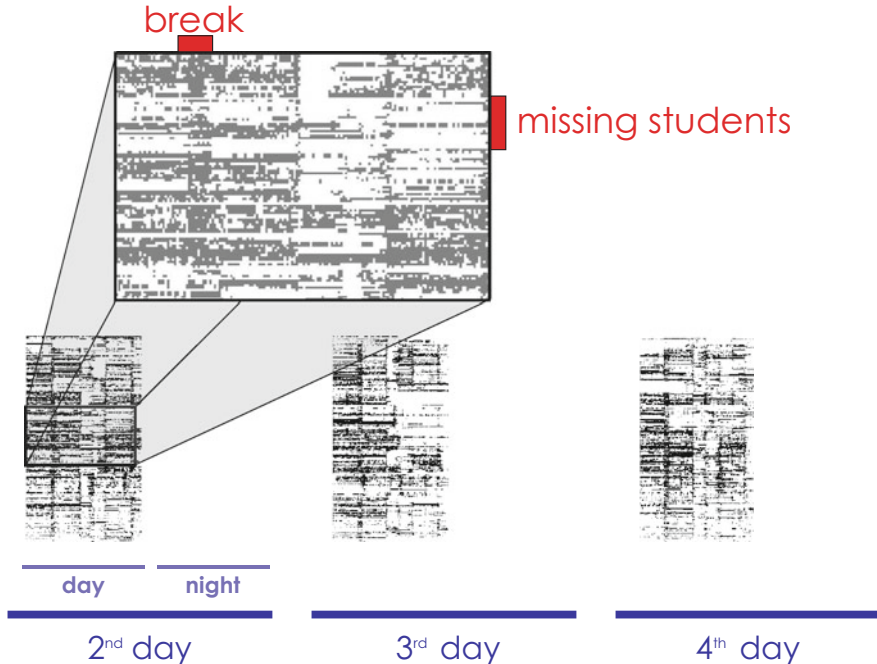


Fig. 7 Temporal activity map for high-school students for 3 days using RN re-ordering strategy. A coloured square indicates that the respective student had a social contact at that time (with the colour gradient indicating the degree $k_i(\tau)$) whereas a white square indicates absence of contact with any other students at the respective time. For all three days, contacts are typically more concentrated in the mornings and no contacts occur at nights. The temporal resolution is $\delta = 3$ min

periods of activity vs. inactivity. The main difference to the previous layout is that node activity is highlighted here. Figure 7 shows the interactions between students (high-school data set) during 3 subsequent days. Sharp transitions are observed when students start (or go home after) their studies with no interactions before or after classes. Interactions after school time could indicate strong friendship ties existing beyond the school environment.⁷ Defining the start/end times is not straightforward in real networks because one cannot easily identify when the first (or last) contact happened (this is called censoring in statistics [40]). Visualisation may improve by using the re-ordering strategy based on the first appearance of the edge (Sect. 3.2). Figure 7 also shows clusters of high activity, capturing the fact that students are divided into various classrooms and thus interactions mostly occur among classmates at certain times. Nevertheless, a relatively higher level of social interactions is observed a few hours after the start of the activity at each day that

⁷In this particular face-to-face experiment, badges were not allowed outside the school.



Fig. 8 Temporal activity map for museum visitors during 1 day using appearance re-ordering strategy. A coloured square indicates that the respective visitor had a social contact at that time (with the colour gradient indicating the degree $k_i(\tau)$) whereas a white square indicates absence of contact with any other visitors at the respective time. The red bar in the x-axis indicates the period of most network activity (most nodes are interacting). The red bar in the y-axis indicates 2 very active nodes that have relatively less intense activity during the period of high network activity (lighter gray). The temporal resolution is $\delta = 2$ min

is likely related to mandatory morning break, for playing and socialising. In day 2 and day 3, the visual analysis suggests that a group of students (not the same in each day) is missing in afternoon sessions, possibly due to self-study time or other activities in which the badges were temporarily removed. A gradient colour scale, linking temporal connectivity ($k_i(\tau)$) to node colour, helps to identify highly active nodes. Figure 8 shows for example that during a period of high connectivity in the museum (several active nodes), a few nodes interacted relatively more than others (see gradients of gray colour), even though less active nodes at those times were active at several other times (their activity is spread over time).

4.4 Dynamic Processes

A useful application of temporal visualisation is the analysis of dynamic processes on networks [22]. For example, the evolution of a diffusion process can be monitored by colouring nodes according to their dynamic state or by colouring edges to highlight specific paths. Two fundamental dynamic processes of theoretical and practical interest are the random walk and the infection (information) spread dynamics. In the random walk model, a node i can be in one out of two states at each time step τ , i.e. occupied $\phi_i(\tau) = O$ or empty $\phi_i(\tau) = E$. All network nodes but one randomly chosen node i_0 start empty at time t_0 . At each τ , the walker decides whether to move via an existing active edge to a neighbour with probability $(1 - p)$ or to remain in the current node with probability p . If there are no active neighbours at τ , the walker simply remains in the node [41, 42]. The process unfolds until $t_f = T$. In the infection dynamics, a node i can be in one out of three states at each

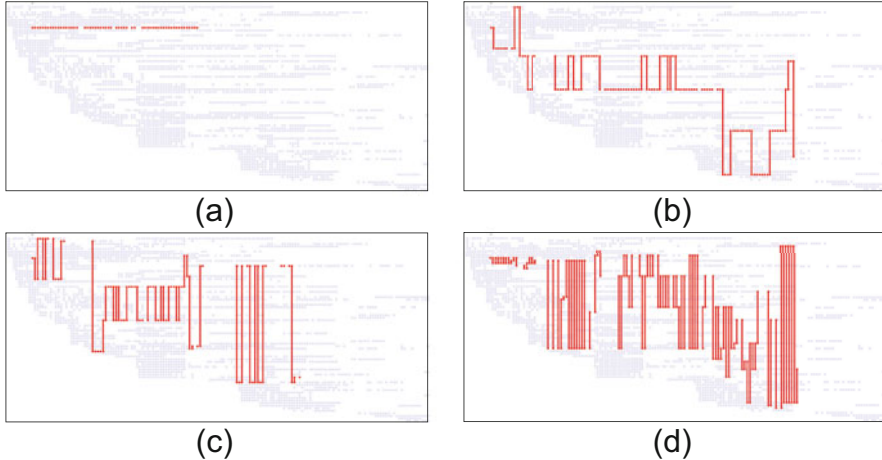


Fig. 9 Random walk trajectories for various stay probability **(a)** $p = 1$, **(b)** $p = 0.75$, **(c)** $p = 0.5$ and **(d)** $p = 0$, for the museum contact network with $\delta = 2$ min. The x-axis represents the temporal dimension. The colour red indicates the nodes occupied by the walker and the edges used to move between nodes at given times. Light gray indicates unoccupied nodes and white indicates absence of activity. Nodes are sorted by order of appearance. The seed is the same for all cases

time step τ , susceptible $\phi_i(\tau) = S$, infected $\phi_i(\tau) = I$, or recovered $\phi_i(\tau) = R$. In this case, all nodes start susceptible and one random node is chosen to be initially infected i_0 at time t_0 (patient zero or seed). In case of active neighbours at time t , an infected node i infects a neighbour j with probability β . An infected node remains infected for t_{infect} time steps and then recovers. Recovered nodes cannot be re-infected or turn back to susceptible state [43, 44].

Figure 9 shows various trajectories of a random walker starting from the same node (seed i_0) but using various probabilities p of staying in the node. In the trivial case, $p = 1$ and the walker simply remains in the initial node i_0 indefinitely. The occupancy of this node by the walker is thus seen until the last activation of the hosting node, that happens well before the end of the observation time T (Fig. 9a). However, for $p \neq 1$, the walker hops between nodes through active edges and a richer diffusion dynamics unfolds in time (Figs. 9b–d). Note that $p = 0$ implies that a walker hops as soon as an active edge becomes available and less hoping (and simpler trajectories) is observed for larger p , as expected. In these particular random cases, the walker is able to reach longer times for $p \neq 1$ in comparison to $p = 1$, and ends up in nodes that entered later in the network (compare last appearance of the walker for different p in Fig. 9). For any $p \neq 1$, the walker remains trapped between two nodes for relatively long periods, an unlikely scenario in static networks where walkers explore larger regions of the network [41]. Since nodes are ordered by time of first activation, one can also identify potential correlations between lifespan and frequency of walker visits. Similar visualisation ideas could be applied to trace higher-order random walks on temporal networks [45].

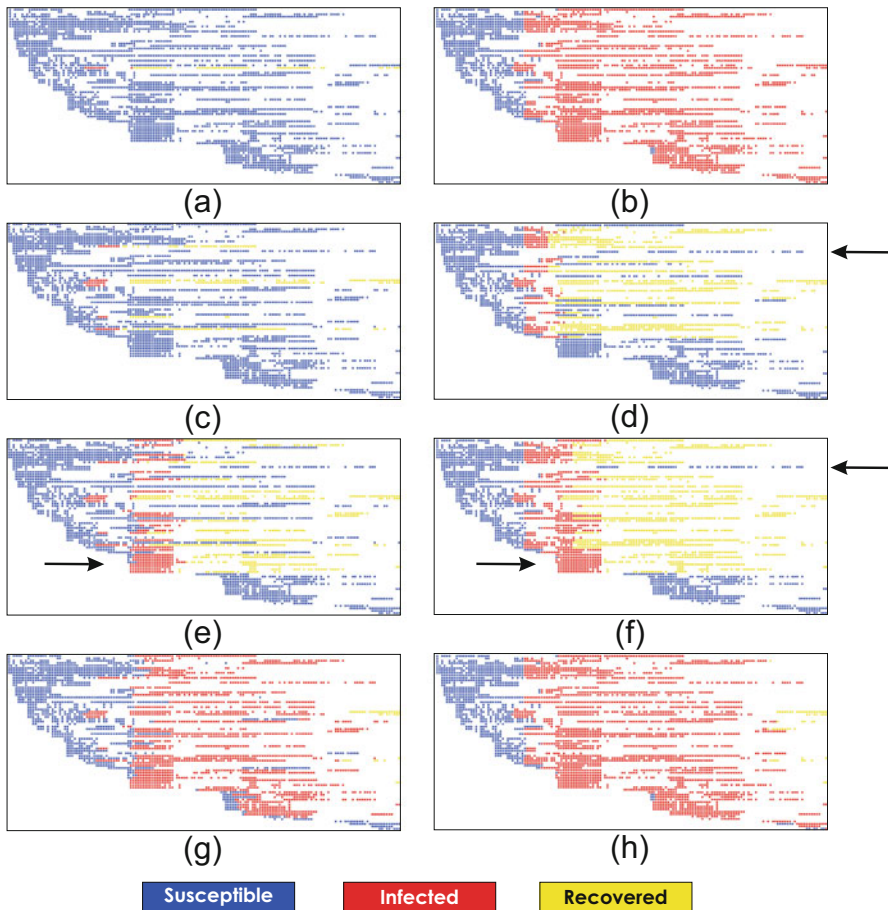


Fig. 10 Infection dynamics for (a) $\beta = 0$ and $t_r = 20$, (b) $\beta = 1$ and $t_r = \infty$, (c) $\beta = 0.01$ and $t_r = 10$, (d) $\beta = 1$ and $t_r = 10$, (e) $\beta = 0.01$ and $t_r = 20$, (f) $\beta = 1$ and $t_r = 20$, (g) $\beta = 0.01$ and $t_r = 100$ and (h) $\beta = 1$ and $t_r = 100$, for the museum contact network with $\delta = 2$ min. Nodes are sorted by order of appearance. The infection seed is the same for all cases

In more elaborated dynamic processes as the infection dynamics, a visualisation may focus on the state of nodes or on transmission paths, or even both but then likely causing cognitive overload [46]. The TAM layout emphasises the node state and is particularly helpful to identify the timings of infection events and how groups of same-state nodes evolve. Figure 10 shows the evolution of the state of all network nodes (for the museum data set) in the SIR infection dynamics for various values of β and t_r . In the trivial case ($\beta = 0$), the infection seed becomes active one more time before turning to the recovery (yellow) state (Fig. 10a). In the worst case scenario ($\beta = 1$ and $t_r = \infty$, Fig. 10b), some nodes remain susceptible for a while after joining the network however everyone eventually becomes infected in this particular

network configuration. Overall, this layout facilitates a global understanding of the impact of certain parameters in the dynamics. One may explore variations in the infection period t_r when β is fixed (Fig. 10c, e, g or Fig. 10d, f, h) or fix t_r and study the infection probability β (Fig. 10c, d, e, f or Fig. 10g, h). For example, a small increase in β or t_r generated a temporal cluster of active infected nodes (see bottom arrows in Fig. 10e, f). In the case of $\beta = 1$, one node (see top arrows in Fig. 10d, f) was active and susceptible before the epidemic outbreak and remained active and susceptible after the end of the outbreak.

The limitation of the previous layout is that information of the transmission paths, i.e. the edges through which infection events occurred, are unavailable. Those edges can be included to create a layout of transmission trees, i.e. the sequence of nodes and edges in which the infection (or information) propagates from the seed, with transparency used on non-infected nodes to reduce information load yet allowing a global view of the nodes' states (see Fig. 11 and compare with Fig. 10c–f using the same parameters). This new layout helps to identify who infected whom and the timings of these infection events. It is particularly useful to visualise the importance of certain nodes and edges to regulate the infection spread, for example, by visualising the transmission trees before and after vaccination, i.e. removal of those nodes or edges. The intensity of edge colour is also used to identify edge overlap but since infection events are rarer than the chance of having a contact in a given time step, overlap (and thus visual clutter) is less of a problem than if all active edges were shown. The layout can be further optimised by ordering nodes according to timings of infection, with earlier infected nodes positioned on the central part of

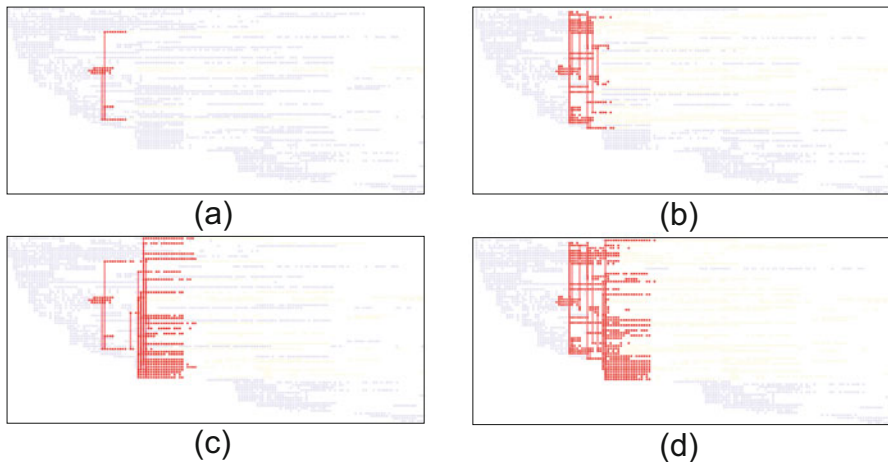


Fig. 11 Infection dynamics for (a) $\beta = 0.01$ and $t_r = 10$, (b) $\beta = 1$ and $t_r = 10$, (c) $\beta = 0.01$ and $t_r = 20$, (d) $\beta = 1$ and $t_r = 20$ for the museum contact network with $\delta = 2$ min. Nodes are sorted by order of appearance. The infection seed is the same for all cases, and the same as for Fig. 10

the layout and those infected later at more peripheral positions. This is similar to the RN algorithm (see Sect. 3.2) however using timings of infection events for ordering nodes.

5 Visual and Computational Limitations

In the temporal layout, node re-ordering methods optimise the distribution of edges, reducing edge overlap (visual clutter) and improving the visualisation. Nevertheless, 2 dimensional spatial constraints also create lengthy edges crossing several in-between nodes and hindering relevant structural information. If activity is relatively high (e.g. a couple of edges active at the same time step) and the network is large (some hundreds of nodes), re-ordering techniques may be insufficient to provide meaningful visualisation [47]. Alternative solutions under development include identifying and removing specific edges, e.g. those edges between or within network communities. Moving to 3D layouts (with 2 dimensions for space and 1 dimension for time) may also improve visualisation by disentangling overlapping edges at the cost of more information being available. The temporal activity map solution is more scalable with network size and density since it removes the issue of edges overlap. Combined with node re-ordering techniques to improve the placement of nodes, this solution may highlight relevant activity and structural patterns with thousands of nodes and any edge density (without showing the edges). The main advantage is the possibility to embed information about the network structure, dynamic processes or meta-data in each node through a colouring scheme with low computational cost.

A crucial step when studying temporal networks is the choice of the observation period (T) and the temporal resolution (δ). Both parameters affect the visualisation since the viewer is effectively looking at a static network on screen. The observation period is in principle less critical since one can zoom in/out or move the network around but since some re-ordering algorithms are based on the cumulative network measures, this period may affect the location of nodes (e.g. longer periods may imply on more edges and thus higher strength [12]). On the other hand, variations in the temporal resolution may substantially change the network structure [12, 35] and thus the information (network structure) being viewed. Although node re-ordering algorithms work for any resolution and easily accommodate all these cases, the viewer has to keep in mind the potential limitations or variations in the structure and activity when performing qualitative visual network analysis.

Since the visualisation per se is static (though can be interactive in a software, see below), the computational bottleneck is the algorithm to calculate node re-ordering, edge removal, or the dynamic process, that are done in a pre-processing stage. Therefore, computational scalability depends more on the specific choice of algorithms than on the visualisation stage. For example, the recurrent neighbours strategy is faster for small-to-medium size networks than the optimised MSV because the first is deterministic and the second runs over several configurations

(simulated annealing) to find the optimal solution [21]. For larger networks (with thousands of nodes), both methods require intensive calculations and naive solutions (e.g. appearance or lexicographic) may work relatively faster. Such computational limitations may also hamper the applicability of such methods on online visualisation of real-time data.

A free software developed in JavaTM implements all methods discussed in this chapter and is available online (www.dynetvis.com). It is multiplatform and runs over the JGraphX library.⁸ The DyNetVis system allows the user to perform interactive visual analysis of temporal networks using either structural (node-edge diagram) or temporal layout, and allows node re-ordering, changes in edge and node colours among other practical functions via interaction tools.

6 Conclusion

Network visualisation provides qualitative visual insights about the network structure to support identifying non-trivial connectivity patterns and developing new statistical measures. The visualisation of dynamic processes unfolding on the network also helps to trace trajectories, transmission paths and the evolution of the states of nodes. The visualisation of temporal networks are particularly helpful since patterns of node and edge activity are typically highly irregular in time. Various visual layouts have been proposed to view temporal networks but all have limitations due to their multiple degrees of freedom. The main challenge is that visual information scales with network size and edge density causing visual clutter due to edge overlap, node proximity and fine temporal resolution. In this chapter we explored a 2D layout where active nodes appear as circles or squares in horizontal lines and vertical lines represent active edges at specific time steps. To avoid edge overlap and to highlight connectivity patterns, colour gradients and node re-ordering strategies were implemented. An effective strategy called recurrent neighbours places highly connected nodes more centrally in the 2D layout and the less active nodes in peripheral locations. Another strategy consists on complete removal of edges and visualisation of node properties (e.g. node activity, structure or states) using colours and gradients on nodes. This layout named temporal activity map is useful to identify activity patterns such as temporal clusters of activity and periods of inactivity. The temporal activity map was also used to simultaneously visualise temporal networks and dynamic processes. This method revealed non-trivial random walker trajectories (e.g. being trapped between two nodes over time), allowed mapping of infection transmission paths and the identification of timings and directions of infection events. The temporal layouts discussed in this chapter are naturally limited to a few thousand nodes, hence alternative scalable strategies are necessary to handle Big network data. Nevertheless, these solutions

⁸Available at <https://github.com/jgraph/jgraphx>. No need of separate installation to run DyNetVis.

have a range of applications on mid-size network data such as those frequently used in social systems (friendship, proximity contacts, opinion dynamics), economics (inter-bank loan networks, transportation, cascade failures), business (enterprise partnerships, corporate board directors), public health (contact tracing, impact of vaccination/intervention, epidemics), or biology (neuronal activity, signaling), to name a few possibilities. Some ideas developed in this chapter may also help to visualise multiplex networks that can be seen as temporal networks containing a few snapshots. Future research efforts however aim to improve methods to filter edges to highlight particular temporal structures, to improve the visual analysis of larger network data sets (scalability issue) and to handle streaming networks, in which the distribution of incoming edges is unknown. The analysis of such cases may require innovative multidimensional layouts involving grouping of nodes and the complete removal of edges.

References

1. Newman, M.: Networks: An Introduction. OUP, Oxford (2010)
2. da Fontoura Costa, L., Oliveira, O.N. Jr., Travieso, G., Rodrigues, F.A., Boas, P.R.V., Antiqueira, L., Viana, M.P., Rocha, L.E.C.: Analyzing and modeling real-world phenomena with complex networks: a survey of applications. *Adv. Phys.* **60**(3), 329–412 (2011)
3. Holme, P., Saramäki, J.: Temporal networks. *Phys. Rep.* **519**, 97–125 (2012)
4. Card, S., Mackinlay, J., Shneiderman, B.: Readings in Information Visualization: Using Vision to Think. Morgan Kaufmann, Los Altos (1999)
5. Sales, T.: Llull as computer scientist, or why llull was one of us. In: Sierra, C., Fidora, A. (eds.) Ramon Llull: From the Ars Magna to Artificial Intelligence, chap. 2, pp. 25–38. Artificial Intelligence Research Institute, Barcelona (2011)
6. Moreno, J.L.: Who Shall Survive? A New Approach to the Problem of Human Interrelations. Nervous and Mental Disease Publishing Co., Washington (1934)
7. Lima, M.: Visual Complexity. Mapping Patterns of Information. Princeton Architectural Press, New York (2011)
8. Ellis, G., Dix, A.: A taxonomy of clutter reduction for information visualisation. *IEEE Trans. Vis. Comput. Graph.* **13**(6), 1216–1223 (2007)
9. Tamassia, R.: Handbook of Graph Drawing and Visualization. Chapman and Hall/CRC, London (2013)
10. Rocha, L.E.C.: Dynamics of air transport networks: a review from a complex systems perspective. *Chin. J. Aeronaut.* **30**, 469–478 (2017)
11. Barabási, A.-L.: The origin of bursts and heavy tails in human dynamics. *Nature* **435**, 207–211 (2005)
12. Rocha, L.E.C., Masuda, N., Holme, P.: Sampling of temporal networks: methods and biases. *Phys. Rev. E* **96**(5), 052302 (2017)
13. Karsai, M., Jo, H.-H., Kaski, K.: Bursty Human Dynamics. Springer, Berlin (2018)
14. Gleicher, M., Albers, D., Walker, R., Jusufi, I., Hansen, C.D., Roberts, J.C.: Visual comparison for information visualization. *Inf. Vis.* **10**(4), 289–309 (2011)
15. Beck, F., Burch, M., Diehl, S., Weiskopf, D.: The state of the art in visualizing dynamic graphs. In: Eurographics Conference on Visualization (EuroVis) (2014)
16. Sazama, P.J.: An overview of visualizing dynamic graphs. Unpublished (2015)
17. Rosvall, M., Bergstrom, C.T.: Mapping change in large networks. *PLoS One* **5**(1), e8694 (2010)

18. Rossetti, G., Cazabet, R.: Community discovery in dynamic networks: a survey. *ACM Comput. Surv.* **51**(2), 35 (2018)
19. Bach, B., Pietriga, E., Fekete, J.-D.: Visualizing dynamic networks with matrixcubes. In: *Proceedings of the 2014 Annual Conference on Human Factors in Computing Systems (CHI2014)*, pp. 877–886. ACM, New York (2014)
20. Jerding, D.F., Stasko, J.T.: The information mural: a technique for displaying and navigating large information spaces. *IEEE Trans. Vis. Comput. Graph.* **4**(3), 257–271 (1998)
21. van den Elzen, S., Holten, D., Blaas, J., van Wijk, J.J.: Dynamic network visualization with extended massive sequence views. *IEEE Trans. Vis. Comput. Graph.* **20**(8), 1087–1099 (2014)
22. Masuda, N., Lambiotte, R.: *A Guide to Temporal Networks*. World Scientific, Singapore (2016)
23. Bach, B.: Unfolding dynamic networks for visual exploration. *IEEE Comput. Graph. Appl.* **36**, 74–82 (2016)
24. Linhares, C.D.G., Travençolo, B.A.N., Paiva, J.G.S., Rocha, L.E.C.: DyNetVis: a system for visualization of dynamic networks. In: *Proceedings of the Symposium on Applied Computing, SAC '17*, (Marrakech, Morocco), pp. 187–194. ACM, New York (2017)
25. Battista, G.D., Eades, P., Tamassia, R., Tollis, I.G.: Algorithms for drawing graphs: an annotated bibliography. *Comput. Geom.* **4**(5), 235–282 (1994)
26. Behrisch, M., Bach, B., Henry Riche, N., Schreck, T., Fekete, J.-D.: Matrix reordering methods for table and network visualization. In: *Computer Graphics Forum*, vol. 35, pp. 693–716. Wiley Online Library (2016)
27. Six, J.M., Tollis, I.G.: A framework and algorithms for circular drawings of graphs. *J. Discrete Algorithms* **4**, 25–50 (2006)
28. Mi, P., Sun, M., Masiane, M., Cao, Y., North, C.: Interactive graph layout of a million nodes. *Informatics* **3**, 23 (2016)
29. Archambault, D., Purchase, H.C.: Can animation support the visualisation of dynamic graphs? *Inf. Sci.* **330**, 495–509 (2016)
30. Cornelissen, B., Holten, D., Zaidman, A., Moonen, L., van Wijk, J.J., van Deursen, A.: Understanding execution traces using massive sequence and circular bundle views. In: *15th IEEE International Conference on Program Comprehension ICPC*, pp. 49–58. IEEE Computer Society, Washington (2007)
31. Ware, C.: *Information Visualization: Perception for Design*, vol. 3. Morgan Kaufmann Publishers Inc., Los Altos (2013)
32. Mucha, P.J., Richardson, T., Macon, K., Porter, M.A., Onnela, J.-P.: Community structure in time-dependent, multiscale, and multiplex networks. *Science* **328**(5980), 876–878 (2010)
33. Holme, P., Liljeros, F.: Birth and death of links control disease spreading in empirical contact networks. *Sci. Rep.* **4**, 4999 (2014)
34. Linhares, C.D.G., Ponciano, J.R., Pereira, F.S.F., Rocha, L.E.C., Paiva, J.G.S., Travençolo, B.A.N.: A scalable node ordering strategy based on community structure for enhanced temporal network visualization. *Comput. Graph.* (2019). <https://doi.org/10.1016/j.cag.2019.08.006>
35. Ribeiro, B., Perra, N., Baronchelli, A.: Quantifying the effect of temporal resolution on time-varying networks. *Sci. Rep.* **3**, 3006 (2013)
36. Zhao, Y., She, Y., Chen, W., Lu, Y., Xia, J., Chen, W., Liu, J., Zhou, F.: EOD edge sampling for visualizing dynamic network via massive sequence view. *IEEE Access* **6**, 53006–53018 (2018)
37. Wilke, C.: *Fundamentals of Data Visualization: A Primer on Making Informative and Compelling Figures*. O'Reilly, Newton (2019)
38. Mastrandrea, R., Fournet, J., Barrat, A.: Contact patterns in a high school: a comparison between data collected using wearable sensors, contact diaries and friendship surveys. *PLOS One* **10**(9), e0136497 (2015)
39. Isella, L., Stehlé, J., Barrat, A., Cattuto, C., Pinton, J.-F., den Broeck, W.V.: What's in a crowd? analysis of face-to-face behavioral networks. *J. Theor. Biol.* **271**, 166–180 (2011)
40. Miller, R.G.: *Survival Analysis*. Wiley, London (1997)
41. Starnini, M., Baronchelli, A., Barrat, A., Pastor-Satorras, R.: Random walks on temporal networks. *Phys. Rev. E* **85**, 056115 (2012)

42. Rocha, L.E.C., Masuda, N.: Random walk centrality for temporal networks. *New J. Phys.* **16**, 063023 (2014)
43. Barrat, A., Barthélémy, M., Vespignani, A.: *Dynamical Processes on Complex Networks*. Cambridge University Press, Cambridge (2008)
44. Rocha, L.E.C., Blondel, V.D.: Bursts of vertex activation and epidemics in evolving networks. *PLOS Comput. Biol.* **9**, e1002974 (2013)
45. Scholtes, I., Wider, N., Fitzner, R., Garas, A., Tessone, C.J., Schweitzer, F.: Causality-driven slow-down and speed-up of diffusion in non-markovian temporal networks. *Nat. Commun.* **5**, 5024 (2014)
46. Huang, W., Eadesband, P., Hong, S.-H.: Measuring effectiveness of graph visualizations: a cognitive load perspective. *Inf. Vis.* **8**(3), 139–152 (2009)
47. Keim, D.: Visual exploration of large data sets. *Commun. ACM* **44**(8), 38–44 (2001)

Weighted Temporal Event Graphs



Jari Saramäki, Mikko Kivelä, and Márton Karsai

1 Introduction

There are two key reasons behind the success of the temporal networks framework [1, 2]. Both have to do with the rich additional information brought by knowing the specific times of interactions between nodes. First, the times of interaction events and their correlations contain detailed information about the dynamics of the entities that form the network. Consider, as an example, studies in computational social science that build on data of human communication: the time stamps of communication events carry far more information on human behaviour than any static network mapping would (see, e.g., [3–7]). Second, the times of events and their correlations can strongly influence dynamical processes taking place on networks. Their effect can be so strong that the static-network picture can become invalid for some dynamical processes [3, 8, 9]. Therefore, more often than not, the times of interactions simply have to be taken into account if one wants to obtain an accurate understanding of the dynamics of processes that unfold on temporal networks.

For both of the above goals—extracting information from the network itself and understanding how the network affects dynamical processes—new kinds of mathematical and computational tools are required. While many static-network

J. Saramäki (✉) · M. Kivelä

Department of Computer Science, Aalto University School of Science, Espoo, Finland

e-mail: jari.saramaki@aalto.fi; mikko.kivela@aalto.fi

M. Karsai

Department of Network and Data Science, Central European University, Budapest, Hungary

Univ Lyon, ENS de Lyon, Inria, CNRS, Université Claude Bernard Lyon 1, LIP, Lyon, France
e-mail: karsaim@ceu.edu

concepts can be extended to temporal networks (at least roughly), the additional degree of freedom due to the temporal dimension complicates things. Computing network measures for temporal networks often requires approaches that are very different from the static case. But even simply defining the measures properly may be less than straightforward. Consider, e.g., shortest paths between nodes: in a static, unweighted network, the only attribute of a shortest path (if it exists) is its length, and it is readily discovered by a breadth-first search. In temporal networks, when considering shortest paths, one has to define “short” first—does it mean the fastest path, or the one with the smallest number of events, or maybe corresponding to the shortest static-network path? Then, additionally, one has to choose the time frame that one is interested in, as paths are fleeting entities that are only brought about by their constituent events: even if there is a path now, there may be none a second later. And then, finally, one has to devise a computational method for empirical data that extracts the shortest temporal paths in a reasonable amount of time.

Nevertheless, it would be convenient to repurpose computational and theoretical methods developed for analyzing static networks for temporal-network studies, because there is an abundance of such methods. This would become possible, e.g., if one was able to cast temporal networks as static entities so that the properties of those static entities correspond to the properties of the original temporal networks (though not necessarily in an one-to-one way). Generally speaking, this is not straightforward; some approaches have been introduced in the literature that typically focus on some chosen subset of the properties of temporal networks (see, e.g., [10]).

In this Chapter, we discuss an approach that maps temporal-network structure onto a weighted static event graph [11] that is directed and acyclic and whose weights encode the time differences between events. This mapping is done so that time-respecting paths of the original network are preserved. Temporal-network event graphs are analogous to line graphs of static networks [12]. In the type of event graphs discussed here, nodes represent events of the original temporal network, directed links connect events that share a node in the temporal network so that their direction follows the direction of time, and the link weights indicate the time difference between the two events that the link connects. As a concrete example, if A calls B who then calls C, the weighted event graph would have two nodes (the AB call and the BC call), so that the AB node is connected to the BC node with a directed link whose weight is the waiting time from the AB call to the BC call.

As its main strength, this approach encodes temporal information as a static network structure. This then allows extraction of temporal-network structures that are constrained by the time differences Δt between successive events, from temporal motifs to time-respecting paths whose events have to follow one another within some time limit and to temporal components defined by connectivity through such time-respecting paths. Additionally, one can use known static-graph-based methods and find these structures in a way that is computationally extremely efficient as compared to brute-force methods applied to the original temporal network. For example, one can use the method developed for percolation studies [13] where one performs sweeps of activating one connection at a time, in this case in the

order of increasing time difference Δt . This method is computationally much more efficient compared to brute-force breadth-first-search approaches, which have been used in temporal-network studies. Such approaches were also used in conventional percolation studies before more efficient methods were discovered [14].

Being able to quickly obtain temporal-network paths and components and sweep through a range of constraints is particularly useful for studying spreading or transportation processes that have to leave a node within some time limit Δt . To mention a few, such processes include variants of the common models of contagion, such as Susceptible-Infectious-Recovered and Susceptible-Infectious-Susceptible, where the recovery/infectiousness time is assumed to be constant or has a clear upper bound. Other types of dynamics include social contagion where information or rumours age, ad-hoc message passing by mobile agents that keep the message only for a limited time, and routing of passengers in transport networks, where both lower and upper limits on the possible or acceptable transfer time may exist.

Once the weighted event graph has been constructed from the temporal network, one can quickly extract subnetworks that correspond to chosen values of Δt ; we shall discuss how this is done below. These subgraphs, being static, can then be approached using static-network methods and algorithms. There can be additional computational advantages because these subnetworks are directed and acyclic, and there are fast methods developed for directed acyclic graphs. Further, as discussed above, because the event graph encodes all time differences between events, one can quickly sweep through a range of differences to see how the maximum (or minimum) difference affects the outcome, for example the existence of temporally connected components.

This Chapter is structured as follows. We begin by providing definitions for concepts related to temporal adjacency and connectivity that are required for constructing the event graphs. We then continue by discussing how temporal networks can be mapped to weighted event graphs, both in theory and in practice. We next talk about how to interpret the structural properties of weighted event graphs: how their topological features (such as directed paths or weakly connected components) map back onto the original temporal networks. This discussion is followed by examples of applications of this framework to temporal motif analysis and to temporal-network percolation studies. Finally, we present our conclusions and discuss possible future directions.

2 Mapping Temporal Networks Onto Weighted Event Graphs

2.1 Definitions: Vertices, Events, Temporal Network

Let us consider a temporal network $G = (V_G, E_G, T)$, where V_G is the set of vertices and $E_G \subset V_G \times V_G \times [0, T]$ is the finite set of interaction events between the vertices with known times, so that the interactions take place within some limited

period of observation $[0, T]$ that can also be considered to be the lifetime of G . We denote an interaction event—simply called an “event” from now on—between vertices i and j at time t with $e(i, j, t)$. Please note that in the following, we require that one node is only allowed to participate in one event at any given point in time.

Note that depending on the context, the events may be directed (e.g., representing an email from i to j in email data) or undirected (e.g., representing a face-to-face conversation between two persons). This choice has consequences on dynamical processes taking place on top of the temporal network: in the case of social contagion, for example, one email or one text message carries information one way only, while a face-to-face conversation can carry information both ways.

There are also cases where the events have a non-zero *duration* that has to be taken into account in temporal-network studies. Examples include the flights in a passenger’s route in an air transport network and phone calls in a communication network—in both cases, a new event (the connecting flight, the next phone call) cannot begin before the first event is finished. When the event duration needs to be taken into account, events are defined as quadruples, $e(i, j, t, \tau)$, where τ indicates the duration of the event.

Depending on the type of events in a temporal network, the time difference is defined in slightly different way:

Definition 1 *Time difference between events.* Given two events e_1 and e_2 , their time difference $\delta t(e_1, e_2)$ is either the difference in times $\delta t(e_1, e_2) = t_2 - t_1$ for *events without duration* or the time from the end of the first event to the start of the second one $\delta t(e_1, e_2) = t_2 - t_1 - \tau_1$ for *events with duration*.

Note that these two definitions become the same if the events have zero duration.

2.2 Definitions: Adjacency and Δt -Adjacency

Our goal is to investigate larger temporal-network structures, from mesoscopic to macroscopic entities, that arise out of the topological and temporal correlations of the network’s constituent events. We begin by defining criteria for events being topologically and temporally close to one another and then move on to defining larger entities based on these criteria. The following concepts of temporal adjacency, temporal connectivity, and temporal subgraphs are the building blocks for temporal-network event graphs as well as their substructures from components to temporal motifs. The concept of temporal adjacency also leads straightforwardly to the notion of time-respecting paths.

Definition 2 (Temporal Adjacency) Two events $e_1(i, j, t_1)$ and $e_2(k, l, t_2)$ are *temporally adjacent*, denoted $e_1 \rightarrow e_2$, if they share (at least) a node, $|\{i, j\} \cap \{k, l\}| > 0$, and they are consecutive (but not simultaneous) in time, i.e. $\delta t(e_1, e_2) > 0$.

Definition 3 (Δt -Adjacency) Two events e_1 and e_2 are Δt -adjacent, denoted $e_1 \xrightarrow{\Delta t} e_2$, if they are temporally adjacent and the time difference between them is $\delta t(e_1, e_2) \leq \Delta t$.

Temporal adjacency and Δt -adjacency are always directed regardless of whether the events themselves are directed or not, and their direction follows the direction of time, from the event that took place first to the event that took place next. Please note that here we use a directed definition of adjacency unlike in [15–17] for reasons that will become apparent later.

Depending on the problem at hand, one may wish to include additional constraints in the definition of temporal adjacency. If the original events are directed and this directionality is important, e.g., because it affects information flows, it can be directly incorporated into the definition of temporal adjacency, so that $e(i, j, t)$ and $e(j, k, t + 1)$ are considered adjacent, while $e(i, j, t)$ and $e(k, j, t + 1)$ are not (see Definition 2). This will also affect time-respecting paths defined according to Definition 10. It is possible to introduce further constraints, e.g., ignoring return events (non-backtracking events only) which might be useful for modelling certain types of spreading dynamics. In this case, the pair $e(i, j, t)$ and $e(j, i, t + 1)$ should not be added to G .

One can also consider allowing simultaneous interactions of the same node by introducing *hyper-events* and an adjacency relationship between them for the definition of a hyper-event graph. In this extension, events happening at the same time and sharing nodes may be grouped in a hyper-event, which this way represents a set of simultaneous events as a single object. Two hyper-events taking place at times t and t' are adjacent if they are consecutive ($t < t'$) and share at least one node from the set of nodes they involve [18].

2.3 Definitions: Temporal Connectivity and Temporal Subgraphs

To study the mesoscopic building blocks of temporal structures, we need to use their local connectivity patterns for identifying meaningful temporal subgraphs in their fabric. Following the approach of [15], we'll use the concept of temporal adjacency defined above to introduce temporal connectivity and temporal subgraphs.

Definition 4 (Weak Temporal Connectivity) Two events e_i and e_j are temporally weakly connected, if without considering the directionality of adjacency, there is a sequence of temporally adjacent events between them.

Definition 5 (Weak Δt -Connectivity) Two events e_i and e_j are weakly Δt -connected if they are temporally connected through Δt -adjacent events, without considering the directionality of Δt -adjacency.

The above definitions of temporal connectivity are weak in the sense that the directions of adjacency do not matter. Their motivation is to ensure that temporal subgraphs—as defined below—are connected both topologically and temporally.

Definition 6 (Connected Temporal Subgraphs) A connected temporal subgraph consists of a set of events where all pairs of events are weakly temporally connected.

Note that in the above definition we have left out the word “weak” because there cannot be strong connectivity between temporal network events (there cannot be any loops in time).

Definition 7 (Δt -Connected Temporal Subgraphs) A Δt -connected temporal subgraph consists of a set of events where all pairs of events are weakly Δt -connected. The subgraph is called *valid* if no events are skipped when constructing the subgraph; i.e., for each node’s time span in the subgraph, all events that can be included are included.

Definition 8 (Maximal Valid Connected Subgraphs) A maximal valid connected temporal subgraph is a connected temporal subgraph that contains all events that can be added to it such that all its event pairs are temporally connected.

Definition 9 (Maximal Valid Δt -Connected Subgraphs) A maximal valid Δt -connected temporal subgraph is a Δt -connected temporal subgraph that contains all events that can be added to it such that all its event pairs are Δt -connected.

Note that by definition, maximal valid Δt -connected subgraphs are themselves subgraphs of maximal valid temporal subgraphs.

2.4 Definitions: Time-Respecting Path and Δt -Constrained Time-Respecting Path

As the final building block before discussing weighted event graphs, we will next focus on temporal-network paths that define which nodes can reach one another and when. Similarly to static-network paths that are sequences of nodes joined by edges, the events of temporal networks form paths in time that connect nodes. For a temporal-network path to be meaningful, it has to respect the direction of time:

Definition 10 (Time-Respecting Path) An alternating sequence of nodes and undirected events $P = [v_1, e_1(i_1, j_1, t_1), \dots, e_n(i_n, j_n, t_n), v_{n+1}]$ is a time-respecting path if the events are consecutive in time and each consecutive pair of events is temporally adjacent, $e_k \rightarrow e_{k+1}$ for all $k < n$, and $v_k, v_{k+1} \in \{i_k, j_k\}$, such that $v_k \neq v_{k+1}$. If the events are directed, then additionally each event’s target node must be the source node of the next event on the path, $j_k = i_{k+1}$. For notational convenience, we can omit the nodes, defining a time-respecting *event path* $P_e = [e_1(i_1, j_1, t_1), \dots, e_n(i_n, j_n, t_n)]$.

For events with zero duration, $P_e = [e_1(i, j, t_1), e_2(j, h, t_2), e_3(h, l, t_3)]$ is a time-respecting path if $t_1 < t_2 < t_3$, in other words, if $\delta t = t_{k+1} - t_k > 0 \forall k = 1, 2, e_k \in P_e$. The inequality follows from the requirement that vertices only participate in at most one event at a time. For events with durations, the next event on the path cannot begin before the first event is finished: $P_e = [e_1(i, j, t_1, \tau_1), e_2(j, h, t_2, \tau_2), e_3(h, l, t_3, \tau_3)]$ is a time-respecting path when $t_1 + \tau_1 < t_2$ and $t_2 + \tau_2 < t_3$. That is, if $\delta t = t_{k+1} - t_k - \tau_k > 0 \forall k = 1, 2, e_i \in P_e$. Note that time-respecting paths are always directed, no matter whether the events themselves are directed or not, and their direction follows the arrow of time.

Finally, as a special case of time-respecting paths, we define a subset of them where the events have to follow one another within some specific time limit Δt .

Definition 11 (Δt -Constrained Time-Respecting Paths) A time-respecting path is Δt -constrained if all its consecutive pairs of events are Δt -adjacent, i.e., all consecutive events follow one another with a time difference of no more than Δt : $\delta t(e_k, e_{k+1}) \leq \Delta t \forall k < n$.

2.5 The Weighted Event Graph D

Armed with the above definitions, our aim is now to map the original temporal network onto a static representation that retains information of the time-respecting paths of the network (Definition 10) as well as the time differences δt between events on such paths. For a temporal network $G = (V_G, E_G, T)$, let $A_G = \{(e_i, e_j) | e_i \rightarrow e_j; e_i, e_j \in E_G\} \subset E_G \times E_G$ be the set of all temporal adjacency relations between the events E_G of G (see Definition 2). We are now ready to define the weighted event graph:

Definition 12 (Weighted Event Graph) The weighted event graph of a temporal network G is a weighted graph $D = (V_D, L_D, w)$, where the nodes $V_D = E_G$, links $L_D = A_G$, and the weights of the edges are given by $w(e_i, e_j) = \delta t(e_i, e_j)$.

In other words, the weighted event graph D is a directed graph whose vertices map to the events of G , whose directed links L_D map to the adjacency relations $e \rightarrow e'$ between G 's events, and whose link weights W indicate for each adjacency relation the time difference δt between the two events. For a schematic example of how D is constructed, see Fig. 1.

Because of how the weighted event graph D is constructed, it is directed, with the direction of its links following the direction of time. Consequently, because there cannot be any loops in time, it is also acyclic and therefore a DAG (Directed, Acyclic Graph). This provides certain computational advantages.

Note that in this mapping, *isolated* events, that is, single events connecting pairs of nodes that have no other events in G , become isolated zero-degree nodes of the event graph D . It may be convenient to entirely remove such zero-degree nodes from D .

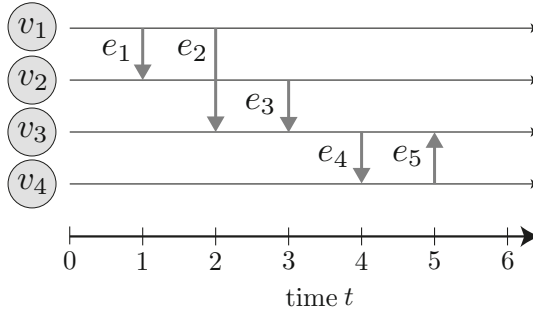
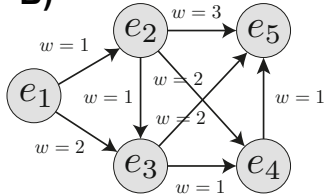
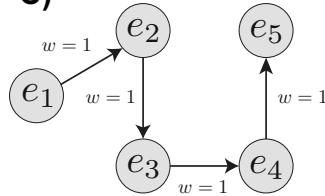
A)**B)****C)**

Fig. 1 Constructing the weighted event graph D . Panel (a) shows the timeline representation of the original temporal network G with vertices v_1 , v_2 , v_3 , and v_4 , and events $e_1 \dots e_5$. Panel (b) shows the weighted event graph D that corresponds to G . Panel (c) displays the thresholded version $D_{\Delta t}$ with $\Delta t = 1$

2.6 Constructing the Weighted Event Graph Computationally

The weighted event graph presentation D of an empirical temporal network G can be constructed computationally by inspecting the timeline of the events of each of G 's nodes separately. For practical purposes, to save memory, we recommend setting a maximum value of the time difference between events, Δt_{\max} , above which two events will not be connected in D . Typically, the problem at hand yields a natural time scale, e.g. when studying processes of contagion it is not necessarily meaningful to connect events that take place several months apart. However, if memory consumption is not a problem, one can use the entire available time range and set $\Delta t_{\max} = T$, where T is the largest time in the data set.

As the temporal adjacency of two events requires that the events share at least a single temporal-network node, it is convenient to compute the adjacencies around each of these nodes separately. For instantaneous events (that is, events that have no durations), one can construct a time-ordered sequence of events containing node i : $\{e_{i1}, e_{i2}, \dots, e_{ik}\}$. Then, it is straightforward to iterate over this sequence: begin at each event e_{il} and scan forward until the time cap Δt_{\max} is met, that is, $t_{in} - t_{il} > \Delta t_{\max}$. While scanning, connect each intermediate event e_{im} with the focal event with the weight $w_{il,im} = \delta(e_{il}, e_{im}) = t_{im} - t_{il}$ (unless they are already connected

by a previous sweep, which is possible for repeated events between the same pair of nodes). Rather similar but slightly more complicated algorithms can be used for temporal networks with events that have durations or even higher-order events that contain more than two nodes.

Creating these sequences of events and sorting them can be done in $\mathcal{O}(|E_G| \log |E_G|)$ time. Because each step of the algorithms yields one connection in D (note that some links may be visited twice), the total runtime of the algorithm is $\mathcal{O}(|E_G| \log |E_G| + |E_D|)$. However, even though the computation of event graphs is quite economic, this representation can have significantly higher memory complexity than the original temporal network representation. While a temporal network can be represented as an event sequence, which requires $\mathcal{O}(|E_G|)$ of memory, event graphs can occupy way more memory than such sequences. In the worst case, their memory complexity is $\mathcal{O}(|E_G|a)$, where a is the maximum number of events a node participates in.

If one is only interested in the connectivity, that is, in knowing whether there is a path between two events regardless of the rest of the paths, then it is possible to use the directed and acyclic nature of the event graph D as an advantage when doing the computations. The directed connectivity in a DAG is a transitive relationship, which means that one can always remove edges whose source and target nodes are connected by some other path without affecting the overall connectivity (weak or directed). Taken to the extreme, this will lead to the *transitive reduction* of D . For all edges removed in this way, the weight of the removed edge is smaller than the weights of the edges in the indirect path. This is a useful fact when thresholding the network (as is done in Sect. 2.7).

A computationally convenient way of removing some (but not necessarily all) of the transitively redundant edges from D is to simply stop the above described algorithm after the first iteration for each node [12]. This trick will only work for weighted temporal event graphs built with undirected adjacency relations, but it will bound the out-degree of the nodes to 2, which can dramatically reduce the time and memory complexity of the network creation algorithms in some cases.

2.7 Thresholding the Weighted Event Graph

A key strength of the weighted event graph approach is that the event graph D can be quickly thresholded so that the resulting graph $D_{\Delta t}$ only contains directed links between events that follow one another within a time Δt in the original temporal network G . Formally, $D_{\Delta t}$ is defined as follows: let $G = (V_G, E_G, T)$ be a temporal network and $A_{G, \Delta t} \subset E_G \times E_G$ the set of all Δt -adjacency relations between its events E_G . We can now define thresholded event graph Δt :

Definition 13 (Thresholded Event Graph $D_{\Delta t}$) The thresholded event graph $D_{\Delta t}$ of G is the graph $D_{\Delta t} = (V_{D_{\Delta t}}, L_{D_{\Delta t}}, w)$ with vertices $V_{D_{\Delta t}}$, directed links $L_{D_{\Delta t}}$, and link weights $W_{D_{\Delta t}}$, so that $V_{D_{\Delta t}} = E_G$, $L_{D_{\Delta t}} = A_{G, \Delta t}$, and $w(e_i, e_j) = \delta t(e_i, e_j) \leq \Delta t$.

In other words, $D_{\Delta t}$'s nodes are again vertices of G , its directed links are Δt -adjacency relations between the events of G , and its link weights are the time differences δt between Δt -adjacent events where by definition $\delta t \leq \Delta t$. Therefore, $D_{\Delta t}$ is a subgraph of D that only contains links between events that follow one another within $\delta t \leq \Delta t$.

While $D_{\Delta t}$ can in principle be constructed directly from G using Δt -adjacency relations from the beginning, this is not the fastest approach if one wants to vary Δt . Rather, it is much faster to first construct D up to the maximum Δt_{\max} and then threshold it to $D_{\Delta t}$ by discarding all links with weights above the chosen value of Δt . This is how the thresholded weighted event graph $D_{\Delta t}$ is always constructed in practice.

Typical use cases for the thresholded event graph $D_{\Delta t}$ include setting maximal values of the allowed time difference between events to account for processes such as deterministic SIR (Susceptible-Infectious-Recovered) or SIS (Susceptible-Infectious-Susceptible), defined so that an infectious node can only infect other nodes through events that take place within a certain constant time since the time of its infection. For modelling certain transport processes, e.g. passenger trips through public transport networks or the air transport network, limiting the allowed range of δt from both above and below might be appropriate instead of using an upper limit Δt only. In such cases, the lower limit would indicate the shortest possible transfer time between vehicles, and the upper limit would correspond to the maximum time that the passengers are willing to wait for their connection.

It is often useful to sweep through a range of allowed values of δt , as in the temporal-network percolation studies discussed later in this Chapter. When thresholding so that all links of D with weights below the limit Δt are retained while varying Δt , one can obtain huge savings in computational time by the following procedure: (1) order the links of D in increasing order of weight, (2) begin with an empty network, (3) add links one by one, (4) after each link addition, mark down current the threshold value Δt and compute the quantities of interest such the sizes of components in the network. Here, one can easily and quickly keep track of component sizes by initially assigning each node to its own component and then always checking if the newly entered link merges two components or not. In fact, with the help of disjoint-sets forest data structure, one does not even need to actually construct the network: it is enough to keep track of the component mergings and their sizes. This procedure is similar to the ones used for analysing connectivity of static networks in percolation studies [13, 19].

3 How to Interpret and Use Weighted Event Graphs

3.1 How the Basic Features of D and $D_{\Delta t}$ Map onto Features of G

Let us begin dissecting the weighted event graphs by mapping out simple correspondences between some features of D and features of G . In the following, for the sake of simplicity, we shall consider the original temporal network G 's events as undirected and instantenous. Further, we assume that the weighted event graph D has been constructed using the whole available time range, that is, with time differences up to $\Delta t_{\max} = T$. By definition, the thresholded version of the event graph $D_{\Delta t}$ only contains links between Δt -adjacent events, that is, events with time differences less than Δt .

First, as already evident, the elements of D map to the elements of G so that the nodes of D are events in G , the links of D are temporal adjacency relations between the events of G , and the link weights of D indicate the times between adjacent events in G . The *in- and out-degrees* of a node of D indicate the numbers of *temporal adjacency relations* between the corresponding event of G and previous/future events of the two nodes that the event connects: the in-degree of node e_i of D (event e_i of G) is the number of events that took place earlier than e_i and involved either or both of the connected nodes. The out-degree is the number of similar future events. For $D_{\Delta t}$, the in- and out-degrees of nodes correspond to the numbers of past and future events of the event's endpoint nodes in G within a time Δt . This latter property could be useful, e.g., for studying temporal threshold models (see, e.g., [20–22]) where the process of contagion is triggered by infection from multiple sources within some short time range.

Due to D 's construction, a *directed path* in D is a *time-respecting path* in G , and vice versa. If we define (without the loss of generality) a vertex path P_v in a graph as a sequence of vertices joined by an edge, then we can formalize this relationship:

Theorem 1 (Path Equivalence) *A path P is a vertex path in D if and only if P is a time-respecting event path in G .*

Put in another way, if $\mathcal{P}_v(D)$ is the set of all vertex paths in the graph D , and $\mathcal{P}_e(G)$ is the set of all time-respecting event paths in G , then $\mathcal{P}_v(D) = \mathcal{P}_e(G)$.

For $D_{\Delta t}$, the corresponding time-respecting path in G is in addition Δt -constrained and so the time difference between its consecutive events is always less than Δt (see Definition 11).

Theorem 2 (Constrained Path Equivalence) *A path P is a vertex path in $D_{\Delta t}$ if and only if P is a Δt -constrained time-respecting event path in G .*

Now, if in addition we denote by $\mathcal{P}_e(G, \Delta t)$ the set of all Δt -constrained time-respecting event paths in G , then $\mathcal{P}_v(D_{\Delta t}) = \mathcal{P}_e(G, \Delta t)$.

If the events are instantaneous, then, additionally, the sum of link weights of a path in D equals the *latency* or *temporal distance* of the corresponding path

in G , i.e., its duration. This property can be rather useful: e.g. for undirected, instantaneous events, the lowest-weight path from e_i to e_j in D equals the fastest time-respecting path in G from event e_i to event e_j (again, expressing time-respecting paths in terms of events rather than nodes). Hence, it is possible to directly use D for computing centrality measures that are defined in terms of time-respecting paths or shortest time-respecting paths.

Because of the above, *the set of downstream nodes in D* reached by following the directed links of D from its node e_i equals the reachable set of event e_i in G , in other words, the set of all events in G that can be reached from e_i through time-respecting paths (its “future light-cone”). Likewise, *the set of upstream nodes* that can be reached by following D ’s links in reverse direction equals the set of all events in G that can lead to e_i through time-respecting paths: the set of events that may influence e_i (“past light-cone”). For Δt , the sets of upstream/downstream nodes come with the additional constraint that they must be reachable through Δt -constrained time-respecting paths.

Finally, the weakly connected components of D (more on components later) correspond by definition to maximal valid temporal subgraphs in G (Definition 8); for $D_{\Delta t}$, the weakly connected components correspond to maximal valid Δt -connected subgraphs (Definition 9).

All the above correspondences are summarized in Table 1 for D and in Table 2 for $D_{\Delta t}$.

3.2 Temporal Motifs and D

The concepts of Δt -adjacency, Δt -connectivity and temporal subgraphs are intimately related to *temporal motifs* [15–17]. The concept of *network motifs* was originally introduced for static networks by Milo et al. [23] in 2002. They defined

Table 1 Correspondence between features of the weighted event graph D and the original temporal graph G

Feature in D	Feature in G
Node V_D	Event E_G
Link L_D	Temporally adjacent pair of events $e_1 \rightarrow e_2$
Link weight w	Time difference δt between adjacent events
In-degree k_{in}	# of previous events of the event’s endpoint nodes
Out-degree k_{out}	# of future events of the event’s endpoint nodes
Directed vertex path P_v	Time-respecting event path P_e
Sum of weights on path P	Duration of time-resp. path P (if events instantaneous)
Set of downstream nodes for v_D	Set of events reachable from e_G (“future light-cone”)
Set of upstream nodes for v_D	Set of events that can influence event e_G (“past light-cone”)
Weakly connected component	Maximal valid temporal subgraph

Table 2 Correspondence between features of the Δt -thresholded event graph $D_{\Delta t}$ and the original temporal graph G

Feature in $D_{\Delta t}$	Feature in G
Node v_D	Event e_G
Link l_D	Δt -adjacent pair of events $e_1 \xrightarrow{\Delta t} e_2$
Link weight w	Time difference δt between adjacent events
In-degree k_{in}	# of previous events of the event's endpoint nodes within Δt
Out-degree k_{out}	# of future events of the event's endpoint nodes within Δt
Directed vertex path P_v	Δt -constrained time-respecting path P_e
Sum of weights on path P	Duration of time-resp. path P (if events instantaneous)
Set of downstream nodes for v_D	Set of events reachable from e_G through Δt -constrained time-respecting paths
Set of upstream nodes for v_D	Set of events that can influence event e_G through Δt -constrained time-respecting paths
Weakly connected component	Maximal valid Δt -connected subgraph

network motifs as classes of isomorphic induced subgraphs with cardinality higher in the data than in a reference system, usually the configuration model. Milo et al. showed that similar networks had similar characteristic network motifs, suggesting that motif statistics are informative of the function of the system and could be used to define universality classes of networks [24].

Similarly to static-network motifs, temporal motifs are one way of looking at frequent, characteristic patterns in networks. In this case, the patterns are defined in terms of both topology and time. For temporal motifs, a natural starting point is to use the definition of Δt -connected subgraphs (Definition 7), and to look at temporal-network entities where a sequence of interaction events unfolds in the same way. As an example, the sequence where A calls B calls C calls A forms a triangular Δt -connected subgraph if all calls follow one another with a time difference of no more than Δt . Note that here we consider the events to be directed, but using undirected events is also possible.

Such temporal-topological patterns reflect the dynamics of the system in question. Therefore, their characterization can improve our understanding of various complex systems, e.g., of temporal networks whose structure reflects the nature of human social interactions and information processing by groups of people. As an example, Ref. [17] showed that there is a tendency of similar individuals to participate in temporal communication patterns beyond what would be expected on the basis of their average interaction frequencies or static-network structure, and that the temporal patterns differed between dense and sparse regions of the network. These observations relied on the timings of the communication events, reflected in their Δt -connectivity.

Temporal motifs are formally defined as equivalence classes of isomorphic Δt -connected, valid temporal subgraphs (Definition 7), where the isomorphism takes into account both the topology of the subgraph and the temporal order of events.

With this definition, the two-call sequences A calls B calls C and D calls E calls F both belong to the same two-event equivalence class (if the Δt -adjacency condition is met).

The temporal-topological isomorphism problem can be solved using a trick that combines the event graph approach presented in this Chapter with the topology of the subgraph in the original network: a “virtual” node is added onto each (event) link, analogous with an event node in D . This virtual node is then connected with a directed arrow to the event that immediately follows it [15, 16]; this is a limited version of temporal adjacency, as only the next event is considered. The directed arrows between the virtual nodes determine the order of events in the subgraph. The virtual nodes are then assigned a “color” different than the original nodes, and the isomorphism problem is finally solved using static-network algorithms for directed, coloured graphs, such as Bliss [25].

The procedure for obtaining temporal-motif statistics from empirical temporal networks with time-stamped events is as follows [15], for a given value of Δt and a chosen motif size s measured in events:

- i Find all maximal Δt -connected subgraphs E_{\max}^* of G .
- ii Find all valid temporal subgraphs $E^* \subset E_{\max}^*$ of size s .
- iii Solve the isomorphism problem to find equivalence classes for all E^* .
- iv Count the number of motif instances in each equivalence class, and compare against a chosen null model.

For details including pseudocode for the required algorithms, we refer the reader to [15, 16].

Here, if one wants to compare motif statistics for a range of values of Δt , as is often the case, the weighted event graph approach helps to substantially reduce computational time for step (i) of the above procedure. While it is possible to generate the maximal Δt -connected subgraphs for each value of Δt separately from G ’s events using brute force, the threshold sweep approach outlined in Sect. 2.7 is a much better solution.

With this approach, one simply needs to generate the weighted event graph D and then threshold it by discarding all edges with weights above each Δt . If one wants to compute motif statistics for, say $\Delta t_1 < \Delta t_2 < \dots < \Delta t_{\max}$, the fastest way is to begin with an empty network and sort links by increasing weight. Then, one add links up to link weight Δt_1 and either store $D_{\Delta t_1}$ or compute the quantities of interest, then add more links up to Δt_2 and do the same, and repeat up to Δt_{\max} . Note that here, one does not initially need to construct the whole D which might cause memory problems: building it up to $\delta t = \Delta t_{\max}$ is sufficient.

3.3 Components of D and Temporal-Network Percolation

3.3.1 Measuring Component Size

Let us next discuss the components of D (and $D_{\Delta t}$) in more detail. First, because the event graph D is directed, the usual complications of defining components in directed networks apply. However, because D is also acyclic, there cannot be any strongly connected components, where all nodes are reachable from all other nodes. Therefore, connected components of D ($D_{\Delta t}$) can only be weakly connected by definition.

For the purposes of our interest, we can focus on three types of components: (i) maximal *weakly connected* components of D , where all nodes of D are joined by a path if the directions of D 's links are ignored and no more nodes can be added, corresponding to maximal valid temporal subgraphs of G (Definition 6); (ii) maximal *out-components*, uniquely defined for each node v_D of D , so that all nodes in the out-component can be reached from the focal node v_D , and (iii) maximal *in-components*, again defined uniquely for each v_D , so that the focal node can be reached from all of the component's nodes. These definitions do not change if we use $D_{\Delta t}$ (however, the thresholded $D_{\Delta t}$ is of course expected to have a different component structure, generally with more components than D). In the following, we will for simplicity talk about D only, but everything holds for $D_{\Delta t}$ as well.

Let us next discuss the properties—in particular, the concept of size—for components of D defined using any of the above definitions.

First, the most straightforward way to define component size is to count the number $S_E(\mathbb{C})$ of the event graph D 's nodes that belong to the component \mathbb{C} . This is equal to the number of events in the original temporal network G that belong to the same component, and $S_E(\mathbb{C}) \in [0, |E_G|]$. For a schematic illustration, see Fig. 2, panel a.

Second, one can map the nodes of D in component \mathbb{C} back to the events of the temporal network G and count the number of vertices involved in the events, $S_V(\mathbb{C}) \in [0, |V_G|]$. This is the “spacelike” definition of size (see Fig. 2, panel b).

Third, because the event nodes in D come with time stamps—the events take place at specified times—one may think of a “timelike” size: the *duration* (that is, the lifetime) of the component $S_t(\mathbb{C}) \in [0, T]$, the time difference between \mathbb{C} 's last and first event. This is illustrated in Fig. 2, panel c.

Note that these measures of size may or may not be correlated in a temporal network. In a random, Erdős-Rényi-like temporal network they on average are (see Ref. [11]). In this case, one can think of a single “giant” temporal component that encompasses most of the events in D and nodes in G and that lives for the entire observation period of the temporal network. However, this is a special case, and one can equally well think of networks where the different types of “giant” components are separated. As an example, there can be a short-lived, “spacelike” component that spans most of the nodes in G but contains only a small fraction of the nodes in D because of its short lifetime. There may also be several such components during the

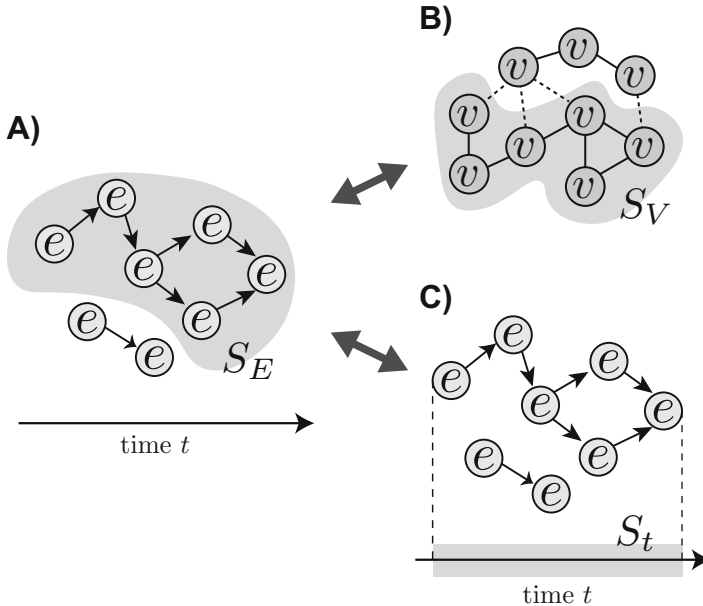


Fig. 2 Panel **a**: The shaded area indicates the size S_E of a component of D , measured in the number of nodes of D (events of G) involved in the component. Panel **b**: the size S_V of the same component, measured as the number of involved vertices in the original graph G as indicated by the shaded area. Panel **c**: The third way of measuring component size, the lifetime S_t of the component measured as the time difference between its last and first events

lifetime of the network. Further, one can also envision a persistent component that spans the whole time range but involves only a small number nodes that repeatedly and frequently interact: this component is large in S_t but vanishingly small in S_E and S_V . Again, multiple such components may coexist.

3.3.2 Temporal-Network Percolation Analysis with $D_{\Delta t}$

When the event graph D is thresholded, its component structure depends on the threshold weight. If the criterion for retaining D 's edges is that their weight is below some chosen value of the time difference Δt , then this parameter can be viewed as the *control parameter* of a percolation problem. The value of the control parameter Δt determines the event graph's component structure, in particular its largest component, similarly to the edge weight threshold used in percolation studies on static, weighted networks (see, e.g., [19]).

In network percolation, there is a critical value of the control parameter that separates the connected and disconnected phases of the network. When the control parameter reaches this value, connectivity suddenly emerges, reflected in the emergence of a giant connected component that spans a finite fraction of the

network. This is measured either as the fraction of nodes or links included in the largest component; whichever measure is used, it is called the the *order parameter* of the percolation problem.

Here, since the control parameter Δt operates on the event graph D , the most obvious choice for the order parameter would be the relative size of D 's largest (weakly connected) component. As discussed above, its size can be measured as the number S_E of its constituent event nodes in D , so that the corresponding order parameter

$$\rho_E(\Delta t) = \frac{1}{|E|} \max S_E, \quad (1)$$

where $|E|$ is the number of (event) nodes in D and we've made the dependence on Δt explicit. As such, this definition works in a straightforward way and $\rho_E(\Delta t)$ can be expected to behave as a typical order parameter would.

The size of the components other than the largest component is often used in percolation studies to detect the critical point. Using the above definition of size S_E , one can define the *susceptibility*

$$\chi_E = \frac{1}{|E|} \sum_{S_E < \max S_E} n_{S_E} S_E^2, \quad (2)$$

where n_{S_E} is the number of components of size S_E and the sum is over all components except the largest. The susceptibility diverges at the critical point that separates the connected and fragmented phase, as small components are absorbed into the emerging giant component.

However, as discussed above, one can measure the size of a component of D in two other ways. The “spacelike” way is to count the number of nodes S_V of the original network G that are involved in the component through D 's event nodes. Using this definition of component size, we arrive at the order parameter that measures what fraction of G is associated with D 's component:

$$\rho_V(\Delta t) = \frac{1}{|V|} \max S_V, \quad (3)$$

where $|V|$ is the number of nodes in G . For this order parameter, while one could naively define the corresponding susceptibility-like measure as

$$\chi_V = \frac{1}{|V|} \sum_{S_V < \max S_V} n_{S_V} S_V^2, \quad (4)$$

which may behave in hard-to-predict ways at the critical point—if something that can be called a critical point even exists. This is because a node $v \in V_G$ that participates in multiple connected events will appear multiple times in the

corresponding component of D . The nodes of the original network G may, for similar reasons, also belong to multiple components occurring at different times. In other words, the sum $\sum_{S_V < \max S_V} n_{S_V}$ is not a conserved quantity.

The third component size definition captures the time length of components in D , leading to an order parameter:

$$\rho_t(\Delta t) = \frac{1}{T} \max S_t , \quad (5)$$

where T is the observation period, i.e., the lifetime of G . While one could in principle again define a susceptibility-like measure for this control parameter, as in Eq. (4), this measure would not be too useful. This is because multiple components of D can easily co-exist, overlapping in time, and there can be a number of long-lived simultaneous components.

When interpreting the results of percolation studies using weighted event graphs, one should bear in mind that the components of D are weakly connected, that is, all pairs of nodes in the component are connected through a path if the directions of the links are discarded. This means that, in the context of spreading processes, the interpretation of component structure and percolation points is that the component size is an upper bound for the number of nodes that can be infected by the process if it begins inside the component. So for processes constrained from above so that the spreading agent has to move forward from a node within δt , the observed critical Δt is a lower bound: one can only be certain that the spreading process would not percolate below this threshold.

3.3.3 Temporal-Network Percolation: Empirical Examples

To illustrate the behaviour of the order parameter and the susceptibility as a function of the event-graph threshold Δt , we'll next recap some of the results originally published in [11], obtained for three data sets: a large dataset of time-stamped mobile-telephone calls [3], a dataset on sexual interactions from a study of prostitution [26], and an air transportation network in the US [27]. See [11] for more details on the datasets.

Two versions of relative largest component size (order parameter) and the susceptibility are shown for all datasets in Fig. 3. The first version is based on the event-graph component size S_E and the second on the number of involved vertices in the original graph, S_V . For these data sets, the critical points indicated by the diverging susceptibility are fairly similar for both measures, with the exception of small difference for the air transport network where χ_V peaks slightly earlier than χ_E . For these datasets, the “timelike” order parameter of Eq. (5) (not shown) does not produce meaningful results; it does not behave like an order parameter for reasons discussed in Sect. 3.3.2.

The identified critical points are related to characteristic time scales in the systems in question; as an example, they indicate how long a spreading process

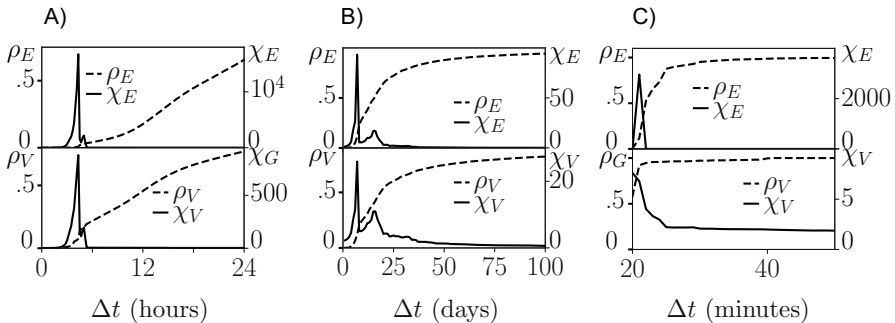


Fig. 3 The behaviour of the relative largest component size ρ and the susceptibility χ as a function of Δt , for three data sets and two variants of the measures. ρ_E and χ_E are for component size measured in event-graph nodes and ρ_V and χ_V for size measured in the number of temporal-network nodes involved in the component's events. Panel **a**: mobile telephone calls, displaying a critical point at around 4 h 20 min. Panel **b**: sexual interactions, with a critical point at around 7 days (followed by a second peak at ~ 16 days). Panel **c**: US air transport, with a critical point at ~ 20 min. Figure adapted from the original in [11]

would typically need to survive in order to eventually reach most of the network. In the case of mobile communication networks, if we imagine, e.g. a rumour spreading through the phone calls, the cascade will die out unless the rumour is still relevant and worth spreading for each node after 4 h and 20 min have passed since the node received it. For the sexual contact network, a sexually transmitted disease can become an epidemic and spread through the network if it remains infectious for longer than 7 days since being infected. For the air transport network, the identified characteristic time of approximately 20 min is related to the synchronization of connecting flights at airports.

4 Discussion and Conclusions

Because temporal networks carry information of the times of the interactions between the network's nodes, they allow for the detection of patterns that would be lost were the networks aggregated into static structures. This has led to increased understanding of the dynamics of network structures and processes that unfold on top of networks. The downside of this framework is that it naturally complicates network analysis, because of the additional degrees of freedom brought by the temporal dimension. Temporal networks are, in a way, mixtures of graphs and time series: therefore, if one is not satisfied with studying one of these aspects only, entirely new ways of looking at their structure are required.

In this Chapter, we have presented an approach that projects important features of temporal network dynamics into a static line graph structure: the weighted event graph. Weighted event graphs can be used both to understand the structural features

of the temporal networks they encode, as well as to investigate dynamical processes taking place on temporal networks. The weighted event graph framework maps temporal-topological structures onto weighted, directed, acyclic graphs. This is an information-lossless representation of temporal networks, which preserves the time-respecting paths of the original network as well as the timing differences between consecutive events on those paths. Weighted event graphs are particularly useful for studying paths, structures, and processes where one wants to set constraints to the times between successive events (Δt -connectivity), in other words, where the events have to follow one another quickly enough.

Beyond the examples discussed in this Chapter (temporal motifs, temporal-network percolation), one can envision many uses for weighted event graphs. In theory, any method or approach, which has been developed around the concepts of paths or walks could benefit from being viewed as a topological problem in weighted event graphs instead of a dynamical problem in temporal networks. Looking beyond the surface, it is clear that many important topics and measures in network science are at least partly based on the path structure of networks, including several approaches in dynamic models on networks, community detection, and centrality measures. As is evident from the cases of percolation analysis and temporal motifs, weighted temporal event graphs can be useful for both defining understandable concepts and measures as well as providing access to computationally efficient methods for solving temporal-network problems.

There is one rather obvious use of weighted event graphs that we have not discussed yet: the issue of *centrality measures*. The computation of various temporal-network centralities should greatly benefit from weighted event graphs, as they encapsulate the whole set of time-respecting paths (or their Δt -constrained subset). Such centralities could straightforwardly be computed using definitions and algorithms developed for static networks but in this case, applied to the event graphs instead. As a bonus, because of the event graph's construction, these measures would be computed for *events* of the original network instead of its vertices. It can be argued that this is—at least in some cases—more meaningful than computing quantities for the nodes. Any centrality measure for a node should come with the additional constraint on its valid time range: e.g., because time-respecting paths constantly change, should the “temporal betweenness centrality” of a node be a quantity that characterizes the node’s properties over some time range (up to the entire range of observation of the temporal network), or at some specific point in time, building on the paths that pass through the node at that point? However, with events, the definition is more straightforward: temporal betweenness centrality should depend on the number of (fastest) temporal paths passing through the event. Therefore, at least for instantaneous events, it can be directly and simply calculated from the event graph’s directed path structure.

Acknowledgements J.S. acknowledges support from the Academy of Finland, project “Digital Daily Rhythms” (project n:o 297195). M.K. acknowledges support from the Aalto Science Institute and the SoSweet ANR project (ANR-15-CE38-0011-01).

References

1. Holme, P., Saramäki, J.: Temporal networks. *Phys. Rep.* **519**(3), 97–125 (2012)
2. Holme, P.: Modern temporal network theory: a colloquium. *Eur. Phys. J. B* **88**(9), 234 (2015)
3. Karsai, M., Kivelä, M., Pan, R.K., Kaski, K., Kertész, J., Barabási, A.-L., Saramäki, J.: Small but slow world: how network topology and burstiness slow down spreading. *Phys. Rev. E* **83**, 025102 (2011)
4. Jo, H.-H., Karsai, M., Kertész, J., Kaski, K.: Circadian pattern and burstiness in human communication activity. *New J. Phys.* **14**, 013055 (2012)
5. Miritello, G., Lara, R., Cebrian, M., Moro, E.: Limited communication capacity unveils strategies for human interaction. *Sci. Rep.* **3**, 1950 (2013)
6. Aledavood, T., López, E., Roberts, S.G.B., Reed-Tsochas, F., Moro, E., Dunbar, R.I.M., Saramäki, J.: Daily rhythms in mobile telephone communication. *PLoS One* **10**, e0138098 (2015)
7. Navarro, H., Miritello, G., Canales, A., Moro, E.: Temporal patterns behind the strength of persistent ties. *EPJ Data Sci.* **6**, 31 (2017)
8. Iribarren, J.L., Moro, E.: Impact of human activity patterns on the dynamics of information diffusion. *Phys. Rev. Lett.* **103**, 038702 (2009)
9. Horváth, D.X., Kertész, J.: Spreading dynamics on networks: the role of burstiness, topology and non-stationarity. *New J. Phys.* **16**, 073037 (2014)
10. Nicosia, V., Musolesi, M., Russo, G., Mascolo, C., Latora, V.: Components in time-varying graphs. *Chaos* **22**, 023101 (2012)
11. Kivelä, M., Cambe, J., Saramäki, J., Karsai, M.: Mapping temporal-network percolation to weighted, static event graphs. *Sci. Rep.* **8**, 12357 (2018)
12. Mellor, A.: The temporal event graph. *J. Complex Netw.* **6**, 639–659 (2017)
13. Newman, M.E.J., Ziff, R.M.: Fast Monte Carlo algorithm for site or bond percolation. *Phys. Rev. E* **64**(1), 016706 (2001)
14. Leath, P.L.: Cluster size and boundary distribution near percolation threshold. *Phys. Rev. B* **14**, 5046 (1976)
15. Kovanen, L., Karsai, M., Kaski, K., Kertész, J., Saramäki, J.: Temporal motifs in time-dependent networks. *J. Stat. Mech. Theory Exp.* **2011**, P11005+ (2011)
16. Kovanen, L., Karsai, M., Kaski, K., Kertész, J., Saramäki, J.: Temporal motifs. In: Holme, P., Saramäki, J. (eds.) *Temporal Networks*, pp. 119–134. Springer, Heidelberg (2013)
17. Kovanen, L., Kaski, K., Kertész, J., Saramäki, J.: Temporal motifs reveal homophily, gender-specific patterns, and group talk in call sequences. *Proc. Natl. Acad. Sci.* **110**(45), 18070–18075 (2013)
18. Karsai, M., Noiret, A., Brovelli, A.: work in progress (2019)
19. Onnela, J.-P., Saramäki, J., Hyvönen, J., Szábo, G., Lazer, D., Kaski, K., Kertész, J., Barabási, A.-L.: Structure and tie strengths in mobile communication networks. *Proc. Natl. Acad. Sci. USA* **104**, 7332 (2007)
20. Karimi, F., Holme, P.: Threshold model of cascades in temporal networks. *Phys. A* **392**, 3476 (2013)
21. Takaguchi, T., Masuda, N., Holme, P.: Bursty communication patterns facilitate spreading in a threshold-based epidemic dynamics. *PLoS One* **8**, e68629 (2013)
22. Backlund, V.-P., Saramäki, J., Pan, R.K.: Effects of temporal correlations on cascades: threshold models on temporal networks. *Phys. Rev. E* **89**, 062815 (2014)
23. Milo, R., Shen-Orr, S., Itzkovitz, S., Kashtan, N., Chklovskii, D., Alon, U.: Network motifs: simple building blocks of complex networks. *Science* **298**(5594), 824–827 (2002)
24. Milo, R.: Superfamilies of evolved and designed networks. *Science* **303**(5663), 1538–1542 (2004)

25. Junttila, T., Kaski, P.: Engineering an efficient canonical labeling tool for large and sparse graphs. In: Applegate, D., Brodal, G.S., Panario, D., Sedgewick, R. (eds) Proceedings of ALENEX 2007, p. 135. SIAM, Philadelphia (2007)
26. Rocha, L.E., Liljeros, F., Holme, P.: Simulated epidemics in an empirical spatiotemporal network of 50,185 sexual contacts. PLoS Comput. Biol. **7**, e1001109 (2011)
27. Bureau of Transportation Statistics. www.bts.gov (2017)

Exploring Concurrency and Reachability in the Presence of High Temporal Resolution



Eun Lee, James Moody, and Peter J. Mucha

1 Introduction

Variation in epidemic spreading stems in part from the diversity of temporal contact patterns between subjects, whether such changes are a direct result of individual state changes (as in, e.g., [2, 22, 23]) or more general temporal variation (see, e.g., [11, 20]). For example, the distribution of the lifespan of edges can significantly affect the speed and eventual spread of an infection [10, 17, 21]. The increased availability of detailed, digitized temporal contact patterns supports and accelerates new investigations about the effects of temporal details, including analysis of properties such as fat-tailed inter-event time distributions [7, 13, 32, 33]. Indeed, the ‘burstiness’ of inter-event times can either slow down [13] or speed up dynamics [7, 32]. Meanwhile, such apparently contradictory effects provide a clue that there may be other elements controlling the dynamics beyond the bursty inter-event times.

Holme and Liljeros [10] investigated the changes to the observed outbreak sizes from various selected shifts to the contact histories: “beginning intervals neutralized” (BIN) shifts all contact pairs to first appear at the same time, “end intervals neutralized” (EIN) shifts the last contact between all pairs to the same time, and “interevent intervals neutralized” (IIN) replaces the heterogeneous intervals of contact between a pair to a uniform step size in time (keeping start and end times the same). For 12 empirical temporal networks, they found that BIN and EIN resulted in more significant differences in the outbreak size compared with differences obtained

E. Lee · P. J. Mucha (✉)
University of North Carolina, Chapel Hill, NC, USA
e-mail: eunfeel@email.unc.edu; mucha@unc.edu

J. Moody
Duke University, Durham, NC, USA
e-mail: jmoody77@soc.duke.edu

from IIN. A possible explanation for the relatively larger effect of these BIN and EIN modifications could be in the resulting changes in the concurrency of contacts. That is, by shifting all contacts to start (BIN) or end (EIN) at the same time, there is presumably greater temporal overlap between different contact intervals, augmenting the temporally consistent paths in the network over which the infection may spread.

Further supporting this possible interpretation, Li et al. [17] analyzed the transient behavior of reference models with randomly permuted times that either preserve the lifetimes of edges or of the nodes, focusing on changes in spreading speed according to the selected reference model. Their results demonstrate the dependence between the ability of an edge to help spread the infection and the time interval of its lifetime. Together, these results highlight the importance of the overall time interval over which a given pair is in contact, as opposed to the detailed timings of the contacts in those intervals.

Such studies point to the crucial function of the concurrency of edges in infection dynamics. In this chapter, we summarize previous studies related to issues of concurrency and the overall reachability constrained by the network timing details. We then explore the impact of concurrency on reachability by rescaling the start times in a set of empirical temporal networks. Using these empirical networks we then demonstrate the accuracy with which reachability is correctly calculated using a simplified interval representation for each edge that ignores the detailed timings of interevent contacts.

2 Previous Studies on Concurrency and Reachability

Although there exist various definitions for concurrency, its essence is clear: the extent of temporal overlap among the contacts. The significance of concurrency in a temporal network is immediately obvious for governing the reachable extent of any information or infection. Consider for example a simple situation with only three actors $\{A, B, C\}$ with B and C connected by an edge at some early time and A and B connected at a later time. If the temporal extent of these two edges do not overlap, then there is no way for any infection or information that spreads from A to B to continue on to C . However, if the two edges temporally overlap, then C is indeed “accessible” or “reachable” from A . The reachable extent allowed by the edge timings in a temporal network immediately impacts the real spread and modeling of an infectious disease, independent of the details of the dynamical process (e.g., SI, SIR, SEIR, complex contagion, etc.). The expected size of the maximally reachable set can be quantified by “reachability”, defined as the fraction of ordered node pairs with at least one temporally consistent path from the source node to the target node. Such ordered node pairs are “accessible.”

Because the reachability is an underlying property of a temporal network, independent of the spreading process taking place on that network, and since it naturally constrains all spreading processes on the temporal network, reachability

has been used in multiple previous studies [1, 9, 16, 25, 26, 30]. For example, Holme [9] numerically investigated two types of reachability called *reachability time* and *reachability ratio*, to categorize the effectiveness of the real-world contact networks in terms of time and spreading size. Lentz et al. [16] also explored accessibility in empirical networks, proposing the use of *causal fidelity*, defined as the fraction of network paths that can be followed by a sequence of events of strictly increasing times. That is, if all of the temporal contact information is agglomerated into a static network (collecting all edges that ever exist in the data but ignoring their timings), causal fidelity is the fraction of paths in this agglomerated static network that are also available in the full temporal network, thereby quantifying how well the static network representation might approximate the full dynamics.

In a related line of inquiry, the effect of concurrent partnerships has been of key interest for the spread of sexually transmitted diseases (STDs) such as HIV/AIDS [14, 25, 28]. Moody [25] emphasized the substantial effect of concurrency on the reachability in an adolescent romantic network, in that reachability plays the role of an upper bound on the expected outbreak size of an infection spreading on the network. An array of studies have assessed the effect of concurrent relationships for modeling infectious spreading on synthetic networks [3, 4, 24, 30]. The merit in studying synthetic networks is that it enables researchers to control the network's structural properties and the extent of the concurrent partnerships, which are obviously impossible to control in real-life networks. Despite considerable emphasis by different investigators about the role of temporally overlapping contacts, we still lack a general definition of concurrency in that slightly different definitions have been used across these studies. For example, Gursky and Hoffman [8] assumed concurrency based on the lifetime of an edge, following the definition in [34]. Doherty et al. [3] defined concurrency as the proportion of subjects engaging in concurrent relationships within a population. Onaga et al. [30] set concurrency as a fixed number of connections of an individual in time.

Onaga et al. [30] proposed a theoretical framework for the epidemic threshold induced by concurrency. In general, a low epidemic threshold can indirectly indicate a high probability of infection prevalence. Further, the relationship between concurrency and the epidemic threshold can help explain the relationship between concurrency and reachability. Onaga et al. defined the concurrency as a fixed number of links emanating from a node in unit time, and the activation of the links are decided by a node's activity level. The activity level is drawn from uniform and power-law probability distributions. Then, they applied the analytically tractable activity-driven model. Given the star-like network in unit time, the authors derived differential equations for an SIS model to estimate the epidemic threshold. They compared the analytically derived threshold to the numerically estimated threshold, confirming a close match. From the results, the authors found that the transition of the epidemic threshold depended strongly on the extent of the concurrent connections. The results, again, stress the importance of concurrency in adjusting infectious potential.

In the present work, we are motivated by the framework investigated by Moody and Benton [26], which focused on the roles of concurrency and structural

cohesion. They performed numerical experiments simulating edge start times and durations on network structures sampled with a four-step random walk from a collaboration network. Moody and Benton thus obtained 100 sample networks with which they explored different levels of structural cohesion, defined as the average number of node-independent paths between node pairs [27]. The authors controlled the concurrency—quantified by the fraction of connected edges whose temporal intervals overlap in time—by adjusting the distributions of the start times and durations of the edges. Given the sample networks with random start and duration times on each edge, they then measured reachability as a function of concurrency and modeled the relationships with general linear regression models. Moody and Benton showed that the concurrency and structural cohesion both affect reachability in their examples, finding that the role of concurrency is particularly important in low structural cohesion networks because a slight increase in concurrency sharply increases the number of accessible node pairs (that is, ordered node pairs connected via temporally consistent paths). When one considers that networks of low structural cohesion are common in many sexual contact networks, Moody and Benton’s findings stress the importance of concurrency for STD transmission.

Recently, Lee et al. [15] developed tree-like model approximations for the relationship between concurrency and reachability, to further elucidate numerical results like those of Moody and Benton [26]. Lee et al. compared their approximations with numerically-computed reachability in temporal networks obtained with simulated edge timings on various network structures: balanced and unbalanced trees, Erdős–Rényi (ER) networks, exponential degree distribution networks, and four of the sampled networks highlighted in [26]. Because of the nature of their tree-like assumptions, these models well approximate the relationship between reachability and concurrency for small values of structural cohesion, doing particularly well also at small values of concurrency. But their existing models do not do as well in the presence of larger numbers of available alternate paths between nodes. Nevertheless, this study further demonstrates how the overall level of reachability emerges through an interplay between concurrency and structural cohesion.

3 Effects of Concurrency: Empirical Examples

In the remainder of this chapter, we focus on a set of empirical examples to further explore reachability and concurrency, complementing the results in [26] and [15]. As part of our exploration, we transform the detailed contact time information of the edges into an interval representation wherein the distinct contacts between each connected node pair is instead represented simply by a start time (the first observed contact) and an end time (the last contact). That is, we treat each edge as if it was present for the entirety of the interval between the first and last observed contacts. We then measure concurrency and reachability on this simpler interval representation. To perform numerical experiments under different values of concurrency, we modify these time intervals by rescaling the total range of the start

Table 1 Four empirical temporal networks used in the present work

Name of the data	N	M_c	M_d	Δ
High school	180	45,047	2220	20 s
Conference	113	20,818	2196	20 s
DNC email	1890	39,263	4463	1 s
Brazil	6576	8497	8056	5 days

The networks are of size N (number of nodes) with M_c distinct temporal contacts between M_d different node pairs (the number of edges). The resolution of the temporal contacts is denoted by Δ

times in the temporal network while keeping the duration of each edge constant. By doing so, we investigate how concurrency affects reachability and examine whether reachability on the simpler interval representation matches that measured from the original contact times.

The basic characteristics of the four example empirical networks used in this study are described below and in Table 1. In the following subsections, we then describe the transformation to the interval representation, the measurement of concurrency and our method for modifying it in our present simulations, and the calculation of reachability. Using the empirical examples, we then demonstrate the impact of concurrency on reachability as well as the relative accuracy of computing reachability with the simplified interval representation in these examples.

3.1 Data

We used four empirical networks in the present study. The first data set (denoted “High School” here) contains the temporal network of contacts between students in a high school in Marseilles, France, including contacts between the students in five classes during a seven day period (from a Monday to the Tuesday of the following week) in November 2012 [6]. The network includes $N = 180$ nodes and $M_c = 45,047$ distinct contacts between $M_d = 2220$ different node pairs (that is, yielding M_d different edges in the interval representation). The time resolution of the measured contacts is $\Delta = 20$ s.

The second data set (“Conference”) corresponds to the contacts among attendees of the ACM Hypertext 2009 conference [12]. The conference spanned 2.5 days, with the network sampled every $\Delta = 20$ s. The network consists of $N = 113$ attendees and $M_c = 20,818$ contacts between $M_d = 2196$ node pairs.

The third data set (“DNC Email”) is the Democratic National Committee email network, as hacked from the DNC in 2016 (data available online at <http://konect.uni-koblenz.de/networks/dnc-temporalGraph>). Nodes in the network correspond to persons, with each contact along an edge representing an email sent to another person. Although the data are originally directed, we treat edges here as undirected for simplicity. The network includes $N = 1890$ nodes and $M_c = 39,263$ email contacts, connecting $M_d = 4463$ node pairs.

The fourth data set (“Brazil”) is a sexual contact data set obtained from a Brazilian web forum exchanging information about sex sellers between anonymous, heterosexual, male sex buyers between September 2002 and October 2008 [31]. In this web forum, male members grade and categorize their sexual encounters with female escorts in posts using anonymous nicknames. From the posts, Rocha et al. [31] constructed a network connecting every community member (sex buyer) to an escort. The time information of the posts are used here as the temporal contact between a seller and buyer. The entire network’s size is 16,730. However, to save computational cost, we ignored temporal contacts that occurred during the first 1000 days of the data. Additionally, whereas the original data is resolved at the level of days, we down-sampled the resolution of the contacts to $\Delta = 5$ days. As a result, the data we consider includes $N = 6576$ nodes and $M_c = 8497$ distinct contacts along $M_d = 8056$ edges.

3.2 Change to the Interval Representation

The empirical networks include detailed temporal contact patterns like that represented in Fig. 1a: an edge representing the connection between nodes i and j has potentially several time stamps that represent the distinct contacts between i and j . The detailed transmission of any infection occurs during these contacts. However, instantaneous contacts are not necessarily the best way to think about concurrency in these relationships. Consider the motivation to study the spread of STDs: the appropriate notion of concurrency does not require that the contacts occur at precisely the same time, only that they are interleaved in time.

As such, in our present investigation of concurrency and reachability we employ a simplification obtained by transforming the temporal details in the contacts into an interval representation, keeping only the start (t_s) and end time (t_e) of each edge, as shown in Fig. 1b. In panel (b), the contacts of the edge between A and D—which includes contacts at times $\{3,4,6\}$ (see, Fig. 1a)—are converted to the time interval $[3, 6 + \Delta]$. In this transformation, we explicitly add the time resolution Δ to the last

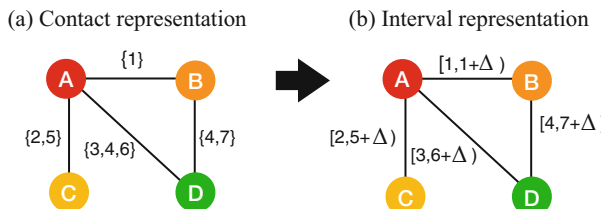


Fig. 1 A toy temporal-network example represented by (a) distinct contacts and (b) the corresponding interval representation. The interval of each edge starts with the first observed contact. To account for temporal resolution, we set a strict inequality (open interval) end time equal to the last observed contact plus the temporal resolution Δ

contact time so that every edge includes a non-zero time interval even if it represents only a single contact at time t [for example, the edge (A,B) in panel (a)]. Consistent with this addition, in our convention the edge only persists for times strictly less than the end time of the interval (open interval on the right).

3.3 Measuring and Controlling Concurrency

In the present work, we measure concurrency as the fraction of edge pairs that overlap in time. In so doing, we first emphasize that the key mechanism through which concurrency plays out is at the level of connected edges (that is, two edges that share a common node). However, in simulations where edge timings are independent and identically distributed, such as those in [26] and [15], the expected measurement of concurrency over all edge pairs is equivalent to that over the subset of connected edge pairs. In practice, in the real world, whether one more naturally defines concurrency over all edge pairs or only connected edge pairs may be directly determined by the nature of surveyed information. For example, if distributions of start times and durations of edges are measured, then the resulting estimate is effectively over all pairs. In contrast, if participants are directly queried about their numbers of concurrent relationships, then the restriction to connected edge pairs may be more natural. For the purposes of the present article, we measure concurrency as the fraction of all edge pairs that overlap in time. This definition enables us to more easily analyze the effect of concurrency on the reachability, particularly in developing models for the effect as in [15].

In our numerical experiments, we control the concurrency by rescaling the edge start times without changing their durations. We identify the minimum start time t_{s,l_i} of each edge—that is, each pair of nodes that are ever in contact—where l_i indicates the i th edge, $i \in [0, 1, \dots, L - 1]$, and L is the total number of edges. (Connecting the notation of this section to our data analysis, we note that $L = M_d$.) For notational convenience, we identify the very first start time $t_{s,\min} = \min t_{s,l_i}$ among all edges and define $\tau_i = t_{s,l_i} - t_{s,\min}$. We can then rescale the distribution of these start times with the parameter r by $t_{s,l'_i} = t_{s,\min} + r\tau_i$, as depicted in Fig. 2a. Meanwhile, we maintain the duration of each edge with $t_{e,l'_i} = t_{s,l'_i} + t_{d,l_i}$ where $t_{d,l_i} = t_{e,l_i} - t_{s,l_i}$ is the edge duration. For example, when we set $r = 0.5$, the interval representation of the original timings depicted in Figs. 1b and 2b (corresponding to $r = 1$) shift to the intervals in Fig. 2c. In particular, note that the edges in panel (c) overlap each other more than the original edges in panel (b).

3.4 Measuring Reachability

Given the interval representation of each edge, we can evaluate the average reachability of the network corresponding to that representation. Consider the

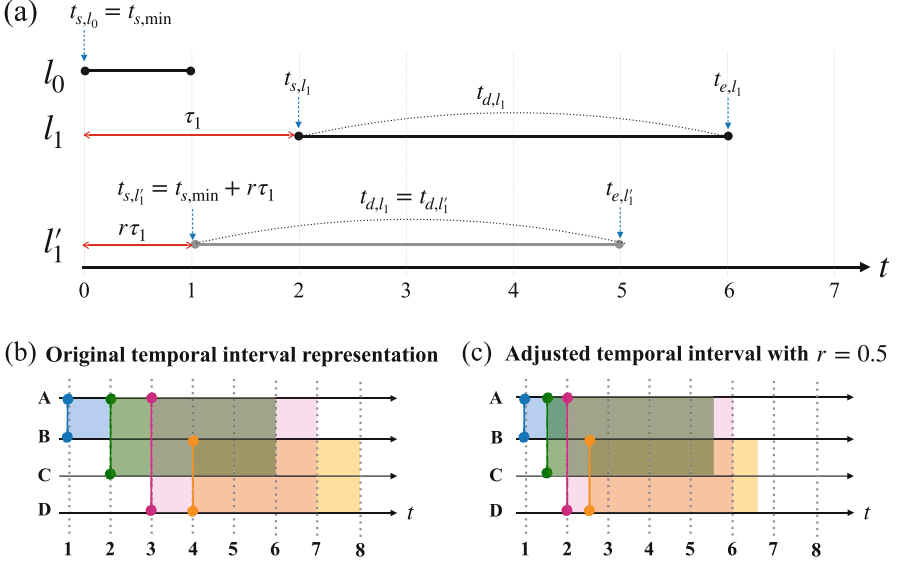


Fig. 2 Controlling concurrency in our toy example. (a) The very first link to appear, l_0 , sets the minimum starting time in the empirical data, $t_{s,\min} = t_{s,l_0}$, and the temporal axis in panel (a) is expressed in time since $t_{s,\min}$. A later link, l_1 , has an empirical start and end time; here $t_{s,l_1} = 1$ and $t_{e,l_1} = 6$, that is, with duration $t_{d,l_1} = 4$. The grey line l'_1 represents the new l_1 after rescaling the start time distribution by $r = 0.5$, with new start time t_{s,l'_1} obtained by pulling the original start time forward by a factor of r . In this rescaling of the start times, the duration of the edge remains the same. Under this rule, the original intervals in panel (b) with time resolution $\Delta = 1$ change under the rescaling $r = 0.5$ to those in panel (c). The concurrency of the intervals in the two panels are $C_{r=1.0} = 3/6 = 0.5$ and $C_{r=0.5} = 4/6 = 0.67$. Further increases in r increase C here until $C = 1$ for $r < 1/3$

(different) toy example in Fig. 3a. In general, all direct contacts such as those connecting (A,B) yield accessible node pairs. Additional pairs like (A,C) and (D,C) in Fig. 3c are accessible because of the temporal ordering of the edges. For example, an infection starting from D at $t = 1$ can reach C by either moving first to A and then on to B, or moving directly to B, and then having B infect C at a later time. However, an infection seeded at C cannot ever reach A or D because of an absence of available connections after the appearance of the (B,C) link at $t = 4$. That is, neither A nor D is accessible from C. (We again emphasize our convention of open intervals on the right, so in the example here the edge between B and D disappears immediately before the edge between B and C starts.) We identify the accessible ordered node pairs with the elements of the accessibility matrix \mathbf{R} , with $R(i, j) = 1$ if and only if j is accessible from i , as shown in Fig. 3d.

To quantify the overall average accessibility across the whole network, we calculate the reachability R as the density of the accessibility graph (i.e., the density of the off-diagonal elements of the accessibility matrix),

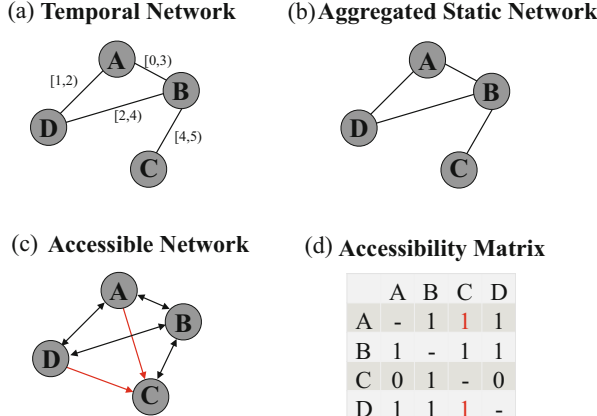


Fig. 3 Schematic representations for establishing accessibility. (a) Each edge in the network of nodes $\{A, B, C, D\}$ is denoted by a start and end time, e.g., the contact between A and D starts at $t = 1$ and continues until (just before) $t = 2$. (b) The static network representation aggregates all contacts that ever appear in the temporal network. (c) The corresponding directed graph of accessibility demonstrates that asymmetric accessibilities (red arrows) are possible. (d) The accessibility matrix encodes whether node j is accessible from node i

$$R = \frac{1}{N(N-1)} \sum_{i \neq j} R(i, j). \quad (1)$$

To calculate the accessibility matrix \mathbf{R} and reachability, we follow the same steps as in [15], generating temporal layers corresponding to the moment immediately before the end of each edge:

1. Sort edges by their end times t_{e,l_w} . Here, $w \in [0, L - 1]$ indexes edges by their end time in ascending order and L is the total number of edges. (We again note $L = M_d$ here.) For example, l_0 is the edge with the earliest end time and l_{L-1} is the last edge to end. (Breaking ties is unimportant for calculating reachability, except it can be used to reduce the number of calculations here, under an appropriate change of notation.)
2. Construct the adjacency matrix \mathbf{T}_w for the w th temporal layer by including edge l_w and all other edges $l_{w'}$ with $w' > w$ (that is, that end after the w th edge) that are also present just before the end time of the w th edge. That is, \mathbf{T}_w includes l_w and all $l_{w'}$ satisfying both $t_{s,l_{w'}} < t_{e,l_w}$ and $t_{e,l_{w'}} \geq t_{e,l_w}$.
3. By repeating step 2, the full set of temporal layer matrices $\mathbf{T}_0, \mathbf{T}_1, \dots, \mathbf{T}_{L-1}$ may be prepared.
4. Multiply the matrix exponentials of each temporal matrix: $\mathbf{R} = \prod_{w=0}^{L-1} e^{\mathbf{T}_w}$.
5. Binarize \mathbf{R} : For all $R_{ij} > 0$, set $R_{ij} = 1$.
6. By using Eq. (1), evaluate the average reachability R .

The matrix exponentials in step 4 provide a simply-expressed formula to indicate connected components within each temporal layer. Multiplying the matrix exponentials from consecutive layers yields (after binarizing) the reachable network associated with that set of layers. While the matrix exponential works conveniently for small data sets, for larger networks a more computationally tractable procedure is to instead directly calculate the connected components of T_w and replace the matrix exponential in step 4 with the binary indicator matrix whose elements specify whether the corresponding pair of nodes are together in the same component at that time. In practice, steps 3 and 4 can be trivially combined to separately consider each temporal layer in isolation from the others. That is, with this procedure the calculation can be performed without forming and holding the entire multilayer representation at one time (cf. breadth-first search on the full multilayer network). For even larger networks whose adjacency matrices must be represented as sparse matrices in order to even fit in memory, the corresponding accessibility graph could instead be constructed one row at a time, updating the running average of the density R to calculate the overall reachability.

The above-described procedure for calculating reachability for the interval representation can be used for the full temporal contact information with only minor modification. Instead of sorting edges by their end times, the reachability due to detailed temporal contacts proceeds by taking each possible contact interval as a separate temporal layer. The adjacency matrix and its exponential (or component indicator) is computed for each temporal layer, multiplying the latter together as in step 4 except that the index runs over all unique contact times.

3.5 Reachability with Concurrency

After transforming the temporal contact information into the interval representation (as described in Sect. 3.2), we measure reachability versus concurrency in the empirical network data sets. We use the parameter r to rescale the start times in order to vary concurrency. In general, reachability increases with increasing concurrency (see Fig. 4) although the details of this relationship between reachability and concurrency depends on the topology of the underlying network.

The High School and Conference examples display only a slight increase in reachability with increasing concurrency for the simple reason that reachability is already so high at zero concurrency. There are so many alternative paths between node pairs in these two networks that almost all pairs have at least one temporally consistent path, even for very small concurrency, and so reachability is almost always close to 1 in these cases (see the inset of Fig. 4). The interval representation of the original edge timings—that is, before we rescale the distribution of start times with the r parameter described above—corresponds to $C = 0.25$ (High School) and $C = 0.4$ (Conference).

In contrast, the DNC email network has larger concurrency in its original edge timings ($C = 0.6$) but much smaller reachability, as seen in Fig. 4. Even as the start

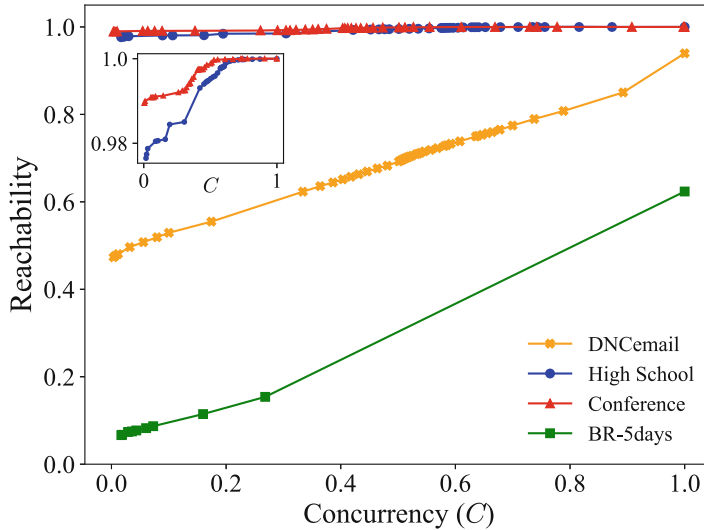


Fig. 4 Reachability of the empirical networks as a function of concurrency. Different levels of concurrency have been obtained here by rescaling the distribution of start times in the original data sets. The inset zooms in on the small deviations of reachability from 1 for the High School and Conference examples. Note that the lines here are only to connect the data points; the lines do not represent a functional relationship

time distribution is compressed (small r), to make the concurrency approach 1, the reachability only approaches 0.94 (not 1). This apparent discrepancy is because the data set includes separate connected components. That is, increasing concurrency all the way to 1 reduces the question of accessibility to connected components in the temporally-aggregated network, with reachability then equal to the fraction of node pairs in the same connected component. In the temporally-aggregated DNC email network, the largest connected component is of size 1833, with another component of size 58.

Similarly, the relatively small value of reachability for the Brazil network as $C \rightarrow 1$ is because the largest connected component includes 5193 (of the 8056 total) nodes. At $r = 1$, the Brazil data has concurrency 0.0172. As such, we can see that increasing the level of concurrency (that is, $r < 1$) can dramatically increase the reachability for this network.

We note in particular the behavior of the High School and the Conference data sets in having reachability values near 1 for all values of concurrency. We point the interested reader back to [26] and [15], where the important role of structural cohesion in the temporally-aggregated graph is demonstrated. We note that the structural cohesion calculated [35] for these two networks are 18.3 (High School) and 28.5 (Conference), quantifying the large number of node-independent paths typically available in these networks. In contrast, the structural cohesion of the DNC email network is 1.28, directly quantifying that it is much more tree-

like, and as such there are typically few (or in many cases no) available detours between nodes. Similarly, the structural cohesion of the Brazil network is 1.21. Given the particularly large values of structural cohesion for the High School and Conference networks, reachability values near 1 are not surprising, even as concurrency approaches zero.

3.6 Accuracy of Reachability from the Interval Representation

To further explore reachability and its dependence on the temporal details of the contacts, we calculate reachability in the four empirical temporal networks, tracing the change in reachability over time in the original data sets (i.e., without modifying start times). Figure 5 demonstrates the different increasing trends of reachability with time t across these networks, setting $t = 0$ in the figure at the appearance of the very first contact. Figure 5 also visualizes this increase in reachability relative to the number of edges $m(t)$ that have appeared by that time (i.e., the number of distinct node pairs that have had contact by that time). The figure includes calculations using the original contact times as well as those from the interval representation wherein each edge is assumed to be present for the full duration from its first appearance to its last. We use subscripts to distinguish between the calculations using the distinct temporal contacts (c) versus the interval representation (d , indicating each edge is assumed to be present for its total duration).

In addition to reachability (R_d , R_c), Fig. 5 includes the largest connected component size (S_d , S_c) and normalized edge count (m_d/M_d , m_c/M_c) as a function of time, considering all edges that have appeared since the very first contact. For ease of comparing different time scales, we re-plot these results for reachability and the size of the largest connected component versus the edge densities in Fig. 6. As observed in the figures, the differences between the calculated values based on full contacts versus the interval representation are relatively small, and in many cases barely distinguishable.

Of course, any error in computing the accessibility of an ordered node pair in the interval representation can only overestimate reachability. That is, an ordered node pair identified as accessible in the full contact representation is necessarily also accessible in the interval representation. However, it is possible that particular paths that appear to be temporally consistent in the interval representation do not actually have an allowed set of distinct contacts. That said, because our reachability calculation in the interval representation only computes results at the end times of edges, a new edge that appears (the node pair have their first contact) at time t does not get accounted for in the interval representation until the first end time that occurs after t . (At that time, this new edge is accounted for, even if its end time is much later.) By showing the results of both calculations, we demonstrate how accurately the interval representation describes reachability in these examples, with good agreement throughout Figs. 5 and 6.

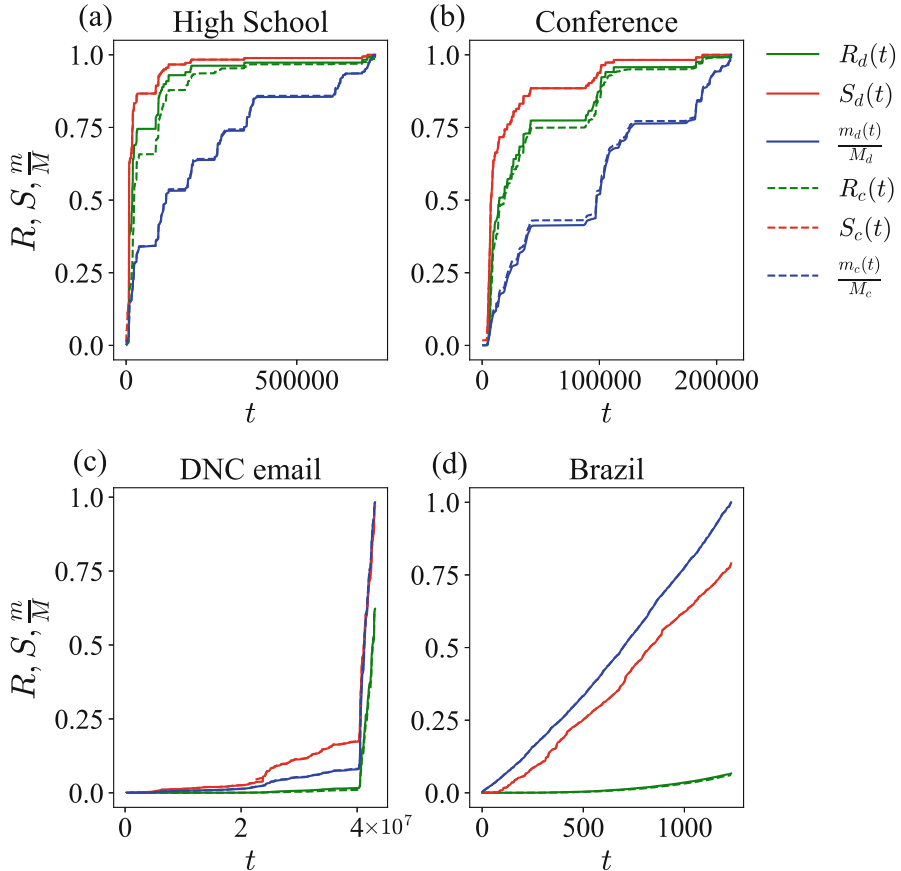


Fig. 5 Temporal traces of reachability (R), the size of the largest component (S) and the normalized edge count (m/M) in four empirical networks as calculated from the contacts (subscripted with c , plotted as dashed lines) and the interval representation (subscripted with d , solid lines). In many cases, the dashed lines are not distinguishable from the corresponding solid lines

In line with the very high structural cohesion of the High School and Conference networks, we observe very sharp increases in reachability at early times, with reachability values only slightly behind the fraction of nodes in the largest connected component. In contrast, we observe in the figure that the reachability of the DNC email and Brazil networks increase more slowly with time, even after redisplaying reachability versus normalized edge count. Remarkably, reachability calculated from the interval representation deviates only slightly from the full calculation using the complete temporal contact details. The most notable differences between the two calculations apparent in Fig. 6 is in the High School data, with the interval representation slightly overestimating reachability through its increase over time.

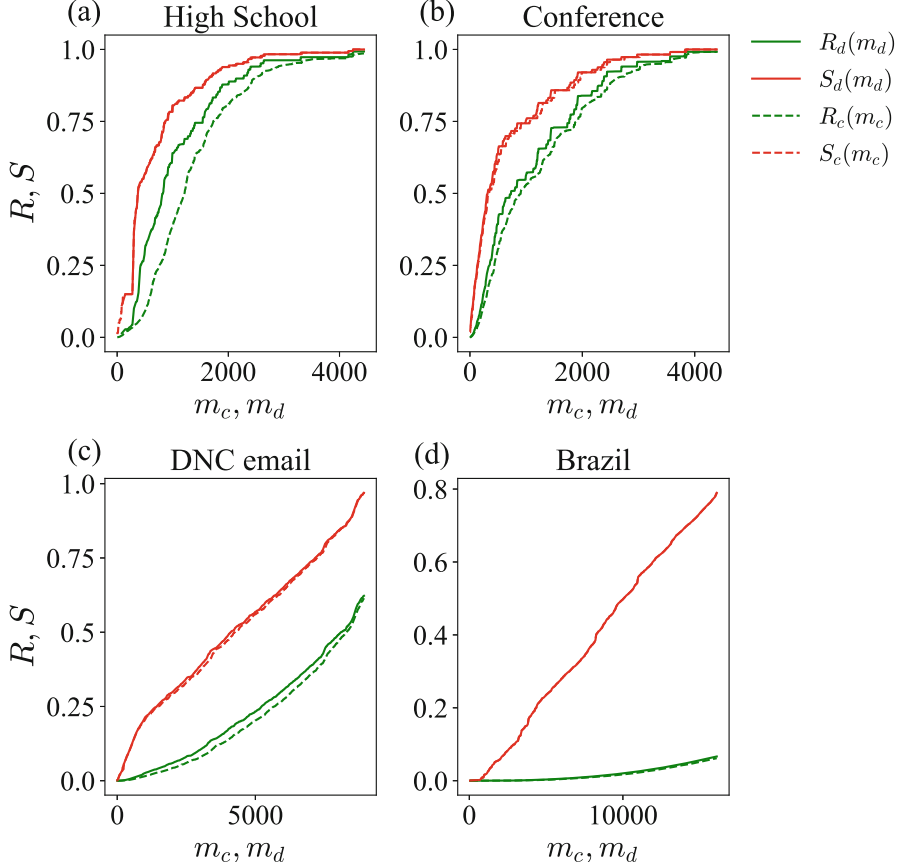


Fig. 6 Temporal traces of reachability (R) and the size of the largest component (S) in the four empirical networks, previously plotted in Fig. 5 are re-plotted here versus the number of edges that have appeared to that point in time. Once again, some of the dashed lines corresponding to calculations with the contacts are indistinguishable from the solid lines obtained from the interval representations

A smaller overestimate is also apparent in the panels for the Conference and DNC email networks.

Considering the importance of reachability as the average of the maximum possible outbreak size (averaging over “patient zero” source nodes), these results provide hope that reachability can be well estimated from the simpler interval representation in most cases, even though the detailed dynamics of a spreading infection surely varies between the true contacts and the interval representation.

4 Final Remarks

The details of edge timings in a temporal network can affect the speed and extent of the spread of diffusive dynamics such as infections or information propagation on the network. But because including temporal details greatly increases the complexity of the system, there has been a much greater amount of study and successful modeling of spreading processes on static networks. With ever greater emphasis on temporal network data, focusing on the role of concurrency appears to be one productive way to accurately summarize the population-level effects of the edge timing details. We here collected references to some previous studies related to the impact of concurrency on spreading processes, including in particular the relationship between concurrency and the average reachability in the temporal network. We have further demonstrated this relationship by calculation of reachability on empirical examples, rescaling the start time distributions in the original edge timing data to consider different levels of concurrency and reachability.

In so doing, we also compare the calculation of reachability on the full contact information against that using a simplified interval representation that treats each edge as present for the entire interval between the appearance of its first contact and its last. We demonstrate with these examples that the level of reachability calculated in the interval representation is nearly identical to that calculated with the full temporal contact information. We note that this result is similar at least in spirit to the findings of [10] where the detailed inter-event timings did not affect the results in their model simulations as much as the start times and end times.

In terms of the temporal trace of reachability, the High School and Conference networks show simultaneous increase of reachability with the size of the largest connected component at early times. In contrast, the DNC email and Brazil networks display a much slower increase in reachability, lagging behind the connected component size, and the reachability in these networks remains relatively low. We confirm with these empirical examples that the effect of concurrency can be quite large in some networks, as seen for the DNC email and Brazil networks.

The importance of concurrency was first identified in the context of the spread of HIV [28]. Conflicting observational works at the national and individual levels have since raised questions about the value of concurrency in the public health context (see, e.g., [5, 18, 19, 29]), but most of this work misunderstands the necessary relation between reachability and diffusion risk highlighted here (and in, e.g., [15, 26]). Whereas increased concurrency increases temporal path accessibility, and this increased reachability must increase diffusion potential, the amount of increase in reachability depends on other network factors, as we have demonstrated. While we have no data to speak directly to these questions about the value of concurrency in the public health context, our results suggest that one contributing factor might be high variance in the levels of structural cohesion in the underlying networks. As such, by analyzing the extent of concurrency in a temporal network and its impact on reachability given the structural properties of the underlying network, one might be able to better choose between different intervention strategies to best mitigate the

spread of an infectious disease or enhance the extent of positive behaviors. We hope this chapter serves to gather relevant previous studies and motivate future work.

Acknowledgements We thank Petter Holme and Jari Saramäki for the invitation to write this chapter. Research reported in this publication was supported by the Eunice Kennedy Shriver National Institute of Child Health and Human Development of the National Institutes of Health under Award Number R01HD075712. Additional support was provided by the James S. McDonnell Foundation 21st Century Science Initiative—Complex Systems Scholar Award (grant #220020315) and by the Army Research Office (MURI award W911NF-18-1-0244). The content is solely the responsibility of the authors and does not necessarily represent the official views of any supporting agency.

References

1. Armbruster, B., Wang, L., Morris, M.: Forward reachable sets: analytically derived properties of connected components for dynamic networks. *Netw. Sci.* **5**(3), 328–354 (2017)
2. Daley, D.J., Kendall, D.G.: Epidemics and rumours. *Nature* **204**(4963), 1118 (1964)
3. Doherty, I.A., Shibuski, S., Ellen, J.M., Adimora, A.A., Padian, N.S.: Sexual bridging socially and over time: a simulation model exploring the relative effects of mixing and concurrency on viral sexually transmitted infection transmission. *Sex. Transm. Dis.* **33**(6), 368–373 (2006)
4. Eames, K.T.D., Keeling, M.J.: Monogamous networks and the spread of sexually transmitted diseases. *Math. Biosci.* **189**(2), 115–130 (2004)
5. Epstein, H., Morris, M.: Concurrent partnerships and HIV: an inconvenient truth. *J. Int. AIDS Soc.* **14**(1), 13 (2011)
6. Fournet, J., Barrat, A.: Contact patterns among high school students. *PLoS One* **9**(9), 1–17 (2014)
7. Gernat, T., Rao, V.D., Middendorf, M., Dankowicz, H., Goldenfeld, N., Robinson, G.E.: Automated monitoring of behavior reveals bursty interaction patterns and rapid spreading dynamics in honeybee social networks. *Proc. Natl. Acad. Sci. U.S.A.* **115**(7), 1433–1438 (2018)
8. Gurski, K., Hoffman, K.: Influence of concurrency, partner choice, and viral suppression on racial disparity in the prevalence of HIV infected women. *Math. Biosci.* **282**, 91–108 (2016)
9. Holme, P.: Network reachability of real-world contact sequences. *Phys. Rev. E* **71**, 046119 (2005)
10. Holme, P., Liljeros, F.: Birth and death of links control disease spreading in empirical contact networks. *Sci. Rep.* **4**(1), 4999 (2015)
11. Holme, P., Saramäki, J.: Temporal networks. *Phys. Rep.* **519**(3), 97–125 (2012)
12. Isella, L., Stehlé, J., Barrat, A., Cattuto, C., Pinton, J.F., den Broeck, W.V.: What's in a crowd? Analysis of face-to-face behavioral networks. *J. Theor. Biol.* **271**(1), 166–180 (2011)
13. Karsai, M., Kivelä, M., Pan, R.K., Kaski, K., Kertész, J., Barabási, A.L., Saramäki, J.: Small but slow world: how network topology and burstiness slow down spreading. *Phys. Rev. E* **83**, 025102 (2011)
14. Kretzschmar, M., Morris, M.: Measures of concurrency in networks and the spread of infectious disease. *Math. Biosci.* **133**(2), 165–195 (1996)
15. Lee, E., Emmons, S., Gibson, R., Moody, J., Mucha, P.J.: Concurrency and reachability in tree-like temporal networks. <http://arxiv.org/abs/1905.08580> (2019)
16. Lentz, H.H.K., Selhorst, T., Sokolov, I.M.: Unfolding accessibility provides a macroscopic approach to temporal networks. *Phys. Rev. Lett.* **110**, 118701 (2013)
17. Li, M., Rao, V.D., Gernat, T., Dankowicz, H.: Lifetime-preserving reference models for characterizing spreading dynamics on temporal networks. *Sci. Rep.* **8**(1), 709 (2018)

18. Lurie, M.N., Rosenthal, S.: The concurrency hypothesis in sub-saharan Africa: Convincing empirical evidence is still lacking. Response to Mah and Halperin, Epstein, and Morris. *AIDS Behav.* **14**(1), 34–37 (2010)
19. Mah, T.L., Halperin, D.T.: The evidence for the role of concurrent partnerships in africa's HIV epidemics: a response to Lurie and Rosenthal. *AIDS Behav.* **14**(1), 25–28 (2010)
20. Masuda, N., Lambiotte, R.: A Guide to Temporal Networks. World Scientific, Singapore (2016)
21. Masuda, N., Klemm, K., Eguíluz, V.M.: Temporal networks: slowing down diffusion by long lasting interactions. *Phys. Rev. Lett.* **111**, 188701 (2013)
22. May, R.M., Anderson, R.M.: Transmission dynainics of HIV infection. *Nature* **326**, 137–142 (1987)
23. May, R.M., Anderson, R.M.: The transmission dynamics of human immunodeficiency virus (HIV). *Trans. R. Soc. Lond. B* **321**, 565–607 (1988)
24. Miller, J.C., Slim, A.C.: Saturation effects and the concurrency hypothesis: insights from an analytic model. *PLoS One* **12**(11), e0187938 (2017)
25. Moody, J.: The importance of relationship timing for diffusion: indirect connectivity and STD infections risk. *Soc. Forces* **81**(1), 25–56 (2002)
26. Moody, J., Benton, R.A.: Interdependent effects of cohesion and concurrency for epidemic potential. *Ann. Epidemiol.* **26**(4), 241–248 (2016)
27. Moody, J., White, D.R.: Structural cohesion and embeddedness: a hierarchical concept of social groups. *Am. Sociol. Rev.* **68**(1), 103–127 (2003)
28. Morris, M., Kretzschmar, M.: Concurrent partnerships and transmission dynamics in networks. *Soc. Netw.* **17**(3), 299–318 (1995)
29. Morris, M., Epstein, H., Wawer, M.: Timing is everything: international variations in historical sexual partnership concurrency and HIV prevalence. *PLoS One* **5**(11), e14092 (2010)
30. Onaga, T., Gleeson, J.P., Masuda, N.: Concurrency-induced transitions in epidemic dynamics on temporal networks. *Phys. Rev. Lett.* **119**, 108301 (2017)
31. Rocha, L.E.C., Liljeros, F., Holme, P.: Information dynamics shape the sexual networks of internet-mediated prostitution. *Proc. Natl. Acad. Sci.* **107**(13), 5706–5711 (2010)
32. Rocha, L.E.C., Liljeros, F., Holme, P.: Simulated epidemics in an empirical spatiotemporal network of 50,185 sexual contacts. *PLoS. Comput. Biol.* **7**(3), 1–9 (2011)
33. Vazquez, A., Rácz, B., Lukács, A., Barabási, A.L.: Impact of non-poissonian activity patterns on spreading processes. *Phys. Rev. Lett.* **98**, 158702 (2007)
34. Watts, C.H., May, R.M.: The influence of concurrent partnerships on the dynamics of HIV/AIDS. *Math. Biosci.* **108**(1), 89–104 (1992)
35. White, D., Newman, M.: Fast approximation algorithms for finding node-independent paths in networks. Santa Fe Institute Working Papers Series (2001). Available at SSRN: <https://ssrn.com/abstract=1831790> or <http://dx.doi.org/10.2139/ssrn.1831790>

Metrics for Temporal Text Networks



Davide Vega and Matteo Magnani

1 Introduction

The concept of communication is fundamental in the study of social systems [13], and the approaches for modeling them as networks make no exception. For example, if we focus on temporal social networks a large majority of the scenarios studied in the literature are clearly describing communication processes, including conversations on social media [14], mobile telephone calls [7], as well as face-to-face interactions [22]. Even when we consider static models of social networks, such as a friendship graphs without any associated temporal information, many of the metrics used to analyze them are still based on the assumption that some information is shared through the network. For example, we can measure the ability of actors or groups of actors to efficiently spread information (closeness, diameter, Page-Rank centrality), or we can identify actors with the ability to influence existing information flows (betweenness centrality). In summary, the most typical application of social network models and in particular temporal social networks is to study systems of communication.

Despite the central role of information in communication systems, the information exchanged through the social ties has often been neglected in network analysis. The most popular methods for the analysis of social networks are only defined on simple graph models, only including actors and their relationships, and hence temporal network analysis methods only rely on the additional availability of time annotations.

Information diffusion processes are often modeled including all three components: the actors propagating the information, the times of the propagation and the

D. Vega · M. Magnani (✉)

InfoLab, Department of Information Technology, Uppsala University, Uppsala, Sweden
e-mail: davide.vega@it.uu.se; matteo.magnani@it.uu.se

content. In practice, however, the content propagated (e.g., the text itself) is used only to define how actors are connected with each other based on, for example, the order of links between blog posts [12], who re-shared the same content in social media [5] or how actors interact with messages shared across multiple social networks [18, 19]. In [23], the authors use the concept of polyadic conversation, a model where chains of Twitter user interactions (replies, mentions and retweets) during a time interval are first grouped into conversation trees, and then aggregated into a static weighted graph of interactions between authors. This type of graph aggregation has recurrently appeared in the literature of network modeling and information retrieval [14], but there is no consensus on either what is the best method to build such model (e.g., how to compute the length of a conversation in terms of time and/or tree's depth) or how the textual content affects the grouping of actors. In summary, studying communication networks without considering *what* is communicated can only allow a partial understanding of the underlying social system.

To allow a more accurate representation of human communication, a model for temporal text networks was recently proposed [25]. This model describes communication events among actors, including the actors exchanging information, the textual representation of this information and the times when the communication happens. While this model is still limited to textual information, text is a very common way to communicate (for example by email, or via Twitter posts) and can also be used to represent other forms of expression, for instance oral communication that can be translated to text either manually or semi-automatically through speech-to-text algorithms, and also images, that can be turned into a set of keywords describing them [24].

While mathematically temporal text networks can be seen as extensions of temporal networks, which are themselves extensions of simple networks, there are two important differences that require the introduction of specific analysis methods. The most intuitive difference is of course the presence of text. An additional and more subtle difference lies in the semantics of the temporal annotations.

In the literature on temporal social networks the time on edges is typically used to indicate when an edge exists, e.g., that during that time the two actors are in contact and can exchange information. An implicit assumption in existing works is that information can be exchanged at any time when an edge is active, and that the exchange of information is instantaneous.

When we explicitly model communication networks, we should make a difference between edges representing the possibility of communicating and edges representing the actual production and consumption of information. In many cases the first type of edges exist between all actors; for example, we can always send an email to an existing email address. Therefore, in this chapter we focus on edges representing communication acts, that is, the actual exchange of information. These acts may have a non-negligible duration, therefore the time annotations in a temporal text network indicate when the transmission of a (text) message starts and when it finishes. Examples where this is important are messages exchanged through physical networks, where the communication channel has a physical delay,

and asynchronous communication such as by email and via social media, where the text is sent at some time but in general only received at a later time.

This different semantics of the temporal edges in temporal networks and in temporal text networks requires the re-definition of some central concepts, such as time-consistent paths, which in turn leads to the definition of new specific metrics.

Finally, it is worth mentioning that NLP¹ methods such as sentiment analysis [3, 16] have been used in the past to study the evolution of tweets, songs, blogs, presidential speeches without requiring information about the underlying communication structure (who exchanges these data sources and how), using only data from time-annotated documents and time series information [11]. The temporal text network model does not only allow researchers to use NLP methods during the analysis, but it provides specific metrics to combine them with other measures from temporal networks.

This chapter introduces the concept of path in temporal text networks and various metrics to characterize them. In Sect. 2 we introduce the temporal text network model to encode communication networks. In Sect. 3 we introduce the concepts of walk and path in temporal text networks, and in Sect. 4 we define alternative ways of summarizing a path, based either on the times when the communication acts happen or on the text exchanged through a path. Finally, in Sect. 5 we conclude with an empirical comparison of some of the measures introduced in this chapter in a sample network formed by the Twitter interactions between Swedish politicians.

2 Representing Temporal Text Networks

From a mathematical point of view, a *temporal text network* [25] can be represented as a triple (G, x, t) where $G = (A, M, E)$ is a directed bipartite graph representing the communication network, $x : M \rightarrow X$ is a mapping between the messages in M and a set of sequences of characters (text) in X and $t : E \rightarrow T$ represents the time associated to each edge, where T is an ordered set of time annotations. The edge directionality indicates the flow of the communication: $(a_i, m_k) \in E$ indicates that actor a_i has produced text m_k , while $(m_k, a_j) \in E$ indicates that actor a_j is the recipient of message m_k . Actors with out-degree larger than 0 are information producers, actors with in-degree greater than 0 are information consumers, and actors with both positive in- and out-degrees are information prossumers.

Figure 1 describes a working example we will use during the remainder of this chapter, representing a temporal text network with $|A| = 8$ actors, $|M| = 6$ messages and $|E| = 15$ edges. It is important to observe that, in most cases, the edges to/from a message have different time attributes; the only restriction imposed by the model is that $(a_i, m), (m, a_j) \in E \Rightarrow t(a_i, m) \leq t(m, a_j)$. In other words, a message can be consumed at different times by each actor (e.g., different social

¹NLP stands for “Natural Language Processing”.

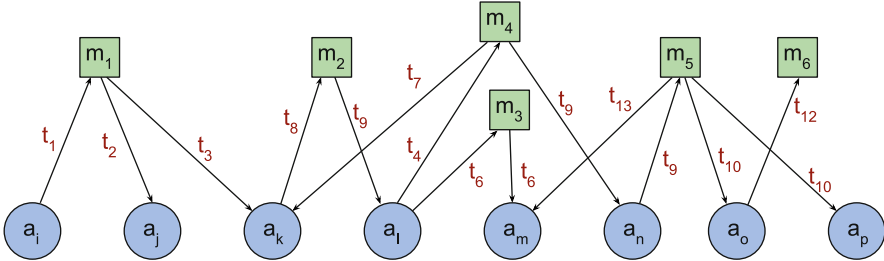


Fig. 1 A temporal text network model. Circles represent actors, squares represent messages and the edges between them represent the production and reception of the messages by the actors. Edges are also annotated with a time attribute $t_i \in T$

media users can visit their notifications page at different times), but can never be received before it has been generated (e.g., a user cannot access information that has not been shared yet).

This simple model can be used to differentiate between so-called unicast (messages m_2 and m_3 in the figure) and multicast (messages m_1 , m_4 and m_5) communication. The model can also be used to represent a variety of communication platforms such as email and Twitter mention networks, and can be easily extended adding edges between actors or between messages to represent additional relationships such as a follower/followee network. Unless we explicitly mention it, in the remainder of the chapter we will ignore these extensions.

A similar model to represent temporal interactions is the *contact sequence* [4, 6] model, which expresses temporal networks as a set of directed edges (called contacts) during a finite span of time. While this model has been successfully used to study spreading processes of information [1, 10] or the structural evolution of social networks [8, 17, 26], the model ignores the role of the content of the messages.

A natural alternative to represent time in networks is to use a sequence of time-annotated graphs, forming a so-called multi-layer network [2, 9]. In time-sliced models [15], for example, each one of the aggregated networks represents a fixed interval of time, and an edge e_{ij} is created if at least one contact has been registered between nodes i and j in the corresponding time interval. The aggregated graphs are sometimes weighted, in which case the edges have an assigned weight attribute w_{ij} proportional to the number of original edges, their frequency or another relevant time summarization function. In longitudinal networks, instead, the relations between the same or similar actors are detected at different points of time [20, 21]. From the modeling point of view there is not much difference between the two models, apart from the fact that in time-sliced networks the time intervals of two adjacent aggregated graphs are contiguous, which is not necessarily true for longitudinal networks.

3 Path-Based Metrics

Metrics for simple networks are based on basic concepts in graph theory, such as adjacency and incidence, and on counting discrete objects such as edges. Temporal networks extend simple networks with time. This requires the extension of some basic concepts in graph theory, and as time is often represented as a real number or interval, then temporal measures also require some additional simple arithmetical operations, such as time difference.

Temporal text networks also contain a text attribute. Text is a much more complex type of data, with a large number of possible operations. For example, the comparison of two texts can be done using different models (edit distance, word overlapping, vector representation, etc.), applying different “normalization” operators (stemming, stop word removal, dictionary based word replacement) or mapping the text to other domains (for example sentiments or topics). While these choices are very important in practice, hard-coding all these details in the metrics would make the model very complex.

Therefore, as discussed in [25], when dealing with temporal text networks we assume to have at least one of the following two types of text functions. The first type corresponds to a so-called *continuous analysis* approach, based on the idea of having different grades of similarity between messages. In this case we assume to have a distance function $d : M \times M \rightarrow [0, \infty)$, indicating how similar two messages are; if $d = 0$, the two messages are considered indistinguishable (for example because they contain the same text), and higher values of d indicate that the two messages are less similar. Notice that one can then plug specific functions into the model based on the text operations described above. An example of a message distance function is the cosine of the angle between vector representations of the two texts.

The second type of functions is targeted to a so-called *discrete analysis* approach, where each message is assigned to 0, 1 or more classes. For each class i we have a function $c_i : M \rightarrow \{0, 1\}$, which returns 1 if the message belongs to class i , 0 otherwise. One example is a topic modelling function with k topics, where $c_i(m) = 1$ if m belongs to topic i . Notice that starting from a discretization function we can also define a text distance function, for example based on how many common topics are shared between the two input messages.

3.1 Incidence and Adjacency

In digraphs two vertices are adjacent if there is an edge between them, and two edges are incident if the tail of the first is the head of the second. In temporal text networks two vertices are adjacent *at time t* if there is an edge between them *at that time*. The concept of adjacency has also been extended to edges (also known as events or contacts): an edge entering a vertex is adjacent to an edge leaving the

same vertex at a later time. This enables the definition of Δt -adjacency between edges, which is satisfied when they are adjacent and the time between them is less or equal than Δt . Note that this terminology is not completely consistent with the one in digraphs, where only vertices can be adjacent.

Temporal text networks differ from the previous cases in two regards. First, we do not need to extend the concept of adjacency to edges: we have two types of vertices (actors and messages), so for example the concept of adjacency between edges in temporal networks corresponds to adjacency between messages. This also means that we can retain the concept of incident edges from the theory of digraphs. Second, the idea of filtering those pairs of vertices that are close enough in time can also be extended to actors. In summary, all the concepts discussed above can be reduced to the following definitions.

Definition 1 (Edge Incidence) Let $e_1 = (v_i, u_k, t_1)$ and $e_2 = (u_k, v_j, t_2)$ be two edges in a temporal text network. We say that e_1 is incident to e_2 if $t_1 \leq t_2$.

Definition 2 (Adjacency) Let $e_1 = (v_i, u_k, t_1)$ and $e_2 = (u_k, v_j, t_2)$ be two edges in a temporal text network. Then:

1. v_i is adjacent to u_k at time t_1 .
2. v_i is Δt -temporally adjacent to v_j if $t_2 - t_1 \leq \Delta t$.
3. v_i is Δx -textually adjacent to v_j if $v_i, v_j \in M$ and $d(v_i, v_j) \leq \Delta x$.

Notice that the definition of incidence and adjacency hold independently of the type of vertices (v_i, u_k and v_j) involved. If $v_i, v_j \in A$ are actors, then their temporal adjacency is defined by the delay between the production and consumption of the message $u_k \in M$. We call an edge from an actor a to a message m a *producer edge* (e_p), while an edge from a message m to an actor a is called a *consumer edge* (e_c). If $v_i, v_j \in M$ are messages, then their temporal adjacency is defined by the delay between when the intermediate actor consumes (e.g., receives) the first message and the time when it produces (e.g., sends) the second. For example, the producer edge $e_4 = (a_l, m_4)$ in Fig. 1 is incident to the consumer edge $e_{10} = (m_4, a_n)$, therefore actor a_l is Δt -adjacent to actor a_n for all $\Delta t \geq t_9 - t_4$.

3.2 Walks and Paths

Definition 3 (Walk) A *walk* in a temporal text network (also called a temporal walk) is a sequence of edges e^1, e^2, \dots, e^l where e^i is incident to e^{i+1} for all i from 1 to $l - 1$.

In the following we will write $a \in w$ to indicate that a vertex (actor or message) is present in walk w .

Notice that the definition above does not constrain the starting and ending vertices of a path to be actors or messages. However, we will often be interested in walks starting from an actor, because every message has a single producer in the model used in this chapter.

Definition 4 (Path) A *path* in a temporal text network (also called a temporal path) is a walk where no vertex (message or actor) is traversed twice.

Each path establishes a precedence relation between actors indicating that the network allows a flow of information between them. Similarly, we have a precedence relation between messages indicating that the two messages can be part of the same flow of information.

Definition 5 (Temporal Precedence) An actor a_i *temporally precedes* another actor a_j if there is a path from a_i to a_j . A message m_i *temporally precedes* another message m_j if there is a path from m_i to m_j .

Figure 2 represents the same temporal text network of Fig. 1 as a temporal sequence of edges between actors and messages. In this example, $w_1 = [e_4, e_7, e_8, e_9]$ and $w_2 = [e_4, e_{10}, e_{11}, e_{12}, e_{14}]$ are two walks of 4 and 5 edges.² The second walk is also a path, starting at an actor and ending in a message m_6 , but the first walk is not a path because the last edge $e_9 = (m_2, a_l, t_9)$ visits for a second time the actor a_l . Finally, notice that in this example a_l precedes actor a_k in path $p_1 = [e_4, e_7]$ and vice-versa in path $p_2 = [e_8, e_9]$, while m_3 precedes m_6 but not otherwise.

In some cases we may want to consider only those paths with a limited delay and with a limited textual difference between adjacent messages. We can thus use the definitions of Δ -adjacency introduced above to select specific paths where sufficiently similar messages are exchanged often enough with respect to some user-defined thresholds.

4 Path Lengths

From now on we will focus on paths starting at an actor and ending at an actor. While a path can also start or end at a message, paths from and to actors are the ones providing the most accurate description of an information flow, because for every message there must always be an actor producing it, and messages that are not consumed by anyone (as message m_6 in our example) do not correspond to any exchange of information.

The length of a path in a temporal text network can be defined based on the topology, on time and on text.

The *topological length* is an unambiguous measure in simple and temporal networks, which are only made of vertices and edges. In a temporal text network a path contains actors, edges and messages, and the definition of length that is compatible with the one used in temporal networks corresponds to the number of

²To simplify the notation, in this chapter we are assuming that $i \leq j \Rightarrow t_i \leq t_j$.

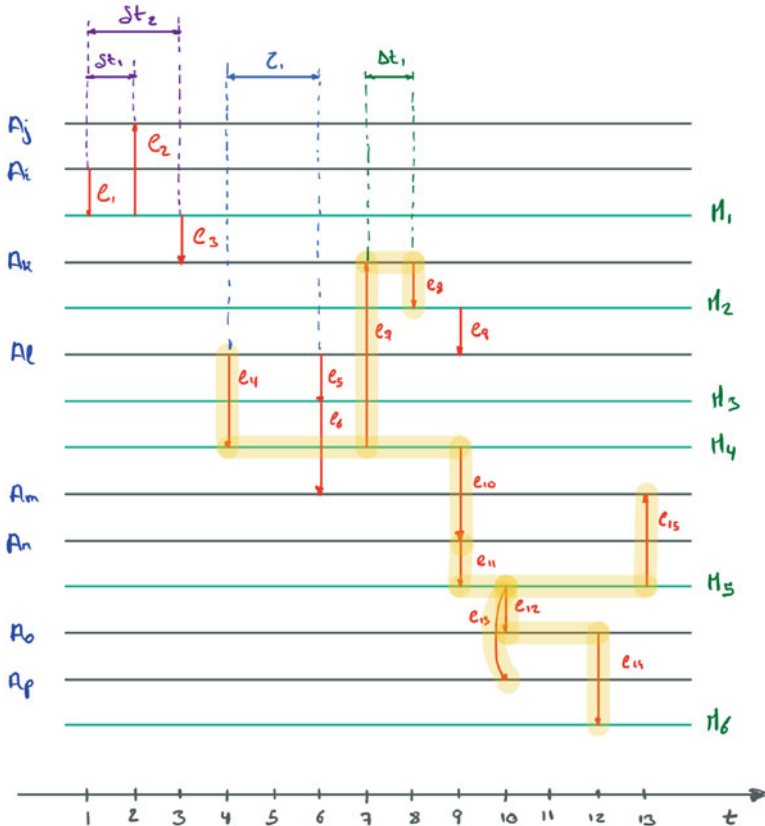


Fig. 2 Temporal text network represented as a sequence of edges. The horizontal lines represent the actors (gray color) and messages (green color) and vertical lines represent the transmission or consumption of a message. The shaded lines indicate all existing paths beginning at actor a_l at the exact time $t = 4$

messages in the path. This is because when a temporal network is translated into a temporal text network every edge is transformed into a message.

The *temporal length*, instead, defines the overall duration of the communication and is computed as the difference between the time of the last consumer edge and the time of the first producer edge in the path.

The topological and temporal length measures we have just described can be used to characterize the several paths that traverse our graph. In Fig. 2 we have highlighted all the existing paths starting at actor a_l at exactly $t = 4$, including those ending in a message. For example if we compare the path $p_1 = [e_4, e_{10}, e_{11}, e_{13}]$ with the path $p_2 = [e_4, e_{10}, e_{11}, e_{15}]$ we can see that both have the same topological length of 2 messages. However, while both paths start at the same time $e_4 = (a_l, m_4, t_4)$, the time of the last consumer edge is different and so their temporal length: $t(e_{13}) = t(m_5, a_p, t_{10}) \leq t(e_{15}) = t(m_5, a_m, t_{15})$.

Interestingly, in temporal text networks the temporal length of a path measures two different types of delays. On the one hand it measures the *transmission time* (δt) as the difference between the time of the consumer edge $t(e_c)$ and the time when the content has been produced $t(e_p)$. On the other hand, it indicates the *idle time* (τ) of the actors involved in the communication between two consecutive edges.

Definition 6 (Transmission Time) Let $e_1 = (a_i, m, t_1)$ and $e_2 = (m, a_j, t_2)$ two incident edges, with $m \in M$. Then the quantity $t_2 - t_1$ is called transmission time.

Definition 7 (Idle Time) Let $e_1 = (m_i, a, t_1)$ and $e_2 = (a, m_j, t_2)$ two incident edges, with $a \in A$. Then the quantity $t_2 - t_1$ is called idle time.

Once one has defined transmission and idle times, one can also compute the sum of all transmission times in a path, the sum of all idle times in a path, as well as the ratio between these values and the temporal length of the path. Back to our previous example, we can observe that the total transmission time of the messages in the first path $\delta_1 = (t_9 - t_4) + (t_{10} - t_9) = 6$ is three units smaller than in the second path $\delta_1 = (t_9 - t_4) + (t_{13} - t_9) = 9$ while their idle time is the same $\tau_F = t_9 - t_9 = 0$; which explains why the first path had a smaller temporal length.

The last type of length concerns the textual content in the path. Every time a message is exchanged, this increases the temporal length of the corresponding amount of time. Similarly, every time a new text is included in the path, this increases the textual information in it.

Definition 8 (Textual Length)

Given a text distance function, the *textual length* of a communication path is defined as the sum of the distances between the texts of all pairs of adjacent messages in the path.

This definition quantifies the variations between adjacent messages. At the same time, it is possible that the texts of the message keep being updated when transmitted through the path, but never significantly deviates from the original message. In this case, an alternative definition of length can be used to compute the maximum distance between any pair of messages.

In the case of discrete text analysis, where each message can belong to some classes (for example topics), this idea of estimating how homogeneous the text is across the path can be computed using a classical measure of entropy, for example the Shannon index:

Definition 9 (Entropy)

Let c_1, \dots, c_n be text discretization functions mapping text into one of n classes. Given a path p , we define $\rho_i(p) = \frac{\sum_{m \in p} c_i(x(m))}{M_p}$, where M_p is the number of messages in p . The textual entropy of path p is then defined as:

$$H(p) = - \sum_{i=1}^L \rho_i(p) \ln \rho_i(p) \quad (1)$$

According to this definition, if all messages that are part of a path belong to the same class (e.g., to the same topic), then the textual entropy will be 0, indicating a homogeneous path when we look at its text. Higher values of entropy would indicate that multiple classes (e.g., topics) are included in the path. This information can be useful in various analysis tasks, including the identification of information flows (when the same textual content is transferred through the network) or community detection, where one wants a community to be homogeneous not only with respect to the topology but also with the exchanged messages.

Once we decide which definition of length to use, this defines what are the shortest paths between any pair of actors, which implies that we can compute all the existing network measures based on shortest paths, including closeness centrality, betweenness centrality, eccentricity, diameter, etc. For the definitions of these metrics we refer the reader to any basic books on network analysis.

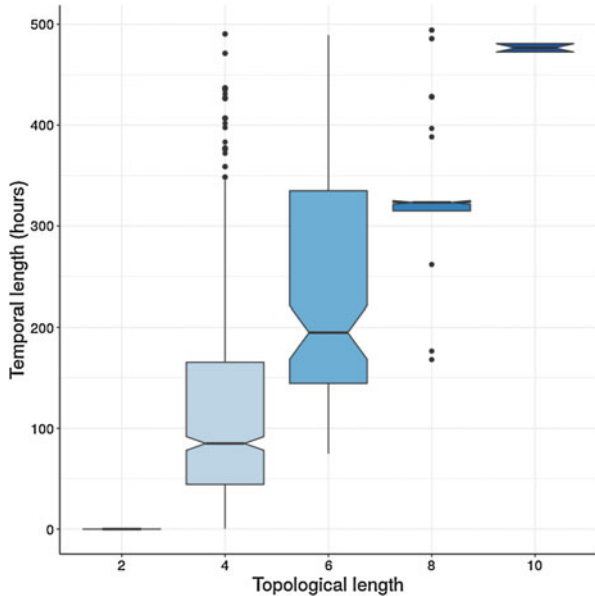
5 Empirical Study

In this section, we show an empirical comparison of the measures introduced in this chapter in a real communication network. Our sample dataset consists of all the public Twitter mentions (messages including another Twitter @username) written by Swedish politicians during January, 2019. The period of observation takes place 4 months after the Swedish general elections in 2018, and includes the time when the new government coalition was formed.³ Our final network consists of $|A| = 886$ actors, including 26 politicians (8 information producers and 18 prosumers) and 860 mentioned users (all of them consumers), $|M| = 1707$ Twitter messages with their corresponding text and $|E| = 4,882$ edges between actors and messages. Modelling the reception time is more difficult, because many social media platforms like Twitter do not provide information about when and who consumed a piece of information. In our experiments we assumed that the consumption time of all messages is the same as the production time, which might not be necessarily true (e.g., users are not always connected to all their social media and, even if they are, the tweet might be lost in the myriad of information provided by the user's wall).

Figure 3 shows, for each one of the 6773 pairs of actors temporally reachable, a comparison of their topological and temporal shortest path length. It includes 5787 (85.4%) paths with only two edges, representing two $\Delta 0$ -textually (and temporally) adjacent actors who have been in direct communication. The average temporal path length of the remaining paths increases with the number of hops (topological length) while its statistical dispersion is reduced, as we usually observe in other type of temporal networks (e.g., contact networks). For example, the 56 pairs of actors connected through 3 messages (6 hops) have an average communication

³We considered only politicians who were either members of the parliament before the elections or were part of an electoral ballot.

Fig. 3 Temporal length. Summary of the temporal length distribution for all shortest paths found in the Swedish politicians network, grouped by their topological path length. All topological paths involve an even number of hops because we are measuring only pairs of reachable actors



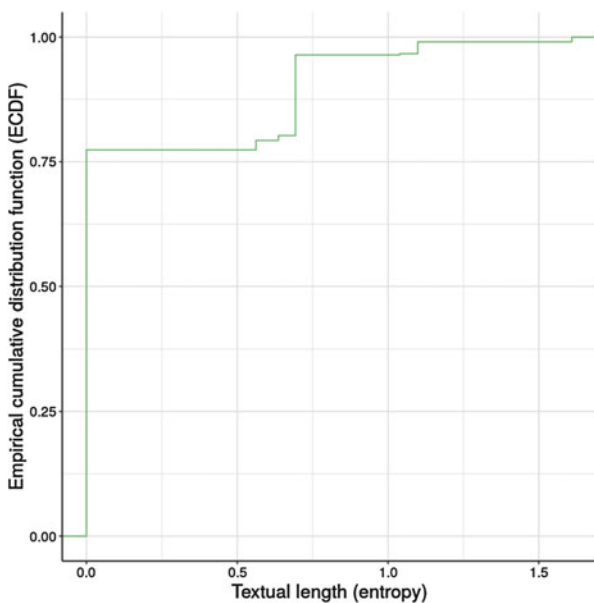
time (shortest temporal length) of approximately 14 days. The order of magnitude of these numbers can be explained by the skewed distribution of roles (producer, consumer and prosumers) of the actors in the data and the small sample of the original social network.

Another important component to understand communication networks is the specific content their members intend to share with each other. For example, in a conversation within a group of close people the content (text) of the messages will be probably different between communications, while news spreading processes will probably have a more similar topic distribution. The consistency of the topics in an information cascade phenomenon, therefore, can be a good metric to describe the dynamics of a complex system.

Following the methodology described in Sect. 4, we have first identified the topics of the messages exchanged in our sample network and then, computed the textual length using the Shannon index described in Eq. (1) to identify the shortest paths of each pair of temporally reachable actors. While identifying the topics, we have used the hashtags as proxies, which is a simple and well accepted solution in many contexts; but as we will see, problematic in practice. As we mentioned in the previous section, the definition of textual length assumes that there is a discretization function mapping the text *into at least one topic*. Hence, because many tweets do not contain any hashtag, their topic assignment is empty.

Figure 4 shows the empirical cumulative distribution function (ECDF) of the textual shortest path in our sample network. In this particular example, only 420 observations of 6773 were computed, as many paths have an unidentified length, either because none of the messages have a topic assigned or because they contain only one message.

Fig. 4 Empirical cumulative distribution function (ECDF) of the textual length



We can observe that more than 75% of the textual paths computed have 0 entropy, indicating that there is one single topic in the messages of the path. A closer look does not indicate any correlation of these results with the topological or temporal length of the paths. The minimum textual length paths include, for example, all the paths with 5 messages (10 hops) and 85.45% of the paths with 4 messages, but less than 50% of the paths with 3 messages.

6 Final Remarks

In this chapter, we have revisited some of the fundamental graph measures for temporal networks and extended them to be compatible with the temporal text network model for communication systems. We have shown that using the proposed model we can directly represent, in a simple but extensible way, all the elements necessary to study communication (time, text and topology), without requiring complex graph transformations. While mathematically temporal text networks are not much different from time-varying graphs, the semantics of its interactions and the presence of textual information in the model, require the introduction of specific analysis methods. In particular, in this chapter we have focused on redefining the idea of connectivity and most of its related measures such as incidence, adjacency, paths and distance, providing alternative metrics for actors and messages when we found it was relevant and necessary. Finally, we have shown how the different distance measures can be used in practice to discover patterns of connectivity.

We believe that, beyond their direct application to different analysis tasks, these measures are fundamental to redefine other relevant measures for studying communication systems such as centrality measures or developing analysis methods like community detection algorithms.

Acknowledgements We would like to thank Prof. Christian Rohner for his comments and suggestions.

This work was partially supported by the European Community through the project “*Values and ethics in Innovation for Responsible Technology in Europe*” (Virt-EU) funded under Horizon 2020 ICT-35-RIA call Enabling Responsible ICT-related Research and Innovation.

References

1. Cheng, J., Adamic, L.A., Kleinberg, J.M., Leskovec, J.: Do cascades recur? In: Proceedings of the 25th International Conference on World Wide Web, pp. 671–681. International WWW Conferences Steering Committee (2016)
2. Dickison, M., Magnani, M., Rossi, L.: Multilayer Social Networks. Cambridge University Press, Cambridge (2016)
3. Dodds, P.S., Danforth, C.M.: Measuring the happiness of large-scale written expression: songs, blogs, and presidents. *J. Happiness Stud.* **11**(4), 441–456 (2010). <https://doi.org/10.1007/s10902-009-9150-9>
4. Gauvin, L., Panisson, A., Cattuto, C., Barrat, A.: Activity clocks: spreading dynamics on temporal networks of human contact. *Sci. Rep.* **3**, 3099 (2013). <https://doi.org/10.1038/srep03099>
5. Gomez Rodriguez, M., Leskovec, J., Krause, A.: Inferring networks of diffusion and influence. In: Proceedings of the 16th ACM SIGKDD International Conference on Knowledge Discovery and Data Mining, KDD’10, pp. 1019–1028. ACM, New York (2010). <http://doi.acm.org/10.1145/1835804.1835933>
6. Holme, P., Saramäki, J.: Temporal networks. *Phys. Rep.* **519**(3), 97–125 (2012). <https://doi.org/10.1016/j.physrep.2012.03.001>
7. Karsai, M., Kivelä, M., Pan, R.K., Kaski, K., Kertész, J., Barabási, A.L., Saramäki, J.: Small but slow world: how network topology and burstiness slow down spreading. *Phys. Rev. E Stat. Nonlinear Soft Matter Phys.* **83**(2), 025102(R) (2011). <https://doi.org/10.1103/PhysRevE.83.025102>
8. Kim, J., Diesner, J.: Over-time measurement of triadic closure in coauthorship networks. *Soc. Netw. Anal. Min.* **7**(1), 9 (2017). <https://doi.org/10.1007/s13278-017-0428-3>
9. Kivelä, M., Arenas, A., Barthelemy, M., Gleeson, J.P., Moreno, Y., Porter, M.A.: Multilayer networks. *J. Complex Netw.* **2**(3), 203–271 (2014)
10. Lambiotte, R., Tabourier, L., Delvenne, J.C.: Burstiness and spreading on temporal networks. *Eur. Phys. J. B* **86**(7), 320 (2013). <https://doi.org/10.1140/epjb/e2013-40456-9>
11. Lavrenko, V., Schmill, M., Lawrie, D., Ogilvie, P., Jensen, D., Allan, J.: Mining of concurrent text and time series. In: SIGKDD Workshop on Text Mining, pp. 37–44 (2000)
12. Leskovec, J., Krause, A., Guestrin, C., Faloutsos, C., VanBriesen, J., Glance, N.: Cost-effective outbreak detection in networks. In: International Conference on Knowledge Discovery and Data Mining (KDD), p. 420 (2007). <https://doi.org/10.1145/1281192.1281239>
13. Luhmann, N.: Social Systems. Stanford University Press, Palo Alto (1995)
14. Magnani, M., Montesi, D., Rossi, L.: Conversation retrieval from microblogging sites. *Inf. Retrieval J.* **15**(3–4) (2012)
15. Mucha, P.J., Porter, M.A.: Communities in multislice voting networks. *Chaos: Interdisciplinary J. Nonlinear Sci.* **20**(4), 041108 (2010). <https://doi.org/10.1063/1.3518696>

16. O'Connor, B., Balasubramanyan, R., Routledge, B.R., Smith, N.A.: From tweets to polls: linking text sentiment to public opinion time series. In: Cohen, W.W., Gosling, S. (eds.) Proceedings of the Eleventh International Conference on Web and Social Media. The AAAI Press, Palo Alto (2010)
17. Paranjape, A., Benson, A.R., Leskovec, J.: Motifs in temporal networks. In: Proceedings of the 10th ACM International Conference on Web Search and Data Mining, WSDM'17, pp. 601–610. ACM, New York (2017). <https://doi.org/10.1145/3018661.3018731>
18. Roth, C., Cointet, J.P.: Social and semantic coevolution in knowledge networks. *Soc. Netw.* **32**(1), 16–29 (2010). <https://doi.org/10.1016/j.socnet.2009.04.005>
19. Salehi, M., Sharma, R., Marzolla, M., Magnani, M., Siyari, P., Montesi, D.: Spreading processes in multilayer networks. *IEEE Trans. Netw. Sci. Eng.* **2**(2), 65–83 (2015). <http://arxiv.org/abs/1405.4329>
20. Snijders, T.A.B.: Models for longitudinal network data. In: P.J. Carrington, J. Scott, S. Wasserman (eds.) Models and Methods in Social Network Analysis, Structural Analysis in the Social Sciences, pp. 215–247. Cambridge University Press, Cambridge (2005). <https://doi.org/10.1017/CBO9780511811395.011>
21. Snijders, T.A.B.: Siena: statistical modeling of longitudinal network data. In: Encyclopedia of Social Network Analysis and Mining, pp. 1718–1725. Springer, New York (2014)
22. Stehlé, J., Voirin, N., Barrat, A., Cattuto, C., Isella, L., Pinton, J.F., Vanhems, P.: High-resolution measurements of face-to-face contact patterns in a primary school. *PLoS One* **6**(8) (2011). <https://doi.org/10.1371/journal.pone.0023176>
23. Tamine, L., Soulier, L., Jabeur, L., Amblard, F., Hanachi, C., Hubert, G., Roth, C.: Social media-based collaborative information access: analysis of online crisis-related twitter conversations. In: HT 2016 - Proceedings of the 27th ACM Conference on Hypertext and Social Media, pp. 159–168 (2016). <https://doi.org/10.1145/2914586.2914589>
24. Vadicalmo, L., Carrara, F., Cimino, A., Cresci, S., Dell'Orletta, F., Falchi, F., Tesconi, M.: Cross-media learning for image sentiment analysis in the wild. In: 2017 IEEE International Conference on Computer Vision Workshops (ICCVW), pp. 308–317 (2017). <https://doi.org/10.1109/ICCVW.2017.45>
25. Vega, D., Magnani, M.: Foundations of temporal text networks. *Appl. Netw. Sci.* **3**(1), 26 (2018). <https://doi.org/10.1007/s41109-018-0082-3>
26. Viard, T., Latapy, M., Magnien, C.: Computing maximal cliques in link streams. *Theor. Comput. Sci.* **609**(1), 245–252 (2016). <https://doi.org/10.1016/j.tcs.2015.09.030>

Bursty Time Series Analysis for Temporal Networks



Hang-Hyun Jo and Takayuki Hiraoka

1 Introduction

Characterizing the interaction structure between constituents of complex systems is crucial to understand not only the dynamics of those systems but also the dynamical processes taking place in them. The topological structure of interaction has been modeled by a network, where nodes and links denote the constituents and their pairwise interactions, respectively [1, 2]. When the interaction is temporal, one can adopt a framework of temporal networks [3–5], where links are considered being existent or activated only at the moment of interaction. The temporal interaction pattern of each link can be described by a series of interaction events or an event sequence. Many empirical event sequences are known to be non-Poissonian or bursty [6–8], e.g., as shown in human communication patterns [9–16], where bursts denote a number of events occurring in short active periods separated by long inactive periods. Such bursty event sequences can be fully understood both by heterogeneous interevent times (IETs) and by correlations between IETs [17, 18]. Here the IET, denoted by τ , is defined by the time interval between two consecutive IETs. The heterogeneities of IETs have been extensively studied in terms of heavy-tailed or power-law IET distributions [8], while the correlations between IETs have been far from being fully explored.

H.-H. Jo (✉)

Asia Pacific Center for Theoretical Physics, Pohang, Republic of Korea

Pohang University of Science and Technology, Pohang, Republic of Korea

Aalto University, Espoo, Finland

e-mail: hang-hyun.jo@apctp.org

T. Hiraoka

Asia Pacific Center for Theoretical Physics, Pohang, Republic of Korea

e-mail: takayuki.hiraoka@apctp.org

In this Chapter, we introduce various measures for bursty time series analysis, such as the IET distribution, the burstiness parameter, the memory coefficient, the bursty train sizes, and the autocorrelation function, to discuss the relation between those measures. Then we show that the correlations between IETs can affect the speed of spreading taking place in temporal networks. Finally, we discuss possible research topics regarding bursty time series analysis for temporal networks.

2 Bursty Time Series Analysis

2.1 Measures and Characterizations

Non-Poissonian, bursty time series or event sequences have been observed not only in the human communication patterns [8], but also in other natural and biological phenomena, including solar flares [19], earthquakes [20, 21], neuronal firings [22], and animal behaviors [23, 24]. Temporal correlations in such event sequences have been characterized by various measures and quantities [8], such as the IET distribution, the burstiness parameter, the memory coefficient, the bursty train sizes, and the autocorrelation function. Each of these five measures captures a different aspect of the bursty time series, while they are not independent of each other. Here we discuss the relation between these five measures, which is conceptually illustrated in Fig. 1.

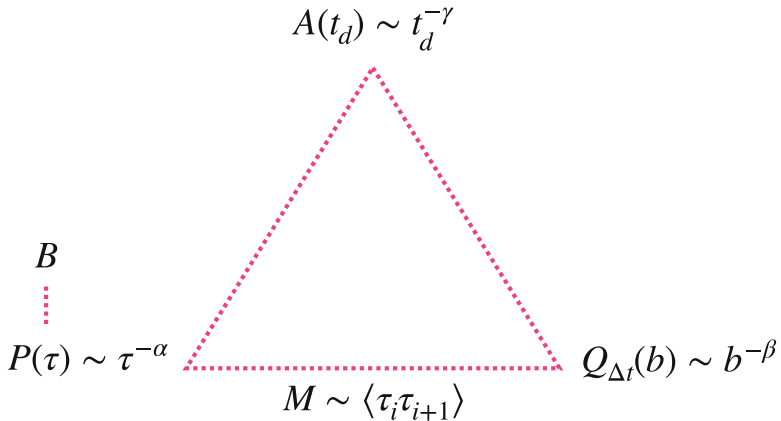


Fig. 1 Conceptual diagram for the relation between the autocorrelation function $A(t_d)$, the interevent time distribution $P(\tau)$, and the burst size distribution for a given time window $Q_{\Delta t}(b)$, together with the burstiness parameter B and the memory coefficient M . The relation between these five measures is discussed in Sect. 2: In particular, for the dependence of γ on α and β , refer to Sect. 2.3, and for the relation between M and $Q_{\Delta t}(b)$, refer to Sect. 2.4

1. The autocorrelation function for an event sequence $x(t)$ is defined with delay time t_d as follows:

$$A(t_d) \equiv \frac{\langle x(t)x(t + t_d) \rangle_t - \langle x(t) \rangle_t^2}{\langle x(t)^2 \rangle_t - \langle x(t) \rangle_t^2}, \quad (1)$$

where $\langle \cdot \rangle_t$ means a time average. The event sequence $x(t)$ can be considered to have the value of 1 at the moment of event occurred, 0 otherwise. For the event sequences with long-term memory effects, one may find a power-law decaying behavior with a decaying exponent γ :

$$A(t_d) \sim t_d^{-\gamma}. \quad (2)$$

Temporal correlations measured by $A(t_d)$ can be understood not only by the heterogeneous IETs but also by correlations between them.

2. The heterogeneous properties of IETs have often been characterized by the heavy-tailed or power-law IET distribution $P(\tau)$ with a power-law exponent α :

$$P(\tau) \sim \tau^{-\alpha}, \quad (3)$$

which may already imply clustered short IETs even with no correlations between IETs. In the case when IETs are fully uncorrelated with each other, i.e., for renewal processes [25], the power spectral density was analytically calculated from power-law IET distributions [26]. Using this result, one can straightforwardly derive the scaling relation between α and γ :

$$\begin{aligned} \alpha + \gamma &= 2 \text{ for } 1 < \alpha \leq 2, \\ \alpha - \gamma &= 2 \text{ for } 2 < \alpha \leq 3. \end{aligned} \quad (4)$$

This relation was also derived in the study of priority queueing models [27]. The relation $\alpha + \gamma = 2$ for $1 < \alpha \leq 2$ has been derived in the context of earthquakes [28] as well as of the hierarchical burst model [29].

3. The degree of burstiness in the event sequence can be measured by a single value derived from the IET distribution, namely, the burstiness parameter B , which is defined as [17]

$$B \equiv \frac{\sigma - \langle \tau \rangle}{\sigma + \langle \tau \rangle}, \quad (5)$$

where σ and $\langle \tau \rangle$ are the standard deviation and mean of IETs, respectively. For the regular event sequence, all IETs are the same, leading to $B = -1$, while for the totally random, Poisson process, since $\sigma = \langle \tau \rangle$, one gets $B = 0$. In the extremely bursty case, characterized by $\sigma \gg \langle \tau \rangle$, one finds $B \rightarrow 1$. However, when analyzing the empirical event sequences of finite sizes, the value of σ is typically limited by the number of events n such that the maximum value of σ

turns out to be $\sigma_{\max} \simeq \langle \tau \rangle \sqrt{n-1}$, allowing to propose an alternative burstiness measure [30]:

$$B_n \equiv \frac{\sqrt{n+1}\sigma - \sqrt{n-1}\langle \tau \rangle}{(\sqrt{n+1}-2)\sigma + \sqrt{n-1}\langle \tau \rangle}, \quad (6)$$

which can have the value of 1 (0) in the extremely bursty case (in the Poisson process) for any n .

4. The correlations between IETs have been characterized by several measures [8]. Among them, we focus on the memory coefficient and bursty train sizes. The memory coefficient M is defined as the Pearson correlation coefficient between two consecutive IETs, whose value for a sequence of n IETs, i.e., $\{\tau_i\}_{i=1,\dots,n}$, can be estimated by [17]

$$M \equiv \frac{1}{n-1} \sum_{i=1}^{n-1} \frac{(\tau_i - \langle \tau \rangle_1)(\tau_{i+1} - \langle \tau \rangle_2)}{\sigma_1 \sigma_2}, \quad (7)$$

where $\langle \tau \rangle_1$ ($\langle \tau \rangle_2$) and σ_1 (σ_2) are the average and the standard deviation of the first (last) $n-1$ IETs, respectively. Positive M implies that the small (large) IETs tend to be followed by small (large) IETs. Negative M implies the opposite tendency, while $M = 0$ is for the uncorrelated IETs. In many empirical analyses, positive M has been observed [17, 31–33].

5. Another notion for measuring the correlations between IETs is the bursty trains [7]. A bursty train is defined as a set of consecutive events such that IETs between any two consecutive events in the bursty train are less than or equal to a given time window Δt , while those between events in different bursty trains are larger than Δt . The number of events in the bursty train is called bursty train size or burst size, and it is denoted by b . The distribution of b would follow an exponential function if the IETs are fully uncorrelated with each other. However, b has been empirically found to be power-law distributed, i.e.,

$$Q_{\Delta t}(b) \sim b^{-\beta} \quad (8)$$

for a wide range of Δt , e.g., in earthquakes, neuronal activities, and human communication patterns [7, 31, 34, 35]. This indicates the presence of higher-order correlations between IETs beyond the correlations measured by M .¹ We note that the exponential distributions of $Q_{\Delta t}(b)$ have also been reported for mobile phone calls of individual users in another work [36].

¹The generalized memory coefficient has also been suggested as the Pearson correlation coefficient between two IETs separated by k IETs [17]. The case with $k = 0$ corresponds to the M in Eq. (7). The relation between the generalized memory coefficients and burst size distributions can be studied for better understanding the correlation structure between IETs.

We show that the statistics of IETs and burst sizes are interrelated to each other [18]. Let us consider an event sequence with $n + 1$ events and n IETs, denoted by $\mathcal{T} \equiv \{\tau_1, \dots, \tau_n\}$. For a given Δt one can detect m bursty trains whose sizes are denoted by $\mathcal{B} \equiv \{b_1, \dots, b_m\}$. The sum of burst sizes must be the number of events, i.e., $\sum_{j=1}^m b_j = n + 1$. With $\langle b \rangle$ denoting the average burst size, we can write

$$m \langle b \rangle = n + 1 \simeq n, \quad (9)$$

where $n \gg 1$ is assumed. The number of bursty trains is related to the number of IETs larger than Δt , i.e.,

$$m = |\{\tau_i | \tau_i > \Delta t\}| + 1. \quad (10)$$

It is because each burst size, say b , requires $b - 1$ consecutive IETs less than or equal to Δt and one IET larger than Δt . In the case with $n, m \gg 1$, we get

$$m \simeq n F(\Delta t), \quad (11)$$

where $F(\Delta t) \equiv \int_{\Delta t}^{\infty} P(\tau') d\tau'$ denotes the complementary cumulative distribution function of $P(\tau)$. By combining Eqs. (9) and (11), we obtain a general relation as

$$\langle b \rangle F(\Delta t) \simeq 1, \quad (12)$$

which holds for arbitrary functional forms of $P(\tau)$ and $Q_{\Delta t}(b)$ [18].

2.2 Correlation Structure and the Bursty-Get-Burstier Mechanism

We pay special attention to the empirical observation that the tail parts of burst size distributions are characterized by the same power-law exponent for a wide range of time windows, e.g., ranging from a few minutes to the order of 1 h in mobile phone communication patterns [7]. To better understand this observation, let us begin with a simple example in Fig. 2. For each given time window Δt_l with “level” $l = 0, 1, 2$, one can obtain the corresponding set of burst sizes, denoted by $\{b^{(l)}\}$. Here we observe that several bursty trains at the level l are merged to make one bursty train at the level $l + 1$. In other words, one burst size in $\{b^{(l+1)}\}$ is typically written as a sum of several burst sizes in $\{b^{(l)}\}$. By characterizing this merging pattern one can get insight into the correlation structure between IETs. In particular, we raise a question: In order to find the power-law tail as $Q_{\Delta t_l}(b^{(l)}) \sim b^{(l)-\beta}$ for every l , which burst sizes in $\{b^{(l)}\}$ should be merged to make one burst size in $\{b^{(l+1)}\}$?

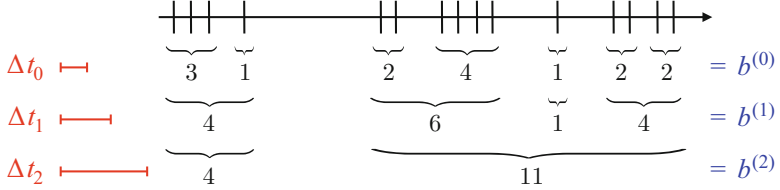


Fig. 2 Schematic diagram for the hierarchical organization of bursty trains at various timescales with 15 events, denoted by vertical lines. These events are clustered using time windows Δt_l with $l = 0, 1, 2$, and the sizes of bursty trains or burst sizes are denoted by $b^{(l)}$, e.g., $\{b^{(1)}\} = \{4, 6, 1, 4\}$

One possible answer to this question has recently been suggested, which is called the bursty-get-burstier (BGB) mechanism [18], indicating that the bigger (smaller) bursty trains tend to follow the bigger (smaller) ones.

We introduce one implementation method of the BGB mechanism following Ref. [18], where $P(\tau)$ and $Q_{\Delta t_0}(b^{(0)})$ are assumed to be given. Although this method has been suggested for arbitrary forms of $P(\tau)$ and $Q_{\Delta t_0}(b^{(0)})$, we focus on the case with power-law tails for both distributions. Precisely, we consider a power-law $P(\tau)$ with a power-law exponent $\alpha > 1$ and a lower bound of IET τ_{\min} , i.e.,

$$P(\tau) = (\alpha - 1)\tau_{\min}^{\alpha-1}\tau^{-\alpha}\theta(\tau - \tau_{\min}), \quad (13)$$

and a power-law distribution of burst sizes at the zeroth level ($l = 0$) as

$$Q_{\Delta t_0}(b^{(0)}) = \zeta(\beta)^{-1}b^{(0)-\beta} \text{ for } b^{(0)} = 1, 2, \dots, \quad (14)$$

where $\theta(\cdot)$ denotes the Heaviside step function and $\zeta(\cdot)$ does the Riemann zeta function.

We first prepare a set of n IETs, $\mathcal{T} = \{\tau_1, \dots, \tau_n\}$, that are independently drawn from $P(\tau)$ in Eq. (13). This \mathcal{T} is partitioned into several subsets, denoted by \mathcal{T}_l , at different timescales or levels $l = 0, 1, \dots, L$:

$$\begin{aligned} \mathcal{T}_0 &\equiv \{\tau_i | \tau_{\min} \leq \tau_i \leq \Delta t_0\}, \\ \mathcal{T}_l &\equiv \{\tau_i | \Delta t_{l-1} < \tau_i \leq \Delta t_l\} \text{ for } l = 1, \dots, L-1, \\ \mathcal{T}_L &\equiv \{\tau_i | \tau_i > \Delta t_{L-1}\}, \end{aligned} \quad (15)$$

where $\Delta t_l < \Delta t_{l+1}$ for all l s. For example, one can use $\Delta t_l = \tau_{\min} c s^l$ with constants $c, s > 1$. This partition readily determines the number of bursty trains at each level, denoted by m_l , similarly to Eq. (10):

$$m_l = |\{\tau_i | \tau_i > \Delta t_l\}| + 1. \quad (16)$$

Then the sizes of bursty trains for a given Δt_l are denoted by $\mathcal{B}_l \equiv \{b^{(l)}\}$, with $m_l = |\mathcal{B}_l|$. To generate \mathcal{B}_0 , m_0 burst sizes are independently drawn from $Q_{\Delta t_0}(b^{(0)})$ in Eq. (14). Partitioning \mathcal{B}_0 into subsets and summing up the burst sizes in each subset leads to \mathcal{B}_1 . Precisely, for each l , \mathcal{B}_l is sorted, e.g., in a descending order, then it is sequentially partitioned into m_{l+1} subsets of the (almost) same size. The sum of $b^{(l)}$'s in each subset leads to one $b^{(l+1)}$, implying that the bigger bursty trains are merged together, so do the smaller ones. This procedure is repeated until the level L is reached. Using the information on which burst sizes at the level l are merged to get each of burst sizes at the level $l + 1$, one can construct the sequence of IETs by permuting IETs in \mathcal{T} and finally get the event sequence. See Ref. [18] for details. Numerical simulations have shown that the generated event sequences show $Q_{\Delta t_l}(b^{(l)}) \sim b^{(l)-\beta}$ at all levels [18].

We remark that the above method lacks some realistic features observed in the empirical analyses. For example, by the above method the number of burst sizes in each partition at the level l is almost the same as being either $\lfloor \frac{m_l}{m_{l+1}} \rfloor$ or $\lfloor \frac{m_l}{m_{l+1}} \rfloor + 1$, which is not always the case. Therefore more realistic merging processes for the correlation structure between IETs could be investigated as a future work.

2.3 Temporal Scaling Behaviors

The scaling relation between α and γ for the uncorrelated IETs in Eq. (4) implies that the autocorrelation function is solely determined by the IET distribution. We can consider a more general case that the IETs are correlated with each other, in particular, in terms of the power-law burst size distributions. Then the temporal correlations measured by the autocorrelation function $A(t_d)$ can be understood by means of the statistical properties of IETs, $P(\tau)$, together with those of the correlations between IETs, $Q_{\Delta t}(b)$. In terms of scaling behaviors, one can study the dependence of γ on α and β .

The dependence of γ on α and β has been investigated by dynamically generating event sequences showing temporal correlations, described by the power-law distributions of IETs and burst sizes in Eqs. (3) and (8). These generative approaches have been based on two-state Markov chain [7] or self-exciting point processes [37]. One can also take an alternative approach by shuffling or permuting a given set of IETs according to the BGB mechanism described in Sect. 2.2, where power-law distributions of IETs and burst sizes are inputs rather than outputs of the model. Then one can explicitly tune the degree of correlations between IETs to test whether the scaling relation in Eq. (4) will be violated due to the correlations between IETs.

For this, the event sequences are generated using the BGB mechanism for the power-law distributions of IETs and burst sizes, which are then analyzed by measuring autocorrelation functions $A(t_d)$ for various values of α and β . The decaying exponent γ of $A(t_d)$ is estimated based on the simple scaling form of

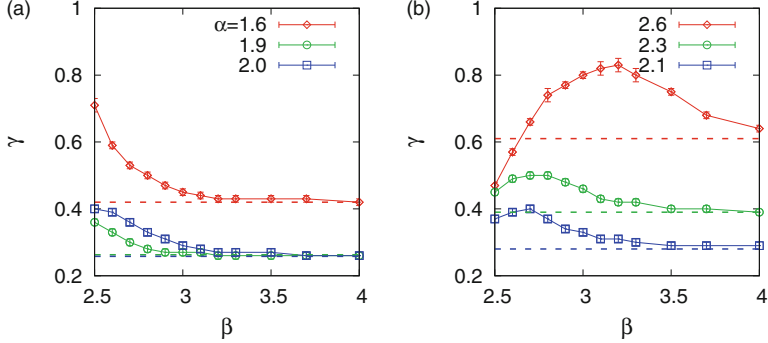


Fig. 3 The values of γ estimated from the numerically obtained autocorrelation functions, for various values of α and β , with horizontal dashed lines corresponding to those for the uncorrelated cases. Reprinted figure with permission from Ref. [18] Copyright (2017) by the American Physical Society

$A(t_d) \sim t_d^{-\gamma}$. The estimated values of γ for various values of α and β are presented in Fig. 3. When $\alpha \leq 2$, it is numerically found that the autocorrelation functions for $\beta < 3$ deviate from the uncorrelated case, implying the violation of scaling relation between α and γ in Eq. (4). Precisely, the smaller β leads to the larger γ , implying that the stronger correlations between IETs may induce the faster decaying of autocorrelation. On the other hand, in the case with $\alpha > 2$, the estimated γ deviates significantly from that for the uncorrelated case for the almost entire range of β , although γ approaches the uncorrelated case as β increases as expected.

One can argue that the deviation (or the violation of $\alpha + \gamma = 2$) observed for $\beta < 3$ is due to the fact that the variance of b diverges for $\beta < 3$. This argument seems to explain why $\alpha + \gamma = 2$ is observed even when $\beta = 3$, for event sequences generated using two-state Markov chain [7].

For better understanding the above results, more rigorous studies need to be done. As the analytical calculation of γ as a function of β is a very challenging task, one can tackle a simplified problem. For example, the effects of correlations only between two consecutive IETs on the autocorrelation function have been analytically studied to find the M -dependence of γ [38].

2.4 Limits of the Memory Coefficient in Measuring Correlations

The memory coefficient, measuring the correlations only between two consecutive IETs, has been used to analyze event sequences in natural phenomena and human activities as well as to test models for bursty dynamics [17, 31, 33, 37]. It has been found that $M \approx 0.2$ for earthquakes in Japan, while M is close to 0 or less than 0.1

for various human activities [17]. In another work on emergency call records in a Chinese city, individual callers are found to show diverse values of M , i.e., a broad distribution of M ranging from -0.2 to 0.5 but peaked at $M = 0$ [31]. Based on these empirical observations, one might conclude that most of human activities do not show strong correlations between IETs. On the other hand, the empirical value of β for the burst size distributions varies from 2.5 for earthquakes in Japan to $2.8\text{--}3.0$ for Wikipedia editing patterns [35] and $3.9\text{--}4.2$ for mobile phone communication patterns [7, 34], while it is found that $\beta \approx 2.21$ in the emergency call dataset [31]. Since the power-law behaviors of burst size distributions for a wide range of time windows imply the complex, higher-order correlations between IETs, this seems to be inconsistent with the weak correlation implied by the observation $M \approx 0$ in human activities.

This puzzling issue has been resolved by deriving the analytical form of M as a function of parameters describing $P(\tau)$ and $Q_{\Delta t}(b)$ [39]. Here we introduce the derivation of M following Ref. [39]. By considering bursty trains detected using one time window or timescale Δt , we divide $\mathcal{T} = \{\tau_1, \dots, \tau_n\}$ into two subsets as

$$\mathcal{T}_0 \equiv \{\tau_i | \tau_i \leq \Delta t\}, \quad (17)$$

$$\mathcal{T}_1 \equiv \{\tau_i | \tau_i > \Delta t\}. \quad (18)$$

The set of all pairs of two consecutive IETs, $\{(\tau_i, \tau_{i+1})\}$, can be divided into four subsets as follows:

$$\mathcal{T}_{\mu\nu} \equiv \{(\tau_i, \tau_{i+1}) | \tau_i \in \mathcal{T}_\mu, \tau_{i+1} \in \mathcal{T}_\nu\}, \quad (19)$$

where $\mu, \nu \in \{0, 1\}$. By denoting the fraction of IET pairs in each $\mathcal{T}_{\mu\nu}$ by $t_{\mu\nu} \equiv \langle |\mathcal{T}_{\mu\nu}| \rangle / (n - 1)$, the term $\langle \tau_i \tau_{i+1} \rangle$ in Eq. (7) can be written as

$$\langle \tau_i \tau_{i+1} \rangle = \sum_{\mu, \nu \in \{0, 1\}} t_{\mu\nu} \tau^{(\mu)} \tau^{(\nu)}, \quad (20)$$

where

$$\tau^{(0)} \equiv \frac{\int_0^{\Delta t} \tau P(\tau) d\tau}{\int_0^{\Delta t} P(\tau) d\tau}, \quad \tau^{(1)} \equiv \frac{\int_{\Delta t}^{\infty} \tau P(\tau) d\tau}{\int_{\Delta t}^{\infty} P(\tau) d\tau}. \quad (21)$$

Here we have assumed that the information on the correlation between τ_i and τ_{i+1} is carried only by $t_{\mu\nu}$, while such consecutive IETs are independent of each other under the condition that $\tau_i \in \mathcal{T}_\mu$ and $\tau_{i+1} \in \mathcal{T}_\nu$. This assumption of conditional independence is based on the fact that the correlation between τ_i and τ_{i+1} with $\tau_i \in \mathcal{T}_\mu$ and $\tau_{i+1} \in \mathcal{T}_\nu$ is no longer relevant to the burst size statistics, because the bursty trains are determined depending only on whether each IET is larger than Δt or not. Then M in Eq. (7) reads in the asymptotic limit with $n \gg 1$

$$M \simeq \frac{\sum_{\mu, \nu \in \{0, 1\}} t_{\mu\nu} \tau^{(\mu)} \tau^{(\nu)} - \langle \tau \rangle^2}{\sigma^2}. \quad (22)$$

Here we have approximated as $\langle \tau \rangle_1 \simeq \langle \tau \rangle_2 \simeq \langle \tau \rangle$ and $\sigma_1 \simeq \sigma_2 \simeq \sigma$, with $\langle \tau \rangle$ and σ denoting the average and standard deviation of IETs, respectively. Note that $\tau^{(0)}$ and $\tau^{(1)}$ are related as follows:

$$\left(1 - \frac{1}{\langle b \rangle}\right) \tau^{(0)} + \frac{1}{\langle b \rangle} \tau^{(1)} \simeq \langle \tau \rangle. \quad (23)$$

For deriving M in Eq. (22), $t_{\mu\nu}$ s need to be calculated. Since each pair of IETs in \mathcal{T}_{11} implies a bursty train of size 1, the average size of \mathcal{T}_{11} is $m Q_{\Delta t}(1)$, with m denoting the number of bursty trains detected using Δt . Thus, the average fraction of IET pairs in \mathcal{T}_{11} becomes

$$t_{11} \equiv \frac{\langle |\mathcal{T}_{11}| \rangle}{n-1} \simeq \frac{Q_{\Delta t}(1)}{\langle b \rangle}, \quad (24)$$

where Eq. (9) has been used. The pair of IETs in \mathcal{T}_{10} (\mathcal{T}_{01}) is found whenever a bursty train of size larger than 1 begins (ends). Hence, the average fraction of \mathcal{T}_{10} , equivalent to that of \mathcal{T}_{01} , must be

$$t_{10} \equiv \frac{\langle |\mathcal{T}_{10}| \rangle}{n-1} \simeq \frac{1}{\langle b \rangle} \sum_{b=2}^{\infty} Q_{\Delta t}(b) = \frac{1 - Q_{\Delta t}(1)}{\langle b \rangle}, \quad (25)$$

which is the same as $t_{01} \equiv \langle |\mathcal{T}_{01}| \rangle / (n-1)$. Finally, for each bursty train of size larger than 2, we find $b-2$ pairs of IETs belonging to \mathcal{T}_{00} , indicating that the average fraction of \mathcal{T}_{00} is

$$t_{00} \equiv \frac{\langle |\mathcal{T}_{00}| \rangle}{n-1} \simeq \frac{1}{\langle b \rangle} \sum_{b=3}^{\infty} (b-2) Q_{\Delta t}(b) = \frac{\langle b \rangle - 2 + Q_{\Delta t}(1)}{\langle b \rangle}. \quad (26)$$

Note that $t_{00} + t_{01} + t_{10} + t_{11} \simeq 1$. Then by using Eqs. (21) and (23) one obtains

$$\sum_{\mu, \nu \in \{0, 1\}} t_{\mu\nu} \tau^{(\mu)} \tau^{(\nu)} = [\langle b \rangle Q_{\Delta t}(1) - 1] (\langle \tau \rangle - \tau^{(0)})^2 + \langle \tau \rangle^2, \quad (27)$$

finally leading to

$$M \simeq \frac{[\langle b \rangle Q_{\Delta t}(1) - 1] (\langle \tau \rangle - \tau^{(0)})^2}{\sigma^2}. \quad (28)$$

This solution has been derived for arbitrary forms of $P(\tau)$ and $Q_{\Delta t}(b)$.

We investigate the dependence of M on $Q_{\Delta t}(b)$, while keeping the same $P(\tau)$. As for the burst size distribution, we consider a power-law distribution as follows:

$$Q_{\Delta t}(b) = \zeta(\beta)^{-1} b^{-\beta} \text{ for } b = 1, 2, \dots . \quad (29)$$

We assume that $\beta > 2$ for the existence of $\langle b \rangle$, i.e., $\langle b \rangle = \zeta(\beta - 1)/\zeta(\beta)$. As for the IET distribution, a power-law distribution with an exponential cutoff is considered:

$$P(\tau) = \frac{\tau_c^{\alpha-1}}{\Gamma(1-\alpha, \tau_{\min}/\tau_c)} \tau^{-\alpha} e^{-\tau/\tau_c} \theta(\tau - \tau_{\min}), \quad (30)$$

where τ_{\min} and τ_c denote the lower bound and the exponential cutoff of τ , respectively. Here $\Gamma(\cdot, \cdot)$ denotes the upper incomplete Gamma function. Figure 4 shows how M varies according to the power-law exponent β for a given α for both cases with diverging and finite τ_c , respectively. For the numerical simulations, the event sequences were generated using the implementation method of the BGB mechanism in Sect. 2.2, but using Eq. (30). We confirm the tendency that the larger positive value of M is associated with the smaller value of β , i.e., the heavier tail. This tendency can be understood by the intuition that the smaller β implies the stronger correlations between IETs, possibly leading to the larger M . We also find that $M \approx 0$ for $\beta \approx 4$, whether τ_c is finite or infinite. This implies that the apparently conflicting observations in human activities are indeed compatible. Hence, we raise an important question regarding the effectiveness or limits of M in measuring higher-order correlations between IETs. Although the definition of M is straightforward and intuitive, it may not properly characterize the complex correlation structure between IETs in some cases.

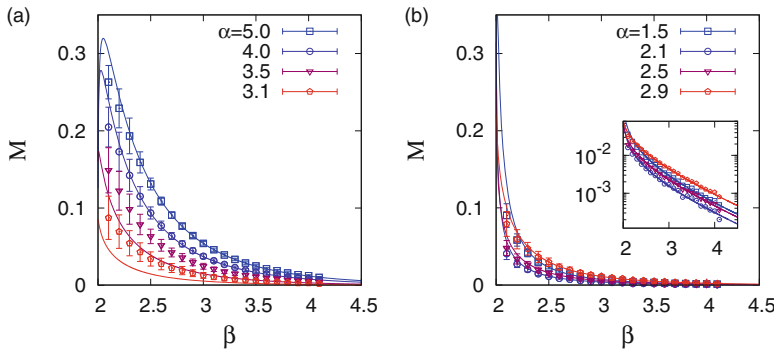


Fig. 4 The analytical solution of M in Eq. (28) as a function of β in Eq. (14) for several values of α in Eq. (30) (solid lines), compared with corresponding numerical results (symbols with error bars). In panel (a) we use the pure power-law distribution of $P(\tau)$ in Eq. (30), with infinite exponential cutoff, i.e., $\tau_c \rightarrow \infty$, while the general form of $P(\tau)$ with $\tau_c = 10^3 \tau_{\min}$ is used in panel (b). The inset shows the same result as in panel (b), but in a semi-log scale. Each point and its standard deviation are obtained from 50 event sequences of size $n = 5 \times 10^5$. Reprinted figure with permission from Ref. [39] Copyright (2018) by the American Physical Society

3 Effects of Correlations Between IETs on Dynamical Processes

The dynamical processes, such as spreading, diffusion, and cascades, taking place in a temporal network of individuals are known to be strongly affected by bursty interaction patterns between individuals [40–53]: In particular, spreading processes in temporal networks have been extensively studied. An important question is what features of temporal networks are most relevant to predict the speed of propagation, e.g., of disease or information. One of the crucial and widely studied features is the heterogeneities of IETs in the temporal interaction patterns. It was shown that the bursty interaction patterns can slow down the early-stage spreading by comparing the simulated spreading behaviors in some empirical networks and in their randomized versions [40, 41, 49]. The opposite tendency was also reported using another empirical network or model networks [44, 45, 48].

In contrast to the effects of heterogeneous IETs on the spreading, yet little is known about the effects of correlations between IETs on the spreading, except for few recent works [52, 54]. This could be partly because the contagion dynamics studied in many previous works, e.g., susceptible-infected (SI) dynamics [51], has focused on an immediate infection upon the first contact between susceptible and infected nodes, hence without the need to consider correlated IETs. In another work [55], probabilistic contagion dynamics, which naturally involves multiple consecutive IETs, was studied by assuming heterogeneous but uncorrelated IETs. Therefore, the effects of heterogeneous and correlated IETs on the spreading need to be systematically studied for better understanding the dynamical processes in complex systems.

To study the spreading dynamics, one can consider one of the extensively studied epidemic processes, i.e., susceptible-infected (SI) dynamics [51]: A state of each node in a network is either susceptible or infected, and an infected node can infect a susceptible node by the contact with it. Here we assume that the contact is instantaneous. One can study a probabilistic SI dynamics, in which an infected node can infect a susceptible node with probability η ($0 < \eta < 1$) per contact, as depicted in Fig. 5a. Due to the stochastic nature of infection, multiple IETs can be involved in the contagion, hence the correlations between IETs in the contact patterns can influence the spreading behavior. The case with $\eta = 1$ corresponds to the deterministic version of SI dynamics: A susceptible node is immediately infected after its first contact with an infected node, see Fig. 5b. Finally, for studying the effect of correlations between IETs on the spreading in a simpler setup, we introduce two-step deterministic SI (“2DSI” in short) dynamics [53] as a variation of generalized epidemic processes [56–59], see Fig. 5c. Here a susceptible node first changes its state to an intermediate state upon its first contact with an infected node; it then becomes infected after the second contact with the same or another infected node. Below we only introduce the results for 2DSI dynamics from Ref. [53].

For modeling the interaction structure in a population, we focus on Bethe lattices as networks of infinite size, where each node has k neighbors. As for the temporal

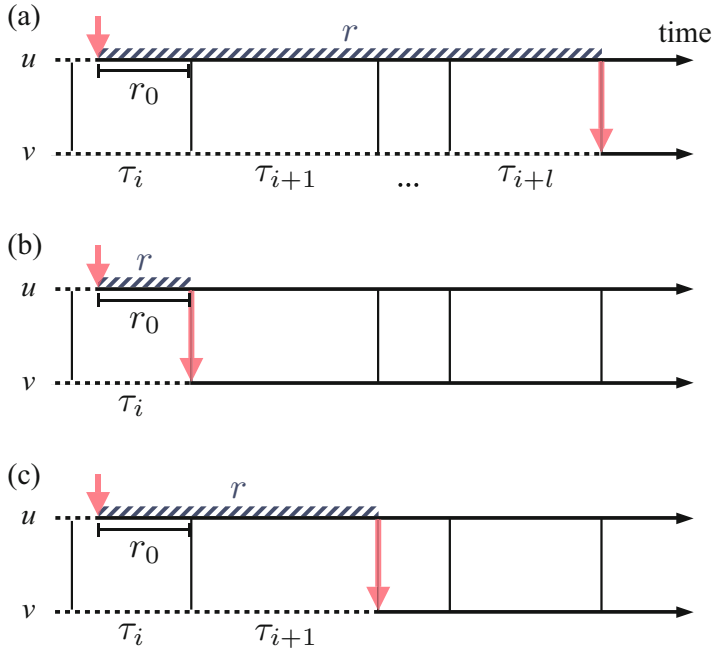


Fig. 5 Schematic diagrams for (a) the probabilistic susceptible-infected (SI) dynamics, (b) the one-step deterministic SI dynamics, and (c) the two-step deterministic SI dynamics. For each node, the susceptible or intermediate state is represented by a dashed horizontal line, while the infected state is by a solid horizontal line. In each panel, a node u gets infected in the time denoted by an upper vertical arrow, then it tries to infect its susceptible neighbor v whenever they make contact (vertical lines). The successful infection of v by u is marked by a lower vertical arrow. The time interval between the infection of u and that of v (striped band) defines the transmission time r . For the definitions of r_0 and τ_s , see the text. Figure in Ref. [53] by Takayuki Hiraoka and Hang-Hyun Jo is licensed under CC BY 4.0

contact patterns, we assume that the contacts between a pair of nodes or on a link connecting these nodes are instantaneous and undirected. Moreover, the contact pattern on each link is assumed to be independent of the states of two end nodes as well as of contact patterns on other links. The contact pattern on each link is modeled by a statistically identical event sequence with heterogeneous and correlated IETs. For this, the shape of IET distribution $P(\tau)$ and the value of memory coefficient M are given as inputs of the model. As for the IET distribution, we adopt $P(\tau)$ in Eq. (30). We fix $\tau_{\min} = 1$ without loss of generality and set $\tau_c = 10^3$ in our work. Based on the empirical findings for α [8], we consider the case with $1.5 \leq \alpha \leq 3$. Secondly, only the positive memory coefficient M is considered, precisely, $0 \leq M < 0.4$, based on the empirical observations [17, 31–33].

Precisely, for each link, we draw n random values from $P(\tau)$ to make an IET sequence $\mathcal{T} = \{\tau_1, \dots, \tau_n\}$, for sufficiently large n . Using Eq. (7), we measure the memory coefficient from \mathcal{T} , denoted by \tilde{M} . Two IETs are randomly chosen in \mathcal{T} and swapped only when this swapping makes \tilde{M} closer to M , i.e., the target

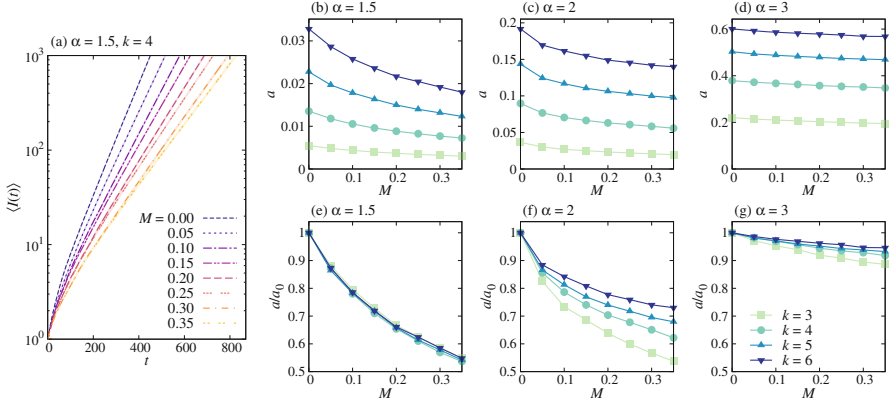


Fig. 6 Two-step deterministic SI dynamics in Bethe lattices: (a) Average numbers of infected nodes as a function of time, $\langle I(t) \rangle$, in Bethe lattices with $k = 4$ for the same IET distribution with power-law exponent $\alpha = 1.5$ in Eq. (30), but with various values of memory coefficient M . For each value of M , the average (dashed curve) and its standard error (shaded area) were obtained from 10^3 runs with different initial conditions. (b–g) Estimated exponential growth rates a , defined in Eq. (31) (top panels) and their relative growth rates a/a_0 with $a_0 \equiv a(M = 0)$ (bottom panels) are plotted for various values of k , α , and M . The lines are guides to the eye. Figure in Ref. [53] by Takayuki Hiraoka and Hang-Hyun Jo is licensed under CC BY 4.0

value. By repeating the swapping, we obtain the IET sequence whose \tilde{M} is close enough to M , and from this IET sequence we get the sequence of contact timings for each link.² Then the temporal network can be fully described by a set of contact timings for all links. Each simulation begins with one node infected at random in time, which we set as $t = 0$, while all other nodes are susceptible at this moment. For each simulation, we measure the number of infected nodes as a function of time, $I(t)$. The average number of infected nodes $\langle I(t) \rangle$ is found to exponentially increase with time, e.g., as shown in Fig. 6a:

$$\langle I(t) \rangle \sim e^{at}, \quad (31)$$

where $a = a(k, \alpha, M)$ denotes the exponential growth rate, known as the Malthusian parameter [61]. a turns out to be a decreasing function of M , indicating the slowdown of spreading due to the positive correlation between IETs, see Fig. 6b–d. The slowdown can be more clearly presented in terms of the relative growth rate a/a_0 with $a_0 \equiv a(M = 0)$ for all cases of k and α , as shown in Fig. 6e–g. We summarize the main observations from the numerical simulations as follows:

1. a decreases with M .
2. a increases with α .

²Another algorithm for generating bursty time series using the copula has recently been suggested [60].

3. a increases with k .
4. The deviation of a/a_0 from 1 tends to be larger for smaller α .

For understanding these observations, we provide an analytical solution for the transmission time in a single link setup. Let us consider a link connecting nodes u and v , see Fig. 5. If u gets infected from its neighbor other than v in time t_u , and later it infects v in time t_v , the time interval between t_u and t_v defines the transmission time $r \equiv t_v - t_u$. Here we assume that v is not affected by any other neighbors than u , for the sake of simplicity. In order for the infected u to infect the susceptible v , u must wait at least for the next contact with v . This waiting or residual time is denoted by r_0 . For the 2DSI dynamics, the transmission process involves two consecutive IETs. If the infection of u occurs during the IET of τ_i , then the transmission time is written as

$$r = r_0 + \tau_{i+1}, \quad (32)$$

with τ_{i+1} denoting the IET following τ_i . Information on the correlations between τ_i and τ_{i+1} is carried by the joint distribution $P(\tau_i, \tau_{i+1})$ or the conditional distribution $P(\tau_{i+1}|\tau_i)$. Using $P(\tau_{i+1}|\tau_i)$ with $\tau_{i+1} = r - r_0$, the transmission time distribution is written as

$$R(r) = \frac{1}{\langle \tau \rangle} \int_0^r dr_0 \int_{r_0}^{\infty} d\tau_i P(\tau_i) P(r - r_0|\tau_i), \quad (33)$$

where it is obvious from Eq. (32) that $\tau_i \geq r_0$ and $0 \leq r_0 \leq r$. The average transmission time is calculated as

$$\langle r \rangle \equiv \int_0^{\infty} dr r R(r) = \frac{1}{2} \left(\langle \tau \rangle + \frac{\sigma^2}{\langle \tau \rangle} \right) + \frac{1}{\langle \tau \rangle} \langle \tau_i \tau_{i+1} \rangle, \quad (34)$$

where

$$\langle \tau_i \tau_{i+1} \rangle \equiv \int_0^{\infty} d\tau_i \int_0^{\infty} d\tau_{i+1} \tau_i \tau_{i+1} P(\tau_i, \tau_{i+1}). \quad (35)$$

In order to relate this result to the memory coefficient in Eq. (7), we define a parameter as

$$M \equiv \frac{\langle \tau_i \tau_{i+1} \rangle - \langle \tau \rangle^2}{\sigma^2} \quad (36)$$

to finally obtain the analytical result of the average transmission time:

$$\langle r \rangle = \frac{3}{2} \langle \tau \rangle + \left(\frac{1}{2} + M \right) \frac{\sigma^2}{\langle \tau \rangle}. \quad (37)$$

We remark that our result in Eq. (37) is valid for arbitrary functional forms of IET distributions as long as their mean and variance are finite. M is coupled with $\sigma^2/\langle\tau\rangle$, implying that the impact of correlations between IETs becomes larger with broader IET distributions. More importantly, we find that a stronger positive correlation between consecutive IETs leads to a larger average transmission time. This can be understood in terms of the role of the variance of IETs in the average transmission time. That is, the variance of the sum of two consecutive IETs is amplified by the positive correlation between those IETs. Based on the result of the single-link analysis, we can understand the numerical results in Fig. 6: The decreasing a with M is expected from Eq. (37), so is the increasing a with α as both $\langle\tau\rangle$ and $\sigma^2/\langle\tau\rangle$ decrease with α . The observation that the deviation of a/a_0 from 1 tends to be larger for smaller α implies that the effect of M becomes larger for smaller α , which can be roughly understood by a larger value of $\sigma^2/\langle\tau\rangle$ coupled to M in Eq. (37). Finally, the increasing a with the degree k is trivial, while the analytical approach to this dependency is not trivial, calling for more rigorous investigation.

4 Discussion

In this Chapter, we have introduced various measures and characterizations for bursty time series analysis and showed how they can be related to each other. Yet more rigorous studies need to be done for understanding such relation comprehensively. In the context of temporal networks, the superposition of event sequences of links incident to a node can result in the event sequence of the node. Then bursty behaviors of a node can be understood in terms of those of links incident to the node. For analyzing the relation between bursty behaviors in nodes and links, one can adopt the notion of contextual bursts by which the scaling behaviors of IET distributions of nodes and links can be systematically understood [62]. Researchers can also study how the correlations between IETs in one node or link are related to those in other nodes or links, how such inter-correlations can be properly characterized, and how they can affect the dynamical processes taking place in temporal networks.

Acknowledgements The authors were supported by Basic Science Research Program through the National Research Foundation of Korea (NRF) funded by the Ministry of Education (NRF-2018R1D1A1A09081919).

References

1. Albert, R., Barabási, A.-L.: Statistical mechanics of complex networks. *Rev. Mod. Phys.* **74**(1), 47–97 (2002)
2. Newman, M.E.J.: Networks: An Introduction, 1st edn. Oxford University Press, Oxford (2010)
3. Holme, P., Saramäki, J.: Temporal networks. *Phys. Rep.* **519**(3), 97–125 (2012)

4. Masuda, N., Lambiotte, R.: A Guide to Temporal Networks. Series on Complexity Science. World Scientific, New Jersey (2016)
5. Gauvin, L., Génois, M., Karsai, M., Kivelä, M., Takaguchi, T., Valdano, E., Vestergaard, C.L.: Randomized reference models for temporal networks. arXiv:1806.04032 (2018)
6. Barabási, A.-L.: The origin of bursts and heavy tails in human dynamics. *Nature* **435**(7039), 207–211 (2005)
7. Karsai, M., Kaski, K., Barabási, A.-L., Kertész, J.: Universal features of correlated bursty behaviour. *Sci. Rep.* **2**, 397 (2012)
8. Karsai, M., Jo, H.-H., Kaski, K.: Bursty Human Dynamics. Springer, Cham (2018)
9. Eckmann, J.-P., Moses, E., Sergi, D.: Entropy of dialogues creates coherent structures in e-mail traffic. *Proc. Natl. Acad. Sci.* **101**(40), 14333–14337 (2004)
10. Malmgren, R.D., Stouffer, D.B., Campanharo, A.S.L.O., Amaral, On universality in human correspondence activity. *Science* **325**(5948), 1696–1700 (2009)
11. Cattuto, C., Van den Broeck, W., Barrat, A., Colizza, V., Pinton, J.-F., Vespignani, A.: Dynamics of person-to-person interactions from distributed RFID sensor networks. *PLoS One* **5**(7), e11596 (2010)
12. Jo, H.-H., Karsai, M., Kertész, J., Kaski, K.: Circadian pattern and burstiness in mobile phone communication. *New J. Phys.* **14**(1), 013055 (2012)
13. Rybski, D., Buldyrev, S.V., Havlin, S., Liljeros, F., Makse, H.A.: Communication activity in a social network: relation between long-term correlations and inter-event clustering. *Sci. Rep.* **2**, 560 (2012)
14. Jiang, Z.-Q., Xie, W.-J., Li, M.-X., Podobnik, B., Zhou, W.-X., Stanley, H.E.: Calling patterns in human communication dynamics. *Proc. Natl. Acad. Sci.* **110**(5), 1600–1605 (2013)
15. Stopczynski, A., Sekara, V., Sapiezynski, P., Cuttone, A., Madsen, M.M., Larsen, J.E., Lehmann, S.: Measuring large-scale social networks with high resolution. *PLoS One* **9**(4), e95978 (2014)
16. Panzarasa, P., Bonaventura, M.: Emergence of long-range correlations and bursty activity patterns in online communication. *Phys. Rev. E* **92**(6), 062821 (2015)
17. Goh, K.-I., Barabási, A.-L.: Burstiness and memory in complex systems. *Europhys. Lett.* **81**, 48002 (2008)
18. Jo, H.-H.: Modeling correlated bursts by the bursty-get-burstier mechanism. *Phys. Rev. E* **96**(6), 062131 (2017)
19. Wheatland, M.S., Sturrock, P.A., McTiernan, J.M.: The waiting-time distribution of solar flare hard x-ray bursts. *Astrophys. J.* **509**, 448–455 (1998)
20. Corral, Á.: Long-term clustering, scaling, and universality in the temporal occurrence of earthquakes. *Phys. Rev. Lett.* **92**, 108501 (2004)
21. de Arcangelis, L., Godano, C., Lippiello, E., Nicodemi, M.: Universality in solar flare and earthquake occurrence. *Phys. Rev. Lett.* **96**(5), 051102 (2006)
22. Kemuriyama, T., Ohta, H., Sato, Y., Maruyama, S., Tandai-Hiruma, M., Kato, K., Nishida, Y.: A power-law distribution of inter-spike intervals in renal sympathetic nerve activity in salt-sensitive hypertension-induced chronic heart failure. *BioSystems* **101**(2), 144–147 (2010)
23. Sorribes, A., Armendariz, B.G., Lopez-Pigozzi, D., Murga, C., de Polavieja, G.G.: The origin of behavioral bursts in decision-making circuitry. *PLoS Comput. Biol.* **7**(6), e1002075 (2011)
24. Boyer, D., Crofoot, M.C., Walsh, P.D.: Non-random walks in monkeys and humans. *J. R. Soc. Interface* **9**(70), 842–847 (2012)
25. Mainardi, F., Gorenflo, R., Vivoli, A.: Beyond the Poisson renewal process: a tutorial survey. *J. Comput. Appl. Math.* **205**(2), 725–735 (2007)
26. Lowen, S.B., Teich, M.C.: Fractal renewal processes generate 1/f noise. *Phys. Rev. E* **47**, 992–1001 (1993)
27. Vajna, S., Tóth, B., Kertész, J.: Modelling bursty time series. *New J. Phys.* **15**(10), 103023 (2013)
28. Abe, S., Suzuki, N.: Violation of the scaling relation and non-Markovian nature of earthquake aftershocks. *Phys. A: Stat. Mech. Appl.* **388**(9), 1917–1920 (2009)

29. Lee, B.-H., Jung, W.-S., Jo, H.-H.: Hierarchical burst model for complex bursty dynamics. *Phys. Rev. E* **98**(2), 022316 (2018)
30. Kim, E.-K., Jo, H.-H.: Measuring burstiness for finite event sequences. *Phys. Rev. E* **94**, 032311 (2016)
31. Wang, W., Yuan, N., Pan, L., Jiao, P., Dai, W., Xue, G., Liu, D.: Temporal patterns of emergency calls of a metropolitan city in China. *Phys. A: Stat. Mech. Appl.* **436**, 846–855 (2015)
32. Guo, F., Yang, D., Yang, Z., Zhao, Z.-D., Zhou, T.: Bounds of memory strength for power-law series. *Phys. Rev. E* **95**(5), 052314 (2017)
33. Böttcher, L., Woolley-Meza, O., Brockmann, D.: Temporal dynamics of online petitions. *PLoS One* **12**(5), e0178062 (2017)
34. Karsai, M., Kaski, K., Kertész, J.: Correlated dynamics in egocentric communication networks. *PLoS One* **7**(7), e40612 (2012)
35. Yasseri, T., Sumi, R., Rung, A., Kornai, A., Kertész, J.: Dynamics of conflicts in Wikipedia. *PLoS One* **7**(6), e38869 (2012)
36. Jiang, Z.-Q., Xie, W.-J., Li, M.-X., Zhou, W.-X., Sornette, D.: Two-state Markov-chain Poisson nature of individual cellphone call statistics. *J. Stat. Mech. Theory Exp.* **2016**(7), 073210 (2016)
37. Jo, H.-H., Perotti, J.I., Kaski, K., Kertész, J.: Correlated bursts and the role of memory range. *Phys. Rev. E* **92**(2), 022814 (2015)
38. Jo, H.-H.: Analytically solvable autocorrelation function for weakly correlated interevent times. *Phys. Rev. E* **100**, 012306 (2019)
39. Jo, H.-H., Hiraoka, T.: Limits of the memory coefficient in measuring correlated bursts. *Phys. Rev. E* **97**(3), 032121 (2018)
40. Vazquez, A.: Impact of memory on human dynamics. *Phys. A Stat. Mech. Appl.* **373**, 747–752 (2007)
41. Karsai, M., Kivelä, M., Pan, R.K., Kaski, K., Kertész, J., Barabási, A.-L., Saramäki, J.: Small but slow world: how network topology and burstiness slow down spreading. *Phys. Rev. E* **83**(2), 025102 (2011)
42. Miritello, G., Moro, E., Lara, R.: Dynamical strength of social ties in information spreading. *Phys. Rev. E* **83**(4), 045102 (2011)
43. Iribarren, J.L., Moro, E.: Impact of human activity patterns on the dynamics of information diffusion. *Phys. Rev. Lett.* **103**(3), 038702 (2009)
44. Rocha, L.E.C., Liljeros, F., Holme, P.: Simulated epidemics in an empirical spatiotemporal network of 50,185 sexual contacts. *PLOS Comput. Biol.* **7**(3), e1001109 (2011)
45. Rocha, L.E.C., Blondel, V.D.: Bursts of vertex activation and epidemics in evolving networks. *PLOS Comput. Biol.* **9**(3), e1002974 (2013)
46. Takaguchi, T., Masuda, N., Holme, P.: Bursty communication patterns facilitate spreading in a threshold-based epidemic dynamics. *PLoS One* **8**(7), e68629 (2013)
47. Masuda, N., Holme, P.: Predicting and controlling infectious disease epidemics using temporal networks. *F1000Prime Rep.* **5**, 6 (2013)
48. Jo, H.-H., Perotti, J.I., Kaski, K., Kertész, J.: Analytically solvable model of spreading dynamics with non-poissonian processes. *Phys. Rev. X* **4**(1), 011041 (2014)
49. Perotti, J.I., Jo, H.-H., Holme, P., Saramäki, J.: Temporal network sparsity and the slowing down of spreading. *arXiv:1411.5553* (2014)
50. Delvenne, J.-C., Lambiotte, R., Rocha, L.E.C.: Diffusion on networked systems is a question of time or structure. *Nat. Commun.* **6**, 7366 (2015)
51. Pastor-Satorras, R., Castellano, C., Van Mieghem, P., Vespignani, A.: Epidemic processes in complex networks. *Rev. Mod. Phys.* **87**(3), 925–979 (2015)
52. Artíme, O., Ramasco, J.J., Miguel, M.S.: Dynamics on networks: competition of temporal and topological correlations. *Sci. Rep.* **7**, 41627 (2017)
53. Hiraoka, T., Jo, H.-H.: Correlated bursts in temporal networks slow down spreading. *Sci. Rep.* **8**(1), 15321 (2018)
54. Masuda, N., Rocha, L.E.C.: A Gillespie algorithm for non-Markovian stochastic processes. *SIAM Rev.* **60**(1), 95–115 (2018)

55. Gueuning, M., Delvenne, J.-C., Lambiotte, R.: Imperfect spreading on temporal networks. *Eur. Phys. J. B* **88**(11), 282 (2015)
56. Janssen, H.-K., Müller, M., Stenull, O.: Generalized epidemic process and tricritical dynamic percolation. *Phys. Rev. E* **70**(2), 026114 (2004)
57. Dodds, P.S., Watts, D.J.: Universal behavior in a generalized model of contagion. *Phys. Rev. Lett.* **92**(21), 218701 (2004)
58. Bizhani, G., Paczuski, M., Grassberger, P.: Discontinuous percolation transitions in epidemic processes, surface depinning in random media, and Hamiltonian random graphs. *Phys. Rev. E* **86**(1), 011128 (2012)
59. Chung, K., Baek, Y., Kim, D., Ha, M., Jeong, H.: Generalized epidemic process on modular networks. *Phys. Rev. E* **89**(5), 052811 (2014)
60. Jo, H.-H., Lee, B.-H., Hiraoka, T., Jung, W.-S.: Copula-based algorithm for generating bursty time series. *Phys. Rev. E* **100**, 022307 (2019)
61. Kimmel, M., Axelrod, D.E.: *Branching Processes in Biology*, vol. 19. Springer, New York (2002)
62. Jo, H.-H., Pan, R.K., Perotti, J.I., Kaski, K.: Contextual analysis framework for bursty dynamics. *Phys. Rev. E* **87**, 062131 (2013)

Challenges in Community Discovery on Temporal Networks



Remy Cazabet and Giulio Rossetti

1 Introduction

The modular nature of networks is one of the most studied aspects of network science. In most real-world networks, a mesoscale organization exists, with nodes belonging to one or several *modules* or *clusters* [29]: think of groups in social networks (groups of friends, families, organizations, countries, etc.), or biological networks such as brain networks [27]. The term *community* is commonly used in the network science literature to describe a *set* of nodes that are grouped for *topological* reasons (e.g., they are strongly connected together and more weakly connected to the rest of the network). Other topological criteria exist, such as having a high internal clustering, similar connection patterns, etc. See Sect. 3 for more on this topic). The literature on the topic is large and diverse, not only on the topic of automatic community discovery but also on community evaluation, analysis, or even generation of networks with realistic community structure. In the last 10 years, many works have focused on adapting those problems to temporal networks [36]. In this chapter, we present an overview of the active topics of research on dynamic communities. For each of these topics, when relevant, we highlight some current challenges.

The chapter is organized into five parts. In the first one, we discuss the definition of dynamic *clusters* in temporal networks, and how to represent them. In the second section, we concentrate on the specificity of dynamic communities, in particular focusing on *smoothness*, *identity* and *algorithmic complexity*. Section 4

R. Cazabet (✉)

University of Lyon, UCBL/CNRS, Lyon, France
e-mail: remy.cazabet@gmail.com

G. Rossetti

Knowledge Discovery and Data Mining Lab, ISTI-CNR, Pisa, Italy

focuses on the differences between communities in different types of dynamic networks such as link streams or snapshot sequences. In Sect. 5, we discuss the evaluation of dynamic communities, using internal and external evaluation—requiring appropriate synthetic benchmarks. Finally, in Sect. 6, we briefly introduce existing tools to work with dynamic communities.

2 Representing Dynamic Communities

The first question to answer when dealing with communities is: *what is a good community?* There is no universal consensus on this topic in the literature; thus, in this article, we adopt a definition as large as possible:

Definition 1 (Community) A (static) community in a graph $G = (V, E)$ is (i) a *cluster* (i.e., a *set*) of nodes $C \subseteq V$ (ii) having *relevant* topological characteristics as defined by a community detection algorithm.

The second part of this definition will be discussed in Sect. 3, and is concerned by the question of the *quality* of a set of nodes as a community, based on a topological criterion. On the contrary, this section discusses the transposition of the first part of this definition to temporal networks, i.e., the definition of *dynamic node clusters* themselves, independently of any quality criteria. We use the term cluster in its data analysis meaning, i.e., clusters are groups of items defined such as those items are more similar (in some sense) to each other than to those in other groups (clusters).

To define dynamic clusters, we first need to define what is a temporal network. This question will be discussed in detail in Sect. 4. For now, let's adopt a generic definition provided in [22], representing in an abstract way any type of temporal network:

Definition 2 (Temporal Network) A temporal network, or stream graph, is defined as $S = (T, V, W, E)$, with V a set of nodes, T a set of time instants (continuous or discrete), $W \subseteq T \times V$, and $E \subseteq T \times V \otimes V$.

2.1 Fixed Membership Cluster in Temporal Networks

The first possible transposition of static clusters to temporal networks is to consider memberships as fixed:

Definition 3 (Fixed Membership Cluster) A fixed membership cluster is defined on a temporal network $S = (T, V, W, E)$ as a cluster of nodes $C \subseteq V$

In fixed membership clusters, nodes cannot change community along time. Communities identified using this definition in a temporal network are usually considered relevant when the clustering they induce would be considered relevant according to a static definition of communities (e.g., modularity) in most times t of the temporal

network. Those communities are different from static ones found in the aggregated graph in that they take into account the *temporal order* of edges. Note that in some algorithms such as stochastic block models, in which communities are defined not only by sets of nodes but also by properties of relations between communities, those properties might evolve, while membership themselves stay unchanged (e.g., [26]). This approach can also be combined with *change point detection* to find periods of the graph with *stable* community structures [32].

2.2 Evolving-Membership Clusters in Temporal Networks

In this second transposition of the definition of cluster, nodes can change membership along time. Note that, for methods based on *crisp* communities, each node must belong to one (and only one) community at each step, while less constrained methods allow having nodes not belonging to any community (conversely, belonging to several communities), in some or all steps.

Definition 4 (Evolving-Membership Cluster) An evolving-membership cluster is defined on a temporal network $S = (T, V, W, E)$ as a cluster $C = \{(t, v), (t, v) \subseteq W\}$

Dynamic communities using this type of clusters are usually considered relevant when (i) the clusters it defines at each t would be considered relevant according to a static definition of communities (e.g., modularity) at each step t , and (ii) the clusters it defines at time t are relatively similar to those belonging to the same dynamic cluster at $t - 1$ and $t + 1$. This is related to the notion of dynamic community *smoothness* discussed in Sect. 3.1.

2.2.1 Persistent-Labels Formalism

The usual way to implement this definition is by using what we call the *persistent labels* formalism: community identifiers—labels—are associated with some nodes over some periods. There is, therefore, no notion of being an *ancestor/descendent* of another community: two nodes can either share a common label, and therefore be part of the same dynamic community, or not. This representation is the most widespread, used for instance in [11, 28].

2.3 Evolving-Membership Clusters with Events

One of the most interesting features of dynamic communities is that they can undergo *events*. Their first formal categorization was introduced in [31], which listed six of them (birth, death, growth, contraction, merge, and split). A seventh

operation, continue, is sometimes added to these. In [6], an eighth operation was proposed (resurgence). These events, illustrated in Fig. 1, are the following:

- **Birth:** The first appearance of a new community composed of any number of nodes.
- **Death:** The vanishing of a community: all nodes belonging to the vanished community lose this membership.
- **Growth:** New nodes increase the size of a community.
- **Contraction:** Some nodes are lost by a community, thus reducing its size.
- **Merge:** Two communities or more merge into a single one.
- **Split:** A community, as a consequence of node/edge vanishing, splits into two or more components.
- **Continue:** A community remains unchanged in consecutive time steps.
- **Resurgence:** A community vanishes for a period, then comes back without perturbations as if it has never stopped existing. This event can be seen as a fake death-birth pair involving the same node set over a lagged period (e.g., seasonal behaviors).

Not all operations are necessarily handled by a generic Dynamic Community Detection algorithm.

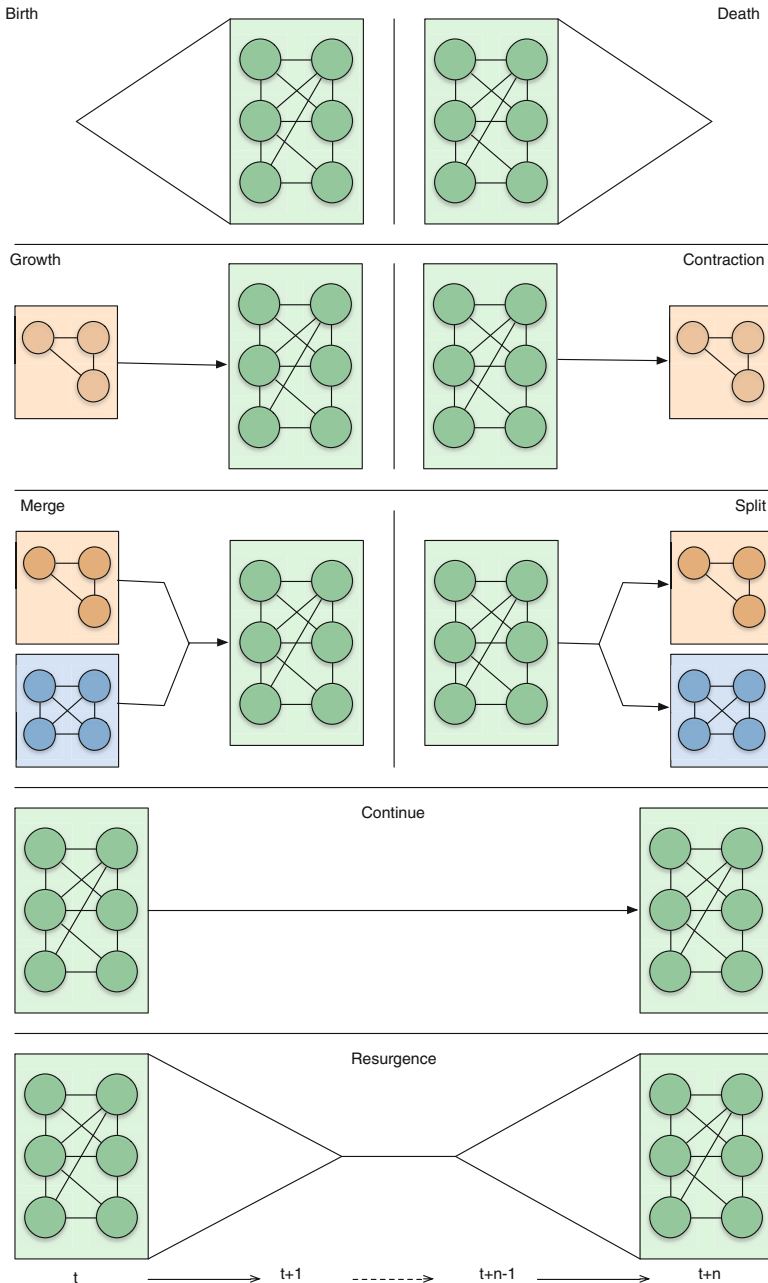
Let's consider a situation in which two communities merge at time t . Using the *persistent-labels* formalism introduced previously, this event can be represented in two ways: either both clusters disappear at time t and a new one—the result of the merge—is created, or one of the clusters becomes the merged one from time t , and the other—considered absorbed—disappear. In both cases, important information is lost. A third definition of evolving membership can be used to solve this problem:

Definition 5 (Evolving-Membership Clusters with Events) Evolving membership cluster with events are defined on a temporal network $S = (T, V, W, E)$ as a set of *fixed-membership Cluster* defined at each time t (or as a set of *evolving-membership clusters*), and a set of community events F . Those events can involve several clusters (merge, split), or a single one (birth, death, shrink, etc.)

2.3.1 Event-Graph Formalism

In practice, most algorithms that do detect events record them in an ad-hoc manner (e.g., the same event can be recorded as: “a split event occurred to community c_1 at time t , yielding communities c_1 and c_2 ” or “community c_2 was born at time t , spawn from c_1 ”). Different representations might even be semantically different. A few works, notably [17], have used an alternative way to represent dynamic communities and events, using what we call here an *event-graph*. We define it as follows:

Definition 6 (Event Graph) An event graph is an oriented graph representing dynamic communities of the temporal network $S = (T, V, W, E)$, in which each node corresponds to a pair $\langle C, t \rangle$, with $C \subseteq V, t \subseteq T$, and each directed edge

**Fig. 1** Different types of community events

represents a relation of continuity between two communities, directed from the earlier to the latter.

Using this representation, some events can be characterized using nodes in/out degrees:

- **In-degree = 0** represents new-born communities
- **In-degree ≥ 2** represents merge events
- **Out-degree = 0** represents death events
- **Out-degree ≥ 2** represents split events

Events represented by an event graph can be much more complex than simple merge/split, since, for instance, a node-community can have multiple out-going links towards node-community having themselves multiple incoming ones.

Both representations, *event-graph* and *persistent labels*, have advantages and drawbacks. The former can represent any event or relation between different communities at different times, while the later can identify which community is *the same as* which other one in a different time.

2.4 Community Life-Cycle

Identified events allow to describe for each cluster the *life-cycle* of its corresponding community:

Definition 7 (Community Life-Cycle) Given a community C , its life-cycle (which univocally identifies C 's complete evolution history) is composed of the directed acyclic graph (DAG) such that (i) the roots are birth events of C , and of its potential predecessors if C has been implicated in merge events; (ii) the leafs are death events, corresponding to deaths of C and of its successors, if C has been implicated in split events; and (iii) the central nodes are the remaining actions of C , its successors, and predecessors. The edges of the tree represent transitions between subsequent actions in C life.

Challenges

Usual events such as birth, merge or shrink were designed to describe a few steps of evolution in the context of snapshot graphs, but are not well suited to describe complex dynamics in networks studied at a fine temporal granularity. In real scenarios, communities are susceptible to evolve gradually. A *shrink* event might corresponds to different scenarios, such as a node switching to another community, a node leaving the system (disappearing), or the community spouting a newborn community composed of a subset of its nodes—and maybe, of other nodes. The usual representation with only labels, even with the addition of some simple events, might be too limited to represent the full range of possible community life-cycle. Defining a complete framework to represent formally complex community evolution scenarios therefore represents a challenge for researchers in the field.

3 Detecting Dynamic Communities

Defining what are good communities in networks is already a challenge in itself. Community discovery is often used as an umbrella term for several related problems, not sharing the same formal objective. It stems from earlier, well-defined problems, in particular, *graph partitioning*, which consists, for a graph and given properties of a partition (number and size of clusters), to find affiliations of nodes minimizing the number of inter-cluster edges. This problem is well-defined, in that its objective can be expressed unequivocally in mathematical terms, and has no trivial solution. But having to provide the number and size of communities was considered too constraining when working with real networks having unknown properties. New methods were therefore introduced, based on ideas such as the modularity [30], compression of random walks [38], stochastic block models (SBM) and minimal description length (MDL) [34], intrinsic properties of communities, and so on. While some of them—e.g., modularity—are based on the same principle of keeping (exceptionally) low the number of inter-community edges, other techniques are searching for completely different things, such as methods based on the Stochastic Block Model framework, in which *blocks* are groups of nodes sharing a similar pattern of connections with nodes belonging to other groups. Furthermore, communities are often categorized in overlapping—one node can belong to several communities—and non-overlapping (crisp) clustering methods. In this chapter, we make abstraction of those differences: each algorithm has a definition of what are *good* static communities, and what we focus on are challenges introduced when going from static to dynamic ones, in particular the notions of temporal smoothness, of identity preservation, and finally the problem of scalability of existing algorithms.

3.1 *Different Approaches of Temporal Smoothness*

In the process of searching for communities over an evolving topology, one of the main questions that need to be answered is: how can the stability of the identified solution be ensured? In static contexts, it has been shown that a generic algorithm executed on the same network that experienced a few topological variations—or even none in case of stochastic algorithms—might lead to different results [1]. The way Dynamic Community Discover (henceforth, DCD) algorithms take into account this problem plays a crucial role in the degree of stability of the solutions they can identify, i.e., on their *smoothness*. In [36] DCD algorithms were grouped in three main categories, depending on the degree of smoothness they aim for:

- Instant Optimal: it assumes that communities existing at time t only depend on the current state of the network at t . Matching communities found at different steps might involve looking at communities found in previous steps, or considering all steps, but communities found at t are considered optimal

concerning the topology of the network at t . By definition, algorithms falling in this family are not temporally smoothed. Examples of Instant Optimal algorithms are [9, 31, 39, 43].

- Temporal Trade-off: it assumes that communities defined at time t depend not only on the topology of the network at t but also on the past topology, past identified partitions, or both. Communities at t are therefore defined as a trade-off between an optimal solution at t and the known past. They do not depend on future topological perturbations. Conversely, from Instant Optimal approaches, the Temporal Trade-off ones are incrementally temporally smoothed. Examples of Temporal Trade-off algorithms are [7, 12, 15, 37].
- Cross-Time: algorithms of this class focus on searching communities relevant when considering the whole network evolution. Methods of this class search a single temporal partition that encompasses all the topological evolution of the observed network: communities identified at time t depend on both past and future network structures. Methods in this class produce communities that are completely temporally smoothed. Examples of Cross-Time algorithms are [2, 13, 20, 25, 44].

All three classes of approaches have advantages and drawbacks; none is superior to the other since they model different DCD problem definition. Nevertheless, we can observe how each one of them is more suitable for some specific use cases. For instance, if the final goal is to provide on-the-fly community detection on a network that will evolve in the future, Instant Optimal and Temporal Trade-off approaches represent the most suitable fit since they do not require to know in advance all the topological history of the analyzed network. Moreover, if the context requires working with a fine temporal granularity, therefore modeling the observed phenomena with link streams instead of snapshots, it is suggested to avoid methods of the first class, which are usually defined to handle well defined—stable—topologies.

Temporal smoothness and partition quality often play conflicting roles. We can observe, for instance that, usually:

- Instant Optimal approaches are the best choice when the final goal is to provide communities that are as good as possible at each step of the evolution of the network;
- Cross-Time approaches are the best choice when the final goal is to provide communities that are coherent in time, particularly over the long term;
- Temporal Trade-off approaches represent a trade-off between these other two classes: they are the best choice in the case of continuous monitoring, rapidly evolving data, and in some cases, limited memory applications. However, they can be subject to “avalanche” effects due to the limited temporal information they leverage to identify communities (i.e., partitions evolve based on local temporal-optimal solutions that, on the long run may degenerate).

3.2 Preservation of Identity: The Ship of Theseus Paradox

The smoothness problem affects the way nodes are split into communities at each time. A different notion is the question of identity preservation along time, which arises in particular in case of a continued slow evolution of communities. It is well illustrated by the paradox of the *ship of Theseus*. It is originally an ancient thought experiment introduced by Plutarch about the identity of an object evolving through time. It can be formulated as follows:

Let's consider a famous ship, the *ship of Theseus*, composed of planks, and kept in a harbor as a historical artifact. As time passes, some planks deteriorate and need to be replaced by new ones. After a long enough period, all the original planks of the ship have been replaced. Can we consider the ship in the harbor to still be *the same* ship of Theseus? If not, at which point exactly did it ceased to be the same ship?

Another aspect of the problem arises if we add a second part to the story. Let's consider that the removed planks were stored in a warehouse, cleaned, and that a new ship, identical to the original one, is built with them. Should this ship, just built out, be considered as the *real* ship of Theseus, because it is composed of the same elements?

Let's call the original ship A , the ship that is in the harbor after all replacements B , and the reconstructed from original pieces, C . In terms of dynamic community detection, this scenario can be modeled by a slowly evolving community $c_1 (c_1 = A)$, from which nodes are removed one after the others, until all of them have been replaced ($c_1 = B$). A new community c_2 appearing after that, composed of the same nodes as the original community ($c_2 = C$). See Fig. 2 for an illustration. A static algorithm analyzing the state of the network at every step would be able to discover that there is, at each step, a community (c_1 , slowly evolving), and, at the

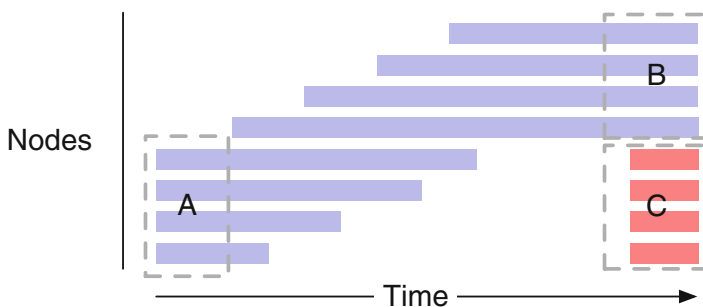


Fig. 2 Illustration of the ship of Theseus paradox. Each horizontal line represents a node. A same color represents nodes belonging to the same community according to a topological criterion (e.g., SBM). The community A is progressively modified until reaching state B . Community C is composed of the same nodes as the other community at its start. Which cluster (B or C) has the same identity as A ? What if all details of the evolution are not known?

end of the experiment, two communities (c_1 and c_2). But the whole point of dynamic community detection is to yield a longitudinal description, and therefore, to decide when two ships at different points in time are *the same* or not.

This problem has barely been considered explicitly in the literature. However, each algorithm has implicitly to make a choice between which ship is the *true* ship of Theseus. For instance, methods that are based on a successive match of communities, such as [17], consider that A and B are the same boats, but not A and C . On the contrary, a method that matches similar clusters without the constraint of being consecutive, such as [11], consider that C is more likely than B to be the same ship than A . Finally, methods such as [28] allow to set what is the influence of time on similarity, and therefore, to choose between those two extreme solutions.

Challenges

The question of identity preservation in dynamic communities has been little discussed and experimented in the literature. For the sake of simplicity, most proposed methods use a mechanism of iterative matching or update of communities and therefore ignore the similarity between ships A and C . However, this situation is probably very common in real networks, for instance, when confronted with seasonal or other cyclical patterns, where groups can disband and reform later. Developing new methods aware of the choice made in terms of identity preservation is, therefore, a challenge for the community.

3.3 Scalability and Computational Complexity

Early methods for community detection in static graphs had high computational complexity (e.g., [14]), thus were not scalable to large graphs. One part of the success of methods such as louvain [4] or infomap [38] is that they can handle networks of thousands of nodes and millions of edges.

Dynamic graphs represent a new challenge in terms of complexity. Among existing algorithms, we can distinguish different categories

- Those whose complexity depends on the *average size of the graph*
- Those whose complexity depends on the *number of graph changes*.

Let's consider the example of a (large) graph composed of n nodes and m edges at time t , and which is evolving at the speed of k changes every step, for s steps. Algorithms in the first category, such as *identify & match* methods, needs to first compute communities at every step, thus their complexity is proportional to $s\mathcal{O}^{CD}(n, m) + (s - 1)\mathcal{O}^{\rightarrow}(n)$ with $\mathcal{O}^{CD}(n, m)$ the complexity of the algorithm used at each step, and $\mathcal{O}^{\rightarrow}(n)$ the complexity of the matching process for communities found on the n nodes.

Conversely, the complexity of an algorithm that update communities at each step such as [7] is roughly proportional (after the initial detection) to $s\mathcal{O}^{+=(k)}$, with $\mathcal{O}^{+=(k)}$ the complexity of updating the community structure according to k

changes. As a consequence, the first category is more efficient in situations where k is large, and n/m are small, while the second is more efficient when n/m are large and k small. The complexity is not necessarily imposed by the adopted definition of community. For instance, algorithms proposed in [31] and [5] yields rigorously the same dynamic communities, but they belong respectively to the first and second categories, as studied in [5].

Another aspect to consider is parallelization. Although the computation of \mathcal{O}^{CD} on many steps might seem expensive, this task can straightforwardly be processed in parallel. On the contrary, methods involving smoothing, or updating the structure in order, cannot be parallelized, as they need to know the communities at time t to compute communities at time $t + 1$. One must, therefore, consider the properties of a temporal network to know which method will or will not be computationally efficient on it.

Challenges

The complexity of DCD algorithms has barely been explored and represents an important challenge to consider in future works. It is important to note that when dynamic networks are considered at a fine temporal resolution as in link streams, the number of edges (interactions) can be much larger than the number of nodes. For instance, in the SocioPatterns Primary School dataset [42], more than 77,000 interactions are observed in a period spanning 2 days, despite having only 242 nodes. Algorithms developed for static algorithms use the sparsity of networks to improve their efficiency, but such an approach might be less rewarding in temporal networks. Analyzing the complexities of existing algorithms and developing new ones adapted to fine temporal resolution is, therefore, a challenge for researchers of the field.

4 Handling Different Types of Temporal Networks

Temporal networks can be modeled in different ways. Among the most common framework, we can cite:

- **Snapshot sequences**, in which the dynamic is represented as an ordered series of graphs
- **Interval graphs** (or series of change) [19], in which intervals of time are associated with edges, and sometimes nodes
- **Link streams** [22], in which edges are associated with a finite set of transient interaction times.

Each DCD algorithm is designed to work on a particular type of network representation. For instance, *Identify & Match* approaches consists of first identifying communities in each snapshot, and then matching similar communities across snapshots. Such a method is therefore designed to work (only) with snapshot sequences. However, as it has been done in several articles, datasets can be

transformed from one representation to the other, for instance by aggregating link streams into snapshots (e.g., [28]), or into interval graphs (e.g., [8]); thus the *representation* of the dynamic graph does not necessarily limit our capacity to use a particular algorithm on a particular dataset.

We think however, that one aspect of the problem, related to representation, has not yet been considered in the literature. Methods working with snapshots and with interval graphs make the implicit assumptions that *the graph any point in time is well defined*, i.e., that each snapshot—or the graph defined by all nodes and edges present at any time t —is not null, has a well-defined community structure, and is somewhat similar to neighboring snapshots. Said differently, those methods expect *progressively evolving* graphs. To the best of our knowledge, this question has not been studied in the literature. A practitioner creating a snapshot sequence from a link stream using a too short sliding window (e.g., a window of 1 h in a dataset of email exchanges) might obtain a well-formed dynamic graph on which an *Identify & Match* method can be applied, but the results would be inconsistent, as the community structure would not persist at such scales. The same dataset analyzed using longer sliding windows might provide insightful results. The problem is particularly pregnant for interval graphs, that can represent real situations of very different nature. For instance, an interval graph could represent relations (friend/follower relation in social networks) as well as interactions (phone calls, face-to-face interactions, etc.). It is clear that both networks should not be processed in the same way.

Challenges

A challenge in the field will be to define the conditions of applicability of different methods better, and theoretical grounds to define when a network needs transformation to become suitable to be analyzed by a given method.

5 Evaluation of Dynamic Communities

We have seen in previous sections that several approaches and methods exist to discover communities in temporal networks. In this section, we first discuss the evaluation of community quality. This process often requires the generation of dynamic networks with community structures, the topic of the second part of the section.

5.1 Evaluation Methods and Scores

As already discussed, there is not a single, universal definition of what is a good community and, consequently, no unique and universal way to evaluate their quality. Nevertheless, for static communities, many functions have been proposed,

to evaluate them either (i) intrinsically (internal evaluation), by means of quality functions, (e.g., Modularity, Conductance, etc.) and (ii) Relatively to a reference partition (external evaluation), using a similarity function (e.g., NMI, aNMI, etc.). Both approaches have pros and cons that have been thoroughly discussed in the literature [33, 45]. Few works have been done to extend those functions to the dynamic case.

5.1.1 Internal Evaluation

In most works, static quality functions are optimized at each step, often adding a trade-off of similarity with temporally adjacent partitions to improve community smoothness (see Sect. 3.1). Some works are based on a longitudinal adaptation of the modularity [1, 28], but they require to create a new graph with added inter-snapshot edges, and therefore cannot be used to evaluate algorithms based on different principles. Works based on Stochastic Block Model [25, 46] also optimize a custom longitudinal quality function.

5.1.2 External Evaluation

Articles doing external evaluation requires to have a reference partition. Since few annotated datasets exist, a synthetic generator is used (see Sect. 5.2). The comparison often uses the average of a static measure (e.g., NMI) computed at each temporal step [3], eventually weighted to take into account the evolution of network properties [35]. A notable exception is found in [16], where windowed versions of similarity functions (Jaccard, NMI, NVI) are introduced, by computing their contingency table on two successive snapshots at the same time.

Challenges

The evaluation of the quality of dynamic communities, both internally and externally, certainly represents a challenge for future works in dynamic community detection. Methods directly adapted from the static case do not consider the specificity of dynamic communities, in particular, the problems of smoothness and community events. This question is of utmost importance, since, despite the large variety of methods already proposed, their performances on real networks besides the ones they have been designed to work on is still mostly unknown.

5.2 Generating Dynamic Graphs with Communities

Complex network modeling studies gave birth to a new field of research: synthetic network generators. Generators allow scientists to evaluate their algorithms on synthetic data whose characteristics resemble the ones that can be observed in

real-world networks. The main reason behind the adoption of network generators while analyzing the performance of a dynamic community detection (DCD) algorithm is the ability to produce benchmark datasets that enable (i) Controlled environment testing, e.g., in term on network size, dynamics, structural properties, etc., and (ii) comparison with a planted ground-truth.

Two families of network generators have been described to provide benchmarks for DCD algorithms: generators that produce static graphs-partitions and generators that describe dynamic graphs-partitions. Static graphs are used to evaluate the quality of the detection at a single time t , and cannot inform about the smoothness of communities. The most known are the GN benchmark [14], the LFR benchmark [21] and planted partitions according to the stochastic block model.

Several methods have been proposed to generate dynamic networks with communities. The network can be composed of a sequence of snapshots, as in [3], in which, at each step, the community structure (based on an SBM) drifts according to a user-defined inter-layer dependency. Another approach consists in having an initial partition yielded by a static algorithm (LFR in [17], GN in [24]), and to make it evolves randomly [17] or until reaching an objective network with a different community structure [24].

Finally, another class of methods generates slowly evolving networks whose changes are driven by community events—merge, split, etc.—that can be tuned with parameters such as the probability of event occurrences. One of these methods is RDyn [35], whose communities are based on a similar principle than LFR. Another method has been proposed in Sengupta et al. [41], which has the particularity of generating overlapping community structures.

Challenges

As we have seen, various methods already exist to generate dynamic graphs with slowly evolving communities. They have different properties, such as community events, stable edges, or overlapping communities. Active challenges are still open in this domain, among them (i) The generation of link streams with community structures, (ii) The empirical comparison of various DCD methods on those benchmarks, and (iii) An assessment on the realism of communities generated with such benchmarks, compared with how empirical dynamic communities behave.

6 Libraries and Standard Formats to Work with Dynamic Communities

In recent years, many tools and software have been developed to manipulate and process network data. Many of those tools have implemented community detection algorithms. Among the best known, we can cite networkx [18], iGraph [10] and snap [23], which propose a wide variety of network analysis tools, among them community detection algorithms, and related quality functions and scores. Some

libraries are even designed specifically for community detection such as CDlib.¹ However, none of them can deal with dynamic networks. Very recently, a few libraries have been introduced to work with dynamic networks, such as tacoma² and pathpy [40] but do not include community detection algorithms.

Furthermore, no standard format has yet emerged to represent dynamic communities and their evolution, which is particularly a problem to compare solutions yielded by different methods. This lack of common tools and standard representation certainly represents an obstacle, and a challenge to overcome for the DCD research community.

7 Conclusion

In this chapter, we have introduced the theoretical aspects of dynamic community detection and highlighted some of the most interesting challenges in the field. Among them, we think that a better formalism to represent the evolution of dynamic clusters and their events, in particular in the context of gradually evolving communities, would facilitate the comparison and the evaluation of communities and detection methods. The scalability of existing approaches is also a concern, again, in the context of *link streams* or other temporal networks studied at fine temporal scales. Finally, a recently introduced technique *graph embedding*, has attracted a lot of attention in various domains. Applications exist to temporal networks, although no work has focused on the dynamic community detection problem yet, to the best of our knowledge. Using this new technique to propose scalable methods could be another challenge worthy of investigation.

References

1. Aynaud, T., Guillaume, J.L.: Static community detection algorithms for evolving networks. In: Proceedings of the 8th International Symposium on Modeling and Optimization in Mobile, Ad Hoc and Wireless Networks (WiOpt), pp. 513–519. IEEE, Piscataway (2010)
2. Aynaud, T., Guillaume, J.L.: Multi-step community detection and hierarchical time segmentation in evolving networks. In: Proceedings of the 5th SNA-KDD Workshop (2011)
3. Bazzi, M., Jeub, L.G., Arenas, A., Howison, S.D., Porter, M.A.: Generative benchmark models for mesoscale structure in multilayer networks. arXiv preprint arXiv:1608.06196 (2016)
4. Blondel, V.D., Guillaume, J.L., Lambiotte, R., Lefebvre, E.: Fast unfolding of communities in large networks. *J. Stat. Mech: Theory Exp.* **2008**(10), P10,008 (2008)
5. Boudebza, S., Cazabet, R., Azouaou, F., Nouali, O.: Olepm: an online framework for detecting overlapping communities in dynamic social networks. *Comput. Commun.* **123**, 36–51 (2018)

¹<https://github.com/GiulioRossetti/cdlib/tree/master/cdlib>.

²<https://github.com/benmaier/tacoma>.

6. Cazabet, R., Amblard, F.: Dynamic community detection. In: Encyclopedia of Social Network Analysis and Mining, pp. 404–414. Springer, Berlin (2014)
7. Cazabet, R., Amblard, F., Hanachi, C.: Detection of overlapping communities in dynamical social networks. In: 2010 IEEE Second International Conference on Social Computing, pp. 309–314. IEEE, Piscataway (2010)
8. Cazabet, R., Takeda, H., Hamasaki, M., Amblard, F.: Using dynamic community detection to identify trends in user-generated content. *Soc. Netw. Anal. Min.* **2**(4), 361–371 (2012)
9. Chen, Z., Wilson, K.A., Jin, Y., Hendrix, W., Samatova, N.F.: Detecting and tracking community dynamics in evolutionary networks. In: 2010 IEEE International Conference on Data Mining Workshops, pp. 318–327. IEEE, Piscataway (2010)
10. Csardi, G., Nepusz, T.: The igraph software package for complex network research. *Inter. J. Complex Syst.* **16**95 (2006). <http://igraph.org>
11. Falkowski, T., Bartelheimer, J., Spiliopoulou, M.: Mining and visualizing the evolution of subgroups in social networks. In: IEEE/WIC/ACM International Conference on Web Intelligence (WI), pp. 52–58. IEEE, Piscataway (2006)
12. Folino, F., Pizzuti, C.: Multiobjective evolutionary community detection for dynamic networks. In: GECCO '10 Proceedings of the 12th Annual Conference on Genetic and Evolutionary Computation, pp. 535–536 (2010)
13. Ghaseemian, A., Zhang, P., Clauset, A., Moore, C., Peel, L.: Detectability thresholds and optimal algorithms for community structure in dynamic networks. *Phys. Rev. X* **6**(3), 031,005 (2016)
14. Girvan, M., Newman, M.E.: Community structure in social and biological networks. *Proc. Natl. Acad. Sci.* **99**(12), 7821–7826 (2002)
15. Görke, R., Maillard, P., Staudt, C., Wagner, D.: Modularity-driven clustering of dynamic graphs. In: International Symposium on Experimental Algorithms, pp. 436–448. Springer, Berlin (2010)
16. Granell, C., Darst, R.K., Arenas, A., Fortunato, S., Gómez, S.: Benchmark model to assess community structure in evolving networks. *Phys. Rev. E* **92**(1), 012,805 (2015)
17. Greene, D., Doyle, D., Cunningham, P.: Tracking the evolution of communities in dynamic social networks. In: International conference on Advances in Social Networks Analysis and Mining (ASONAM), pp. 176–183. IEEE, Piscataway (2010)
18. Hagberg, A., Swart, P., S Chult, D.: Exploring network structure, dynamics, and function using networkX. Tech. rep., Los Alamos National Lab. (LANL), Los Alamos, NM (United States) (2008)
19. Holme, P., Saramäki, J.: Temporal networks. *Phys. Rep.* **519**(3), 97–125 (2012)
20. Jdidia, M.B., Robardet, C., Fleury, E.: Communities detection and analysis of their dynamics in collaborative networks. In: 2007 2nd International Conference on Digital Information Management, vol. 2, pp. 744–749. IEEE, Piscataway (2007)
21. Lancichinetti, A., Fortunato, S.: Benchmarks for testing community detection algorithms on directed and weighted graphs with overlapping communities. *Phys. Rev. E* **80**(1), 016,118 (2009)
22. Latapy, M., Viard, T., Magnien, C.: Stream graphs and link streams for the modeling of interactions over time. *CoRR abs/1710.04073* (2017). <http://arxiv.org/abs/1710.04073>
23. Leskovec, J., Sosić, R.: Snap: a general-purpose network analysis and graph-mining library. *ACM Trans. Intell. Syst. Technol.* **8**(1), 1 (2016)
24. Lin, Y.R., Chi, Y., Zhu, S., Sundaram, H., Tseng, B.L.: Facetnet: a framework for analyzing communities and their evolutions in dynamic networks. In: Proceedings of the 17th International Conference on World Wide Web (WWW), pp. 685–694. ACM, New York (2008)
25. Matias, C., Miele, V.: Statistical clustering of temporal networks through a dynamic stochastic block model. *J. R. Stat. Soc. Ser. B (Stat Methodol.)* **79**(4), 1119–1141 (2017)
26. Matias, C., Rebafka, T., Villers, F.: Estimation and clustering in a semiparametric Poisson process stochastic block model for longitudinal networks (2015)
27. Meunier, D., Lambiotte, R., Bullmore, E.T.: Modular and hierarchically modular organization of brain networks. *Front. Neurosci.* **4**, 200 (2010)

28. Mucha, P.J., Richardson, T., Macon, K., Porter, M.A., Onnela, J.P.: Community structure in time-dependent, multiscale, and multiplex networks. *Science* **328**(5980), 876–878 (2010)
29. Newman, M.E.: Modularity and community structure in networks. *Proc. Natl. Acad. Sci.* **103**(23), 8577–8582 (2006)
30. Newman, M.E., Girvan, M.: Finding and evaluating community structure in networks. *Phys. Rev. E* **69**(2), 026,113 (2004)
31. Palla, G., Barabási, A.L., Vicsek, T.: Quantifying social group evolution. *Nature* **446**(7136), 664–667 (2007)
32. Peel, L., Clauset, A.: Detecting change points in the large-scale structure of evolving networks. *CoRR* abs/1403.0989 (2014). <http://arxiv.org/abs/1403.0989>
33. Peel, L., Larremore, D.B., Clauset, A.: The ground truth about metadata and community detection in networks. *Sci. Adv.* **3**(5), e1,602,548 (2017)
34. Peixoto, T.P.: Hierarchical block structures and high-resolution model selection in large networks. *Phys. Rev. X* **4**(1), 011,047 (2014)
35. Rossetti, G.: Rdyn: graph benchmark handling community dynamics. *J. Complex Networks* **5**(6), 893–912 (2017). <https://doi.org/10.1093/comnet/cnx016>
36. Rossetti, G., Cazabet, R.: Community discovery in dynamic networks: a survey. *ACM Comput. Surv.* **51**(2), 35 (2018)
37. Rossetti, G., Pappalardo, L., Pedreschi, D., Giannotti, F.: Tiles: an online algorithm for community discovery in dynamic social networks. *Mach. Learn.* **106**(8), 1213–1241 (2017)
38. Rosvall, M., Bergstrom, C.T.: Maps of random walks on complex networks reveal community structure. *Proc. Natl. Acad. Sci.* **105**(4), 1118–1123 (2008)
39. Rosvall, M., Bergstrom, C.T.: Mapping change in large networks. *PloS One* **5**(1), e8694 (2010)
40. Scholtes, I.: When is a network a network?: Multi-order graphical model selection in pathways and temporal networks. In: Proceedings of the 23rd ACM SIGKDD International Conference on Knowledge Discovery and Data Mining, pp. 1037–1046. ACM, New York (2017)
41. Sengupta, N., Hamann, M., Wagner, D.: Benchmark generator for dynamic overlapping communities in networks. In: 2017 IEEE International Conference on Data Mining (ICDM), pp. 415–424. IEEE, Piscataway (2017)
42. Stehlé, J., Voirin, N., Barrat, A., Cattuto, C., Isella, L., Pinton, J., Quaggiotto, M., Van den Broeck, W., Régis, C., Lina, B., Vanhemps, P.: High-resolution measurements of face-to-face contact patterns in a primary school. *PloS One* **6**(8), e23,176 (2011). <http://dx.doi.org/10.1371/journal.pone.0023176>
43. Takaffoli, M., Sangi, F., Fagnan, J., Zaïane, O.R.: Modelc-modeling and detecting evolutions of communities. In: 5th International Conference on Weblogs and Social Media (ICWSM), pp. 30–41. AAAI, Menlo Park (2011)
44. Viard, T., Latapy, M., Magnien, C.: Computing maximal cliques in link streams. *Theor. Comput. Sci.* **609**, 245–252 (2016)
45. Yang, J., Leskovec, J.: Defining and evaluating network communities based on ground-truth. *Knowl. Inf. Syst.* **42**(1), 181–213 (2015)
46. Yang, T., Chi, Y., Zhu, S., Gong, Y., Jin, R.: A bayesian approach toward finding communities and their evolutions in dynamic social networks. In: Proceedings of the International Conference on Data Mining, pp. 990–1001. SIAM, Philadelphia (2009)

Information Diffusion Backbone



From the Union of Shortest Paths to the Union of Fastest Path Trees

Huijuan Wang and Xiu-Xiu Zhan

1 Introduction

Many types of complex networks are designed to serve the diffusion of information, traffic, epidemic or behavior, ranging from telecommunications networks, social networks to railway transportation networks. How information (traffic or epidemic) propagates on a network has been modeled by various processes whereas the underlying network can be static or evolving over time i.e. temporal. For example, transport on e.g. the Internet and transportation networks such as railway, airline and roadway networks is mainly carried along the shortest paths. In a weighted network, the shortest path between two nodes is the path that minimizes the sum of the weights along the path, where the weight of a link may represent the time delay, distance or cost when information traverses the link. We consider the Internet and transportation networks static since the evolution of their topology is far slower than the information diffusion process. Social networks can be considered to be static where nodes represent the individuals and where links indicate the relationship between nodes such as friendship [1]. The information diffusion process on a social network has been modeled by e.g., independent cascade models [43], threshold models [13] and epidemic spreading models [21, 28, 29, 31, 42, 45]. Take the Susceptible-Infected (SI) model as an example. Each individual can be in one of the two states: susceptible (S) or infected (I) where the infected state means that the node possesses the information. An infected node could spread the information to a susceptible neighbor with a rate β . An infected individual remains infected forever. Recently, the temporal nature of contact networks have been taken into account in the spreading processes, i.e., the contacts or connection

H. Wang (✉) · X.-X. Zhan
Delft University of Technology, Delft, The Netherlands
e-mail: H.Wang@tudelft.nl; X.Zhan@tudelft.nl

between a node pair occur at specific time stamps (the link between nodes is time dependent) and information could possibly propagate only through contacts (or temporal links) [15, 16, 34, 37, 46]. In the SI spreading process on a temporal network [28, 45], a susceptible node could get infected with an infection probability β via each contact with an infected node.

Significant progress has been made in understanding how the network topology affects emergent properties such as the distribution of the shortest path length [6], the prevalence of (percentage of nodes reached by) an epidemic or information [28, 30, 31]. In this work, we explore another, less-studied problem: which links (i.e. the static or temporal connection of which node pairs) are likely to contribute to the actual diffusion of information, i.e., appear in a diffusion trajectory? To solve this problem, we will firstly introduce how to construct the information diffusion backbone, a weighted network to represent the probability for each link to appear in an information diffusion trajectory. Our research question is equivalent to how the probability that a link appears in an diffusion trajectory (the weight of the link in the backbone) is related to local network properties of the link or its two ending nodes.

To address this question, we consider two scenarios as examples: (i) the shortest path transport on a static network and (ii) the SI spreading process on a temporal network. These scenarios correspond to a deterministic process on a static network and a stochastic process on a temporal network. Information is assumed to diffuse along the shortest path and the fastest path trees respectively.

2 Network Representation

The topology of a static network G can be represented by an adjacency matrix A consisting of elements $A(i, j)$ that are either one or zero depending on whether node i is connected to j or not. If the network is weighted, the adjacency matrix is also weighted. In this case, each element $A(i, j)$ is equal to the weight of the link if i is connected to j or is equal to zero when i is not connected to j .

A temporal network $\mathcal{G} = (\mathcal{N}, \mathcal{L})$ records the contacts between each node pair at each time step within a given observation time window $[0, T]$. \mathcal{N} is the set of nodes, whose size, i.e., the number of nodes is $N = |\mathcal{N}|$, and $\mathcal{L} = \{l(j, k, t), t \in [0, T], j, k \in \mathcal{N}\}$ is the set of contacts, where the element $l(j, k, t)$ indicates that the nodes j and k have a contact at time step t . A temporal network can also be described by a three-dimensional binary adjacency matrix $\mathcal{A}_{N \times N \times T}$, where the elements $\mathcal{A}(j, k, t) = 1$ and $\mathcal{A}(j, k, t) = 0$ represent, respectively, that there is a contact or no contact between the nodes j and k at time step t .

An integrated weighted network $G_W = (\mathcal{N}, \mathcal{L}_W)$ can be derived from a temporal network \mathcal{G} by aggregating the contacts between each node pair over the entire observation time window T . In other words, two nodes are connected in G_W if there is at least one contact between them in \mathcal{G} . Each link $l(j, k)$ in \mathcal{L}_W is associated with a weight w_{jk} counting the total number of contacts between node j and k in \mathcal{G} .

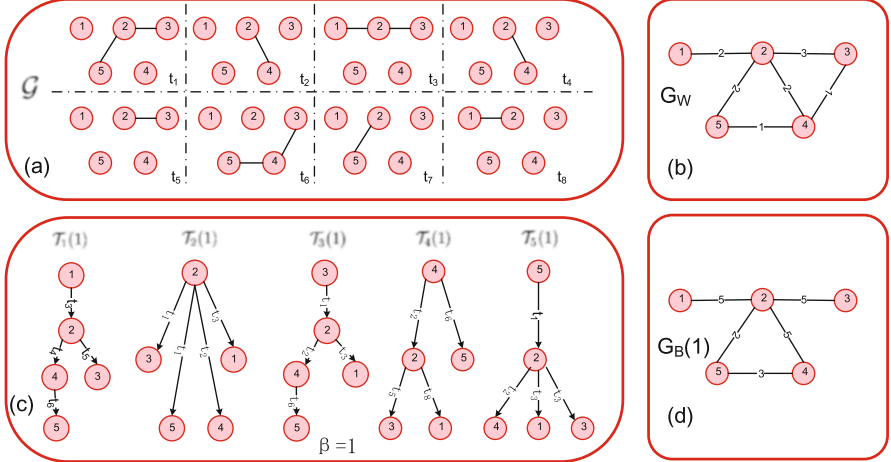


Fig. 1 (a) A temporal network \mathcal{G} with $N = 5$ nodes and $T = 8$ time steps. (b) The integrated weighted network G_W , in which a link exists between a node pair in G_W as long as there is at least one contact between them in \mathcal{G} . The weight of a link in G_W is the number of contacts between the two nodes in \mathcal{G} . (c) Diffusion or fastest path tree $\mathcal{T}_i(\beta)$, where node i is the seed and infection rate is $\beta = 1$. (d) Diffusion backbone $G_B(1)$, where the infection probability $\beta = 1$ in the SI diffusion process. The weight of a node pair represents the number of times it appears in all the diffusion path trees

The integrated weighted network G_W can therefore be described by a weighted adjacency matrix $A_{N \times N}$, with its element

$$A(j, k) = \sum_{t=1}^T \mathcal{A}(j, k, t) \quad (1)$$

counting the number of contacts between a node pair. An example of a temporal network \mathcal{G} and its integrated weighted network G_W are given in Fig. 1a, b, respectively.

3 Shortest Paths in Static Networks

3.1 Construction of the Backbone

We construct the information diffusion backbone as the union of links that possibly appear in an information diffusion trajectory where the weight of each link in the backbone represents the probability that the link appears in an information diffusion trajectory. In case of the shortest path transport on a weighted network G , the information diffusion trajectory between a node pair is the shortest path, the path

that minimizes the sum of the weights over all the links in that path. The topology of the information diffusion backbone G_B is the union of the shortest paths between all possible node pairs. The betweenness of a link in the underlying network is the total number of shortest paths between all node pairs that traverse this link [11, 40]. Hence, the link weight in the backbone is the betweenness of that link in the underlying network normalized by the total number of node pairs ($N(N - 1)/2$).

If the underlying network is unweighted, the topology of the backbone is the same as the topology of the underlying network, because every link in the static network is the shortest path between its two ending nodes. If the underlying network is weighted, the topology of the backbone is possibly a sub-graph of the underlying network. Links in the underlying network that have a zero betweenness do not appear in the backbone.

3.2 Network with i.i.d./Polynomial Link Weights

As an example, we consider the weight w of each link in G is an independently identically distributed (i.i.d.) random variable, that follows the polynomial distribution,

$$F_w(x) = \Pr[w \leq x] = x^\alpha 1_{x \in [0,1]} + 1_{x \in [1,\infty)}, \quad \alpha > 0, \quad (2)$$

where the indicator function 1_z is one if z is true else it is zero. The corresponding probability density is $f_w(x) = \alpha x^{\alpha-1}$, $0 < x < 1$. The exponent

$$\alpha = \lim_{x \downarrow 0} \frac{\log F_w(x)}{\log x}$$

is called the *extreme value index* of the probability distribution. One motivation to consider the polynomial distribution is that link weights around zero primarily influence shortest paths. The polynomial distribution can capture distinct behavior for small values by tuning the α . If $\alpha \rightarrow \infty$, we can obtain $w = 1$ almost surely for all links according to Eq. (2). We can consider the network as unweighted. When $\alpha \rightarrow 0$, all link weights will be close to 0, but, relatively, they differ significantly with each other. When $\alpha = 1$, the polynomial distribution becomes a uniform distribution.

The Minimum Spanning Tree MST on a weighted network is a tree that spans over all the nodes and for which the sum of the weights of all its links is minimal. If the weight of each link is independently identically distributed and if the link weight distribution is sufficiently broad that it reaches the strong disorder region, the backbone topology equals the MST on the underlying network G . Van Mieghem and Magdalena [38] have found that, by tuning the extreme value index α of the polynomial link weight distribution, a phase transition occurs around a critical extreme value α_c . The critical extreme value α_c is defined through the relation

$H(\alpha_c) = \frac{1}{2}$ where $H(\alpha) = \Pr[G_{\cup \text{spt}(\alpha)} = \text{MST}]$ and $G_B = G_{\cup \text{spt}(\alpha)}$ is the backbone topology i.e. the union of all the shortest path trees. When $\alpha > \alpha_c$, the backbone contains more than $N - 1$ links whereas for $\alpha < \alpha_c$, the backbone equals the MST, consisting of $N - 1$ links.

Van Mieghem and Wang found the same phase transition curve $H(\alpha) = \Pr[G_B = \text{MST}]$ versus α/α_c , in diverse types of networks (see Fig. 2) [39]. As α increases, the transport is more likely to traverse over more links and the backbone $G_{\cup \text{spt}(\alpha)}$ will less likely become a tree. This finding strengthens the belief that the curve $F_T(\alpha) \approx 2^{-\left(\frac{\alpha}{\alpha_c}\right)^2}$ is universal for all networks that are not trees.

Which kind of links in G tend to have a high link betweenness, equivalently a high weight in the backbone? Does a low link weight implies a high link betweenness in G ? Table 1 shows the linear correlation coefficient between the

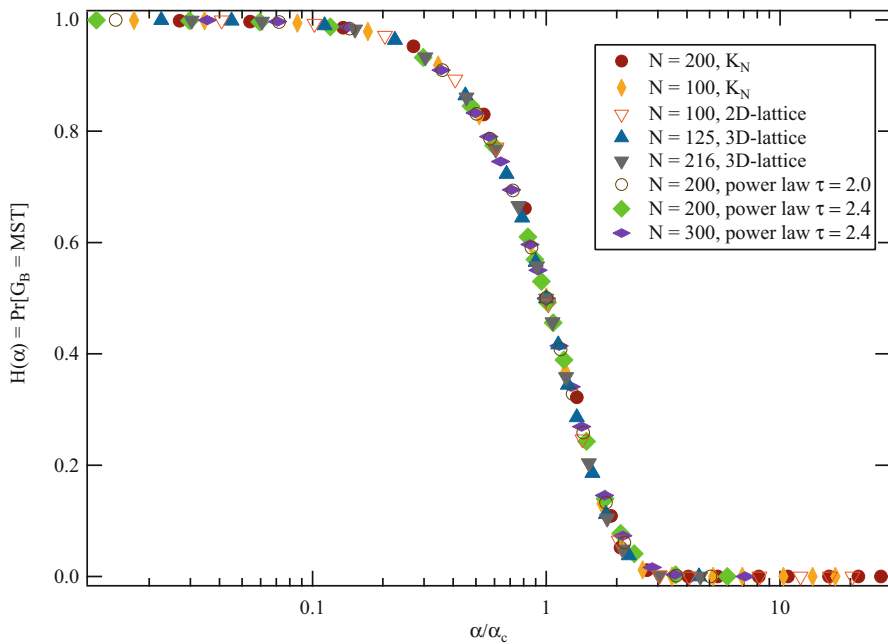


Fig. 2 The probability $H(\alpha) = \Pr[G_B = \text{MST}]$ that the backbone topology equals the MST as a function of α/α_c . Three classes of networks are considered: complete graphs K_N with N nodes, 2D- and 3D lattice and Havel-Hakimi power law networks [4, 5]

Table 1 The correlation coefficient between weight and betweenness of a link

	$\alpha = 0.2$	$\alpha = 1.0$	$\alpha = 2.0$	$\alpha = 4.0$	$\alpha = 8.0$	$\alpha = 16.0$
$G_{\cup \text{spt}}$ on $G_{0.4}(100)$	-0.06	-0.61	-0.70	-0.78	-0.84	-0.84
$G_{\cup \text{spt}}$ on 2D-lattice $N = 100$	-0.22	-0.53	-0.54	-0.53	-0.53	-0.53
$G_{\cup \text{spt}}$ on 3D-lattice $N = 125$	-0.18	-0.60	-0.66	-0.67	-0.68	-0.68
$G_{\cup \text{spt}}$ on BA $N = 100, m = 3$	-0.12	-0.53	-0.66	-0.60	-0.50	-0.49

weight and betweenness of a link in different network models for different index values α [40]. The critical extreme value index $\alpha_c \leq 0.1$ in 2D-lattice with $N = 100$ nodes and 3D-lattice with $N = 125$ nodes [39] and $\alpha_c = 0.2$ in Erdős-Rényi random graphs [38]. When link weights are relatively weakly disordered, i.e., $\alpha \geq 1$, the link weight and betweenness are evidently and negatively correlated, implying a link with a low weight tends to have a high betweenness, a high weight in the backbone. When link weights are in relatively strong disorder e.g. when $\alpha_c = 0.2$, the correlation strength is relatively weak, because the weight of a path i.e. the sum of the link weight over all the links in that path is dominated by the largest link weight [2]. Furthermore, the correlation is shown to be dependent on the underlying graph as well as on the extreme value index α . For homogeneous network models such as the Erdős-Rényi random graphs, the correlation strength increases monotonically as α increases. When $\alpha \rightarrow \infty$, all links have the same weight and almost the same betweenness. As α decreases, or equivalently as the strength of the disorder in link weight increases, a link with a low link weight tends to have a high betweenness. However, in a non-homogeneous topology such as the Barabási-Albert (BA) power law networks, the betweenness of a link depends on both the weight and the connectivity of the link. That is why the correlation strength decreases after a maximum has been reached as α increases. When the underlying network is unweighted, i.e., $\alpha \rightarrow \infty$, how the betweenness of link is related to the local network features, e.g., of the two end nodes of the link is still far from well understood [11, 40].

Besides the number of links and the link weights in the backbone that we focus on in this chapter, other network properties of the backbone such as the degree distribution, the spectrum and the path length of a shortest path have been explored [6, 39].

3.3 Link Weight Scaling

We assume information diffuses along the shortest path, where the weight of a link may represent the distance, delay, monetary cost etc. In functional brain networks, the correlation between the activities measured at any two brain regions by e.g. magnetoencephalography (MEG) can be defined and derived [41]. To compute the shortest paths, the weight of the link between the two regions/nodes can be defined as e.g. one minus the correlation value or the reciprocal of the correlation value [33]. Different choices of the link weight including the correlation may lead to different features of the backbone. We will illustrate the choice of the link weight by the following theorem.

Let $w > 0$ be a weight of an arbitrary link in a given weighted network $G(N, L)$ with N nodes and L links. We construct a new graph $G_{\alpha_1}(N, L)$ by scaling the weight w of each link as $w^{\frac{1}{\alpha_1}}$, where $\alpha_1 > 0$ but without changing the network topology. The backbone of $G_{\alpha_1}(N, L)$ is denoted as $G_B(\alpha_1)$. Similarly, we can

obtain weighted network $G_{\alpha_2}(N, L)$ by scaling each link weight as $w^{\frac{1}{\alpha_2}}$, whose backbone is $G_B(\alpha_2)$ and $\alpha_2 > 0$. The following theorem shows that backbone with a smaller value of α is always included in the backbone with a larger value of α . In other words, all links in $G_B(\alpha_2)$ belong to $G_B(\alpha_1)$ if $\alpha_1 \geq \alpha_2 > 0$.

Theorem 1 *If $\alpha_1 \geq \alpha_2 > 0$, then $G_B(\alpha_2) \subset G_B(\alpha_1)$.*

Proof We order the original set of link weights in $G(N, L)$ as $w_{(1)} \geq w_{(2)} \geq \dots \geq w_{(L)}$, where $w_{(i)}$ denotes the $i - th$ smallest link weight and $1 \leq i \leq L$. The ordering of the link weights in G_{α_1} after link weight transformation with parameter α_1 is unchanged, $w_{(1)}^{\alpha_1} \geq w_{(2)}^{\alpha_1} \geq \dots \geq w_{(L)}^{\alpha_1}$. The same holds for G_{α_2} . The ordering of the weight of all the links is independent of $\alpha > 0$. Our proof is by contradiction. Assume that there exist a link with rank k in G_{α_2} that belongs to $G_B(\alpha_2)$, but this link in G_{α_1} does not belong to $G_B(\alpha_2)$. The link with rank k connects the nodes A and B in both $G_B(\alpha_1)$ and $G_B(\alpha_2)$. The fact that $k \notin G_B(\alpha_1)$ means that there exists a path \mathcal{P}_{AB} between nodes A and B , such that

$$w_k^{\frac{1}{\alpha_1}} > \sum_{i \in \mathcal{P}_{AB}; i < k} w_i^{\frac{1}{\alpha_1}} \quad (3)$$

where, importantly, the rank condition $i < k$ for a link implies that each link in \mathcal{P}_{AB} must have a smaller weight than the link with rank k . Since $w_{(i)}^{\frac{1}{\alpha_1}} = w_{(i)}^{\frac{1}{\alpha_2}} w_{(i)}^{\frac{\alpha_2 - \alpha_1}{\alpha_1 \alpha_2}}$, inequality (3) can be rewritten as

$$w_{(k)}^{\frac{1}{\alpha_1}} = w_{(k)}^{\frac{1}{\alpha_2}} w_{(k)}^{\frac{\alpha_2 - \alpha_1}{\alpha_1 \alpha_2}} > \sum_{i \in \mathcal{P}_{AB}; i < k} w_{(i)}^{\frac{1}{\alpha_2}} w_{(i)}^{\frac{\alpha_2 - \alpha_1}{\alpha_1 \alpha_2}}$$

Since $i < k$, $\alpha_1 \geq \alpha_2$, it holds that $w_{(i)}^{\frac{\alpha_2 - \alpha_1}{\alpha_1 \alpha_2}} > w_{(k)}^{\frac{\alpha_2 - \alpha_1}{\alpha_1 \alpha_2}}$ and

$$\sum_{i \in \mathcal{P}_{AB}; i < k} w_{(i)}^{\frac{1}{\alpha_2}} w_{(i)}^{\frac{\alpha_2 - \alpha_1}{\alpha_1 \alpha_2}} > w_{(k)}^{\frac{\alpha_2 - \alpha_1}{\alpha_1 \alpha_2}} \sum_{i \in \mathcal{P}_{AB}; i < k} w_{(i)}^{\frac{1}{\alpha_2}}$$

Hence,

$$w_{(k)}^{\frac{1}{\alpha_2}} > \sum_{i \in \mathcal{P}_{AB}, i < k} w_{(i)}^{\frac{1}{\alpha_2}}$$

which contradicts the hypothesis that the link with rank $k \in G_B(\alpha_2)$.

This inclusion theorem illustrates the effect of the choice of the link weights, specifically the scaling of the link weights on the link density of the backbone. This

finding is in line with what we have observed before: link weights in strong disorder or with a high variance tends to lead to a sparse backbone or heterogeneous traffic distribution.

4 SI Spreading Process on Temporal Networks

We explore further the other extreme scenario, where a stochastic process, e.g., the SI spreading process unfolds on a temporal network [44].

4.1 Construction of the Backbone

We first construct the backbone when the infection probability of the SI spreading process is $\beta = 1$. At time step $t = 0$, the seed node i is infected and all the other nodes are susceptible. The trajectory of the SI diffusion on \mathcal{G} started from root i can be recorded by a *diffusion path tree* $\mathcal{T}_i(\beta)$, also called the fastest path tree. The diffusion path tree $\mathcal{T}_i(\beta)$ records the union of contacts, via which information reaches each of the rest $N - 1$ nodes in the earliest time. A diffusion tree, composed of maximally $N - 1$ contacts is actually the union of fastest paths to reach the rest $N - 1$ nodes. We define the diffusion backbone $G_B(\beta) = (\mathcal{N}, \mathcal{L}_B(\beta))$ as the union of all diffusion/fastest path trees, i.e., $\bigcup_{i=1}^N \mathcal{T}_i(\beta)$, that start at each node as the seed node. The node set of $G_B(\beta)$ equals the node set \mathcal{N} in the underlying temporal network $\mathcal{G} = (\mathcal{N}, \mathcal{L})$. Nodes are connected in $G_B(\beta)$ if they are connected in any diffusion path tree. Each link in $\mathcal{L}_B(\beta)$ is associated with a weight w_{jk}^B , which denotes the number of times link (j, k) (i.e. contact between j and k) appears in all diffusion path trees. An example of how to construct the diffusion backbone is given in Fig. 1c, d for $\beta = 1$. The ratio $\frac{w_{jk}^B}{N}$ indicates the probability that link (j, k) appears in a diffusion trajectory starting from an arbitrary seed node.

When $0 < \beta < 1$, the diffusion process is stochastic. In this case, we construct the backbone as the average of a number of realizations of the backbones. In each realization, we perform the SI process starting from each node serving as the seed for information diffusion, obtain the diffusion path trees and construct one realization of the diffusion backbone. The weight w_{jk}^B of a link in $G_B(\beta)$ is the average weight of this link over the h realizations. The computational complexity of constructing $G_B(\beta)$ is $\mathcal{O}(N^3 Th)$, where T is the length of the observation time window of the temporal network in number of time steps.

4.2 Real-World Temporal Networks

4.2.1 Description and Basic Features

We consider a large number of empirical temporal networks that capture two types of contacts, i.e., (face-to-face) proximity and electronic communication (mailing and messaging) contacts. These temporal networks and their basic statistical properties are provided in Table 2. The networks are measured at discrete time steps, whereas the duration of a time step differs among the datasets. We have removed the time steps without any contact in order to consider the steps that are relevant for information diffusion and to avoid the periods that have no contact due to technical errors in measurements.

4.2.2 Observation Time Windows

We aim to understand which node pairs are likely to be connected in the backbone, thus to contribute to a diffusion process and how such connection in the backbone is related to this node pair's local temporal connection properties. However, real-world temporal networks are measured for different lengths T of time windows as showing in Table 2. If a diffusion process has a relatively high spreading probability and the temporal network has a relatively long observation time window, most nodes

Table 2 Basic properties of a list of empirical networks: The number of nodes (N), the original length of the observation time window (T in number of steps), the total number of contacts ($|\mathcal{C}|$), the number of links ($|\mathcal{L}_W|$) in G_W and contact type

Network	N	T	$ \mathcal{C} $	$ \mathcal{L}_W $	Contact type
Reality mining (RM) [8, 32]	96	33,452	1,086,404	2539	Proximity
Hypertext 2009 (HT2009) [17, 19]	113	5246	20,818	2196	Proximity
High school 2011 (HS2011) [9]	126	5609	28,561	1710	Proximity
High school 2012 (HS2012) [9]	180	11,273	45,047	2220	Proximity
High school 2013 (HS2013) [23]	327	7375	188,508	5818	Proximity
Primary school (PS) [36]	242	3100	125,773	8317	Proximity
Workplace (WP) [10]	92	7104	9827	755	Proximity
Manufacturing email (ME) [22, 24]	167	57,791	82,876	3250	Electronic communication
Email eu (EEU) [20]	986	207,880	332,334	16,064	Electronic communication
Haggle [3, 14]	274	15,662	28,244	2124	Proximity
Infectious [18]	410	1392	17,298	2765	Proximity
DNC email (DNC) [7]	1866	18,682	37,421	4384	Electronic communication
Collegemsg [27]	1899	58,911	59,835	13,838	Electronic communication

can be reached within a short time. The temporal contacts happened afterwards will not contribute to the diffusion process. Hence, we will select the time windows such that all contacts within each selected time window could possibly contribute, or equivalently, are relevant to a diffusion process. On the other hand, we will consider several time windows for each temporal network. This will allow us to understand how the time window of a temporal network may influence the relation between the backbones of different spreading probabilities and relation between a node pair's local connection properties and its connection in the backbone. We select the observation time windows for each measured temporal network within its original time window $[0, T]$ as follows. On each measured temporal network with its original observation time window $[0, T]$, we conduct the SI diffusion process with $\beta = 1$ by setting each node as the seed of the information diffusion process and plot the average prevalence ρ as a function of time, which is the time step t normalized by the original length of observation window T (see Fig. 3). The average prevalence at the end of the observation is recorded as $\rho(t/T = 1)$. The time to reach the steady state varies significantly across the empirical networks. The prevalence curves ρ of the last four networks in the list (i.e., *Haggle*, *Infectious*, *DNC* and *Collegemsg*) increase slowly and approximately linearly over the whole period. In the other networks, however, the diffusion finishes or stops earlier and contacts happened afterwards are not relevant for the diffusion process.

For each real-world temporal network with its original length of observation time window T , we consider the following lengths of observation time windows: the time $T_p\%$ when the average prevalence reaches $p\%$, where $p \in \{10, 20, \dots, 90\}$

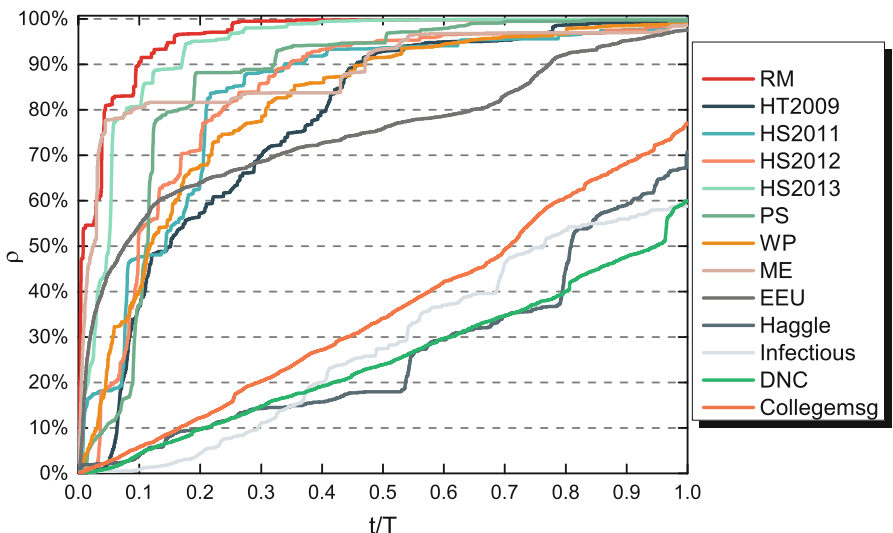


Fig. 3 Average prevalence ρ of the SI spreading process with $\beta = 1$ on each original empirical temporal network over time. The time steps are normalized by the corresponding observation time window T of each network

and $p\% < \rho(t = T)$. For a given empirical temporal network $\mathcal{G} = (\mathcal{N}, \mathcal{L})$, we consider maximally nine observation time windows. For each length $T_{p\%}$, we construct a sub-temporal network, $\mathcal{G}_{p\%} = (\mathcal{N}, \mathcal{L}_{p\%})$, in which $\mathcal{L}_{p\%}$ include contacts in \mathcal{L} that occur earlier than $T_{p\%}$. The lengths of observation time window $T_{p\%}$ for the empirical networks are given in [44]. For a network like *RM*, we can get nine sub-networks and for network like *Infectious*, we can only obtain five sub-networks. In total, we obtain 106 sub-networks. Contacts in all these sub-networks are possibly relevant for a SI diffusion process with any spreading probability β . Without loss of generality, we will consider all these sub-networks with diverse lengths of observation time windows and temporal network features to study the relationship between diffusion backbones and temporal connection features.

4.3 Relationship Between Diffusion Backbones

What are the relationships among the backbones $G_B(\beta)$ with different spreading probabilities $\beta \in [0, 1]$ on the same temporal network? When the infection probability $\beta \rightarrow 0$, the backbone $G_B(\beta \rightarrow 0)$ approaches the integrated weighted network G_W if the network is finite regarding to its size and number of contacts, as proved in [44].

We denote $G_B(\beta \rightarrow 0) \triangleq G_B(\beta = 0) = G_W$ except that the weight of each node pair in the two networks are scaled. When the infection probability β is small, node pairs with more contacts are more likely to appear in the backbone. The backbone $G_B(\beta)$ varies from $G_B(0) = G_W$ when $\beta \rightarrow 0$ to $G_B(1)$ when $\beta = 1$. $G_B(\beta = 0)$ well approximates the backbones with a small β . Similarly, $G_B(1)$ well approximates the backbones with a large β . When the observation time window of a temporal network is small, the backbones with different β are relatively similar in topology.

4.3.1 Degree of a Node in Different Backbones

From now on, we focus on the two extreme backbones $G_B(0) = G_W$ and $G_B(1)$. A node pair that has at least one contact may not necessarily contribute to a diffusion process. Hence, the degree of a node in $G_B(0)$ is larger or equal to its degree in $G_B(1)$. A universal finding is that the degree of a node in these two backbones tend to be linearly and positively correlated in all the empirical networks, where the linear correlation coefficient between the degree of a node in these two backbones is above 0.7 for all networks [44]. Since $G_B(1)$ is a sub-graph of G_W , the degrees of a node in these two backbones tend to be correlated if these two backbones have a similar number of links. However, the two backbones may differ much in number of links in many temporal networks, especially those with a long observation window. Figure 4 shows the scatter plot of the degree of each node in G_W and $G_B(1)$ respectively for the network with the longest observation window from two datasets respectively. In

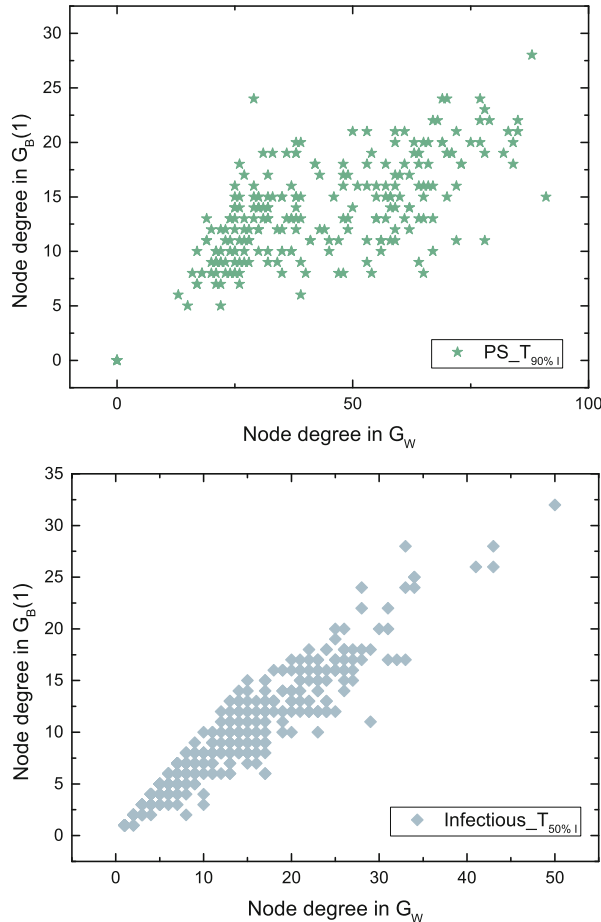


Fig. 4 Scatter plots of each node's degree in G_W and in $G_B(1)$ for networks *PS* and *Infectious* with the longest observation window respectively

both cases, the backbone G_W and $G_B(1)$ differ much in the number of links. Our observation suggests that a node that has contacts with many others tends to be able to propagate the information directly to many others.

4.4 Identifying the Diffusion Backbone $G_B(1)$

In this section, we investigate how to identify the (large weight) links in the backbone $G_B(1)$ based on local and/or temporal connection properties of each node pair. The key objective to understand how local and temporal connection features of a node pair are related to its role in the diffusion backbone $G_B(1)$. Our investigation

may also allow us to approximate the backbone, whose computational complexity is high ($\mathcal{O}(N^3 T)$) base on local temporal features whose computational complexity is low.

We propose to consider systematically a set of local temporal features of a node pair and examine whether node pairs having a higher value of each feature/metric tend to be connected in the backbone $G_B(1)$. Some of these properties are derived from the integrated network G_W whereas the feature *Time-scaled Weight* that we will propose encodes also the time stamps of the contacts between a node pair. These node pair properties or metrics are:

- *Time-scaled Weight* of a node pair (j, k) is defined as

$$\phi_{jk}(\alpha) = \sum_{m=1}^n \left(\frac{1}{t_{jk}^{(m)}} \right)^\alpha \quad (4)$$

where n is the total number of contacts between j and k over the given observation window and $t_{jk}^{(i)}$ is the time stamp when the i 'th contact occurs and α is the scaling parameter to control the contribution of temporal information. For the node pairs that have no contact, their temporal weights are assumed to be zero. The motivation to consider this metric is that when each node is set as the seed of a diffusion process at time $t = 0$, contacts that happen earlier have a higher probability to contribute to the actual diffusion, i.e. appear in $G_B(1)$. When $\alpha = 0$, $\phi_{jk}(0) = w_{jk}^B(\beta = 0)$ degenerates to the weight of the node pair in G_W . When α is larger, node pairs with early contacts have a relatively higher time-scaled weight.

- *Degree Product* of a node pair (j, k) is the product $d_j(\beta = 0) \cdot d_k(\beta = 0)$ of the degrees of j and k in the integrated network G_W . Two nodes that are not connected in G_W , have a degree product zero. Given the degree of each node in $G_B(1)$ and if the links are randomly placed as in the configuration model [26], the probability that a node pair (j, k) is connected in $G_B(1)$ is proportional to $d_j(\beta = 1) \cdot d_k(\beta = 1)$, which approximates $d_j(\beta = 0) \cdot d_k(\beta = 0)$ since the degrees of a node in G_W and $G_B(1)$ are found to be strongly and positively correlated and only node pairs connected in G_W are possible to be connected in $G_B(1)$.
- *Strength Product* of a node pair (j, k) is defined as the product $s_j(\beta = 0) \cdot s_k(\beta = 0)$ of the node strengths of j and k in G_W , where the strength $s_j(\beta = 0) = \sum_{i \in \mathcal{N}} A(j, i)$ of a node in G_W equals the total weight of all the links incident to this node [12, 41]. Two nodes that are not connected in G_W are considered to have Strength Product zero.
- *Betweenness* of a link in G_W counts the number of shortest paths between all node pairs that traverse the link. The distance of each link, based on which the shortest path is computed, is considered to be $\frac{1}{w_{jk}^B(\beta = 0)}$, inversely proportional to its link weight in G_W , because a node pair with more contacts tend to propagate information faster [25, 40]. If two nodes are not connected in G_W , they have a

zero betweenness. Although betweenness is not a local topological property, we consider it as a benchmark property that has been widely studied.

We explore further whether these node pair features could well identify the links in $G_B(1)$. According to the definition of the aforementioned metrics, a higher value of a metric may suggest the connection of the corresponding node pair in $G_B(1)$. According to each metric, we rank the node pairs and the $|\mathcal{L}_B(1)|$ node pairs with the highest values are identified as the links in $G_B(1)$. The identification quality of a metric, e.g. the time-scaled weight $\phi_{jk}(\alpha)$, is quantified as the overlap r between the identified link set $\mathcal{L}_B(\phi_{jk}(\alpha))$ and the link set $\mathcal{L}_B(1)$ in $G_B(1)$

$$r = r(\mathcal{L}_B(\phi_{jk}(\alpha)), \mathcal{L}_B(1)) = \frac{|\mathcal{L}_B(\phi_{jk}(\alpha)) \cap \mathcal{L}_B(1)|}{|\mathcal{L}_B(1)|}, \quad (5)$$

We focus first on the time-scaled weight $\phi_{jk}(\alpha)$ and explore how the quality of identifying links in $G_B(1)$ by using this metric is influenced by the scaling parameter α . As shown in Fig. 5, the quality differs mostly when $0 \leq \alpha \leq 2$ and

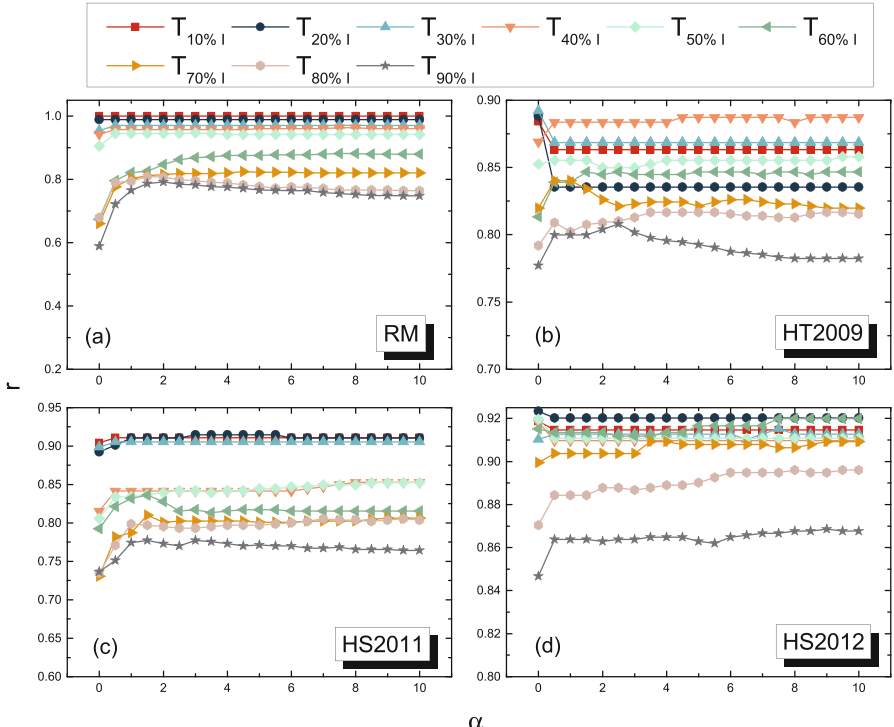
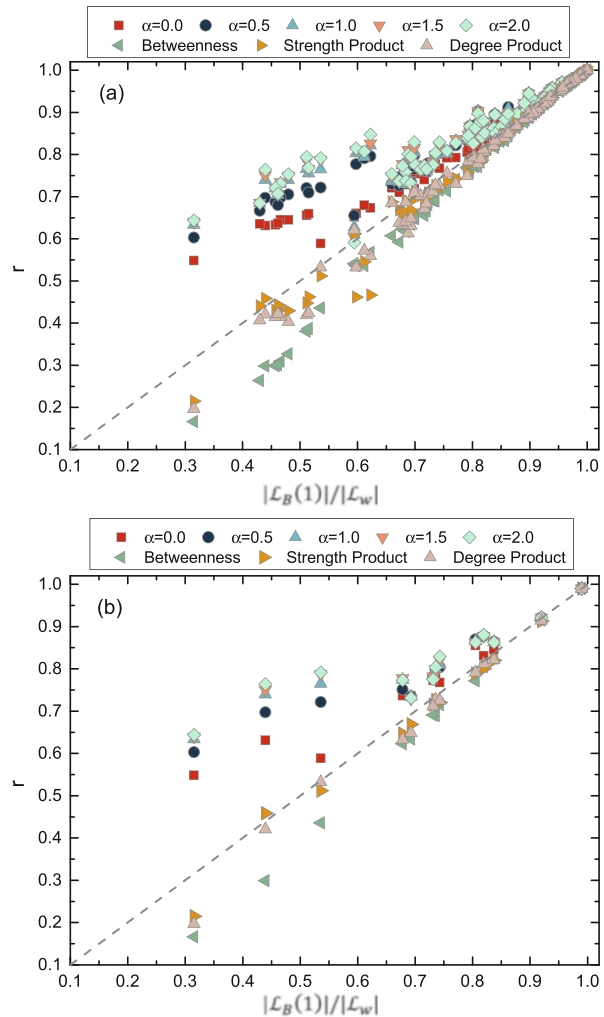


Fig. 5 The quality of identifying links in $G_B(1)$ by using the time-scaled weight $\phi_{jk}(\alpha)$ in relation to α in temporal networks derived from datasets (a) RM, (b) HT2009, (c) HS2011 and (d) HS2012

Fig. 6 The quality of identifying links in $G_B(1)$ by using each metric for (a) all the networks with all possible observation windows; (b) all the networks with longest observation windows. The time-scaled weight with different α values are considered



remains relatively the same when $\alpha \geq 2$ in all temporal networks. Hence, we will confine ourselves to the range $0 \leq \alpha \leq 2$.

The identification quality r by using each metric versus the ratio $\frac{|\mathcal{L}_B(1)|}{|\mathcal{L}_w|}$ of the number of links in $G_B(1)$ to that in G_w are plotted in Fig. 6 for all the empirical temporal networks, with different lengths of the observation time windows. The diagonal curve $r = \frac{|\mathcal{L}_B(1)|}{|\mathcal{L}_w|}$ corresponds to the quality of the random identification, where $|\mathcal{L}_B(1)|$ links are randomly selected from the links in G_w as the identified links in $G_B(1)$. Degree product, strength product and betweenness perform, in general, worse than or similarly to the random identification. Even if the connections in $G_B(1)$ were random given the degree of each node in $G_B(1)$, the quality r of identifying links in $G_B(1)$ by using the degree product can be close to the

quality of the random identification, if the distribution of the degree product is relatively homogeneous or if the $\frac{|\mathcal{L}_B(1)|}{|\mathcal{L}_W|}$ is large. The degree distribution in $G_B(1)$ is indeed relatively homogeneous and $\frac{|\mathcal{L}_B(1)|}{|\mathcal{L}_W|}$ is large in most empirical networks. This explains why the degree product performs similarly to the random identification. The link weight in G_W , equivalently, $\phi_{jk}(\alpha = 0)$, outperforms the random identification, whereas the time-scaled weight $\phi_{jk}(\alpha)$ with a larger α performs better. Node pairs with many contacts that occur early tend to contribute to the actual information propagation, i.e., be connected in $G_B(1)$. This observation suggests that the temporal information is essential in determining the role of nodes in a spreading process.

We investigate further whether these metrics can identify the links with the highest weights in $G_B(1)$. We choose the top $f|\mathcal{L}_B(1)|$ node pairs according to each metric as the identification of the top f fraction of links in $G_B(1)$ with the highest weights. The quality r of identifying the top f fraction of links with the highest weight in $G_B(1)$ is plotted in Fig. 7 for the networks with the longest observation

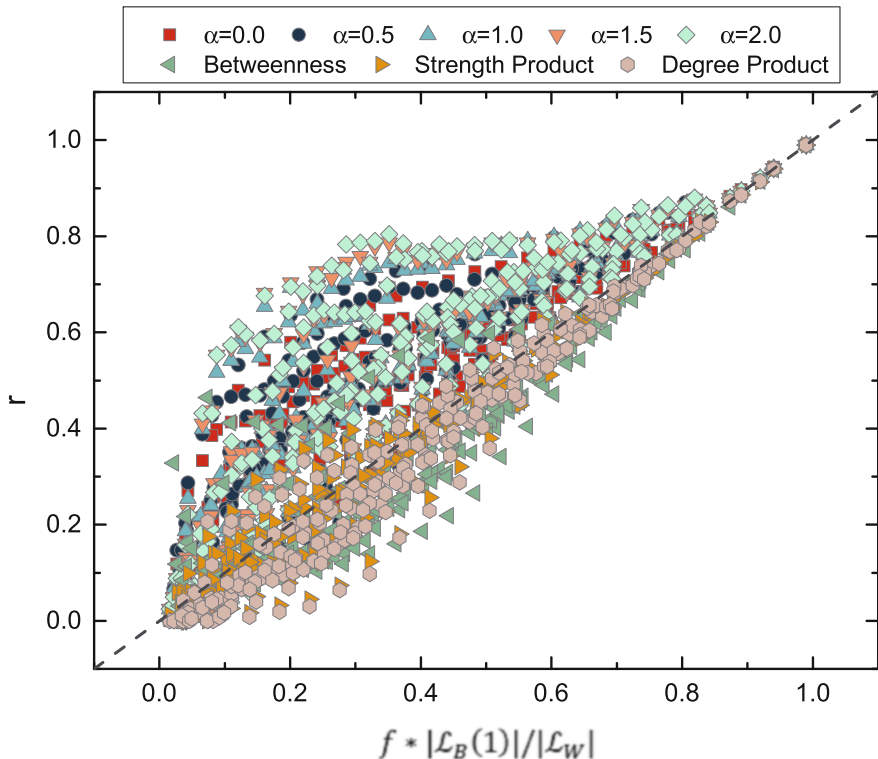


Fig. 7 The quality r of identifying top f fraction weighted links in $G_B(1)$ by using each metric for each network with the longest observation window in each dataset. We consider the time-scaled weight with $\alpha \in [0, 2]$

window from each dataset. The line $r = f \frac{|\mathcal{L}_B(1)|}{|\mathcal{L}_W|}$ corresponds to the quality of the random identification. Similar to the identification of all the links in $G_B(1)$, the time-scaled weight $\phi_{jk}(\alpha)$ with a large α performs the best in identifying highly weighted links in $G_B(1)$, emphasizing again the important role of the temporal information of contacts.

5 Conclusion and Discussions

In this chapter, we address a generic question, namely, which links (either static or temporal) are more likely to appear in an information diffusion trajectory. We construct the backbone as the union of links that possibly appear in a diffusion trajectory. Each link in the backbone is associated with a weight representing the probability that the link appears in a diffusion trajectory. When information diffuses along the shortest path on a static weighted network, the backbone is the union of shortest paths. Both numerical simulations and our theory point out the importance of the link weight in determining the a link's probability to appear in a diffusion trajectory. When information propagates through the fastest path trees governed by the SI spreading model, the backbone is the union of the fastest path trees rooted at every possible seed node. The temporal information of the contacts between a node pair turns out to be crucial in determining the node pair's weight in the backbone. A node pair with many early contacts tends to have a high weight in the backbone. Still, using such local topological properties to predict the links that tend to appear in the backbone or have a high weight in the backbone is far from accurate.

The backbones can be defined or constructed differently to capture various roles of links in diverse types of diffusion trajectories. Grady et al. [35] considered the shortest path routing on a weighted network. They defined the salience of a link as the probability that it appears in a shortest path tree rooted at an arbitrary node. The difference between link salience and link betweenness has been discussed in [35]. Considering unweighted static networks, Zhang et al. [47] defined the link transmission centrality, which can be used to identify weak ties in social networks and is shown to be correlated with link betweenness. How link salience and transmission centrality are related to local topological properties remains a non-trivial question. Our question which links are more likely to appear in an information diffusion trajectory is challenging and interesting for the Susceptible-Infected-Susceptible epidemic spreading process on a static network. An epidemic spreads through a link only when one end node of the link is susceptible whereas the other is infected. The relation between the infection probability of a node and its local topological properties is still far from well understood. The correlation between the states (infected or not) of two neighboring nodes introduces extra complexity.

References

1. Barabási, A.L.: Network Science. Cambridge University Press, Cambridge (2016)
2. Braunstein, L., Wu, Z., Chen, Y., Buldyrev, S., Kalisky, T., Sreenivasan, S., Cohen, R., López, E., Havlin, S., Stanley, H.: Optimal path and minimal spanning trees in random weighted networks. I. J. Bifurcation and Chaos **17**, 2215–2255 (2007). <https://doi.org/10.1142/S0218127407018361>
3. Chaintreau, A., Hui, P., Crowcroft, J., Diot, C., Gass, R., Scott, J.: Impact of human mobility on opportunistic forwarding algorithms. IEEE Trans. Mob. Comput. **6**(6), 606–620 (2007)
4. Chartrand, G., Lesniak, L.: Graphs and Digraphs. Chapman and Hall/CRC, London/Boca Raton (1996)
5. Chartrand, G., Oellermann, O.R.: Applied and Algorithmic Graph Theory. McGraw-Hill College, New York City (1992)
6. Chen, Y., López, E., Havlin, S., Stanley, H.E.: Universal behavior of optimal paths in weighted networks with general disorder. Phys. Rev. Lett. **96**, 068,702 (2006). <https://doi.org/10.1103/PhysRevLett.96.068702>
7. Dnc emails network dataset – KONECT. <http://konect.uni-koblenz.de/networks/dnc-temporalGraph>
8. Eagle, N., (Sandy) Pentland, A.: Reality Mining: sensing complex social systems. Pers. Ubiquitous Comput. **10**(4), 255–268 (2006)
9. Fournet, J., Barrat, A.: Contact patterns among high school students. PloS One **9**(9), e107878 (2014)
10. Génois, M., Vestergaard, C.L., Fournet, J., Panisson, A., Bonmarin, I., Barrat, A.: Data on face-to-face contacts in an office building suggest a low-cost vaccination strategy based on community linkers. Net. Sci. **3**(3), 326–347 (2015)
11. Goh, K.I., Oh, E., Jeong, H., Kahng, B., Kim, D.: Classification of scale-free networks. Proc. Natl. Acad. Sci. **99**(20), 12,583–12,588 (2002). <https://doi.org/10.1073/pnas.202301299>
12. Grady, D., Thiemann, C., Brockmann, D.: Robust classification of salient links in complex networks. Nat. Commun. **3**, 864 (2012)
13. Granovetter, M.: Threshold models of collective behavior. Am. J. Sociol. **83**(6), 1420–1443 (1978)
14. Haggle network dataset – KONECT. <http://konect.uni-koblenz.de/networks/contact>
15. Holme, P.: Modern temporal network theory: a colloquium. Eur. Phys. J. B **88**(9), 234 (2015)
16. Holme, P., Saramäki, J.: Temporal networks. Phys. Rep. **519**(3), 97–125 (2012)
17. Hypertext 2009 network dataset – KONECT. <http://konect.uni-koblenz.de/networks/sociopatterns-hypertext>
18. Isella, L., Stehlé, J., Barrat, A., Cattuto, C., Pinton, J.F., Van den Broeck, W.: What's in a crowd? analysis of face-to-face behavioral networks. J. Theor. Biol. **271**(1), 166–180 (2011)
19. Isella, L., Stehlé, J., Barrat, A., Cattuto, C., Pinton, J.F., den Broeck, W.V.: What's in a crowd? analysis of face-to-face behavioral networks. J. Theor. Biol. **271**(1), 166–180 (2011)
20. Leskovec, J., Kleinberg, J., Faloutsos, C.: Graph evolution: densification and shrinking diameters. ACM Trans. Knowl. Discov. Data **1**(1), 2 (2007)
21. Liu, C., Zhan, X.X., Zhang, Z.K., Sun, G.Q., Hui, P.M.: How events determine spreading patterns: information transmission via internal and external influences on social networks. New J. Phys. **17**(11), 113,045 (2015)
22. Manufacturing emails network dataset – KONECT. http://konect.uni-koblenz.de/networks/radoslaw_email
23. Mastrandrea, R., Fournet, J., Barrat, A.: Contact patterns in a high school: a comparison between data collected using wearable sensors, contact diaries and friendship surveys. PloS One **10**(9), e0136,497 (2015)
24. Michalski, R., Palus, S., Kazienko, P.: Matching organizational structure and social network extracted from email communication. In: Lecture Notes in Business Information Processing, vol. 87, pp. 197–206. Springer, Berlin (2011)

25. Newman, M.E.: Scientific collaboration networks. ii. shortest paths, weighted networks, and centrality. *Phys. Rev. E* **64**(1), 016,132 (2001)
26. Newman, M.E.J., Strogatz, S.H., Watts, D.J.: Random graphs with arbitrary degree distributions and their applications. *Phys. Rev. E* **64**(2), 026,118 (2001)
27. Panzarasa, P., Opsahl, T., Carley, K.M.: Patterns and dynamics of users' behavior and interaction: network analysis of an online community. *J. Assoc. Inf. Sci. Technol.* **60**(5), 911–932 (2009)
28. Pastor-Satorras, R., Castellano, C., Van Mieghem, P., Vespignani, A.: Epidemic processes in complex networks. *Rev. Mod. Phys.* **87**(3), 925 (2015)
29. Pastor-Satorras, R., Castellano, C., Van Mieghem, P., Vespignani, A.: Epidemic processes in complex networks. *Rev. Mod. Phys.* **87**, 925–979 (2015)
30. Qu, B., Wang, H.: Sis epidemic spreading with correlated heterogeneous infection rates. *Physica A: Stat. Mech. Appl.* **472**, 13–24 (2017)
31. Qu, B., Wang, H.: Sis epidemic spreading with heterogeneous infection rates. *IEEE Trans. Netw. Sci. Eng.* **4**, 177–186 (2017)
32. Reality mining network dataset – KONECT. <http://konect.uni-koblenz.de/networks/mit>
33. Rubinov, M., Sporns, O.: Complex network measures of brain connectivity: uses and interpretations. *NeuroImage* **52**(3), 1059–1069 (2010). Computational Models of the Brain
34. Scholtes, I., Wider, N., Pfizner, R., Garas, A., Tessone, C.J., Schweitzer, F.: Causality-driven slow-down and speed-up of diffusion in non-markovian temporal networks. *Nat. Commun.* **5**, 5024 (2014)
35. Shekhtman, L.M., Bagrow, J.P., Brockmann, D.: Robustness of skeletons and salient features in networks. *J. Complex Networks* **2**(2), 110–120 (2014)
36. Stehlé, J., Voirin, N., Barrat, A., Cattuto, C., Isella, L., Pinton, J.F., Quaggiotto, M., Van den Broeck, W., Réglis, C., Lina, B., et al.: High-resolution measurements of face-to-face contact patterns in a primary school. *PloS One* **6**(8), e23,176 (2011)
37. Valdano, E., Ferreri, L., Poletto, C., Colizza, V.: Analytical computation of the epidemic threshold on temporal networks. *Phys. Rev. X* **5**(2), 021,005 (2015)
38. Van Mieghem, P., Magdalena, S.M.: A phase transition in the link weight structure of networks. *Phys. Rev. E* **72**, 056,138 (2005)
39. Van Mieghem, P., Wang, H.: The observable part of a network. *IEEE/ACM Trans. Networking* **17**(1), 93–105 (2009). <https://doi.org/10.1109/TNET.2008.925089>
40. Wang, H., Hernandez, J.M., Van Mieghem, P.: Betweenness centrality in a weighted network. *Phys. Rev. E* **77**, 046,105 (2008)
41. Wang, H., Douw, L., Hernández, J.M., Reijneveld, J.C., Stam, C.J., Van Mieghem, P.: Effect of tumor resection on the characteristics of functional brain networks. *Phys. Rev. E* **82**, 021,924 (2010)
42. Wang, H., Li, Q., D'Agostino, G., Havlin, S., Stanley, H.E., Van Mieghem, P.: Effect of the interconnected network structure on the epidemic threshold. *Phys. Rev. E* **88**, 022,801 (2013)
43. Watts, D.J.: A simple model of global cascades on random networks. *Proc. Natl. Acad. Sci. USA* **99**(9), 5766–5771 (2002)
44. Zhan, X.X., Hanjalic, A., Wang, H.: Information diffusion backbones in temporal networks. *Sci. Rep.* **9**(1), 6798 (2019)
45. Zhang, Z.K., Liu, C., Zhan, X.X., Lu, X., Zhang, C.X., Zhang, Y.C.: Dynamics of information diffusion and its applications on complex networks. *Phys. Rep.* **651**, 1–34 (2016)
46. Zhang, Y.Q., Li, X., Vasilakos, A.V.: Spectral analysis of epidemic thresholds of temporal networks. *IEEE Trans. Cybern.* (to be published). <https://doi.org/10.1109/TCYB.2017.2743003>
47. Zhang, Q., Karsai, M., Vespignani, A.: Link transmission centrality in large-scale social networks. *EPJ Data Sci.* **7**(1), 33 (2018)

Continuous-Time Random Walks and Temporal Networks



Renaud Lambiotte

1 Introduction

Random walks are a paradigmatic model for stochastic processes, finding applications in a variety of scientific domains [1, 2], and helping to understand how the random motion of particles leads to diffusive processes at the macroscopic scale. Classically defined on infinitely large regular lattices or on continuous media, random walks have long been studied on non-trivial topologies, as different parts of the system, adjacent or not, are connected through a predefined transition probability. In a finite and discrete setting, random walks are equivalent to Markov chains [3], whose behaviour is entirely encoded in their transition matrix. The matrix allows to characterise the succession of states visited by the walker, whose dynamics is seen as a discrete-time process and where time is measured by the number of jumps experienced by the walker. However, the complete description of a trajectory requires an additional input about the statistical properties of the timings at which the jumps take place, usually under the form of a waiting-time distribution for the walker. Taken together, the modelling of whereto and when the next step will be forms the core of the theory of continuous-time random walks.

Random walks also play a central role within the field of network science, and provide a simple framework for understanding the relation between their structure and dynamics. Random walks on networks have been used to model diffusion of ideas in social networks, or diffusion of people in location networks, for instance [4]. In their dual form, they are also used for the modelling of decentralised consensus [5]. In addition, random walks have been exploited to extract non-local information from the underlying network structure. Take Pagerank for instance,

R. Lambiotte (✉)
Mathematical Institute, University of Oxford, Oxford, UK
e-mail: renaud.lambiotte@maths.ox.ac.uk

defined as the density of walkers on a node at stationarity [6]; or random walk-based kernels defining a similarity measure between nodes, and embedding nodes in low-dimensional space [7]; or community detection where clusters are defined in terms of their tendency to trap a walker for long times [8–10]. In each of these examples, the properties of the process at a slow time scale are essentially used to capture large-scale information in the system. Importantly, these works usually rely on discrete-time random walks or on basic Poisson processes in their continuous counterpart.

The structure of networks has been the subject of intense investigation since the early works on small-world or scale-free networks [11]. This activity has originally been driven by the availability of large relational datasets in a variety of disciplines, leading to the design of new methods to uncover their properties and of models to reproduce the empirical findings. Yet, a vast majority of datasets have only provided static snapshots of networks, or information about their growth in certain conditions. It is only more recently that the availability of fine-grained longitudinal data has motivated the study of the temporal properties of networks [12–14]. Several works have shown that the dynamics of real-world networks are non-trivial and exhibit a combination of temporal correlations and non-stationarity.

In this chapter, we will focus on a particular aspect that has attracted much attention in the literature, the presence of burstiness in the temporal series of network activity [15]. Take a specific node, or a specific edge, and look at the sequence of events associated to that object. The resulting distribution of inter-event times has been shown to differ significantly from an exponential, even after discarding confounding factors [16]. After a short introduction on relevant concepts, and a clarification of the differences between active and passive diffusion, we will use the language of continuous-time random walks to identify how the shape of temporal distributions affects diffusion. In analogy with static networks, where deviations from a binomial degree distribution play a central role, we will focus on renewal processes whose inter-event time distribution differs from an exponential. Finally, we will widen the scope and discuss possible generalisations of the models, for instance in the case of non-conservative spreading processes.

2 Models of Graphs and of Temporal Sequences

Random models play an important role when analysing real-world data. The main purpose of this section is to introduce simple random models for graphs and for temporal sequences. Both sub-sections are organised in mirror to highlight the similarities between the models.

2.1 Random Graphs

The most fundamental model of random graph is the Erdős-Rényi model. Usually denoted by $\mathcal{G}(N, q)$, it takes as parameters the number of nodes N , and the probability q that two distinct nodes are connected by a link. By construction, each pair of node is a Bernoulli process, whose realisation is independent from that of other pairs in the graph. The Erdős-Rényi model, as any random graph model, has to be considered as an ensemble of graphs, whose probability of being realised depends on the model parameters. Due to the independence between the processes defined on each edge, several properties of the model can be computed exactly. This includes the degree distribution, expected to take the form of the binomial distribution

$$p(k) = \binom{N-1}{k} q^k (1-q)^{N-1-k}, \quad (1)$$

but also the number of cliques of any size, or the percolation threshold. The underlying assumptions of a Erdős-Rényi model are often violated in empirical data. Take connections in a social network, where triadic closure induces correlations between neighbouring edges for instance. Yet, the model's simplicity and analytical tractability naturally make it a baseline model, and more realistic network models can be developed systematically by relaxing its assumptions. Well-known examples include:

- *The configuration model.* Real-life networks tend to present a strong heterogeneity in their degrees, associated to fat tailed distributions very different from a binomial. The configuration model is defined as a random graph in which all possible configurations appear with the same probability, with the constraint that each node i has a prescribed degree k_i , that is with a tuneable degree distribution.
- *Stochastic block models.* Real-life networks are not homogeneous and their nodes tend to be organised in groups revealing their function in the system. These groups may take the form of assortative or disassortative communities and may be reproduced by stochastic block models where the nodes are divided into k classes, and the probability p_{ij} for two nodes i, j , belonging to class c_i and c_j , to be connected is encoded in an affinity matrix $\Omega_{c_i c_j}$.

Note that both models can be combined to form so-called degree-corrected stochastic block models [17]. In essence, both models assume that the processes on each edge are independent but break the assumption that they are identical. Certain pairs of nodes are more or less likely to be connected within this framework. Models questioning the independence of different edges include

- *The preferential attachment model.* In this mechanistic model for growing networks, nodes are added one at a time and tend to connect with a higher probability to high degree nodes. The resulting networks naturally produce fat-tailed degree distributions and exhibit correlations building in the course of the

process. Variations of the model include divergence-duplication models [18], or copying models [19], whose correlations produce a high density of triangles, and cliques of all size, that are negligible in the afore-mentioned models.

2.2 Poisson and Renewal Processes

Let us now turn our attention to the modelling of temporal sequences of events. Examples include the sequences of retweets of an original tweet, of meeting a cat in the street, or of nuclei to disintegrate in a radioactive material. As a first order approximation, these systems can be modelled by a Poisson process, assuming that events are independent of each other and that their rate is constant over time. As in case of the Erdős-Rényi model, these assumptions are often unrealistic, but the resulting simplicity allows us to derive analytically its statistical properties. For Poisson processes, the inter-event time between two consecutive events, usually denoted by τ , is exponentially distributed according to

$$\psi(\tau) = \lambda e^{-\lambda\tau}, \quad (2)$$

where λ is the rate at which events occur. Likewise, the distribution of the number of events observed within a given time window is readily found to be

$$p(n, t) = \frac{(\lambda t)^n}{n!} e^{-\lambda t} \quad (3)$$

for any $n \geq 0$. Deviations from these distributions in empirical data indicate that the assumptions of a Poisson process are not verified and that a more complicated process is at play. Generalised models relaxing some of these assumptions include:

- *Renewal processes.* Empirical data often show fat-tailed inter-event time distributions, which can be captured by renewal processes. In a renewal process, inter-event times are independent of each other and drawn from the same distribution $\psi(\tau)$. When $\psi(\tau) = \lambda e^{-\lambda\tau}$, we recover a Poisson process. The properties of renewal processes are usually best analysed in the frequency domain. After defining the Laplace transform

$$\hat{\psi}(s) = \int_0^\infty \psi(\tau) e^{-s\tau} d\tau \quad (4)$$

and noting that a convolution in time translates into a product in the Laplace domain, one readily finds the probability of having observed n events at time t

$$\hat{p}(n, s) = [\hat{\psi}(s)]^n \frac{1 - \hat{\psi}(s)}{s}. \quad (5)$$

As we will see below, this quantity is critical, as it relates two ways to count time: one in terms of the number of events, n , and the other in terms of the physical time, t .

- *Non-homogeneous Poisson processes.* Real-life time series are often non-stationary, which can be incorporated in a Poisson process with a time-dependent event rate $\lambda(t)$. For a non-homogeneous Poisson process, (3) is extended as

$$p(n, t) = \frac{\Lambda(t)^n}{n!} e^{-\Lambda(t)}, \quad (6)$$

where

$$\Lambda(t) = \int_0^t \lambda(t') dt'. \quad (7)$$

Similarly, the distribution of inter-event times is given by

$$\psi(\tau) = \lambda(\tau) e^{-\Lambda(\tau)}, \quad (8)$$

and leads to time-dependent, non-exponential distributions in general.

The previous two generalisations assume that successive inter-event times are independent processes, which is expected to be invalid in many situations. Take discussion threads between individuals for instance, or cascades of events in social media. This type of situation can instead be modelled by

- *Self-exciting processes.* The underlying idea is that an event induces an additional event rate for future events. This property is at the core of Hawkes processes [20, 21] where, in their simplest form, the event rate at time t is given by

$$\lambda(t) = \lambda_0 + \sum_{\ell, t_\ell \leq t} \chi(t - t_\ell), \quad (9)$$

where t_ℓ is the time of the ℓ th event. The model incorporates a baseline rate λ_0 independent of self excitation and a memory kernel $\chi(t)$ describing the additional rate incurred by an event. It is generally assumed that $\chi(t)$ peaks at $t = 0$ and monotonically decay towards zero as t increases.

As in the case of random graph models, different generalisations can be combined to form more realistic models. This is the case of TideH, for instance, a model for retweet dynamics combining ingredients from Hawkes processes and non-homogeneous Poisson processes [22].

3 Trajectories on Networks

3.1 Discrete-Time Dynamics

Let us now turn to the case of static networks and the description of trajectories on their nodes. A canonical example could be one-dollar bill transiting between individuals forming a large social network [23]. For the sake of simplicity, we will assume that social interactions are undirected and unweighted, and that the whole network forms a connected component. The structure of the network is encoded through its adjacency matrix \mathbf{A} , whose element A_{ij} determines the presence of an edge between nodes i and j . As a first step, we consider the case when the random walk process takes place at the discrete times n . A trajectory on the network is thus characterised by a sequence $X_0, X_1, \dots, X_n, \dots$, where X_n is a random variable denoting the node visited by the walker at time n . In general, the state X_{n+1} may depend on all preceding states of the dynamics and the probability of visiting a certain node i requires information about the full history of the process

$$p(X_{n+1} = i_{n+1} | X_n = i_n, \dots, X_1 = i_1, X_0 = i_0). \quad (10)$$

The process simplifies drastically in situations when the system is stationary and the conditional probability depends only on the state at time n . The process then takes the form of a Markov chain, and is fully described by its initial state and the $N \times N$ transition matrix

$$p(X_{n+1} = j | X_n = i) \equiv T_{ij} = \frac{A_{ij}}{k_i}, \quad (11)$$

where k_i is, as before, the degree of node i . For instance, the probability that state i is visited at time n , denoted by $P_i(n)$, evolves according to

$$P_j(n+1) = \sum_{i=1}^N P_i(n) T_{ij} \quad (12)$$

or, in matrix notations,

$$\mathbf{P}(n+1) = \mathbf{P}(n) \mathbf{T}, \quad (13)$$

yielding the formal solution

$$\mathbf{P}(n) = \mathbf{P}(0) \mathbf{T}^n. \quad (14)$$

When the underlying network is connected and the corresponding Markov chain is ergodic, it can be shown that any initial condition converges to the stationary density $P_i^* = k_i/2m$ solution of

$$\mathbf{P}^* = \mathbf{P}^* \mathbf{T}. \quad (15)$$

3.2 Fourier Modes

The solution, Eq. (14), involves products of matrices, which can be simplified by rewriting the system in the basis formed by the eigenvectors of the transition matrix. This operation is sometimes called the graph Fourier transform [24], and it allows to replace the matrix products by algebraic products for amplitudes associated to the different dynamical modes. To show this, we consider the symmetric matrix

$$\tilde{A}_{ij} = \frac{A_{ij}}{\sqrt{k_i k_j}}, \quad (16)$$

and its spectral decomposition

$$\tilde{A}_{ij} = \sum_{\ell=1}^N \lambda_{\ell} u_{\ell} u_{\ell}^{\top}, \quad (17)$$

where u_{ℓ} is the normalised eigenvector of eigenvalue λ_{ℓ} , and where we have assumed that all eigenvalues are distinct to avoid unnecessary complications. By construction, the eigenvectors verify $\langle u_{\ell}, u_{\ell'} \rangle = \delta_{\ell\ell'}$ and form a proper basis for signals defined on the nodes of the network. One should also note that the eigenvalues are in the interval $[-1, 1]$, that the multiplicity of the dominant eigenvalue 1 gives the number of connected components in the graph, and that an eigenvalue equal to -1 indicates that the graph is bipartite. It is straightforward to show that the left and right eigenvectors of T are given by

$$u_{\ell}^L = \left((u_{\ell})_1 \sqrt{k_1} \cdots (u_{\ell})_N \sqrt{k_N} \right), \quad (18)$$

$$u_{\ell}^R = \left((u_{\ell})_1 / \sqrt{k_1} \cdots (u_{\ell})_N / \sqrt{k_N} \right)^{\top} \quad (19)$$

respectively which implies, after some algebra, that the state of the random walk after n steps is given by a linear combination of the eigenmodes

$$P_i(n) = \sum_{\ell=1}^N a_{\ell}(n) (u_{\ell}^L)_i, \quad (20)$$

where the amplitude of the modes evolves as

$$a_{\ell}(n) = \lambda_{\ell}^n a_{\ell}(0). \quad (21)$$

and $a_{\ell}(0) \equiv \langle P(0), u_{\ell}^R \rangle$ is given by the initial condition.

The spectral decomposition (20) helps to understand how the structure of a network affects the diffusion of a random walker. The stationary density corresponds to the mode with $\lambda_\ell = 1$, assumed to be unique as the network is connected. In addition, in situations when the network is non-bipartite, and no eigenvalue is equal to -1 , all the other modes asymptotically decay to 0, each one with a time-scale associated to its eigenvalue. The long-time relaxation to the stationary density is determined by the eigenmode associated to $\lambda_{2\text{nd}}$, the second largest eigenvalue, which is related to the spectral gap $1 - \lambda_{2\text{nd}}$. A small spectral gap entails slow relaxation and the presence of a bottleneck between communities in the network, as shown by the Cheeger inequality [25].

3.3 Continuous-Time Dynamics

We have described the trajectory of the walker in terms of the number of jumps so far. We now turn to the situation when the jumps take place in continuous time, which motivates the use of continuous-time random walk processes. The passage from discrete to continuous time is usually done by modelling the sequence of jumps of the walker as a renewal process: the walker waits between two jumps for a duration τ given by the probability density function $\psi(\tau)$ before performing a transition according to the Markov chain. We have assumed here that the waiting time distribution is identical on each node. The position of the walker at time t is given by

$$P_i(t) = \sum_{n=0}^{\infty} P_i(n) p(n, t), \quad (22)$$

where we have used the fact that arriving at node i in n steps, and performing n steps in time t are independent processes.

By going into the Laplace domain and combining (5) and (14), we find

$$\hat{P}(s) = \frac{1 - \psi(s)}{s} P(0) \left[\mathbf{I} - \mathbf{T}\hat{\psi}(s) \right]^{-1}, \quad (23)$$

whose inverse Laplace transform provides the probability $P_i(t)$ for the walker to be on node i at time t . The latter usually involves convolutions in time, reflecting the lack of Markovianity of the process for general renewal process. (23) also takes the equivalent form

$$\left(\frac{1}{\psi(s)} - 1 \right) \hat{P}(s) = \left(\frac{1}{\psi(s)} - 1 \right) \frac{1}{s} P(0) + \hat{P}(s) \mathbf{L} \quad (24)$$

where $\mathbf{L} = \mathbf{T} - \mathbf{I}$ is the normalised Laplacian of the network. This expression simplifies drastically in the case when the renewal process is a Poisson process, and

$\psi(\tau) = \lambda e^{-\lambda\tau}$, leading to the standard rate equation

$$\frac{dP(t)}{dt} = P(t)\mathbf{L}. \quad (25)$$

It is important to emphasise that (24) provides an exact solution to the problem and that it departs from (25) through its causal operator $\left(\frac{1}{\psi(s)} - 1\right)$, which translates the input from the neighbours of a node into a change of its state, different from a usual $\frac{d}{dt}$. Note that this operator asymptotically behaves like a fractional derivative in situations when the waiting time distribution has a power-law tail [26].

This solution also helps us to clarify the impact of the shape of the waiting time distribution on the speed of diffusion. In the basis of the eigenvectors of the transition matrix, it is straightforward to generalise (21) to obtain

$$\hat{P}(s) = \frac{1 - \hat{\psi}(s)}{s} \sum_{\ell=1}^N \frac{a_\ell(0)}{1 - \lambda_\ell \hat{\psi}(s)} u_\ell^L. \quad (26)$$

In other words, the time evolution of the amplitude of each mode is given by

$$\hat{a}_\ell(s) = \frac{1 - \hat{\psi}(s)}{s \left[1 - \lambda_\ell \hat{\psi}(s) \right]} a_\ell(0), \quad (27)$$

which is, in general, different from an exponential decay. The asymptotic behaviour can be obtained by performing a small s expansion

$$\hat{\psi}(s) = 1 - \langle \tau \rangle s + \frac{1}{2} \langle \tau^2 \rangle s^2 + o(s^2) \quad (28)$$

and assuming a finite mean and variance, yielding the dominant terms

$$a_\ell(s) = \frac{\langle \tau \rangle}{1 - \lambda} \left[1 - s \left(\frac{\lambda_\ell \langle \tau \rangle}{1 - \lambda_\ell} + \frac{\langle \tau^2 \rangle}{2 \langle \tau \rangle} \right) \right] \quad (29)$$

and thus a characteristic time t_ℓ ,

$$t_\ell = \langle \tau \rangle \left(\frac{1}{\epsilon_\ell} + \beta \right), \quad (30)$$

where $\epsilon_\ell = 1 - \lambda_\ell$ is an eigenvalue of the normalised Laplacian and

$$\beta = \frac{\sigma_\tau^2 - \langle \tau \rangle^2}{2 \langle \tau \rangle^2} \quad (31)$$

is the variance of τ . Poisson processes yield $\beta = 0$ and this expression clearly shows that negative values of β tend to accelerate the relaxation of each mode, while larger values slow them down. The former happens in the case of discrete-time dynamics for instance, when $\psi(\tau)$ is a delta distribution. The latter is when the distribution has a fat tail. Importantly, (30) shows that a combination of structural and temporal information determines the temporal properties of the process.

4 Diffusion on Temporal Networks

4.1 Active Versus Passive Walks

What about temporal networks? The results derived in the previous section focus on random walks on static networks. They are nonetheless instructive to model and understand diffusion on temporal networks. As a first step, we should emphasise that the distinction between the dynamics on the network and the dynamics of the network is not always clear-cut [27, 28]. The temporal nature of a network usually comes from time series of events taking place on nodes or edges. There are situations when it is the diffusive process itself that defines the temporal network. Take the action of sending an email or an SMS to a friend, and the modelling of information diffusion in the resulting network. In this case of **active** diffusion, the motion of the random walker is defining the temporal patterns of activity on links existing, as transition trigger the activation of a potential edge. The model of Sect. 3.3 is then a good candidate to explore the interplay between structure and dynamics in the resulting temporal network. Note that even the Poisson model described by (25) can then be seen as generating a temporal network, even if it is not a very interesting one.

There are other situations, however, when the motion of the walker does not trigger the connections between nodes, but it is instead constrained by their temporal patterns. A good example would that of a person random walking a public transportation network, or of a disease spreading in a contact network. In that case, the temporal sequence of edges restrains the time-respecting paths that are available for the walker and one talks of **passive** diffusion. As we will see, passive random walks can also be mapped to continuous-time random walks to some extent, but this operation must be performed more carefully. As a simple model of temporal networks supporting diffusion, let us consider a stochastic temporal network. The network is modelled as a set of potential edges between nodes, each one evolving as an independent renewal process, with a distribution of inter-event times $\phi(\tau)$. A random walker located on a node i performs a jump as soon as an edge appears, for instance to node j , where it waits until the next available edge.

4.2 Bus Paradox and Backtracking Transitions

When considering passive random walks, it is critical to clearly distinguish the waiting-time distribution $\psi(\tau)$ from the inter-event time distribution $\phi(\tau)$. The former characterises the times that a walker has to wait on a node before its next move. The latter gives the time between edge activations in the renewal process defining the stochastic temporal network. The inter-event time distribution is a parameter of the network model but the motion of the walker is directly affected by the waiting-time distribution, and it should thus be estimated. To do so, let us first focus on the case of a walker arriving at a node j from i and calculating the time before an edge to another edge k appears. Assuming the independence between the act of arriving at node j and the appearance of the edge to k , one finds that both distributions are related as

$$\psi(\tau) = \frac{1}{\langle \tau \rangle_\phi} \int_\tau^\infty \phi(\tau') d\tau', \quad (32)$$

where $\langle \tau \rangle_\phi$ is the average inter-event time distribution. Most strikingly, the average waiting time is

$$\langle \tau \rangle_\psi = \frac{1}{2} \frac{\langle \tau^2 \rangle_\phi}{\langle \tau \rangle_\phi} \quad (33)$$

and it depends on the variance of the inter-activation time. At a fixed value of $\langle \tau \rangle_\phi$, the waiting time can thus be arbitrarily large if the variance of $\phi(\tau)$ is sufficiently large. The waiting-time paradox is a standard result in queuing theory [29] and is an example of length-biased sampling. It is often called the bus paradox, after the observation that the average waiting time at a bus stop tends to be longer than half of the average interval between two buses expected from the timetable.

As a second step, it is important to note that the approximation behind the derivation of (32) is, in general, not respected if the walker passes several times by the same edge, as information about the previous passage time may help to predict the next activation time. This effect is most apparent in (but is not limited to) the case of undirected networks. Consider a walker taking an edge from node i to node j . The time before the next activation of the edge back to i is clearly not given by $\psi(\tau)$ in (32), but simply by $\phi(\tau)$. The waiting time for a backtracking edge is therefore typically different, and shorter for fat-tailed distributions, than the waiting time of a non-backtracking edge. This difference is particularly critical because edges are in competition with each other [27]. When a walker waits on a node, the model specifies that it takes the first edge to appear. For this reason, the prevalence of an edge over another may bias the trajectory of the walker, and make the process non-Markovian [28].

Let us quantify this effect when the walker arrives on a node j with degree k_j , and consider the probability of the time t at which the walker takes a specific

edge. As before, the inter-event times of the links are identically and independently distributed according to $\phi(\tau)$. Starting from the time when the walker arrived on j , the time of the next activation for a backtracking step is simply $\phi(\tau)$. The time for another edge to activate is instead determined by the waiting-time distribution $\psi(\tau)$, where we assume that the approximation (32) is valid. For the walker to take an edge at time t , no other edge can have appeared in $[0, t]$. Therefore, we obtain

$$f_{\text{back}}(t) \approx \phi(t) \left[\int_t^\infty \psi(\tau) d\tau \right]^{k_i-1} \quad (34)$$

$$f_{\text{non-back}}(t) \approx \psi(t) \left[\int_t^\infty \psi(\tau) d\tau \right]^{k_i-2} \int_t^\infty \phi(\tau) d\tau \quad (35)$$

As we discussed, if ψ has a fat tail, the waiting time is larger than the inter-event time on average and the walker preferentially backtracks, thereby leading to non-Markovian trajectories. Here, we should clarify the distinction between two types of non-Markovianity that can be induced on temporal networks. In (24), the sequence of nodes visited by the walker is described by a Markov chain, but the statistical properties of the timings induce long-term memory effects. In (34), instead, the sequence of nodes visited by the walker cannot be produced by a first-order Markov process.

To summarise, when considering passive diffusion on a stochastic temporal network, the rate at which the random walker explores the network is slowed down in three ways when the inter-event time distribution has a fat tail, namely through:

- *the bus paradox*, because the waiting time of the walker on the nodes tends to be longer on average. As the speed of diffusion is controlled by the sum of the waiting times of the walker, this effect leads to a slow down of diffusion.
- *the backtracking bias*. The random walker tends to backtrack, which hinders its exploration of the network and can be shown to increase the mixing time of the process [30, 31].
- *the variance of the waiting-time distribution*. On top of the slow down due to the bus paradox, and an increase of the average waiting time, the variance of the waiting time also slows down diffusion through the same mechanisms as for active random walks, in (30).

5 Perspectives

The main purpose of this chapter was to provide an overview on theoretical results for diffusion on temporal networks. As we discussed, the problem may be understood through the lens of continuous-time random walks, after carefully distinguishing between waiting time and inter-event time, on the one hand, and active versus passive walks, on the other hand. An analytical approach allows us to

identify unambiguously the mechanisms accelerating or slowing down the diffusion, and also helps to warn against caveats that could be met with numerical simulations. A good example concerns the use of null models to determine how the temporal nature of a real-world network affects diffusion. A popular solution consists in comparing numerical simulations of diffusion on the original data and on different versions of randomised data [32]. The results from Sect. 4.2 show that randomised null models in which temporal correlations are removed yet have the tendency towards backtracking, and thus to slow down the exploration of the network.

The results presented in this chapter also open different perspectives for future research. As we discussed in Sect. 2.1, different types of random graph models have been proposed for static networks. A model like the stochastic temporal network incorporates temporal activity on a given network structure, which opens the question of how to properly define generalisations of the configuration model or stochastic block model in this context. Answers may be found by clarifying the connections with activity-driven models, where the dynamics can also be generated by general renewal processes [33, 34]. The temporal networks presented in this chapter also suffer from limitations that may hinder their applicability. Those include their stationarity, the absence of correlations between edges and the instantaneity of the interactions. To address the last two limitations, we point the reader to the possibility to use higher-order Markov models for the data [35, 36], and recent generalisations based on continuous-time random walks allowing for interactions with a finite duration [37]. The latter emphasises a critical aspect of temporal networks, which are characterised by different processes and their corresponding time scales. Those time scales include one associated to the motion of the random walker, one to the time between successive activity periods of the edges and another to the duration of the activity periods. Depending on the model parameter, one process may dominate the others and lead to mathematical simplifications for the dynamics.

As a final comment, we would also like to come back on our observation that temporal networks may be generated by active diffusive processes. This chapter was limited to conservative spreading processes, where the number of diffusing entities is preserved in time. There are many practical situations, however, when this is not the case. Take the spreading of viruses in human populations or of hashtags in online social networks for instance. In that case, other spreading models should be considered to generate more realistic temporal networks. A promising candidate is multivariate Hawkes processes, generalising (9) to interacting entities, and whose equation of evolution takes a form very similar to (24):

$$\lambda(s) = \frac{\lambda_0}{s} + \chi(s)\lambda(s)\mathbf{A}, \quad (36)$$

where the vector $\lambda(s)$ is the Laplace transform of the average rate of activity on each node, $\chi(s)$ of the memory kernel and \mathbf{A} is the adjacency matrix of the network. The presence of the adjacency matrix instead of the Laplacian is a clear sign of the epidemic nature of the spreading. Note also that a heterogeneous mean-

field, *à la configuration model*, version of the model has been considered for the modelling of retweet cascades [38]. Alternatively, the related family of Bellman-Harris branching processes could be used, where a node i remains infected for a duration t , determined by a distribution $\rho(t)$, before infecting its neighbours, leading to

$$\lambda(s) = \frac{1 - \rho(s)}{s} + \rho(s)\lambda(s)A. \quad (37)$$

In each case, the active process allows for the formation of a growing cascade of infections, and includes a non-trivial causal operator.

Acknowledgements I would like to thank my many collaborators without whom none of this work would have been done and, in particular, Naoki Masuda for co-writing [14] that was a great inspiration for this chapter.

References

1. Balescu, R.: Statistical Dynamics: Matter Out of Equilibrium. Imperial College, London (1997)
2. Klafter, J., Sokolov, I.M.: First Steps in Random Walks: From Tools to Applications. Oxford University Press, New York (2011)
3. Lovász, L., et al.: Random walks on graphs: a survey. Combinatorics, Paul Erdos is Eighty 2(1), 1–46 (1993)
4. Masuda, N., Porter, M.A., Lambiotte, R. Random walks and diffusion on networks. Phys. Rep. **716**, 1–58 (2017)
5. Blondel, V.D., Hendrickx, J.M., Olshevsky, A., Tsitsiklis, J.N.: Convergence in multiagent coordination, consensus, and flocking. In: Proceedings of the 44th IEEE Conference on Decision and Control, pp. 2996–3000. IEEE, Piscataway (2005)
6. Brin, S., Page, L.: Anatomy of a large-scale hypertextual web search engine. In: Proceedings of the Seventh International World Wide Web Conference, pp. 107–117 (1998)
7. Fouss, F., Saerens, M., Shimbo, M.: Algorithms and Models for Network Data and Link Analysis. Cambridge University Press, Cambridge (2016)
8. Rosvall, M., Bergstrom, C.T.: Maps of random walks on complex networks reveal community structure. Proc. Natl. Acad. Sci. USA **105**, 1118–1123 (2008)
9. Delvenne, J.C., Yaliraki, S.N., Barahona, M.: Stability of graph communities across time scales. Proc. Natl. Acad. Sci. USA **107**, 12755–12760 (2010)
10. Lambiotte, R., Delvenne, J.C., Barahona, M.: Random walks, Markov processes and the multiscale modular organization of complex networks. IEEE Trans. Netw. Sci. Eng. **1**, 76–90 (2014)
11. Newman, M.: Networks: An Introduction. Oxford University Press, Oxford (2010)
12. Holme, P., Saramäki, J.: Temporal networks. Phys. Rep. **519**(3), 97–125 (2012)
13. Holme, P.: Modern temporal network theory: a colloquium. Eur. Phys. J. B **88**(9), 1–30 (2015)
14. Masuda, N., Lambiotte, R.: A Guide to Temporal Networks. World Scientific, London (1996)
15. Barabasi, A.-L.: The origin of bursts and heavy tails in human dynamics. Nature **435**(7039), 207 (2005)
16. Malmgren, R.D., Stouffer, D.B., Motter, A.E., Amaral, L.A.N.: A poissonian explanation for heavy tails in e-mail communication. Proc. Natl. Acad. Sci. **105**(47), 18153–18158 (2008)
17. Karrer, B., Newman, M.E.J.: Stochastic blockmodels and community structure in networks. Phys. Rev. E **83**(1), 016107 (2011)

18. Ispolatov, I., Krapivsky, P.L., Yuryev, A.: Duplication-divergence model of protein interaction network. *Phys. Rev. E* **71**(6), 061911 (2005)
19. Lambiotte, R., Krapivsky, P.L., Bhat, U., Redner, S.: Structural transitions in densifying networks. *Phys. Rev. Lett.* **117**(21), 218301 (2016)
20. Hawkes, A.G.: Point spectra of some mutually exciting point processes. *J. R. Stat. Soc. B* **33**, 438–443 (1971)
21. Masuda, N., Takaguchi, T., Sato, N., Yano, K.: Self-exciting point process modeling of conversation event sequences. In: *Temporal Networks*, pp. 245–264. Springer, Berlin (2013)
22. Kobayashi, R., Lambiotte, R.: Tideh: time-dependent hawkes process for predicting retweet dynamics. In: *Tenth International AAAI Conference on Web and Social Media* (2016)
23. Brockmann, D., Hufnagel, L., Geisel, T.: The scaling laws of human travel. *Nature* **439**(7075), 462 (2006)
24. Perraudin, N., Vanderghenst, P.: Stationary signal processing on graphs. *IEEE Trans. Signal Process.* **65**(13), 3462–3477 (2017)
25. Chung, F.R.K., Graham, F.C.: *Spectral Graph Theory*. Number 92. American Mathematical Society, Providence (1997)
26. De Nigris, S., Hastir, A., Lambiotte, R.: Burstiness and fractional diffusion on complex networks. *Eur. Phys. J. B* **89**(5), 114 (2016)
27. Hoffmann, T., Porter, M.A., Lambiotte, R.: Generalized master equations for non-Poisson dynamics on networks. *Phys. Rev. E* **86**, 046102 (2012)
28. Speidel, L., Lambiotte, R., Aihara, K., Masuda, N.: Steady state and mean recurrence time for random walks on stochastic temporal networks. *Phys. Rev. E* **91**, 012806 (2015)
29. Allen, A.O.: *Probability, Statistics, and Queueing Theory: With Computer Science Applications*, 2nd edn. Academic Press, Boston (1990)
30. Saramäki, J., Holme, P.: Exploring temporal networks with greedy walks. *Eur. Phys. J. B* **88**(12), 334 (2015)
31. Gueuning, M., Lambiotte, R., Delvenne, J.-C.: Backtracking and mixing rate of diffusion on uncorrelated temporal networks. *Entropy* **19**(10), 542 (2017)
32. Karsai, M., Kivelä, M., Pan, R.K., Kaski, K., Kertész, J., Barabási, A.-L., Saramäki, J.: Small but slow world: how network topology and burstiness slow down spreading. *Phys. Rev. E* **83**(2), 025102 (2011)
33. Moinet, A., Starnini, M., Pastor-Satorras, R.: Random walks in non-poissonian activity driven temporal networks. *arXiv preprint arXiv:1904.10749* (2019)
34. Moinet, A., Starnini, M., Pastor-Satorras, R.: Burstiness and aging in social temporal networks. *Phys. Rev. Lett.* **114**(10), 108701 (2015)
35. Scholtes, I., Wider, N., Pfitzner, R., Garas, A., Tessone, C.J., Schweitzer, F.: Causality-driven slow-down and speed-up of diffusion in non-markovian temporal networks. *Nat. Commun.* **5**, 5024 (2014)
36. Lambiotte, R., Rosvall, M., Scholtes, I.: From networks to optimal higher-order models of complex systems. *Nat. Phys.* **1** (2019)
37. Petit, J., Gueuning, M., Carletti, T., Lauwens, B., Lambiotte, R.: Random walk on temporal networks with lasting edges. *Phys. Rev. E* **98**(5), 052307 (2018)
38. Zhao, Q., Erdogan, M.A., He, H.Y., Rajaraman, A., Leskovec, J.: Seismic: a self-exciting point process model for predicting tweet popularity. In: *Proceedings of the 21th ACM SIGKDD International Conference on Knowledge Discovery and Data Mining*, pp. 1513–1522. ACM, New York (2015)

Spreading of Infection on Temporal Networks: An Edge-Centered Perspective



Andreas Koher, James P. Gleeson, and Philipp Hövel

1 Introduction

The foundation of modern theoretical epidemiology was established at the beginning of the twentieth century, mainly by health physicians such as Ross, Hamer, McKendrick, and Kermack who introduced the *compartment model* [1–3]. This approach separates individuals within a population into epidemic categories or compartments, depending on their health status such as susceptible, infected, and recovered. Since the early years, development in the field of mathematical epidemiology has accelerated, not least due to the seminal works of Bailey [4], Anderson & May [5] and Hethcote [6]. Modern models include stochasticity [7–10], non-Markovian dynamics [11–15], demographic structures, vaccinations, disease vectors and quarantine (see references in [6] for details). Thus, the field of research ranges from simple explanatory models that reveal hidden patterns and reproduce fundamental observations to elaborate numerical models that provide realistic predictions [16].

In recent years, we witnessed a second *golden age* [17] of epidemiological modeling. The driving forces behind this development are increasing computing power and an unprecedented amount of mobility data. The combination of both

A. Koher

Institut für Theoretische Physik, Technische Universität Berlin, Berlin, Germany
e-mail: andreas.koher@tu-berlin.de

J. P. Gleeson

MACSI, Department of Mathematics and Statistics, University of Limerick, Limerick, Ireland
e-mail: james.gleeson@ul.ie

P. Hövel (✉)

School of Mathematical Sciences, University College Cork, Cork, Ireland
e-mail: philipp.hoevel@ucc.ie

allows scientists to simulate the behavior of entire populations at the level of single individuals [18–24] and thus to advise policy makers by means of quantitative models.

One of the cornerstones of network-based disease models is the *individual-based* (IB) approach. It is a drastic simplification of the exact description using a master equation, because it assumes that the epidemiological states of neighboring nodes are statistically independent. Under this approximation, one can define a set of dynamic equations for the marginal probability to find a node in a given disease state [10, 25–31]. This method is widely employed, because it offers an intuitive and analytically tractable approach to integrate the underlying contact network. As a particularly important result, we mention that the largest eigenvalue of the adjacency matrix, which represents the topology of the network, determines the critical disease parameters that separate local and global outbreaks [26, 28].

Karrer & Newman substantially improved previous models of uni-directional diseases, such as the generic susceptible-infected-recovered (SIR) model, using the message-passing framework [13]. This approach dates back to the computer scientist Pearl [32], who formulated an exact inference algorithm on trees. Karrer & Newman proposed an integro-differential equation as a model for non-Markovian disease dynamics and improved previous estimates of the critical disease parameters on static networks [33]. A crucial conceptual difference to earlier works is that edges instead of nodes appear as central elements of the model. This idea has influenced considerably further research on network epidemiology [12, 34–37].

The *dynamic message-passing* model [35] is a particularly application-oriented variant for Markovian SIR dynamics and has been extended recently to networks with time-varying topologies [37]. This novel approach for epidemics on temporal networks, termed the *contact-based* (CB) model, focuses on edge-based quantities that are updated in discrete time and thus allows for a seamless integration of temporal networks that are sampled at a constant rate. Importantly, the authors in [37] derive a critical condition that improves previous estimates of the epidemic threshold [26], which is an valuable risk measure for public health institutions.

Another important research branch in theoretical epidemiology focuses not on a single realization of a graph but on an ensemble of random networks. A particularly accurate and compact model of epidemic spreading on this class of random networks has been proposed in [34] and is termed *edge-based compartmental* (EBC) model. The original work focused not only on the configuration model for static networks, but also on different classes of random graphs with time-varying topologies. Since then, several extensions have been proposed, such as non-Markovian recovery dynamics [12] and arbitrary initial conditions [38]. Moreover, studies in [39, 40] investigated links to other existing models such as *pair-approximations* [41], the *effective degree model* [42] and *message-passing* [13].

In this chapter, we will derive a continuous-time formulation of the CB model for temporal networks, analyze the low-prevalence limit and explore links to previously proposed models. To this end, we will briefly summarize in Sect. 2 the discrete-time version proposed in [37]. Then, we extend the dynamic equations to the

continuous-time case in Sect. 3 and determine in Sect. 4 the epidemic threshold from a stability analysis of the disease-free fixed point. Moreover, we will link the continuous-time results to existing models and in particular to the *edge-based compartmental model* in Sect. 5 and the *message-passing* framework in Sect. 6.

2 Discrete-Time Description

The dynamic equations of the contact-based model appeared first in [35] and [37] for static and temporal networks, respectively. In the following, we will briefly re-derive the discrete-time model, which will then serve as the starting point for a continuous-time formulation in the main part of this chapter.

We begin by introducing our notational convention and consider a network $G(t)$, whose topology can change at any time $t \in [0, T]$. Next we sample T_s snapshots of the graph with a constant interval Δt . The resulting sequence $[G_0, G_1, \dots, G_{T_s-1}]$ is an approximation of the continuous-time network, which approaches the exact representation in the limit $\Delta t \rightarrow 0$.

Let us denote with \mathcal{N} and $\mathcal{C} \subset \mathcal{T} \times \mathcal{N} \times \mathcal{N}$ the set of all nodes ($|\mathcal{N}| = N$) and time-resolved contacts, respectively, where $\mathcal{T} = \{0, 1, \dots, T_s - 1\}$ represents the set of sampling times. To emphasize the difference between temporal and static elements, we will refer to edges as static links $(k, l) \in \mathcal{E} \subset \mathcal{N} \times \mathcal{N}$ of the time-aggregated graph and denote the number of edges with $E = |\mathcal{E}|$. In other words, an edge exists if and only if at least one contact was recorded between the corresponding nodes. We assume a directed network and hence represent a potential undirected contact through two reciprocal elements. Finally, it is helpful to define an indicator function that returns whether or not a contact from k to l exists at sampling time t :

$$a_{k \rightarrow l}(t) = \begin{cases} 1, & \text{if } (t, k, l) \in \mathcal{C} \\ 0, & \text{otherwise.} \end{cases} \quad (1)$$

Here we use the notation $k \rightarrow l$ to denote quantities defined on the set of edges \mathcal{E} , thus preventing potential confusion with node-based elements.

As a model for disease spreading, we consider the generic susceptible-infected-recovered (SIR) dynamic as a paradigmatic model for infections that lead to permanent immunity. In this modeling framework, a susceptible node (S) contracts the disease from an infected neighbor (I) with a constant and uniform rate β . The transition to the recovered state (R) follows with a likewise universal rate μ .

After this formal introduction we can now start with the actual modeling and to this end, we begin with the marginal probability $P_l^S(t)$ that node l is susceptible at time t . We observe that l is susceptible if it has been so already at the beginning $t = 0$ (with a corresponding probability of z_l) and hence did not contract the infection

from any of its neighbors up to the observation time t . We denote the probability of the latter event with $\Phi_l(t)$, which leads to the following relation:

$$P_l^S(t) = z_l \Phi_l(t). \quad (2)$$

In order to determine the central quantity $\Phi_l(t)$, we make the simplifying assumption that the undirected, time-aggregated graph has a tree structure. In other words, ignoring the directionality, the static backbone does not contain loops and hence all branches emanating from the root node l can be considered independently of each other.

In order to factorize the probability $\Phi_l(t)$, we also need to introduce a concept that is sometimes referred to as *test node* [34], *cut-vertex* [43], or *cavity state* [13, 35]. To understand why this concept is helpful, imagine the case that a disease appears in one branch and hence may spread into another branch via the root node l . As a consequence, the probability that l will be infected by either of the two infected neighbors is clearly correlated and therefore cannot factorize. However, this case requires l to be already infected and hence appears as an artefact. In order to exclude this event we remove (virtually) all edges emanating from l , which prevents a disease transmission from one branch to another. We refer to vertex l as being in the *cavity state* or simply a *cavity node*. This intervention does not change the dynamics of l , as the node can still be infected and once it is, it recovers regardless of the network structure. Furthermore, we call this modification *virtual* because we restore the topological modification as soon as we focus on the dynamics of another node. This method ensures that $\Phi_l(t)$ factorizes and thus we arrive at

$$P_l^S(t) = z_l \prod_{k \in \mathcal{N}_l} \theta_{k \rightarrow l}(t). \quad (3)$$

Here, the product iterates through all neighbors $k \in \mathcal{N}_l$ of node l and with $\theta_{k \rightarrow l}(t)$ we denote the probability that cavity node l has not contracted the disease from k up to the observation time.

The conceptual change from a node-based to an edge-based modeling approach requires new auxiliary dynamic variables. Besides $\theta_{k \rightarrow l}(t)$, we will introduce additional quantities that are defined on the set of edges \mathcal{E} and following our convention, we use the index notation *source* \rightarrow *target*. In order to avoid repetition, we also note that in all cases the target node is considered to be in the cavity state.

To set up a dynamic equation for $\theta_{k \rightarrow l}(t)$, we observe that the value can only decrease precisely when (i) a contact indicated by $a_{k \rightarrow l}(t)$ exists and (ii) the source node k is infected and has not yet transmitted the disease to l . We denote the corresponding probability for event (ii) with $I_{k \rightarrow l}(t)$. Together with the probability $\beta \Delta t$ to contract the disease within the time step Δt , we obtain our first, discrete-time dynamic equation:

$$\theta_{k \rightarrow l}(t + \Delta t) = \theta_{k \rightarrow l}(t) - \beta \Delta t a_{k \rightarrow l}(t) I_{k \rightarrow l}(t). \quad (4)$$

As the initial condition we choose $\theta_{k \rightarrow l}(t) = 1$ for all edges $(k, l) \in \mathcal{E}$.

Next, we investigate $I_{k \rightarrow l}(t)$ and observe that the value can change due to three independent events: (i) Node k recovers, with probability $\mu \Delta t$; (ii) Node l contracts the disease from k upon a contact, with probability $\beta \Delta t$, whereby both events, i.e. (i) and (ii), can also occur simultaneously with probability $\beta \mu(\Delta t)^2$; (iii) Source node k is newly infected by one of its incident neighbors, excluding the cavity node l with probability $-\Delta S_{k \rightarrow l}(t) = S_{k \rightarrow l}(t + \Delta t) - S_{k \rightarrow l}(t)$. Here, $S_{k \rightarrow l}(t)$ denotes the probability to find k in the susceptible state. Balancing all probabilities, we obtain the following dynamic equation:

$$I_{k \rightarrow l}(t + \Delta t) = (1 - \mu \Delta t)[1 - \beta \Delta t a_{k \rightarrow l}(t)] I_{k \rightarrow l}(t) - \Delta S_{k \rightarrow l}(t). \quad (5)$$

The initial condition is given by $I_{k \rightarrow l}(0) = 1 - z_k$ for all edges.

We determine the probability $S_{k \rightarrow l}(t)$ in the same manner as Eq. (2), i.e., we find that k is susceptible if (i) it has been initially with probability z_k and (ii) with probability $\Phi_{k \rightarrow l}$ no pathogens were transmitted from one of its neighbors $j \in \mathcal{N}_k \setminus \{l\}$, excluding the cavity node l . Hence, we find $S_{k \rightarrow l}(t) = z_k \Phi_{k \rightarrow l}$. Moreover, the authors in [44] demonstrated that $\Phi_{k \rightarrow l}$ factorizes under the assumption of a tree topology and thus, similar to Eq. (3), we obtain:

$$S_{k \rightarrow l}(t) = z_k \prod_{j \in \mathcal{N}_k \setminus \{l\}} \theta_{j \rightarrow k}(t). \quad (6)$$

We can now substitute Eq. (6) into Eq. (5) and together with Eq. (4) we thus obtain a closed system of $2E$ dynamical equations that determine the disease progression.

Finally, we return to node-centric quantities. To this end, we follow [13] and note first that Eq. (3) determines already the probability $P_l^S(t)$ that node l is susceptible at the time t . Then, we obtain the corresponding probability $P_l^I(t)$ for the infected state from the conservation condition, i.e., a node can assume only one of the three possible states $X \in \{S, I, R\}$:

$$P_l^I(t) = 1 - P_l^S(t) - P_l^R(t). \quad (7)$$

The remaining marginal probability $P_l^R(t)$ can only increase due to a transition from the infected to the recovered state, which is given by $\mu \Delta t P_l^I(t)$. Hence, the third node-centric equation reads

$$P_l^R(t + \Delta t) = P_l^R(t) + \mu \Delta t P_l^I(t). \quad (8)$$

After this brief review of the discrete-time case that has been first derived in [37], we will elaborate on a continuous-time version next.

3 Continuous-Time Description

In the continuous-time limit $\Delta t \rightarrow 0$, Eq. (4) leads to

$$\frac{d}{dt} \theta_{k \rightarrow l}(t) = -\beta a_{k \rightarrow l}(t) I_{k \rightarrow l}(t). \quad (9)$$

We focus on $S_{k \rightarrow l}(t + \Delta t)$ from Eq. (6) and using the definition of $\theta_{j \rightarrow k}(t + \Delta t)$ (cf. Eq. (4)), we obtain:

$$S_{k \rightarrow l}(t + \Delta t) = z_k \prod_{j \in \mathcal{N}_k \setminus \{l\}} \theta_{j \rightarrow k}(t + \Delta t) \quad (10a)$$

$$= z_k \prod_{j \in \mathcal{N}_k \setminus \{l\}} [\theta_{j \rightarrow k}(t) - \beta \Delta t a_{k \rightarrow l}(t) I_{j \rightarrow k}(t)]. \quad (10b)$$

For a sufficiently small sampling interval Δt , such that $\theta_{j \rightarrow k}(t) \gg \beta \Delta t a_{k \rightarrow l}(t) I_{k \rightarrow l}(t)$, we can linearize Eq. (10b) and thus arrive at:

$$S_{k \rightarrow l}(t + \Delta t) = z_k \prod_{j \in \mathcal{N}_k \setminus \{l\}} \theta_{j \rightarrow k}(t) \cdot \left[1 - \sum_{j' \in \mathcal{N}_k \setminus \{l\}} \frac{\beta \Delta t a_{k \rightarrow l}(t) I_{j' \rightarrow k}(t)}{\theta_{j' \rightarrow k}(t)} \right] \quad (11a)$$

$$= S_{k \rightarrow l}(t) \left[1 - \beta \Delta t \sum_{j' \in \mathcal{N}_k \setminus \{l\}} a_{k \rightarrow l}(t) \frac{I_{j' \rightarrow k}(t)}{\theta_{j' \rightarrow k}(t)} \right]. \quad (11b)$$

In Eq. (11b) we inserted the definition of $S_{k \rightarrow l}(t)$ from Eq. (6) and this leads directly to our second continuous-time dynamic equation

$$\frac{d}{dt} S_{k \rightarrow l}(t) = -\beta S_{k \rightarrow l}(t) \sum_{j \in \mathcal{N}_k \setminus \{l\}} a_{k \rightarrow l}(t) \frac{I_{j \rightarrow k}(t)}{\theta_{j \rightarrow k}(t)}. \quad (12)$$

The quotient $I_{j \rightarrow k}(t)/\theta_{j \rightarrow k}(t)$ can be interpreted as the conditional probability that j is infected *given* that cavity node k has not yet contracted the disease from j . It is worth noting that Eq. (12) is well defined because we start from the initial condition $\theta_{j \rightarrow k}(t) = 1$ for all edges $k \rightarrow j$ and Eq. (9) asserts positivity for $\theta_{j \rightarrow k}(t)$ for all finite observation times t . The remaining discrete-time Eq. (5) can be immediately written down in terms of a difference quotient $\Delta X(t) = [X(t + \Delta t) - X(t)]/\Delta t$:

$$\frac{\Delta I_{k \rightarrow l}(t)}{\Delta t} = [-\mu - \beta a_{k \rightarrow l}(t) + \mu \beta \Delta t a_{k \rightarrow l}(t)] I_{k \rightarrow l}(t) - \frac{\Delta S_{k \rightarrow l}(t)}{\Delta t}. \quad (13)$$

In the continuous-time limit, the higher order term $\mu\beta\Delta t a_{k \rightarrow l}(t)$ vanishes, leading to

$$\frac{d}{dt} I_{k \rightarrow l}(t) = [-\mu - \beta a_{k \rightarrow l}(t)] I_{k \rightarrow l}(t) - \frac{d}{dt} S_{k \rightarrow l}(t). \quad (14)$$

At last it is also instructive to formulate the dynamic equation for $R_{k \rightarrow l}(t)$, i.e., the probability that node k has recovered at time t without transmitting the disease to cavity node l . The value of $R_{k \rightarrow l}(t)$ can only increase over time and the corresponding in-flux at time t is given by (i) the probability $I_{k \rightarrow l}(t)$ that node k is in state I and has not infected its neighbor l together with (ii) the probability $\mu\Delta t$ to recover within the time step Δt . With this, we obtain:

$$R_{k \rightarrow l}(t + \Delta t) = R_{k \rightarrow l}(t) + \mu\Delta t I_{k \rightarrow l}(t). \quad (15)$$

The corresponding continuous-time equation thus reads

$$\frac{d}{dt} R_{k \rightarrow l}(t) = \mu I_{k \rightarrow l}(t). \quad (16)$$

Unlike the discrete-time model, it is now obvious that the dynamic Eqs. (9), (12), (14), and (16) satisfy the conservation condition

$$\theta_{k \rightarrow l}(t) = S_{k \rightarrow l}(t) + I_{k \rightarrow l}(t) + R_{k \rightarrow l}(t) \quad (17)$$

at every time t . Moreover, we can rescale time according to $\mu t \mapsto t$ and rewrite the continuous-time contact-based model in terms of the dimensionless epidemic parameter $\gamma = \beta/\mu$:

$$\frac{d}{dt} \theta_{k \rightarrow l}(t) = -\gamma a_{k \rightarrow l}(t) I_{k \rightarrow l}(t) \quad (18a)$$

$$\frac{d}{dt} S_{k \rightarrow l}(t) = -\gamma S_{k \rightarrow l}(t) \sum_{j \in \mathcal{N}_k \setminus \{l\}} a_{j \rightarrow k}(t) \frac{I_{j \rightarrow k}(t)}{\theta_{j \rightarrow k}(t)} \quad (18b)$$

$$\frac{d}{dt} I_{k \rightarrow l}(t) = -[1 + \gamma a_{k \rightarrow l}(t)] I_{k \rightarrow l}(t) - \frac{d}{dt} S_{k \rightarrow l}(t) \quad (18c)$$

$$\frac{d}{dt} R_{k \rightarrow l}(t) = I_{k \rightarrow l}(t). \quad (18d)$$

We can further reduce the set of dynamic equations using the conservation condition in Eq. (17). To this end, we first substitute $S_{k \rightarrow l}(t)$ in Eq. (17) with the definition from Eq. (6):

$$I_{k \rightarrow l}(t) = \theta_{k \rightarrow l}(t) - z_k \prod_{j \in \mathcal{N}_k \setminus \{l\}} \theta_{j \rightarrow k}(t) - R_{k \rightarrow l}(t). \quad (19)$$

With this, we replace $I_{k \rightarrow l}(t)$ in Eqs. (18a) and (18d) and thus we obtain a closed set of $2E$ dynamic equations that determine the disease progression of the continuous-time CB model.

Returning to node-centric quantities, i.e., the probability that a given node l is susceptible, infected or recovered, the continuous-time equivalent formulation to Eqs. (3), (7), and (8) reads

$$P_l^S(t) = z_l \prod_{k \in \mathcal{N}_l} \theta_{k \rightarrow l}(t) \quad (20a)$$

$$P_l^I(t) = 1 - P_l^S(t) - P_l^R(t) \quad (20b)$$

$$\frac{d}{dt} P_l^R(t) = P_l^I(t). \quad (20c)$$

4 Spectral Properties of the Continuous-Time Model

In this section, we evaluate the low prevalence limit of Eq. (18) in order to derive a spectral criterion that determines the epidemic threshold. To this end, we assume $\theta_{k \rightarrow l}(t) = 1 - \delta_{k \rightarrow l}(t)$, where $\delta_{k \rightarrow l}(t) \ll 1$ as well as $I_{k \rightarrow l} \ll 1$. With this, we linearize Eq. (18b) and obtain

$$\frac{d}{dt} S_{k \rightarrow l}(t) = -\gamma \left[1 - \sum_{j \in \mathcal{N}_k \setminus \{l\}} \delta_{j \rightarrow k}(t) \right] \cdot \sum_{j \in \mathcal{N}_k \setminus \{l\}} a_{k \rightarrow l}(t) \frac{I_{j \rightarrow k}(t)}{1 - \delta_{k \rightarrow l}(t)} \quad (21a)$$

$$= -\gamma \sum_{j \in \mathcal{N}_k \setminus \{l\}} a_{k \rightarrow l}(t) I_{j \rightarrow k}(t). \quad (21b)$$

In Eq. (21b), we keep only linear terms in $\delta_{k \rightarrow l}(t)$ and $I_{j \rightarrow k}(t)$. This allows us to decouple the set of dynamic equations and express Eq. (18c) only in terms of $I_{k \rightarrow l}(t)$:

$$\frac{d}{dt} I_{k \rightarrow l}(t) = [-1 - \gamma a_{k \rightarrow l}(t)] I_{k \rightarrow l}(t) + \gamma \sum_{j \in \mathcal{N}_k \setminus \{l\}} a_{k \rightarrow l}(t) I_{j \rightarrow k}(t). \quad (22)$$

Next, we vectorize Eq. (22) and to this end, we define the vectors $\mathbf{I}(t)$ and $\mathbf{a}(t)$ with elements $I_{k \rightarrow l}(t)$ and $a_{k \rightarrow l}(t)$, respectively. In order to rewrite $\sum_{j \in \mathcal{N}_k \setminus \{l\}} a_{j \rightarrow k}(t) I_{k \rightarrow l}(t)$ from Eq. (22) in terms of a matrix that acts on the state

vector $\mathbf{I}(t)$, we introduce the time-dependent non-backtracking operator $\mathbf{B}(t)$ as in [37]:

$$B_{k \rightarrow l, j \rightarrow k'}(t) = \begin{cases} a_{j \rightarrow k'}(t), & \text{if } k' = k, \text{ and } j \neq l \\ 0, & \text{otherwise.} \end{cases} \quad (23)$$

Expressed in words, we find $B_{k \rightarrow l, j \rightarrow k'}(t) = 1$ if the contact (t, j, k') is incident on the edge (k, l) , implying $k' = k$, and additionally $j \neq l$. The latter constraint prevents a probability flow back to the initially infected node and constitutes the non-backtracking property. In all other cases, we find $B_{k \rightarrow l, j \rightarrow k'}(t) = 0$. Unlike the static definition in [33, 45], we have to differentiate between the first and second index of the $L \times L$ dimensional matrix \mathbf{B} : The first index, i.e. $(k, l) \in \mathcal{E}$, corresponds to an edge in the aggregated graph, thus reflecting a potential path for future infections. The second index $(t, j, k') \in \mathcal{C}$, however, is a (temporal) contact from node j to k' at time t .

Moreover, we define the diagonal matrix $\text{diag}(\mathbf{a}(t))$ with elements $a_{k \rightarrow l}(t)$ for all edges $(k, l) \in \mathcal{E}$ on the diagonal and, additionally, we denote with $\mathbb{1}$ the identity matrix. Similar to the discrete-time derivation in [37], we thus obtain:

$$\frac{d}{dt} \mathbf{I}(t) = [-\mathbb{1} - \gamma \text{diag}(\mathbf{a}(t)) + \gamma \mathbf{B}(t)] \mathbf{I}(t). \quad (24)$$

The only structural difference to the discrete-time result in [37] is that the higher order term $\beta a_{k \rightarrow l}/\mu$ does not appear, because the simultaneous event of infection and recovery does not need to be accounted for in the continuous-time formulation.

Within the open interval $[t_n, t_{n+1})$ where the boundaries t_n and t_{n+1} , respectively, mark subsequent change points of the network topology, we integrate Eq. (24) and obtain

$$\mathbf{I}(t_{n+1}) = \mathbf{M}_n(\gamma) \mathbf{I}(t_n) \quad (25a)$$

$$\mathbf{M}_n(\gamma) = \exp \left(\int_{t_n}^{t_{n+1}} d\tau [-\mathbb{1} - \gamma \text{diag}(\mathbf{a}(\tau)) + \gamma \mathbf{B}(\tau)] \right). \quad (25b)$$

Using the initial condition $\mathbf{I}(0)$, we can formally state the explicit solution as follows:

$$\mathbf{I}(T) = \prod_{n=0}^{N_G-1} \mathbf{M}_n(\gamma) \mathbf{I}(0). \quad (26)$$

Here, N_G is the total number of discrete changing points of the network topology. Following [46] we can state the propagator $\mathbf{M}(\gamma) = \prod_{n=0}^{N-1} \mathbf{M}_n(\gamma)$ in a compact

notation using Dyson's time ordering operator $\mathsf{T} \mathbf{B}(\tau_1) \mathbf{B}(\tau_2) = \mathbf{B}(\tau_1) \mathbf{B}(\tau_2) \Theta(\tau_1 - \tau_2) + \mathbf{B}(\tau_2) \mathbf{B}(\tau_1) \Theta(\tau_2 - \tau_1)$, where $\Theta(x)$ denotes the Heaviside function:

$$\mathbf{M}(\gamma) = \mathsf{T} \exp \left(\int_0^t d\tau \left[-\mathbb{1} - \gamma \text{diag}(\mathbf{a}(\tau)) + \gamma \mathbf{B}(\tau) \right] \right). \quad (27)$$

Any small initial perturbation will decrease exponentially if the largest eigenvalue λ_1 , i.e., the spectral radius satisfies $\lambda_1[\mathbf{M}(\gamma)] < 1$. This result corresponds to [46] where the epidemic propagator $\mathbf{M}(\gamma)$ has been derived within the IB framework and reads

$$\mathbf{M}(\gamma) = \mathsf{T} \exp \left(\int_0^t d\tau \left[-\mathbb{1} + \gamma \mathbf{A}(\tau) \right] \right). \quad (28)$$

In Eq. (28), we denote with $\mathbf{A}(\tau)$ the time-dependent adjacency matrix and here, $\mathbb{1}$ is the $N \times N$ dimensional identity matrix.

In many cases, the temporal network is sampled with equidistant time steps Δt and in this case, we can simplify the propagator Eq. (28) to

$$\mathbf{M}(\gamma) = \prod_{n=0}^{N_G-1} \exp \left(\Delta t \left[-\mathbb{1} - \gamma \text{diag}(\mathbf{a}(n)) + \gamma \mathbf{B}(t_n) \right] \right). \quad (29)$$

The CB result in Eq. (29) is akin to the IB formulation that was first derived in [47]. In the *quenched limit*, when the disease evolves on a much faster time scale than the temporal network, we can assume a static underlying topology and thus identify $\text{diag}(\mathbf{a}(t)) \equiv \mathbb{1}$ and $\mathbf{B}(t) \equiv \mathbf{B}(1) \equiv \mathbf{B}$. Then, the linearized result in Eq. (24) simplifies to

$$\frac{d}{dt} \mathbf{I}(t) = [-(1 + \gamma)\mathbb{1} + \gamma \mathbf{B}] \mathbf{I}(t). \quad (30)$$

Finally, Eq. (30) is asymptotically stable if the largest eigenvalue λ_1 of the infection operator $\mathbf{M}(\gamma) = (1 + \gamma)\mathbb{1} + \gamma \mathbf{B}$ is negative. Hence, we recover the continuous-time threshold as previously derived within the more general message-passing framework on static networks [13, 33]:

$$\frac{\gamma}{\gamma + 1} = \frac{1}{\lambda_1(\mathbf{B})}. \quad (31)$$

For non-Markovian infection and recovery processes the generalized criticality condition reads $T = 1/\lambda_1(\mathbf{B})$ (see [13, 33]), where the transmissibility T is given by

$$T = \int_0^\infty s(\tau) \left(\int_\tau^\infty r(\tau') d\tau' \right) d\tau. \quad (32)$$

Intuitively, T can be interpreted as the probability that a newly infected node transmits the disease to a given neighbor prior to recovery [13, 48]. Within this general formulation $s(\tau)d\tau$ is the probability that an infected node passes the disease to a neighbor within a time interval $[\tau, \tau + d\tau]$ after contracting the infection. Similarly, we define the probability $r(\tau)d\tau$ that a node recovers in the interval $[\tau, \tau + d\tau]$ after it has been infected. For a constant infection and recovery rate, i.e., for the Markovian dynamics that we assumed in this article, we find $s(\tau) = \beta \exp(-\beta\tau)$ and $r(\tau) = \mu \exp(-\mu\tau)$. This particularly simple and widely studied choice then leads to $T = \gamma/(\gamma + 1)$ and thus to Eq. (31).

For temporal networks, we cannot separate in general the transmissibility T from the network topology in order to find a similarly elegant results like Eq. (31). The reason is that the probability to infect a given neighbor depends on the timing of contacts and as a consequence the transmissibility T would have to be both edge- and time-dependent even in the Markovian case.

5 Relation to the Edge-Based Compartmental Model

An important branch in theoretical epidemiology focuses on random graphs, i.e., an ensemble of networks derived from a generating model, instead of a single realization. In this context, the *edge-based compartmental* (EBC) model [34] is a particularly compact and accurate approach to model infections with permanent immunity. In this section, we will explore the relation between the CB model presented in Sect. 3 and the EBC framework for static random graphs.

To this end, we will focus on random networks with unweighted and undirected edges that are derived from the *configuration model* [49, 50]. This widely used generative model allows to study the effect of the degree distribution on the spread of infections [48]. For this, we have to create an ensemble of networks with the same degree distribution that are otherwise maximally random. This can be done according to the Bender-Canfield algorithm [49], which begins with a set of N vertices. To each node we assign a number of k (undirected) *stubs*, i.e., edges with no target node that are drawn independently from the given degree distribution $p(k)$. In the next step, we connect two randomly chosen stubs which then form a proper edge between the corresponding nodes. The step is repeated until no more stubs are available and if initially the number of stubs were found to be odd then the we would replace one node repeatedly until the sum is even.

Before we proceed with the ensemble average, we restate for convenience the relevant dynamic equations of the continuous-time model, i.e., Eqs. (18a) and (18d), for a network with a static topology. In this case, $a_{k \rightarrow l} \equiv 1$ for all edges $(k, l) \in \mathcal{E}$ and thus we obtain

$$\frac{d}{dt}\theta_{k \rightarrow l}(t) = -\gamma I_{k \rightarrow l}(t) \quad (33a)$$

$$\frac{d}{dt} R_{k \rightarrow l}(t) = I_{k \rightarrow l}(t) \quad (33b)$$

and close the set of equations with the conservation condition from Eq. (19):

$$I_{k \rightarrow l}(t) = \theta_{k \rightarrow l}(t) - z_k \prod_{j \in \mathcal{N}_k \setminus \{l\}} \theta_{j \rightarrow k}(t) - R_{k \rightarrow l}(t). \quad (34)$$

For static networks, we can further simplify the dynamic equations by substituting $I_{k \rightarrow l}(t)$ in Eq. (33a) with Eq. (33b) and integrating the result:

$$\frac{d}{dt} R_{k \rightarrow l}(t) = -\frac{1}{\gamma} \frac{d}{dt} \theta_{k \rightarrow l}(t) \quad (35a)$$

$$R_{k \rightarrow l}(t) = \frac{1}{\gamma} (1 - \theta_{k \rightarrow l}(t)). \quad (35b)$$

From Eqs. (33a), (34), and (35b), we obtain a coupled set of E dynamic equations that determine the progression of an SIR epidemic on a static graph:

$$\frac{d}{dt} \theta_{k \rightarrow l}(t) = 1 - (1 + \gamma) \theta_{k \rightarrow l}(t) + \gamma z_k \prod_{j \in \mathcal{N}_k \setminus \{l\}} \theta_{j \rightarrow k}(t). \quad (36)$$

The result in Eq. (36) constitutes a message-passing equation as derived in [13]. We will explore the connection to the more general message-passing framework for epidemics with non-Markovian dynamics in Sect. 6. Here, we continue instead with the ensemble average over random networks, thereby following closely the approach outlined in [13]. We start with the following crucial observation: The state of a given edge $k \rightarrow l$ in a single realization of a graph displays a characteristic trajectory in state space, i.e., a time-dependent curve given by $\theta_{k \rightarrow l}(t)$ from Eq. (36). As we perform an average over the ensemble of graphs, our selected edge $k \rightarrow l$ will assume every position within a network. As a consequence the averaged state trajectory is identical to the one that we would obtain if we had started with a different edge initially and then performed the average. In other words, it is sufficient to determine the ensemble averaged probabilities for *one representative edge*:

$$\frac{d}{dt} \theta(t) \equiv \frac{d}{dt} \langle \theta_{k \rightarrow l}(t) \rangle \quad (37a)$$

$$= 1 - (1 + \gamma) \theta(t) + \gamma \left\langle z_k \prod_{j \in \mathcal{N}_k \setminus \{l\}} \theta_{j \rightarrow k}(t) \right\rangle. \quad (37b)$$

Next, we focus on the second term in Eq. (37b). A crucial property of large networks that are generated by the configuration model is that they are locally tree-like in the sense that the average length of the smallest cycle diverges with increasing network

size. Hence, we can assume in the limit $N \rightarrow \infty$ that different branches emerging from k can be treated independently. The average over the product thus equals the product over averages. Moreover, we remember that ensemble averaged dynamic quantities are equal for all edges and in particular $\theta_{j \rightarrow k}(t) \equiv \theta(t)$ for all edges $(j, k) \in \mathcal{N}_k \setminus \{l\}$. With this the product in Eq. (37b) simplifies to $[\theta(t)]^{k_e}$, where k_e is the average number of next nearest neighbors, or equally, the *excess degree* [13]. From a given degree distribution p_n in the configuration model, we can derive the excess degree distribution q_n according to $q_n = (n+1)p_{n+1}/k$ [50], where $k = \langle n \rangle$ denotes the average degree. Finally, we make use of the corresponding generating function $G_1(x) = \sum_n q_n x^n$ and thus the second term in Eq. (37b) simplifies to

$$\left\langle z_k \prod_{j \in \mathcal{N}_k \setminus \{l\}} \theta_{j \rightarrow k}(t) \right\rangle = z \sum_{n=0}^N q_n [\theta(t)]^n \quad (38a)$$

$$= z G_1(\theta(t)). \quad (38b)$$

Here, $z = \langle z_k \rangle$ denotes the probability that a randomly chosen node is initially susceptible. With Eqs. (37b) and (38b), we obtain the following ensemble averaged dynamic equation for θ :

$$\frac{d}{dt} \theta(t) = 1 - (1 + \gamma)\theta(t) + \gamma z G_1(\theta(t)). \quad (39)$$

This compact result captures the disease dynamic with high accuracy as demonstrated in [13] within the message-passing framework and later in [34] as a special case of the edge-based compartmental model. The authors in [34] also investigated alternative random graph models with time-varying topologies.

We close the section with a linear stability analysis of Eq. (39). Similar to the derivation in Sect. 4, we start with a small initial perturbation: $\theta(t) = 1 - \delta(t)$ with $\delta(t) \ll 1$ and $z = 1$. We then expand the generating function $G_1(1 - \delta(t))$ to the first order in $\delta(t)$:

$$G_1(1 - \delta(t)) = \sum_n p_n (1 - \delta(t))^n \quad (40a)$$

$$= 1 + \langle n \rangle_q (1 - \delta(t)) + \mathcal{O}(\delta(t)^2). \quad (40b)$$

Here, we used two properties of the generating function, namely $G_1(1) = \sum_n q_n = 1$ and $G'_1(1) = \sum_n n q_n = \langle n \rangle_q$, where $\langle n \rangle_q = k_e$ denotes the mean excess degree. With this, the linearization of Eq. (39) around the disease-free stable fixed point reads:

$$\frac{d}{dt} \delta(t) = -(1 + \gamma - \gamma \langle n \rangle_q) \delta(t). \quad (41)$$

From Eq.(41) we can easily see that a transition occurs from local to global outbreaks if $1 + \gamma - \gamma \langle n \rangle_q < 0$. Commonly, $\langle n \rangle_q$ is expressed in terms of the first and second moment of the degree distribution, i.e. $\langle n \rangle = \sum_n np_n$ and $\langle n^2 \rangle = \sum_n n^2 p_n$, respectively. For that we take the definition $\langle n \rangle_q = \sum_n n q_n$ and substitute the relation $q_n = (n+1)p_{n+1}/\langle n \rangle$ (see [50] for details). With this, we recover the well-known criticality condition from [48, 51]:

$$\frac{\gamma}{\gamma + 1} = \frac{\langle n \rangle}{\langle n^2 \rangle - \langle n \rangle}. \quad (42)$$

This result is related to the epidemic threshold in Eq.(31), where we studied a single realization of a static graph and hence expressed the right hand side of Eq.(42) through the spectral radius $\lambda_1(\mathbf{B})$ of the non-backtracking matrix \mathbf{B} .

6 Relation to the Message-Passing Framework

In the seminal work of Karrer & Newman [13], the authors proposed a general model for SIR spreading processes on sparse networks with non-Markovian infection and recovery dynamics. The integro-differential formulation in [13] is a foundation of our CB model and therefore we will discuss in this section the relation to their message-passing approach. For that we first propose a generalization of the CB model to non-Markovian dynamics and then, taking the static network limit, we will arrive at the previously proposed result.

As a first step, we transform the dynamic equations in Eqs.(9), (12), (14), and (16) that define the continuous-time CB model to an integro-differential equation. To this end, we notice first that Eq.(14) is of the form

$$\frac{d}{dt} I_{k \rightarrow l}(t) = -\lambda_{k \rightarrow l}(t) I_{k \rightarrow l}(t) - \frac{d}{dt} S_{k \rightarrow l}(t). \quad (43)$$

For notational convenience, we use the short-hand notation $\lambda_{k \rightarrow l}(\tau) = \mu + \beta a_{k \rightarrow l}(\tau)$ and $\Lambda_{k \rightarrow l}(t, t_k) = \exp[-\int_{t_k}^t \lambda_{k \rightarrow l}(\tau) d\tau]$. The former denotes the probability that node k recovers or infects the cavity node l within the time interval $[\tau, \tau + dt]$ after contracting the disease and the latter corresponds to the probability that no such event took place between the time of infection and the observation time t_k and t , respectively. Here, we denote the absolute and relative time after infection with t and τ , respectively. Together with the initial condition $I_{k \rightarrow l}(0) = 1 - z_k$ the solution to the differential equation is given by

$$I_{k \rightarrow l}(t) = (1 - z_k) \Lambda_{k \rightarrow l}(t, 0) + \int_0^t \left[-\frac{d}{dt} S_{k \rightarrow l}(t_k) \right] \Lambda_{k \rightarrow l}(t, t_k) dt_k. \quad (44)$$

In words, Eq. (44) states that node k has contracted the disease but not infected its neighbor l by absolute time t if (i) node k was infected initially but has neither recovered nor passed the infection or (ii) it was susceptible initially, contracted the disease at time t_k and has then neither recovered nor infected its neighbor up to the observation time t .

Next, we integrate Eq. (9) and using the initial condition $\theta_{k \rightarrow l}(0) = 1$ we get

$$1 - \theta_{k \rightarrow l}(t) = \int_0^t \beta a_{k \rightarrow l}(t') I_{k \rightarrow l}(t') dt' \quad (45a)$$

$$\begin{aligned} &= (1 - z_k) \int_0^t dt' f_{k \rightarrow l}(t'|0) \\ &\quad + \int_0^t \int_0^{t'} dt' dt_k \left[-\frac{d}{dt_k} S_{k \rightarrow l}(t_k) \right] f_{k \rightarrow l}(t'|t_k). \end{aligned} \quad (45b)$$

In Eq. (45b) we used $I_{k \rightarrow l}(t)$ from Eq. (44) and we also introduced the transmission probability $f_{k \rightarrow l}(t'|t_k) = \beta a_{k \rightarrow l}(t') \Lambda_{k \rightarrow l}(t', t_k)$: Given that node k contracted the infection at absolute time t_k , $f_{k \rightarrow l}(t'|t_k)$ gives the probability that the same node passes the disease to its neighbor l at absolute time t' . In the context of static networks the quantity $\int_{t_k}^{\infty} f_{k \rightarrow l}(t'|t_k) dt'$ is frequently referred to as *transmissibility* and plays a crucial role in linking epidemic spreading to a percolation process [13, 48]. Note that the transmissibility can be smaller than one as node k might recover before passing on the infection and for temporal networks, unlike the static case, the value is edge- and time-dependent as we discussed already at the end of Sect. 4.

The message-passing framework in [13] assumes a non-Markovian infection and recovery process. Similarly, our result in Eq. (45b) demonstrates how a general epidemic model on *temporal networks* can be formulated by redefining $f_{k \rightarrow l}(t'|t_k)$ as proposed in [13] (see also Eq. (32)).

In order to demonstrate the reduction to the message-passing formulation of [13], we reformulate Eq. (45b) for a static underlying topology. With $a_{k \rightarrow l}(t) \equiv 1$ the transmission probability $f_{k \rightarrow l}(t|t_k) \rightarrow f(\tau)$ depends only on the relative time $\tau = t - t_k$ after infection and becomes an identical function for all edges $k \rightarrow l$. Using this simplification we obtain

$$\begin{aligned} 1 - \theta_{k \rightarrow l}(t) &= (1 - z_k) \int_0^t d\tau f(\tau) \\ &\quad + \int_0^t \int_0^{\tau} d\tau d\tau_i f(\tau - \tau_i) \left[-\frac{d}{d\tau_i} S_{k \rightarrow l}(\tau_i) \right]. \end{aligned} \quad (46)$$

Integrating the second term in Eq. (46) by parts, and using the fact that the double integral can be reordered as

$$\int_0^t d\tau \int_0^{\tau} d\tau_i = \int_0^t d\tau_i \int_{\tau_i}^t d\tau, \quad (47)$$

we arrive at the message-passing formulation equivalent to that in [13]:

$$\theta_{k \rightarrow l}(t) = 1 - \int_0^t d\tau f(\tau)(1 - S_{k \rightarrow l}(t - \tau)). \quad (48)$$

With this we have linked the continuous-time CB model with a previously introduced message-passing framework for general non-Markovian epidemic models in the case of a static underlying graph.

7 Summary

We have presented a continuous-time description of a contact-based model. The discussed theoretical framework allows us to study the spreading of epidemics and extends the dynamic message-passing approach to networks with a time-varying topology. At the center of the contact-based model is a shift in perspective from node- to edge-centric quantities. This allows to accurately model, e.g., susceptible-infected-recovered outbreaks on time-varying trees, that is, temporal networks with a loop-free underlying topology. We have shown that on arbitrary graphs, the proposed contact-based (edge-centric) model incorporates potential structural and temporal heterogeneities of the underlying contact network and improves analytic estimations with respect to the individual-based (node-centric) approach at a low computational and conceptual cost. Within this new framework, we have derived an analytical expression for the epidemic threshold on temporal networks.

We have taken a decidedly theoretical and analytical approach to the proposed framework. This will facilitate the application to both empirical data sets and generic classes of networks.

Acknowledgements AK and PH acknowledge the support by Deutsche Forschungsgemeinschaft (DFG) in the framework of Collaborative Research Center 910. AK acknowledges further support by German Academic Exchange Service (DAAD) via a short-term scholarship. JPG acknowledges the support by Science Foundation Ireland (grant numbers 16/IA/4470 and 16/RC/3918).

References

1. Hamer, W.H.: Lancet **1**, 733 (1906)
2. Ross, R.: The Prevention of Malaria, E.P. Dutton, New York (1910)
3. Kermack, W.O., McKendrick, A.G.: Proc. R. Soc. A **115**(772), 700 (1927)
4. Bailey, N.T.J.: The Mathematical Theory of Epidemics. Hafner, Royal Oak (1957)
5. Anderson, R.H., May, R.M.: Infectious Diseases of Humans: Dynamics and Control. Oxford University Press, Oxford (1992)
6. Hethcote, H.W.: SIAM Rev. **42**(4), 599 (2000)
7. van Kampen, N.G.: Stochastic Processes in Physics and Chemistry. North-Holland, Amsterdam (1981)

8. Bailey, N.T.J.: The mathematical theory of infectious diseases and its applications. In Mathematics in Medicine Series. Charles Griffin & Company Ltd., Bucks (1975)
9. Simon, P.L., Taylor, M., Kiss, I.Z.: *J. Math. Biol.* **62**(4), 479 (2011)
10. Van Mieghem, P., Omic, J., Kooij, R.: *IEEE/ACM Trans. Netw.* **17**(1), 1 (2009)
11. Kiss, I.Z., Röst, G., Vizi, Z.: *Phys. Rev. Lett.* **115**(7), 078701 (2015)
12. Sherborne, N., Miller, J.C., Blyuss, K.B., Kiss, I.Z.: *J. Math. Biol.* **76**(3), 755 (2018)
13. Karrer, B., Newman, M.E.J.: *Phys. Rev. E* **82**, 016101 (2010)
14. Gonçalves, S., Abramson, G., Gomes, M.F.C.: *Eur. Phys. J. B* **81**(3), 363 (2011)
15. Van Mieghem, P., van de Bovenkamp, R.: *Phys. Rev. Lett.* **110**, 108701 (2013)
16. Keeling, M.J., Rohani, P.: Modeling Infectious Diseases in Humans and Animals. Princeton University Press, Princeton (2008)
17. Pastor-Satorras, R., Castellano, C., Van Mieghem, P., Vespignani, A.: *Rev. Mod. Phys.* **87**, 925 (2015)
18. Balcan, D., Colizza, V., Gonçalves, B., Hu, H., Ramasco, J.J., Vespignani, A.: *Proc. Natl. Acad. Sci.* **106**(51), 21484 (2009)
19. Eubank, S., Guclu, H., Kumar, V.S.A., Marathe, M.V., Srinivasan, A., Toroczkai, Z., Wang, N.: *Nature* **429**, 180 (2004)
20. Ferguson, N.M., Cummings, D.A.T., Cauchemez, S., Fraser, C., Riley, S., Meeyai, A., Iamsirithaworn, S., Burke, D.S.: *Nature* **437**(7056), 209 (2005)
21. Halloran, M.E., Ferguson, N.M., Eubank, S., Longini, I.M., Cummings, D.A.T., Lewis, B., Xu, S., Fraser, C., Vullikanti, A., Germann, T.C., Wagener, D., Beckman, R., Kadri, K., Barrett, C., Macken, C.A., Burke, D.S., Cooley, P.: *Proc. Natl. Acad. Sci.* **105**(12), 4639 (2008)
22. Chao, D.L., Halloran, M.E., Obenchain, V.J., Longini Jr., I.M.: *PLOS Comput. Biol.* **6**(1), 1 (2010)
23. Longini, I.M., Nizam, A., Xu, S., Ungchusak, K., Hanshaoworakul, W., Cummings, D.A.T., Halloran, M.E.: *Science* **309**(5737), 1083 (2005)
24. Merler, S., Ajelli, M., Pugliese, A.: *PLOS Comput. Biol.* **7**(9), 1 (2011)
25. Wang, Y., Chakrabarti, D., Wang, C., Faloutsos, C.: In: Proceedings 22nd International Symposium on Reliable Distributed Systems, 2003 (2003), pp. 25–34
26. Valdano, E., Ferreri, L., Poletto, C., Colizza, V.: *Phys. Rev. X* **5**, 021005 (2015)
27. Rocha, L.E.C., Masuda, N.: *Sci. Rep.* **6**, 31456 (2016)
28. Chakrabarti, D., Wang, Y., Wang, C., Leskovec, J., Faloutsos, C.: *ACM Trans. Inf. Syst. Secur.* **10**(4), 1–26 (2008)
29. Ganesh, A., Massoulié, L., Towsley, D.: In Proceedings IEEE INFOCOM 2005. 24th Annual Joint Conference of the IEEE Computer and Communications Societies, vol. 2, pp. 1455–1466. IEEE, Piscataway (2005)
30. Gómez, S., Arenas, A., Borge-Holthoefer, J., Meloni, S., Moreno, Y.: *Europhys. Lett.* **89**(3), 38009 (2010)
31. Youssef, M., Scoglio, C.: *J. Theor. Biol.* **283**(1), 136 (2011)
32. Pearl, J.: In: Proceedings of the Second AAAI Conference on Artificial Intelligence, AAAI'82, pp. 133–136. AAAI Press, Menlo Park (1982)
33. Karrer, B., Newman, M.E.J., Zdeborová, L.: *Phys. Rev. Lett.* **113**, 208702 (2014)
34. Miller, J.C., Slim, A.C., Volz, E.M.: *J. Royal Soc. Interface* **9**(70), 890 (2012)
35. Lokhov, A.Y., Mézard, M., Ohta, H., Zdeborová, L.: *Phys. Rev. E* **90**(1), 012801 (2014)
36. Wilkinson, R.R., Ball, F.G., Sharkey, K.J.: *J. Math. Biol.* **75**(6), 1563 (2017)
37. Koher, A., Lentz, H.H.K., Gleeson, J.P., Hövel, P.: *Phys. Rev. X* **9**, 031017 (2019)
38. Miller, J.C.: *PLoS One* **9**(7), 1 (2014)
39. Miller, J.C., Volz, E.M.: *J. Math. Biol.* **67**(4), 869 (2013)
40. Miller, J.C., Kiss, I.Z.: *Math. Model. Nat. Phenom.* **9**(2), 4 (2014)
41. Eames, K.T.D., Keeling, M.J.: *Proc. Natl. Acad. Sci.* **99**(20), 13330 (2002)
42. Lindquist, J., Ma, J., van den Driessche, P., Willeboordse, F.H.: *J. Math. Biol.* **62**(2), 143 (2011)
43. Kiss, I.Z., Morris, C.G., Sélley, F., Simon, P.L., Wilkinson, R.R.: *J. Math. Biol.* **70**(3), 437 (2015)

44. Lokhov, A.Y.: Dynamic cavity method and problems on graphs. Theses, Université Paris Sud – Paris XI (2014)
45. Krzakala, F., Moore, C., Mossel, E., Neeman, J., Sly, A., Zdeborová, L., Zhang, P.: Proc. Natl. Acad. Sci. **110**(52), 20935 (2013)
46. Valdano, E., Fiorentin, M.R., Poletto, C., Colizza, V.: Phys. Rev. Lett. **120**(6), 068302 (2018)
47. Speidel, L., Klemm, K., Eguiluz, V.M., Masuda, N.: New J. Phys. **18**(7), 073013 (2016)
48. Newman, M.E.J.: Phys. Rev. E **66**(1), 016128 (2002)
49. Molloy, M., Reed, B.: Random Struct. Algoritm. **6**(2–3), 161 (1995)
50. Newman, M.E.J., Strogatz, S.H., Watts, D.J.: Phys. Rev. E **64**, 026118 (2001)
51. Miller, J.C.: Phys. Rev. E **76**, 010101 (2007)

The Effect of Concurrency on Epidemic Threshold in Time-Varying Networks



Tomokatsu Onaga, James P. Gleeson, and Naoki Masuda

1 Introduction

How infectious diseases and information spread on contact networks may considerably depend on temporal dynamics as well as static structural properties of the underlying networks. While earlier research has focused on the understanding of epidemic processes on static networks, an overarching aim of what one could call “temporal network epidemiology” is to reveal qualitative and quantitative changes that the time-dependent nature of the network introduces to epidemic processes on networks [1–4].

Concurrency in epidemiology is a notion proposed in mid 1990s that concerns the number of contacts that a node has simultaneously [5–7]. In a static network, all edges exist concurrently (i.e., at the same time) such that if a node has degree k , the k edges incident to the node are simultaneously present over time. This is not necessarily the case for temporal networks, in which edges appear and disappear. In a temporal network in which each node never has more than one edge at any point of time, one can say that the temporal network completely lacks concurrency. In general, although it depends on how to measure the concurrency, temporal networks are considered to have lower concurrency than the corresponding static networks.

T. Onaga

The Frontier Research Institute for Interdisciplinary Sciences and Graduate School of Information Sciences, Tohoku University, Sendai, Japan

e-mail: onaga@se.is.tohoku.ac.jp

J. P. Gleeson

MACSI, Department of Mathematics and Statistics, University of Limerick, Limerick, Ireland
e-mail: james.gleeson@ul.ie

N. Masuda (✉)

Department of Engineering Mathematics, University of Bristol, Bristol, UK
e-mail: naoki.masuda@bristol.ac.uk

However, different temporal networks can have different levels of concurrency even if they are reduced to the same aggregate static network when the time information about the edges is ignored. Consider two temporal networks shown in Fig. 1a, b, both of which have $N = 5$ nodes and 10 discrete time points. The temporal network shown in Fig. 1a lacks concurrency because all edges appear in isolation. Each node has at most $m = 1$ edge at any given time. In contrast, the temporal network shown in Fig. 1b has high concurrency because some time points contain a star network and the hub in the star has $m = 4$ edges that exist simultaneously. In fact, these two temporal networks have the same aggregated network, which is defined as the time-averaged network (Fig. 1c). In Fig. 1c, the edges are shown by thin lines because they should have smaller weights than the edges shown in Fig. 1a, b to ensure that each edge is used for the same “weight \times time”. Specifically, assume that each edge in Fig. 1a, b is of unit weight and each edge in Fig. 1c is of weight $1/5$. In Fig. 1a, b, an edge of unit weight appears between each node pair in two out of the 10 discrete time points. In Fig. 1c, an edge of weight $1/5$ appears between each node pair in all the 10 discrete time points. Then, in each of the three networks shown in Fig. 1, each edge in the complete graph is used for a total of two “weight \times time” units across the ten discrete time points.

In the present chapter, we pose the following question: how do different levels of concurrency in temporal networks (e.g., Fig. 1a versus b) impact epidemic spreading in temporal networks? We address this question by theoretically analysing

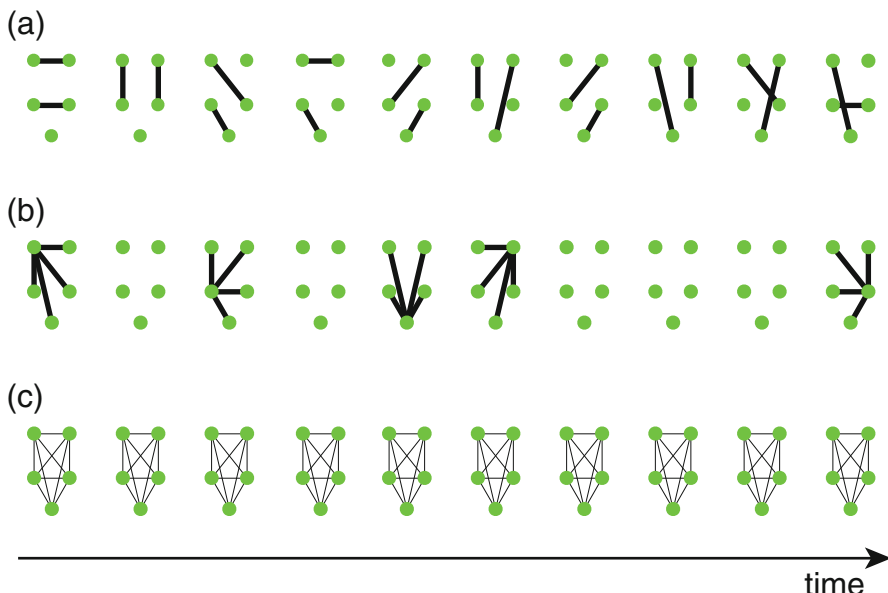


Fig. 1 (a) A temporal network lacking concurrency. (b) A temporal network having a high concurrency. (c) The aggregate network corresponding to the temporal networks shown in (a) and (b)

a susceptible-infected-susceptible (SIS) model on a temporal network model based on activation of cliques (rather than stars as in Fig. 1).

2 Model

We consider the following continuous-time SIS model on a variant of the activity-driven model of temporal networks (see [8] for the original activity-driven model), which we call the clique-based activity-driven network. For the modelling and analysis of the epidemic threshold in the case of the original activity-driven network model, see Ref. [9].

We denote the number of nodes by N . We assign each node i ($1 \leq i \leq N$) an activity potential a_i , drawn from a probability density $F(a)$ ($0 < a \leq 1$). Activity potential a_i is the probability with which node i is activated in each time window of constant period τ and is fixed over time. If activated, node i creates a clique with m uniformly randomly selected other nodes in the network (Fig. 2), modelling a group conversation event [10–12]. If two cliques overlap and share at least two nodes, we only create a single edge between each pair of the nodes shared by the different cliques. However, for large N and relatively small a_i , such events seldom occur. At the end of each time window of length τ , all cliques are discarded. Then, in the next time window, each node is again activated with probability a_i , independently of the activity in the previous time window, and creates a clique with m uniformly randomly selected nodes. We repeat this procedure. The present network model is an example of a switching network [13–16]. A large τ implies that the dynamics of network structure are slow compared to epidemic dynamics. In the limit of $\tau \rightarrow 0$, the network changes infinitesimally fast, enabling the dynamical process on networks to be approximated by that on the time-averaged static network [15].

In the SIS model, each node takes either the susceptible or infected state. At any time, each susceptible node contracts infection according to the Poisson process with rate β per infected neighbouring node. Each infected node recovers to transit to the susceptible state at rate μ irrespectively of the neighbours' states. Changing τ to $c\tau$ ($c > 0$) is equivalent to changing β and μ to β/c and μ/c , respectively, while leaving τ unchanged. Hence, we set $\mu = 1$ without loss of generality.

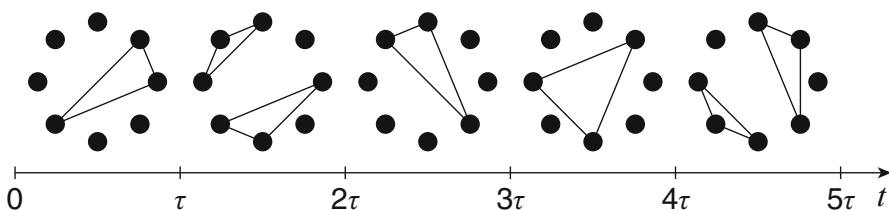


Fig. 2 Schematic of a clique-based activity-driven network with $m = 2$

3 Analysis

In this section, we calculate the epidemic threshold for the SIS model on the clique-based activity-driven network as follows. First, we analyse SIS dynamics on a static clique spanning a single time window of length τ by explicitly considering extinction effects (Sect. 3.1). Second, we obtain a linear mapping that transforms the network state at the beginning of the time window to that at the end of the time window, which coincides with the beginning of the next time window (Sect. 3.2). Third, we obtain the epidemic threshold as the root of an implicit function using a moment closure method. For expository purposes, we confine ourselves to a simplified model where the activity potential of all nodes is the same (Sect. 3.3). In Sect. 3.4, we consider the general case in which the activity potential depends on the node.

For the sake of the theoretical analysis, we assume that cliques generated by an activated node are disjoint from each other. Because a clique created by node i overlaps with another clique with probability $\approx m \sum_{j \neq i} a_j(m+1)/N \propto m^2 \langle a \rangle$, where $\langle a \rangle \equiv \int da F(a)a$ is the mean activity potential, we impose $m^2 \langle a \rangle \ll 1$ for this assumption to be valid.

3.1 SIS Dynamics on a Clique and Extinction Effects

In this section, we examine the SIS dynamics of a clique of size $m+1$. We explicitly calculate the effect of stochastic extinction in the following analysis. For demonstration purposes, we consider SIS dynamics on a clique of size 3 (Fig. 3a). We denote the probability with which there are i infected nodes on a clique at time t by $\rho_i^{\text{clique}}(t)$. The master equation for $\rho_i^{\text{clique}}(t)$ is given by

$$\frac{d}{dt} \begin{pmatrix} \rho_0^{\text{clique}} \\ \rho_1^{\text{clique}} \\ \rho_2^{\text{clique}} \\ \rho_3^{\text{clique}} \end{pmatrix} = \begin{pmatrix} 0 & 1 & 0 & 0 \\ 0 & -2\beta - 1 & 2 & 0 \\ 0 & 2\beta & -2\beta - 2 & 3 \\ 0 & 0 & 2\beta & -3 \end{pmatrix} \begin{pmatrix} \rho_0^{\text{clique}} \\ \rho_1^{\text{clique}} \\ \rho_2^{\text{clique}} \\ \rho_3^{\text{clique}} \end{pmatrix}. \quad (1)$$

By solving Eq. (1), one can obtain $\{\rho_0^{\text{clique}}(t), \rho_1^{\text{clique}}(t), \rho_2^{\text{clique}}(t), \rho_3^{\text{clique}}(t)\}$ as a function of the state of the clique at the beginning of the time window, i.e., $\{\rho_0^{\text{clique}}(0), \rho_1^{\text{clique}}(0), \rho_2^{\text{clique}}(0), \rho_3^{\text{clique}}(0)\}$. With $\beta = 2$, the values of $\rho_i^{\text{clique}}(t)$ for a range of t are shown in Fig. 3b. Because the employed infection rate is relatively large, infection initially spreads over a clique, causing the increase in ρ_2^{clique} and ρ_3^{clique} . However, at larger t , ρ_0^{clique} grows dramatically. Because the present dynamics are a Markov process with a unique, disease-free absorbing state, ρ_0^{clique} approaches 1 for any infection rate. Therefore, on the clique-based activity-driven network, an infection would die out, for any infection rate if the length of the time window, τ , is large.

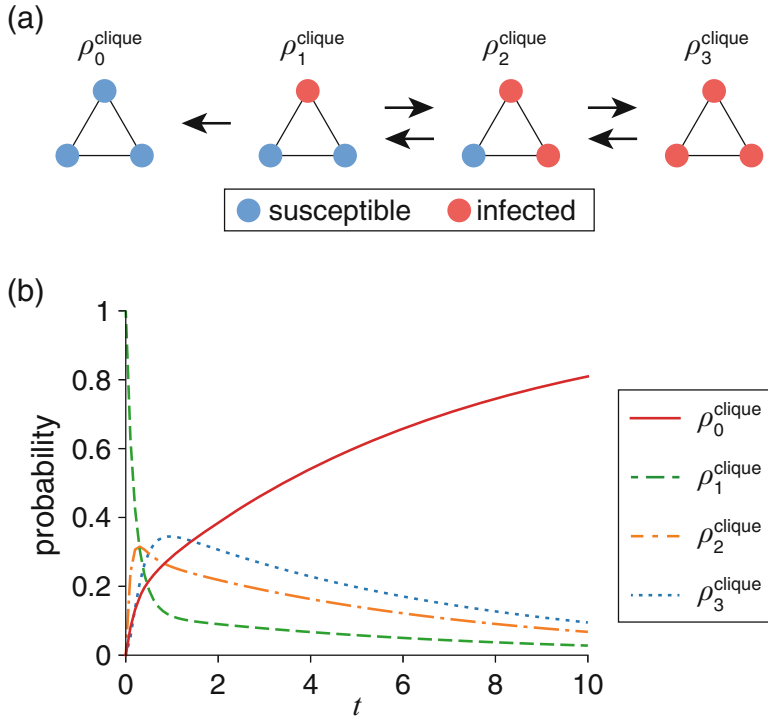


Fig. 3 Stochastic SIS dynamics on a clique of size 3. (a) Four possible states of the clique and the transitions between them. (b) Time course of the probability of each state of the clique. The initial condition is set to $\rho_1^{\text{clique}}(0) = 1$ and $\rho_i^{\text{clique}}(0) = 0$ for $i \neq 1$. We set $\beta = 2$

The most common approach to SIS dynamics in statistical physics and mathematical biology is perhaps the mean-field theory [17]. However, in temporal networks, only a small number of contacts may be simultaneously present such that stochastic extinction effects are not negligible. In this case, we need to use the master equation or other approaches that explicitly deal with the stochastic dynamics including extinction effects [18–22]. We note that the so-called individual-based mean-field approximation is also a method aiming to track the evolution of the probability that each node is infected [17, 21]. That method assumes that the state of each node is independent from each other. For this reason, the approximation may fail to capture the probability of the extinction state. Note that the extinction effect becomes stronger for smaller m and that the mean-field theory and the individual-based mean-field approximation are accurate in the limit $m \rightarrow \infty$, where the extinction effects can be safely ignored. Within the present modelling approach, the master-equation approach as opposed to the mean-field approaches is better when m is roughly less than ten in practice. The analysis presented in this section suggests that, for large values of τ , infection tends to vanish even if the infection rate is large. Therefore, the epidemic threshold β_c for the clique-based activity-driven networks is expected to be large when τ is large.

3.2 Linear Mapping of the Network State Across a Time Window of Length τ

To calculate the epidemic threshold for the entire SIS model, we first formulate SIS dynamics on a static clique with $m + 1$ nodes using a master equation. Let us denote the state of the clique by $\{x, y, z\}$ ($x, y \in \{S, I\}$, $0 \leq z \leq m - 1$), where x and y are the states of the activated node and another specific node, respectively, and z is the number of infected nodes among the other $m - 1$ nodes. Although a general network with $m + 1$ nodes has 2^{m+1} states, using this notation, we can describe SIS dynamics on a clique by a continuous-time Markov process with $4m$ states [19].

We denote the $4m \times 4m$ transition rate matrix of the Markov process by \mathbf{M} . By definition, the element $M_{\{x', y', z'\}, \{x, y, z\}}$ of \mathbf{M} is equal to the rate of transition from state $\{x, y, z\}$ to state $\{x', y', z'\}$. The diagonal elements of \mathbf{M} are given by

$$M_{\{x, y, z\}, \{x, y, z\}} = - \sum_{\{x', y', z'\} \neq \{x, y, z\}} M_{\{x', y', z'\}, \{x, y, z\}}. \quad (2)$$

The transition rates owing to a recovery event are given by

$$M_{\{S, y, z\}, \{I, y, z\}} = 1, \quad (3)$$

$$M_{\{x, S, z\}, \{x, I, z\}} = 1, \quad (4)$$

$$M_{\{x, y, z-1\}, \{x, y, z\}} = z \quad (z \geq 1), \quad (5)$$

because the recovery rate μ has been set to 1. The transition rates owing to an infection event are given by

$$M_{\{I, S, z\}, \{S, S, z\}} = z\beta, \quad (6)$$

$$M_{\{S, I, z\}, \{S, S, z\}} = z\beta, \quad (7)$$

$$M_{\{I, I, z\}, \{S, I, z\}} = (z + 1)\beta, \quad (8)$$

$$M_{\{I, I, z\}, \{I, S, z\}} = (z + 1)\beta, \quad (9)$$

$$M_{\{S, S, z+1\}, \{S, S, z\}} = z(m - 1 - z)\beta \quad (z \leq m - 2), \quad (10)$$

$$M_{\{I, S, z+1\}, \{I, S, z\}} = (z + 1)(m - 1 - z)\beta \quad (z \leq m - 2), \quad (11)$$

$$M_{\{S, I, z+1\}, \{S, I, z\}} = (z + 1)(m - 1 - z)\beta \quad (z \leq m - 2), \quad (12)$$

$$M_{\{I, I, z+1\}, \{I, I, z\}} = (z + 2)(m - 1 - z)\beta \quad (z \leq m - 2). \quad (13)$$

The remaining elements of \mathbf{M} are equal to 0.

Let $p_{\{x, y, z\}}(t)$ be the probability for a clique to be in state $\{x, y, z\}$ at time t . Because

$$\dot{\mathbf{p}}(t) = \mathbf{M} \mathbf{p}(t), \quad (14)$$

where $\mathbf{p}(t)$ is the $4m$ -dimensional column vector whose elements are $p_{\{x,y,z\}}(t)$, one obtains

$$\mathbf{p}(t) = \exp(\mathbf{M}t)\mathbf{p}(0). \quad (15)$$

Using Eq. (15), we obtain a linear mapping for the state of the entire temporal network, i.e., mapping from the network state before a time window to the network state after the time window, as follows.

Let c_1 be the probability that the activated node in an isolated clique is infected at time $t + \tau$, when the activated node is the only infected node at time t and a new time window of length τ is started exactly at time t . Note that c_1 is the probability with which $x = I$ at time τ when the initial state is $\{I, S, 0\}$. Therefore, using Eq. (15), one obtains

$$c_1(\beta, \tau, m) = \sum_{y,z} [\exp(\mathbf{M}\tau)_{\{I,y,z\},\{I,S,0\}}]. \quad (16)$$

Let c_2 be the probability that the activated node is infected at $t + \tau$ when another single node but no other node is infected at t . One obtains

$$c_2(\beta, \tau, m) = \sum_{y,z} [\exp(\mathbf{M}\tau)_{\{I,y,z\},\{S,I,0\}}]. \quad (17)$$

Let $\rho(a, t)$ be the probability that a node with activity potential a is infected at time t . The fraction of infected nodes in the entire network at time t is given by

$$\langle \rho(t) \rangle \equiv \int da F(a) \rho(a, t). \quad (18)$$

Denoting by ρ_1 the probability that an activated node with activity potential a is infected after the duration τ of the clique, one obtains

$$\rho_1(a, t + \tau) = c_1 \rho(a, t) + c_2 m \langle \rho(t) \rangle, \quad (19)$$

where the first term on the right-hand side of Eq. (19) corresponds to the situation in which the activated node with activity potential a is infected after duration τ , when only that node is infected at time t . The second term corresponds to the situation in which the activated node is infected after duration τ , when only another single node in the clique is infected at time t . In deriving Eq. (19), we assumed that the value of β is selected close to the epidemic threshold such that at most one node is infected in the clique at time t (and hence $\rho(a, t), \langle \rho(t) \rangle \ll 1$).

Let ρ_2 be the probability that a node with activity potential a in a clique triggered by activation of a different node with activity potential a' is infected after time τ . One obtains

$$\rho_2(a, a', t + \tau) = c_1 \rho(a, t) + c_2 \rho(a', t) + c_2(m - 1) \langle \rho(t) \rangle, \quad (20)$$

where the first term on the right-hand side of Eq. (20) corresponds to the situation in which the node with activity potential a is infected after duration τ , when that node is the unique infected node in the clique at time t . The second term corresponds to the situation in which the node with activity potential a is infected after duration τ , when the activated node with activity potential a' is the unique infected node in the clique at time t . The third term corresponds to the situation in which the node with activity potential a is infected after duration τ , when a different node is infected at time t .

Finally, the probability that an isolated node with activity potential a is infected after time τ is given by $e^{-\tau} \rho(a, t)$.

By combining these contributions, one obtains

$$\begin{aligned}\rho(a, t + \tau) &= a\rho_1(a, t + \tau) + \int da' F(a')ma'\rho_2(a, a', t + \tau) \\ &\quad + (1 - a - m\langle a \rangle)e^{-\tau} \rho(a, t) \\ &= [e^{-\tau} + (a + m\langle a \rangle)(c_1 - e^{-\tau})] \rho(a, t) \\ &\quad + [ma + m(m - 1)\langle a \rangle] c_2 \langle \rho(t) \rangle + mc_2 \langle a \rho(a, t) \rangle.\end{aligned}\quad (21)$$

3.3 Epidemic Threshold When All Nodes Have the Same Activity Potential

Consider the special case in which all nodes have the same activity potential a . In this case, Eq. (21) is reduced to the one-dimensional map given by

$$\rho(t + \tau) = T(\beta, \tau, m)\rho(t), \quad (22)$$

where

$$T(\beta, \tau, m) = e^{-\tau} + (m+1)a [c_1(\beta, \tau, m) - e^{-\tau}] + m(m+1)ac_2(\beta, \tau, m) \quad (23)$$

and we have omitted the argument a from $\rho(a, t)$. A positive prevalence $\rho(t)$ (i.e., a positive fraction of infected nodes in the equilibrium state) occurs only if scalar T exceeds 1. Therefore, the epidemic threshold β_c is given by the solution of the following implicit function:

$$f(\beta_c, \tau, m) \equiv T(\beta_c, \tau, m) - 1 = 0. \quad (24)$$

Equation (24) in the limit $\tau \rightarrow 0$ is reduced to

$$\beta_c = \frac{1}{m(m+1)a} = \frac{1}{\bar{k}}, \quad (25)$$

where $\bar{k} = m(m + 1)a$ is the degree of a node averaged over realisations of the network structure generated by clique-based activity-driven networks. When the network blinks infinitesimally fast (i.e., $\tau \rightarrow 0$), the epidemic dynamics are equivalent to those occurring on the time-averaged network [15]. The time-averaged network of the clique-based activity-driven network is the complete graph with edge weight $\bar{k}/(N - 1)$. Therefore Eq. (25) is consistent with the result for the well-mixed population.

For $m = 1$, Eq. (24) for any τ value is reduced to

$$2ae^{\frac{(\beta_c-1)\tau}{2}} \left[\cosh\left(\frac{\kappa_c\tau}{2}\right) + \frac{1+3\beta_c}{\kappa_c} \sinh\left(\frac{-\kappa_c\tau}{2}\right) \right] - e^\tau + 1 - 2a = 0, \quad (26)$$

where $\kappa_c = \sqrt{\beta_c^2 + 6\beta_c + 1}$.

We calculated the epidemic threshold by numerically solving Eq. (24) for $m = 10$ and Eq. (26) for $m = 1$. The epidemic threshold for a range of τ is indicated by the solid lines in Fig. 4a, b. Note that we have kept the mean number of edges in the network the same between $m = 1$ and $m = 10$. Therefore, β_c at $\tau \rightarrow 0$ is the same between the two cases and is given by Eq. (25). The prevalence values obtained by direct numerical simulations of the stochastic SIS model are also shown in the same figures in different colours. The figures suggest that Eqs. (24) and (26) describe results obtained by numerical simulations fairly well.

For $m = 1$, the epidemic threshold increases with τ and diverges at $\tau \approx 0.1$ (Fig. 4a). The network dynamics (i.e., larger values of τ) reduce the prevalence for all values of β . In contrast, for $m = 10$, the epidemic threshold initially decreases, then increases and finally diverges, as τ increases (Fig. 4b). Depending on the level of concurrency (i.e., $m = 1$ versus $m = 10$), the network dynamics impact the epidemic threshold in qualitatively different manners.

The phase diagram for the epidemic threshold when τ and m are varied is shown in Fig. 5a. The colour indicates the β_c values that we calculated by numerically solving Eq. (24). Note that β_c has the same value for all m at $\tau = 0$. Depending on the value of m , network dynamics (i.e., finite τ) increase or decrease the epidemic threshold as τ increases from zero.

Two boundaries partitioning the different phases are given as follows. First, we derive the boundary between the “hindered” and “extinct” phases, which is shown by the solid line in Fig. 5a. In Fig. 5a, the epidemic threshold diverges at $\tau = \tau_*$. In the limit $\beta_c \rightarrow \infty$, infection seeded by a single infected node immediately infects the entire clique, leading to $c_1 \rightarrow 1$ and $c_2 \rightarrow 1$. By substituting $c_1, c_2 \rightarrow 1$ in Eq. (23), we obtain $f(\beta_c \rightarrow \infty, \tau_*, m) = 0$, where

$$\tau_* = \ln \frac{1 - (1 + m)a}{1 - (1 + m)^2 a} \approx \bar{k}. \quad (27)$$

In Eq. (27), we used the approximation $\ln(1 - x) \approx -x$ for $x \ll 1$. For $\tau > \tau_*$ (i.e., “extinct” phase), infection always dies out even if the infection rate is infinite. This is because, in a finite network (i.e., a finite clique in the present case), infection always dies out after a sufficiently long time because of stochasticity (Sect. 3.1).

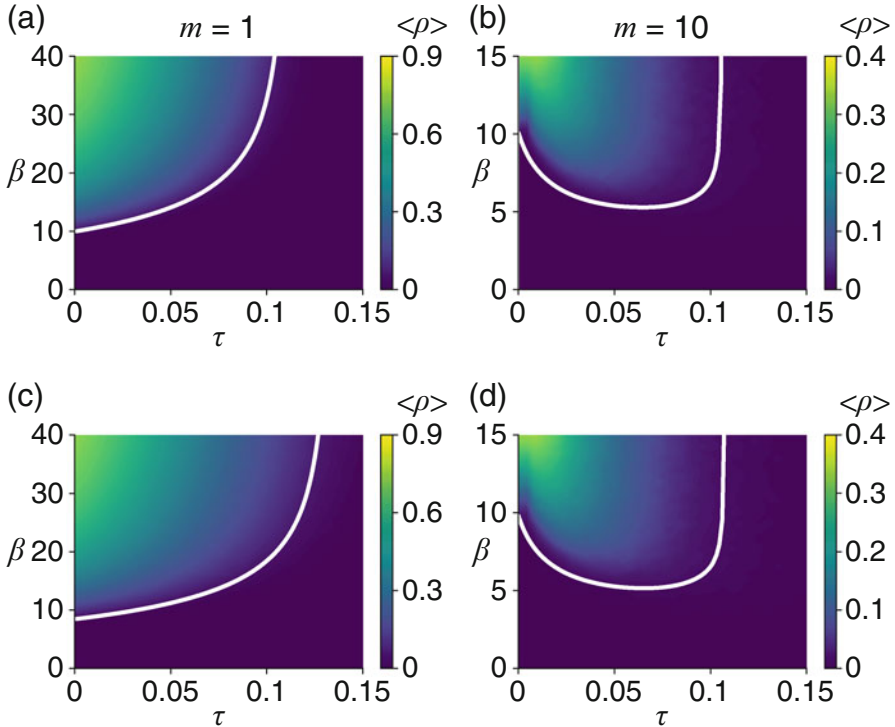


Fig. 4 Epidemic threshold and the numerically simulated prevalence when $m = 1$ ((a) and (c)) and $m = 10$ ((b) and (d)). In (a) and (b), all nodes have the same activity potential value a . In (c) and (d), the activity potential ($\epsilon \leq a_i \leq 0.9, 1 \leq i \leq N$) is assumed to obey a power-law distribution with exponent 3. The solid lines represent the analytical estimate of the epidemic threshold given by Eq. (26) in (a), Eq. (24) in (b) and Eq. (35) in (c) and (d). We set $N = 2000$ and adjust the values of a and ϵ such that the mean degree is the same (i.e., $\langle k \rangle = 0.1$) for the four cases. We simulated the stochastic SIS dynamics using the quasistationary state method [23], as we did in our previous studies [9, 16], and calculated the prevalence as an average over 100 realisations after discarding the first 15,000 time steps ($\Delta t = 0.005$)

Second, there may exist τ_c such that β_c at $\tau < \tau_c$ is smaller than the β_c value at $\tau = 0$. The comparison between the behaviour of β_c at $m = 1$ and $m = 10$ (Figs. 4a, b) leads us to hypothesise that $\tau_c (> 0)$ exists only for $m > m_c$ for a positive value of m_c between 1 and 10. We should obtain

$$\frac{d\beta_c}{d\tau} = 0 \quad (28)$$

at $(\tau, m) = (0, m_c)$. The derivative of Eq. (24) with respect to τ gives

$$\frac{\partial f}{\partial \tau} + \frac{\partial f}{\partial \beta_c} \frac{d\beta_c}{d\tau} = 0. \quad (29)$$

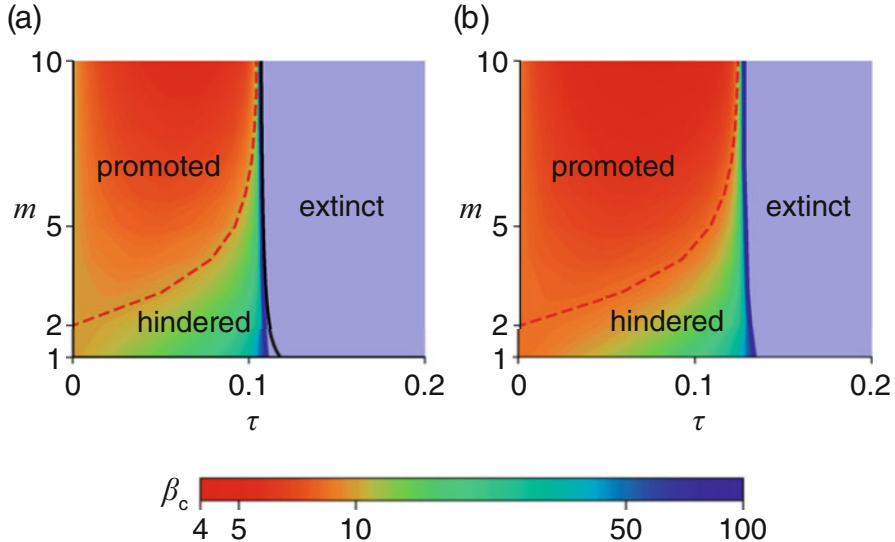


Fig. 5 Epidemic threshold β_c for the clique-based activity-driven network model. In (a), we set the activity potential to a for all nodes. In (b), the activity potential ($\epsilon \leq a_i \leq 0.9$, $1 \leq i \leq N$) obeys a power-law distribution with exponent 3. We set $\langle k \rangle = 0.1$ for $m = 1$ and adjusted the values of a (in (a)) or ϵ (in (b)) such that the value of β_c at $\tau = 0$ is independent of m . In the “extinct” phase, the epidemic threshold β_c is effectively infinity such that infection eventually dies out for any finite β . In the “hindered” phase, β_c is finite and is larger than the value at $\tau = 0$. In the “promoted” phase, β_c is smaller than the value at $\tau = 0$. The solid and dashed lines represent τ_* (Eq. (27)) and τ_c , respectively. The “extinct” regions are determined as the regions in which $\beta_c > 100$

By combining Eqs. (28) and (29), one obtains $\frac{\partial f}{\partial \tau} = 0$, leading to

$$m_c = 2. \quad (30)$$

When $m \leq m_c$, any finite value of τ increases the epidemic threshold and reduces the risk of the prevalence. When $m > m_c$, a small positive τ reduces the epidemic threshold and increases the risk of the prevalence, whereas a larger τ increases the epidemic threshold and reduces the prevalence.

3.4 General Activity Distributions

To obtain the epidemic threshold for general distributions of the activity potential, we use a moment closure method in this section. Note that a generating function approach, which is more complicated than the present moment closure method, yields the epidemic threshold without approximations [9]. By averaging Eq. (21)

over the nodes having various activity potentials distributed according to $F(a)$, we obtain

$$\begin{aligned}\langle \rho(t + \tau) \rangle &= \left[e^{-\tau} + m\langle a \rangle(c_1 - e^{-\tau}) + m^2\langle a \rangle c_2 \right] \langle \rho(t) \rangle \\ &\quad + (c_1 - e^{-\tau} + mc_2)\langle a\rho(a, t) \rangle.\end{aligned}\quad (31)$$

By multiplying Eq. (21) by a and averaging over a , we obtain

$$\begin{aligned}\langle a\rho(a, t + \tau) \rangle &= \left[m\langle a^2 \rangle + m(m-1)\langle a \rangle^2 \right] c_2 \langle \rho(t) \rangle \\ &\quad + \left[e^{-\tau} + m\langle a \rangle(c_1 - e^{-\tau}) + m\langle a \rangle c_2 \right] \langle a\rho(a, t) \rangle \\ &\quad + (c_1 - e^{-\tau})\langle a^2 \rho(a, t) \rangle.\end{aligned}\quad (32)$$

To close the system of equations given by Eqs. (31) and (32), we approximate $\langle a^2 \rho(a, t) \rangle$ by $\langle a \rangle \langle a\rho(a, t) \rangle$. Then, we obtain

$$\begin{pmatrix} \langle \rho(t + \tau) \rangle \\ \langle a\rho(a, t + \tau) \rangle \end{pmatrix} = \mathbf{T} \begin{pmatrix} \langle \rho(t) \rangle \\ \langle a\rho(a, t) \rangle \end{pmatrix}, \quad (33)$$

where

$$\mathbf{T} = \begin{pmatrix} e^{-\tau} + m\langle a \rangle(c_1 - e^{-\tau}) + m^2\langle a \rangle c_2 & c_1 - e^{-\tau} + mc_2 \\ \left[m\langle a^2 \rangle + m(m-1)\langle a \rangle^2 \right] c_2 & e^{-\tau} + (m+1)\langle a \rangle(c_1 - e^{-\tau}) + m\langle a \rangle c_2 \end{pmatrix}. \quad (34)$$

A positive prevalence $\langle \rho(t) \rangle$ is expected if and only if the largest eigenvalue of $\mathbf{T}(\beta_c, \tau, m)$ exceeds 1. This condition results in the implicit equation for the epidemic threshold given by

$$\begin{aligned}f(\beta_c, \tau, m) &\equiv m(m+1)\langle a \rangle^2 q^2 + \left[(m^2 + m + 1) \langle a \rangle^2 - \langle a^2 \rangle \right] qr + \left[\langle a \rangle^2 - \langle a^2 \rangle \right] r^2 \\ &\quad - (2m+1)\langle a \rangle q - (m+1)\langle a \rangle r + 1 = 0,\end{aligned}\quad (35)$$

where

$$q(\beta, \tau, m) = \frac{c_1(\beta, \tau, m) - e^{-\tau}}{1 - e^{-\tau}}, \quad (36)$$

$$r(\beta, \tau, m) = \frac{mc_2(\beta, \tau, m)}{1 - e^{-\tau}}. \quad (37)$$

By solving the Eq. (35), one can obtain the epidemic threshold β_c for any combination of τ and m . If the activity potentials of all nodes are the same such that $\langle a^2 \rangle = \langle a \rangle^2$, Eq. (35) is reduced to Eq. (24).

In Fig. 4c, d, the epidemic threshold given as the numerical solution of Eq. (35) (solid lines) is compared with the prevalence obtained by direct numerical simulations of the stochastic dynamics of the model. Although we employed the moment closure approximation, our theory describes the numerical results fairly well. The dependence of β_c on τ and m is similar to when the activity potential is the same for all nodes (Fig. 4a, b).

The phase diagram of epidemic threshold is shown in Fig. 5b. The figure indicates that the network dynamics (i.e., finite positive τ) always suppress epidemics when $m < 2$, whereas small positive values of τ enhance epidemics when $m > 2$. If τ is large enough, infection always vanishes.

4 Clique-Based Activity-Driven Networks with Attractiveness

In this section, we consider a generalisation of the clique-based activity-driven networks. In social networks, the chance for nodes to be selected by active nodes, i.e., attractiveness, may depend on the nodes. As a variant of the activity-driven network model, we consider the model in which each node is assigned a positive attractiveness b_i ($1 \leq i \leq N$) [24, 25]. When a node is activated, it creates a clique with m nodes randomly selected with probability $b_i/(\langle b \rangle N)$. In general, a node is assigned with activity a_i and attractiveness b_i that are drawn from the joint probability density $H(a, b)$. We focus on the special case in which activity and attractiveness have a deterministic relationship given by $b \sim a^\gamma$, i.e., $H(a, b) = F(a)\delta(b - a^\gamma)$, where $\delta(x)$ is the Dirac delta function [24, 25]. We also assume that a_i is distributed according to the same power law as that used in Fig. 4c, d.

The prevalence obtained by direct numerical simulations is shown in Fig. 6 for two values of m , three values of γ and a range of τ and β . When the activity potential and attractiveness are negatively correlated (Fig. 6a, b), the results are qualitatively the same as the cases without attractiveness (Fig. 6c, d), which are equivalent to the colour maps shown in Fig. 4c, d. In contrast, a positive correlation between the activity potential and attractiveness yields larger prevalence (Fig. 6e, f). In this case, for a wider range of τ , the prevalence is positive for both $m = 1$ and $m = 10$. In addition, for $m = 10$ (Fig. 6f), the prevalence is positive even at relatively small values of β . These results imply that the epidemic threshold is smaller when the activity potential and attractiveness are positively correlated than otherwise. This is consistent with the previous result that positive correlation between the activity potential and attractiveness facilitates epidemics [25].

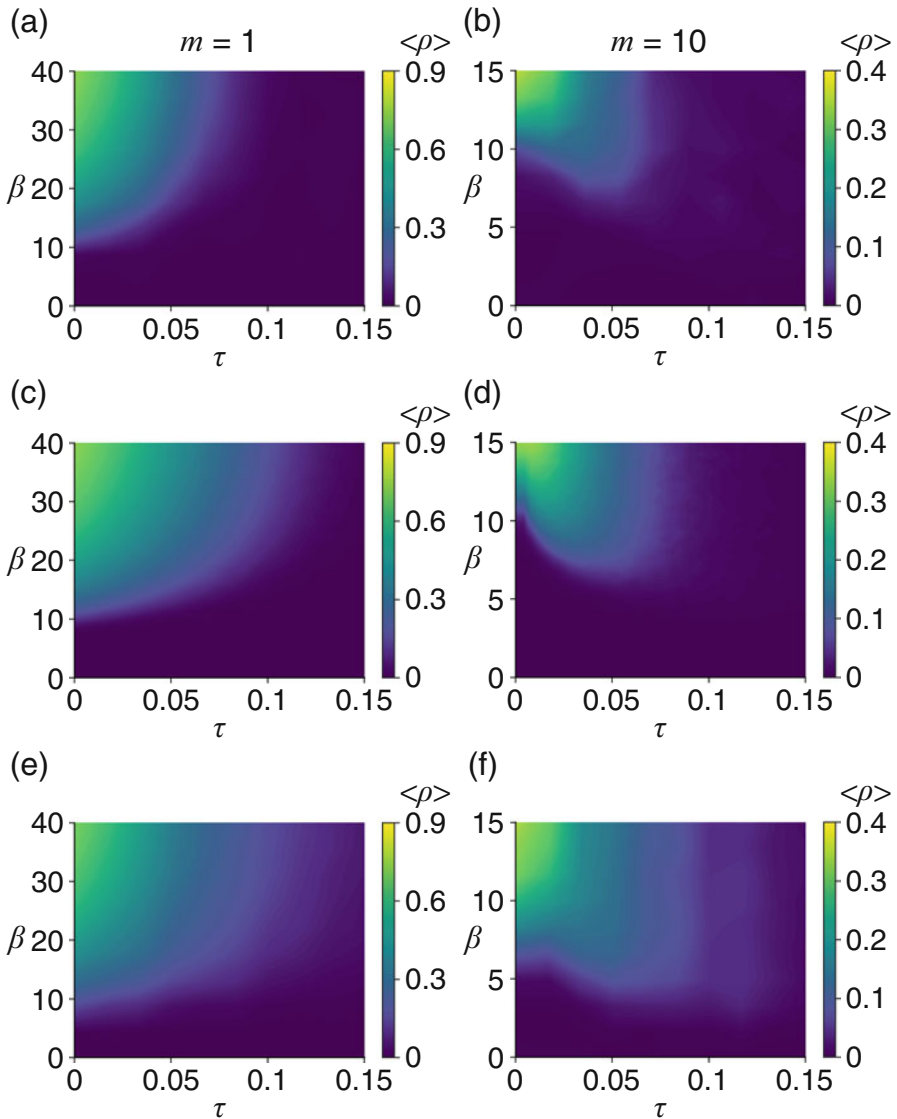


Fig. 6 Numerically simulated prevalence on clique-based activity-driven networks with attractiveness of nodes. (a) $\gamma = -1$, $m = 1$. (b) $\gamma = -1$, $m = 10$. (c) $\gamma = 0$, $m = 1$. (d) $\gamma = 0$, $m = 10$. (e) $\gamma = 1$, $m = 1$. (f) $\gamma = 1$, $m = 10$. The activity potential ($\epsilon \leq a_i \leq 0.9$, $1 \leq i \leq N$) obeys a power-law distribution with exponent 3. The colour indicates the prevalence. We set $N = 2000$ and adjust the value of ϵ such that the mean degree $\langle k \rangle$ is the same in all the cases

5 Conclusions

We introduced a theoretical approach to stochastic SIS dynamics on a switching temporal network model and its extension, which are variants of the activity-driven network model. We found that the epidemic threshold and prevalence, and how they compare with the case of static networks, mainly depend on the level of concurrency and the distribution of attractiveness.

Acknowledgements T.O. acknowledges the support provided through JSPS KAKENHI Grant Number JP19K14618 and JP19H01506. J.G. acknowledges the support provided through Science Foundation Ireland (Grants No. 16/IA/4470 and No. 16/RC/3918). N.M. acknowledges the support provided through JST, CREST, and JST, ERATO, Kawarabayashi Large Graph Project.

References

1. Bansal, S., Read, J., Pourbohloul, B., Meyers, L.A.: *J. Biol. Dyn.* **4**, 478–489 (2010)
2. Masuda, N., Holme, P.: *F1000Prime Rep.* **5**, 6 (2013)
3. Holme, P.: *Eur. Phys. J. B* **88**, 234 (2015)
4. Masuda, N., Holme, P. (eds.): *Temporal Network Epidemiology*. Springer, Singapore (2017)
5. Morris, M., Kretzschmar, M.: *Soc. Networks* **17**, 299–318 (1995)
6. Kretzschmar, M., Morris, M.: *Math. Biosci.* **133**, 165–195 (1996)
7. Morris, M., Kretzschmar, M.: *AIDS* **11**, 641–648 (1997)
8. Perra, N., Gonçalves, B., Pastor-Satorras, R., Vespignani, A.: *Sci. Rep.* **2**, 469 (2012)
9. Onaga, T., Gleeson, J.P., Masuda, N.: *Phys. Rev. Lett.* **119**, 108301 (2017)
10. Tantipathananandh, C., Berger-Wolf, T., Kempe, D.: In: *Proceedings of the Thirteenth ACM SIGKDD International Conference on Knowledge Discovery and Data Mining*, pp. 717–726. ACM, New York (2007)
11. Stehlé, J., Barrat, A., Bianconi, G.: *Phys. Rev. E* **81**, 035101(R) (2010)
12. Zhao, K., Karsai, M., Bianconi, G.: *PLoS One* **6**, e28116 (2011)
13. Liberzon, D.: *Switching in systems and control*. In: *Systems and Control: Foundations and Applications*. Birkhäuser, Boston (2003)
14. Masuda, N., Klemm, K., Eguíluz, V.M.: *Phys. Rev. Lett.* **111**, 188701 (2013)
15. Hasler, M., Belykh, V., Belykh, I.: *SIAM J. Appl. Dyn. Syst.* **12**, 1031–1084 (2013)
16. Speidel, L., Klemm, K., Eguíluz, V.M., Masuda, N.: *New J. Phys.* **18**, 073013 (2016)
17. Pastor-Satorras, R., Castellano, C., Van Mieghem, P., Vespignani, A.: *Rev. Mod. Phys.* **87**, 925–979 (2015)
18. Keeling, M.J., Ross, J.V.: *J. R. Soc. Interface* **5**, 171–181 (2008)
19. Simon, P.L., Taylor, M., Kiss, I.Z.: *J. Math. Biol.* **62**, 479–508 (2011)
20. Hindes, J., Schwartz, I.B.: *Phys. Rev. Lett.* **117**, 028302 (2016)
21. Kiss, I.Z., Miller, J.C., Simon, P.L.: *Mathematics of Epidemics on Networks: From Exact to Approximate Models*. Springer, Cham (2017)
22. Van Mieghem, P., Omic, J., Kooij, R.: *IEEE Trans. Netw.* **17**, 1–14 (2009)
23. De Oliveira, M.M., Dickman, R.: *Phys. Rev. E* **71**, 016129 (2005)
24. Alessandretti, L., Sun, K., Baronchelli, A., Perra, N.: *Phys. Rev. E* **95**, 052318 (2017)
25. Pozzana, I., Sun, K., Perra, N.: *Phys. Rev. E* **96**, 042310 (2017)

Dynamics and Control of Stochastically Switching Networks: Beyond Fast Switching



Russell Jeter, Maurizio Porfiri, and Igor Belykh

1 Introduction

Collective behavior within networks has received a considerable amount of attention in the literature, from animal grouping to robotic motion [71, 77]. One type of collective behavior, synchronization, is particularly important in how prevalent it is in real-world systems [3, 10, 59]. Synchronization is one of the most basic instances of collective behavior, and one of the easiest to diagnose: it occurs when all of the nodes in a network act in unison. Typically, it manifests in ways similar to a school of fish moving as one larger unit to confuse or escape from a predator [15], or a collection of neurons firing together during an epileptic seizure [53].

Significant attention has been devoted to the interplay between node dynamics and network topology which controls the stability of synchronization [6, 46, 54, 57]. Most studies have looked at networks whose connections are static; networks with a dynamically changing network topology, called temporal or evolving networks, are only recently appearing into the scientific literature [1, 5, 7, 17–20, 20–22, 24, 27, 28, 29, 30–32, 38, 47–51, 60, 61, 63, 67, 69, 70, 72–74, 76, 79, 80] (see the recent books [36, 37] for additional references).

R. Jeter

Department of Biomedical Informatics, Emory University, Atlanta, GA, USA
e-mail: rjeter@emory.edu

M. Porfiri

Department of Mechanical and Aerospace Engineering, New York University Tandon School of Engineering, Brooklyn, NY, USA
e-mail: mperfiri@nyu.edu

I. Belykh (✉)

Department of Mathematics and Statistics and Neuroscience Institute, Georgia State University, Atlanta, GA, USA
e-mail: ibelykh@gsu.edu

A particular class of evolving dynamical networks is represented by on-off switching networks, called “blinking” networks [5, 69] where connections switch on and off randomly and the switching time is fast, with respect to the characteristic time of the individual node dynamics. As summarized in a recent review [8], different aspects of synchronization, consensus, and multistability in stochastically blinking networks of continuous-time and discrete-time oscillators have been studied in the fast-switching limit where the dynamics of a stochastically switching network is close to the dynamics of a static network with averaged, time-independent connections. While a mathematically rigorous theory of synchronization in fast-switching blinking networks is available [5, 7, 30–32, 39, 60, 61, 63, 67, 69, 70, 72], the analysis of synchronization in non-fast switching networks of continuous-time oscillators has proven to be challenging and often elusive.

Non-fast switching connections yield a plethora of unexpected dynamical phenomena, including (i) the existence of a significant set of stochastic sequences and optimal frequencies for which the trajectory of a multistable switching oscillator can converge to a “wrong” ghost attractor [7] and (ii) bounded windows of intermediate switching frequencies (“windows of opportunity”) in which synchronization becomes stable in a switching network over bounded intervals of the switching frequency, which may not include the fast switching limit [39]. As a result, networks that do not synchronize in the fast switching limit may synchronize for non-fast switching, and then lose synchronization as the frequency is further reduced. Found numerically in networks of continuous-time Rössler and Duffing oscillators [39] and Rosenzweig-MacArthur food chain models [40], the emergence of windows of opportunity calls for a rigorous explanation of unexpected synchronization from non-fast switching. Blinking networks of discrete-time systems (maps) with non-fast switching offer such a mathematical treatment [26, 41, 42, 62, 66]. More precisely, the switching period in discrete-time networks can be quantified as a number of the individual map’s iterates such that rescaling of time yields a new, multi-iterate map that is more convenient to work with. This enables the formulation of a rigorous mathematical framework for the analysis of the stochastic stability of synchronization as a function of the switching period.

The purpose of this chapter is to give a detailed overview of this rigorous mathematical framework and reveal the central role of non-fast switching which may provide opportunity for stochastic synchronization in a range of switching periods where fast switching fails to synchronize the maps. We start with a historical perspective and a short review of the existing fast-switching theory for networks of continuous-time oscillators and discuss a motivating example of coupled Rössler oscillators with non-fast switching (Sect. 2). Then, we present the stochastic model of coupled maps and introduce the mean square stability of the transverse dynamics. To isolate the delicate mechanisms underpinning stochastic synchronization, we consider two coupled maps with independent identically distributed stochastic switching and study the stability of synchronization as a function of the switching period (Sect. 3). In Sect. 4, we extend our rigorous toolbox to assess the mean-square stability of controlled synchronization in broadcaster-network systems. We examine the feasibility of on-off broadcasting from a single reference node to

induce synchronization in a target network with connections from the reference node that stochastically switch in time with an arbitrary switching period. Internal connections within the target network are static and promote the network's resilience to externally induced synchronization. Through rigorous mathematical analysis, we uncover a complex interplay between the network topology and the switching period of stochastic broadcasting, fostering or hindering synchronization to the reference node. With coupled chaotic tent maps as our test-bed, we prove the emergence of “windows of opportunity” where only non-fast switching periods are favorable for synchronization. The size of these windows of opportunity is shaped by the Laplacian spectrum such that the switching period needs to be manipulated accordingly to induce synchronization. Surprisingly, only the zero and the largest eigenvalues of the Laplacian matrix control these windows of opportunities for tent maps within a wide parameter region.

2 The Blinking Network Model: Continuous-Time Systems

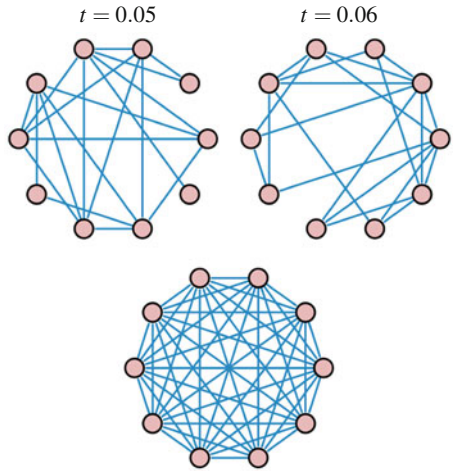
“Blinking” networks were originally introduced for continuous-time oscillators in the context of network synchronization in [5]. A blinking network consists of N oscillators interconnected pairwise via a stochastic communication network:

$$\frac{d\mathbf{x}_i}{dt} = \mathbf{F}_i(\mathbf{x}_i) + \varepsilon \sum_{j=1}^N s_{ij}(t) P(\mathbf{x}_j - \mathbf{x}_i), \quad (1)$$

where $\mathbf{x}_i(t) \in \mathbb{R}^d$ is the state of oscillator i , $\mathbf{F}_i : \mathbb{R}^d \rightarrow \mathbb{R}^d$ describes the oscillators' individual dynamics, $\varepsilon > 0$ is the coupling strength. The $d \times d$ matrix P determines which variables couple the oscillators, $s_{ij}(t)$ are the elements of the time-varying connectivity (Laplacian) matrix $G(t)$. The existence of an edge from vertex i to vertex j is determined randomly and independently of other edges with probability $p \in [0, 1]$. Expressed in words, every switch in the network is operated independently, according to a similar probability law, and each switch opens and closes in different time intervals independently. All possible edges $s_{ij} = s_{ji}$ are allowed to switch on and off so that the communication network $G(t)$ is constant during each time interval $[k\tau, (k+1)\tau)$ and represents an Erdős-Rényi graph of N vertices. Figure 1 gives an example of a “blinking” graph.

The switching network (1) is a relevant model for stochastically changing networks such as information processing cellular neural networks [30] or epidemiological networks [24, 40, 70]. For example, independent and identically distributed (i.i.d.) stochastic switching of packet networks communicating through the Internet comes from the fact that network links have to share the available communication time slots with many other packets belonging to other communication processes and the congestion of the links by the other packets can also occur independently.

Fig. 1 (Top). Two subsequent instances of the switching network. Probability of an edge $p = 0.5$, the switching time step $\tau = 0.01$. (Bottom). The corresponding averaged network where the switching connections of strength ε are replaced with static all-to-all connections of strength pe , representing their mean value



As far as network synchronization is concerned, local computer clocks, that are required to be synchronized throughout the network, are a representative example. Clock synchronization is achieved by sending information about each computer's time as packets through the communication network [5]. The local clocks are typically implemented by an uncompensated quartz oscillator. As a result, the clocks can be unstable/inaccurate and need to receive synchronizing signals, that aim to reduce the timing errors. These signals must be sufficiently frequent to guarantee sufficient precision of synchronization between the clocks. At the same time, the communication network must not be overloaded by the administrative signals. This is a compromise between the precision of synchronization and the traffic load on the network. Remarkably, this blinking network administration can provide precise functioning of a network composing of imprecise elements. It also indicates the importance of optimal switching frequencies that ensure this compromise.

2.1 Historical Perspective: Fast Switching Theory

Over the years, various aspects of synchronization in fast switching networks of continuous-time oscillators have been extensively investigated [5, 39, 61, 63, 67, 69, 70, 72]. In particular, it was rigorously proved in both continuous and discrete-time cases that if the switching frequency is sufficiently high, with respect to the characteristic time of the individual oscillators (fast switching limit), the stochastically blinking network can synchronize even if the network is disconnected at every instant of time.

Beyond synchronization, a rigorous theory for the behavior of stochastic switching networks of continuous-time oscillators in the fast switching limit was developed in [7, 30–32]. In general, it was proved in [31, 32] that for switching dynamical

systems of this type, if the stochastic variables switch sufficiently fast, the behavior of the stochastic system will converge to the behavior of the averaged system in finite time, where the dynamical law is given by the expectation of the stochastic variables. These studies have also helped clarify a number of counterintuitive findings about the relationship between the stochastic network and its time-averaged counterpart. While intuition suggests that the switching network should follow the averaged system in the fast switching limit, this is not always the case, especially when the averaged system is multistable and its attractors are not invariant under the switching system. These attractors act as ghost attractors for the switching system, whereby the trajectory of the switching system can only reach a neighborhood of the ghost attractor, and remains close most of the time with high probability when switching is fast. In a multistable system, the trajectory may escape to another ghost attractor with low probability [32]. This theory uses the Lyapunov function method along with large deviation bounds to derive explicit conditions that connect the probability of converging towards an attractor of a multistable blinking network, the fast switching frequency, and the initial conditions. As the switching frequency decreases, it was shown that there is a range of “resonant” frequencies where the trajectory of a multistable switching oscillator receives enough kicks in the wrong direction to escape from the ghost attractor against all odds [7].

Indeed, there are circumstances for which not converging to the averaged system is favorable, and the present fast-switching theory is not able to make definitive claims about the behavior of the stochastic system. This leads us to explore the effects of non-fast-switching on the dynamics of the switching network.

2.2 *Beyond Fast Switching: A Motivating Example*

We begin with a numerical example of the stochastic Erdős-Rényi network (1) composed of ten x -coupled Rössler oscillators:

$$\begin{cases} \dot{x}_i = -(y_i + z_i) + \varepsilon \sum_{j=1}^{10} s_{ij}(t)(x_j - x_i) \\ \dot{y}_i = x_i + ay_i \\ \dot{z}_i = b + z_i(x_i - c). \end{cases} \quad (2)$$

Hereafter, the intrinsic parameters are chosen and fixed as follows: $a = 0.2$, $b = 0.2$, $c = 7$. The averaged network is an all-to-all network with a fixed coupling strength $p\varepsilon$. Synchronization in a network of x -coupled Rössler systems is known [57] to destabilize after a critical coupling strength ε^* , which depends on the eigenvalues of the connectivity matrix G . We choose the coupling strengths in the stochastic network such that the coupling in the averaged network is defined by one of the three values, marked in Fig. 2. In particular, for $\varepsilon = 1$, synchronization in the averaged network is unstable. As a result, synchronization in the fast-switching network is also unstable. Surprisingly, there is a window of intermediate switching frequencies for which synchronization becomes stable (see Fig. 3). In fact, the

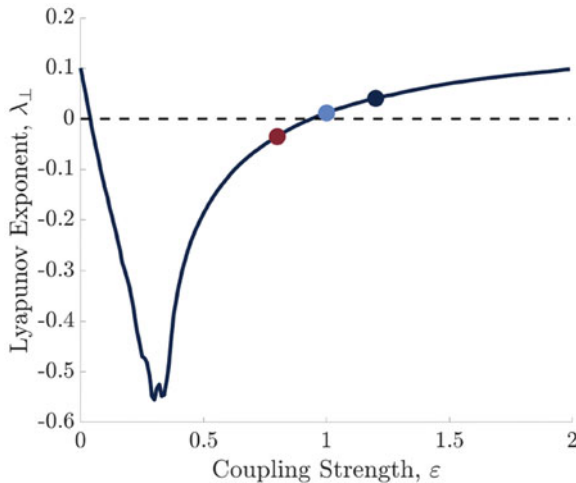


Fig. 2 Transversal stability of synchronization in the averaged ten-node x -coupled Rössler system, expressed via the largest transversal Lyapunov exponent. Synchronization is stable within the interval $\varepsilon^- < \varepsilon < \varepsilon^+$ [not shown]. The values of ε used in Fig. 3 are marked with dot in red, light blue, and navy

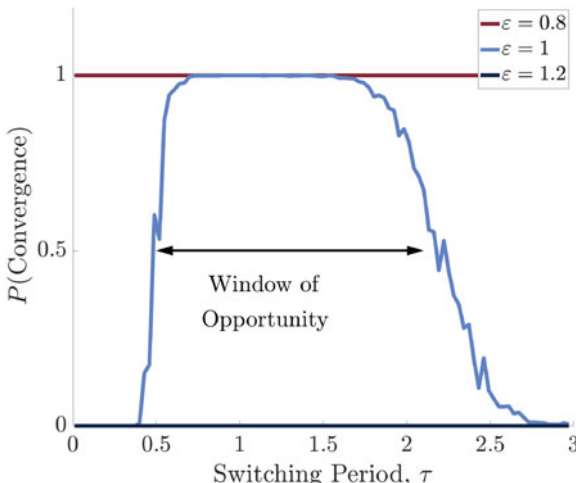


Fig. 3 Probability of synchronization in the ten-node stochastic Rössler network with differing coupling strengths, showing the effects of varying τ . These are coupling strengths for which synchronization in the averaged system is stable (red), weakly unstable (light blue), and strongly unstable (navy), respectively (cf. Fig. 2 for the values marked with appropriately colored dots). The bell-shaped curve corresponds to an optimal range of non-fast switching $0.6 < \tau < 2.2$ (the “window of opportunity”), where synchronization in the stochastic network becomes stable with high probability, whereas synchronization in the corresponding averaged system is unstable ($\varepsilon = 1$). Switching probability $p = 0.5$. Probability calculations are based on 1000 trials

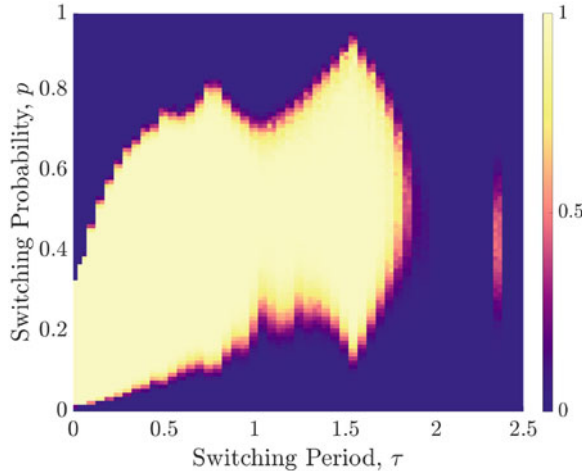


Fig. 4 Probability of synchronization in the two-node Rössler network (2) as a function of the switching probability p and switching period τ . Yellow (lighter) colors correspond to higher probability of convergence (with light yellow at probability 1) and blue (darker) colors correspond to lower probabilities (dark blue at probability 0). The coupling strength of the connection is fixed at $\varepsilon = 7$. As p increases, $p\varepsilon$, the effective coupling in the averaged/fast-switching network progresses through the window of synchrony indicated in Fig. 2. For the two-node network this interval is $p\varepsilon \in [0.08, 2.2]$, yielding the stability range $p \in [0.011, 0.31]$ (the yellow interval on the y -axis) for $\varepsilon = 7$ and small τ . Probability calculations are based on 1000 trials

stochastic network switches between topologies whose large proportion does not support synchronization or is simply disconnected.

To better isolate the above effect and gain insight into what happens when switching between a connected network in which the synchronous solution is unstable, and a completely disconnected network in which the nodes' trajectories behave independently of one another, we consider a two-node Rössler network (2). Figure 4 demonstrates the emergence of synchronization windows for various intermediate values of τ for which the fast-switching network does not support synchronization. In essence, the system is switching between two *unstable* systems, and yet when the switching period τ is in a favorable range within a window of opportunity, the system stabilizes.

Observed numerically in the network of continuous-time oscillators, this phenomenon calls for a more rigorous study to isolate the principal mechanisms underpinning unexpected synchronization from non-fast switching. The following sections aim at establishing such an analytical insight in more analytically tractable networks of discrete-time oscillators.

3 Revealing Windows of Opportunity in Two Stochastically Coupled Maps

We focus on a *discrete-time* setting, where the coupling between the maps is held fixed for a finite number of time steps (switching period) and then it stochastically switches, independent of the time history. In this case, non-fast switching can be studied by re-scaling the time variable and consequently modifying the individual dynamics of the coupled maps. This enables the formulation of a rigorous mathematical framework for the analysis of the stochastic stability of synchronization as a function of the switching period. We restrict our analysis to two coupled maps with the two-fold aim of: (i) providing a clear demonstration for the origin of this phenomenon, which may be hidden by topological factors in large networks and (ii) establishing a toolbox of closed-form results for the emergence of windows of opportunity.

3.1 Network Model

We study the stochastic synchronization of two maps characterized by the state variables $x_i \in \mathbb{R}$, $i \in \{1, 2\}$. We assume that the individual dynamics of each node evolves according to $x_i(k+1) = F(x_i(k))$, where $k \in \mathbb{Z}^+$ is the time step and $F: \mathbb{R} \rightarrow \mathbb{R}$ is a smooth nonlinear scalar function. The maps are linearly coupled through the stochastic gains $\varepsilon_1(k), \varepsilon_2(k) \in \mathbb{R}$, such that

$$\begin{bmatrix} x_1(k+1) \\ x_2(k+1) \end{bmatrix} = \begin{bmatrix} F(x_1(k)) + \varepsilon_1(k)(x_2(k) - x_1(k)) \\ F(x_2(k)) + \varepsilon_2(k)(x_1(k) - x_2(k)) \end{bmatrix}. \quad (3)$$

Each of the sequences of coupling gains, $\varepsilon_1(0), \varepsilon_1(1), \varepsilon_1(2), \dots$ and $\varepsilon_2(0), \varepsilon_2(1), \varepsilon_2(2), \dots$, is assumed to be switching stochastically with the same period $m \in \mathbb{Z}^+ \setminus \{0\}$. Every m time steps, the coupling gains simultaneously switch, such that $\varepsilon_1(mk) = \varepsilon_1(mk+1) = \dots = \varepsilon_1(mk+m-1) = \tilde{\varepsilon}_1(k)$ and $\varepsilon_2(mk) = \varepsilon_2(mk+1) = \dots = \varepsilon_2(mk+m-1) = \tilde{\varepsilon}_2(k)$ for every time step k , where $\tilde{\varepsilon}_1(0), \tilde{\varepsilon}_1(1), \dots$ and $\tilde{\varepsilon}_2(0), \tilde{\varepsilon}_2(1), \dots$ are two sequences of independent and identically distributed random variables.

The evolution of the coupled maps in Eq. (3) is determined by the random variables $\tilde{\varepsilon}_1$ and $\tilde{\varepsilon}_2$, from which the coupling gains are drawn. In general, these random variables may be related to each other and may not share the same distribution. For example, in the case of uni-directional stochastic coupling, one of the random variables is zero; on the other hand, for bi-directional interactions, the two random variables coincide.

The majority of the work on stochastic synchronization of coupled discrete maps is largely limited to the case $m = 1$, for which the coupling gains switch at every time step [60]. In this case, the random variables $\varepsilon_i(0), \varepsilon_i(1), \varepsilon_i(2), \dots$, for $i \in$

$\{1, 2\}$, are mutually independent. For each value of k , $x_1(k+1)$ and $x_2(k+1)$ are functions only of the previous values $x_1(k)$ and $x_2(k)$, and Eq. (3) reduces to a first order Markov chain with explicit dependence on time through the individual dynamics. In the case of $m > 1$, the random variables $\varepsilon_i(0), \varepsilon_i(1), \varepsilon_i(2), \dots$, for $i \in \{1, 2\}$, are no longer independent, which poses further technical challenges for the analysis of the system, while opening the door for rich behavior to emerge from the stochastically driven coupling.

The oscillators synchronize at time step k if their states are identical, that is, $x_1(k) = x_2(k)$. From Eq. (3), once the oscillators are synchronized at some time step, they will stay synchronized for each subsequent time step. The common synchronized trajectory $s(k)$ is a solution of the individual dynamics, whereby $s(k+1) = F(s(k))$. The linear stability of synchronization can be studied through the following variational equation, obtained by linearizing Eq. (3) in the neighborhood of the synchronization manifold:

$$\xi(k+1) = [F'(s(k)) - d(k)]\xi(k), \quad (4)$$

where prime indicates differentiation, $d(k) = \varepsilon_1(k) + \varepsilon_2(k)$ is the net coupling, and $\xi(k) = x_1(k) - x_2(k)$ is the synchronization error at time step k . Equation (4) defines the linear transverse dynamics of the coupled oscillators, measured with respect to the difference between their states $\xi(k)$. This quantity is zero when the two oscillators are synchronized. Equation (4) relies on the assumption that the mapping governing the individual dynamics, F , is differentiable everywhere. This assumption can be relaxed, however, to functions that are differentiable almost everywhere [58].

Only the sum of the two coupling gains $\varepsilon_1(k)$ and $\varepsilon_2(k)$ affects the transverse dynamics, thereby only the statistics of the random variable $d(k)$ modulate the linear stability of the synchronization manifold. To simplify the treatment of the variational problem in Eq. (4), we can rescale the time variable with respect to the switching period as follows:

$$\tilde{\xi}(k+1) = \prod_{i=0}^{m-1} (F'(s(mk+i)) - \tilde{d}(k))\tilde{\xi}(k), \quad (5)$$

where $\tilde{\xi}(k) = \xi(mk)$ and $\tilde{d}(k) = \tilde{\varepsilon}_1(k) + \tilde{\varepsilon}_2(k)$. Equation (5) casts the variational dynamics in the form of a first order time-dependent Markov chain, generated by a linear time-varying stochastic finite difference equation [23, 44].

It is important to emphasize that the synchronization manifold $x_1(k) = x_2(k)$ is an invariant set of the stochastic Eq. (3). Therefore, the dynamics of the synchronization manifold is governed by an attractor of the mapping function $F(s(k))$.

3.2 Mean Square Stability of Synchronization

In determining the stability of the synchronous state, various criteria can be considered, such as almost sure, in probability, and mean square [23, 44, 66]. The concept of mean square stability is particularly attractive, due to its practicality of implementation and its inclusiveness with respect to other criteria. Mean square stability of the synchronous state is ascertained through the analysis of the temporal evolution of the second moment of the error $E[\tilde{\xi}^2]$, where $E[\cdot]$ indicates expectation with respect to the σ -algebra generated by the switching. By taking the square of each side of Eq. (5) and computing the expectation, we obtain

$$E\left[\tilde{\xi}^2(k+1)\right] = E\left[\prod_{i=0}^{m-1} (F'(s(mk+i)) - \tilde{d}(k))^2\right] E\left[\tilde{\xi}^2(k)\right]. \quad (6)$$

This recursion is a linear, time-varying, deterministic finite difference equation whose initial condition is $\tilde{\xi}^2(0)$, which is treated as a given value and not as a random variable. We say that Eq. (5) is mean square asymptotically stable if Eq. (6) is asymptotically stable, that is, if the Lyapunov exponent λ of Eq. (6) is negative. This implies that any small difference between the states of the oscillators will converge to zero in the mean square sense as time increases.

The Lyapunov exponent is a function of the switching period m and can be computed from Eq. (6) as follows [58]:

$$\lambda(m) = \lim_{k \rightarrow \infty} \frac{1}{k} \ln \prod_{j=0}^{k-1} E\left[\prod_{i=0}^{m-1} (F'(s(mj+i)) - \tilde{d}(j))^2\right]. \quad (7)$$

In general, the stability of the synchronization manifold depends on the underlying synchronous solution, whereby $\lambda(m)$ in Eq. (7) explicitly depends on $s(k)$. In what follows, we focus on the case where $s(k)$ is a chaotic trajectory. We comment that our approach is based on the linearized dynamics in Eq. (4), which describes small perturbations from the synchronous state. Thus, our analysis is only applicable to the study of local stability of the synchronization manifold, and initial conditions cannot be arbitrarily selected in the basin of attraction.

3.3 Preliminary Claims

We assume that $\tilde{d}(k)$ takes values on a finite sample space $D = \{d_1, d_2, \dots, d_n\}$ of cardinality n . For $l = 1, \dots, n$, the probability that the net coupling is equal to d_l is chosen to be equal to p_l . For example, in the case of simple on-off connections, the individual coupling gains take values 0 and ε with corresponding probabilities p and $1 - p$. Therefore, the net coupling gain $\tilde{d}(k)$ takes values $d_1 = 0, d_2 = \varepsilon,$

and $d_3 = 2\varepsilon$ with corresponding probabilities $p_1 = p^2$, $p_2 = 2p(1 - p)$ and $p_3 = (1 - p)^2$.

From the individual values of the net coupling and their probabilities, we can evaluate the Lyapunov exponent in Eq. (7) as

$$\lambda(m) = \lim_{k \rightarrow \infty} \frac{1}{k} \sum_{j=0}^{k-1} \ln \left[\sum_{l=1}^n p_l \prod_{i=0}^{m-1} (F'(s(mj + i)) - d_l)^2 \right]. \quad (8)$$

One of the central objectives of this study is to understand the relationship between the synchronizability of the coupled maps when statically coupled through the net coupling gains in D and their stochastic synchronizability when the net coupling randomly switches at a period m . Toward this aim, we adjust Eq. (8) to the case of statically coupled maps with a net coupling d^*

$$\lambda^{\text{st}}(d^*) = \lim_{k \rightarrow \infty} \frac{1}{k} \sum_{j=0}^{k-1} \ln \left[(F'(s(j)) - d^*)^2 \right]. \quad (9)$$

For convenience, we write $\lambda_l^{\text{st}} = \lambda^{\text{st}}(d_l)$ for $l = 1, \dots, n$. Depending on the value of d_l , the statically coupled systems may synchronize or not, that is, the corresponding error dynamics may be asymptotically stable or unstable.

If all of the Lyapunov exponents of the statically coupled systems are finite, then we can establish the following relationship between the Lyapunov exponent of the stochastic error dynamics (8) and $\{\lambda_r^{\text{st}}\}_{r=1}^n$:

$$\lambda(m) = m\lambda_r^{\text{st}} + \lim_{k \rightarrow \infty} \frac{1}{k} \sum_{j=0}^{k-1} \ln \left[\frac{\sum_{l=1}^n p_l \prod_{i=0}^{m-1} (F'(s(mj + i)) - d_l)^2}{\prod_{i=0}^{m-1} (F'(s(mj + i)) - d_r)^2} \right]. \quad (10)$$

Equation (10) is derived from Eq. (8) by: (i) dividing and multiplying the argument of the logarithm by $\prod_{i=0}^{m-1} (F'(s(mj + i)) - d_r)^2$; (ii) using the product rule of logarithms; and (iii) applying Eq. (9) upon rescaling of the time variable by the period m .

By multiplying both sides of Eq. (10) by p_r and summing over r , we obtain the following compact relationship between the Lyapunov exponent of the stochastic dynamics and the individual Lyapunov exponents for statically coupled maps:

$$\lambda(m) = m \sum_{l=1}^n p_l \lambda_l^{\text{st}} + \lim_{k \rightarrow \infty} \frac{1}{k} \sum_{j=0}^{k-1} \ln \frac{\sum_{l=1}^n p_l \zeta_l(j)}{\prod_{l=1}^n \zeta_l^{p_l}(j)}. \quad (11)$$

Here, we have introduced:

$$\xi_l(j) = \prod_{i=0}^{m-1} (F'(s(mj + i)) - d_l)^2, \quad (12)$$

which we assume to be different than zero to ensure that the Lyapunov exponent stays finite.

The first summand on the right-hand side of Eq.(11) is linearly proportional to the switching period m and the “effective” Lyapunov exponent $\bar{\lambda} = \sum_{l=1}^n p_l \lambda_l^{\text{st}}$, which corresponds to the average of the Lyapunov exponents associated with the statically coupled maps, weighted by the probability of the corresponding switching. The second summand is a residual quantity, which is always nonnegative and encapsulates the complex dependence of the transverse dynamics on the switching period beyond the linear dependence associated with the first summand.

3.4 Necessary Condition for Mean Square Synchronization

Proposition 3.1 *The synchronization of the stochastic system (3) is mean square stable only if the effective Lyapunov exponent $\bar{\lambda}$ is negative.*

Proof A lower bound for the Lyapunov exponent $\lambda(m)$ can be obtained by applying the weighted arithmetic-geometric mean inequality [13]

$$\prod_{l=1}^n \xi_l^{p_l} \leq \sum_{l=1}^n p_l \xi_l. \quad (13)$$

From inequality (13), it follows that the argument of the logarithm in Eq.(11) is larger than or equal to 1. As a result, we obtain

$$\lambda(m) \geq m\bar{\lambda}. \quad (14)$$

This inequality establishes that for $\lambda(m)$ to be negative, $\bar{\lambda}$ must also be negative. \square

Remark 1 From the previous claim, we posit if none of the Lyapunov exponents $\{\lambda_r^{\text{st}}\}_{r=1}^n$ are negative, synchronization is not feasible for any selection of m and $\{p_r\}_{r=1}^n$. Thus, stochastic synchronization cannot be achieved without at least one coupling configuration to support synchronization. This is in contrast with observations from continuous-time systems which indicate the possibility of stable synchronization even if none of the coupling configurations support synchronization [39, 40].

Remark 2 The weighted arithmetic and geometric mean, introduced in (13), are equal if and only if $\xi_1 = \xi_2 = \dots = \xi_n$. Thus, inequality (14) reduces to an equality if and only if

$$\prod_{i=0}^{m-1} (F'(s(mj+i)) - d_1)^2 = \prod_{i=0}^{m-1} (F'(s(mj+i)) - d_2)^2 = \quad (15)$$

$$\dots = \prod_{i=0}^{m-1} (F'(s(mj+i)) - d_n)^2 \quad (16)$$

holds for any $j \in \mathbb{Z}^+$. For the case of chaotic dynamics, where $s(k)$ does not evolve periodically in time, this condition cannot be satisfied and Eq. (15) is a strict inequality.

For continuous-time systems [5, 30, 63–65, 67–70], it was shown that under fast switching conditions the synchronizability of stochastically switching system can be assessed from the synchronizability of the averaged system. Here, we re-examine this limit in the case of coupled maps, whereby the averaged system is obtained by replacing the switching gain by its expected values. The synchronizability of the averaged system is ascertained by studying the Lyapunov exponent obtained by replacing d^* with $E[d]$ in Eq. (9), that is,

$$\lambda^{\text{aver}} = \lim_{k \rightarrow \infty} \frac{1}{k} \sum_{j=0}^{k-1} \ln \left[(F'(s(j)) - E[d])^2 \right]. \quad (17)$$

In what follows, we demonstrate through examples that the weighted average Lyapunov exponent $\bar{\lambda}$ can be positive or negative, *independent* of the value of λ^{aver} . Therefore, the averaged system does not offer valuable insight on the stability of the synchronization manifold of the stochastically coupled maps. For the sake of illustration, we consider the case in which the individual dynamics corresponds to the identity, such that

$$\begin{bmatrix} x_1(k+1) \\ x_2(k+1) \end{bmatrix} = \begin{bmatrix} x_1(k) + \varepsilon_1(k)(x_2(k) - x_1(k)) \\ x_2(k) + \varepsilon_2(k)(x_1(k) - x_2(k)) \end{bmatrix}. \quad (18)$$

In this case, the transverse dynamics in (4) takes the simple form

$$\xi(k+1) = [1 - d(k)] \xi(k). \quad (19)$$

Statically coupled identity maps should have a Lyapunov exponent given by (9) with $F'(s(j)) = 1$, that is,

$$\lambda^{\text{st}}(d^*) = \ln \left[(1 - d^*)^2 \right]. \quad (20)$$

Suppose that the net switching gain is a random variable that takes values $d_1 = 1$ and $d_2 = -1$ with equal probabilities 0.5. Then, using Eq. (20) we compute

$$\bar{\lambda} = \frac{1}{2} (\lambda^{\text{st}}(1) + \lambda^{\text{st}}(-1)) = -\infty, \quad (21\text{a})$$

$$\lambda^{\text{aver}} = \lambda^{\text{st}}(0) = 0 > \bar{\lambda}. \quad (21\text{b})$$

Thus, the average coupling does not support synchronization, even though the effective Lyapunov exponent is negative.

Now, we assume $d_1 = 0$ and $d_2 = 2$ with the same probability 0.5, which yields

$$\bar{\lambda} = \frac{1}{2} (\lambda^{\text{st}}(0) + \lambda^{\text{st}}(2)) = 0, \quad (22\text{a})$$

$$\lambda^{\text{aver}} = \lambda^{\text{st}}(1) = -\infty < \bar{\lambda}. \quad (22\text{b})$$

This posits that the stochastically coupled maps cannot synchronize for any selection of the period m , even though the average coupling affords synchronization in a single time step.

If the difference between the possible values of the net coupling gain in D is sufficiently small, the stability of the stochastic system can be related to the stability of the error dynamics of the averaged system. In this case, if for all $l = 1, \dots, n$, we can write $F'(x) - d_l$ as $F'(x) - \Delta d_l + E[d]$, where $|\Delta d_l| \ll |F'(x) - E[d]|$ is the deviation of the stochastic switching with respect to their expected value. Thus, we obtain

$$\begin{aligned} \bar{\lambda} &= \sum_{l=1}^n p_l \lim_{k \rightarrow \infty} \frac{1}{k} \sum_{j=0}^{k-1} \ln \left[(F'(s(j)) - E[d] + \Delta d_l)^2 \right] \approx \\ &\lim_{k \rightarrow \infty} \frac{1}{k} \sum_{j=0}^{k-1} \left(\ln \left[(F'(s(j)) - E[d])^2 \right] \right) + \sum_{l=1}^n \lim_{k \rightarrow \infty} \sum_{j=0}^{k-1} \frac{2p_l \Delta d_l}{F'(s(j)) - E[d]} = \lambda^{\text{aver}}, \end{aligned} \quad (23)$$

where we have expanded the logarithm in series in the neighborhood of $F'(s(j)) - E[d]$ and we have used the fact that $\sum_{l=1}^n p_l \Delta d_l = 0$ by construction.

3.5 Chaotic Dynamics

Direct computation of the Lyapunov exponent as a limit of a time series from Eqs. (8) or (11) may be challenging or even not feasible; for example, if $F'(x)$ is undefined on a finite set of points x . Following the approach of [33], we replace the summation with integration using Birkhoff's ergodic theorem [14].

Toward this aim, we introduce $\rho(x)$ as the probability density function of the map $F(x)$, defined on a set B and continuously differentiable on B except for a finite number of points. The probability density function of each map can be found analytically or numerically [9, 12]. Using Birkhoff's ergodic theorem, Eqs. (8), (9), and (11) can be written as

$$\lambda_l^{\text{st}} = \int_B \ln \left[(F'(t) - d_l)^2 \right] \rho(t) dt, \quad (24a)$$

$$\lambda(m) = \int_B \ln \sum_{l=1}^n p_l Y_l(t, m) \rho(t) dt, \quad (24b)$$

$$\lambda(m) = m \sum_{l=1}^n p_l \lambda_l^{\text{st}} + \int_B \ln \frac{\sum_{l=1}^n p_l Y_l(t, m)}{\prod_{l=1}^n Y_l^{p_l}(t, m)} \rho(t) dt. \quad (24c)$$

Here, we have introduced the function of time and switching period

$$Y_l(t, m) = \prod_{i=0}^{m-1} (F'(F^i(t)) - d_l)^2, \quad (25)$$

where $F^i(t) = [F \circ F \circ \dots \circ F](t)$ is the composite function of order i .

If the analytical expression of the probability density function is known, the Lyapunov exponents can be found explicitly as further detailed in what follows when we study coupled tent maps. Numerical analysis can also benefit from the above formulation, which obviates with computational challenges related to uncertainties in rounding variables in Eqs. (8), (9), and (11) for large values of k . This may be especially evident for large curvatures of the individual map, which could result in sudden changes in the synchronization dynamics.

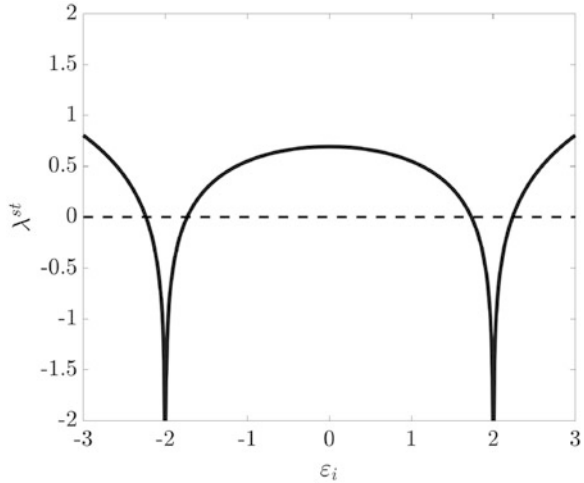
Remark 3 Equation set (24) can be used to explore the synchronizability of an N -periodic trajectory $s(Nk + i) = s_i$, where $i = 0, 1, \dots, N - 1$, $k \in \mathbb{Z}^+$, and $N \in \mathbb{Z}^+/\{0\}$, by using the appropriate probability density function [12] $\rho(s) = \frac{1}{N} \sum_{i=0}^{N-1} \delta(s - s_i)$, where $\delta(\cdot)$ denotes the Dirac delta distribution. Specifically, from (24a) and (24b), we establish

$$\lambda(m) = \frac{1}{N} \sum_{i=0}^{N-1} \ln \sum_{l=1}^n p_l Y_l(s_i, m). \quad (26)$$

3.6 A Representative Example: Coupled Tent Maps

To illustrate our approach, we use the paradigm of two linearly coupled one-dimensional tent maps. Statically coupled tent maps are known to have two

Fig. 5 Transversal Lyapunov exponent, λ^{st} , for stability of synchronization in the static network of tent maps (3), calculated through (28) as a function of coupling ε



symmetric ranges of positive and negative coupling for which synchronization is locally stable [33] (see Fig. 5). In our setting, we let the coupling stochastically switch between values within and outside these stability regions to explore the emergence of windows of opportunity. We will demonstrate that while fast switching, occurring at each time step may not synchronize the maps, there can be a range of lower frequencies that yields stable synchronization. We argue that this is possible for coupled maps where the probability of switching between stable and unstable configurations is uneven, inducing a non-trivial balance between the dynamics of the coupled maps and the switching periods.

The chaotic tent map, described by the equation

$$x(k+1) = F(x(k)) = \begin{cases} ax(k), & x(k) < 1/2 \\ a(1-x(k)), & x(k) \geq 1/2 \end{cases} \quad (27)$$

with parameter $a = 2$ is known to have a constant invariant density function $\rho(t) = 1$ [33].

3.6.1 Statically Coupled Maps

The stability of synchronization in a static network (3) of tent maps (27) is controlled by the sign of the transversal Lyapunov exponent [33]

$$\lambda^{st} = \ln |2 - \varepsilon| + \ln |2 + \varepsilon|. \quad (28)$$

Figure 5 indicates two disjoint regions given by $\varepsilon \in [-\sqrt{5}, -\sqrt{2}]$ and $\varepsilon \in [\sqrt{2}, \sqrt{5}]$ in which $\lambda^{st} < 0$ and synchronization is stable.

3.6.2 Stochastically Coupled Maps

To elucidate synchronizability of stochastically coupled tent maps, we assume that the net coupling gain d takes values d_1 and d_2 with corresponding probabilities p_1 and $p_2 = 1 - p_1$. The numerical computation of the Lyapunov exponent in (8) is performed for different values of d_2 from -4 to 4 with a step of 0.01 and m from 1 to 25 with a step of 1 . The probability p_1 is held fixed to 0.5 and the net coupling gain d_1 to -1.90 .

This wide parameter selection allows for exploring the connection between the stability of synchronization for static coupling and the resulting stochastic synchronization. We consider different cases, where stochastic switching is implemented on coupling gains which could individually support or hamper synchronization for statically coupled maps. Specifically, we contemplate the case in which: none (case I), one (case II), or both (case III) of the coupling gains yield synchronization.

A closed-form expression for the Lyapunov exponent of coupled tent maps can be derived from Eq. (24b) using the probability density function $\rho(t) = 1$, see [26] for a precise derivation,

$$\lambda(m) = \frac{1}{2^m} \sum_{i=0}^m \binom{m}{i} \ln \left(\sum_{l=1}^n p_l (2 - d_l)^{2(m-i)} (2 + d_l)^{2i} \right). \quad (29)$$

We comment that for large m the binomial coefficient grows as $2^m / \sqrt{m}$ according to Stirling's formula, which ensures that the summation is well behaved in the slow switching limit [55].

Figure 6 (top) provides the Lyapunov exponent of two stochastically tent maps, analytically computed from Eq. (29). The effective Lyapunov exponent is directly computed from Eq. (28), which for the select parameters, $p_1 = p_2 = 0.5$ and $d_1 = -1.90$, yield the following intervals for

$$d_2 : \left(-\sqrt{4 + \frac{1}{0.39}}, -\sqrt{4 - \frac{1}{0.39}} \right) \cup \left(\sqrt{4 - \frac{1}{0.39}}, \sqrt{4 + \frac{1}{0.39}} \right).$$

Importantly, analytical results for large periods in Fig. 6 (bottom) confirm that slow switching in case III favors stochastic synchronization. Figure 6 (bottom) also confirms the existence of a thin green zone surrounding the blue bands, where synchronization is stable even though one of the coupling gains does not support synchronization (case II). For example, in the case of fast switching, $m = 1$, these regions are $(-2.33, -2.24)$ and $(-1.73, -1.64)$ from the closed-form expressions in Eqs. (28) and (29).

The analytical solution in Eq. (29) allows for shedding further light on the possibility of synchronizing coupled maps in case II. Specifically, in Fig. 7 we consider switching between coupling gains $d_1 = -1.9999$ and $d_2 = 1.7000$, which are associated with $\lambda_1^{\text{st}} = -7.82$ (strongly stable synchronization) and $\lambda_2^{\text{st}} = 0.10$ (weakly unstable synchronization). We systematically vary the probability of

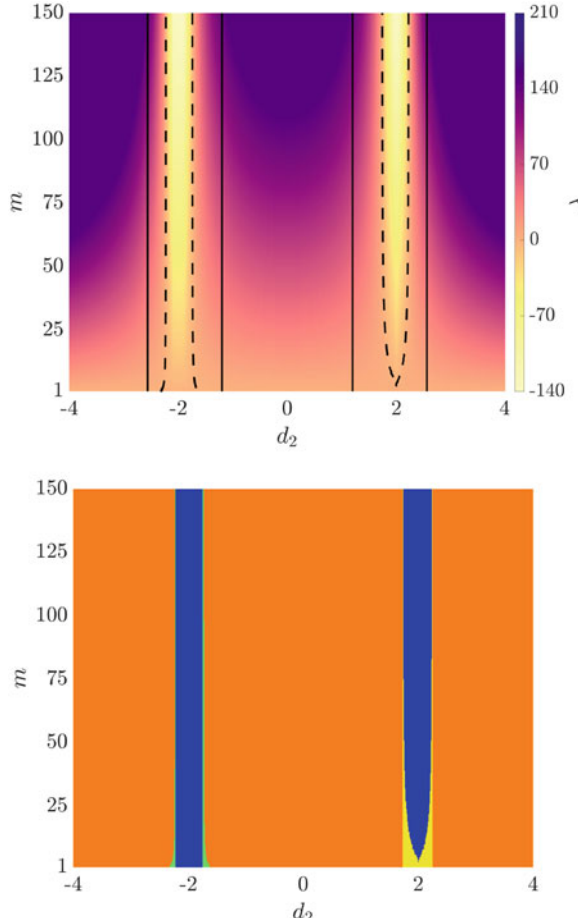
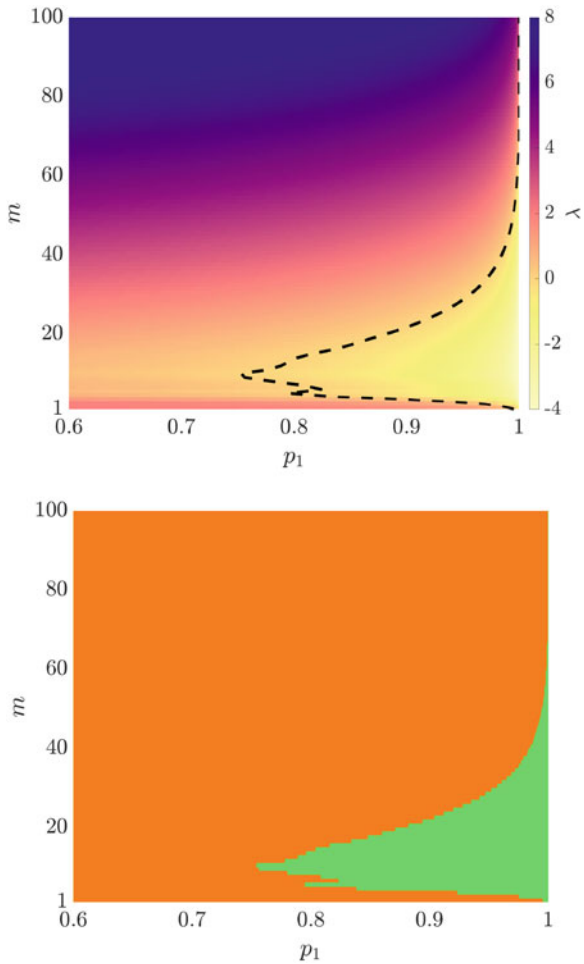


Fig. 6 Analytical demonstration of synchronization through non-fast switching. (Top) Lyapunov exponent of two stochastically tent maps, where the net coupling is switching with equal probability between $d_1 = -1.90$ and d_2 at a period m , analytically computed from Eq. (29). Color illustrates the range of Lyapunov exponents attained for each value of γ . The dashed line identifies the values of d_2 and m for which the Lyapunov exponent is zero; the regions within such contours correspond to negative values of the Lyapunov exponent and thus stochastic synchronization. The solid lines refer to the values of d_2 and m for which the effective Lyapunov exponent is zero. The vertical bands identified by such solid lines correspond to regions where stochastic synchronization is feasible, as predicted by Proposition 3.1. (Bottom) Interplay between synchronization in stochastically and statically coupled tent maps. The partition into cases I, II, and III is based on the sign of the Lyapunov exponent in Eq. (28), corresponding to the net couplings d_1 and d_2 . The regions are colored as follows: orange (case II without stochastic synchronization); yellow (case III without stochastic synchronization); green (case II with stochastic synchronization); and blue (case III with stochastic synchronization)

Fig. 7 Analytical demonstration of emergence of windows of opportunity. (Top) Lyapunov exponent of two stochastically tent maps as a function of the switching probability p_1 and the period m , analytically computed from Eq. (29) with $d_1 = -1.9999$ and $d_2 = 1.7000$. The color bar illustrates the range of Lyapunov exponents attained for each value of γ . The dashed line identify the values of d_2 and m for which the Lyapunov exponent is zero; the regions within such contours correspond to negative values of the Lyapunov exponent and thus stochastic synchronization. (Bottom) Interplay between synchronization in stochastically and statically coupled tent maps. For the select values of the net couplings, $\lambda_1^{\text{st}} = -7.82$ and $\lambda_2^{\text{st}} = 0.10$, which correspond to case II. The regions are colored as follows: orange (case II without stochastic synchronization) and green (case II with stochastic synchronization)



switching p_1 from 0.6 to 1 with a step 0.001, so that when the coupled maps spend most of the time with the coupling gain that would support synchronization. In this case, the effective Lyapunov exponent is always negative, and synchronization may be attained everywhere in the parameter space.

Surprisingly, under fast switching conditions, synchronization is not attained if $p_1 \lesssim 1$ as shown in Fig. 7. Although the maps spend most of the time in a configuration that would strongly support synchronization, the sporadic ($p_2 \approx 0$) occurrence of a coupling gain which would lead to weak instability hampers stochastic synchronization under fast switching. Increasing the switching period, synchronization may be attained for $p_1 > 0.995$ (see the “Pinocchio nose” in Fig. 7 (bottom)). For $0.753 < p_1 < 0.795$, we observe a single window of opportunity, whereby synchronization is achieved in a compact region around $m = 10$. For $0.795 \lesssim p_1 \lesssim 0.824$, a second window of opportunity emerges for smaller values

of m around 5. The two windows ultimately merge for $p_1 \approx 0.83$ in a larger window that grows in size as p_1 approaches 1.

In summary, we have studied the stochastic stability of the transverse dynamics using the notion of mean square stability, establishing a mathematically-tractable form for the Lyapunov exponent of the error dynamics. We have demonstrated the computation of the stochastic Lyapunov exponent from the knowledge of the probability density function. A necessary condition for stochastic synchronization has been established, aggregating the Lyapunov exponents associated with each static coupling configuration into an effective Lyapunov exponent for the stochastic dynamics. For tent maps, we have established a closed-form expression for the stochastic Lyapunov exponent, which helps dissecting the contribution of the coupling gains, switching probabilities, and switching period on stochastic synchronization.

We have demonstrated that non-fast switching may promote synchronization of maps whose coupling alternates between one configuration where synchronization is unstable and another where synchronization is stable (case II). These windows of opportunity for the selection of the switching period may be disconnected and located away from the fast switching limit, where the coupling is allowed to change at each time step.

In contrast to one's expectations, fast switching may not even be successful in synchronizing maps that are coupled by switching between two configurations that would support synchronization (case III). However, a sufficiently slow switching that allows the maps to spend more time in one of the two stable synchronization states will induce stochastic synchronization. The emergence of a lower limit for the switching period to ensure stochastic synchronization is highly non-trivial, while the stabilization of synchronization by slow switching in the dwell time limit should be expected as the maps will spend the time necessary to synchronize in one of the stable configurations, before being re-wired to the other stable configuration.

4 Network Synchronization Through Stochastic Broadcasting

Building on our results from the previous section on the stochastic synchronization of two intermittently coupled maps, in this section, we go further and address an important problem of how non-fast switching can be used to control synchronization in a target network through stochastic broadcasting from a single external node.

This problem of controlling synchronous behavior of a network towards a desired common trajectory [52] arises in many technological and biological systems where agents are required to coordinate their motion to follow a leader and maintain a desired formation [71]. In our setting, each node of the target network, implemented as a discrete-time map, is coupled to the external node with connections that stochastically switch in time with an arbitrary switching period. The network is

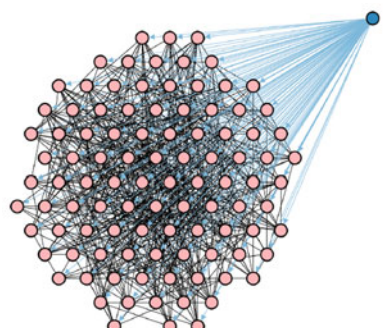
harder to synchronize than its isolated nodes, as its structure contributes to resilience to controlled synchronization probed by the externally broadcasting node.

In the following, we will rigorously study the mean square stability of the synchronous solution in terms of the error dynamics and provide an explicit dependence of the stability of controlled synchronization on the network structure and the properties of the underlying broadcasting signal, defined by the strength of broadcasting connections and their switching period and probability. Via an analytical treatment of the Lyapunov exponents of the error dynamics and the use of tools from ergodic theory, we derive a set of stability conditions that provide an explicit criterion on how the switching period should be manipulated to overcome network resilience to synchronization as a function of the Laplacian spectrum of the network [25].

Through the lens of chaotic tent maps, we discover that the network topology shapes the windows of opportunity of favorable non-fast switching in a highly non-linear fashion. In contrast to mutual synchronization with a network whose stability is determined by the second smallest and largest eigenvalue of the Laplacian matrix via the master stability function, [57] controlled synchronization by the external node is defined by *all its eigenvalues*, including the zero eigenvalue. In the case of chaotic tent maps, the zero and the largest eigenvalue appear to effectively control the size of these windows of opportunity. This leads to the appearance of a persistent window of favorable switching periods where all network topologies sharing the largest eigenvalue become more prone to controlled synchronization.

We study the synchronization of a network of N discrete-time oscillators given by the state variables $y_i \in \mathbb{R}$ for $i = 1, 2, \dots, N$ ¹ that are driven by an external reference node given by $x \in \mathbb{R}$ via a signal that is stochastically broadcasted to all of the nodes in the network. The topology of the network is undirected and unweighted. It is described by the graph $\mathcal{G} = (\mathcal{V}, \mathcal{E})$, where \mathcal{V} is the set of vertices and \mathcal{E} is the set of edges. The broadcaster-network system is depicted in Fig. 8. The evolution of the oscillators in the network and the reference node are given

Fig. 8 The reference node (blue) stochastically broadcasts a signal to each of the nodes in a static network of N oscillators (pink)



¹These results generalize for $y_i \in \mathbb{R}^n$.

by the same mapping function $F : \mathbb{R} \rightarrow \mathbb{R}$, such that $x(k+1) = F(x(k))$. The switching of the broadcasted signal is an independent and identically distributed (i.i.d) stochastic process that re-switches every m time steps. That is, the coupling strength of the reference node $\varepsilon(mk) = \varepsilon(mk+1) = \dots = \varepsilon(m(k+1)-1)$ is drawn randomly from a set of n coupling strengths $\{\varepsilon_1, \dots, \varepsilon_n\}$ with probabilities p_1, \dots, p_n , respectively ($\sum_{l=1}^n p_l = 1$).

The evolution of the discrete-time broadcaster-network system can be written compactly as

$$\begin{aligned} x(k+1) &= F(x(k)), \\ y(k+1) &= \mathbf{F}(y(k)) - \mu L y(k) - \varepsilon(k) I_N (y(k) - x(k) \mathbf{1}_N), \end{aligned} \quad (30)$$

where \mathbf{F} is the natural vector-valued extension of F , μ is the coupling strength within the network, $\mathbf{1}_N$ is the vector of ones of length N , I_N is the $N \times N$ identity matrix, and L is the Laplacian matrix of \mathcal{G} i.e., $L_{ij} = -1$ for $ij \in \mathcal{E}$, $L_{ii} = -\sum_{j=1, j \neq i}^N L_{ij}$, $i = 1, 2, \dots, N$. Without loss of generality, we order and label the Laplacian spectrum of L : $\gamma_1 = 0 \leq \gamma_2 \leq \dots \leq \gamma_N$.

We study the stability of the stochastic synchronization of the network about the reference node's trajectory, or $y_1(k) = y_2(k) = \dots = y_N(k) = x(k)$. Towards this goal, it is beneficial to re-format the problem and study the evolution of the error dynamics $\xi(k) = x(k)\mathbf{1}_N - y(k)$. When all of the nodes $y_i(k)$ have converged to the reference trajectory, $\xi(k) = x(k)\mathbf{1}_N - y(k) = \mathbf{0}_N$. To study the stability of synchronization, we linearize the system about the reference trajectory

$$\dot{\xi}(k+1) = [DF(x(k))I_N - \mu L - \varepsilon(k)I_N] \xi(k), \quad (31)$$

where $DF(x(k))$ is the Jacobian of F evaluated along the reference trajectory $x(k)$. As is typical of linearization, we assume that the perturbations $\xi_i(k)$ in the variational Eq. (31) are small and in directions transversal to the reference trajectory. Convergence to the reference trajectory along these transversal directions ensures the local stability of the synchronous solution. Despite the stochastic and time-dependent nature of the broadcasting signal $\varepsilon(k)$, it only appears on the diagonal elements underlying the evolution of the error vector $\xi(k)$. Because μL is the only matrix in (31) that is not diagonal, we can diagonalize (31) with respect to the eigenspaces of the Laplacian matrix.

We obtain the stochastic master stability equation

$$\zeta(k+1) = [DF(x(k)) - \mu \gamma - \varepsilon(k)] \zeta(k), \quad (32)$$

where $\gamma \in \{\gamma_1, \dots, \gamma_N\}$ and $\zeta \in \mathbb{R}$ is a generic perturbation along the eigendirection of L . Notice that $\gamma_1 = 0$ corresponds to the evolution of the error dynamics in the absence of a network. Lastly, in order to simplify the analysis of the evolution of the variational equations, we re-scale the time variable with respect to the switching period

$$\tilde{\xi}(k+1) = \prod_{i=0}^{m-1} [DF(x(mk+i)) - \mu\gamma - \tilde{\varepsilon}(k)] \tilde{\xi}(k), \quad (33)$$

where $\tilde{\xi}(k) = \xi(mk)$ and $\tilde{\varepsilon}(k) = \varepsilon(mk)$. This scalar equation provides the explicit dependence of the synchronization error on the network topology (via $\mu\gamma$) and the strength of the broadcasted signal (via ε). With this in mind, we continue by discussing the stability of the synchronization to the reference trajectory.

Definition 4.1 The synchronous solution $y_i(k) = x(k)$ for $i = 1, 2, \dots, N$ in the stochastic system (30) is *locally mean square asymptotically stable* if $\lim_{k \rightarrow \infty} E[\tilde{\xi}^2(k)] = 0$ for any $\tilde{\xi}(0)$ and $\gamma \in \{\gamma_1, \dots, \gamma_N\}$ in (33), where $E[\cdot]$ denotes expectation with respect to the σ -algebra generated by the stochastic process underlying the switching.

Mean square stability of the stochastic system in (33), and by extension synchronization in the original system (30), corresponds to studying the second moment of $\tilde{\xi}(k)$. We take the expectation of the square of the error in (33)

$$E[\tilde{\xi}^2(k+1)] = \sum_{l=1}^n p_l \left(\prod_{i=0}^{m-1} [DF(x(mk+i)) - \mu\gamma - \varepsilon_l] \right)^2 E[\tilde{\xi}^2(k)]. \quad (34)$$

Reducing the stochastically switching system (30) to a deterministic system (34) allows for the use of standard tools from stability theory, such as Lyapunov exponents [56]. The Lyapunov exponent for (34) is computed as

$$\lambda = \lim_{k \rightarrow \infty} \frac{1}{k} \ln \left[\frac{E[\tilde{\xi}^2(k)]}{\tilde{\xi}^2(0)} \right] = \lim_{j \rightarrow \infty} \frac{1}{j} \sum_{k=1}^j \ln [E[\tilde{\xi}^2(k+1)]]. \quad (35)$$

There are numerous pitfalls that can undermine the numerical computation of Lyapunov exponent from a time series, such as $E[\tilde{\xi}^2]$ falling below numerical precision in a few time steps and incorrectly predicting stochastic synchronization for trajectories that would eventually diverge. With the proper assumptions, one can use Birkoff's ergodic theorem [56] to avoid these confounds and form the main analytical result of this section.

Proposition 4.1 *The synchronous solution $x(k)$ of the stochastic system (30) is locally mean square asymptotically stable if*

$$\lambda = \int_B \ln \left[\sum_{l=1}^n p_l \left(\prod_{i=0}^{m-1} [DF(t) - \mu\gamma - \varepsilon_l] \right)^2 \right] \rho(t) dt \quad (36)$$

is negative for $\forall \gamma \in \{\gamma_1, \dots, \gamma_N\}$. Here, B is the region for which the invariant density $\rho(t)$ of F is defined.

Proof Assuming F is ergodic with invariant density $\rho(t)$, one can avoid computing the Lyapunov exponent from a time series using Birkoff's ergodic theorem to replace the averaging over time with averaging over the state. This amounts to replacing the summation with integration in (35). Then, by virtue of (35) and the definition of a Lyapunov exponent, stability of the stochastic system reduces to monitoring the sign of this Lyapunov exponent. \square

Remark 4 We reduce studying the stability of synchronization in (30) to monitoring the sign of the Lyapunov exponents in (36), with a different exponent for each eigenvalue γ . If each of these Lyapunov exponents is negative, the dynamics of the network in the original system (30) converges to the dynamics of the reference trajectory. Furthermore, this allows the stability of stochastic synchronization to be studied explicitly in the network and broadcasting parameters $\mu, \{\gamma_1, \dots, \gamma_N\}, \{\varepsilon_1, \dots, \varepsilon_n\}, \{p_1, \dots, p_n\}$, and m .

Remark 5 There are two notable consequences of the Laplacian spectrum on the stability conditions given by the sign of (36): (i) $\mu\gamma = 0$ is always an eigenvalue, such that it is necessary that the nodes in the network pairwise synchronize to the reference node in the absence of a network topology, and (ii) if the network is disconnected, fewer stability conditions need to be satisfied, whereby there will be repeated zero eigenvalues. In light of these consequences, a network is inherently resilient to broadcasting synchronization, in that it necessitates satisfying more stability conditions, and synchronization in the absence of a network is always one of the stability conditions.

4.1 Tent Maps Revisited

To explore some of the theoretical implications of the general stability criterion (36), we consider the broadcaster-network system (30) composed of chaotic tent maps. In this context, the general criterion (36) can be written in a compact form that depends only on the network and broadcasting parameters.

Proposition 4.2 A stochastic system (30) of chaotic tent maps is locally mean square asymptotically stable if

$$\lambda = \frac{1}{2^m} \sum_{i=0}^m \binom{m}{i} \ln \left[\sum_{l=1}^n p_l Y(i, m, \mu\gamma, \varepsilon_l) \right] \quad (37)$$

is less than zero, where $Y(i, m, \mu\gamma, \varepsilon_l)$ is given by $(2 + \mu\gamma + \varepsilon_l)^{2i} (2 - \mu\gamma - \varepsilon_l)^{2(m-i)}$ and $\binom{m}{i} = \frac{m!}{(m-i)!i!}$.

Remark 6 The closed-form analytical expression (37) for the Lyapunov exponents indicates the explicit dependence of the stability of controlled synchronization on the network coupling strength μ , the eigenvalues of the Laplacian matrix for the network, the switching period m , the stochastically switching coupling strengths $\{\varepsilon_1, \dots, \varepsilon_n\}$, and their respective probabilities $\{p_1, \dots, p_n\}$. For controlled synchronization to be mean square stable, the Lyapunov exponent for each eigenvalue in the Laplacian spectrum must be negative.

To illustrate the power of our explicit criterion (37) for controlled synchronization and clearly demonstrate of the emergence of windows of opportunity, we limit our attention to stochastic broadcasting between two coupling strengths ε_1 (with probability p) and ε_2 (with probability $1 - p$).

To choose the coupling strengths ε_1 and ε_2 , we consider two statically coupled tent maps (27)

$$\begin{aligned} x(k+1) &= f(x(k)), \\ y(k+1) &= f(y(k)) + \varepsilon(x(k) - y(k)). \end{aligned} \quad (38)$$

This network (38) describes a pairwise, directed interaction between the dynamics of the broadcasting map $x(k)$ and a single, isolated map $y(k)$ from the network where the switching broadcasting coupling is replaced with a static connection of strength ε . The stability of synchronization in the static network (38) is controlled by the sign of the transversal Lyapunov exponent [33] given in (28). Figure 5 indicates two disjoint regions given by $\varepsilon \in [-\sqrt{5}, -\sqrt{2}]$ and $\varepsilon \in [\sqrt{2}, \sqrt{5}]$ in which $\lambda^{st} < 0$ and synchronization is stable.

4.2 Stochastic Broadcasting: Fast Switching ($m = 1$)

When switching occurs at every time step, the condition described in Proposition 4.2 can be simplified to the following corollary, which we state without additional proof.

Corollary 4.1 *The Lyapunov exponent for the mean square stability of the synchronous solution in the fast-switching system represented by (30) of chaotic tent maps is*

$$\begin{aligned} \lambda &= \ln [(2 - \mu\gamma)^2 + 2(\mu\gamma - 2)\mathbb{E}[\varepsilon(k)] + \mathbb{E}[\varepsilon^2(k)]] \\ &\quad \cdot [(-2 - \mu\gamma)^2 + 2(\mu\gamma + 2)\mathbb{E}[\varepsilon(k)] + \mathbb{E}[\varepsilon^2(k)]], \end{aligned} \quad (39)$$

where $\mathbb{E}[\varepsilon(k)] = p_1\varepsilon_1 + p_2\varepsilon_2$ and $\mathbb{E}[\varepsilon^2(k)] = p_1\varepsilon_1^2 + p_2\varepsilon_2^2$.

4.2.1 Master Stability Function

The Lyapunov exponent (39) demonstrates the explicit dependence of the stability of stochastic synchronization on the node-to-node coupling strength, the eigenvalues of the Laplacian matrix, and the stochastically switching coupling strengths along with their respective probabilities.

Figure 9 illustrates the dependence of λ on ε_1 and $\mu\gamma$. The dashed curve in Fig. 9 indicates the boundary between positive and negative Lyapunov exponents, identifying the onset of mean square stability of the error dynamics. In order for the network to synchronize to the reference node, the point $(\varepsilon_1, \mu\gamma)$ must fall within the dashed curve for *every* eigenvalue in the spectrum of the Laplacian matrix. In agreement with our predictions, we find that as $\mu\gamma$ increases the range of values of ε_1 which affords stable synchronization becomes smaller and smaller. This suggests that the resilience of the network to synchronize improves with $\mu\gamma$.

Remark 7 While the nonlinear dependence of the stability boundary on ε_1 and $\mu\gamma$ is modulated by the nonlinearity in the individual dynamics, it should not be deemed as a prerogative of nonlinear systems. As shown in Remark 4, the stochastic stability of synchronization in the simplest case of a linear system is also nonlinearly related to the spectrum of the Laplacian matrix and to the expectation and variance of the broadcasting signal—even for classical consensus with $\alpha = 1$ [16].

Remark 8 In this example of a chaotic tent map, the stability boundary is a single curve, defining a connected stability region. To ensure stable synchronization of

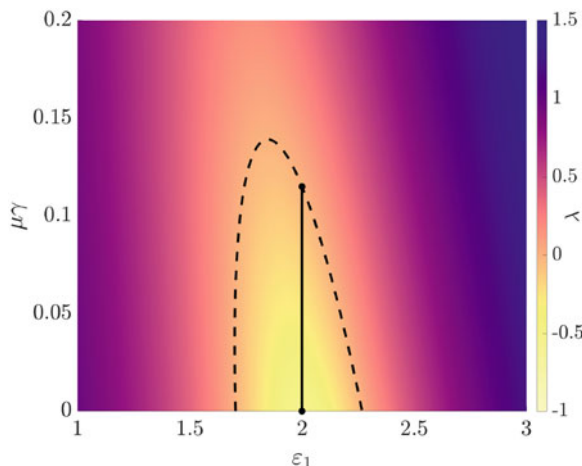


Fig. 9 Master stability function for stochastic synchronization of chaotic tent maps, for $\varepsilon_2 = 2.2$, $m = 1$, and $p_1 = p_2 = 0.5$. For synchronization to be stable, each eigenvalue of the Laplacian matrix must correspond to a negative Lyapunov exponent (indicated by the yellow color, isolated by the black dashed curve). For example, the black vertical line shows the range of admissible values of $\mu\gamma$ that would guarantee stability at $\varepsilon_1 = 2$

a generic network, it is thus sufficient to monitor the largest eigenvalue of the Laplacian matrix, γ_N , such that $(\varepsilon_1, \mu\gamma)$ will fall within the stability region. This is in contrast with the master stability function for uncontrolled, spontaneous synchronization [57], which would typically require the consideration of the second smallest eigenvalue, often referred to as the algebraic connectivity [25]. However, similar to master stability functions for uncontrolled, spontaneous synchronization [75], we would expect that for different maps, one may find several disjoint regions in the $(\varepsilon_1, \mu\gamma)$ -plane where stable stochastic synchronization can be attained.

4.2.2 Role of Network Topology

The master stability function in Fig. 9 shows that both μ and γ contribute to the resilience of the network to synchronization induced by stochastic broadcasting. For a given value of the node-to-node coupling strength μ , different networks will exhibit different resistances based on their topology. Based on the lower bound by Grone and Merris [29] and the upper bound by Anderson and Morley [2], for a graph with at least one edge, we can write $\max\{d_i, i = 1, \dots, N\} + 1 \leq \gamma_N \leq \max\{d_i + d_j, ij \in \mathcal{E}\}$, where d_i is the degree of node $i = 1, \dots, N$. While these bounds are not tight, they suggest that the degree distribution has a key role on γ_N . For a given number of edges, one may expect that networks with highly heterogeneous degree distribution, such as scale-free networks [11], could lead to stronger resilience to broadcasting as compared to regular or random networks, with more homogenous degree distributions [11].

In Fig. 10, we illustrate this proposition by numerically computing the largest eigenvalue of the graph Laplacian for three different network types:

- (i) A $2K$ -regular network, in which each node is connected to $2K$ nearest neighbors, such that the degree is equal to $2K$. As K increases, the network approaches a complete graph.
- (ii) A scale-free network [4] which is grown from a small network of q nodes. At each iteration of the graph generation algorithm, a node is added with q edges to nodes already in the network. The probability that an edge will be connected to a specific node is given by the ratio of its degree to the total number of edges in the network. Nodes are added until there are N nodes in the network. When q is small, there are a few hub nodes that have a large degree and many secondary nodes with small degree, whereas when q is large, the scale-free network is highly connected and similar to a complete graph.
- (iii) A random Erdős-Rényi network which takes as input the probability, p , of an edge between any two nodes. When p is small, the network is almost surely disconnected, and when p approaches 1, it is a complete graph.

We fix N to 100 and vary K , q , and p in (i), (ii), and (iii), respectively, to explore the role of the number of edges.

As expected from the bounds in [2, 29], for a given number of edges, the scale-free network tends to exhibit larger values of γ_N . This is particularly noticeable

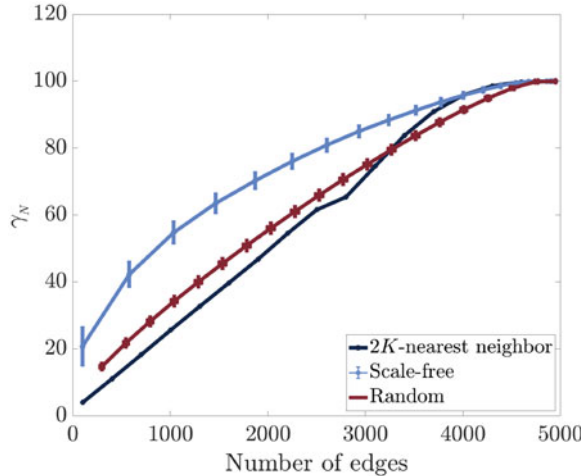


Fig. 10 Largest eigenvalue γ_N of the Laplacian matrix as a function of the number of edges for three different types of networks of 100 nodes: a $2K$ -regular network (navy curve), scale-free (light blue curve), and random Erdős-Rényi (red curve) networks. Scale-free and random networks are run 10,000 times to compute means and standard deviations, reported herein—note that error bars are only vertical for scale-free networks since the number of edges is fully determined by q , while for random networks also horizontal error bars can be seen due to the process of network assembly

for networks of intermediate size, whereby growing the number of edges will cause the three network types to collapse on a complete graph of N nodes. As the largest eigenvalue of the Laplacian matrix fully controls the resilience of the network to broadcasting-induced synchronization (in the case of linear and chaotic tent maps), we may argue that, given a fixed number of edges, the network can be configured such that it is either more conducive (regular graph) or resistant (scale-free graph) to synchronization. The increased resilience of scale-free networks should be attributed to the process of broadcasting-induced synchronization, which globally acts on all nodes simultaneously, without targeting critical nodes (low or high degree) like in pinning control [16, 78].

4.3 Stochastic Broadcasting: Beyond Fast Switching ($m > 1$)

Returning to the stochastically switching broadcaster-network system, but without the limitation of $m = 1$, we use the master stability function of Fig. 5 to choose $\varepsilon_1 = -1.999$ from a stability region and $\varepsilon_2 = -1.7$ from an instability region such that the connection from the broadcasting node to the network switches between the two values where one value supports controlled synchronization whereas the other destabilizes it. In this way, the broadcaster sends two conflicting messages to the network to follow and not to follow its trajectory.

We pay particular attention to the case where the switching probability of the stabilizing coupling, ε_1 is higher ($p > 0.5$.) One's intuition would suggest that fast-switching between the stable and unstable states of controlled synchronization with probability ($p > 0.5$), that makes the system spend more time in the stable state, would favor the stability of synchronization. However, the master stability function of Fig. 11 calculated through the analytical expression for the Lyapunov exponent (37) shows that this is not the case. Our results reveal the presence of a stability zone (black area) which, in terms of the switching periods m , yields a window of opportunity when non-fast switching favors controlled synchronization, whereas fast or slow switching does not. The fact that slower switching at $m > 25$ at the switching probability $p = 0.9$ (see the transition from point A to B) desynchronizes the system is somewhat unexpected, as the system is likely to stay most of the time in the stable state, defined by ε_1 .

The exact cause of this effect remains to be studied; however, we hypothesize that this instability originates from a large disparity between the time scale of weak convergence in the vicinity of the synchronization state during the (long) time lapse when the stabilizing coupling ε_1 is on and the time scale of strong divergence from the synchronization solution far away from it when the destabilizing coupling ε_2 finally switches on. As a result, this unbalance between the convergence and divergence makes synchronization unstable.

The window of opportunity displayed in Fig. 11 appears as a result of intersections between the boundaries (dashed curves) of the stability zones where each boundary is calculated from the criterion (37) when the Lyapunov exponent is zero for each eigenvalue of the Laplacian matrix. The red curve for $\gamma_1 = 0$ shows the stability region in the absence of a network, and is therefore a necessary condition for controlled synchronization in the presence of the network. In the general case of N distinct eigenvalues, there will be N curves. Each curve adds a constraint and, therefore, one would expect each eigenvalue $\gamma_1, \dots, \gamma_N$ to play a role in reducing the size of the stability zone and shaping the window of opportunity as a function of network topology.

In contrast to these expectations, Fig. 11 provides a convincing argument that the stability zone is essentially defined by two curves, corresponding to the zero eigenvalue, γ_1 (red dashed curve) and the largest eigenvalue, γ_N (black dashed curve). All the other curves offer a very minor contribution to shaping the stability region. As a consequence, windows of opportunity should be relatively robust to topological changes, preserving the maximum largest eigenvalue of the Laplacian spectrum. For example, the set of four distinct eigenvalues (0, 1, 3, 10) in Fig. 11 corresponds to a star network of 10 nodes with an additional edge connecting two outer nodes. In this case, the removal of the additional link reduces the spectrum to three distinct eigenvalues (0, 1, 10) and eliminates the curve for $\gamma = 3$ which, however, does not essentially change the stability region. This observation suggests that the addition of an edge to a controlled network, which would be expected to help a network better shield from the external influence of the broadcasting node, might not necessarily improve network resilience to synchronization.

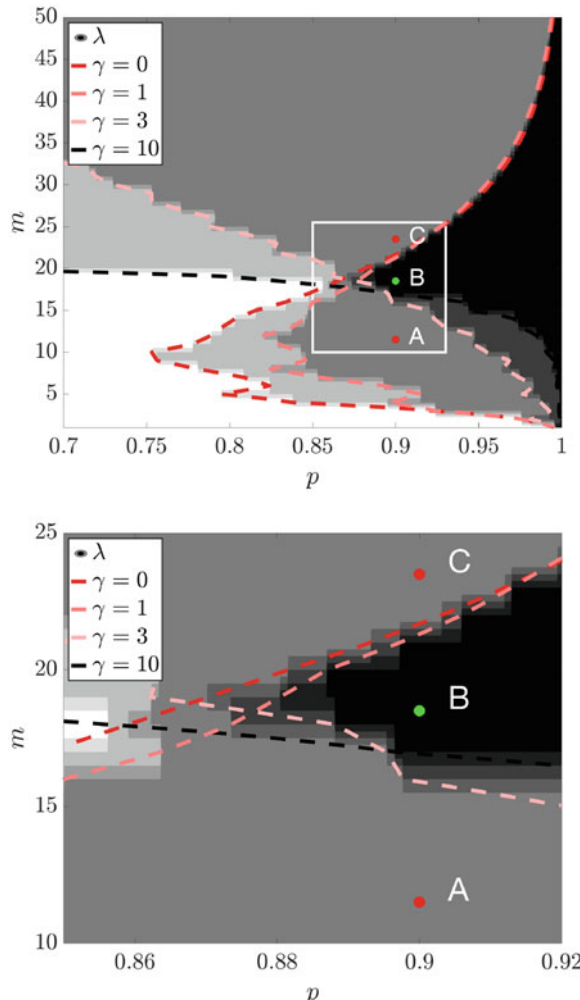


Fig. 11 Analytical calculation of the master stability function (37) for controlled synchronization of tent maps as a function of the switching probability p and switching period m for $\varepsilon_1 = -1.9999$, $\varepsilon_2 = 1.7$, and $\mu = 0.01$. (Top). The black region indicates the stability of controlled synchronization, and the dashed lines represent the boundaries for the stability region for various eigenvalues γ of a network's Laplacian matrix. Notice that the size of the stability region is primarily controlled by only two curves, corresponding to $\gamma = 0$ (red dashed) and $\gamma = 10$ (black dashed) such that the addition of curves for eigenvalues $\gamma \in (0, 10)$ only affects the small cusp part of the stability region (see the zoomed-in area). (Bottom). Zoom-in of the region marked by the white rectangle in (top). Points A, B, and C indicate pairs (p, m) for which synchronization is unstable, stable, and unstable, respectively for different values of the switching period m . Note the window of favorable frequencies m which includes point B in the vertical direction from A to C. Remarkably, the size of the stability region remains persistent to changes of the intra-network coupling μ (not shown), suggesting the existence of soft, lower and upper thresholds for favorable switching frequencies between $m = 20$ and 30

Similarly, the removal of an edge from an all-to-all network with two distinct eigenvalues $(0, N)$ changes the spectrum to $(0, N - 1, N)$, which according to Fig. 11 does not significantly alter the stability region either. For general topologies, one may look at the degree distribution to gather insight on the largest eigenvalue [2, 29], thereby drawing conclusions on the switching periods that guarantee the success of the broadcaster to synchronize the network. Put simply, “you can run but you cannot hide:” the broadcaster will identify suitable switching rates to overcome the resilience of the network.

5 Conclusions

While the study of stochastically switching networks has gained significant momentum, most analytical results have been obtained under the assumption that the characteristic time scales of the intrinsic oscillators and evolving connections are drastically different, enabling the use of averaging and perturbation methods. In regard to on-off stochastically switching systems, these assumptions typically yield two extremes, fast or slow (dwell-time [35]) switching, for which rigorous theory has been developed [5, 7, 31, 32, 63, 67, 69, 70]. However, our understanding of dynamical networks with non-fast switching connections is elusive, and the problem of an analytical treatment of the dynamics and synchronization in non-fast switching network remains practically untouched.

In this chapter, we sought to close this gap by presenting an analytical approach to characterize the stability of synchronization in stochastically switching networks of discrete-time oscillators as a function of network topology and switching period. We first focused on the simplest stochastic network composed of two maps and studied the stability of synchronization by analyzing the linear stability of an augmented system, associated with the linear mean square transverse dynamics. We performed a detailed analysis of the Lyapunov exponent of the transverse dynamics, based on the knowledge of the probability density function for the synchronized trajectory. We established a necessary condition for stochastic synchronization in terms of the synchronizability of the coupled maps with a static coupling. The necessary condition can be used to demonstrate that switching between configurations which do not individually support synchronization will not stabilize stochastic synchronization for any switching frequencies. This is in contrast with networks of continuous-time oscillators where windows of opportunity for stable synchronization may appear as a result of switching between *unstable states* [39, 40]. Through closed-form and numerical findings, we have demonstrated the emergence of windows of opportunity and elucidated their nontrivial relationship with the stability of synchronization under static coupling.

While the details of the mechanisms for the appearance of windows of opportunity in stochastically switching networks are yet to be clarified, it is tenable to hypothesize that this effect is related to the dynamic stabilization of an unstable state. From a mechanics perspective, this can be loosely explained by an analogy

to the dynamics of Kapitza's pendulum. Kapitza's pendulum is a rigid pendulum in which the pivot point vibrates in a vertical direction, up and down [43]. Stochastic vibrations of the suspension are known to stabilize Kapitza's pendulum in an upright vertical position, which corresponds to an otherwise unstable equilibrium in the absence of suspension vibrations. By this analogy, stochastic switching between stable and unstable configurations can be proposed to perform a similar stabilizing role.

Extending our analysis of synchronization of two maps, we then established a rigorous toolbox for assessing the mean-square stability of controlled synchronization in a static network of coupled maps induced by stochastic broadcasting from a single, external node. We studied the conditions under which a reference broadcasting node can synchronize a target network by stochastically transmitting sporadic, possibly conflicting signals. We demonstrated that manipulating the rate at which the connections between the broadcasting node and the network stochastically switch can overcome network resilience to synchronization. Through a rigorous mathematical treatment, we discovered a nontrivial interplay between the network properties that control this resilience and the switching rate of stochastic broadcasting that should be adapted to induce synchronization. Unexpectedly, non-fast switching rates controlling the so-called windows of opportunity guarantee stable synchrony, whereas fast or slow switching leads to desynchronization, even though the networked system spends more time in a state favorable to synchronization.

In contrast to classical master stability functions for uncontrolled synchronization, where both the algebraic connectivity and the largest eigenvalue of the Laplacian matrix determine the onset of synchronization, we report that the algebraic connectivity has no role on broadcasting-induced synchronization of chaotic tent maps. Specifically, the resilience of the network to broadcasting synchronization increases with the value of the largest eigenvalue of the Laplacian matrix. Heterogenous topologies with hubs of large degree should be preferred over homogenous topologies, when designing networks that should be resilient to influence from a broadcasting oscillator. On the contrary, homogenous topologies, such as regular or random topologies, should be preferred when seeking networks that could be easily tamed through an external broadcasting oscillator. Interestingly, these predictions would be hampered by a simplified analysis based on averaging, which could lead to false claims regarding the stability of synchronous solutions.

Our approach is directly applicable to high-dimensional maps whose invariant density measure can calculated explicitly. These systems include two-dimensional diffeomorphisms on tori such as Anosov maps [34], for which the invariant density measure can be calculated analytically, and volume-preserving two-dimensional standard maps whose invariant density function can be assessed through computer-assisted calculations [45]. Although our work provides an unprecedented understanding of network synchronization beyond the fast switching limit, we have hardly scratched the surface of temporal dynamical networks theory. This work immediately raises the following questions: (i). What if the i.i.d process underlying the switching was relaxed to be a more general Markov process? (ii). What if the

underlying topology of the broadcasting was more complex? Both of these questions are of interest, but provide their own technical challenges and require further study. We anticipate that combining our recent work on synchronization of two maps under Markovian switching with memory [62] with the approach presented in this chapter should make progress toward unraveling a complex interplay between switching memory and network topology for controlled synchronization.

Acknowledgements This work was supported by the U.S. Army Research Office under Grant No. W911NF-15-1-0267 (to I.B., R.J., and M.P.), the National Science Foundation (USA) under Grants DMS-1009744, DMS-1616345 (to I.B and R.J.), and DMS-1909924 (to I.B.), and CMMI 1561134, CMMI 1505832, and CMMI 1433670 (to M.P.).

References

1. Abaid, N., Porfiri, M.: Consensus over numerosity-constrained random networks. *IEEE Trans. Autom. Control* **56**(3), 649–654 (2011)
2. Anderson Jr, W.N., Morley, T.D.: Eigenvalues of the laplacian of a graph. *Linear and Multilinear Algebra* **18**(2), 141–145 (1985)
3. Arenas, A., Díaz-Guilera, A., Kurths, J., Moreno, Y., Zhou, C.: Synchronization in complex networks. *Phys. Rep.* **469**(3), 93–153 (2008)
4. Barabási, A.L., Albert, R.: Emergence of scaling in random networks. *Science* **286**(5439), 509–512 (1999)
5. Belykh, I.V., Belykh, V.N., Hasler, M.: Blinking model and synchronization in small-world networks with a time-varying coupling. *Physica D: Nonlinear Phenom.* **195**(1), 188–206 (2004)
6. Belykh, V.N., Belykh, I.V., Hasler, M.: Connection graph stability method for synchronized coupled chaotic systems. *Physica D: Nonlinear Phenom.* **195**(1), 159–187 (2004)
7. Belykh, I., Belykh, V., Jeter, R., Hasler, M.: Multistable randomly switching oscillators: the odds of meeting a ghost. *Eur. Phys. J. Spec. Top.* **222**(10), 2497–2507 (2013)
8. Belykh, I., Di Bernardo, M., Kurths, J., Porfiri, M.: Evolving dynamical networks. *Physica D: Nonlinear Phenome.* **267**(1), 1–6 (2014)
9. Billings, L., Boltt, E.: Probability density functions of some skew tent maps. *Chaos, Solitons Fractals* **12**(2), 365–376 (2001)
10. Boccaletti, S., Kurths, J., Osipov, G., Valladares, D., Zhou, C.: The synchronization of chaotic systems. *Phys. Rep.* **366**(1), 1–101 (2002)
11. Boccaletti, S., Latora, V., Moreno, Y., Chavez, M., Hwang, D.U.: Complex networks: Structure and dynamics. *Phys. Rep.* **424**(4), 175–308 (2006)
12. Boltt, E.M., Santitissadeekorn, N.: Applied and Computational Measurable Dynamics. SIAM (2013)
13. Bullen, P.S., Mitrinovic, D.S., Vasic, M.: Means and Their Inequalities, vol. 31. Springer Science & Business Media, Berlin (2013)
14. Bunimovich, L., Dani, S., Dobrushin, R., Jakobson, M., Kornfeld, I., Maslova, N., Pesin, Y.B., Smillie, J., Sukhov, Y.M., Vershik, A.: Dynamical Systems, Ergodic Theory and Applications, vol. 100. Springer Science & Business Media, Berlin (2000)
15. Camazine, S., Deneubourg, J.L., Franks, N.R., Sneyd, J., Bonabeau, E., Theraulaz, G.: Self-Organization in Biological Systems, vol. 7. Princeton University Press, Princeton (2003)
16. Cao, Y., Yu, W., Ren, W., Chen, G.: An overview of recent progress in the study of distributed multi-agent coordination. *IEEE Trans. Ind. Inf.* **9**(1), 427–438 (2013)
17. Chen, M., Shang, Y., Zhou, C., Wu, Y., Kurths, J.: Enhanced synchronizability in scale-free networks. *Chaos: Interdiscip. J. Nonlinear Sci.* **19**(1), 013105 (2009)

18. De Lellis, P., di Bernardo, M., Garofalo, F.: Synchronization of complex networks through local adaptive coupling. *Chaos: Interdiscip. J. Nonlinear Sci.* **18**(3), 037110 (2008)
19. DeLellis, P., Di Bernardo, M., Garofalo, F.: Adaptive pinning control of networks of circuits and systems in lur'e form. *IEEE Trans. Circuits Syst. Regul. Pap.* **60**(11), 3033–3042 (2013)
20. DeLellis, P., Di Bernardo, M., Garofalo, F., Porfiri, M.: Evolution of complex networks via edge snapping. *IEEE Trans. Circuits Syst. Regul. Pap.* **57**(8), 2132–2143 (2010)
21. DeLellis, P., Di Bernardo, M., Gorochowski, T.E., Russo, G.: Synchronization and control of complex networks via contraction, adaptation and evolution. *IEEE Circuits Syst. Mag.* **10**(3), 64–82 (2010)
22. Dorogovtsev, S.N., Mendes, J.F.: Evolution of networks. *Adv. Phys.* **51**(4), 1079–1187 (2002)
23. Fang, Y.: Stability analysis of linear control systems with uncertain parameters. Ph.D. thesis, Case Western Reserve University (1994)
24. Frasca, M., Buscarino, A., Rizzo, A., Fortuna, L., Boccaletti, S.: Synchronization of moving chaotic agents. *Phys. Rev. Lett.* **100**(4), 044102 (2008)
25. Godsil, C., Royle, G.F.: Algebraic Graph Theory, vol. 207. Springer Science & Business Media, Berlin (2013)
26. Golovneva, O., Jeter, R., Belykh, I., Porfiri, M.: Windows of opportunity for synchronization in stochastically coupled maps. *Physica D: Nonlinear Phenom.* **340**, 1–13 (2017)
27. Gorochowski, T.E., Bernardo, M.D., Grierson, C.S.: Evolving dynamical networks: a formalism for describing complex systems. *Complexity* **17**(3), 18–25 (2012)
28. Gorochowski, T.E., di Bernardo, M., Grierson, C.S.: Evolving enhanced topologies for the synchronization of dynamical complex networks. *Phys. Rev. E* **81**(5), 056212 (2010)
29. Grone, R., Merris, R.: The laplacian spectrum of a graph ii. *SIAM J. Discrete Math.* **7**(2), 221–229 (1994)
30. Hasler, M., Belykh, I.: Blinking long-range connections increase the functionality of locally connected networks. *IEICE Trans. Fundam. Electron. Commun. Comput. Sci.* **88**(10), 2647–2655 (2005)
31. Hasler, M., Belykh, V., Belykh, I.: Dynamics of stochastically blinking systems. Part I: finite time properties. *SIAM J. Appl. Dyn. Syst.* **12**(2), 1007–1030 (2013)
32. Hasler, M., Belykh, V., Belykh, I.: Dynamics of stochastically blinking systems. Part II: asymptotic properties. *SIAM J. Appl. Dyn. Syst.* **12**(2), 1031–1084 (2013)
33. Hasler, M., Maistrenko, Y.L.: An introduction to the synchronization of chaotic systems: coupled skew tent maps. *IEEE Trans. Circuits Syst. I: Fundam. Theory Appl.* **44**(10), 856–866 (1997)
34. Hasselblatt, B., Katok, A.: Handbook of Dynamical Systems. Elsevier, Amsterdam (2002)
35. Hespanha, J.P., Morse, A.S.: Stability of switched systems with average dwell-time. In: Conference on Decision and Control, 1999. Proceedings of the 38th IEEE, vol. 3, pp. 2655–2660. IEEE, Piscataway (1999)
36. Holme, P., Saramäki, J.: Temporal networks. *Phy. Rep.* **519**(3), 97–125 (2012)
37. Holme, P., Saramäki, J.: Temporal Networks. Springer, Berlin (2013)
38. Ito, J., Kaneko, K.: Spontaneous structure formation in a network of chaotic units with variable connection strengths. *Phy. Rev. Lett.* **88**(2), 028701 (2001)
39. Jeter, R., Belykh, I.: Synchronization in on-off stochastic networks: windows of opportunity. *IEEE Trans. Circuits Syst. Regul. Pap.* **62**(5), 1260–1269 (2015)
40. Jeter, R., Belykh, I.: Synchrony in metapopulations with sporadic dispersal. *Int. J. Bifurcation Chaos* **25**(07), 1540002 (2015)
41. Jeter, R., Porfiri, M., Belykh, I.: Network synchronization through stochastic broadcasting. *IEEE Control Syst. Lett.* **2**(1), 103–108 (2018).
42. Jeter, R., Porfiri, M., Belykh, I.: Overcoming network resilience to synchronization through non-fast stochastic broadcasting. *Chaos: Interdiscip. J. Nonlinear Sci.* **28**(7), 071104 (2018)
43. Kapitza, P.L.: Dynamic stability of a pendulum when its point of suspension vibrates. *Sov. Phys. - JETP* **21**, 588–592 (1951)
44. Kushner, H.J.: Introduction to Stochastic Control. Holt, Rinehart and Winston, New York (1971)

45. Levnajić, Z., Mezić, I.: Ergodic theory and visualization. i. mesochronic plots for visualization of ergodic partition and invariant sets. *Chaos: Interdiscip. J. Nonlinear Sci.* **20**(3), 033114 (2010)
46. Li, Z., Chen, G.: Global synchronization and asymptotic stability of complex dynamical networks. *IEEE Trans. Circuits Syst. Express Briefs* **53**(1), 28–33 (2006)
47. Lu, W.: Adaptive dynamical networks via neighborhood information: synchronization and pinning control. *Chaos: Interdiscip. J. Nonlinear Sci.* **17**(2), 023122 (2007)
48. Lu, J., Chen, G.: A time-varying complex dynamical network model and its controlled synchronization criteria. *IEEE Trans. Autom. Control* **50**(6), 841–846 (2005)
49. Masuda, N., Holme, P.: *Temporal Network Epidemiology*. Springer, Berlin (2017)
50. Masuda, N., Klemm, K., Eguíluz, V.M.: Temporal networks: slowing down diffusion by long lasting interactions. *Phys. Rev. Lett.* **111**(18), 188701 (2013)
51. Mondal, A., Sinha, S., Kurths, J.: Rapidly switched random links enhance spatiotemporal regularity. *Phys. Rev. E* **78**(6), 066209 (2008)
52. Motter, A.E.: Networkcontrology. *Chaos: Interdiscip. J. Nonlinear Sci.* **25**(9), 097621 (2015)
53. Netoff, T.I., Schiff, S.J.: Decreased neuronal synchronization during experimental seizures. *J. Neurosci.* **22**(16), 7297–7307 (2002)
54. Nishikawa, T., Motter, A.E.: Network synchronization landscape reveals compensatory structures, quantization, and the positive effect of negative interactions. *Proc. Natl. Acad. Sci.* **107**(23), 10342–10347 (2010)
55. Olver, F., Lozier, D., Boisvert, R., Clark, C.: *Nist Handbook of Mathematical Functions*. Cambridge University Press, Cambridge (2010)
56. Ott, E.: *Chaos in Dynamical Systems*. Cambridge University Press, Cambridge (2002)
57. Pecora, L.M., Carroll, T.L.: Master stability functions for synchronized coupled systems. *Phys. Rev. Lett.* **80**(10), 2109 (1998)
58. Pikovsky, A., Politi, A.: *Lyapunov Exponents: A Tool to Explore Complex Dynamics*. Cambridge University Press, Cambridge (2016)
59. Pikovsky, A., Rosenblum, M., Kurths, J.: *Synchronization: A Universal Concept in Nonlinear Sciences*, vol. 12. Cambridge University Press, Cambridge (2003)
60. Porfiri, M.: A master stability function for stochastically coupled chaotic maps. *Europhys. Lett.* **96**(4), 40014 (2011)
61. Porfiri, M.: Stochastic synchronization in blinking networks of chaotic maps. *Phys. Rev. E* **85**(5), 056114 (2012)
62. Porfiri, M., Belykh, I.: Memory matters in synchronization of stochastically coupled maps. *SIAM J. Appl. Dyn. Syst.* **16**(3), 1372–1396 (2017)
63. Porfiri, M., Fiorilli, F.: Global pulse synchronization of chaotic oscillators through fast-switching: theory and experiments. *Chaos, Solitons & Fractals* **41**(1), 245–262 (2009)
64. Porfiri, M., Fiorilli, F.: Node-to-node pinning control of complex networks. *Chaos: Interdiscip. J. Nonlinear Sci.* **19**(1), 013122 (2009)
65. Porfiri, M., Fiorilli, F.: Experiments on node-to-node pinning control of chua's circuits. *Physica D: Nonlinear Phenom.* **239**(8), 454–464 (2010)
66. Porfiri, M., Jeter, R., Belykh, I.: Windows of opportunity for the stability of jump linear systems: almost sure versus moment convergence. *Automatica* **100**, 323–329 (2019)
67. Porfiri, M., Pigliacampo, R.: Master-slave global stochastic synchronization of chaotic oscillators. *SIAM J. Appl. Dyn. Syst.* **7**(3), 825–842 (2008)
68. Porfiri, M., Stilwell, D.J.: Consensus seeking over random weighted directed graphs. *IEEE Trans. Autom. Control* **52**(9), 1767–1773 (2007)
69. Porfiri, M., Stilwell, D.J., Bollett, E.M.: Synchronization in random weighted directed networks. *IEEE Trans. Circuits Syst. Regul. Pap.* **55**(10), 3170–3177 (2008)
70. Porfiri, M., Stilwell, D.J., Bollett, E.M., Skufca, J.D.: Random talk: random walk and synchronizability in a moving neighborhood network. *Physica D: Nonlinear Phenom.* **224**(1), 102–113 (2006)
71. Ren, W., Beard, R.W.: *Distributed Consensus in Multi-Vehicle Cooperative Control*. Springer, Berlin (2008)

72. Skufca, J.D., Boltt, E.M.: Communication and synchronization in disconnected networks with dynamic topology: moving neighborhood networks. *Math. Biosci. Eng.(MBE)* **1**(2), 347–359 (2004)
73. So, P., Cotton, B.C., Barreto, E.: Synchronization in interacting populations of heterogeneous oscillators with time-varying coupling. *Chaos: Interdiscip. J. Nonlinear Sci.* **18**(3), 037114 (2008)
74. Sorrentino, F., Ott, E.: Adaptive synchronization of dynamics on evolving complex networks. *Phys. Rev. Lett.* **100**(11), 114101 (2008)
75. Stefański, A., Perlikowski, P., Kapitaniak, T.: Ragged synchronizability of coupled oscillators. *Phys. Rev. E* **75**(1), 016,210 (2007)
76. Stojanovski, T., Kocarev, L., Parlitz, U., Harris, R.: Sporadic driving of dynamical systems. *Phy. Rev. E* **55**(4), 4035 (1997)
77. Sumpter, D.J.: *Collective Animal Behavior*. Princeton University Press, Princeton, NJ (2010)
78. Tang, Y., Qian, F., Gao, H., Kurths, J.: Synchronization in complex networks and its application—a survey of recent advances and challenges. *Annu. Rev. Control* **38**(2), 184–198 (2014)
79. Yu, W., DeLellis, P., Chen, G., Di Bernardo, M., Kurths, J.: Distributed adaptive control of synchronization in complex networks. *IEEE Trans. Autom. Control* **57**(8), 2153–2158 (2012)
80. Zanette, D.H., Mikhailov, A.S.: Dynamical systems with time-dependent coupling: clustering and critical behaviour. *Physica D: Nonlinear Phenom.* **194**(3), 203–218 (2004)

The Effects of Local and Global Link Creation Mechanisms on Contagion Processes Unfolding on Time-Varying Networks



Kaiyuan Sun, Enrico Ubaldi, Jie Zhang, Márton Karsai, and Nicola Perra

1 Introduction

Think about the last conference you attended. In particular, focus on the social interactions you had throughout the week. Chances are that you spent a disproportionate fraction of time chatting with old and current collaborators as well as with long time colleagues you typically meet in such settings. Chances are that you also networked with new people. Most of these interactions were probably short and spontaneous exchanges maybe while waiting in line for coffee or after your presentation. Others might have been with editors, to whom you were trying to push your new idea for a book, or with one of the keynote speakers after her inspiring talk. Bear with us and think about last time you visited Twitter. Chances are that you read and interacted with the posts of popular users, which you don't know personally, but follow avidly. Finally, chances are that you also interacted with your personal friends you follow.

K. Sun

MOBS Lab, Network Science Institute, Northeastern University, Boston, MA, USA

E. Ubaldi

Sony Computer Science Laboratories, Paris, France

J. Zhang

Networks and Urban Systems Centre, University of Greenwich, London, UK

e-mail: jie.zhang@gre.ac.uk

M. Karsai

Department of Network and Data Science, Central European University, Budapest, Hungary

Univ Lyon, ENS de Lyon, Inria, CNRS, Université Claude Bernard Lyon 1, LIP, Lyon, France
e-mail: karsaim@ceu.edu

N. Perra (✉)

Networks and Urban Systems Centre, University of Greenwich, London, UK

e-mail: n.perra@gre.ac.uk

These two scenarios highlight how both face-to-face and digital interactions are temporal acts driven by intricate social mechanisms. Among them we can identify two categories. The first, refers to frequent reciprocated connections with individuals in your close social circle(s). These are interactions you reinforce and activate over time. The second refers to (mostly) one-sided interactions with popular individuals. These are connections you initiate with people who, thanks to their status and fame, are able to attract a large share of the attention from many others. The first category encompasses *local* mechanisms that do not depend on the behavior of people outside your social circle. The second instead, *global* mechanisms that depend on the behavior of, potentially, a large fraction of individuals.

Let's go back to your last conference. Many of the interactions you probably had were with people that, conference after conference, dinner after dinner, paper after paper, entered in your close social circle. These are individuals that you know very well and that are likely part of the same community. Some of the other interactions instead were probably with popular and influential people such as the keynote speakers or editors with whom many other participants wanted to speak to. The first type of interactions were driven by *social closeness*, the second instead by *popularity*.

A large literature, mostly built on a time-aggregated (static) data, substantiates this picture. In particular, it is well known that social ties (both offline and online) can be categorized as strong or weak [1–8]. The first describes a small subset of ties which are activated frequently. The second instead describes sporadic (such as the person you met while waiting for coffee) interactions. A classic signature of this tendency is found in the distributions of link's weights which are heterogeneous. There is more. In fact, as alluded above, people with whom we share strong ties are likely to be also connected in tight communities [3, 9–11]. Thus, strong ties are clustered around groups of people characterized by large links' overlap [3, 12]. Some of the weak ties instead, bridge such groups [3, 13]. Another well known property of real networks is the heterogeneity in the distribution of number of ties (the degree) [14, 15]. In fact, networks are typically sparse. Many nodes are poorly connected. Few of them instead are able to attract a disproportionate amount of connections. It is important to stress how strong and weak ties, communities, and hubs emerge and evolve over time [16, 17]. Which model(s) can be used to reproduce such features? How do they affect contagion phenomena taking place on their fabric? These are the main questions we will tackle in this chapter. In particular, we aim to revise and discuss a set of models that have been proposed to capture the evolution of social ties as function of time. In particular, we will consider both local and global approaches able to reproduce the formation of strong ties, communities, as well as the presence of popular individuals. From this stand point, we will then study how they affect contagion (epidemic) processes unfolding on such networks.

2 The Activity-Driven Framework

To explore the effects of local and global link formation mechanisms on epidemic spreading processes, we will consider several variations of the activity-driven framework [18]. These are models of time-varying networks, based on the same fundamental scheme. In particular, when one is tasked to describe the evolution of the connections between N nodes, needs to specify (at least) which nodes are involved in interactions at each time step. In the activity-driven framework this prescription is divided in two steps: (i) activation, (ii) partners selection. The first describes, which nodes are *active* and willing to connect. The second instead describes how such active nodes select the partners to whom interact. The modeling of the activation process, which will be the same for all the different variations of the framework we discuss here, is based on the intuition that not all nodes are equally willing to create or be part of social interactions. This has been confirmed with a range of observations in real datasets capturing very different type of interactions ranging from scientific collaborations to R&D alliances between firms [18–24]. In particular, it turns out that the activity rate (measured in series of time windows of size Δt) is very heterogeneous. Furthermore, the distribution of activity is largely independent on the choice of Δt . In other words, if we measure the propensity of nodes to be involved in a social interaction by splitting the data in time windows of size Δt or $\Delta t'$ we will get very extremely similar distributions. The partner selection process instead describes the mechanism behind the formation of links. Here, we will revise and consider three different models that capture popularity and social closeness mentioned above. In addition, we will consider a basic version of the model in which link creation is random. This will serve as null model (baseline). In all cases, we will first discuss the details of the link formation mechanism and then their effect on epidemic processes unfolding on the network at comparable time scale respect to the evolution on the graph's structure.

The general setting of activity driven models is the following. N nodes are described by at least one variable: their activity a . This quantity regulates their propensity to be active and willing to initiate social interactions at each time step. Activities are extracted and assigned to nodes from a distribution $F(a)$, which in the following we consider as a power-law. Thus $F(a) = Ca^{-\gamma}$ with $\epsilon \leq a \leq 1$ to avoid divergences for small values of activities. At each time step t the network G_t starts completely disconnected. Each node i is active with a probability $a_i \Delta t$. Active nodes create m connections with others. As mentioned above we will consider four link creation mechanisms. At time $t + \Delta t$ each link is deleted and the process restart and a network $G_{t+\Delta t}$ is generated. It is important to stress how all the links are deleted at the end of each iteration and thus links do not persist across time steps unless they are re-formed.

2.1 Model 1: Baseline

The simplest link formation mechanism is random [18] (see Fig. 1a). In this very unrealistic scenario partners are selected homogeneously across the entire system. While, very active nodes are likely to initiate connections in adjacent time steps, the probability that the same link is activated more than one time, the weight in a time integrated network, follows a Poisson distribution which, as mentioned in the introduction, is quite far from real observations. However, it is possible to show that integrating links over T time steps, the degree distribution follows the functional form of the activity [25]. Thus, the heterogeneous propensity to initiate social interactions results in a heterogeneous degree distribution. It is important to

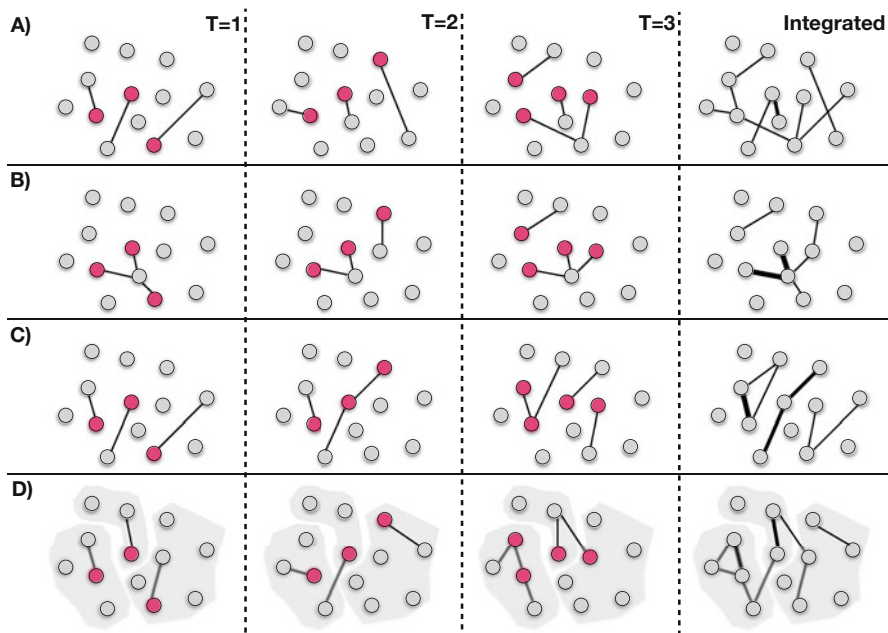


Fig. 1 Schematic representation of the four different variations of the activity-driven framework. The first three columns describe three time-steps of the evolution of network. The final column describes the union of links created in the three time steps. At each time, for all the networks, we assume that the same nodes are active (nodes in red), but the link creation process is instead different. For simplicity we assume $m = 1$, the width of the link in the final column is proportional to how many time each link was activated. The first row (**a**) shows the case of random link creation (model 1). The second (**b**) describe the global link creation mechanism based on popularity (model 2). In this representation, one of nodes (the node with degree 4 in the integrated network) is the most attractive node. The third row (**c**) describes the local link creation mechanism based on the social memory (model 3). The final row (**d**) describes the local link creation mechanism driven by the presence of communities which are depicted by shaded areas (model 4)

stress however, that each G_t network is mostly constituted by a set of disconnected stars formed around active nodes. Hubs emerge in time due the active engagement of such nodes.

2.2 Model 2: Global Links Formation Process Driven By Popularity

The second link formation we consider aims to capture a global, popularity based, mechanism [23] (see Fig. 1b). The basic intuition here is that not all nodes are equally *attractive*. Keynotes in conferences and celebrities in Twitter attract a disproportionate fraction of the connections in the system. To account for this, we assume that nodes, besides the activity, are characterized by another feature: the attractiveness b . Observations in different online social platforms suggest that indeed the propensity of people to attract connections is heterogeneously distributed [23]. All these aspects can be modeled within the activity-driven framework as follows. Nodes are assigned with two features: activity a and attractiveness b . These two quantities are extracted from a joint distribution $H(a, b)$. Interestingly, observations on online social platforms indicate that active people are also more attractive, thus the two features are in general positively correlated [23]. In these settings the dynamics of the networks are very similar as those described above. At each time step t , the network G_t starts disconnected. Each node is active with probability $a\Delta t$ and connects to m other nodes. Each partner j is selected following a simple preferential attachment, thus with probability $b_j/\langle b \rangle N$. At time $t + \Delta t$ all links are deleted and the process starts from scratch. It is possible to show that also in this case the degree distribution, obtained integrating links over time, is heterogeneous. However, the presence of attractiveness introduces some levels of heterogeneity in the weight distribution [23].

2.3 Model 3: Local Links Formation Process Driven by Social Memory

The third link formation mechanism is local and based on the idea of social closeness (see Fig. 1c). The intuition is that, due to the need for close social connection, cognitive and temporal constraints, large part of our interactions take place within a small social circle [4, 26–31]. These are strong ties that we remember (hence social memory) and activate frequently. We do also have sporadic, weak, interactions with people outside the circle such as the conference participants we met waiting for coffee in the hypothetical scenario described in the introduction. Observations across collaboration and communication networks corroborate this picture [3, 13, 20, 22–24]. Indeed, the probability that the next social act, for nodes

that have already contacted k distinct individuals in the past, will result in the establishment of a new, $k+1$ -th, tie follows this function $p(k) = (1 + \frac{k}{c})^{-\eta}$ [20, 22]. This implies that the larger the size of social circle the smaller the probability of increasing it. Consequently, social acts are frequently repeated within small circles of nodes. Remarkably, the behavior of large number of individuals can be modeled using one single value of c (that captures the off-set after which the memory effects become effective) and a single (or multiple within a small region) value of η (that captures the memory strength) [20, 22]. We can modify the activity-driven framework to account for the function $p(k)$ that regulates the tendency towards new/old connections (social memory). The evolution of these networks, driven by such local link formation mechanism, is modeled as follows. At each time t the network G_t starts completely disconnected. Each node i activates with probability $a_i \Delta t$ and creates m connections. Each of these is created towards a randomly selected node never contacted before with probability $p(k_i)$ (where k_i is the number of nodes already in the social circle of i) and with probability $1 - p(k_i)$ towards a node already connected before. It is possible to show how both emergent degree and weight distributions are heterogeneous and function of η [20, 22].

2.4 Model 4: Local Links Formation Process Driven By Communities

The fourth, and final, mechanism is also based on a local link formation process. As mentioned in the introduction, not only our social ties are organized around strong and weak ties but people in our social circles are likely to be friends. In networks terms, social circles are communities formed by groups of tightly connected people [9]. It is important to notice how the local mechanism described above (model 3) does not account for this important aspect. Indeed, triangles (i.e. a friend of my friend is my friend), which are crucial aspects of real communities, might emerge but are not likely by construction. There has been multiple proposals on how to model emergent clusters using the activity-driven framework [32, 33]. Here, we will consider the approach developed in Ref. [33] (see Fig. 1d). Observations in real networks show how the size of communities is heterogeneous [9]. Thus, we can set a distribution $P(s) \sim s^{-\alpha}$ with $s_{min} \leq s \leq s_{max}$ to describe the size, s , of communities in the system. Each node is then associated to a community. In these settings, we can easily modify the activity-driven framework to account for communities. As before, at each time step t the network G_t starts completely disconnected. Each node i is active with probability $a_i \Delta t$ and creates m connections. With probability q each of these is directed towards nodes in the same community (at random). With probability $1 - q$ instead links are created randomly outside the community. The parameter q regulates the modularity of the time-aggregated network. Clearly, if $q = 0$ the community structure does not play any role on the dynamics of the network. Instead, if $q = 1$ the system is formed by disconnected

communities. Values in between connect these two limits. It is possible to show how, for moderately high values of q , the degree and weight distribution are heterogeneous [33].

3 Epidemic Spreading on Activity-Driven Networks: Analytical Approach

After this preamble, we are in the position to investigate how global and local link formation mechanisms affect epidemic spreading. To this end, we will consider a prototypical contagion process: the Susceptible-Infected-Susceptible model [34–36]. Here, nodes are divided in two compartments according to their disease status. Susceptible, S for short, are healthy nodes that might be infected. Infected, I for short, are infectious nodes. The natural history of the disease is described by two transitions. The first is the infection process which is linked to a contact between S and I nodes. In particular, a susceptible node in contact with an infected one gets infected with probability λ : $S + I \xrightarrow{\lambda} 2I$. The second is instead the recovery process. Infected nodes spontaneously recover and become susceptible again with rate μ : $I \xrightarrow{\mu} S$. A key quantity, that can be used to study the spreading of a disease with a given λ and μ in a given network, is the epidemic threshold. The disease will be able to spread, and reach an endemic state, only above a critical value (which is determined by the features of the network where the process unfolds). Below such critical value the disease will die out and affect only a small fraction of the population. Before going forward we need another piece. In particular, how do we go about estimating, numerically, the epidemic threshold? The classic approach is to study I_∞ as function of λ/μ [35, 37]. As already mentioned, above the threshold the process reaches an endemic state. This is a dynamical equilibrium in which the total number of infected nodes is constant. Thus above threshold $I_\infty > 0$, while below threshold $I_\infty = 0$. Due to the stochastic nature of the process, the estimation of the threshold by looking at the behavior of I_∞ is quite hard. We will adopt an alternative and recent approach, which looks at the *life time*, L , of the process [38]. This quantity is defined as the time the disease needs either to die out or to reach a finite fraction, Y , of the population. Indeed, well below the threshold the disease will quickly die out. Well above the threshold the disease will be able to reach the fraction Y quite quickly. For values between these two regimes the life time increases and reaches a peak for values in proximity of the real threshold. In the language of phase transitions, the life time acts as the susceptibility χ [38].

We have now all the ingredients to study a contagion process unfolding on different versions of activity-driven networks which capture local and global link formation dynamics. Before jumping to the details we summarize the key features of the various models in Table 1.

Table 1 Summary of the four different activity driven models and their key features

Model	Links creation mechanism	Key variable(s)
1	Random	Activity a
2	Global: driven by popularity	Activity a and attractiveness b
3	Local: driven by social memory	Activity a , social ties reinforcement parameters c and η
4	Local: driven by communities	Activity a , details of communities sizes distribution, probability q to select partners in the same community

3.1 SIS Epidemic Processes Unfolding on Model 1: Baseline

As first step, let us consider the basic model where links are created randomly. This is the baseline which will highlight the effects of heterogeneous activity patterns (since the link formation is featureless). We can assume that nodes in the same activity class are statistically equivalent. Furthermore, we can differentiate them according to their disease status. Thus we will refer to S_a , and I_a as the number of susceptible and infected nodes in activity class a . As we are considering a fixed population $N_a = S_a + I_a$ at all times. In order to derive the conditions for the spreading, we can study the evolution of the infected population. In particular, we can write the number of infected nodes at time $t + \Delta t$ as:

$$I_a(t + \Delta t) = I_a(t) - \mu I_a(t)\Delta t + m\lambda S_a(t)a\Delta t \int da' \frac{I_{a'}(t)}{N} + m\lambda S_a(t) \int da' a' \Delta t \frac{I_{a'}(t)}{N}. \quad (1)$$

In particular, this is given by the number of infected nodes at time t (first term on the r.h.s.), minus the nodes that recover (second term on the r.h.s.), plus susceptible nodes that are active, get in contact with infected nodes in other classes and get infected as result (third term on the r.h.s.), plus susceptible nodes that get contacted and infected by active infectious nodes in other categories of activity (fourth term on the r.h.s.). It is important to stress that as each m link is created randomly, the probability of selecting a node in a particular class is simply m/N . By dividing for Δt in the limit of $\Delta t \rightarrow 0$ we can write:

$$d_t I_a = -\mu I_a + m\lambda \frac{N_a - I_a}{N} a I + m\lambda \frac{N_a - I_a}{N} \Theta, \quad (2)$$

where for simplify the notation we removed the explicit dependence of time, wrote $S_a = N_a - I_a$, defined $\Theta = \int a I_a da$ and considered that $I = \int I_a da$ is the total number of infected nodes. Since we are interested at the early stages of the spreading we can move forward linearizing the expression by assuming that $N_a \sim S_a$ and by keeping just the first order terms in I_a . Thus we get

$$d_t I_a = -\mu I_a + m\lambda \frac{N_a}{N} a I + m\lambda \frac{N_a}{N} \Theta. \quad (3)$$

By summing over all classes of activity we get

$$d_t I = -\mu I + m\lambda \langle a \rangle I + m\lambda \Theta, \quad (4)$$

since $\langle a \rangle = \int a N_a / N da = \int a F(a) da$. The expression is now function of two variables of I and Θ . In order to understand their behavior we need to get an expression for Θ . To this end, we multiply Eq. 3 by a and sum over all activity classes:

$$d_t \Theta = -\mu \Theta + m\lambda \langle a^2 \rangle I + m\lambda \langle a \rangle \Theta. \quad (5)$$

At this stage, we obtained a system of two differential equations, one in I one in Θ . The disease will be able to spread only if the largest eigenvalue of the Jacobian of the system is larger than zero. In fact, this will imply that the region where we developed the system is unstable. The Jacobian matrix can be written as

$$J_m = \begin{pmatrix} -\mu + \lambda m \langle a \rangle & \lambda m \\ \lambda m \langle a^2 \rangle & -\mu + \lambda m \langle a \rangle \end{pmatrix},$$

with eigenvalues

$$\Lambda_{(1,2)} = m \langle a \rangle \lambda - \mu \pm \lambda m \sqrt{\langle a^2 \rangle}. \quad (6)$$

Thus, the epidemic threshold can be simply written as [18]

$$\frac{\lambda}{\mu} > \frac{1}{m} \frac{1}{\langle a \rangle + \sqrt{\langle a^2 \rangle}} \quad (7)$$

We can define β as the per capita rate at which people get infected. This is equal to $\beta = \lambda \langle k \rangle$. The average degree at each time step is equal to $\langle k \rangle = 2m \langle a \rangle$. Thus we can write

$$\frac{\beta}{\mu} > \xi_r \equiv \frac{2 \langle a \rangle}{\langle a \rangle + \sqrt{\langle a^2 \rangle}}, \quad (8)$$

where we defined ξ_r as the epidemic threshold for the random link creation process. It is interesting to notice how the threshold is function of the first and second moments of the activity distribution and that it has been derived using also other methods [25, 39, 40]. As the process is unfolding as the network changes structure the threshold is not function of the integrated degree distribution but only of the quantities describing the activation of each node at each time step.

3.2 SIS Epidemic Processes in Model 2: The Effects of Popularity

Let us now shift gears and analyze the first not random link creation mechanism. In particular, following the previous order, let us consider the global mechanism based on popularity. To this end, nodes are characterized by two features extracted from a general joint distribution $H(a, b)$. As before a describes the activity, b instead the attractiveness. In these settings, it is necessary to divide nodes according to these two features. Thus, the number of susceptible, and infected nodes of activity a and attractiveness b at time t is indicated as $S_{a,b}$ and $I_{a,b}$ respectively. The evolution of the number of infected nodes can be written as:

$$d_t I_{a,b} = -\mu I_{a,b} + \frac{\lambda m}{N\langle b \rangle} S_{a,b} \left[a \iint da' db' b' I_{a',b'} + b \iint da' db' a' I_{a',b'} \right]. \quad (9)$$

The first term on the r.h.s. accounts for the recovery process. The second describes susceptible nodes that are active and select (with probability $b/(b)N$) infected nodes in other classes getting infected. The third term finally describes susceptible nodes selected by active and infected nodes in other classes and that become infectious as result. It is interesting to notice the symmetry of the last two terms. To move forward, let us define two functions $\theta = \iint a I_{a,b} dadb$ and $\phi = \iint b I_{a,b} dadb$. The previous expression becomes:

$$d_t I_{a,b} = -\mu I_{a,b} + \frac{\lambda m}{N\langle b \rangle} S_{a,b} [a\phi + b\theta]. \quad (10)$$

As before, we can assume that at the early stages of the spreading $N_{a,b} \sim S_{a,b}$ and neglect the terms at the second order in $I_{a,b}$ thus we are left with

$$d_t I_{a,b} = -\mu I_{a,b} + \frac{\lambda m}{N\langle b \rangle} N_{a,b} [a\phi + b\theta]. \quad (11)$$

From the last expression, we can obtain a system of three equations necessary to study the behavior of the number of infected nodes in the early stages. In particular, we can obtain an expression for (i) I by summing all activity and attractiveness classes, (ii) θ by multiplying both sides for a and summing all classes, and iii) ϕ by multiplying both sides for b and summing all classes. Doing so, we obtain the following system of differential equations:

$$d_t I = -\mu I + \frac{\lambda m}{\langle b \rangle} [\langle a \rangle \phi + \langle b \rangle \theta], \quad (12)$$

$$d_t \theta = -\mu \theta + \frac{\lambda m}{\langle b \rangle} [\langle a^2 \rangle \phi + \langle ab \rangle \theta], \quad (13)$$

$$d_t \phi = -\mu \phi + \frac{\lambda m}{\langle b \rangle} [\langle ab \rangle \phi + \langle b^2 \rangle \theta]. \quad (14)$$

The eigenvalues of the Jacobian matrix read:

$$\Lambda_1 = -\mu, \quad \Lambda_{(2,3)} = \frac{\lambda m}{\langle b \rangle} \left(\langle ab \rangle \pm \sqrt{\langle a^2 \rangle \langle b^2 \rangle} \right) - \mu. \quad (15)$$

As before, the disease is able to spread if the largest eigenvalue is larger than zero. This condition implies [41]:

$$\frac{\beta}{\mu} > \xi_{att} \equiv \frac{2\langle a \rangle \langle b \rangle}{\langle ab \rangle + \sqrt{\langle a^2 \rangle \langle b^2 \rangle}}. \quad (16)$$

It is important to notice how the threshold has been computed without any assumption on the form of the distribution $H(a, b)$, thus it is valid for any (integrable) form. A comparison between ξ_r and ξ_{att} reveals how the general structure of the threshold is similar. In particular, the second moments are under the square root in the denominator. However, note how the details of the correlation between the two features appear explicit in the term $\langle ab \rangle$. To gather a deeper understanding on the differences between the two thresholds, let us first consider the uncorrelated case thus $H(a, b) = F(a)G(b)$. In this case, we can re-write the threshold as:

$$\xi_{att} = \frac{2}{1 + \sqrt{\frac{\langle a^2 \rangle \langle b^2 \rangle}{\langle a \rangle^2 \langle b \rangle^2}}}. \quad (17)$$

As the dependence of the threshold on the two moments is symmetric, the case with constant attractiveness and generic $F(a)$ (baseline) can be mapped to the one with constant activity and attractiveness distribution $F(b)$. Clearly the symmetry would be broken in case of directed networks, since the activity would regulate out-links while the attractiveness in-links. Furthermore, as $\langle b^2 \rangle \geq \langle b \rangle^2$ always holds, the threshold can only be lower than or equal to the one found in first model. This means that the introduction of any amount of heterogeneity in the attractiveness helps the epidemic spreading pushing the threshold to smaller values. As mentioned in the introduction, observations in real networks suggest that activity and attractiveness are correlated. The relation between the two, in two online communication networks, can be modeled as $a \sim b^{\gamma_c}$ with γ_c close to one. What happens to the threshold in this case? To answer this question, we can study the case of deterministic correlation between the two variables imposing:

$$H(a, b) = F(a)\delta(b - q(a)), \quad (18)$$

where $\delta(x)$ is the Dirac delta and $q(a)$ is the function that determines the attractiveness of a node given its activity: $b_i = q(a_i)$, $\forall i$. Using the relation $G(b) = F(a)|da/db|$, we can obtain an expression for $G(b)$:

$$G(b) = F(q^{-1}(b)) \left| \frac{dq^{-1}(b)}{db} \right|. \quad (19)$$

To account for the observations mentioned above, we can set $q(a) = a^{\gamma_c}$, $\gamma_c > 0$. Since the activity is distributed according to a power-law ($F(a) \propto a^{-\gamma_a}$), the attractiveness will be distributed as $G(b) \propto b^{-1+\frac{1-\gamma_a}{\gamma_c}}$. In these settings, a generic moment of the joint distribution can be expressed as:

$$\langle a^n b^m \rangle = \langle a^{n+\gamma_c m} \rangle, \quad (20)$$

thus the epidemic threshold becomes:

$$\xi_{att} = \frac{2\langle a \rangle \langle a^{\gamma_c} \rangle}{\langle a^{1+\gamma_c} \rangle + \sqrt{\langle a^2 \rangle \langle a^{2\gamma_c} \rangle}}.$$

Generally speaking (this is controlled by the value of γ_c) the threshold is not only smaller than ξ_r but also smaller than the uncorrelated case. In fact, the disease is able to spread faster when popular people, that are able to attract the connection from many others, are also very active in contacting other nodes.

3.3 SIS Epidemic Processes in Model 3: The Effects of Social Memory

The third model, based on the local reinforcement of previously activated ties (social memory), does not allow (to the best of our knowledge) a derivation of a closed expression for the threshold as we did in the previous two cases. Exact numerical methods, based on the spectral properties of matrices obtained from G_t , can be used to derive it, but these do not allow to gather an explicit expression [42, 43]. However, a recent paper by Tizzani et al. [44] provides an analytical treatment with some approximations. While we refer the interested reader to the original paper for details, here we provide a summary of their derivation as it nicely complements the techniques we discussed above. First of all, they adopted an individual based approach, in which rather than considering classes of activity each node is considered explicitly. In fact, the memory effects for each node make the interactions with a given social circle more likely. Thus nodes in the same activity class cannot be considered statistically equivalent as their behavior depends on their memory of past interactions. In the individual based approach, the focus goes from the study of the evolution of the number of infected nodes in a given activity class to the study of the probability $\rho_i(t)$ that the node i is infected at time t . This can be written as [44]:

$$\begin{aligned}
d_t \rho_i(t) = & -\mu \rho_i(t) + \lambda [1 - \rho_i(t)] \left[\sum_j a_i [1 - p(k_i)] \frac{A_{ij}(t)}{k_i} \rho_j(t) + \right. \\
& + \sum_{j \neq i} a_i p(k_i) \frac{\rho_j(t)}{N - k_i - 1} + \sum_j a_j [1 - p(k_j)] \frac{A_{ij}(t)}{k_j} \rho_j(t) \\
& \left. + \sum_{j \neq i} a_j p(k_j) \frac{\rho_j(t)}{N - k_j - 1} \right], \tag{21}
\end{aligned}$$

where $A_{ij}(t)$ is the adjacency matrix of the integrated graph up to time t , and $\not\sim$ selects only the nodes j not yet connected to i . By construction this is $N - k_j(t) - 1$. The first term on the r.h.s. describes the recovery rate of the node. All the other terms describe the infection processes, which depend on the infection probability λ and the probability that the node is susceptible ($1 - \rho_i(t)$). The first two terms in the large brackets account for the fact that the node i is active and connects with a node j that has already contacted before (first term) or that has never seen (second term). The last two terms are the same but in this case they account for the fact that the other nodes are active and connect to i [44]. It is important to notice that this expression underlies an approximation: the state of every node is independent of the state of the neighbors. Clearly, this neglects the correlation between nodes. The challenges induced by the memory are clear thinking that the adjacency matrix and the social circle of each node are function of time. Thus, the unfolding of the disease is clearly function of its starting point in time. As Tizzani et al. noted, if we consider the limit in which $1 \ll k_i(t) \ll N$, thus if the disease starts spreading when the degree of each node is far from one and from N , hence at large times (but not too large), the expression can be reduced as (see Ref. [44] for details):

$$d_t \rho(t) = -\mu \rho(t) + \lambda [1 - \rho(t)] \sum_j A_{ij}(t) \left(\frac{a_i}{k_i} + \frac{a_j}{k_j} \right) \rho_j(t). \tag{22}$$

In order to find a solution to this expression, Tizzani et al. transitioned from the time integrated connectivity patterns (A_{ij}) to an annealed form ($P_{ij}(t)$) which describes the probability that i and j have been connected in the past. Interestingly, they show that

$$P_{ij}(t) = (1 + \eta) \frac{t^{\frac{1}{1+\eta}}}{N} [g(a_i) + g(a_j)], \tag{23}$$

where they defined $g(x) = x/(Cx)^\eta$. The strength of the memory η regulates the expression as well as the activity of the two nodes. From here Tizzani et al. can move from the probability that a node i is infected at time t to the probability that

a node of activity a at time t is infected (thanks to the annealed approximation). In particular, they obtain [44]:

$$\begin{aligned} d_t \rho(a, t) = & -\mu \rho(a, t) + \lambda [1 - \rho(a, t)] \left[\frac{ag(a)}{g(a) + \langle g \rangle} \int da' F(a') \rho(a', t) \right. \\ & + \frac{a}{g(a) + \langle g \rangle} \int da' F(a') \rho(a', t) g(a') + g(a) \int da' F(a') \frac{a'}{g(a') + \langle g \rangle} \rho(a', t) \\ & \left. + \int da' F(a') \frac{a' g(a')}{g(a') + \langle g \rangle} \rho(a', t) \right], \end{aligned} \quad (24)$$

where interestingly we find similar terms from the two previous cases. This expression is rather complex. However, the conditions for the spreading can be found, conceptually as before, by linearizing it at early times and studying the Jacobian of the system of four differential equations obtained for it (see Ref. [44] for the derivation). While the condition can be obtained fairly easily numerically, the nature of the terms, and the size of the matrix does not allow for a simple closed expression. Nevertheless, in case a disease start spreading in a *mature* social network in which nodes have build social circles, this analytical treatment works extremely well [44]. However, the general case, does not have a general closed solution, yet.

3.4 SIS Epidemic Processes in Model 4: The Effects of Communities

Finally, let us turn our attention to the last model where the link creation dynamic is influenced by the membership to specific communities. In particular, active nodes select (at random) a connection with nodes in their community with probability q , and outside their community with probability $1 - q$. Although we will not be able to solve them, it is instructive to write the dynamical equations describing the contagion process in these settings. Similarly to what we did before, let us define $S_{a,s}$ and $I_{a,s}$ as the number of susceptible and infected individuals, respectively, in the class of activity a and community of size s at time t . We can then write [33]:

$$\begin{aligned} d_t I_{a,s} = & -\mu I_{a,s} + \lambda a S_{a,s} \left[q \frac{I_s}{s} + (1 - q) \frac{I}{N} \right] \\ & + \lambda \int da' a' \left[q I_{a',s} \frac{S_{a,s}}{s} + (1 - q) I_{a',s} \frac{S_{a,s}}{N} \right], \end{aligned} \quad (25)$$

where I_s and I are the number of infected in communities of size s and in the whole network, respectively. As usual, the first term in the r.h.s accounts for the recovery of infected individuals. The second and third terms describe susceptible nodes that are active and select infected nodes in their community or outside. The fourth and fifth

terms are similar but consider that active nodes and infected nodes select susceptible nodes of class a in community of size s . For simplicity, we consider that $N - s \sim N$ and, at least initially, $I - I_s \sim I$. Summing over all the activities and community sizes, and considering only the first order terms in a , $I_{a,s}$ and their products, we obtain

$$d_t I = -\mu I + \lambda \langle a \rangle I + \lambda \theta + \lambda q \sum_s (\langle a \rangle_s - \langle a \rangle) I_s, \quad (26)$$

$$\begin{aligned} d_t \theta = & -\mu \theta + \lambda \langle a^2 \rangle I + \lambda \langle a \rangle \theta + \\ & + \lambda q \sum_s \left[(\langle a^2 \rangle_s - \langle a^2 \rangle) I_s + (\langle a \rangle_s - \langle a \rangle) \theta_s \right], \end{aligned} \quad (27)$$

where we defined as before $\theta = \int a I_a da$, and $\theta_s = \int a I_{a,s} da$. The term $\langle a^x \rangle_s = \int da N_{a,s} a^x / s$ describes the moments of the activity distribution in any community of size s . That is the average activity in a community of size s . As before, the second, auxiliary, equation is obtained from the first by multiplying both sides by a and summing over all s and a . The epidemic threshold, at least in principle, can be derived evaluating the largest eigenvalue of the Jacobian matrix of the system of differential equations in I and θ . Unfortunately, a closed expression, to the best of our knowledge, has not been derived yet. Nevertheless, we can point out some interesting observations. First of all, the terms in q weight a comparison between the moments of the activity distribution in the whole network with the corresponding values computed inside each community. In case the fluctuations of these terms are negligible, due for example to very large community sizes or to narrow distribution of activity, the equations become equivalent to the case $q = 0$ (which is equivalent, for small community sizes, to a random link creation mechanism). Similarly, in case $q \rightarrow 0$, the network has no modular structure, and the threshold becomes equal to the first simple model. In the opposite limit $q \rightarrow 1$ the large majority of connections take place inside each community. Thus the coupling between clusters becomes very weak. Especially when the average size of communities is small, the probability of selecting the same node as partner increases significantly.

Before moving to a more direct comparison between the thresholds in the four different models, let us spend few words about another important, and prototypical, contagion process: the SIR model [34–36]. While the infection mechanism is equivalent to the SIS, the recovery is radically different. In fact, there is another compartment, R , describing infected nodes that recover. These cannot be infected again as they acquire a permanent immunity. It is easy to show that, in case at early stages the population is fully susceptible and thus $R \sim 0$, the threshold for the SIR model unfolding on activity-driven networks with random or global link creation dynamics is equivalent to that of a SIS process. However, the symmetry breaks in case of local link creation mechanisms (for the last model in the limit of high q and small community sizes) [33, 45]. In fact, the presence of memory in the connectivity patterns induced by the reinforcement of previously activated ties or by high modularity have opposite effects in SIR and SIS models. The repetition of

a small number of connections hinders the spreading power of SIR processes. In fact, as soon as a node recovers, links towards it cannot result in further infections. However, such repetition (as will see more in details in the next section) favors SIS dynamics since it allows the disease to survive in small patches (infected nodes will eventually be susceptible again).

4 Epidemic Spreading on Activity-Driven Networks: Numerical Simulations

In Fig. 2 we show the normalized lifetime, L_n , for the different variations of the activity-driven framework discussed above. The normalization is done dividing each curve by its maximum, i.e. $L_n = L / \max L$. In the plot we considered two versions of the model with heterogenous attractiveness (model 2). In the first, attractiveness and activity, for each node, are extracted independently (uncorrelated scenario). In the second instead, attractiveness and activity are equal (correlated scenario). In the case of social memory (model 3), we set $c = 1$ and $\eta = 1$, thus previously activated ties are repeated with probability $1 - p(k) = \frac{k}{1+k}$. We also considered two different versions of the model with communities (model 4). In the first, we set $q = 0.45$, thus only 45% of the links are created within each community. In the second instead, we set $q = 0.9$, a much higher value. In both scenarios, community sizes are extracted from a power-law distribution $P(s) s^{-2.1}$ with $10 \leq s \leq \sqrt{N}$.

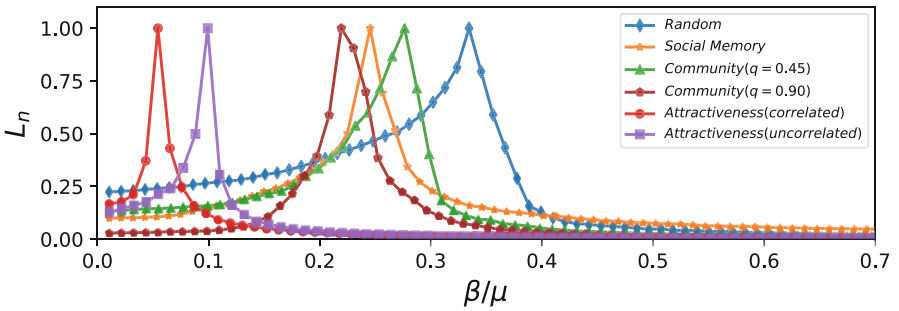


Fig. 2 We show the normalized lifetime of SIS processes unfolding on different variations of the activity driven framework as function of β/μ . In all cases, we set $N = 10^5$, $m = 1$, $F(a) a^{-2.1}$, $\epsilon = 10^{-3}$, $\mu = 10^{-2}$, $Y = 0.25$, start each simulations with 1% of randomly selected seeds, and each point is the average of 10^2 independent simulations. In the models with attractiveness, we set the distribution of popularity as $G(b) b^{-2.1}$ and considered two scenarios: (1) $H(a, b) = F(a)G(b)$ (uncorrelated case), (2) $H(a, b) = F(a)\delta(b - a)$ (correlated case). In the model with social memory, we set $c = 1$ and $\eta = 1$, thus a node that contacted already k nodes will connect to a new tie with probability $p(k) = \frac{1}{k+1}$ and will reinforce a previously activated link with probability $1 - p(k) = \frac{k}{k+1}$. Finally, in the models with community structure, we extracted communities sizes for a power-law distribution $P(s) s^{-2.1}$ with $10 \leq s \leq \sqrt{N}$ and considered two values of q

In order to compare the different scenarios, we fixed (across the board) all the other parameters (see legend of Fig. 2 for details). In these settings, several observations are in order. First, all global and local links creation mechanisms result in smaller values of the epidemic threshold respect to the baseline (random links' creation). Second, global, popularity-driven, mechanisms based on heterogenous distributions of attractivity (model 2) push the threshold to much smaller values respect to local mechanisms based on social closeness principles (models 3 and 4). Interestingly, correlations between activity and attractiveness help the spreading of the disease even further respect to uncorrelated scenarios. Third, the effects of communities depend on the value of q . In particular, high values of this quantity help the spreading more than smaller values of it. In fact, the repetition of connections within each cluster, helps the disease to survive for smaller values of the spreading rate. Finally, social memory, thus the repetition of previously activated ties, helps the spreading respect to medium-low values of modularity ($q = 0.45$), but not as much as larger values of it. In order to gather a deeper understanding on the dynamics, in Fig. 3 we show, as function of β/μ , the fraction of infected population evaluated at the time step equal to the life time, I_L . This quantity provides complimentary information respect to the previous plot by showing the prevalence of the disease at the moment the conditions that define the lifetime are met (i.e. disease either dies out or reaches a cumulative fraction Y of the population). Several observations are in order. First, the presence of heterogeneity in nodes' attractiveness (model 2) not only results in the lower value of the threshold (as shown in Fig. 2), but affects a larger fraction of the population respect to all the other links creation mechanisms. The effects of correlations between activity and attractiveness are not as visible as for the threshold. Second, despite in case of strong modularity ($q = 0.9$) the threshold is smaller than in case of social memory, the latter has a larger impact on the population. Indeed, while the presence of tightly connected communities allows for the survival of the disease for smaller values of the spreading rate, high values of modularity confine the impact of the virus in small patches. It is important to notice that this effect is dependent on the average community size and the distribution of

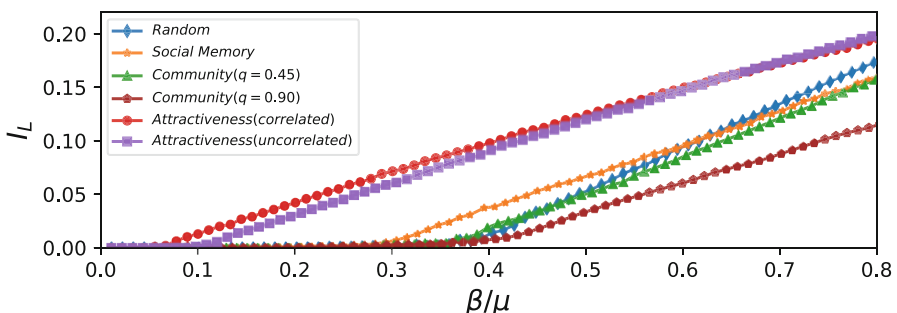


Fig. 3 We show I_L for the different version of activity-driven models. This quantity describes the fraction of infected nodes at time $t = L$. The parameters for all different cases are the same used in Fig. 2

sizes. Intuitively, in case nodes are arranged in few and very large communities such effects would be reduced as the repetition of ties would be much less likely. Finally, social memory (model 3), thus the reinforcement of previously activated ties, has a large impact on the system respect to random and other local mechanisms for values of β/μ closer to the epidemic threshold. As β/μ increases we enter in a region of the phase space where the repetition of the same connections hampers the spreading power of the disease respect to randomly activated ties or to networks with low modularity (model 4). In this regime, the spreading rate is high and having connections with a large number nodes, rather than repeating the links with few of them, helps the unfolding of the disease.

5 Conclusions

In this chapter we have investigated the effects of different link creation mechanisms on contagion processes unfolding on time-varying networks. In particular, we focused on two main classes: global and local mechanisms. We modeled the first considering that the propensity of nodes to attract social interactions is heterogeneous. We modeled the second, considering two different approach: (i) ties activated in the past are more likely to be re-activated than new ones (social memory), (ii) social ties are typically organized in tight communities poorly connected between them. The first mechanism is inspired by popularity (attractiveness) the second by social closeness mechanisms. Furthermore, as null model, we considered the simple, and unrealistic, case in which links are created randomly (baseline). We first provided details about how to analytically tackle the spreading of SIS processes in these models. We then presented a more direct numerical comparison between them. Interestingly, we found that global link creation mechanisms, driven by heterogenous distributions of attractivity, drastically reduce the epidemic threshold respect to the case of homogenous distribution of such quantity (baseline) and to the case of local mechanisms driven by social closeness. Thus, the presence of globally popular nodes, able to attract a large share of the interactions, facilitates the spreading respect to the local correlated dynamics induced by social closeness mechanisms. In fact, as soon such popular hubs get infected they affect a large fraction of the population that connects to them, even for small values of the spreading rate. The effect of communities is function of the modularity. High values of modularity push the threshold to smaller values respect to low values of it and to the social memory mechanism based on the repetition of previously activated ties. However, social memory might have a large impact on system in terms of disease's prevalence in the population. In fact, for values of the spreading rates close to the threshold we observe an interesting phenomenology where the fraction of infected nodes is larger respect to the case of communities as well as to the baseline. While the presence of communities allows the disease to survive for smaller values of the spreading rate, it confines the disease in smaller patches respect to case of social memory.

Arguably, all the mechanisms considered here are not mutually exclusive. In fact, both offline and online social networks are driven by their interplay. Here, we shown that even taken singularly they introduced no-trivial dynamics on contagion processes. More research should be conducted to study their interplay and trade-off in the future.

References

1. Granovetter, M.: The strength of weak ties. *Am. J. Sociol.* **78**, 1360–1380 (1973)
2. Granovetter, M.: Getting a Job: A Study of Contacts and Careers. University of Chicago Press, Chicago (1995)
3. Onnela, J.-P., Saramaki, J., Hyvonen, J., Szabo, G., Lazer, D., Kaski, K., Kertesz, J., Barabasi, A.-L.: Structure and tie strengths in mobile communication networks. *Proc. Natl. Acad. Sci. U.S.A.* **104**, 7332 (2007)
4. Saramäki, J., Leicht, E.A., López, E., Roberts, S.G., Reed-Tsochas, F., Dunbar, R.I.: Persistence of social signatures in human communication. *Proc. Natl. Acad. Sci.* **111**(3), 942–947 (2014)
5. Bakshy, E., Rosenn, I., Marlow, C., Adamic, L.: The role of social networks in information diffusion. In: Proceedings of the 21st International Conference on World Wide Web, pp. 519–528 (2012)
6. Levin, D.Z., Cross, R.: The strength of weak ties you can trust: the mediating role of trust in effective knowledge transfer. *Manag. Sci.* **50**(11), 1477–1490 (2004)
7. Friedkin, N.: A test of structural features of granovetter's strength of weak ties theory. *Soc. Networks* **2**(4), 411–422 (1980)
8. Brown, J.J., Reingen, P.H.: Social ties and word-of-mouth referral behavior. *J. Consum. Res.* **14**(3), 350–362 (1987)
9. Fortunato, S.: Community detection in graphs. *Phys. Rep.* **486**, 75–174 (2010)
10. Karsai, M., Ihiguez, G., Kaski, K., Kertész, J.: Complex contagion process in spreading of online innovation. *J. R. Soc. Interface* **11**(101), 20140694 (2014)
11. Karsai, M., Kivelä, M., Pan, R.K., Kaski, K., Kertész, J., Barabási, A.L., Saramäki, J.: Small but slow world: How network topology and burstiness slow down spreading. *Phys. Rev. E* **83**(2), 025102 (2011)
12. Weng, L., Karsai, M., Perra, N., Menczer, F., Flammini, A.: Attention on weak ties in social and communication networks. In: Complex Spreading Phenomena in Social Systems, pp. 213–228. Springer, Berlin (2018)
13. Burt, R.S.: Structural holes: The Social Structure of Competition. Harvard University Press, Cambridge (2009)
14. Newman, M.E.J.: Networks. An Introduction. Oxford University Press, Oxford (2010)
15. Barabási, A.-L., et al.: Network Science. Cambridge University Press, Cambridge (2016)
16. Holme, P.: Modern temporal network theory: a colloquium. *Eur. Phys. J. B* **88**(9), 1–30 (2015)
17. Holme, P., Saramäki, J.: Temporal networks. *Phys. Rep.* **519**(3), 97–125 (2012)
18. Perra, N., Gonçalves, B., Pastor-Satorras, R., Vespignani, A.: Activity driven modeling of time-varying networks. *Sci. Rep.* **2**, 469 (2012)
19. Ribeiro, B., Perra, N., Baronchelli, A.: Quantifying the effect of temporal resolution on time-varying networks. *Sci. Rep.* **3**, 3006 (2013)
20. Karsai, M., Perra, N., Vespignani, A.: Time varying networks and the weakness of strong ties. *Sci. Rep.* **4**, 4001 (2014)
21. Tomasello, M. V., Perra, N., Tessone, C. J., Karsai, M., Schweitzer, F.: The role of endogenous and exogenous mechanisms in the formation of R&D networks. *Sci. Rep.* **4**, 5679 (2014)

22. Ubaldi, E., Perra, N., Karsai, M., Vezzani, A., Burioni, R., Vespignani, A.: Asymptotic theory of time-varying social networks with heterogeneous activity and tie allocation. *Sci. Rep.* **6**, 35724 (2016)
23. Alessandretti, L., Sun, K., Baronchelli, A., Perra, N.: Random walks on activity-driven networks with attractiveness. *Phys. Rev. E* **95**(5), 052318 (2017)
24. Ubaldi, E., Vezzani, A., Karsai, M., Perra, N., Burioni, R.: Burstiness and tie activation strategies in time-varying social networks. *Sci. Rep.* **7**, 46225 (2017)
25. Starnini, M., Pastor-Satorras, R.: Temporal percolation in activity driven networks. *Phys. Rev. E* **89**, 032807 (2014)
26. Holt-Lunstad, J., Smith, T. B., Layton, J. B.: Social relationships and mortality risk: a meta-analytic review. *PLoS Med.* **7**(7), e1000316 (2010)
27. Dunbar, R.I.M.: The social brain hypothesis and its implications for social evolution. *Ann. Hum. Biol.* **36**(5), 562–572 (2009)
28. Miritello, G., Moro, E., Lara, R.: Dynamical strength of social ties in information spreading. *Phys. Rev. E* **83**, 045102 (2011)
29. Stiller, J., Dunbar, R.I.M.: Perspective-taking and memory capacity predict social network size. *Soc. Networks* **29**(1), 93–104 (2007)
30. Powell, J., Lewis, P.A., Roberts, N., García-Fiñana, M., Dunbar, R.I.M.: Orbital prefrontal cortex volume predicts social network size: an imaging study of individual differences in humans. *Proc. R. Soc. Lond. B Biol. Sci.* **279**, 2157–2162 (2012)
31. Gonçalves, B., Perra, N., Vespignani, A.: Modeling users' activity on twitter networks: validation of dunbar's number. *PloS one* **6**(8), e22656 (2011)
32. Laurent, G., Saramäki, J., Karsai, M.: From calls to communities: a model for time-varying social networks. *Eur. Phys. J. B* **88**(11), 1–10 (2015)
33. Nadini, M., Sun, K., Ubaldi, E., Starnini, M., Rizzo, A., Perra, N.: Epidemic spreading in modular time-varying networks. *Sci. Rep.* **8**(1), 2352 (2018)
34. Keeling, M.J., Rohani, P.: *Modeling Infectious Disease in Humans and Animals*. Princeton University Press, Princeton (2008)
35. Barrat, A., Barthélémy, M., Vespignani, A.: *Dynamical Processes on Complex Networks*. Cambridge University Press, Cambridge (2008)
36. Pastor-Satorras, R., Castellano, C., Van Mieghem, P., Vespignani, A.: Epidemic processes in complex networks. *Rev. Mod. Phys.* **87**(3), 925 (2015)
37. Wang, Z., Bauch, C.T., Bhattacharyya, S., d'Onofrio, A., Manfredi, P., Perc, M., Perra, N., Salathé, M., Zhao, D.: Statistical physics of vaccination. *Phys. Rep.* **664**, 1–113 (2016)
38. Boguña, M., Castellano, C., Pastor-Satorras, R.: Nature of the epidemic threshold for the susceptible-infected-susceptible dynamics in networks. *Phys. Rev. Lett.* **111**, 068701 (2013)
39. Rizzo, A., Frasca, M., Porfiri, M.: Effect of individual behavior on epidemic spreading in activity driven networks. *Phys. Rev. E* **90**, 042801 (2014)
40. Zino, L., Rizzo, A., Porfiri, M.: Continuous-time discrete-distribution theory for activity-driven networks. *Phys. Rev. Lett.* **117**(22), 228302 (2016)
41. Pozzana, I., Sun, K., Perra, N.: Epidemic spreading on activity-driven networks with attractiveness. *Phys. Rev. E* **96**(4), 042310 (2017)
42. Valdano, E., Ferreri, L., Poletto, C., Colizza, V.: Analytical computation of the epidemic threshold on temporal networks. *Phys. Rev. X* **5**(2), 021005 (2015)
43. Prakash, B.A., Tong, H., Valler, M., Faloutsos, M.: Virus propagation on time-varying networks: theory and immunization algorithms. *Mach. Learn. Knowl. Discovery Databases Lect. Notes Comput. Sci.* **6323**, 99–114 (2010)
44. Tizzani, M., Lenti, S., Ubaldi, E., Vezzani, A., Castellano, C., Burioni, R.: Epidemic spreading and aging in temporal networks with memory. *Phys. Rev. E* **98**(6), 062315 (2018)
45. Sun, K., Baronchelli, A., Perra, N.: Contrasting effects of strong ties on sir and sis processes in temporal networks. *Eur. Phys. J. B* **88**(12), 1–8 (2015)

Supracentrality Analysis of Temporal Networks with Directed Interlayer Coupling



Dane Taylor, Mason A. Porter, and Peter J. Mucha

1 Introduction

Quantifying the importances of nodes through the calculation of ‘centrality’ measures is a central topic in the study of networks [1]. It is important in numerous and diverse applications, including identification of influential people [2–5], ranking web pages in searches [6–8], ranking teams and individual athletes in sports [9–11], identification of critical infrastructures that are susceptible to congestion or failure [12, 13], quantifying impactful judicial documents [14–16] and scientific publications [17], revealing drug targets in biological systems [18], and much more.

Because most networks change in time [19–21], there is much interest in extending centralities to temporal networks [22]. Past efforts have generalized quantities such as betweenness centrality [23–27], closeness centrality [23–25, 28], Bonacich and Katz centrality [29, 30], win/lose centrality [31], communicability [27, 32–36], dynamic sensitivity [37], coverage centrality [38], PageRank [39–43], and eigenvector centrality [44–46]. A common feature of these extensions is that they illustrate the importance of using methods that are designed explicitly for temporal networks, as opposed to various alternatives: aggregating a temporal network into a single ‘time-independent’ network; independently analyzing the temporal network at different instances in time; or binning the temporal network

D. Taylor (✉)

University at Buffalo, State University of New York, Buffalo, NY, USA

e-mail: danet@buffalo.edu

M. A. Porter

University of California, Los Angeles, CA, USA

e-mail: mason@math.ucla.edu

P. J. Mucha

University of North Carolina, Chapel Hill, NC, USA

e-mail: muchap@unc.edu

into time windows and analyzing those windows independently. In the first case, it is not even possible to study centrality trajectories (i.e., how centrality changes over time).

Because one can derive many centralities by studying walks on a network, some of the above temporal generalizations of centrality involve the analysis of so-called ‘time-respecting paths’ [47, 48]. There are multiple ways to define a time-respecting path, including the possibility of allowing multiple edge traversals per time step for a discrete-time temporal network. There are also multiple ways to quantify the length of a time-respecting path [25], because such a path can describe the number of edges that are traversed by a path, latency between the initial and terminal times of a path, or a combination of these ideas. In particular, it is necessary to make choices even to define a notion of a ‘shortest path’ (from which one can formulate several types of centrality). Consequently, some of the diversity in the various temporal generalizations of centrality measures arises from the diversity in defining and measuring the length of a time-respecting path.

In the present work, we examine a notion *supracentrality* [49, 50], which one can calculate by representing a temporal network as a sequence of network layers and coupling those layers to form a multilayer network (specifically, a multiplex network [51, 52]). See Fig. 1 for illustrative examples. The sequence of network layers, which constitute *time layers*, can represent a discrete-time temporal network at different time instances or a continuous-time network in which one bins (i.e., aggregates [53]) the network’s edges to form a sequence of time windows with interactions in each window. This approach is motivated by the use of a multiplex-network representation to detect communities in temporal networks through maximization of multilayer modularity [54–57]. We note in passing that there is also widespread interest in generalizing centrality measures to multilayer networks more generally [58–74].

Our supracentrality framework generalizes a family of centralities for time-independent networks called *eigenvector-based* centralities, which are defined by the property of calculating centralities as the entries of an eigenvector (the so-called ‘dominant’ eigenvector) that corresponds to the largest-magnitude eigenvalue (the ‘dominant’ eigenvalue) of a *centrality matrix* $C(\mathbf{A})$, which one defines by some function of a network adjacency matrix \mathbf{A} . Different choices for the centrality matrix recover some of the most popular centrality measures, including eigenvector centrality (by using $C(\mathbf{A}) = \mathbf{A}$) [2], hub and authority scores (by using $C(\mathbf{A}) = \mathbf{A}\mathbf{A}^T$ for hubs and $\mathbf{A}^T\mathbf{A}$ for authorities) [8], and PageRank [7] (see Sect. 2.2). Given a discrete-time temporal network in the form of a sequence of adjacency matrices $\mathbf{A}^{(t)} \in \mathbb{R}^{N \times N}$ for $t \in \{1, \dots, T\}$, where $A_{ij}^{(t)}$ denotes a directed edge from entity i to entity j in time layer t , examining supracentralities involves two steps:

1. Construct a supracentrality matrix $\mathbb{C}(\omega)$, which couples centrality matrices $C(\mathbf{A}^{(t)})$ of the individual time layers $t = 1, t = 2, t = 3, \dots$
2. Compute and interpret the dominant eigenvector of $\mathbb{C}(\omega)$.

For a temporal network with N nodes and T time layers, $\mathbb{C}(\omega)$ is a square matrix of size $NT \times NT$. We require the set of nodes to be the same for all time layers.

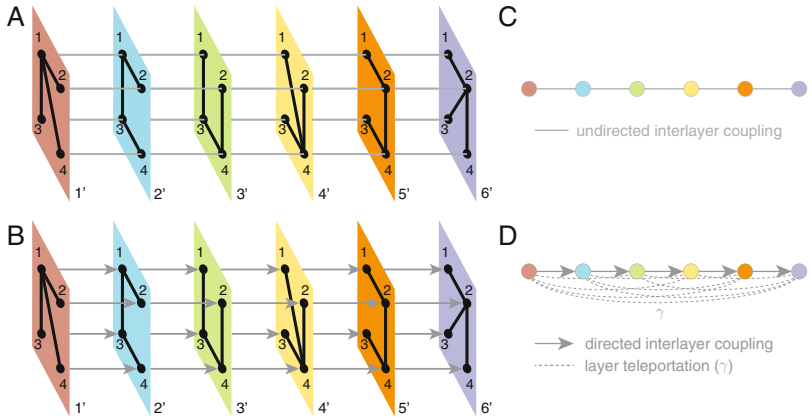


Fig. 1 Multiplex-network representations of a discrete-time temporal network. Given a temporal network with $N = 4$ nodes and $T = 6$ times, we represent the network at each time by a ‘time layer’ with adjacency matrix $\mathbf{A}^{(t)} \in \mathbb{R}^{N \times N}$ for $t \in \{1, \dots, T\}$. (a, b) We represent the network as a multiplex network by coupling the layers with ‘interlayer edges’ (gray edges) that we encode in an interlayer-adjacency matrix $\tilde{\mathbf{A}} \in \mathbb{R}^{T \times T}$. Panel (a) illustrates interlayer coupling in the form of an undirected chain, and panel (b) depicts directed coupling between layers. In panels (c) and (d), we show visualizations of the networks that are associated with $\tilde{\mathbf{A}}$ for panels (a) and (b), respectively. In panel (d), there are directed interlayer edges between consecutive time layers, so these interlayer edges respect the direction of time. Additionally, we construct connections of weight $\gamma > 0$ between corresponding nodes from all pairs of layers to ensure that $\tilde{\mathbf{A}}$ corresponds to a strongly connected network, which in turn ensures that the centralities are positive and unique. By analogy to ‘node teleportation’ in PageRank [75], we refer to this coupling as ‘layer teleportation’

However, it is easy to accommodate the appearance and disappearance of nodes by including extra instances of the entities in layers in which they otherwise do not appear (but without including any associated intralayer edges). The parameter ω scales the weights of the interlayer coupling to control the strength of the connection between time layers. It thus provides a ‘tuning knob’ to control how rapidly centrality trajectories can change over time.

An important aspect of the first step is that one must choose a topology to couple layers to each other. To do this, we define an interlayer-adjacency matrix $\tilde{\mathbf{A}} \in \mathbb{R}^{T \times T}$, where the entry $\tilde{A}_{tt'}$ encodes the coupling from time layer t to time layer t' . In Fig. 1, we illustrate two possible choices for coupling the time layers. In the upper row, $\tilde{\mathbf{A}} \in \mathbb{R}^{T \times T}$ encodes an undirected chain, which couples the time layers with *adjacent-in-time* coupling but neglects the directionality of time. In the lower row, by contrast, we couple the time layers with a directed chain that reflects the directionality of time. In addition to the directed, time-respecting edges, Fig. 1(d) also illustrates that we include weighted, undirected edges between corresponding nodes in all pairs of layers. This implements ‘layer teleportation’, which is akin to the well-known ‘node teleportation’ of the PageRank algorithm [75]. Similar to the motivation for node teleportation, layer teleportation ensures that supracentralities are well-behaved (specifically, that they are positive and unique).

The second step of our supracentrality framework involves studying the dominant right eigenvector of the supracentrality matrix $\mathbb{C}(\omega)$, which characterizes the *joint centrality* of each node-layer pair (i, t) —that is, the centrality of node i in time layer t —and thus reflects the importances of both node i and layer t . From the joint centralities, one can calculate *marginal centralities* for only the nodes (or only the time layers). One can also calculate *conditional centralities* that measure a node’s centrality at time t relative only to the other nodes’ centralities in that particular time layer t . These concepts, which are inspired by ideas from probability theory, allow one to develop a rich characterization for how node centralities change over time.

In this chapter, we describe the supracentrality framework that we developed in [49, 50] and extend these papers with further numerical explorations of how interlayer coupling topology affects supracentralities. We apply this approach to a data set, which we studied in [49] and is available at [76], that encodes the graduation and hiring of Ph.D. recipients between mathematical-sciences doctoral programs in the United States. We focus our attention on five top universities and examine how they are affected by the value of ω and the choice of $\tilde{\mathbf{A}}$. Specifically, we compare the two strategies for interlayer coupling in Fig. 1, and we explore the effect of reversing the directions of all directed edges. Our experiments reveal how to use ω and $\tilde{\mathbf{A}}$ to tune the extent to which centrality trajectories of nodes are influenced by the oldest time layers, the newest time layers, and the direction of time.

2 Background Information

We now give some background information on multiplex networks and eigenvector-based centralities. Our supracentrality framework involves representing a temporal network as a multiplex network (see Sect. 2.1). In Sect. 2.2, we review eigenvector-based centrality measures.

2.1 Analysis of Temporal Networks with Multiplex-Network Representations

We study discrete-time temporal networks, for which we provide a formal definition.

Definition 1 (Discrete-Time Temporal Network) A *discrete-time temporal network* consists of a set $\mathcal{V} = \{1, \dots, N\}$ of nodes and sets $\mathcal{E}^{(t)}$ of weighted edges that we index (using t) in a sequence of network layers. We denote such a network either as $\mathcal{G}(\mathcal{V}, \{\mathcal{E}^{(t)}\})$ or by the sequence $\{\mathbf{A}^{(t)}\}$ of adjacency matrices, where $A_{ij}^{(t)} = w_{ij}^t$ if $(i, j, w_{ij}^t) \in \mathcal{E}^{(t)}$ and $A_{ij}^{(t)} = 0$ otherwise.

As we illustrated in Fig. 1, we represent a discrete-time temporal network as a multiplex network with weighted and possibly directed coupling between the time layers. We restrict our attention to the following type of multiplex network.

Definition 2 (Uniformly and Diagonally Coupled (i.e., Layer-Coupled) Multiplex Network) Let $\mathcal{G}(\mathcal{V}, \{\mathcal{E}^{(t)}\}, \tilde{\mathcal{E}})$ be a T -layer multilayer network with node set $\mathcal{V} = \{1, \dots, N\}$ and interactions between node-layer pairs that are encoded by the sets $\{\mathcal{E}^{(t)}\}$ of weighted edges, where $(i, j, w_{ij}^t) \in \mathcal{E}^{(t)}$ if and only if there is an edge (i, j) with weight w_{ij}^t in layer t . The set $\tilde{\mathcal{E}} = \{(s, t, \tilde{w}_{st})\}$ encodes the topology and weights for coupling separate instantiations of the same node between a pair $(s, t) \in \{1, \dots, T\} \times \{1, \dots, T\}$ of layers. Equivalently, one can encode a multiplex network as a set $\{\mathbf{A}^{(t)}\}$ of adjacency matrices, such that $A_{ij}^{(t)} = w_{ij}^t$ if $(i, j, w_{ij}^t) \in \mathcal{E}^{(t)}$ and $A_{ij}^{(t)} = 0$ otherwise, along with an interlayer-adjacency matrix $\tilde{\mathbf{A}}$ with entries $\tilde{A}_{st} = \tilde{w}_{st}$ if $(s, t, \tilde{w}_{st}) \in \tilde{\mathcal{E}}$ and $\tilde{A}_{st}^{(t)} = 0$ otherwise.

The coupling in Definition 2 is ‘diagonal’ in that the only interlayer edges are ones that couple a node in one layer with that same node in another layer. It is ‘uniform’ in that the coupling between two layers is identical for all nodes in those two layers. A multilayer network with both conditions is called ‘layer-coupled’ [51].

As we illustrate in Fig. 1, we focus our attention on two choices for coupling time layers:

(A) $\tilde{\mathbf{A}}$ encodes an undirected chain:

$$\tilde{A}_{tt'} = \begin{cases} 1, & |t' - t| = 1, \\ 0, & \text{otherwise;} \end{cases} \quad (1)$$

(B) $\tilde{\mathbf{A}}$ encodes a directed chain with layer teleportation:

$$\tilde{A}_{tt'} = \begin{cases} 1 + \gamma, & t' - t = 1, \\ \gamma, & \text{otherwise,} \end{cases} \quad (2)$$

where $\gamma > 0$ is the *layer-teleportation probability*. In Sect. 4, we compare the effects on centrality trajectories of these two choices for $\tilde{\mathbf{A}}$.

2.2 Eigenvector-Based Centrality for Time-Independent Networks

Arguably the most notable—and certainly the most profitable—type of centrality is PageRank, which provided the mathematical foundation for the birth of the web-search algorithm of the technology giant Google [6, 7, 75]. PageRank quantifies the importances of nodes in a network (e.g., a directed network that encodes hyperlinks between web pages) by computing the dominant eigenvector of the ‘PageRank matrix’ (or ‘Google matrix’ [77])

$$\mathbf{C}^{(PR)} = \sigma \mathbf{A}^T \mathbf{D}^{-1} + (1 - \sigma) N^{-1} \mathbf{1} \mathbf{1}^T, \quad (3)$$

where N is the number of nodes, $\mathbf{1} = [1, \dots, 1]^T$ is a length- N vector of ones, and \mathbf{A} is an adjacency matrix in which each entry A_{ij} encodes a directed (and possibly weighted) edge from node i to node j . The matrix $\mathbf{D} = \text{diag}[d_1^{\text{out}}, \dots, d_N^{\text{out}}]$ is a diagonal matrix that encodes the node out-degrees $d_i^{\text{out}} = \sum_j A_{ij}$.

The PageRank matrix's dominant right eigenvector is a natural choice for ranking nodes, as it encodes a random walk's stationary distribution (which estimates the fraction of web surfers on each web page in the context of a web-search engine¹). The term $\mathbf{A}^T \mathbf{D}^{-1}$ is a transition matrix that operates on column vectors that encode the densities of random walkers [78]. The term $N^{-1} \mathbf{1} \mathbf{1}^T$ is a *teleportation matrix*; it represents a transition matrix in a network with uniform all-to-all coupling between nodes. The *teleportation parameter* $\sigma \in (0, 1)$ implements a linear superposition of the two transition matrices and yields an irreducible matrix, even when the transition matrix $\mathbf{A}^T \mathbf{D}^{-1}$ is reducible. Because we introduced the concept of layer teleportation in Sect. 2.1, we henceforth refer to the traditional teleportation in PageRank as ‘node teleportation’.

It is common to define the PageRank matrix as the transpose of Eq. (3); in that case, one computes the dominant left eigenvector instead of the dominant right one. However, we use the right-eigenvector convention to be consistent with a broader class of centrality measures called ‘eigenvector-based centralities’, in which one encodes node importances in the elements of the dominant eigenvector of some centrality matrix. In addition to PageRank, prominent examples of eigenvector-based centralities include (vanilla) eigenvector centrality [2] and hub and authority (i.e., HITS) centralities [8]. We now provide formal definitions.

Definition 3 (Eigenvector-Based Centrality) Let $\mathbf{C} = C(\mathbf{A})$ be a centrality matrix, which we obtain from some function $C : \mathbb{R}^{N \times N} \mapsto \mathbb{R}^{N \times N}$ of the adjacency matrix \mathbf{A} , of a network $\mathcal{G}(\mathcal{V}, \mathcal{E})$. Consider the dominant right eigenvector \mathbf{u} , which satisfies

$$\mathbf{Cu} = \lambda_{\max} \mathbf{u}, \quad (4)$$

where $\lambda_{\max} \in \mathbb{R}_+$ is the largest eigenvalue of \mathbf{C} . (Note that this eigenvalue is guaranteed to be positive.) The i th entry u_i specifies the *eigenvector-based centrality* of node $i \in \mathcal{V}$ that is associated with the function C .

Definition 4 (PageRank [7, 75]) When \mathbf{C} is given by Eq. (3), we say that Eq. (4) yields *PageRank* centralities $\{u_i^{(\text{PR})}\}$.

Remark 1 It is also common to compute PageRank centralities from a left eigenvector [75]. In the present paper, we use a right-eigenvector formulation to be consistent with the other eigenvector-based centralities. One can recover the other formulation by taking the transpose of Eq. (4).

¹Note that PageRank has had intellectual impact well beyond web searches [75].

3 Supracentrality Framework

We now describe the supracentrality framework that we presented in [50]. The present formulation generalizes our formulation of supracentrality from [49] that required interlayer coupling to take the form of an undirected chain. (See the top row of Fig. 1.) To aid our presentation, we summarize our mathematical notation in Table 1.

3.1 Supracentrality Matrices

We first describe a supracentrality matrix from [50].

Definition 5 (Supracentrality Matrix) Let $\{\mathbf{C}^{(t)}\}$ be a set of T centrality matrices for a discrete-time temporal network with a common set $\mathcal{V} = \{1, \dots, N\}$ of nodes; and assume that $C_{ij}^{(t)} \geq 0$. Let $\tilde{\mathbf{A}}$, with entries $\tilde{A}_{ij} \geq 0$, be a $T \times T$ interlayer-adjacency matrix that encodes the interlayer couplings. We define a family of *supracentrality matrices* $\mathbb{C}(\omega)$, which are parameterized by the interlayer-coupling strength $\omega \geq 0$, of the form

$$\mathbb{C}(\omega) = \hat{\mathbf{C}} + \omega \hat{\mathbb{A}} = \begin{bmatrix} \mathbf{C}^{(1)} & \mathbf{0} & \mathbf{0} & \dots \\ \mathbf{0} & \mathbf{C}^{(2)} & \mathbf{0} & \dots \\ \mathbf{0} & \mathbf{0} & \mathbf{C}^{(3)} & \ddots \\ \vdots & \vdots & \ddots & \ddots \end{bmatrix} + \omega \begin{bmatrix} \tilde{A}_{11}\mathbf{I} & \tilde{A}_{12}\mathbf{I} & \tilde{A}_{13}\mathbf{I} & \dots \\ \tilde{A}_{21}\mathbf{I} & \tilde{A}_{22}\mathbf{I} & \tilde{A}_{23}\mathbf{I} & \dots \\ \tilde{A}_{31}\mathbf{I} & \tilde{A}_{32}\mathbf{I} & \tilde{A}_{33}\mathbf{I} & \dots \\ \vdots & \vdots & \vdots & \ddots \end{bmatrix}, \quad (5)$$

where $\hat{\mathbf{C}} = \text{diag}[\mathbf{C}^{(1)}, \dots, \mathbf{C}^{(T)}]$ and $\hat{\mathbb{A}} = \tilde{\mathbf{A}} \otimes \mathbf{I}$ is the Kronecker product of $\tilde{\mathbf{A}}$ and \mathbf{I} .

Table 1 Summary of our mathematical notation for objects with different dimensions

Typeface	Class	Dimension
\mathbb{M}	Matrix	$NT \times NT$
\mathbf{M}	Matrix	$N \times N$
M	Matrix	$T \times T$
\mathbf{v}	Vector	$NT \times 1$
\mathbf{v}	Vector	$N \times 1$
\mathbf{v}	Vector	$T \times 1$
M_{ij}	Scalar	1
v_i	Scalar	1

For layer t , the matrix $\mathbf{C}^{(t)}$ can represent any matrix whose dominant eigenvector is of interest. In our discussion, we focus on PageRank (see Definition 4), but one can alternatively choose eigenvector centrality [2], hub and authority centralities [8], or something else.

The $NT \times NT$ supracentrality matrix $\mathbb{C}(\omega)$ encodes the effects of two distinct types of connections: the layer-specific centrality entries $\{C_{ij}^{(t)}\}$ in the diagonal blocks relate centralities between nodes in layer t ; and entries in the off-diagonal blocks encode coupling between layers. The matrix $\hat{\mathbf{A}} = \tilde{\mathbf{A}} \otimes \mathbf{I}$ implements uniform and diagonal coupling. The matrix \mathbf{I} encodes diagonal coupling; and any two layers t and t' are uniformly coupled, because all interlayer edges between them have the identical weight $\omega \tilde{A}_{tt'}$.

3.2 Joint, Marginal, and Conditional Centralities

As we indicated earlier, we study the dominant right eigenvalue equation for supracentrality matrices. That is, we solve the eigenvalue equation

$$\mathbb{C}(\omega)\mathbf{v}(\omega) = \lambda_{\max}(\omega)\mathbf{v}(\omega), \quad (6)$$

and we interpret entries in the dominant right eigenvector $\mathbf{v}(\omega)$ as scores that measure the importances of node-layer pairs $\{(i, t)\}$. Because the vector $\mathbf{v}(\omega)$ has a block form—its first N entries encode the joint centralities for layer $t = 1$, its next N entries encode the joint centralities for layer $t = 2$, and so on—it is useful to reshape $\mathbf{v}(\omega)$ into a matrix.

Definition 6 (Joint Centrality of a Node-Layer Pair [49]) Let $\mathbb{C}(\omega)$ be a supracentrality matrix given by Definition 5, and let $\mathbf{v}(\omega)$ be its dominant right eigenvector. We encode the *joint centrality* of node i in layer t via the $N \times T$ matrix $\mathbf{W}(\omega)$ with entries

$$W_{it}(\omega) = \mathbf{v}_{N(t-1)+i}(\omega). \quad (7)$$

We refer to $W_{it}(\omega)$ as a ‘joint centrality’ because it reflects the importance both of node i and of layer t .

Definition 7 (Marginal Centralities of Nodes and Layers [49]) Let $\mathbf{W}(\omega)$ encode the joint centralities given by Definition 6. We define the *marginal layer centrality* (MLC) and *marginal node centrality* (MNC), respectively, by

$$\begin{aligned} x_t(\omega) &= \sum_i W_{it}(\omega), \\ \hat{x}_i(\omega) &= \sum_t W_{it}(\omega). \end{aligned} \quad (8)$$

Definition 8 (Conditional Centralities of Nodes and Layers [49]) Let $\{W_{it}(\omega)\}$ be the joint centralities given by Definition 6; and let $\{x_t(\omega)\}$ and $\{\hat{x}_i(\omega)\}$, respectively, be the marginal layer and node centralities given by Definition 7. We define the *conditional centralities* of nodes and layers by

$$\begin{aligned} Z_{it}(\omega) &= W_{it}(\omega)/x_t(\omega), \\ \hat{Z}_{it}(\omega) &= W_{it}(\omega)/\hat{x}_i(\omega), \end{aligned} \quad (9)$$

where $Z_{it}(\omega)$ gives the centrality of node i conditioned on layer t and $\hat{Z}_{it}(\omega)$ gives the centrality of layer t conditioned on node i . The quantity $Z_{it}(\omega)$ indicates the importance of node i relative just to the other nodes in layer t .

We ensure that the supracentralities are well-defined (i.e., unique, positive, and finite) with the following theorem.

Theorem 1 (Uniqueness and Positivity of Supracentralities [50]) Let $\mathbb{C}(\omega)$ be a supracentrality matrix given by Eq. (5). Additionally, suppose that $\tilde{\mathbf{A}}$ is an adjacency matrix for a strongly connected graph and that $\sum_t \mathbf{C}^{(t)}$ is an irreducible, nonnegative matrix. It then follows that $\mathbb{C}(\omega)$ is irreducible, nonnegative, and has a simple largest positive eigenvalue $\lambda_{\max}(\omega)$, with corresponding left eigenvector $\mathbf{u}(\omega)$ and right eigenvector $\mathbf{v}(\omega)$ that are each unique and positive. The centralities $\{W_{it}(\omega)\}$, $\{x_t(\omega)\}$, $\{\hat{x}_i(\omega)\}$, $\{Z_{it}(\omega)\}$, and $\{\hat{Z}_{it}(\omega)\}$ are then positive and finite. If we also assume that $\mathbb{C}(\omega)$ is aperiodic, it follows that $\lambda_{\max}(\omega)$ is a unique dominant eigenvalue.

In Fig. 2, we show the joint and marginal centralities for the network in panel (a) of Fig. 1. We have normalized the vector $\mathbf{v}(\omega)$ using the 1-norm.

	layer index							
	1	2	3	4	5	6	MNC	
node index	1	0.0305	0.0461	0.0493	0.0460	0.0360	0.0195	0.2272
	2	0.0198	0.0368	0.0480	0.0501	0.0471	0.0308	0.2326
	3	0.0249	0.0491	0.0592	0.0520	0.0402	0.0212	0.2466
	4	0.0238	0.0465	0.0660	0.0744	0.0552	0.0275	0.2935
MLC	0.0990	0.1784	0.2225	0.2225	0.1784	0.0990		

Fig. 2 Joint centralities $\{W_{it}(\omega)\}$ of Definition 6 (white cells), with corresponding marginal layer centralities (MLC) $\{x_t(\omega)\}$ and marginal node centralities (MNC) $\{\hat{x}_i(\omega)\}$ from Definition 7 (gray cells), for the network in panel (a) of Fig. 1 with $\omega = 1$. The centrality matrices of the layers are PageRank centrality matrices (see Eq. (3)) with a node-teleportation parameter of $\sigma = 0.85$

4 Application to a Ph.D. Exchange Network

We apply our supracentrality framework to study centrality trajectories for a temporal network that encodes the graduation and hiring of mathematicians between $N = 231$ mathematical-sciences doctoral programs in the United States during the years {1946, ..., 2010} [49]. Each edge $A_{ij}^{(t)}$ in the temporal network encodes the number of Ph.D. recipients who graduated from university j in year t and subsequently supervised a Ph.D. student at university i . The edge directions, where $A_{ij}^{(t)}$ is an edge from university i to university j , point in the opposite direction to the flow of people who earn their Ph.D. degrees. We define edge directions in this way to indicate that university i effectively selects the output of university j when they hire someone who received their Ph.D. from j [79–81]. With this convention for the direction of edges, $\{\mathbf{C}^{(t)}\}$ encodes the PageRank matrices of the layers; and the highest-ranking universities are the ones that are good sources for the flow of Ph.D. recipients. The network, which we constructed using data from the Mathematics Genealogy Project [82], is available at [76].

We focus our discussion on five U.S. universities: Harvard, Massachusetts Institute of Technology (MIT), Princeton, Stanford, and University of California at Berkeley. They have the largest PageRank centralities (using a node-teleportation parameter of $\sigma = 0.85$) for a temporally aggregated network with adjacency matrix $\sum_t \mathbf{A}^{(t)}$. In all of our experiments, we assume that the layers' centrality matrices are given by PageRank matrices, as defined in Eq. (3). As in our previous explorations [49, 50], we vary the interlayer coupling strength ω to adjust how rapidly centralities change over time. In the present work, our primary focus is investigating the effects on supracentralities of undirected and directed interlayer coupling. See Eqs. (1) and (2) for the definitions of these interlayer-coupling schemes; see Fig. 1 for visualizations of these two types of interlayer coupling.

We first consider undirected interlayer coupling, so we define $\tilde{\mathbf{A}}$ by Eq. (1). In Fig. 3, we plot the joint and conditional centralities for the five universities. The columns show results for interlayer-coupling strengths $\omega \in \{1, 10, 10^2, 10^3\}$. In the bottom row, we see that progressively larger values of ω yield progressively smoother conditional-centrality trajectories. In the top row, we observe that as one increases ω , the joint centrality appears to limit to one arc of a sinusoidal curve. We prove this result in Sect. 5. The most striking results occur in the bottom row of the third column. Based on conditional node centrality, we see that MIT becomes the top-ranked university in the 1950s and then remains so in our data set. Stanford and UC Berkeley develop gradually larger conditional centralities over the 64 years in the data set, whereas those of Princeton and Harvard decrease gradually over this period. When considering all universities, these five universities have conditional node centralities in the top-10 values throughout all years of the data set. This is consistent with our results in [49, 50].

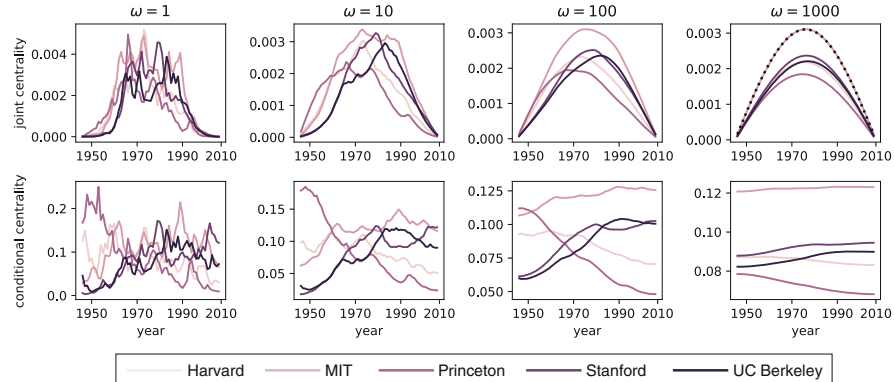


Fig. 3 Trajectories of node centralities using undirected interlayer coupling for mathematical-sciences Ph.D. programs at five top universities. The top and bottom rows illustrate joint and conditional node centralities, respectively, that we compute with centrality matrices based on PageRank with a node-teleportation parameter of $\sigma = 0.85$ and undirected interlayer coupling \tilde{A} given by Eq. (1) with $\omega \in \{1, 10, 100, 1000\}$. The dotted black curve in the rightmost top panel is the result of an asymptotic approximation that we present in Sect. 5

We now examine directed interlayer coupling, and we take \tilde{A} to correspond to a directed chain with layer teleportation. See Eq. (2) for the specific formula and the bottom row of Fig. 1 for an associated visualization. In each panel of Fig. 4, we plot the joint centralities and conditional node centralities. The columns give results for interlayer coupling strengths of $\omega \in \{0.1, 1, 10, 100\}$, and the three panels indicate different choices for the layer-teleportation probabilities: (a) $\gamma = 0.0001$; (b) $\gamma = 0.001$; and (c) $\gamma = 0.01$. The dotted black curves in the rightmost column indicate large- ω asymptotic approximations that we will present in Sect. 5.

To understand the main effect of directed interlayer coupling, we first compare the joint centralities in Fig. 4 to those in Fig. 3. To help our discussion, we focus on the rightmost column of both figures. Comparing Fig. 4 to Fig. 3, we observe that the joint-centrality trajectories tend to decay with time for directed interlayer coupling, whereas they are peaked and attain their largest values near $t = 1978$ for undirected interlayer coupling. Therefore, directed interlayer coupling tends to “boost” the joint centralities of earlier time layers in comparison to undirected coupling. Comparing panels (a)–(c) of Fig. 4 (and again focusing on the rightmost column), we observe that the rate of decay is fastest for $\gamma = 0.0001$ (panel (a)) and slowest for $\gamma = 0.01$ (panel (c)).

The conditional centralities are also affected by directed interlayer coupling. Consider $\omega = 10$ in Fig. 3, and observe that the conditional centrality of Princeton decreases monotonically in time. By contrast, observe in Fig. 4(a, b) for $\omega = 10$ that the conditional centrality of Princeton now decreases between $t = 1946$ and about $t = 1988$, but then it increases.

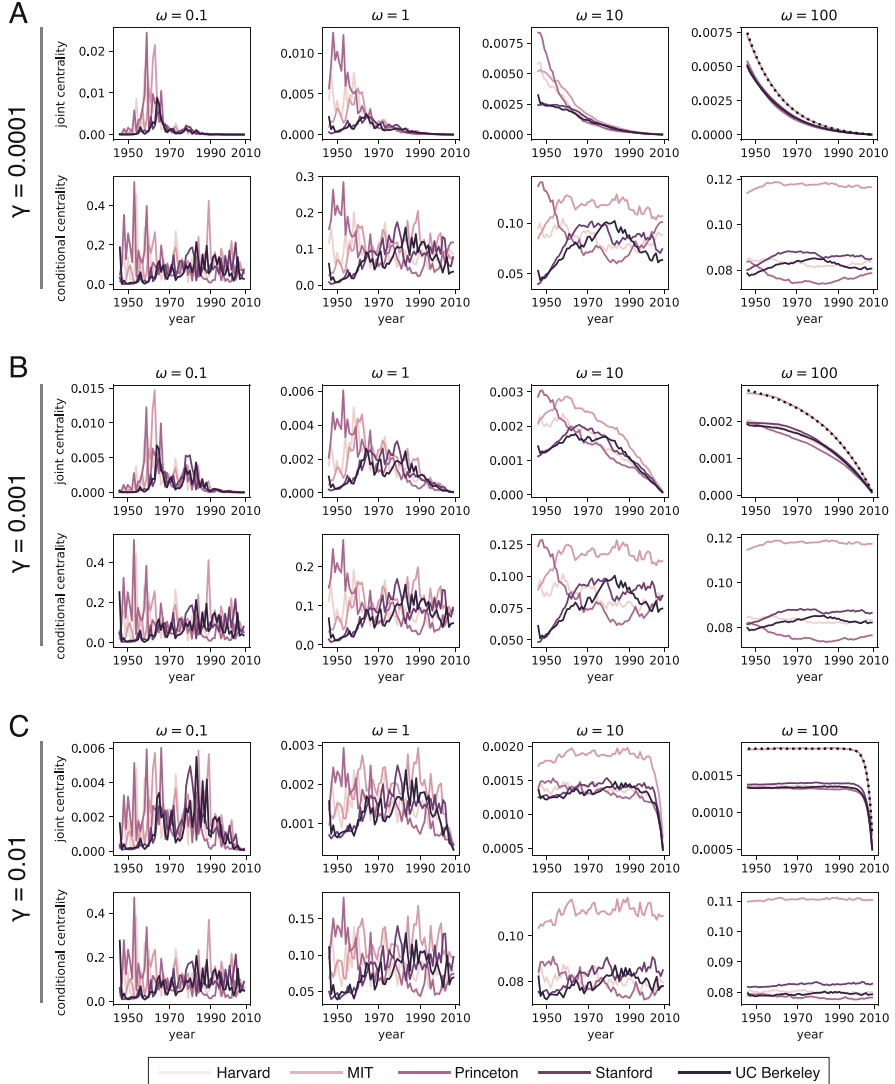


Fig. 4 Trajectories of node centralities using directed interlayer coupling for mathematical-sciences Ph.D. programs at five top universities. This figure is similar to Fig. 3, except that the interlayer-adjacency matrix \tilde{A} is now given by Eq. (2), which corresponds to a directed chain with layer teleportation with rate γ . Panels (a), (b), and (c) show results for $\gamma = 0.0001$, $\gamma = 0.001$, and $\gamma = 0.01$, respectively. The dotted black curves in the rightmost top subpanels of panels (a)–(c) are the result of an asymptotic approximation that we present in Sect. 5. For sufficiently large ω and sufficiently small γ , observe that the joint centralities decrease with time

For our last experiment, we examine how reversing the direction of interlayer edges changes the results of our supracentrality calculations. Specifically, we repeat the previous experiment with directed interlayer edges, except that now we set $\tilde{\mathbf{A}}$ to be the transpose of the matrix that we defined by Eq. (2). One motivation is that for some applications, the most recent time layers are more important than the earliest time layers. One can incorporate this idea into our supracentrality framework by reversing the direction of interlayer edges. In Fig. 5, we plot the same quantities as in Fig. 4, except that now we take the directed interlayer edges to have the opposite direction (so we have reversed the arrow of time). Observe that the joint centralities now tend to increase with time, as opposed to Fig. 4, where they tended to decrease with time. These trends are most evident in the rightmost columns. We also observe differences for the conditional centralities. For example, focusing on $\omega = 10$ in the third column of Fig. 5, we see that Princeton never has the largest conditional centrality. By contrast, for $\omega = 10$ in Figs. 3 and 4(a, b), Princeton has the largest conditional centrality for the earliest time steps (specifically, for $t \in \{1946, \dots, 1954\}$).

Understanding how the weights, topologies, and directions of interlayer coupling affect supracentralities is essential to successfully deploying supracentrality analysis to reveal meaningful insights. The above experiments highlight that one can tune the weights and topology of interlayer coupling to emphasize either earlier or later time layers. Specifically, one can adjust the parameters ω and γ , as well as the direction of interlayer edges, to cater a study to particular data sets and particular research questions. In our investigation in this section, we considered both the case in which \mathbf{A} is given by Eq. (2) and that in which it is given by the transpose of the matrix that we determine from Eq. (2). It is worth considering how these different choices of interlayer edge directions are represented in the supracentrality matrix $\mathbb{C}(\omega)$ and the consequences of these choices. Specifically, each layer's PageRank matrix $\mathbf{C}^{(t)}$ is defined in Eq. (3) using the transpose of the layer's adjacency matrix $\mathbf{A}^{(t)}$, yet when coupling the centrality matrices, we do not take the transpose of $\tilde{\mathbf{A}}$ when defining $\mathbb{C}(\omega)$ in Eq. (5). Accordingly, one may worry that the matrix $\mathbb{C}(\omega)$ effectively acts in the forward direction for the intralayer edges, but in the opposite direction for the interlayer edges. However, this does not lead to any inherent contradiction, as the meanings of the directions in these two types of edges are fundamentally different: the direction of intralayer edges dictates the flow of random walkers, whereas the direction of interlayer edges couples the centralities of the different layers. In other applications, it may be necessary to encode the directions of the interlayer and intralayer edges in the same way, but there is no reason why one cannot encode directions of interlayer and intralayer edges in different ways in a supracentrality formalism. As we have demonstrated by considering both $\tilde{\mathbf{A}}$ and its transpose—and thus by treating the effect of the interlayer edges in opposite ways in these two calculations—both uses are meaningful. They also probe different aspects of temporal data.

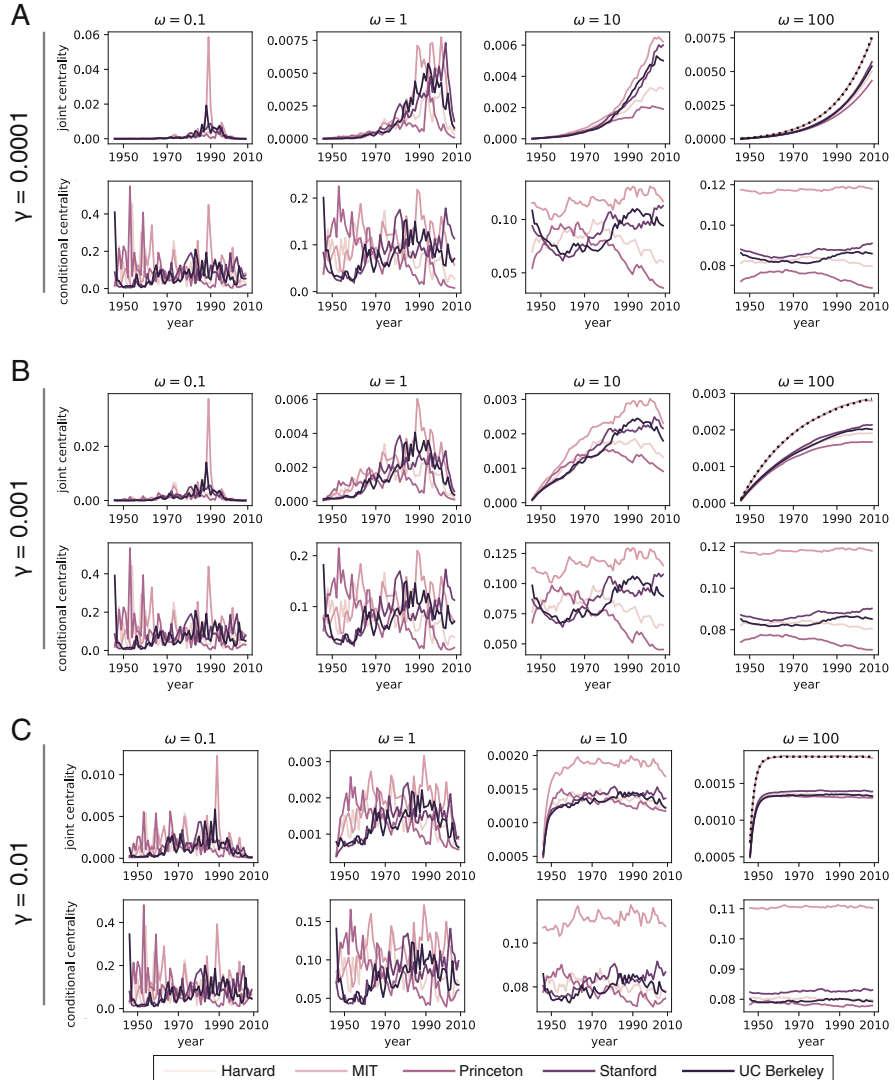


Fig. 5 Trajectories of node centralities using reversed directed interlayer coupling for mathematical-sciences Ph.D. programs at five top universities. This figure is identical to Fig. 4, except that \tilde{A} is now given by the transpose of the matrix from Eq. (2), such that the directed chain points backwards in time. For sufficiently large ω and sufficiently small γ , observe that the joint centralities now increase with time

5 Asymptotic Behavior for Small and Large Interlayer-Coupling Strength ω

In this section, we summarize the asymptotic results from [50] that reveal the behavior of supracentralities in the limit of small and large ω . In our present discussion, we focus on dominant right eigenvectors.

To motivate our asymptotic analysis, consider the top-right subpanels in each panel of Figs. 3, 4, and 5. In each of these subpanels, we plot (in dotted black curves) the results of an asymptotic analysis of the dominant right eigenvector $\tilde{\mathbf{v}}^{(1)}$ of $\tilde{\mathbf{A}}$ for the joint centrality of MIT in the limit of large ω . We observe excellent agreement with our numerical calculations. Therefore, for sufficiently large ω , one can understand the effects of both undirected and directed interlayer couplings (as encoded in an interlayer-adjacency matrix $\tilde{\mathbf{A}}$) by examining the dominant right eigenvector of $\tilde{\mathbf{A}}$. For large values of ω , this eigenvector captures the limit of the joint centralities as a function with a peak for undirected coupled (see Fig. 3), decay in time for directed coupling (see Fig. 4), and growth in time for directed coupling when reversing the arrow of time (see Fig. 5).

5.1 Layer Decoupling in the Limit of Small ω

We begin with some notation. Let $\tilde{\mu}_1$ be the dominant eigenvalue (which we assume to be simple) of $\tilde{\mathbf{A}}$, and let $\tilde{\mathbf{u}}^{(1)}$ and $\tilde{\mathbf{v}}^{(1)}$ denote its corresponding left and right eigenvectors. Given a set $\{\mathbf{C}^{(t)}\}$ of centrality matrices, we let $\mu_1^{(t)}$ be the dominant eigenvalue (which we also assume to be simple) of $\mathbf{C}^{(t)}$; and $\mathbf{u}^{(1,t)}$ and $\mathbf{v}^{(1,t)}$ are the corresponding left and right eigenvectors. Let $\{\mu_1^{(t)}\}$ denote the set of spectral radii, where $\lambda_{\max}(0) = \max_t \mu_1^{(t)}$ is the maximum eigenvalue over all layers. (Recall that $\lambda_{\max}(\omega)$ is the dominant eigenvalue of the supracentrality matrix $\mathbb{C}(\omega)$.) Let $\mathcal{P} = \{t : \mu_1^{(t)} = \lambda_{\max}(0)\}$ denote the set of layers whose centrality matrices achieve the maximum. When the layers' centrality matrices $\{\mathbf{C}^{(t)}\}$ are PageRank matrices given by Eq. (3), it follows that $\mu_1^{(t)} = 1$ for all t (i.e., $\mathcal{P} = \{1, \dots, T\}$), the corresponding left eigenvector is $\mathbf{u}^{(1,t)} = [1, \dots, 1]^T / N$, and $\mathbf{v}^{(1,t)}$ is the PageRank vector for layer t . Furthermore, for each t , we define the length- NT “block” vector $\mathbf{v}^{(1,t)} = \mathbf{e}^{(t)} \otimes \mathbf{v}^{(1,t)}$, which consists of zeros, except for block t , which equals $\mathbf{v}^{(1,t)}$. (The vector $\mathbf{e}^{(t)}$ is a length- T unit vector that consists of zeros, except for entry t , which is 1.)

We now present a theorem from [50], although we restrict our attention to the part that describes the right dominant eigenvector.

Theorem 2 (Weak-Coupling Limit of Dominant Right Eigenvectors [50]) *Let $\mathbf{v}(\omega)$ be the dominant right eigenvector of a supracentrality matrix that is normalized using the 1-norm and satisfies the assumptions of Thm. 1. Additionally, let*

$\mathcal{P} = \{t : \mu_1^{(t)} = \lambda_{\max}(0)\}$ denote the set of indices associated with the eigenvalues of $\mathbf{C}^{(t)}$ that equal the largest eigenvalue $\lambda_{\max}(0)$ of $\mathbb{C}(0)$. We assume that each layer's dominant eigenvalue $\mu_1^{(t)}$ is simple. It then follows that the $\omega \rightarrow 0^+$ limit of $\mathbf{v}(\omega)$ satisfies

$$\mathbf{v}(\omega) \rightarrow \sum_{t \in \mathcal{P}} \alpha_t \mathbf{v}^{(1,t)}, \quad (10)$$

where the vector $\boldsymbol{\alpha} = [\alpha_1, \dots, \alpha_T]^T$ has nonnegative entries and is the unique solution to the dominant eigenvalue equation

$$\mathbf{X}\boldsymbol{\alpha} = \lambda_1 \boldsymbol{\alpha}. \quad (11)$$

The eigenvalue λ_1 needs to be determined, and the entries of \mathbf{X} are

$$X_{tt'} = \tilde{A}_{t,t'} \frac{\langle \mathbf{u}^{(1,t)}, \mathbf{v}^{(1,t')} \rangle}{\langle \mathbf{u}^{(1,t)}, \mathbf{v}^{(1,t)} \rangle} \chi(t) \chi(t'), \quad (12)$$

where $\chi(t) = \sum_{t' \in \mathcal{P}} \delta_{tt'}$ is an indicator function: $\chi(t) = 1$ if $t \in \mathcal{P}$ and $\chi(t) = 0$ otherwise. The vector $\boldsymbol{\alpha}$ must also be normalized to ensure that the right-hand side of Eq. (10) is normalized (by setting $\|\boldsymbol{\alpha}\|_p = 1$ for normalization with a p -norm).

5.2 Layer Aggregation in the Limit of Large ω

To study the $\omega \rightarrow \infty$ limit, it is convenient to divide Eq. (6) by ω and define $\epsilon = 1/\omega$ to obtain

$$\tilde{\mathbb{C}}(\epsilon) = \epsilon \mathbb{C}(\epsilon^{-1}) = \epsilon \hat{\mathbb{C}} + \hat{\mathbb{A}}, \quad (13)$$

which has right eigenvectors $\tilde{\mathbf{v}}(\epsilon)$ that are identical to those of $\mathbb{C}(\omega)$ (specifically, $\tilde{\mathbf{v}}(\epsilon) = \mathbf{v}(\epsilon^{-1})$). Its eigenvalues $\{\tilde{\lambda}_i\}$ are scaled by ϵ , so $\tilde{\lambda}_i(\epsilon) = \epsilon \lambda_i(\epsilon^{-1})$.

Before presenting results from [50], we define a few additional concepts. Let $\tilde{\mathbf{v}}^{(1,j)} = \tilde{\mathbf{e}}^{(j)} \otimes \tilde{\mathbf{v}}^{(1)}$ denote a block vector that consists of zeros, except for block j , which equals the dominant right eigenvector $\tilde{\mathbf{v}}^{(1)}$ of $\tilde{\mathbb{A}}$. (The vector $\tilde{\mathbf{e}}^{(j)}$ is a length- N unit vector that consists of zeros, except for entry j , which is 1.) We also define the stride permutation matrix

$$[\mathbb{P}]_{kl} = \begin{cases} 1, & l = \lceil k/N \rceil + T [(k-1) \bmod N], \\ 0, & \text{otherwise}, \end{cases} \quad (14)$$

where the ceiling function $\lceil \theta \rceil$ denotes the smallest integer that is at least θ and ‘mod’ denotes the modulus function (i.e., $a \bmod b = a - b \lceil a/b - 1 \rceil$).

Theorem 3 (Strong-Coupling Limit of Dominant Eigenvectors [50]) *Let $\tilde{\mathbf{A}}$, $\tilde{\mu}_1$, $\tilde{\mathbf{u}}^{(1)}$, and $\tilde{\mathbf{v}}^{(1)}$ be defined as above, with the same assumptions as in Theorem 1. It then follows that the dominant eigenvalue $\tilde{\lambda}_{\max}(\epsilon)$ and the associated eigenvector $\tilde{\mathbf{v}}(\epsilon)$ of $\mathbb{C}(\epsilon)$ converge as $\epsilon \rightarrow 0^+$ to the following expressions:*

$$\begin{aligned}\tilde{\lambda}_{\max}(\epsilon) &\rightarrow \tilde{\mu}_1, \\ \tilde{\mathbf{v}}(\epsilon) &\rightarrow \sum_j \tilde{\alpha}_j \mathbb{P}_{\tilde{\mathbf{V}}}^{(1,j)},\end{aligned}\tag{15}$$

where the constants $\{\tilde{\alpha}_i\}$ solve the dominant eigenvalue equation

$$\tilde{\mathbf{X}}\tilde{\boldsymbol{\alpha}} = \tilde{\mu}_1\tilde{\boldsymbol{\alpha}},\tag{16}$$

with

$$\tilde{X}_{ij} = \sum_t C_{ij}^{(t)} \frac{\tilde{u}_t^{(1)} \tilde{v}_t^{(1)}}{\langle \tilde{\mathbf{u}}^{(1)}, \tilde{\mathbf{v}}^{(1)} \rangle}.\tag{17}$$

Note that we normalize the vector $\tilde{\boldsymbol{\alpha}}$ to ensure that the right-hand side of Eq. (15) is normalized.

Equation (17) indicates that the strong-coupling limit effectively aggregates the centrality matrices $\{\mathbf{C}^{(t)}\}$ across time via a weighted average, with weights that depend on the dominant left and right eigenvectors of $\tilde{\mathbf{A}}$. When $\tilde{\mathbf{A}}$ encodes an undirected chain from Eq. (1) (see the top row of Fig. 1), it follows that [49]

$$\tilde{\mathbf{X}} = \sum_t \mathbf{C}^{(t)} \frac{\sin^2\left(\frac{\pi t}{T+1}\right)}{\sum_{t=1}^T \sin^2\left(\frac{\pi t}{(T+1)}\right)}.\tag{18}$$

The dotted black curve in the top-right subpanel of Fig. 3 shows a scaled version of $\tilde{\mathbf{v}}^{(1)}$, which is defined by the normalized sinusoidal weightings in Eq. (18). The dotted black curves in the top-right subpanels of each panel of Figs. 4 and 5 also show $\tilde{\mathbf{v}}^{(1)}$ (specifically, when $\tilde{\mathbf{A}}$ is given by Eq. (2) or by the transpose of the matrix that we obtain from Eq. (2), respectively), which we scale to normalize the joint centralities.

6 Discussion

We presented a supracentrality framework to study how the importances of nodes in a temporal network change over time. Our approach involves representing a temporal sequence of networks as time layers in a multiplex network and using the

strength and topology of coupling between time layers to tune centrality trajectories. A key feature of our approach is that it simultaneously yields the centralities of all nodes at all times by computing the dominant right eigenvector of a supracentrality matrix.

Inspired by ideas from probability theory, we examined three types of eigenvector-based supracentralities:

- (i) the joint centrality for a node-layer pair (i, t) ; this captures the combined importance of node i and time layer t ;
- (ii) the marginal centrality of node i or time t ; these capture separate importances of a node or a time layer; and
- (iii) the conditional centrality of a node i at time t ; this captures the importance of a node relative only to other nodes at that particular time.

Because our approach involves analyzing the dominant eigenvector of a centrality matrix, it generalizes eigenvector-based centralities, such as PageRank, hub and authority centralities, and (vanilla) eigenvector centrality. Naturally, it is desirable to extend supracentralities to analyze networks that are both temporal and multiplex [51]. Another important generalization of centrality analysis is the study of continuous-time temporal networks and streaming network data [30, 83], and it will be insightful to extend supracentralities to such situations.

Acknowledgements We thank Petter Holme and Jari Saramäki for the invitation to write this chapter. We thank Deryl DeFord, Tina Eliassi-Rad, Des Higham, Christine Klymko, Marianne McKenzie, Scott Pauls, and Michael Schaub for fruitful conversations. DT was supported by the Simons Foundation under Award #578333. PJM was supported by the James S. McDonnell Foundation 21st Century Science Initiative—Complex Systems Scholar Award #220020315.

References

1. Newman, M.E.J.: Networks, 2nd edn. Oxford University Press, Oxford (2018)
2. Bonacich, P.: J. Math. Sociol. **2**(1), 113 (1972)
3. Faust, K.: Soc. Networks **19**(2), 157 (1997)
4. Borgatti, S.P., Jones, C., Everett, M.G.: Connections **21**(2), 27 (1998)
5. Kempe, D., Kleinberg, J., Tardos, É.: In: Proceedings of the Ninth ACM SIGKDD International Conference on Knowledge Discovery and Data Mining, pp. 137–146. ACM, New York, NY (2003)
6. Brin, S., Page, L.: In: Proceedings of the Seventh International World Wide Web Conference, pp. 107–117 (1998)
7. Page, L., Brin, S., Motwani, R., Winograd, T.: The PageRank citation ranking: bringing order to the Web. Technical Report 1999-66. Stanford InfoLab (1999)
8. Kleinberg, J.: J. ACM **46**(5), 604 (1999)
9. Callaghan, T., Porter, M.A., Mucha, P.J.: Am. Math. Mon. **114**(9), 761 (2007)
10. Saavedra, S., Powers, S., McCotter, T., Porter, M.A., Mucha, P.J.: Physica A **389**(5), 1131 (2010)
11. Chartier, T.P., Kreutzer, E., Langville, A.N., Pedings, K.E.: SIAM J. Sci. Comput. **33**(3), 1077 (2011)

12. Holme, P.: *Adv. Complex Syst.* **6**(02), 163 (2003)
13. Guimerà, R., Mossa, S., Turtschi, A., Amaral, L.A.N.: *Proc. Natl. Acad. Sci. U. S. A.* **102**(22), 7794 (2005)
14. Leicht, E.A., Clarkson, G., Shedden, K., Newman, M.E.J.: *Eur. Phys. J. B* **59**(1), 75 (2007)
15. Fowler, J.H., Johnson, T.R., Spriggs II, J.F., Jeon, S., Wahlbeck, P.J.: *Policy Anal.* **15**(3), 324 (2007)
16. Fowler, J.H., Jeon, S.: *Soc. Networks* **30**(1), 16 (2008)
17. Bergstrom, C.T., West, J.D., Wiseman, M.A.: *J. Neurosci.* **28**(45), 11433 (2008)
18. Jeong, H., Mason, S.P., Barabási, A.L., Oltvai, Z.N.: *Nature* **411**(6833), 41 (2001)
19. Holme, P., Saramäki, J.: *Phys. Rep.* **519**(3), 97 (2012)
20. Holme, P., Saramäki, J. (eds.): *Temporal Networks*. Springer-Verlag, Berlin (2013)
21. Holme, P.: *Eur. Phys. J. B* **88**(9), 234 (2015)
22. Liao, H., Mariani, M.S., Medo, M., Zhang, Y.C., Zhou, M.Y.: *Phys. Rep.* **689**, 1 (2017)
23. Tang, M.Y., Musolesi, M., Mascolo, C., Latora, V., Nicosia, V.: In: *Proceedings of the 3rd Workshop on Social Network Systems—SNS '10*, pp. 1–6 (2010)
24. Kim, H., Tang, J., Anderson, R., Mascolo, C.: *Comput. Netw.* **56**(3), 983 (2012)
25. Williams, M.J., Musolesi, M.: *R. Soc. Open Sci.* **3**(6) (2016)
26. Alsayed, A., Higham, D.J.: *Chaos, Solitons Fractals* **72**, 35 (2015)
27. Fenu, C., Higham, D.J.: *SIAM J. Matrix Anal. Appl.* **38**(2), 343 (2017)
28. Pan, R., Saramäki, J.: *Phys. Rev. E* **84**(1), 016105 (2011)
29. Lerman, K., Ghosh, R., Kang, J.H.: In: *Proceedings of the Eighth Workshop on Mining and Learning with Graphs*, pp. 70–77. ACM, New York, NY (2010)
30. Grindrod, P., Higham, D.J.: *Proc. R. Soc. A* **470**(2165), 20130835 (2014)
31. Motegi, S., Masuda, N.: *Sci. Rep.* **2**, 904 (2012)
32. Grindrod, P., Parsons, M.C., Higham, D.J., Estrada, E.: *Phys. Rev. E* **83**(4), 046120 (2011)
33. Estrada, E.: *Phys. Rev. E* **88**(4), 042811 (2013)
34. Grindrod, P., Higham, D.J.: *SIAM Rev.* **55**(1), 118 (2013)
35. Chen, I., Benzi, M., Chang, H.H., Hertzberg, V.S.: *J. Complex Networks* **5**(2), 274 (2016)
36. Arrigo, F., Higham, D.J.: *Appl. Network Sci.* **2**(1), 17 (2017)
37. Huang, D.W., Yu, Z.G.: *Sci. Rep.* **7**, 41454 (2017)
38. Takaguchi, T., Yano, Y., Yoshida, Y.: *Eur. Phys. J. B* **89**(2), 1 (2016)
39. Walker, D., Xie, H., Yan, K.K., Maslov, S.: *J. Stat. Mech.* **2007**(06), P06010 (2007)
40. Mariani, M.S., Medo, M., Zhang, Y.C.: arXiv preprint, arXiv: 1608.08414 (2016)
41. You, K., Tempo, R., Qiu, L.: *IEEE Trans. Autom. Control* **62**(5), 2080 (2017)
42. Rossi, R.A., Gleich, D.F.: *Algorithms and Models for the Web Graph*, pp. 126–137. Springer, Berlin (2012)
43. Mariani, M.S., Medo, M., Zhang, Y.C.: *Sci. Rep.* **5**, 16181 (2015)
44. Praprotnik, S., Batagelj, V.: *Ars Mat. Contemp.* **11**(1), 11 (2015)
45. Huang, Q., Zhao, C., Zhang, X., Wang, X., Yi, D.: *Europhys. Lett.* **118**(3), 36001 (2017)
46. Flores, J., Romance, M.: *J. Comput. Appl. Math.* **330**, 1041 (2018)
47. Kossinets, G., Kleinberg, J., Watts, D.: In: *Proceedings of the 14th ACM SIGKDD International Conference on Knowledge Discovery and Data Mining*, pp. 435–443. ACM, New York, NY (2008)
48. Kostakos, V.: *Physica A* **388**(6), 1007 (2009)
49. Taylor, D., Myers, S.A., Clauset, A., Porter, M.A., Mucha, P.J.: *Multiscale Model. Simul.* **15**(1), 537 (2017)
50. Taylor, D., Porter, M.A., Mucha, P.J.: arXiv preprint arXiv:1904.02059 (2019)
51. Kivelä, M., Arenas, A., Barthelemy, M., Gleeson, J.P., Moreno, Y., Porter, M.A.: *J. Complex Networks* **2**(3), 203 (2014)
52. Porter, M.A.: *Not. Am. Math. Soc.* **65**(11), 1419 (2018)
53. Taylor, D., Caceres, R.S., Mucha, P.J.: *Phys. Rev. X* **7**(3), 031056 (2017)
54. Mucha, P.J., Porter, M.A.: *Chaos* **20**(4), 041108 (2010)
55. Bassett, D.S., Porter, M.A., Wymbs, N.F., Grafton, S.T., Carlson, J.M., Mucha, P.J.: *Chaos* **23**(1), 013142 (2013)

56. Weir, W.H., Emmons, S., Gibson, R., Taylor, D., Mucha, P.J.: *Algorithms* **10**(3), 93 (2017)
57. Pamfil, A.R., Howison, S.D., Lambiotte, R., Porter, M.A.: *SIAM J. Math. Data Sci.* (in press) arXiv:1804.01964
58. Magnani, M., Rossi, L.: In: *2011 International Conference on Advances in Social Networks Analysis and Mining (ASONAM)*, pp. 5–12. IEEE, Piscataway, NJ (2011)
59. De Domenico, M., Solé-Ribalta, A., Cozzo, E., Kivelä, M., Moreno, Y., Porter, M.A., Gómez, S., Arenas, A.: *Phys. Rev. X* **3**(4), 041022 (2013)
60. Battiston, F., Nicosia, V., Latora, V.: *Phys. Rev. E* **89**(3), 032804 (2014)
61. Tavassoli, S., Zweig, K.A.: In: *2016 Third European Network Intelligence Conference (ENIC)*, pp. 25–32. IEEE, Wrocław, Poland (2016)
62. Magnani, M., Micenková, B., Rossi, L.: arXiv preprint arXiv:1303.4986 (2013)
63. Solé-Ribalta, A., De Domenico, M., Gómez, S., Arenas, A.: In: *Proceedings of the 2014 ACM Conference on Web Science*, pp. 149–155. ACM, New York, NY (2014)
64. Chakraborty, T., Narayanan, R.: In: *2016 IEEE 32nd International Conference on Data Engineering (ICDE)*, pp. 397–408. IEEE, Piscataway, NJ (2016)
65. Solé-Ribalta, A., De Domenico, M., Gómez, S., Arenas, A.: *Physica D* **323**, 73 (2016)
66. Spatocco, C., Stilo, G., Domeniconi, C.: arXiv preprint arXiv:1801.08026 (2018)
67. Rahmede, C., Iacoviacci, J., Arenas, A., Bianconi, G.: *J. Complex Networks* **6**(5), 733 (2017)
68. Tudisco, F., Arrigo, F., Gautier, A.: *J. SIAM Appl. Math.* **78**(2), 853 (2018)
69. Solá, L., Romance, M., Criado, R., Flores, J., del Amo, A.G., Boccaletti, S.: *Chaos* **23**(3), 033131 (2013)
70. DeFord, D.R., Pauls, S.D.: *J. Complex Networks* **6**(3), 353 (2017)
71. DeFord, D.R.: In: *International Workshop on Complex Networks and their Applications*, pp. 1111–1123. Springer, Berlin (2017)
72. Ng, M.K.P., Li, X., Ye, Y.: In: *Proceedings of the 17th ACM SIGKDD International Conference on Knowledge Discovery and Data Mining*, pp. 1217–1225. ACM, New York, NY (2011)
73. Halu, A., Mondragón, R.J., Panzarasa, P., Bianconi, G.: *PLoS ONE* **8**(10), e78293 (2013)
74. Ding, C., Li, K.: *Neurocomputing* **312**, 263 (2018)
75. Gleich, D.F.: *SIAM Rev.* **57**(3), 321 (2015)
76. Taylor, D.: Data release: Ph.D. exchange in the Mathematical Genealogy Project. Available at <https://sites.google.com/site/danetaylorresearch/data>
77. Langville, A.N., Meyer, C.D.: *Google’s PageRank and Beyond: The Science of Search Engine Rankings*. Princeton University Press, Princeton, NJ (2006)
78. Masuda, N., Porter, M.A., Lambiotte, R.: *Phys. Rep.* **716–717**, 1 (2017)
79. Burris, V.: *Am. Sociol. Rev.* **69**(2), 239 (2004)
80. Myers, S.A., Mucha, P.J., Porter, M.A.: *Chaos* **21**(4), 041104 (2011)
81. Clauset, A., Arbesman, S., Larremore, D.B.: *Sci. Adv.* **1**(1), e1400005 (2015)
82. The Mathematics Genealogy Project. Available at <http://www.genealogy.ams.org>; data provided 19 October 2009
83. Ahmad, W., Porter, M.A., Beguerisse-Díaz, M.: arXiv preprint arXiv:1805.00193 (2018)

Approximation Methods for Influence Maximization in Temporal Networks



Tsuyoshi Murata and Hokuto Koga

1 Introduction

Diffusion of rumors (or information) can be represented as information propagation in a social network where its nodes are people and its edges are contacts among the people. The scale of information propagation depends on where and when to start the propagation. In order to propagate information as much as possible, starting nodes should be carefully selected. Selecting starting nodes for large-scale information propagation is important as one of the methods for viral marketing.

From given network, selecting such starting nodes for large-scale information propagation was formalized as “influence maximization problem” by Kempe et al. [20]. The original formalization is for static networks. However, nodes and edges can be newly added or deleted in many real social networks. Therefore, influence maximization problem in temporal networks should be considered. Since the influence maximization problem in temporal networks is NP-hard, computing the best solution in realistic time is computationally intractable. Therefore, many approximation schemes based on Monte-Carlo simulation and other heuristic methods have been proposed. Methods based on Monte-Carlo simulation are more accurate but computationally expensive. On the other hand, other heuristic methods are fast but they are less accurate.

In order to find better solutions for the information maximization problem, we propose three new methods for temporal networks as the extension of the methods for static networks. Dynamic Degree Discount is a heuristic method based on node degree. Dynamic CI is a method based on a node’s degree and the degrees of reachable nodes from the node within specific time. Dynamic RIS uses many similar

T. Murata (✉) · H. Koga

Department of Computer Science, School of Computing, Tokyo Institute of Technology, Meguro, Tokyo, Japan

e-mail: murata@c.titech.ac.jp

networks generated by random edge removal. We compare the proposed methods with previous methods. Although the performance of MC greedy was better than the three methods, it was computationally expensive and intractable for large-scale networks. The computational time of our proposed methods was more than 10 times faster than MC greedy. When compared with Osawa, the performances of the three methods were better for most of the cases.

We discuss extended methods for influence maximization in temporal networks [25, 26]. This chapter includes detailed explanation of background knowledge, discussions of the effect of different values of parameters in the proposed methods, and detailed analysis of the advantages and disadvantages of the proposed methods.

The structure of this chapter is as follows. Section 2 shows related work. Section 3 presents proposed methods (Dynamic Degree Discount, Dynamic CI and Dynamic RIS), Sect. 4 explains our experiments, and Sect. 5 shows the experimental results. Section 6 shows discussions about the experimental results, and Sect. 7 concludes the chapter.

2 Related Work

2.1 Model of Information Propagation

We use the SI model as the model of information propagation on networks. In the SI model, each node in networks is either in state S (susceptible) or in state I (infected). Nodes in state S do not know the information and those in state I know the information. At the beginning of information propagation (at time $t = 1$), a set of nodes in state I is fixed as the seed nodes. For all edges (t, u, v) at time $t = 1, 2, \dots, T$, the following operations are performed. If node u is in state I and node v in state S, information is propagated from u to v with probability λ , which means the state of v is changed from S to I at time $t+1$. Probability λ is the parameter of susceptibility, and it controls the percentage of information propagation. At time $t = T + 1$, information propagation is terminated.

Based on the above notations, we can formulate influence maximization problem as follows. We define $\sigma(S)$ as the expected number of nodes of state I at time $T + 1$ when information propagation started at time 1 from seed nodes S of state I based on SI model. (Please keep in mind that S in $\sigma(S)$ is a set of seed nodes, and S in SI model is susceptible state.) Influence maximization problem in a temporal network is to search for a set of seed nodes S of size k that maximizes $\sigma(S)$ when a temporal network G , duration of the network T , susceptibility of SI model λ and the size of seed nodes k are given.

2.2 Problems Related to Influence Maximization in Temporal Networks

There are some problems related to influence maximization in temporal networks. Instead of giving item (or information) to seed nodes for free, revenue maximization [2] is the problem of finding seed customers (nodes) and offering discounts to them in order to increase total revenue. Although the problem is important in the field of marketing, it is more complicated than influence maximization problem since seed nodes are not treated as equal, and the amount of discount for each node may not be equal. The number of possible parameters increases greatly especially in the case of temporal networks.

Opinion formation [1, 16, 17] is another problem related to influence maximization problem. Each agent (node) has an opinion which might be a continuous or a discrete quantity. The underlying network represents the society where the agents have interactions. Each agent has an opinion in the society that is influenced by the society. Analyzing the increase and decrease of each opinion is important for modeling the dynamics of opinion formation and for opinion polarization [10].

It is often pointed out that the properties of temporal networks are quite different from those in static networks. Braha and Bar-Yam [4, 5] pointed out the overlap of the centrality in temporal networks and that in the aggregated (static) network is very small. Hill and Braha [13] propose dynamic preferential attachment mechanism that reproduce dynamic centrality phenomena. Holme presents good surveys of temporal networks [14, 15].

2.3 Influence Maximization Methods for Static Networks

Jalili presents a survey on spreading dynamics of rumor and disease based on centrality [18]. There are roughly three approaches for influence maximization problem in static networks. The first is Monte-Carlo simulation methods, the second is heuristic-based methods and the third is the methods to generate a large number of networks with random edge removal and select seed nodes based on the generated networks.

Monte-Carlo simulation method is proposed by Kempe et al. [20]. In Kepme's method, $\sigma(S)$ is estimated by repeating Monte-Carlo simulations. When S is given as a set of seed nodes, simulations of information propagation are repeated R times and the average number of infected nodes is defined as $\sigma(S)$. Next, the node v which maximizes the difference $\sigma(S \cup \{v\}) - \sigma(S)$ is added to seed nodes greedily based on the estimated $\sigma(S)$. This operation is repeated until $|S| = k$.

Since $\sigma(\cdot)$ is a monotonic and submodular function, when we denote strict solution of seed nodes as S^* , the seed nodes obtained by the above greedy algorithm S_{greedy} are proved to satisfy $\sigma(S_{\text{greedy}}) \geq (1 - 1/e)\sigma(S^*)$ [20]. Because of this property, qualities of the solutions by Kempe's method are good. However, more and more repetition of Monte-Carlo simulation is needed in order to estimate $\sigma(S)$ accurately. Since the computational cost for finding seed nodes with this method is high, it is not possible to find seed nodes in realistic time for large scale networks.

Heuristic methods are proposed in order to search for seed nodes at high speed. Chen et al. [7] proposes PMIA to find seed nodes focusing on the paths with high information propagation ratio. Jiang et al. [19] proposed SAEDV which searches for seed nodes by annealing method to obtain $\sigma(\cdot)$ from adjacent nodes in seed nodes. Chen et al. [8] proposed Degree Discount based on node degree where the nodes adjacent to already selected node are given penalty. This is because when node v is selected as one of seed nodes and u is its neighbor, it is highly likely that v propagates information to u , so selecting nodes other than u as seed nodes is better for information diffusion.

Algorithm of Degree Discount is shown as follows. t_i in the algorithm shows the penalty of node i . dd_i is the degree of node i after giving penalty. dd_i is smaller when the value of t_i is bigger.

Algorithm 1 Degree discount

InputsStatic network G The size of seed nodes k Susceptibility λ **Outputs**Seed nodes S **Algorithm**

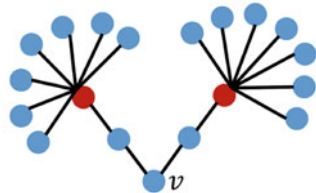
- (1) Initialize seed nodes as $S = \emptyset$, and initialize $dd_i = k_i$, $t_i = 0$ for each node i . k_i is the degree of node i in network G .
- (2) Add node v to seed nodes S such that $v = \operatorname{argmax}_i \{dd_i | i \in V \setminus S\}$. V is the nodes in network G .
- (3) Update dd_u and t_u for all nodes u adjacent to v .

$$t_u = t_u + 1$$

$$dd_u = k_u - 2t_u - (k_u - t_u)t_u\lambda$$

- (4) Repeat (2) and (3) until $|S| = k$.
-

Fig. 1 Example for explaining $\text{CI}_l(v)$. When $l = 2$, $\text{CI}_l(v) = 14$



Morone and Makse [24] proposed a method for finding seed nodes considering the degrees of distant nodes. The method calculates the following $\text{CI}_l(v)$ for each node and selects seed nodes based on the values:

$$\text{CI}_l(v) = (k_v - 1) \sum_{u \in \partial \text{Ball}(v, l)} (k_u - 1).$$

$\partial \text{Ball}(v, l)$ in the above formula represents nodes where the distance from node v is l . The example of $\text{CI}_l(v)$ is explained in Fig. 1. $\partial \text{Ball}(v, 2)$ when $l = 2$ are two nodes with distance 2 from node v and the degrees of both nodes are 8. Therefore, $\text{CI}_2(v) = (2 - 1) \times \{(8 - 1) + (8 - 1)\} = 14$.

The degree of node v itself is low in the network in Fig. 1, but the node v is effective for information propagation because it is connected with some high degree nodes with distance two. This method thus selects seed nodes causing wider propagation compared with the cases when seed nodes are selected based on the degree of node v only.

These heuristic methods compute seed nodes faster than the methods based on Monte-Carlo simulation. However, it is experimentally confirmed that the scale of propagation of the methods depends on network structures and parameters.

Ohsaka et al. [27] proposed a method to generate many networks with random edge removal in order to solve this problem. Ohsaka's method is based on "coin flip" mentioned in Kempe's paper [20]. The distribution of nodes to which information is propagated from seed nodes S in static network G is set as $D_G(S)$. And distribution of nodes where information is propagated from seed nodes S on network where edges are removed at constant ratio from the network G is set as $D'_G(S)$. "Coin flip" states as $D_G(S)$ equals to $D'_G(S)$ in this situation. $\sigma(\cdot)$ can be estimated by generating many networks with edges removed at constant ratio, not by repeating Monte-Carlo simulation. Ohsaka's method estimates $\sigma(\cdot)$ by acquiring Strongly Connected Component (SCC) in each network generated by RR numbers of networks with edges removed at constant ratio. SCC is a subgraph where each node in the subgraph can be reachable to and from any other nodes.

Borgs et al. [3] and Tang et al. [30] also propose methods similar to Ohsaka's method. The difference from Ohsaka's method is $\sigma(\cdot)$, which is not estimated directly from generated networks. Reachable nodes from randomly selected node v are computed, and then seed nodes are selected based on the nodes. More specifically, the algorithm is as follows.

Algorithm 2 Algorithm by Borgs and Tang

Input

Static network G
 The size of seed nodes k
 Susceptibility λ
 Generated number of networks θ

Outputs

Seed nodes S

Algorithm

- (1) Initialize $S = \emptyset, U = \emptyset$. U is a set of all RR .
 - (2) Select node v at random.
 - (3) Remove edges with probability $1 - \lambda$ from network G and set as G_p .
 - (4) Acquire nodes RR reachable to v by G_p . Add RR to U .
 - (5) Repeat θ times from (2) to (4).
 - (6) Add node u with the highest frequency in U to S .
 - (7) Delete all RR containing u from U .
 - (8) Repeat (6) and (7) until $|S| = k$.
-

There are other approaches for influence maximization problem in different problem setting. Chen et al. [6] proposed a method to solve the problem with time limit. Feng et al. [9] solves the influence maximization problem in a situation where freshness of the information degrades as it spreads. Mihara et al. [23] proposed a method to influence maximization problem where the whole network structure is unknown.

2.4 Degrees in Temporal Networks

Notations of edges and paths in temporal networks are the same as the ones in [28]. (t, u, v) represents an edge from node u to v at time t . A path from node v_1 to v_k of length $k - 1$ is represented as $(t_1, v_1, v_2), (t_2, v_2, v_3), \dots, (t_{k-1}, v_{k-1}, v_k)$, where $t_1 < t_2 < \dots < t_{k-1}$ and $\forall i, j (i \neq j), v_i \neq v_j$. Duration of time from the start to the end of a path $t_{k-1} - t_1$ is the length of time of the path, and the smallest one is the minimum length of time.

Habiba et al. [12] define degrees in temporal network using symmetric difference of past connections and future connections. However, diffusion in temporal networks is from past to future only, and it is not bidirectional. We therefore define degree $D_T(v)$ of node v in temporal network as follows:

$$D_T(v) = \sum_{1 < t \leq T} \frac{|N(v, t-1) \setminus N(v, t)|}{|N(v, t-1) \cup N(v, t)|} |N(v, t)|,$$

where $N(v, t)$ is a collection of nodes adjacent to node v at time t . Figures 2 and 3 illustrate the examples of degrees on temporal networks. In Fig. 2, adjacent

Fig. 2 Example of low degree nodes in a temporal network. Nodes adjacent to node A do not change over time ($\{B, C\} \rightarrow \{B, C\} \rightarrow \{B, C\}$)

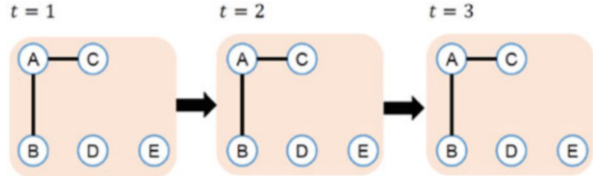
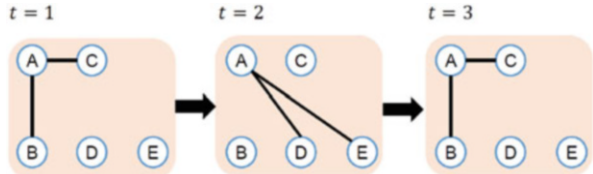


Fig. 3 Example of high degree nodes in a temporal network. Nodes adjacent to node A change at each time ($\{B, C\} \rightarrow \{D, E\} \rightarrow \{B, C\}$)



nodes of node A do not change during the period. The difference of adjacent nodes $N(A, 1) \setminus N(A, 2)$ and $N(A, 2) \setminus N(A, 3)$ are empty. Therefore, the degree of node A in Fig. 2 is calculated as follows.

$$\begin{aligned} D_3(A) &= \frac{|N(A, 1) \setminus N(A, 2)|}{|N(A, 1) \cup N(A, 2)|} |N(A, 2)| + \frac{|N(A, 2) \setminus N(A, 3)|}{|N(A, 2) \cup N(A, 3)|} |N(A, 3)| \\ &= \frac{0}{2} * 2 + \frac{0}{2} * 2 = 0 \end{aligned}$$

On the other hand, in Fig. 3, nodes adjacent to node A change over time. So the degree of node A is bigger than that in Fig. 2.

$$\begin{aligned} D_3(A) &= \frac{|N(A, 1) \setminus N(A, 2)|}{|N(A, 1) \cup N(A, 2)|} |N(A, 2)| + \frac{|N(A, 2) \setminus N(A, 3)|}{|N(A, 2) \cup N(A, 3)|} |N(A, 3)| \\ &= \frac{2}{4} * 2 + \frac{2}{4} * 2 = 2 \end{aligned}$$

In Figs. 2 and 3, the number of adjacent nodes of node A is the same every time, so the average degree of node A is the same in Figs. 2 and 3. On the other hand, if we employ $D_T(v)$ as the definition of node degree, $D_3(A) = 0$ in Fig. 2 and $D_3(A) = 2$ in Fig. 3. $D_T(v)$ captures the number of newly adjacent nodes, and this is important for influence maximization problem. We therefore employ $D_T(v)$ as the definition of node degree in temporal networks.

2.5 Influence Maximization Methods for Temporal Networks

There are two approaches for influence maximization problem in temporal networks: methods based on Monte-Carlo simulation and heuristic-based methods. The

former method is proposed by Habiba. The method estimates the scale of propagation $\sigma(\cdot)$ by repeating Monte-Carlo simulation just the same as in static networks. Since $\sigma(\cdot)$ is monotonic and deteriorated modular also in temporal networks, this method achieves large-scale propagation. However, the computational cost of this method is high as in static networks. Osawa [28] proposed a heuristic method for calculating $\sigma(\cdot)$ at high speed. His algorithm for computing $\sigma(S)$ for seed nodes S is shown as follows.

Algorithm 3 Osawa's algorithm

Input

Temporal network G
Duration of temporal network T
Seed nodes S
Susceptibility λ

Output

The number of state I nodes $\sigma(S)$

Algorithm

- (1) Initialize $\hat{p}_v(1)$ as follows where the probability of node v being in state I is $\hat{p}_v(t)$ in time t ($1 \leq t \leq T + 1$).

$$\hat{p}_v(1) = \begin{cases} 1 & v \in S \\ 0 & v \notin S \end{cases}$$

- (2) Update $\hat{p}_v(t)$ in time t as follows.

$$\hat{p}_v(t + 1) = 1 - (1 - \hat{p}_v(t))R_v(t)$$

$$R_v(t) = \prod_{u \in N(v,t)} (1 - \hat{p}_u(t)\lambda)$$

where $R_v(t)$ is the probability of which information is not propagated to node v from any adjacent nodes at time t . $N(v, t)$ is the set of nodes adjacent to node v at time t .

- (3) $\sigma(S)$ is computed by adding probability $\hat{p}_v(T + 1)$ of each node which is in state I at time $T + 1$.

$$\sigma(S) = \sum_{v \in V} \hat{p}_v(T + 1)$$

After $\sigma(S)$ is computed, seed nodes are obtained by greedy algorithm as in the method by Monte-Carlo simulation. Osawa's method finds seed nodes in realistic computational time. However, the quality of its solution depends on given networks because $\sigma(\cdot)$ is calculated approximately, and it is worse compared with the solutions by Monte-Carlo simulation.

3 Proposed Methods

We propose new methods for influence maximization problem in temporal networks in this section. We propose three new methods (Dynamic Degree Discount, Dynamic CI and Dynamic RIS) which are the extensions of static network methods to temporal network methods. We use the following notations: G : temporal network, T : duration of the temporal network, k : the size of seed nodes, λ : susceptibility, θ : the number of generated networks, and S : seed nodes.

3.1 Dynamic Degree Discount

Dynamic Degree Discount is the extension of Degree Discount by Chen et al. [8] to temporal networks. In Dynamic Degree Discount, definition of degrees and adjacent nodes in the algorithm of Degree Discount are modified for temporal networks. Algorithm 4 shows the algorithm of Dynamic Degree Discount. Underlines show the parts modified from original Degree Discount.

3.2 Dynamic CI

Dynamic CI is an extension of Morone's method [24] for temporal networks. Morone's method focuses on the degree of node v and the degrees of nodes with distance l from v . Dynamic CI defines an index $D_{CI_l}(v)$ in which degree and distance are extended to temporal networks.

$$D_{CI_l}(v) = D_T(v) \sum_{u \in DBall(v,l)} D_T(u)$$

The differences between $CI_l(v)$ and $D_{CI_l}(v)$ are: (1) the definition of degree is changed to that for temporal networks and (2) $\partial Ball(v, l)$ in $CI_l(v)$ is changed to $DBall(v, l)$. $DBall(v, l)$ represents nodes where their shortest duration of time from node v is l . l is a parameter which takes the value within the range $1 \leq l \leq T$. In the algorithm of Dynamic CI, $D_{CI_l}(v)$ is computed for each node and top k nodes are selected as seed nodes.

Algorithm 4 Dynamic degree discount

Input

Temporal network G
Duration of temporal network T
The size of seed nodes k
Susceptibility λ

Output

Seed nodes S

Algorithm

- (1) Initialize seed nodes as $S = \emptyset$. Also initialize the values of each node i as $\underline{dd}_i = D_T(i)$ and $t_i = 0$.
- (2) Add node v where $v = \operatorname{argmax}_i \{\underline{dd}_i | i \in V \setminus S\}$ to S . V is the set of nodes in the network.
- (3) For all nodes u where $u \in N_T(v)$, update \underline{dd}_u and t_u as follows.

$$\begin{aligned} t_u &= t_u + 1 \\ \underline{dd}_u &= \underline{D}_T(u) - 2t_u - (D_T(u) - t_u)t_u\lambda \end{aligned}$$

$N_T(v)$ represents a set of all nodes adjacent to v during the whole period of the temporal network.

$$N_T(v) = \bigcup_{t=1}^T N(v, t)$$

- (4) Repeat (2) and (3) until $|S| = k$.
-

3.3 Dynamic RIS

Dynamic RIS is an extension of Borgs's method [3] and Tang's method [30] for temporal networks.

The difference between Borgs's and Tang's algorithms and Dynamic RIS are where RR in their algorithm is set as $RR(v, d)$ in our algorithm. $RR(v, d)$ is a set of all nodes that are reachable to v within the shortest duration of time d in all durations of temporal networks, which is defined as follows:

$$RR(v, d) = \bigcup_{t=1}^T RR_t(v, d).$$

$RR_t(v, d)$ is a set of nodes which are reachable to “node v at time t ” within the shortest period of d . The computational complexities of these methods are as follows.

Algorithm 5 Dynamic RIS

Inputs

Temporal network G
Duration of the temporal network T
Size of seed nodes k
Susceptibility λ
The number of generated networks θ

Output

Seed nodes S

Algorithm

- (1) Initialize as $S = \emptyset$, $U = \emptyset$, where U is the set containing all $RR(v, d)$.
 - (2) Select node v at random.
 - (3) Remove edges from temporal network G with probability $1 - \lambda$ and set as G_p .
 - (4) Acquire nodes $RR(v, d)$ reachable to v on G_p . Add $RR(v, d)$ to U .
 - (5) Repeat (2) to (4) θ times.
 - (6) Add the most frequent node u in U to S .
 - (7) Remove all $RR(v, d)$ with u from U .
 - (8) Repeat (6) and (7) until $|S| = k$.
-

Dynamic Degree Discount

According to the paper of Chen et al. [8], the computational complexity of Degree Discount is $O(k \cdot \log n + m)$, where k is the number of seed nodes, n is the number of nodes, and m is the number of edges, respectively. Dynamic Degree Discount is an extension of Degree Discount. Static degree is replaced with dynamic one ($D_T(i)$) and Static neighbors is replaced with dynamic one ($N_T(v)$). Computational complexity for dynamic degree and dynamic neighbors are $\frac{T \cdot m}{n}$, where T is the total duration of time of given temporal network. Therefore, the total computational complexity of Dynamic Degree Discount is $O(k \cdot \log n + m + \frac{T \cdot m}{n})$.

Dynamic CI

According to the paper of Morone and Makse [24], the computational complexity of CI is $O(n \cdot \log n)$, where n is the number of nodes. Dynamic CI is an extension of CI. Static degree is replaced with dynamic one ($D_T(i)$), and its computational complexity is $\frac{T \cdot m}{n}$, where T is the total duration of time of given temporal network. Therefore, the total computational complexity of Dynamic CI is $O(n \cdot \log n + \frac{T \cdot m}{n})$.

Dynamic RIS

According to the paper of Tang [30], the computational complexity of RIS is $O(k \cdot l^2(m + n) \log^2 n / \epsilon^3)$ which returns $(1 - \frac{1}{e} - \epsilon)$ -approximate solution with at least $1 - n^{-l}$ probability, where l and ϵ are the constants. Computational complexity of Dynamic RIS heavily depends on the parameters θ and d , which are the number of generated networks and the duration of time for computing $RR(v, d)$, respectively. Therefore, the total computational complexity of Dynamic RIS is $O(\theta \cdot d \cdot k \cdot l^2(m + n) \log^2 n / \epsilon^3)$.

4 Experiments

We perform experiments for comparing the proposed methods with previous ones in order to confirm their effectiveness. Temporal networks used for the experiments are shown in Table 1. These networks are the same as the ones used in previous research. Average degree in Table 1 shows the average of all nodes in the network, which is $\frac{1}{|V|} \sum_{v \in V} D_T(v)$. Hospital [31] is a network about contacts of patients and medical staffs at hospital with time. Primary School [11, 29] is a network about contacts of students and teachers at school. High School 2013 [22] is a network of contacts of students. The unit of the duration in these three datasets is 20 s. Each dataset is available at SocioPatterns (<http://www.sociopatterns.org>).

Methods used in the experiments are previous two methods (Monte-Carlo simulation (MC Greedy) and Osawa) for temporal network explained in Sect. 2.5 and our proposed methods (Dynamic Degree Discount, Dynamic CI and Dynamic RIS) in Sect. 3. Given a network as input, each method computes seed nodes S . The simulation of influence maximization based on SI model is repeated R times with the obtained seed nodes and set the average of the number of nodes in state I as $\sigma(S)$. The values of $\sigma(S)$ are compared in order to evaluate the methods.

Experiments are performed for the following purposes:

- (1) Comparison of $\sigma(S)$ when the size of seed nodes k changes
- (2) Comparison of computational time when the size of seed nodes k changes

Parameters in the experiments are set as follows. The number of repetition of the simulations for information propagation is set as $R = 50$. The number of repetition of Monte-Carlo simulation in MC Greedy is set as 1000. These two parameters are common in all experiments. The size of seed nodes k is set from 0 to 20%. Susceptibility λ is set as $\lambda = 0.01$. It is difficult to perform experiments for all the values as parameter l in Dynamic CI which takes the value of $1 \leq l \leq T$. We use the values $l = 1, 5, 10, 20$ in the experiments. As the parameters θ and d in Dynamic RIS, θ is set as $\theta = 1000$. As for d , values $d = 0, 5, 10, 20$ are used since it is difficult to perform experiments for all the value as in l of Dynamic CI.

CELF [21] is used to speedup the experiments when greedy algorithms are used in MC Greedy and Osawa. CELF is an algorithm used when the greedy algorithm is applied to the problem with inferior modularity, and the solution is the same as in normal greedy algorithm. According to the experiments by Leskovec et al. [21], computational time is 700 times faster than normal greedy algorithm when CELF is used.

Table 1 Dataset for the experiments

	Nodes	Edges	Duration	Ave. deg.
Hospital	75	32,424	9,453	69.3
Primary school	242	125,773	3,100	142.7
High school 2013	327	188,508	7,375	63.0

5 Experimental Results

5.1 Comparison of $\sigma(S)$ When the Size of Seed Nodes k Changes

The results of information propagation for each size of seed nodes k with fixed susceptible $\lambda = 0.01$ of SI model are shown in Fig. 4. The x-axis of the Figure shows the percentage of seed nodes, and the y-axis shows the number of infected nodes. Values of the x-axis is $\frac{k}{|V|} * 100$, the percentage of seed nodes to all nodes in the network. Values of the y-axis is $\frac{\sigma(S)}{|V|} * 100$, the percentage of $\sigma(S)$ to all nodes in the network. The best values of l in Dynamic CI and d in Dynamic RIS are used in our experiments. As shown in Fig. 4, MC Greedy achieves the highest diffusion in all dataset. Diffusion of the proposed methods, Dynamic Degree Discount, Dynamic CI and Dynamic RIS are inferior to MC Greedy, but they are still better than Osawa. The scale of diffusion of Dynamic RIS in High School 2013 achieves 1.5 times as in Osawa.

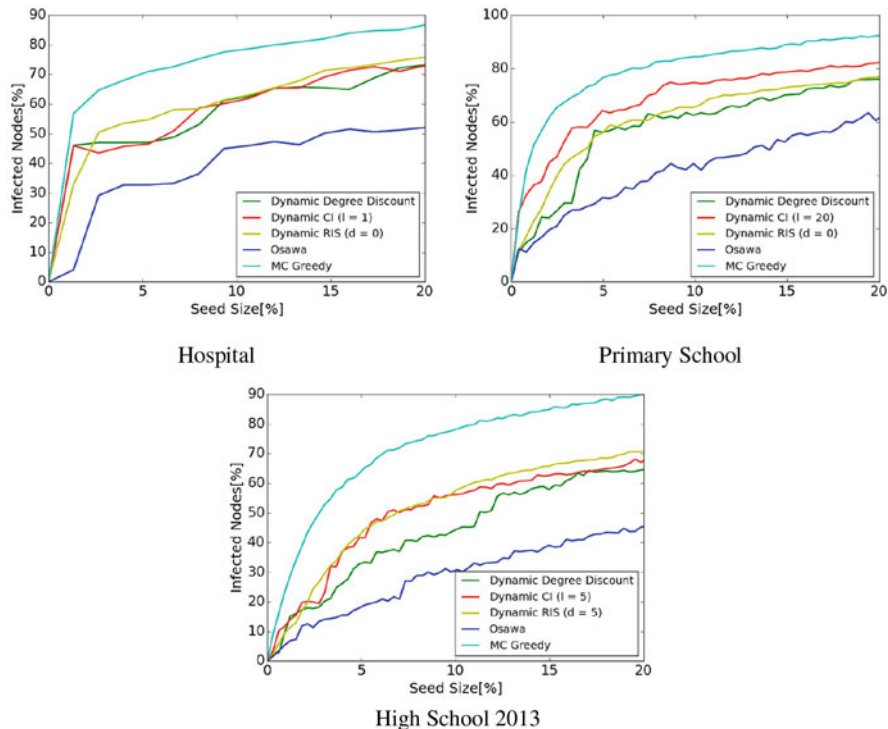


Fig. 4 Comparison of $\sigma(S)$ when the size of seed nodes k changes. Except (computationally expensive) MC Greedy, three proposed methods are better than Osawa

There is not much difference in the scale of diffusion among each of three proposed methods. Dynamic RIS achieves the highest in High School 2013 for example, but the difference among proposed methods is small compared with the difference between proposed methods and previous methods (MC Greedy and Osawa).

5.2 Comparison of $\sigma(S)$ When Susceptibility λ Changes

Figure 5 shows diffusion when the size of seed nodes is fixed as 20% of all nodes in the networks and susceptibility is changed as $\lambda = 0.001, 0.01, 0.05$. The x-axis shows the value of λ , and the y-axis shows the percentage of diffusion. Parameters l and d are the same as the ones used in the previous experiments. As shown in Fig. 5, MC Greedy achieves the highest diffusion regardless of the value of λ . The difference among three proposed methods are small.

As the result of comparison with proposed methods and Osawa, our proposed methods achieve higher scale of diffusion than Osawa in Hospital and High School 2013 when $\lambda = 0.05$. Osawa achieves higher diffusion than Dynamic RIS only in

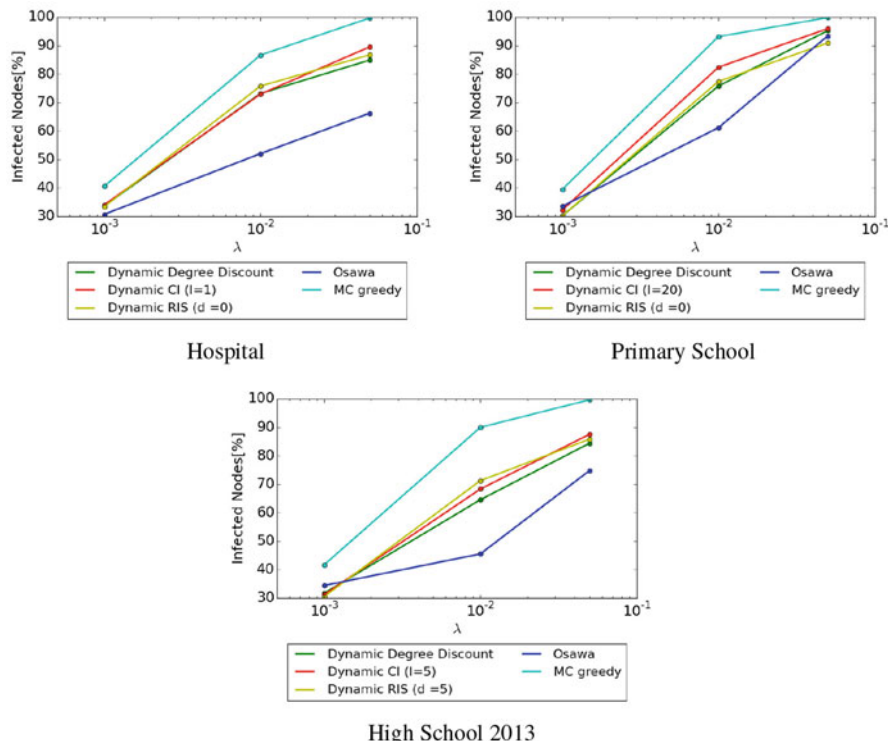


Fig. 5 Comparison of $\sigma(S)$ when susceptibility λ changes. Except (computationally expensive) MC Greedy, three proposed methods are better than Osawa for most of the cases

Primary School. When $\lambda = 0.001$, the difference between proposed methods and Osawa is very small compared with the cases of other λ values.

5.3 Comparison of Computational Time When the Size of Seed Nodes k Changes

Figure 6 shows the computational time when λ is set as $\lambda = 0.01$ and the sizes of seed nodes are changed. A PC of Intel Core i7 (3.4GHz) CPU and 8GB memory is used for the experiments. X-axis shows the percentage of seed nodes, and y-axis shows the computational time (log-scale).

Figure 6 shows that for all datasets, methods other than MC Greedy can compute seed nodes in realistic time. MC Greedy needs several hours to compute seed nodes. This shows that MC Greedy is intractable in realistic time for large scale networks.

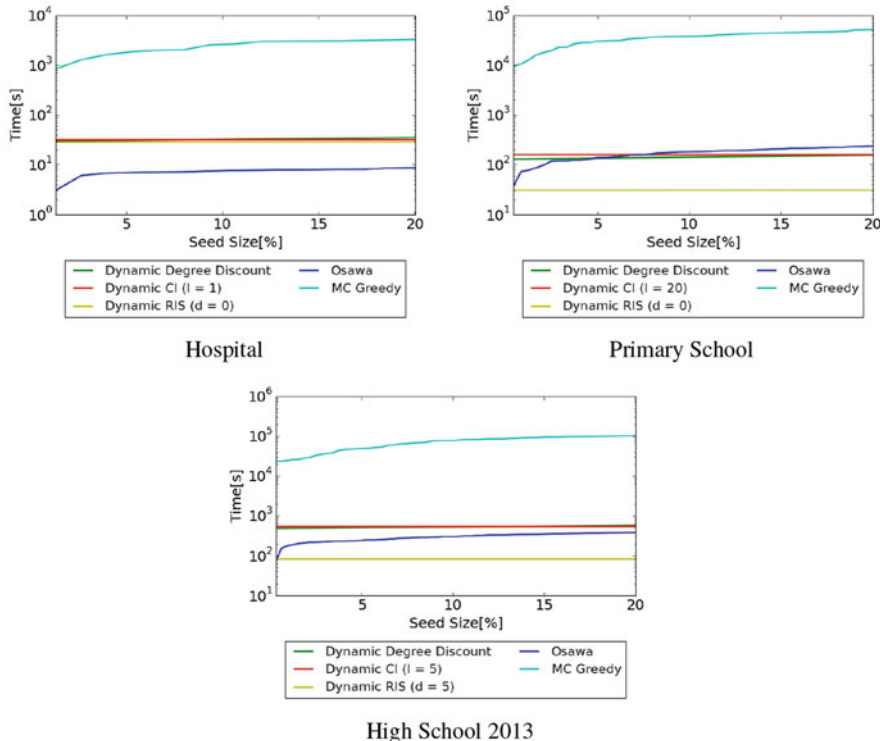


Fig. 6 Comparison of computational time when the size of seed nodes k changes. Methods other than MC Greedy can compute in realistic time

Regarding the comparison among three proposed algorithm, computational time of Dynamic Degree Discount and Dynamic CI are almost the same in all dataset. Dynamic RIS is about the same computational time as the other two proposed methods in Hospital, and is faster in Primary School and High School 2013. Regarding the comparison with proposed methods and Osawa, Dynamic RIS is approximately 7.8 times faster than Osawa except very small network (Hospital).

5.4 Parameters of Dynamic CI and Dynamic RIS

Diffusion of proposed methods with different parameters are shown in this section. We change parameters l of Dynamic CI, and θ and d in Dynamic RIS.

5.4.1 Diffusion and Computational Time of Different l in Dynamic CI

Diffusion and computational time when l in Dynamic CI changes to 1, 5, 10, 20 are shown in Fig. 7. Left line graphs show the size of diffusion when l is changed in each network. Right bar graphs show computational time. Left line graphs show that diffusion depends on the value of l . Therefore, it is important to find appropriate l in Dynamic CI. Since there is no simple correlation between the scale of diffusion and the value of l (such as diffusion becomes larger as l becomes large), diffusion for various values of l should be investigated and compared. Right bar graphs show that there are no big differences of execution time when the value of l changes.

5.4.2 Diffusion and Computational Time of Different θ in Dynamic RIS

In Dynamic RIS, θ is a parameter for the number of generated graphs in $RR(v, d)$. Diffusion and computational time when parameter θ is changed to 500, 1000, 1500, 2000 are shown in Fig. 8. Left line graphs show that diffusion does not change much when θ changes. However, the scale of diffusion is slightly small when $\theta = 500$ in Hospital and High School 2013. This means that bigger θ is desirable from the viewpoint of diffusion. On the contrary, right bar graphs show that higher value of θ results in the increase of computational time. From the viewpoint of computational time, smaller θ is better. Regarding the value of θ , there is a trade-off between the scale of diffusion and the computational time. It is important to find smaller θ for shorter computational time, but too small θ results in small-scale diffusion.

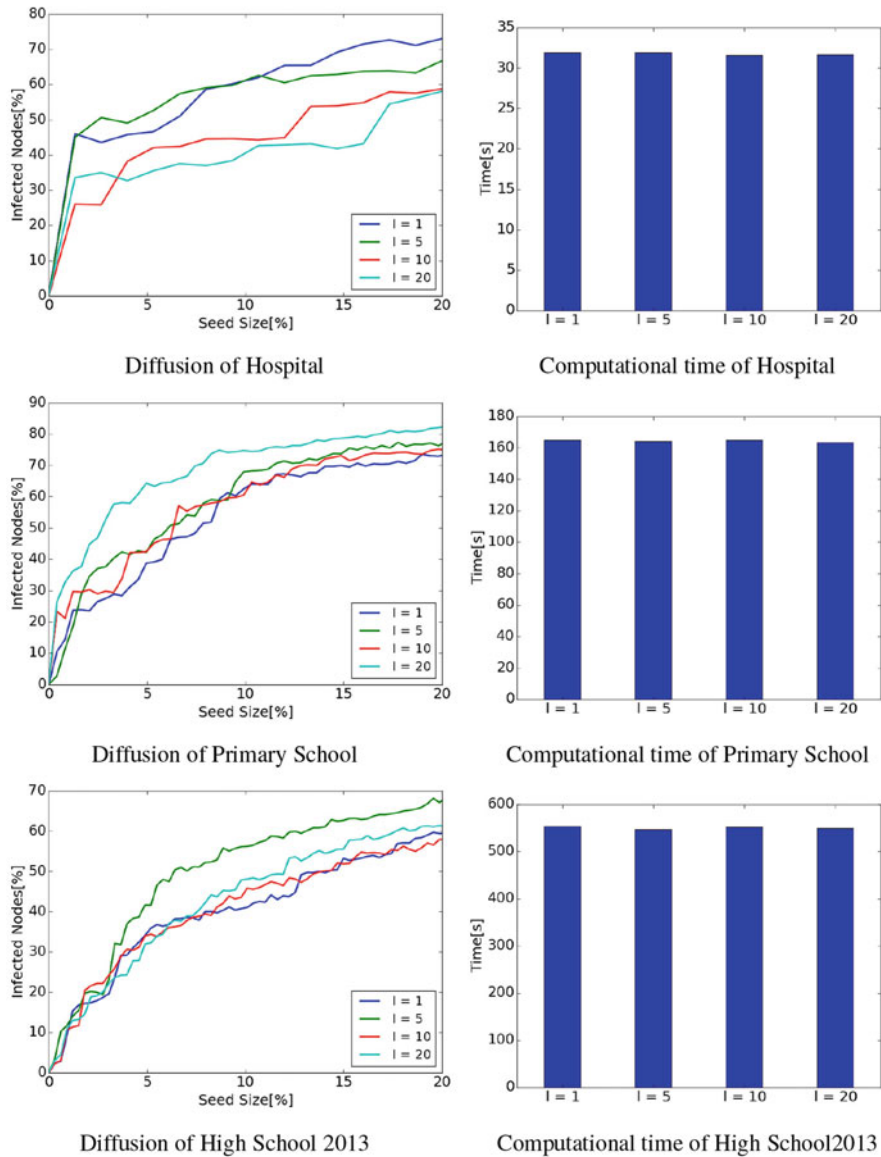


Fig. 7 Diffusion and computational time for different l in Dynamic CI. Left: there is no simple correlation between the scale of diffusion and the value of l . Right: there are no big differences of execution time when the value of l changes

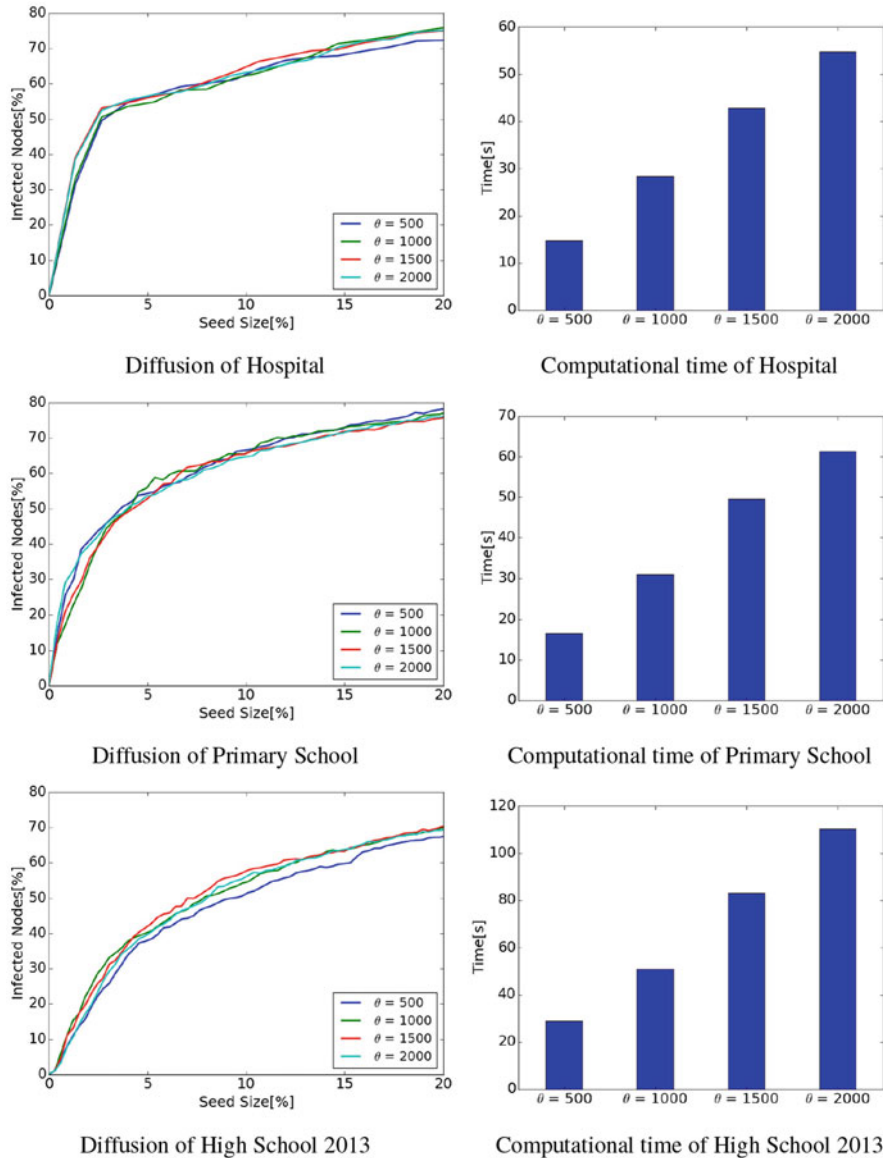


Fig. 8 Diffusion and computational time of different θ in Dynamic RIS. Left: diffusion does not change much when θ changes. Right: higher value of θ results in the increase of computational time

5.4.3 Diffusion and Computational Time of Different d in Dynamic RIS

In Dynamic RIS, d is a parameter for the number of time steps for looking back. Figure 9 shows diffusion and executing time when parameter d changes to

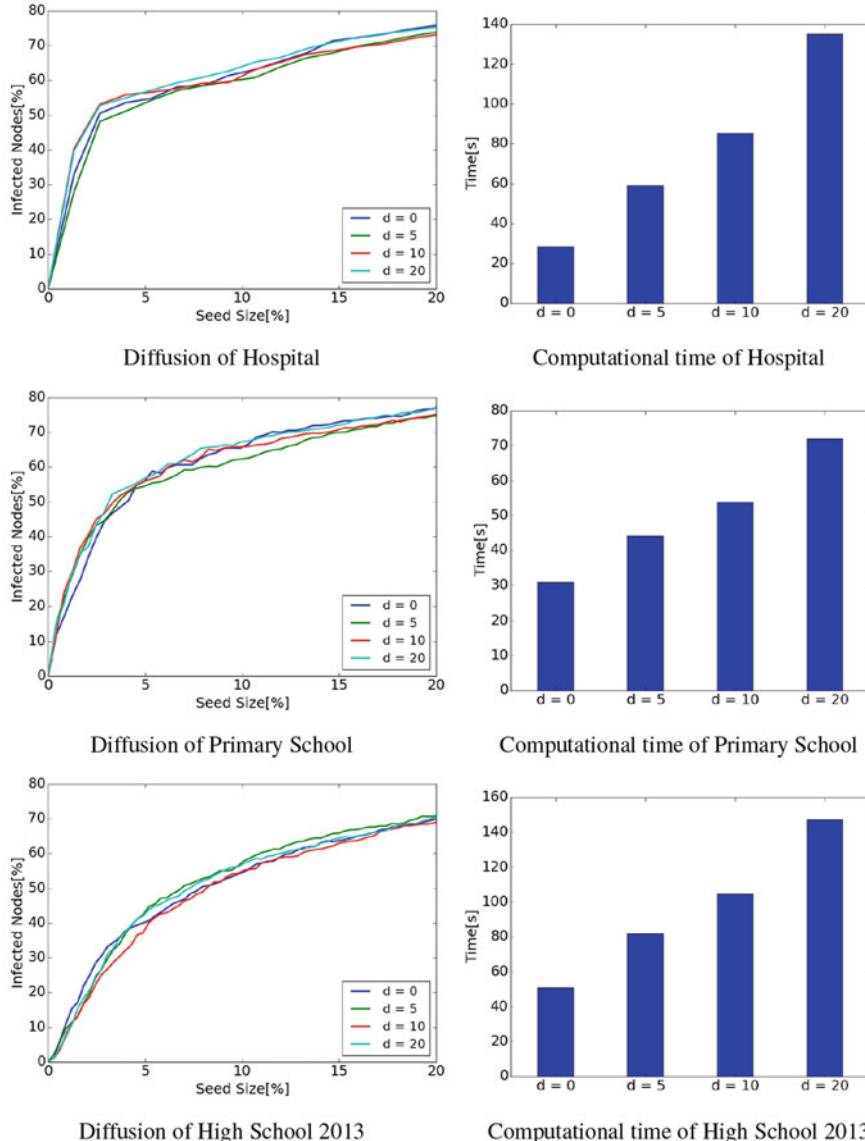


Fig. 9 Diffusion and computational time of different d in Dynamic RIS. Left: there is almost no difference in diffusion when d changes. Right: computational time increases as the value of d becomes bigger

0, 5, 10, 20. Left line graphs show that there is almost no difference in diffusion when d changes, while right bar graphs show that computational time increases as the value of d becomes bigger. The scale of diffusion does not change even if the value of d becomes bigger in our experiments.

6 Discussion

6.1 Analysis Focused on Diffusion of Each Node

In the experiments when susceptibility changes in Sect. 5.2, the difference between the proposed methods and Osawa was small when $\lambda = 0.001$ compared with the experiments with other values of λ . When $\lambda = 0.05$, Osawa outperforms proposed methods only in Primary School. This section discusses these two points.

Figure 10 shows the distribution of diffusion $\sigma(\{v\})$ of each node v when Monte-Carlo simulation is used. X-axis shows the percentage of diffusion from node v to the whole network ($\sigma(\{v\})$), and Y-axis shows the frequency of the nodes with each of the percentage in X-axis. When $\lambda = 0.001$, almost all nodes are less than 5% of diffusion in all networks. This means that there is no big difference of the diffusion from different seed nodes. This is the reason why the difference between proposed methods and Osawa is small in the experiment in Sect. 5.2. On the contrary, there are many nodes with more than 60% of diffusion in Primary School when $\lambda = 0.05$ compared with other two networks. In this case, large scale diffusion is easy to be achieved even if the most appropriate seed nodes are not selected. This is the reason why Osawa outperforms proposed method in Primary School in Sect. 5.2.

6.2 Advantages and Disadvantages of Each of Proposed Methods

Advantages and disadvantages of each of proposed methods are discussed in this section. An advantage of Dynamic Degree Discount is that it contains no parameter, so there is no need to adjust parameter. Its disadvantage is that it is only for SI model, so the method cannot be used for other models. This is because Dynamic Degree Discount is an extension of Chen's Degree Discount which is for SI model. There are other information propagation models such as LT model and Triggering models proposed by Kempe et al. Dynamic Degree Discount cannot be applied to such models.

An advantage of Dynamic CI is that it can be applied to many information propagation models in contrast to Dynamic Degree Discount because Dynamic CI uses only degree information when it calculates seed nodes. Its disadvantage is

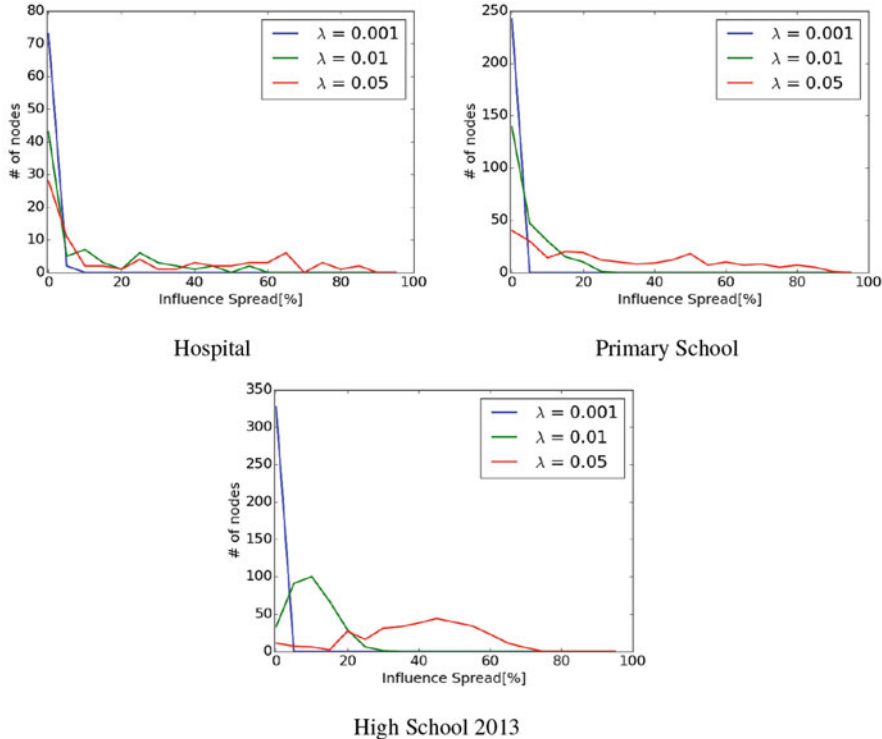


Fig. 10 Distribution of diffusion $\sigma(\{v\})$ of each node v . In the case of Primary School when $\lambda = 0.05$, there are many nodes of high diffusion. Therefore, large scale diffusion is easy to be achieved even if the most appropriate seed nodes are not selected. This is the reason Osawa outperforms proposed method in Primary School

that the ability of diffusion depends on the value of parameter l as mentioned in section 5.4.1. It is necessary to search for appropriate values of l for Dynamic CI. The parameter l takes the value within the range $1 < l < T$, so the search takes time in general.

An advantage of Dynamic RIS is that its computational time is short. As shown in the experimental results, its computational time is shorter than other methods in all networks except Hospital. As the method can be applied to large networks due to its short computational time, this is a big advantage. Disadvantage of Dynamic RIS is that it needs to adjust parameters θ and d . As mentioned in the previous section, computational time becomes bigger as the parameter θ becomes bigger, and the scale of diffusion becomes smaller for too small θ . Therefore, it is necessary to set appropriate value for θ . However, parameter sensitivity of θ and d is not so much compared with the sensitivity of l in Dynamic CI.

7 Conclusion

We propose three new methods for influence maximization problem in temporal networks which are the extensions of the methods for static networks. As the result of experiments for comparing with previous methods, MC Greedy and Osawa, our three proposed methods are better than previous methods in the following sense. Although the performance of MC greedy is better than these three methods, it is computationally expensive and intractable for large scale networks. The computational time of our proposed methods are more than 10 times faster than MC greedy, so they can be computed in realistic time even for large scale temporal networks. As the comparison with Osawa, the performances of these three methods are almost the same as Osawa, but they are approximately 7.8 times faster than Osawa. Based on these facts, the proposed methods are suitable for influence maximization in temporal networks.

The comparison of Dynamic Degree Discount, Dynamic CI and Dynamic RIS is as follows. The choice of the methods should be done based on the following pros and cons.

Dynamic Degree Discount

- It requires no parameter.
- It is applicable to SI model only.

Dynamic CI

- It is applicable to other information propagation models.
- The performance heavily depend on parameter l .

Dynamic RIS

- It is relatively fast among these three methods.
- It requires two parameters to be adjusted (θ and d).

Finding the strategies of choosing suitable method for given temporal network is practically important. It is a challenging open question and is left for our future work. The problem of adjusting the parameters for Dynamic CI and and Dynamic RIS is also left for our future work.

Acknowledgement This work was supported by JSPS Grant-in-Aid for Scientific Research(B) (Grant Number 17H01785).

References

1. Afshar, M., Asadpour, M.: Opinion formation by informed agents. *J. Artif. Soc. Soc. Simul.* **13**(4), 1–5 (2010)
2. Babaei, M., Mirzasoleiman, B., Jalili, M., Safari, M.A.: Revenue maximization in social networks through discounting. *Soc. Netw. Anal. Min.* **3**(4), 1249–1262 (2013)

3. Borgs, C., Brautbar, M., Chayes, J., Lucier, B.: Maximizing social influence in nearly optimal time. In: Proceedings of the Twenty-Fifth Annual ACM-SIAM Symposium on Discrete Algorithms, pp. 946–957. (2014)
4. Braha, D., Bar-Yam, Y.: From centrality to temporary fame: Dynamic centrality in complex networks. *Complexity* **12**(2), 59–63 (2006)
5. Braha, D., Bar-Yam, Y.: Time-dependent complex networks: Dynamic centrality, dynamic motifs, and cycles of social interactions. In: Adaptive Networks: Theory, Models and Applications, pp. 39–50. Springer, Berlin (2009)
6. Chen, W., Lu, W., Zhang, N.: Time-Critical Influence Maximization in Social Networks with Time-Delayed Diffusion Process. In: Proceedings of the Twenty-Sixth AAAI Conference on Artificial Intelligence, pp. 592–598 (2012)
7. Chen, W., Wang, C., Wang, Y.: Scalable influence maximization for prevalent viral marketing in large-scale social networks. In: Proceedings of the 16th ACM SIGKDD international conference on Knowledge discovery and data mining - KDD '10, pp. 1029–1038 (2010)
8. Chen, W., Wang, Y., Yang, S.: Efficient influence maximization in social networks. In: Proceedings of the 15th ACM SIGKDD international conference on Knowledge discovery and data mining - KDD '09, pp. 199–207 (2009)
9. Feng, S., Chen, X., Cong, G., Yifeng, Z., Yeow, Meng, C., Yanping, X.: Influence Maximization with Novelty Decay in Social Networks. In: Proceedings of the Twenty-Eighth AAAI Conference on Artificial Intelligence, pp. 37–43 (2014)
10. Garimella, K., Morales, G.D.F., Mathiouidakis, M., Gionis, A.: Polarization on social media. *Web Conf 2018 Tutorial* **1**(1), 1–191 (2018)
11. Gemmetto, V., Barrat, A., Cattuto, C.: Mitigation of infectious disease at school: targeted class closure vs school closure. *BMC Infect. Dis.* **14**(1), 1 (2014)
12. Habiba, Yu, Y., Berger-Wolf, T.Y., Saia, J.: Finding spread blockers in dynamic networks. In: Advances in Social Network Mining and Analysis, vol. 5498, pp. 55–76 (2010)
13. Hill, S.A., Braha, D.: Dynamic model of time-dependent complex networks. *Phys. Rev. E* **82**(046105), 1–7 (2010)
14. Holme, P.: Modern temporal network theory: a colloquium. *Eur. Phys. J. B* **88**(234), 1–30 (2015)
15. Holme, P., Saramäki, J.: Temporal networks. *Phys. Rep.* **519**(3), 97–125 (2012)
16. Jalili, M.: Effects of leaders and social power on opinion formation in complex networks. *Simulation* **89**(5), 578–588 (2012)
17. Jalili, M.: Social power and opinion formation in complex networks. *Physica A* **392**(4), 959–966 (2013)
18. Jalili, M., Perc, M.: Information cascades in complex networks. *J. Complex Networks* **5**(5), 665–693 (2017)
19. Jiang, Q., Song, G., Cong, G., Wang, Y., Si, W., Xie, K.: Simulated Annealing Based Influence Maximization in Social Networks. In: Proceedings of the Twenty-Fifth AAAI Conference on Artificial Intelligence, pp. 127–132 (2011)
20. Kempe, D., Kleinberg, J., Tardos, É.: Maximizing the spread of influence through a social network. In: Proceedings of the Ninth ACM SIGKDD International Conference on Knowledge Discovery and Data Mining - KDD '03, pp. 137–146 (2003)
21. Leskovec, J., Krause, A., Guestrin, C., Faloutsos, C., VanBriesen, J., Glance, N.: Cost-effective Outbreak Detection in Networks. In: Proceedings of the 13th ACM SIGKDD International Conference on Knowledge Discovery and Data Mining- KDD '07, pp. 420–429 (2007)
22. Mastrandrea, R., Fournet, J., Barrat, A.: Contact patterns in a high school: a comparison between data collected using wearable sensors, contact diaries and friendship surveys. *PloS one* **10**(9), e0136497 (2015)
23. Mihara, S., Tsugawa, S., Ohsaki, H.: Influence Maximization Problem for Unknown Social Networks. In: Proceedings of the 2015 IEEE/ACM International Conference on Advances in Social Networks Analysis and Mining 2015 - ASONAM '15, pp. 1539–1546 (2015)
24. Morone, F., Makse, H.A.: Influence maximization in complex networks through optimal percolation. *Nature* **524**(7563), 65–68 (2015)

25. Murata, T., Koga, H.: Methods for Influence Maximization in Dynamic Networks. In: Proceedings of the 6th International Conference on Complex Networks and Their Applications (Complex Networks 2017), Studies in Computational Intelligence, pp. 955–966. Springer, Berlin (2017)
26. Murata, T., Koga, H.: Extended Methods for Influence Maximization in Dynamic Networks. *Comput. Soc. Networks* **5**(8), 1–21 (2018)
27. Ohsaka, N., Akiba, T., Yoshida, Y., Kawarabayashi, K.i.: Fast and Accurate Influence Maximization on Large Networks with Pruned Monte-Carlo Simulations. In: Proceedings of the Twenty-Eighth AAAI Conference on Artificial Intelligence, pp. 138–144 (2014)
28. Osawa, S., Murata, T.: Selecting Seed Nodes for Influence Maximization in Dynamic Networks. In: Proceedings of the 6th Workshop on Complex Networks (CompleNet 2015), Studies in Computational Intelligence, pp. 91–98. Springer, Berlin (2015)
29. Stehlé, J., Voirin, N., Barrat, A., Cattuto, C., Isella, L., Pinton, J.F., Quaggiotto, M., den Broeck, W., Régis, C., Lina, B., et al.: High-resolution measurements of face-to-face contact patterns in a primary school. *PloS one* **6**(8), e23176 (2011)
30. Tang, Y., Xiao, X., Shi, Y.: Influence maximization: Near-optimal time complexity meets practical efficiency. In: Proceedings of the 2014 ACM SIGMOD International Conference on Management of Data, pp. 75–86 (2014)
31. Vanhemps, P., Barrat, A., Cattuto, C., Pinton, J.F., Khanafer, N., Régis, C., Kim, B.a., Comte, B., Voirin, N.: Estimating potential infection transmission routes in hospital wards using wearable proximity sensors. *PloS one* **8**(9), e73970 (2013)

Index

A

- Active vs. passive walks, 228
- Activity-driven framework
 - baseline, 308–309
 - communities effect, 318–320
 - epidemic spreading process, 307
 - global links formation process, 309
 - local links formation process, 309–311
 - N nodes, 307
 - numerical simulations, 320–322
 - popularity effects, 314–316
 - R&D alliances, 307
 - SIS epidemic processes unfolding, 312–313
 - social memory effect, 316–318
- Activity driven model, 15
- Accessibility, 130, 131, 136, 138
- Adjacent-in-time coupling, 327
- Averaging, 292

B

- Backbone, *see* Information diffusion
- Backtracking transitions, 229–230
- Balanced and unbalanced trees, 132
- Barabási-Albert (BA) power law networks, 204
- Bayesian inference, 66
- Beginning intervals neutralized (BIN) shifts, 129, 130
- Betweenness
 - BA power law networks, 204
 - of link, 211
 - and weight, correlation coefficient, 203
- Birkhoff's ergodic theorem, 282–283
- Bipartite graphs
 - clustering coefficients, 56, 58

defined, 55–57

- information losses, 56
- top/bottom projections, 55, 57
- transitivity, 56

Blinking networks

- clock synchronization, 272
- coupling strength, 271
- defined, 270
- fast switching theory, 272–273
- network synchronization, 271
- nodes' trajectories, 278
- switching network, 271, 272
- synchronization probability, 274
- transversal stability, synchronization, 273, 274

x -coupled Rössler oscillators, 273

- Burstiness parameter, 162, 163
- Bursty-Get-Burstier mechanism, 165–167
- Bursty time series analysis
 - correlation structure, 165–167
 - heterogeneities of IETs, 161
 - human communication patterns, 161
 - measures and characterizations, 162–165
 - memory coefficient, 168–171
 - temporal scaling behaviors, 167–168
- Bursty train size, 162, 164

C

- Centrality, 326
 - adjacent-in-time coupling, 327
 - description, 325
 - discrete-time temporal network, 327
 - eigenvector-based centralities, 326
 - entity, 326

- Centrality (*cont.*)
 marginal and conditional, 328
 Ph.D. exchange network, 334–338
 temporal networks, 325
 ‘time-respecting paths’, 326
- Change points
 empirical dynamic networks, 75
 fitted segments and transition probabilities, 77
 integrated joint likelihood, 77
 maximum-likelihood estimation, 75
 Metropolis-Hastings criterion, 76
 network structures, 79
 number of infected nodes, 78
 occurrence of, 75
 overfitting, 76
 posterior odds ratio, 77
 uniform priors, 76
- Chaotic dynamics, 282–283
- Clique and extinction effects, 256–257
- Clique-based activity-driven networks,
 communication networks
 communities, 38–40
 defined, 25
 dynamic class of, 27, 29
 face-to-face contacts, 25
 frequently asked questions (FAQ) section, 31–33
 fundamental structures, 27
 generative models, 35–36
 link prediction and activity, 36–37
 many-to-many, synchronous networks, 29–31
 one-to-one, one-to-many, many-to-many, 26
 prototypical communicative practices and
 real-world examples, 26
 randomization techniques, 34–35
 the SensibleDTU project, 27
 spreading processes, 37–38
 synchronous vs. asynchronous, 26
 topological properties, 29
 views of, 28
- Communication system, 147
- Community events
 defined, 181, 182
 evolving-membership cluster, 183–184
 fixed membership cluster, 182–183
 temporal network/stream graph, 182
 topological reasons, 181
- Community life-cycle, 186
- Community structure
 empirical temporal networks, 73
 infected nodes over time, 70
 inferred temporal model, 74
 Markov model with, 71
 maximum likelihood parameter, 70
 nodes and edge labels, 72
 parameters, 69
 posterior distribution, 72
 token and memory models, 70
- Compartment model, 235
- Complex networks, *see* Dynamic networks
- Complex systems, *see* Dynamic networks
- Computational social science, 107
- Concurrency
 data, 133–134
 dynamical process, 130
 empirical temporal networks, 133
 interval representation, 134–135, 140–142
 measurement and control, 135
 measurement, reachability, 135–138
 numerically-computed reachability, 132
 reachability of, 138–140
 STDs, 131
 structural cohesion, 131–132
 temporal overlap among contacts, 130, 131
 tractable activity-driven model, 131
 types, 131
- Concurrency effect
 clique and extinction effects, 256–257
 clique-based activity-driven network, 255
 epidemic threshold, 260–263
 in epidemiology, 253
 general activity distributions, 263–265
 model, 255
 network state across time window of
 length, 258–260
 temporal network lacking, 254, 255
- The configuration model, 221
- Connected temporal subgraphs, 112
- Δt -connected temporal subgraphs, 112
- Contact-based (CB) model, 236
- Contact sequence model, 150
- Continuous analysis approach, 151
- Continuous-time description, 240–242
- Continuous-time dynamics, 226–228
- Continuous-time model, 242–245
- Continuous-time Rössler and Duffing
 oscillators, 270
- Continuous-time systems, *see* Blinking
- Control parameter, 122
- Coupled tent maps
 description, 283–284
 statistically coupled maps, 284
 stochastically coupled maps, 284–288

D

- Degree-corrected stochastic block models, 221
 Degree discount, 345, 348
 Diffusion and computational time
 different d in dynamic RIS, 364
 different l in dynamic CI, 360
 different θ in dynamic RIS, 360–363
 Diffusion backbones identification, 210–215
 Diffusion
 active *vs.* passive walks, 228
 bus paradox and backtracking transitions, 229–230
 See also Influence maximization
 Directed acyclic graphs (DAG), 109, 113, 126
 Directed graphs
 defined, 58, 59
 example, 60
 link asymmetry, 59
 out-going and in-coming neighborhoods, 59, 60
 time information and link direction, 60
 transitivity, 61
 Discrete analysis approach, 151
 Discrete-time description, 237–239
 Discrete-time dynamics, 224
 Disease spreading simulation
 applied mathematicians, 12
 contagion event, 12
 infectious period duration, 12
 link-centric and node-centric compartmental models, 13
 mean first passage time, 13
 periodic boundary conditions, 12
 SEIS/SEIR model, 13
 SIR and SIS, 12
 Distance measure, 158
 Driven model, 265–266
 Dynamic communities
 community detection algorithms, 194
 complex network modeling studies, 193–194
 graph partitioning, 187
 methods and scores, 192–193
 SBM and MDL, 187
 scalability and computational complexity, 190–191
 The Ship of Theseus Paradox, 189–190
 temporal smoothness, 187–188
 Dynamic degree discount, 353
 Dynamic graph benchmark, 192
 Dynamic message-passing model, 236

Dynamic networks

- contacts, 7
 controllability, 10
 disease spreading, 12–13
 generalizing centrality measures, 9–10
 influence maximization problem, 11
 links, 7, 8
 node percolation, 11
 nodes, 7
 sentinel surveillance, 11
 vaccination problem, 10

Dynamical processes on time-varying networks, *see* Time-varying networks

- Dynamic CI, 353–354
 Dynamic processes, 97–101
 Dynamic RIS, 354–355

E

- Edge-based compartmental (EBC) model, 236, 245–248
 Edge overlap
 filtering, 90
 node re-ordering methods, 101
 and nodes, 84–85
 redundant coding, 88
 visual clutter, 89
 visual structural information, 90
 Effective degree model, 236
 Eigenvector-based centrality, 329–330
 Empirical cumulative distribution function (ECDF), 157, 158
 Empirical temporal networks, 130
 End intervals neutralized (EIN) shifts, 129, 130
 Epidemic potential, 131
 Epidemics, 100, 103
 Epidemic spreading, 236, 249
 Epidemic threshold, 237, 242, 248, 255–258
 Erdős Rényi (ER) networks, 132
 Erdős-Rényi random graphs, 204
 Event-graph formalism, 184–186
 Evolving-membership cluster, 183–184
 Exponential degree distribution networks, 132
 Extreme value index, 202

F

- Fastest path trees, 206, 215
 Fast switching theory, 272–273
 Fat-tailed inter-event time distributions, 129
 Fixed membership cluster, 182–183
 Fourier modes, 225–226

G

- General activity distributions, 263–265
- Generative models, 35–36
- Global links formation process, 309
- Graph partitioning, 187
- Graph theory
 - defined, 49
 - stream (*see* Stream graphs)

H

- Higher-order Markov chains
 - Bayesian posterior distribution, 67
 - dynamical networks modelling, 67
 - epidemic spreading, 67
 - maximum likelihood, 67
 - posterior distribution, 69
 - proximity events, 66
 - sequence with probability, 66
 - “zero-order”, 68
- Higher-order network models, 7
- Human communication, 148

I

- Identify & Match method, 192
- Individual-based (IB) approach, 236
- Influence maximization
 - degrees in, 350–351
 - diffusion of rumors, 345
 - dynamic degree discount, 345–346
 - information propagation model, 346
 - Monte-Carlo simulation, 345
 - static networks, 347–350
 - temporal networks, 347, 351–353
- Influence maximization problem, 10
- Information diffusion
 - network representation, 200–201
 - SI (*see* Susceptible-infected (SI) model)
 - See also* Shortest paths
- Information propagation model, 346
- Information, *see* Temporal text network
- Information visualisation, 85, 87, 88
- Interevent intervals neutralized (IIN) shifts, 129
- Interevent times (IETs)
 - description, 161
 - dynamical processes, 172–176
 - See also* Bursty time series analysis
- Internet and transportation networks, 199
- Interval graphs, 191

J

- Joint, marginal and conditional centralities, 332–333

L

- Layer aggregation, 340–341
- Layer decoupling, 339–340
- Layouts
 - defined, 86
 - force-based and circular algorithms, 87
 - Gestalt principles, 88
 - MSV, 88
 - redundant coding, 88–89
 - representation methods, 87
- Line graphs, 108, 125
- Link prediction, 17
- Link prediction and activity, 36–37
- Link streams, 191
 - See also* Stream graphs
- Link weight scaling, 204–206
- Local links formation process
 - communities, 310–311
 - social memory, 309–310

M

- Massive sequence view (MSV), 88
- Master stability function, 294–295
- Matrix cube method, 85
- Maximal valid connected subgraphs, 112
- Maximal valid Δt -connected subgraphs, 112
- Mean square synchronization, 280–282
- Memory coefficient
 - analytical solution, 171
 - average fraction, 170
 - empirical observations and values, 169
 - event sequences analysis, 168
 - power-law distribution, 171
 - subsets, 169
- Message-passing, 236, 248–250
- Minimum spanning tree (MST), 202
- Mixing, 230
- Multi-aspect graphs (MAG), 50
- Multicast communication, 150
- Multi-layer network, 150, 326, 328
- Multiplex-network representations, 328–329
- Multiplex networks, 328–329

N

- Network attack/dismantling, 11
- Network model, 276–277

- Network reconstruction, 17, 18
 Network representation, 200–201
Network science
 mesoscopic structures, 8
 nodes/clusters of nodes, 1
 power-law degree distributions/community structure, 15
Network visualisation
 clutter estimation, 91–92
 computational scalability, 101
 connections and inter dependencies, 83
 degree of node, accumulated degree and strength, 86
 dynamic processes, 97–101
 JavaTM implementation, 102
 layouts, 86–89
 mathematical abstraction, 83
 matrix cube method, 85
 multiple edges, 86
 network data, 93
 observation period and temporal resolution, 101
 road and flight networks, 84
 sociogram and ridiculogram, 84
 specific edges, 101
 static network drawings, 84–85
 temporal activity, 94–97
 temporal activity map solution, 101
 temporal structure, 93–94
 transparency and dimensional visualisation, 85
 2D visualisation, 85
 visual clutter, 84, 89–91
Node percolation, 11
Non-backtracking matrix, 248
Non-homogeneous Poisson processes, 223
- Percolation, temporal-network, *see* Temporal-network percolation
Persistent-labels formalism, 183
Popularity effect, 306, 314–316
Precedence, temporal, 153
The preferential attachment model, 221–222
 Preliminary claims, 278–280
- R**
Randomization techniques, 34–35
Random graphs
 The configuration model, 221
 degree-corrected stochastic block models, 221
 Erdős-Rényi model, 221
 The preferential attachment model, 221–222
 stochastic block models, 221
Random walks, 85, 97, 98
 large-scale information, 220
 model diffusion, 219
 paradigmatic model, stochastic process, 219
 Poisson and renewal processes, 222–223
 random graphs, 221–222
 small-world/scale-free networks, 220
See also Diffusion
Reachability graphs, 5
Reachability ratio, 131
Reachability time, 131
Real-world temporal networks
 description, 207
 observation time windows, 207–209
Renewal process, 222–223
Rosenzweig-MacArthur food chain models, 270
- O**
Order parameter, 123
- P**
PageRank algorithm, 325–327, 329, 330, 332–334
Pair-approximations, 236
Path-based metrics
 adjacency and incidence, 151–152
 continuous analysis approach, 151
 discrete analysis approach, 151
 text attribute, 151
 walks and paths, 152–153
Path lengths, 153–156
- S**
Scalability and computational complexity, 190–191
Self-exciting processes, 223
Sentinel surveillance, 11
Sexually transmitted diseases (STDs), 131
The Ship of Theseus Paradox, 189–190
Shortest paths
 backbone construction, 201–202
 network with i.i.d./polynomial link weights, 202–204
SI model, 346, 347
Snapshot sequences, 191
Social closeness, 306
Social memory effect, 316–318

- Social networks, 84, 199
 Spectral radius, 244, 248
 Spreading phenomena, 11
 Spreading processes, 37–38
 Statically coupled maps, 284–288
 Static networks, 347–350
 Stochastic block models, 221
 Stochastic broadcasting
 beyond fast switching, 296–299
 convergence, reference trajectory, 290
 eigenvalues, 289
 fast switching ($m = 1$)
 definition, 293
 master stability function, 294–295
 network topology, 295–296
 Lyapunov exponents, error dynamics, 289
 natural vector-valued extension, 290
 N discrete-time oscillators, 289
 reference node, 289
 synchronous solution, 291–292
 technological and biological systems, 288
 tent maps revisited, 292–293
 Stochastic extinction, 256
 Stochastic stability
 blinking networks, 270
 chaotic dynamics, 282–283
 mean square stability, synchronization, 278
 mean square synchronization, 280–282
 network model, 276–277
 non-fast switching connections, 270
 preliminary claims, 278–280
 synchronization, 269, 271
 temporal/evolving networks, 269
 Static-graph-based methods, 108
 Stream graphs
 defined, 49
 example of, 50
 global positioning, 51
 graph-equivalent, 50
 nature of data, 50
 See also Bipartite graphs; Directed graphs;
 Weighted graphs
 Structural cohesion, 132, 139, 140, 141, 143
 Supracentrality framework
 joint, marginal and conditional centralities,
 332–333
 matrices, 331–332
 Susceptible-infected (SI) model
 backbone construction, 206
 description, 199
 diffusion backbones identification, 210–215
 real-world temporal networks, 207–209
 relationship between diffusion backbones,
 209–210
 Susceptible-infected-susceptible (SIS) model
 activation of cliques, 255
 clique and extinction effects, 256–257
 epidemic threshold, 256
 Synchronization, 269
- T**
- Temporal adjacency, 110–111
 Temporal contacts, 129, 131, 134, 138, 140,
 141
 Temporal correlations, 110
 Temporal/evolving networks, 269
 Temporal motif, 42
 Temporal motifs and D, 118–120
 Temporal-network percolation
 D components
 analysis with D, 122–124
 empirical examples, 124–125
 size measurement, 121–122
 Temporal networks
 boundaries, 3–4
 connectivity, 4–5
 events, 3
 fundamental structures, 9
 Hawkes process, 17
 mathematical and computational
 frameworks, 1, 2
 mesoscopic structures, 7–9
 power-law degree distributions/community
 structure, 15
 procedures, 15
 randomization schemes, 14–15
 research themes, 2
 static networks, projections, 5–7
 See also Dynamic networks; Change
 points; Community structure;
 Higher-order Markov chains;
 Network visualisation
 Temporal precedence, 153
 Temporal scaling behaviors, 167–168
 Temporal smoothness, 187–188
 Temporal text network
 communication processes, 147, 148
 contact sequence model, 150
 edges, 148
 human communication, 148
 information diffusion processes, 147–148
 model, 149, 150
 multi-layer network, 150
 representation, 149
 Twitter user interactions, 148
 unicast and multicast communication, 150
 See also Path-based metrics; Path lengths

- Text, *see* Temporal text network
Theseus ship, 189–190
Time-independent networks, 329–330
Time-respecting path, 112
Time-varying networks (TVG), 12, 50
 activity-driven framework (*see* Activity-driven framework)
 face-to-face and digital interactions, 306
 social approach, 306
 social closeness and popularity, 306
Two-dimensional random walk model, 15
- U**
Unicast communication, 150
- V**
Vaccination problem, 10
Visual clutter, 84, 89–91
- W**
Weak temporal connectivity, 111
Weighted graphs
 approaches, 54
 bipartite graph studies, 53
- clustering coefficients, 52, 54
defined, 51, 53
example, 53
generalizing density, 52, 54
maximal, minimal and average, 52
node strength, 52
transitivity, 53, 55
Weighted network, 200–202
Weighted temporal event graphs
 Δt -adjacency, 111
 connected temporal subgraphs, 112
 Δt -constrained time-respecting paths, 113
 construction, 114–115
 definition, 113–114
 hyper-event graphs, 111
 maximal valid connected subgraphs, 112
 maximal valid Δt -connected subgraphs, 112
 temporal adjacency, 110–111
 temporal motifs and D, 118–120
 threshold, 115–116
 time difference between events, 109–110
 time-respecting path, 112
 weak Δt -connectivity, 111–112
 weak temporal connectivity, 111
 weighted event graph, 113–114
Window of opportunity, 274, 287